NASA Conference Publication 2188
NOAA/NEMP III 81 ABCDFG 0042

Chesapeake Bay Plume Study

Superflux 1980

Proceedings of a symposium held
in Williamsburg, Virginia
January 21-23, 1981

NASA

NASA Conferenc
NOAA/NEMP III 81 ABCDFG 0042

Chesapeake Bay Plume Study

Superflux 1980

Edited by
Janet W. Campbell
Langley Research Center

James P. Thomas
Northeast Fisheries Center

Proceedings of a symposium sponsored by the National Aeronautics and Space Administration and the National Marine Fisheries Service, National Oceanic and Atmospheric Administration, U.S. Department of Commerce and held in Williamsburg, Virginia January 21-23, 1981

NASA
National Aeronautics and Space Administration

Scientific and Technical Information Branch

1981

PREFACE

This conference publication contains the proceedings of a symposium which was held in Williamsburg, Virginia, January 21-23, 1980, on the results of the 1980 Chesapeake Bay Plume Study. The study, called Superflux, was initiated in 1980 to delineate the role of remote sensing in Federal programs concerned with monitoring and assessing the effects of pollution on marine resources.

Sponsored jointly by the Northeast Fisheries Center of the National Marine Fisheries Service - National Oceanic and Atmospheric Administration - and NASA Langley Research Center, the study concentrated on the use of airborne remote sensors to assess the impact of estuarine outflows on shelf ecosystems. The Chesapeake Bay plume was selected as the site for a series of prototype experiments, and a number of state agencies and universities participated in the study. Three interactive aircraft-boat experiments focused on techniques to characterize the spatial extent, variability, and biochemical properties of the plume during periods of high, moderate, and low runoff.

The symposium consisted of three sessions in which the participants presented the results of experiments involving the physical dynamics, geochemistry, and biology of the Chesapeake Bay plume. These experiments also provided the first opportunity for an intercomparison of the operational requirements and data output of different remote sensing instruments. Since the year during which the Superflux experiments took place (1980) was particularly dry, the data collected will be useful as a benchmark, or point of reference, for analysis of other data in these areas which may be collected in the future.

Use of trade names or names of manufacturers in this report does not constitute an official endorsement of such products or manufacturers, either expressed or implied, by the National Aeronautics and Space Administration.

Janet W. Campbell
James P. Thomas

Co-Conveners

CONTENTS

RESULTS III. BIOLOGY
Chairman: Wayne E. Esaias
NASA Langley Research Center

A BENCHMARK MULTI-DISCIPLINARY STUDY OF THE INTERACTION BETWEEN THE CHESAPEAKE BAY AND ADJACENT WATERS OF THE VIRGINIAN SEA

William J. Hargis, Jr.
Virginia Institute of Marine Science
College of William and Mary

Estuaries are by definition coastal bodies of water emptying into the seas or oceans of the world through semi-restricted openings within which the salt water from the sea is diluted by freshwater from land drainage (ref. 1). Such systems, especially large ones, behave like semi-enclosed brackish water reservoirs and have physical, chemical, geological, and biological features different from those of the ocean into which they open and flow and from the freshwater streams which empty into them. Generally speaking, uncontaminated estuaries are extremely fertile, producing large quantities of animal and plant materials (i.e. total biomass) each biological year. Consequently, they are sites of many highly productive and valuable inshore fisheries and the spawning areas or nursery grounds of many species of finfish which range the waters of the continental shelves of the Earth's oceans. They also shelter many plants and invertebrates of ecological or economic significance.

The sheltered waters and extensive tidal shorelines of estuaries also provide ports, industrial and residential sites, recreational opportunities, and tourist attractions. Because of these attractions and amenities, estuarine shorelines are usually the first places to be populated when countries are colonized from the sea or when agricultural and economic development occurs, and they grow rapidly. Urban and industrial development in such areas is common. Consequently multiple-use problems involving conflict among the many users are common in heavily populated areas and they inevitably increase as populations grow. During periods of growing international commerce, estuarine shorelines often experience explosive growth and utilization and natural or traditional uses are "pinched" even further.

In the United States, a look at the major population centers of the East, Gulf, and West coasts demonstrates the accuracy of these statements. Some examples include Boston on the Charles estuary, New York City on the Hudson, Philadelphia, Chester and Wilmington on the Delaware, the principal urban areas of Baltimore, Washington, Richmond-Hopewell and the Hampton Roads complex in the Chesapeake Bay region, Charleston on the estuarine portions of the Ashly and Cooper Rivers and their confluence, New Orleans on the Mississippi, Corpus Christi and San Francisco on the bays of the same names, and the Seattle-Tacoma complex on Puget Sound. Many more could be cited, and this situation applies the world over.

Because of their social and economic importance and associated multiple-use development and management problems, as well as their internal physical, geological, chemical, and biological complexities, estuaries have become the

objects of much scientific study and technological advancement over the last thirty years in the United States and many other countries.

The Chesapeake Bay, the largest estuary in the United States, exemplifies this last point. At present a large array, probably the largest on any similar body of water in the world, of scientific and technological specialists and institutions is engaged in investigation of its natural and socially-related phenomena and problems, and a great deal has been discovered in the last three decades. For example, the Chesapeake Bay Bibliography series (refs. 2 to 6) contains over 6610 entries.

Despite the efforts and the knowledge developed by recent and extant scientists and institutions and their predecessors, much of scientific, technological, and managerial importance remains to be learned. It is not yet possible to answer many of the critical questions which would allow determination of cause and effect or prediction and management.

A number of reasons account for our continuing relative ignorance of certain important features. Estuaries are naturally complex and dynamic, subject to changes of great magnitude, violence, and suddenness in the catastrophic events experienced. They are also subject to the lesser, but still significant, fluctuations which occur over long periods of time, such as dry years, wet years, and years of average annual rainfall, as well as to the smaller but more frequent daily, monthly, and seasonal changes.

Not only has nature made certain estuaries especially large and/or complex, dynamic, complicated, and extremely difficult to grasp, understand, and manipulate, but society has superimposed its own complicating and dynamic effects, all of which make the task of understanding and controlling estuarine environments and resources even more difficult. At times it may seem impossible to develop adequate understandings of such natural systems using traditional means of field sampling (or laboratory observation), analysis, and deduction or induction which have stood the scientific method in such good stead over the years of recorded human history. Only in recent years have techniques of sampling and analysis, e.g. automated samples, instrumented buoys, high-speed computers, sensitive micro-analytical techniques, hydraulic models, wide-area remote sensing, and accurate navigation and positioning developed the power and scope to give encouragement that such systems may soon be better understood.

For some years, science administrators and scientists interested in understanding large systems like the Chesapeake have dreamed of being able to plan and mount large-scale multi-disciplinary field and laboratory efforts designed to gather, analyze, and synthesize biological, chemical, geological, physical, and even socio-economic data taken at the same time (or nearly so) over the entire length and breadth of the Bay, or large segments of it. They have also wished to understand the interactions between the Chesapeake and its tributaries, especially the principal ones, and those between the Bay and the adjacent waters of the Atlantic. Comprehensive synoptic and simultaneous studies of the passage or flux of energy, chemicals, biological entities, turbidity, and other factors into, through, and out of the estuarine system

have been particular dreams. The goal has been to develop a comprehensive understanding in sufficient detail to enable accurate explanation, precise prediction and, hopefully, wiser use and manipulation.

The Chesapeake Bay drains large expanses of four states - New York, Pennsylvania, Maryland and Virginia - and lesser portions of West Virginia and Delaware (fig. 1). Principal inflow from the Susquehanna system provides approximately 50% of all the fresh water entering the system. The rest is provided by the Potomac (18%) and the James (14%), with the remaining (18%) coming from all of the other rivers of the eastern shores (fig. 1). The Bay is 156 n. mi. long and 25.6 n. mi. wide at its widest and encompasses 11.5×10^9 m^2 (2 841 650 acres) of surface area with a volume of 74×10^9 m^3 (11.6 cubic miles) of water. Though its deepest spots in the natural channels are quite deep (i.e. 53 m (175 ft)) it is essentially a shallow body of water, averaging about 8 m (27 ft) in depth in its main body. Including the tributaries, it averages 6 m (21 ft) in depth (ref. 7). Its shallowness renders it subject to violent stirrings by wind. Its waters are frequently quite turbid as a consequence of wind action, river flow, and runoff. Normally the tide ranges about 1 m (3 ft).

Like all great estuaries with a large but varying volume of freshwater inflow, the Chesapeake experiences wide fluctuations in its physical and chemical parameters, which vary considerably at any one spot in the water column. They also fluctuate up and down the Bay and between day and night, as well as seasonally and annually on a regular or sometimes irregular basis (refs. 8 to 11).

Fluctuations in salinity are especially significant indicators of such variability and its importance. Figures 2, 3, and 4, depicting salinity at specific locations and depths and by years, show this quite clearly. For example, figures 2 and 3 compare salinities in several different years at comparable locations in the James and York estuaries. During periods of drought over the drainage basin, higher salinity ranges far up these tidal tributaries. During the extremely dry period of the mid-1960's it moved some 21.7 n. mi. inland, up the tidal James, reaching to the city of Hopewell and threatening municipal and industrial water supplies (fig. 4). Figure 4 also shows that the distribution of the male and female blue crabs (Callinectes sapidus) was affected since there is some sorting by sex of that species with the females remaining in higher salinity waters. Such salinity-related destructions affect a number of economically and ecologically important estuarine species. Similar changes occurred in the main stem of the Bay proper, as shown in figure 5 which depicts salinities during normal (1968) and wet (1972) years at the surface and bottom at the same stations.

The extremely wet years occurred when two tropical storms (i.e. former Gulf coast hurricanes), Camille (August 1969) and Agnes (June 1972), visited the basin. These episodes generally caused marked reductions in salinities throughout the Bay, but the responses were complex and scientifically interesting (ref. 12). An immediate aftermath of Agnes was large-scale freshwater mortalities over the vulnerable low-salinity upstream oysterbeds of the basin. A long-term effect of these salinity changes was a marked reduction in the

abundance of the two oyster-eating snails, Urosalpinx cinerea and Eupleura caudata, and a number of mortality-causing oyster disease organisms. Thus, long-term recovery and survival of oyster populations on higher-salinity beds have been much better than formerly since Agnes visited the area in 1972, at least until 1980-81 when two dry years began to allow salinities in those same places to increase.

The Agnes episode also provided scientists with an opportunity to investigate for the first time the details of the effects of such Bay-wide catastrophic events. An entire volume resulted from the multi-institutional, multi-disciplinary investigations that took place (ref. 12). Agnes not only affected the Chesapeake but also produced low salinities far out over the shelf waters around the mouth of the Chesapeake, mostly northward, as shown in figures 6 and 7 (ref. 12).

Many other important features of the Bay also vary. For example, the currents at any one spot in the system also vary daily and seasonally and, at times, annually. The amount of fresh water entering the system at any one time, in relation to the salt water from the ocean, influences not only salinity (especially) and temperature but currents as well. Other physical features such as turbidity (due to sediment-laden land runoff from above and below the fall line, plankton productivity, and resuspension of particulates from the bottom), color, and transparency are also affected by freshwater inflow from contributing streams and from adjacent highland and lowland areas. Estuarine chemistry is likewise affected by rainfall, temperature, sediment influx and resuspension, biological processes, and other factors, including the chemical contributions from society's many industrial, domestic, and agricultural activities. Additionally, chemical oxygen demand (COD), biological oxygen demand (BOD), nutrients, trace metals, many toxicants, and many other chemicals and chemically-related phenomena are influenced by rainfall and runoff and injections from point-source or non-point-source discharges.

Biological systems within the estuary are influenced directly, indirectly, and inter-reactively by all the physical, chemical, and geological factors mentioned above. Hence, biological productivity may be affected favorably or adversely by changing nutrient levels and types or by toxicants (usually adversely), salinity, temperature, turbidity, transparency, and other factors.

As indicated above, salinity is important to estuarine biological systems since many species are themselves directly salinity-dependent or salinity-limited. Most are indirectly affected as well; for example, the several pathogens and predators (i.e. MSX, Dermocystidium, and other diseases, and the oyster drills Urosalpinx cinerea and Eupleura caudata which damage oysters) may be allowed (or caused) to invade oyster beds previously protected by low salinities when drought causes an increase in the salinity levels in the waters over those beds. Conversely, extremely low salinities caused by a surfeit of freshwater inflow can kill oysters in those same previously productive beds. Many similar fluctuations can occur in the populations of other changeable species of ecological and economic significance.

Scientists have long been interested in the physical, chemical, geological, and biological interactions between the Chesapeake Bay and the waters of the nearby littoral and shelf regions. The integrity and productivity of the Bay is closely dependent upon the Atlantic waters which enter within the approximately 15.6-n.-mi.-wide mouth between Cape Henry and Cape Charles. The tremendous volume of salty ocean water (about 32 parts per thousand of salts at the Bay mouth) obviously influences salinities far into the Bay, and waterborne ocean sediments, animals, and plants play a strong role in productivity of the system. Conversely, the coastal and nearby shelf waters of the Chesapeake Bight of the Mid-Atlantic Bight are known to be greatly influenced by fresh water from the nearby Chesapeake and Delaware Bays. It remains to be determined how much influence each system has on the other, how far these interacting influences extend southward (around Cape Hatteras into the Carolinas) and northward (off of Maryland, Delaware, and New Jersey), what their seaward distribution is, how they change, and what influence the estuarine-generated water, sediments, detritus, contaminants, and biological systems have on coastal and shelf waters.

To understand such complex and dynamic systems and answer the questions involved in developing such understanding involves large-scale, multidisciplinary field and laboratory research efforts. It also involves carrying out such studies over long periods of time because many natural phenomena exhibit not only short-period but long-period variability and studies must be of sufficient duration and extent to cover such periodicities. For example, one must cover normal or average periods as well as abnormal or extreme periods in order to understand the ups and downs of fishery populations, since population levels can be markedly influenced by extremes in physical, chemical, or even biological aspects of their habitats.

In 1979 scientists and employees from a number of scientific institutions joined in a multi-institutional, multi-disciplinary study of the lower Chesapeake Bay and adjacent coastal and shelf waters. The project, called Superflux, the field phases of which were carried out during the period from March to October of 1980, involved personnel from the National Aeronautics and Space Administration's Langley Research Center and Wallops Flight Center; the Virginia Institute of Marine Science (VIMS); Chesapeake Bay Institute of the Johns Hopkins University; the National Marine Fisheries Service of the National Oceanic and Atmospheric Administration (NOAA), Northeast Fisheries Center; NOAA's National Ocean Survey and Atlantic Marine Center; Research Triangle Institute; the College of Marine Studies of the University of Delaware; Old Dominion University; the U.S. Navy (Oceana Naval Air Base, Little Creek Amphibious Base, and the Naval Academy); the Environmental Protection Agency; the U.S. Coast Guard; Anne Arundel Community College; the Department of Natural Resources of the State of Maryland; and the University of Miami.

As frequently happens in scientific research, unforeseen events conspired to make Superflux of special interest. A severe drought (which markedly reduced rainfall and hence river flow) over the entire East Coast throttled the outflow of the major tributaries entering the Mid-Atlantic Bight. For example, rainfall dropped to extremely low levels and riverflow into the Chesapeake was reduced to the lowest since 1966-67, when the salt water

intrusion zone moved upstream some 21.7 n. mi. into the James and other tributaries. That this unusual natural event should occur at a time when scientific forces were marshalled and active in the three segments of Superflux was especially notable.

The severity of the drought which occurred during the Superflux experiments offered an unusual opportunity to observe rainfall-dependent phenomena Bay-wide and in synoptic fashion during an extreme condition. In this sense, the measurements made during Superflux will serve as a benchmark for future monitoring of this area. The results of these experiments demonstrated the influence of extreme low-flow conditions on the mouth of the Chesapeake and the nearby Atlantic using remote sensing techniques and sea truth observations during periods of high and normal flow.

The Superflux experiments were also marked by a notable degree of interdisciplinary scientific and technical coordination, from data collection all the way to analysis and interpretation. Several times in the past, scientists have attempted to plan and carry out large-scale sea truth observations to compare them with the observations made by remote sensing instruments. Attempts have been made to correlate surface and subsurface oceanographic measurements with remote-sensing passes from low, intermediate, and high altitudes as well as satellite overflights. Superflux marks the most successful effort to date in bringing about such a coordinated effort between marine scientists and remote sensing scientists.

Future efforts in ocean research and development should devote high priority to large-scale, multi-disciplinary examinations of estuarine, coastal, and near-shore oceanic regions. Much remains to be learned in order to allow proper scientific understanding, prediction and management. Remote sensing techniques should again be paired with large-scale, synoptic observations of the several important natural and economically- and socially-related phenomena to develop new understandings and predictive models of estuarine and coastal waters in order to enable reasonable selections and sound management and economic decisions. Science and economics will both be served by the resulting improved understanding.

REFERENCES

1. Pritchard, D. W.: What is an Estuary: Physical Viewpoint. Estuaries, G. H. Lauff, ed., AAAS publication no. 83, 1967, pp. 3-5.

2. Barrick, S. O.; Davis, M. B.; Tennyson, P. S.; Wojcik, F. J.; Norcross, J. J.; and Hargis, W. J.: The Chesapeake Bay Bibliography, vol. 1: The James River. Special Scientific Report No. 58, Virginia Institute of Marine Science, 1981.

3. Tennyson, P. S.; Barrick, S. O.; Wojick, F. J.; Norcross, J. J; and Hargis, W. J.: The Chesapeake Bay Bibliography, vol. II: Virginia Waters. Special Scientific Report No. 63, Virginia Institute of Marine Science, 1975.

4. Stauble, J. F.; and Wood, D. H.: The Chesapeake Bay Bibliography, vol. III: Maryland Waters, A Coastal Zone Management Report of the Maryland Department of Natural Resources and the Virginia Institute of Marine Science. Special Scientific Report No. 73, Virginia Institute of Marine Science, 1975.

5. Gleeson, S. A.; and Stauble, J. F.: The Chesapeake Bay Bibliography, vol. IV: Virginia Waters, A Report for Virginia's Coastal Resources Management Program. Special Scientific Report No. 80, Virginia Institute of Marine Science, 1976.

6. Loesch, M. N.: The Chesapeake Bay Bibliography, vol. V. Special Scientific Report No. 107, Virginia Institute of Marine Science, 1981.

7. Cronin, W. B.: Volumetric, Areal, and Tidal Statistics of the Chesapeake Bay Estuary and Its Tributaries. Special Report 20, Reference 7102, Chesapeake Bay Institute, Johns Hopkins University, 1971.

8. Whaley, H. H.; and Hopkins, T. C.: Atlas of the Salinity and Temperature Distribution of Chesapeake Bay 1949-1951. Graphical Summary Report 1, Reference 52-4, Chesapeake Bay Institute, Johns Hopkins University, 1952.

9. Hines, R. I.; Stroup, E. D.; and Seitz, R. C.: Atlas of the Distribution of Dissolved Oxygen and pH in Chesapeake Bay 1949-1961. Graphical Summary Report 3, Reference 63-4, Chesapeake Bay Institute, Johns Hopkins University, 1963.

10. Stroup, E. D.; and Lynn, R. J.: Atlas of Salinity and Temperature Distributions in Chesapeake Bay 1952-1961 and Seasonal Averages 1949-1961. Graphical Summary Report 2, Reference 63-1, Chesapeake Bay Institute, Johns Hopkins University, 1963.

11. Stroup, E. D.; and Wood, J. H.: Atlas of the Distribution of Turbidity, Phosphate, and Chlorophyl in Chesapeake Bay, 1949-1951. Graphical Summary Report 4, Reference 66-1, Chesapeake Bay Institute, Johns Hopkins University, 1966.

12. The Chesapeake Research Consortium, Inc.: The Effects of Tropical Storm Agnes on the Chesapeake Bay Estuarine System. CRC publication no. 54, The Johns Hopkins University Press, 1976.

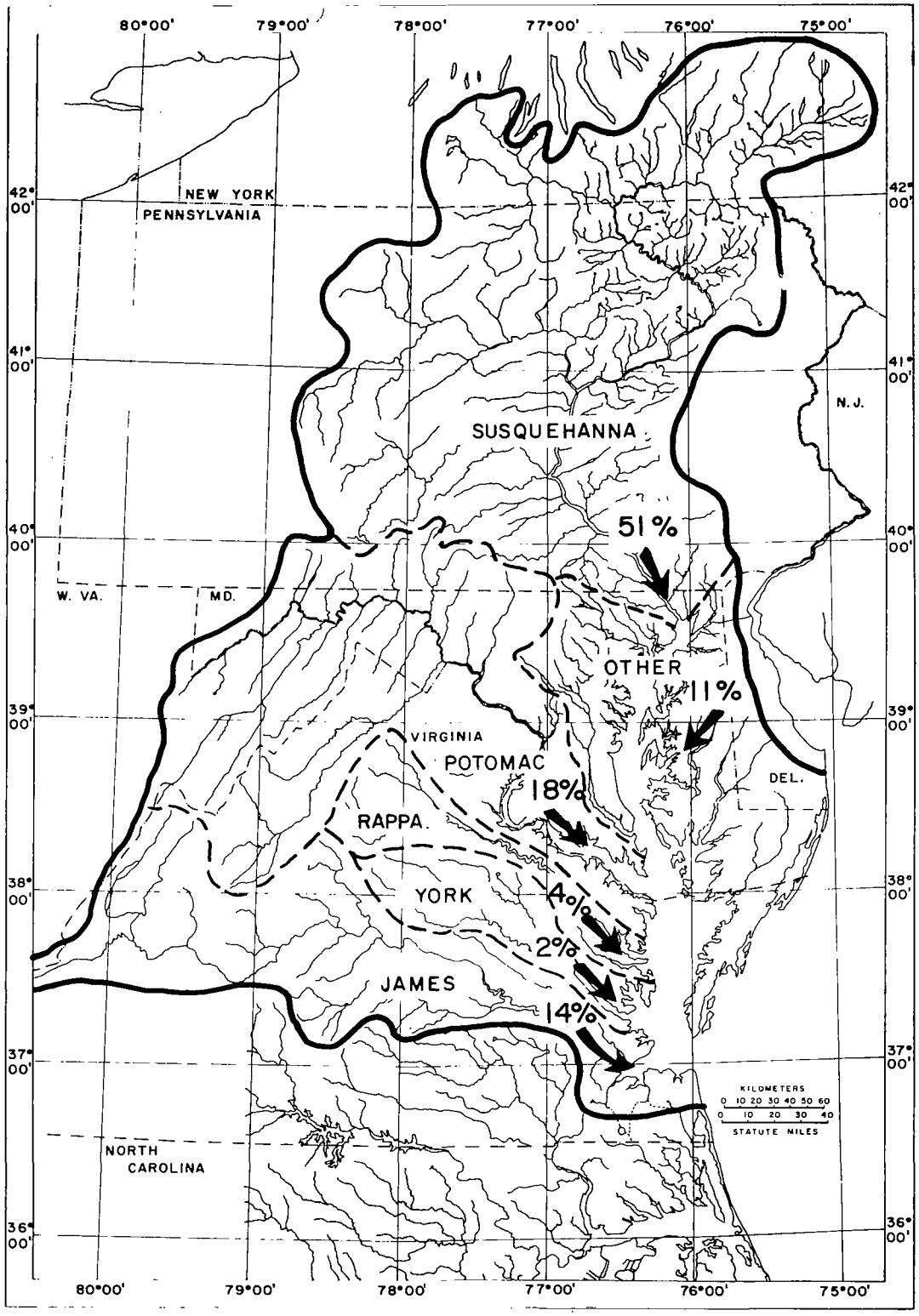

Figure 1.- Chesapeake Bay drainage basin showing sub-basins and approximate freshwater contribution by major tributaries.

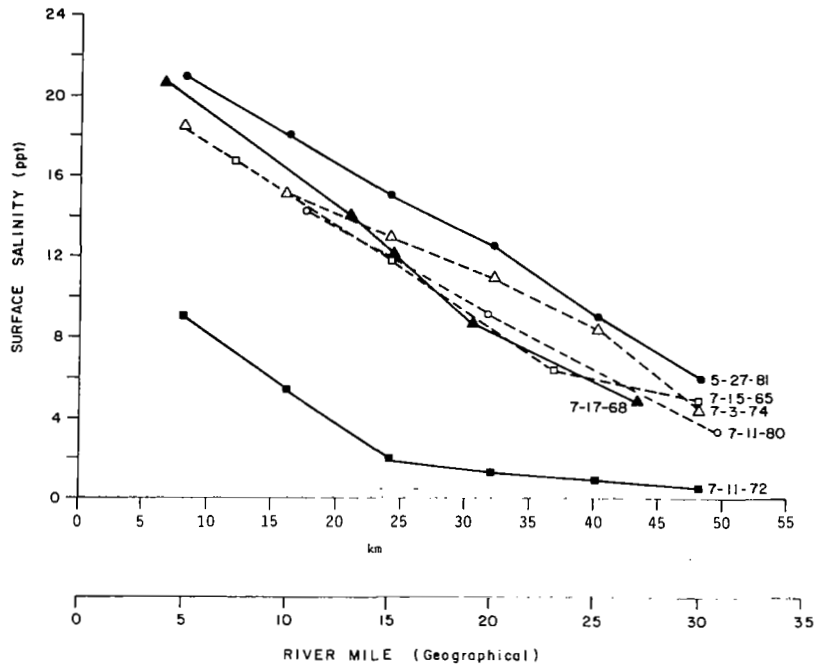

Figure 2.- Surface water salinity of the James River by river mile during periods of high rainfall (1972, tropical storm Agnes), normal rainfall (July 1968), and drought (1965, 1974, and 1980-1981).

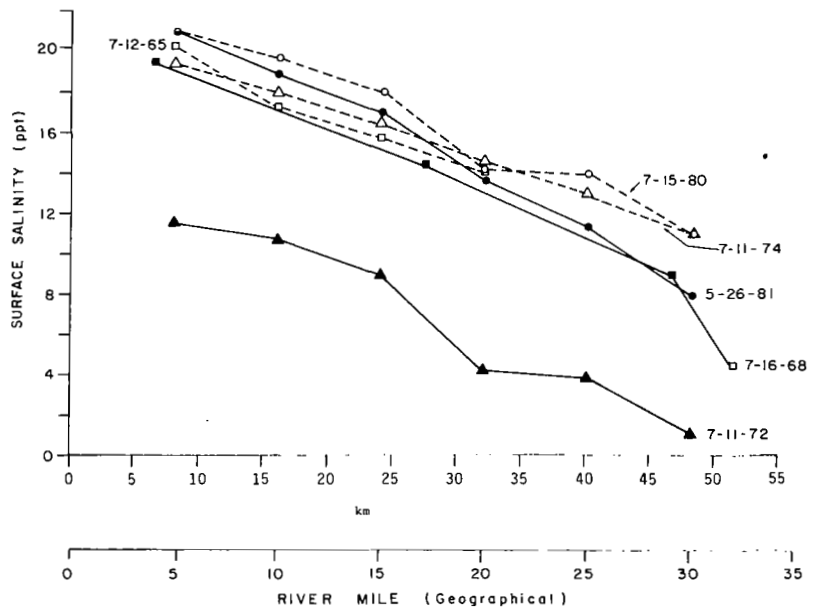

Figure 3.- Surface water salinity of the York River by river mile during periods of high rainfall (1972, tropical storm Agnes), normal rainfall (July 1968), and drought (1965, 1974, and 1980-1981).

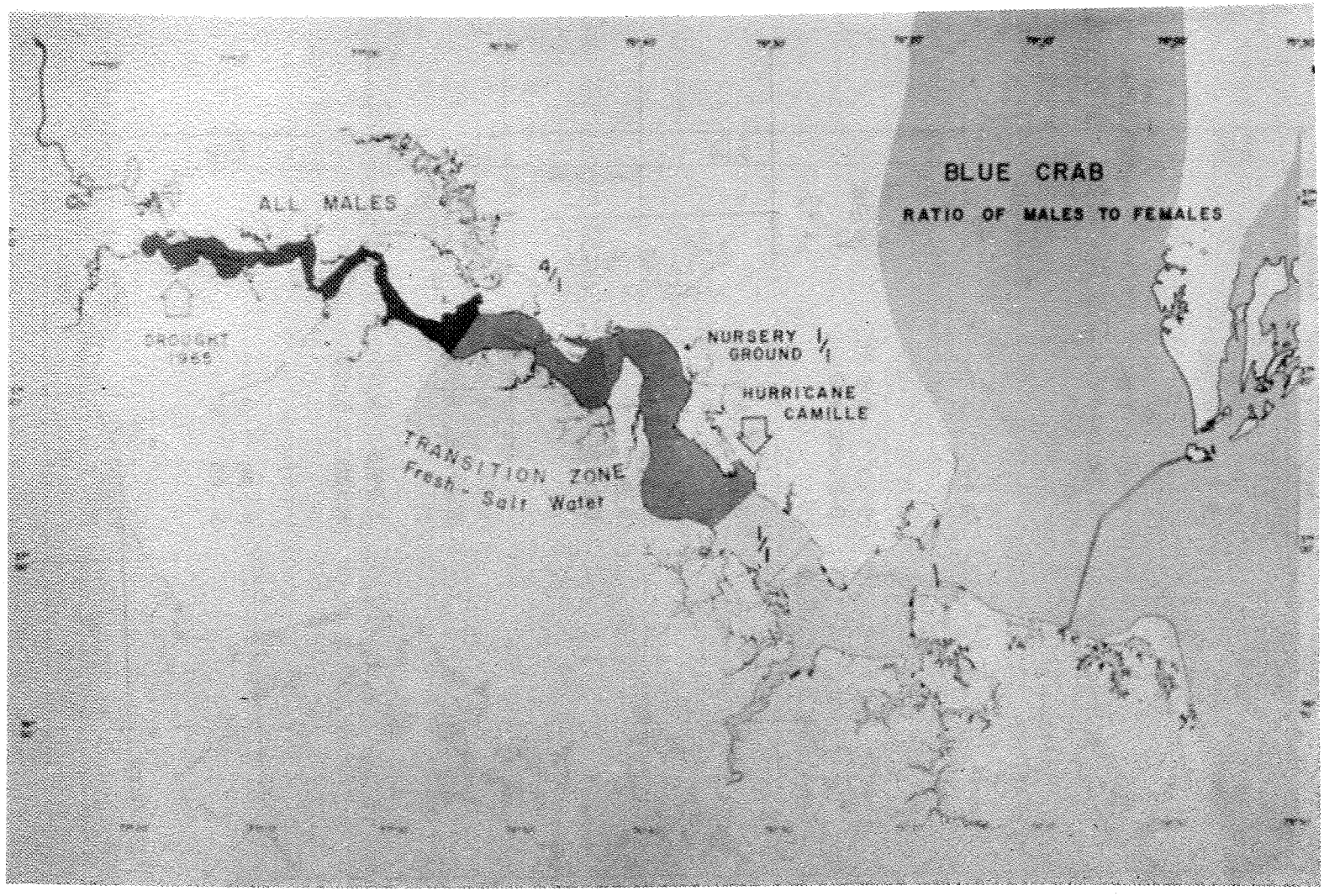

Figure 4.- Influence of drought (1965) and high rainfall (tropical storm Camille, August 1969) on the salinity transition zone and on the ratio of male to female blue crabs in the James River.

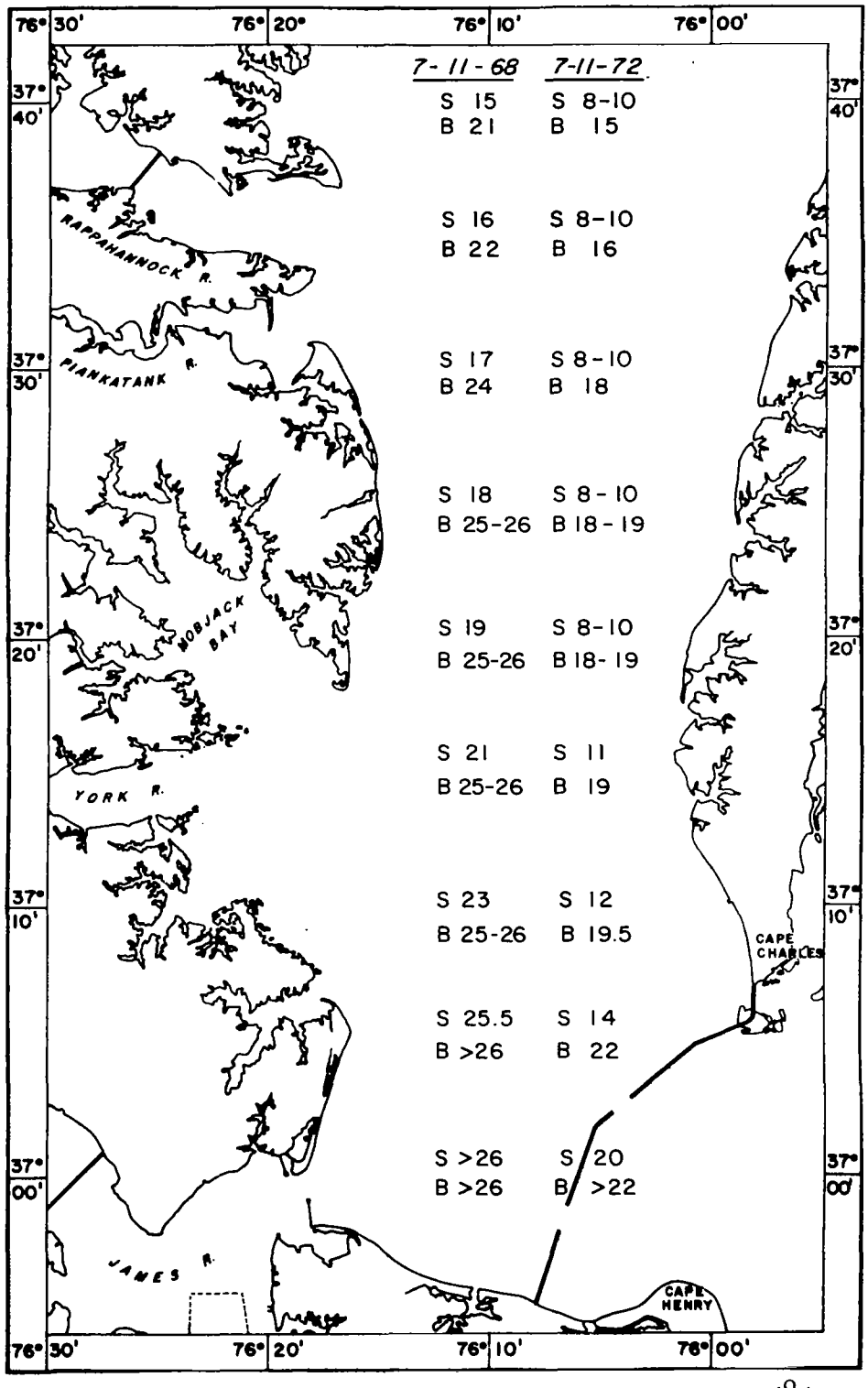

Figure 5.- Distribution of salinity in parts per thousand (^{o}/oo) at the same locations in the Chesapeake Bay during July, 1968 (average to below-average rainfall period) and July 1972 (high rainfall period, tropical storm Agnes).

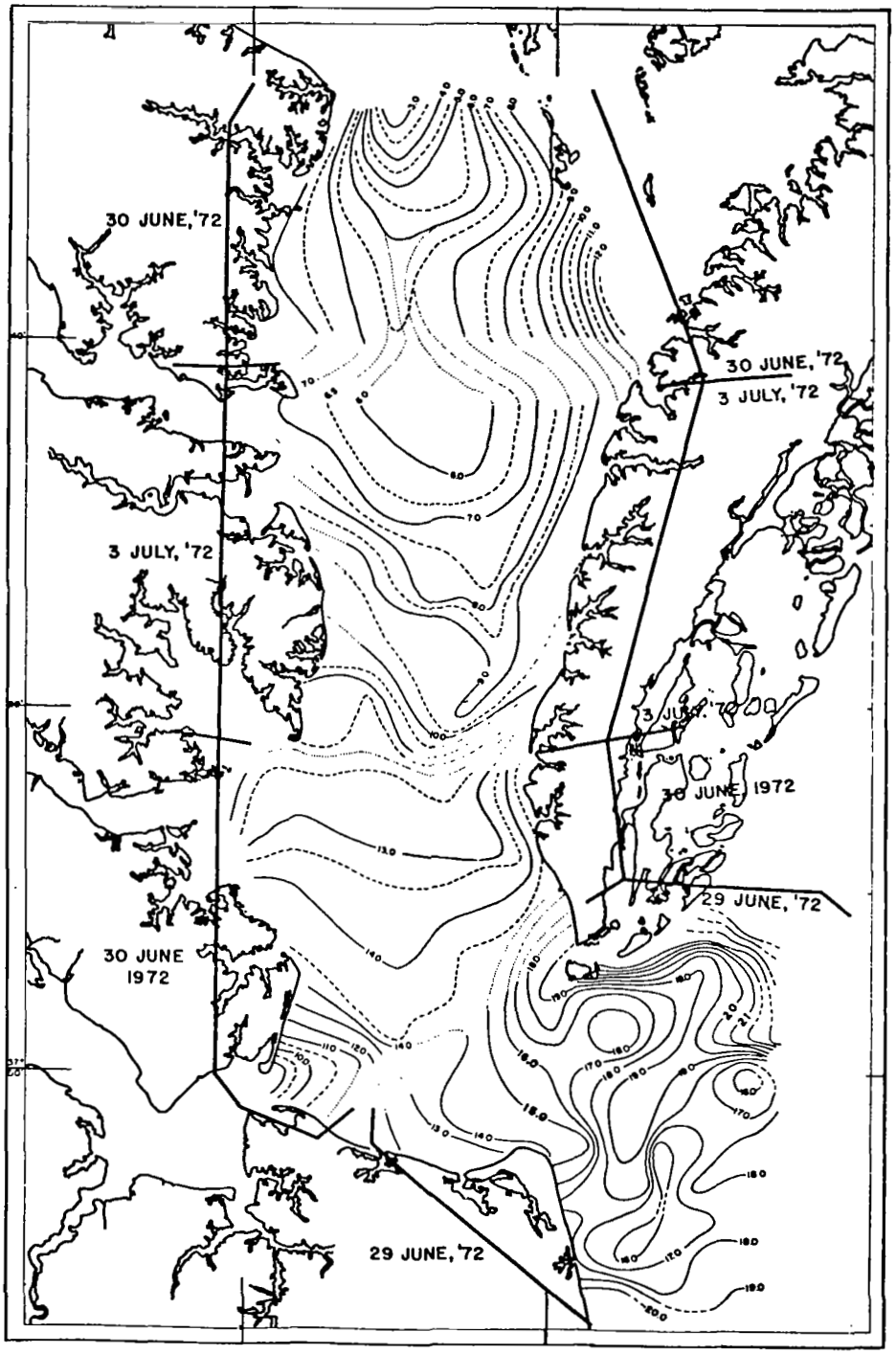

Figure 6.- Surface salinities in the lower Chesapeake Bay one week (June 29 to July 3, 1972) after passage of tropical storm Agnes through the region (June 21 and 22, 1972) (from ref. 12).

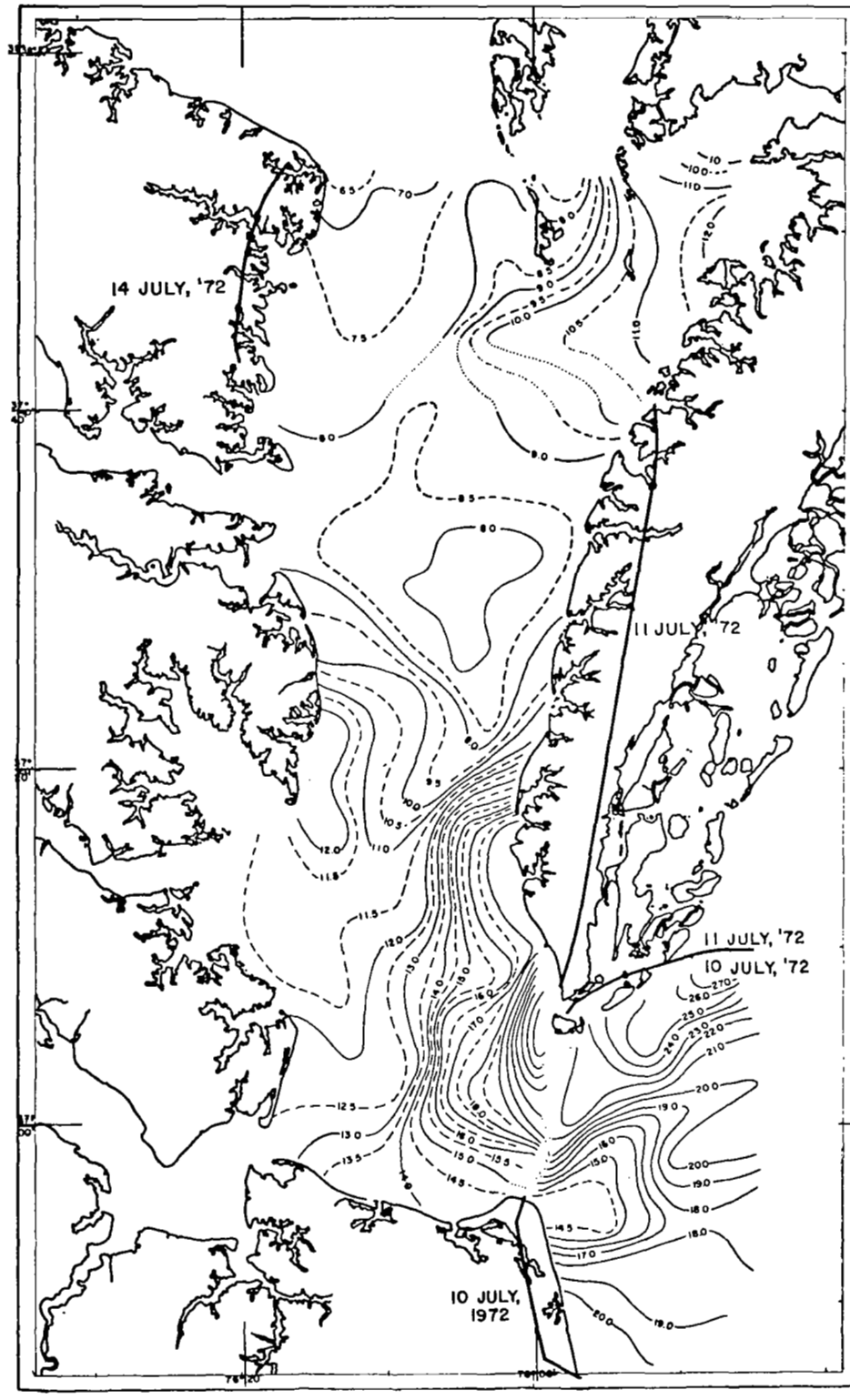

Figure 7.- Surface salinities in the lower Chesapeake Bay two weeks (July 10-14, 1972) after passage of tropical storm Agnes through the Chesapeake Bay region (June 21 and 22, 1972) (from ref. 12).

A MARINE ENVIRONMENTAL MONITORING AND ASSESSMENT PROGRAM

John B. Pearce
Division of Environmental Assessment
National Marine Fisheries Service
Northeast Fisheries Center
Sandy Hook Laboratory
Highlands, New Jersey

During my flight on a Pan Am clipper from Newark to Norfolk, I happened to read the airline magazine called Pan Am Clipper. In the particular issue there was an article entitled, "The future imperfect". The topic of the article had to do with the success of the various pundits and prognosticators to predict what might happen in recent decades. The article noted that the accuracy of many individuals who tended to be pessimistic about the future world, when they were making their predictions some decades ago, was extremely poor; individuals who were talking about the world of 1984 or the "brave new world" of the 60's and 70's generally turned out to be quite wrong. However, the optimists who were making predictions about the world in which citizens of the 1970's and 80's would live free of the worry of starvation, war, or some other disaster were also equally wrong. Many of the so-called futurists had predicted that by this time man would be living in self-contained units at the floor of the sea and would be producing all of the foodstuffs and other of life's requirements that would meet the needs of the world's population.

What turned out to be the case is that where mankind has had modern technology at his disposal he has often, for various reasons, not taken advantage of the technology. In some cases it would be possible to build living units under the sea where the general citizen could carry out his life activity in terms of harvesting living and mineral resources. As we know, in certain cases we are now doing this for limited periods; divers can now acclimate to pressures of 700 to 800 m under the surface of the water, and there are many new techniques for harvesting fish and installing deepwater mineral recovery devices. The reality is, however, that there is no good economic reason at the present time for most of us to dive to these depths or to use new methods of fish harvesting when living resources of the sea are probably already being over-exploited.

The reality though will be that as mankind moves into the 21st century it will be faced with the problem of feeding a world population which will have doubled from the present 4 billion to well over 8 billion people. This increase in population is occurring at a time when many of our agrarian and forestry resources are already being over-harvested and, perhaps, at a time when severe climatic change is already resulting in droughts which will severely reduce the production of food items from the earth's surface. Thus, mankind will have to look to the seas for increased yields of proteins and other foodstuffs. If mankind is already harvesting or over-harvesting

fishery resources, what can be done? As I will show in a few minutes, there are a number of nations that have already begun projects in ecological aquaculture and sea ranching, which is essentially a form of aquaculture pursued in open waters, and without use of ponds, aquaria, and other devices to contain the fishes of interest. New technology will allow us to greatly increase the productivity of the oceans, especially estuaries and coastal habitats.

At the same time that new technology is to be used to develop coastal aquaculture and sea ranching it will be necessary to have in place an intensive monitoring program for the environmental health of the coastal zone, as well as estuaries and the open sea. Monitoring is a topic that today draws mixed reactions. In the mid 70's, the National Academy of Science produced a report on petroleum development on the continental shelf. This report stated that monitoring in the traditional sense was not a fit subject for research in relation to petroleum exploration and development. However, the authors also emphasized at that time that it was important to understand the sources, fate, and effects of pollutants (including petroleum products). At about the same time this report was being developed, several international groups associated with the United Nations and the International Council for the Exploration of the Sea (ICES) had noted that while it was possible at the time to develop a listing of the sources of pollutants and while it was also possible using state-of-the-art technology to approximate or estimate movements of contaminants from their sources, it was not equally easy to understand the effects of various contaminants on living marine resources of interest to man or the food chains which sustain the commercially or recreationally important species.

Thus, the United Nations Group of Experts on the Scientific Aspects of Marine Pollution (UN GESAMP) and ICES established several working groups that were concerned with investigating the best way to carry on biological effects monitoring so as to actually understand how pollutants impacted on living marine resources. Both groups held a number of work sessions and ICES sponsored a major international symposium on biological effects monitoring which was sponsored by NOAA/NMFS and EPA, and held in Beaufort, North Carolina (Duke Marine Laboratory) in February 1979.

The results of these meetings indicate strongly that it is possible, using techniques presently available, to monitor the effects of pollutants on living marine resources. The Beaufort meeting concluded that there is presently, within the disciplines of biochemistry, ecology, behavior, physiology, genetics, pathobiology and bioassays the possibility to determine how pollutants might affect various categories of marine life over extensive areas of the coastal zone and continental shelf (ref. 1).

Within the general area of ecology, it has been seen that in recent years coastal eutrophication has resulted in measurable changes in phytoplankton populations and primary productivity (ref. 2). In coastal waters of the Middle Atlantic Bight, for instance, it has been demonstrated that eutrophication results in unusually high levels of primary production which may result in extensive standing stocks of carbonaceous

material, much of which may not be available to normal food chains culminating in commercially valuable fish. This is largely because in waters such as Raritan Bay the producing organisms are often of unusually small cell size (nanoplankton) and such cells are not easily used as food by many of the zooplankton and other secondary producers. As will be noted later in this talk, organic materials which are not culled from the water column often are attached by bacteria and thus may result in greatly lowered oxygen values.

It is now possible, using either traditional collections and measurements from vessels or remote sensing techniques, to measure levels of standing stocks of chlorophyll over extensive areas of coastal waters. Such measurements, using remote sensing capabilities, can often be performed in a matter of hours, whereas in collections and measurements from vessels literally days are required to census effectively the standing stocks of chlorophyll over the continental shelf area of interest.

In recent years it has become apparent that high technology, as used in remote sensing, can be effectively applied to problems of eutrophication and biostimulation and may also be used in estimating contaminant flow from estuaries, which are probably a principal source of marine pollution. This is a case where, until recently, existing technology has not been applied extensively to help deal with one of mankind's more important problems. Fortunately, during the past two or three years the remote sensing capabilities of NASA have been brought together with the oceanographic and fishery ecology capabilities of the National Marine Fisheries Service (NMFS). Our interactions started on a relatively informal and limited basis in the early 1970's. In 1979 we implemented the first of our joint programs which was called LAMPEX, or Large Area Marine Productivity/Pollution Experiment. This activity indicated convincingly that it was feasible to use remote sensing over extensive portions of the coastline in the Middle Atlantic Bight, as well as Georges Bank and Gulf of Maine, to assess standing stocks of chlorophyll; approximately 20 different institutions participated in this program to demonstrate that it was possible to measure synoptically standing stocks of chlorophyll over broad geographic areas.

More recently, we have begun to use remote sensing techniques to establish the sources, fates and effects of materials being carried from Chesapeake Bay in the form of the so-called Chesapeake Bay plume. It is these recent activities, involving both NASA and NMFS in the Chesapeake Bay plume, that will be reported upon during this meeting.

Since many of the people involved in the present Superflux Symposium are not fully aware of some of the problems which have been dealt with in the past using conventional techniques, I thought it would be most appropriate to indicate briefly some of the problems that have been investigated in the past using more conventional techniques. It is well-known that the population of the northeastern sector of the United States is largely concentrated in the coastal zone. This is demonstrated in figure 1. It is this dense population that produces the extensive amounts of pollutants which enter coastal waterways in several ways. For instance, each day the Hudson River carries seaward approximately one billion gallons of pollutants

which enter the New York Bight apex and may have a residence time of several weeks depending upon prevailing weather conditions. Another source of pollution in our coastal waters is due to extensive dumping activities at two sites approximately 10 to 15 km off the base of Sandy Hook. Dumping includes some 3.8 million cubic meters of sewer sludge and somewhere between 4 and 9 million cubic meters of contaminated dredging spoils each year. In addition a variety of industrial wastes are disposed of at a site in close proximity to the aforementioned dumping areas. Finally, there is extensive surficial runoff from the land mass as well as atmospheric inputs of combustion materials and other pollutants to the seawater/air interface. As I will show in a series of illustrations, there have been numerous effects from the various categories of waste which enter the estuaries and coastal waters of the Middle Atlantic Bight.

In 1979, the International Council for the Exploration of the Sea (ICES) asked me to have investigators located at our major east coast estuaries to develop a series of papers which present the status of these estuaries. Various scientists, including Dr. Peter Larsen in Maine (ref. 3), Mr. Ken Pecci of New Hampshire (ref. 4), Dr. Donald Phelps in Narragansett Bay (ref. 5), Mr. Robert Reid who covered Long Island Sound (ref. 6), Dr. Donald Maurer who dealt with Delaware Bay (ref. 7), and Dr. Robert Lippson who reported on Chesapeake Bay (ref. 8), as well as myself, who developed a paper on Raritan Bay (ref. 9), developed short essays on what was known about these estuaries.

The estuaries on the south shore of the Maine coastline are generally thought to be relatively unpolluted except for harbor areas such as Casco Bay upon which the port of Portland, Maine is located. It was also noted that the central part of the Gulf of Maine was relatively unpolluted, although other investigators have noted that the area off Boston Harbor is extensively affected by a variety of pollutants. Narragansett Bay was shown to be heavily polluted going back to the time of our Revolutionary War (ref. 5). The effects of pollution can be seen and measured in the northern third of the Bay, but the Lower Bay is still relatively free from heavy pollution. Scientists have noted a gradient of effects on mussel populations as they have been investigated from the inner reaches of Narragansett Bay seaward. Long Island Sound also shows a gradient of pollutant effects with the western third of the Sound showing evidence of extensive contamination and changes in the biological populations. Perhaps most important, relatively small harbor areas such as Milford Harbor can be shown to be affected by man's activities, and the larger harbors, as characterized by the New Haven Harbor area, are extensively polluted, to the point that living marine resources cannot legally be harvested. Raritan Bay is, perhaps, the classic example of an estuary which has been over-utilized by man and which can be demonstrated to have a historical record of pollution beginning at the time of the Civil War. In the 1870's, Newark Bay was already so polluted with petroleum products that shellfish and fish taken from this small bay could not be sold for human consumption because they tasted of kerosene. By the time of the First World War, pollution had spread from Newark Bay through Arthur Kill to the western part of Raritan Bay. Shellfish biologists at Rutgers University reported at the time

of the First World War that oysters in Raritan Bay were being affected by heavy metals from industrial wastes. These biologists stated at that time that if something was not done about this pollution the oysters would disappear from the bay; by the 40's this had happened.

Today, we are able to compare the conditions in Raritan Bay which changed between the mid 1950's and the early 1970's. Dean and Haskin reported in their earlier studies of the bay that there were up to 13,000 ampeliscid amphipods (small shrimp-like animals valuable as forage for fish) per square meter at that time (ref. 10). Our studies, conducted in the early 1970's, did not yield a single ampeliscid amphipod even though the number of sampling stations and the frequency of sampling were significantly increased relative to the earlier study (ref. 11).

The changes in Raritan Bay cannot be ascribed to any single pollutant although it is known that the bay is heavily contaminated with petroleum, heavy metals, PCB's, and other wastes that are deleterious to a variety of marine life. Figures 2, 3, 4 and 5 show the levels of petroleum hydrocarbons in sediments and waters as well as the levels of heavy metals found in sediments and waters at the same general localities. It can be seen easily that the western third of Raritan Bay contains levels of contaminants which have been shown in laboratory and field studies to be lethal to a variety of marine life (refs. 12 and 13). The amphipods are known to be particularly vulnerable to petroleum hydrocarbons. Following a spill in Wild Harbor at the western margin of Cape Cod, it has taken over a decade for the fauna (including the vulnerable amphipods) to return to the former levels of abundance (ref. 14).

The waters emanating into the New York Bight from Raritan Bay are, as was previously mentioned, heavily contaminated by a variety of pollutants. Studies done at the sites where ocean dumping is conducted have shown that bottom-dwelling organisms are impacted by the numerous contaminants associated with dumped materials and the high levels of pollutants flowing seaward from the Hudson River estuary. In 1976, there was an event of unparalled proportions. At that time the level of dissolved oxygen declined markedly and much of the bottom-dwelling life of the entire Middle Atlantic Bight off the New Jersey coastline was affected by the extremely low levels of dissolved oxygen. This hypoxia has not been ascribed to any single contaminant or waste, but rather seems to have resulted from complex physical and biological forces, probably associated with intense eutrophication (ref. 15)

It has also been shown since the early 60's that there has been a higher than expected prevalence of disease in fish taken from the New York Bight apex. A wide range of bottom-dwelling and pelagic fish have shown effects of a disease syndrome generally referred to as fin rot disease (figure 6). In addition, a wide range of crustaceans which dwell on the sea floor have also been shown to suffer from a higher than usual incidence of exoskeleton disease. Again, it is difficult to ascribe these syndromes to a particular contaminant, although recent investigations have shown that increases in a toxic trace metal, copper, can result in an increase in

disease of the exoskeleton of shrimp. This metal is found in elevated amounts in the polluted Raritan Bay (ref. 16). There are increasing pieces of evidence suggesting a relationship between fish and shellfish disease and the level of pollution in waters of the Middle Atlantic Bight.

The ICES papers suggest that in Delaware Bay and Chesapeake Bay, there are changes in water quality and concomitant changes in the well-being of biota similar to those which have been demonstrated for the Lower Hudson estuary, Raritan Bay and the New York Bight apex. Investigators in both of these major estuarine systems have reported significant decreases in the production of shellfish in those portions of the bays receiving heavy pollution loads.

It is obvious that the resources (dollars and personnel) available to society to monitor and demonstrate the changes which are occurring in living resources are limited and thus we must look to new ways of rapidly assessing long-term change in habitat quality and consequent effects on living marine resources. One way to do this is to have comprehensive monitoring and assessment studies, on sufficient geographic and temporal scales, in areas which are known to be receiving pollutants as well as in areas which are relatively free from pollution. By establishing benchmarks for present levels of pollutants in the physical and biological compartments, and for the responses of organisms to these pollutants in areas which are heavily impacted and relatively free from pollution, we can begin to gain an understanding of how future change may affect organisms. By having such information at hand, we can more effectively manage the habitats of fishes and the living marine resources themselves at the same time as we are carrying out economic activities such as transportation, ocean dumping, development of mineral resources and the development of offshore energy supplies.

The National Marine Fisheries Service has developed such a program and it has been operating in a pilot mode during the past two years. We are presently developing our first annual report which will be a status of the health of the coastal and shelf environments of the northeast. The report will indicate that materials such as PCB's and coprostanol are spread over a much wider area than might have been expected based on studies conducted during the past few years (figures 7 and 8). Moreover, the study has indicated that a variety of fish are heavily contaminated, i.e. have unexpectedly high body burdens of pollutants such as petroleum hydrocarbons and PCB's. The fish showing these elevated levels of pollution were caught not only near the mouths of estuaries which are known to be polluted, but were taken over the entire continental shelf to the shelf slope-break (ref. 17), areas that are hundreds of kilometers from a source of the pollutant.

At the same time that we have been investigating levels of contaminants in sediments, waters, and biota we have developed a pilot program to look at the different physiological and biochemical responses to a variety of contaminants. We have also been establishing benchmarks for the incidence of genetic anomalies in waters known to be polluted or relatively free from pollution. Finally, we have intensified our studies of the expression of

disease due possibly to increased pollutant loadings. Information to date continues to suggest organisms in heavily polluted habitats show a much higher level of genetic aberration, disease, and changes in physiological and biochemical responses. Our benchmark studies have also shown the aforementioned effects are expressed in changes in the standing stocks of populations of bottom-dwelling organisms. This, in the end, is the kind of change that is most important to mankind; while the change in an individual organism, or a small sector of the population, is an indication of or expression of environmental impact on living resources, it is the large-scale change in populations and communities which is most significant. It is not so significant whether change is seen in an entire benthic community or in the disappearance of a population of amphipods or whether the change occurs in a phytoplankton population or physiological function; in the end, changes in the various trophic levels are manifested in changes in populations of finfish and shellfish which are important to man for food and recreation.

As mentioned earlier, the resources available for the monitoring and assessment of environmental effects are limited. Future activities will have to depend upon new technology and new protocols for carrying out investigations of environmental or habitat change. Techniques such as remote sensing provide us with an opportunity to monitor rapidly and assess significant changes within coastal and shelf habitats. Other papers in this conference publication are concerned with the type of remote sensing devices and their relative efficacy in detecting variables or changes in variables which are of interest to oceanographers and marine ecologists. The coastal zone color scanner and ocean color scanner are apparatus which already can detect variables that may be of immediate significance to oceanographers. The active laser techniques will undoubtedly have paramount application in understanding the quality of various plant pigments which are of interest to man. Changes in the quality of chlorophyll and other plant pigments may well be the immediate indicators of significant change in phytoplankton populations. Such changes can then be related to change in the primary and secondary levels of production within the water column.

Finally, there will be semi-conservative relationships between the presence of suspended material which can be detected by remote sensing systems and the levels of several categories of contaminants. Again, by using remote sensing techniques, it will be possible to monitor rapidly how plumes containing suspended materials and associated contaminants move from the major estuarine systems over the continental shelf and eventually impact on living resources.

We do indeed live in a remarkable time when it will be possible to use modern, extremely sensitive remote sensing techniques to aid us in rapidly and synoptically assessing the relative health and production of coastal waters and estuaries. Today's presentations will be a large step in establishing a solid foundation for the use of remote sensing in basic oceanographic studies and the management of man's wastes; there is little doubt that within this decade satellite imagery will be used on a frequent basis to guide modern waste disposal vessels to appropriate dumping areas,

thus insuring that wastes are not entrained in warm core eddies and other water masses likely to return to shore. Many applications of remote sensing to problems of ocean research and management can now only be guessed at. What is obvious is that we now have in hand a powerful tool which can only be used to maximum levels if marine and space scientists work closely in coherent and cooperative programs such as Superflux.

REFERENCES

1. McIntyre, A. D.; Pearce, J. B. Biological Effects of Marine Pollution. Volume 10, Rapports et Proces-Verbaux, International Council for the Exploration of the Sea, Copenhagen, Denmark, 1980.

2. O'Reilly, J. E.; Thomas, J. P.; Evans, C. Annual primary production (nannoplankton, netplankton, dissolved organic matter) in the Lower New York Bay. 4th Symp. Hudson River Environ. Soc., Paper #19, 1976.

3. Larsen, P. F.; Doggett, L. F. An Overview of Nearshore Environmental Research in the Gulf of Maine. Marine Environmental Quality Comm., C.M. 1979/E:41, International Council for the Exploration of the Sea, 1979.

4. McCarthy, K.; Gross, C.; Cooper, R.; Langton, R.; Pecci, K.; Uzmann, J. Biology and Geology of Jeffreys Ledge and Adjacent Basins: An Unpolluted Inshore Fishing Area, Gulf of Maine, NW Atlantic. Marine Environmental Quality Comm., C.M. 1979/E:44, International Council for the Exploration of the Sea, 1979.

5. Phelps, D. K. A Prognosis for Narragansett Bay. Marine Environmental Quality Comm., C.M. 1979/E:46, International Council for the Exploration of the Sea, 1979.

6. Reid, R. N. Contaminant Concentrations and Effects in Long Island Sound. Marine Environmental Quality Comm., C.M. 1979/E:47, International Council for the Exploration of the Sea, 1979.

7. Maurer, D. A Brief Review of the Status of Selected Pollutants (Pesticides, Hydrocarbons, Trace Metals) in Relation to Benthic Invertebrates in Delaware Bay. Marine Environmental Quality Comm., C.M. 1979/E:43, International Council for the Exploration of the Sea, 1979.

8. Lippson, R. L.; Lippson, A. J. The Condition of Chesapeake Bay - An Assessment of its Present State and its Future. Marine Environmental Quality Comm., C.M. 1979/E:42, International Council for the Exploration of the Sea, 1979.

9. Pearce, J. B. Raritan Bay - A Highly Polluted Estuarine System. Marine Environmental Quality Comm., C.M. 1979/E:45, International Council for the Exploration of the Sea, 1979.

10. Dean, D.; Haskin, H. Benthic Repopulation of the Raritan River Estuary Following Pollution Abatement. Limnol. Oceanogr. 9, 1964, pp. 551-563.

11. McGrath, R. Benthic Macrofaunal Census of Raritan Bay - Preliminary Results. Proceeding 3rd Symp. Hudson River Ecol., Mar. 22-23, 1973, Bear Mountain, New York, Paper No. 24, Hudson River Environ. Soc., 1974.

12. Davies, A. G. Pollution studies with marine plankton. Part II. Heavy metals. Russell, F. S.; Yonge, M. eds. Advances in Marine Biology, Vol. 15, Academic Press, London; 1978:381-508.

13. Corner, E. D. S. Pollution studies with marine plankton. Part I. Petroleum hydrocarbons and related compounds. Russell, F. S.; Yonge, M. eds. Advances in Marine Biology, Vol. 15, Academic Press, London; 1978:290-507.

14. Saunders, H. L., Grassle, J. F.; Hampson, G. R.; Morse, L. S., Garner-Price, S.; Jones, C. C. Anatomy of an oil spill: long-term effects from the grounding of the barge Florida off West Falmouth, MA. J. Mar. Res. 38(2):265; 1980.

15. Swanson, R. L., Sindermann, C. J. (editors). Oxygen Depletion and Associated Benthic Mortalities in New York Bight, 1976. NOAA Prof. Paper 11, U.S. Dept. of Commerce, NOAA, Rockville, Maryland, 1979.

16. Waldhauer, R.; Matte, A.; Tucker, R. E. Lead and Copper in the Waters of Raritan and Lower New York Bays. Mar. Poll. Bull 9(2), 1978, pp.38-42.

17. Boehm, P. New York Bight Benthic Sampling Survey: Coprostanol, Polychlorinated Biphenyl and Polynuclear Aromatic Hydrocarbon Measurements in Sediments. Northeast Monitoring Program (NEMP) Report No. NEMP-III-80-B-0046, NOAA, 1980.

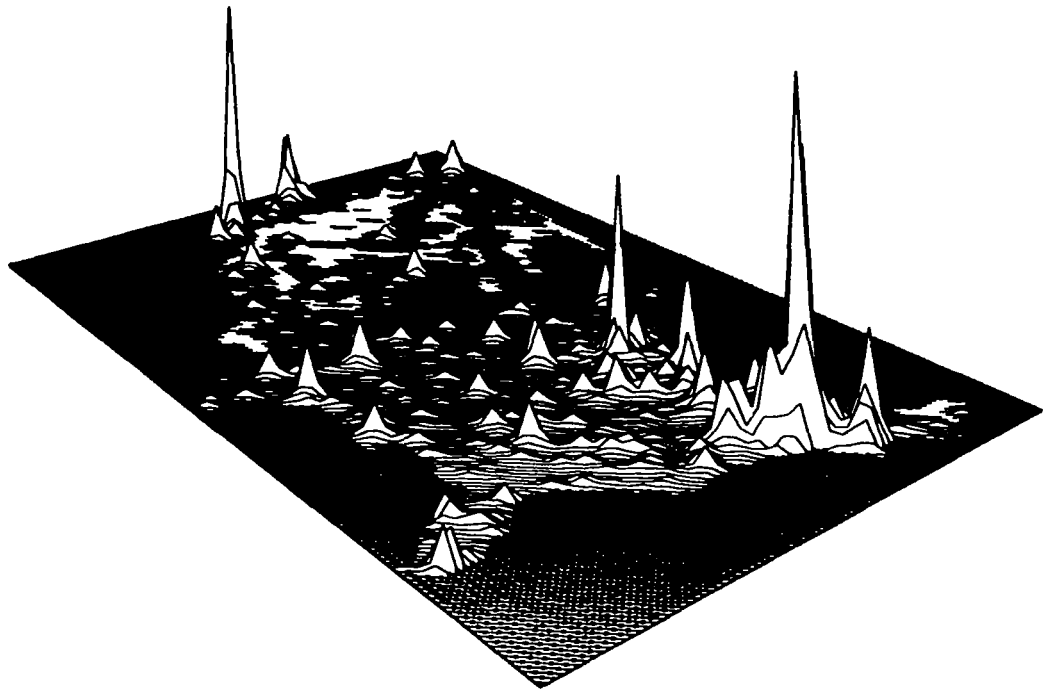

Figure 1. Relief map of population density in U.S. from 1970 census data (courtesy of the Laboratory for Computer Graphics and Spatial Analysis, Harvard University).

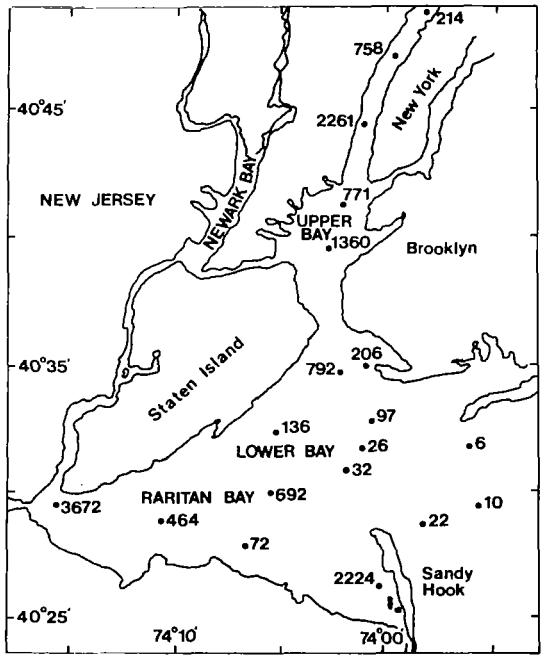

Figure 2. Concentration of C_{15+} hydrocarbons at 19 stations in New York Harbor, Hudson River, and Raritan Bay (expressed in PPM by weight of dry sediment).

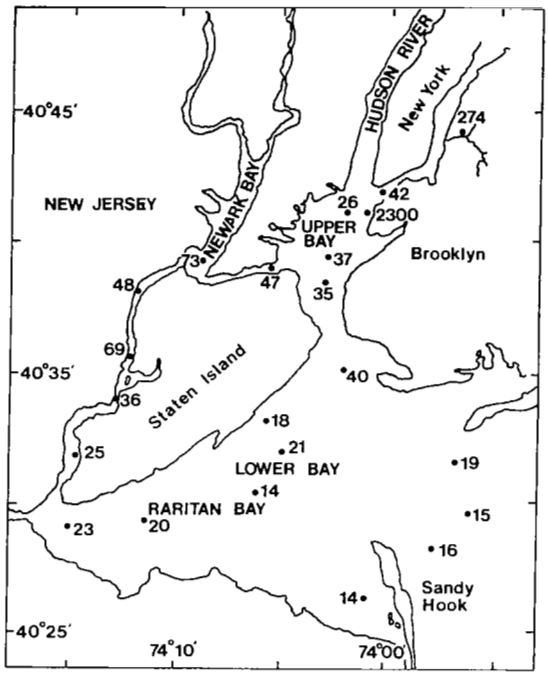

Figure 3. Concentrations of hydrocarbons in water samples collected from New York Harbor, the Hudson and East Rivers, and Raritan Bay (expressed in µg/l).

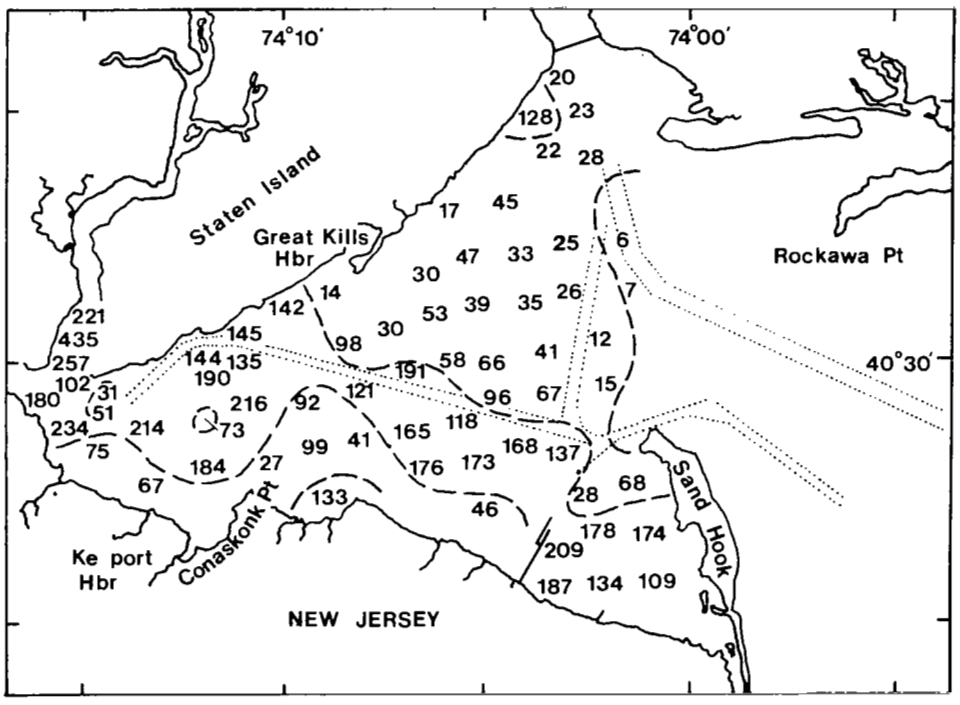

Figure 4. Contour lines depicting arithmetic mean metals value (obtained by combining each of the individual values (in PPM) for metal species) for sediments collected in Raritan Bay.

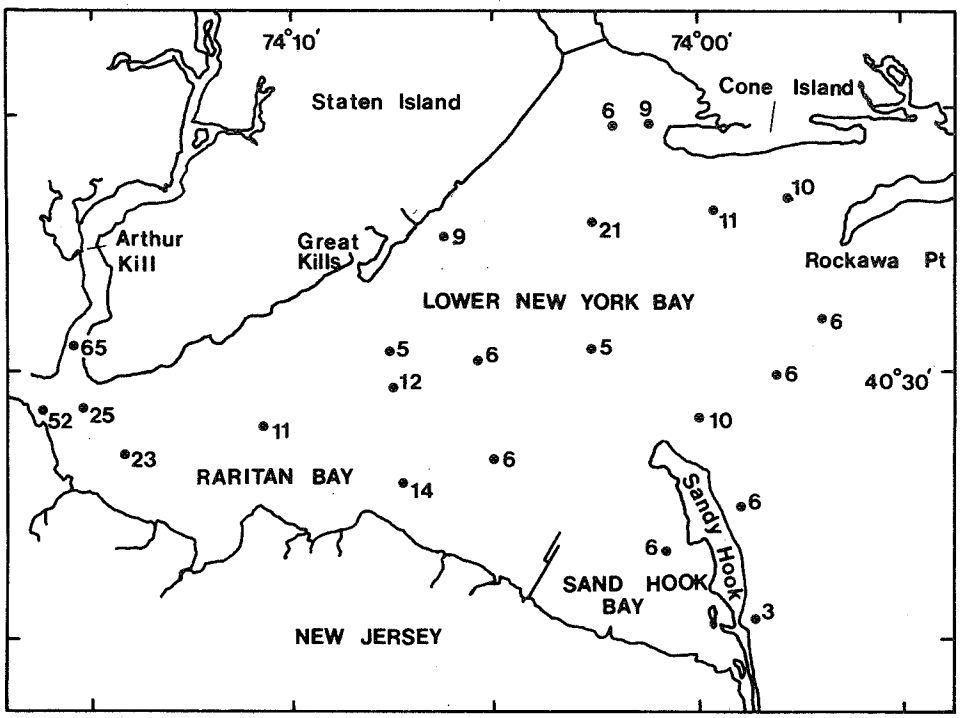

Figure 5. Concentrations of copper in bottom waters of Raritan Bay ($\mu g l^{-1}$).

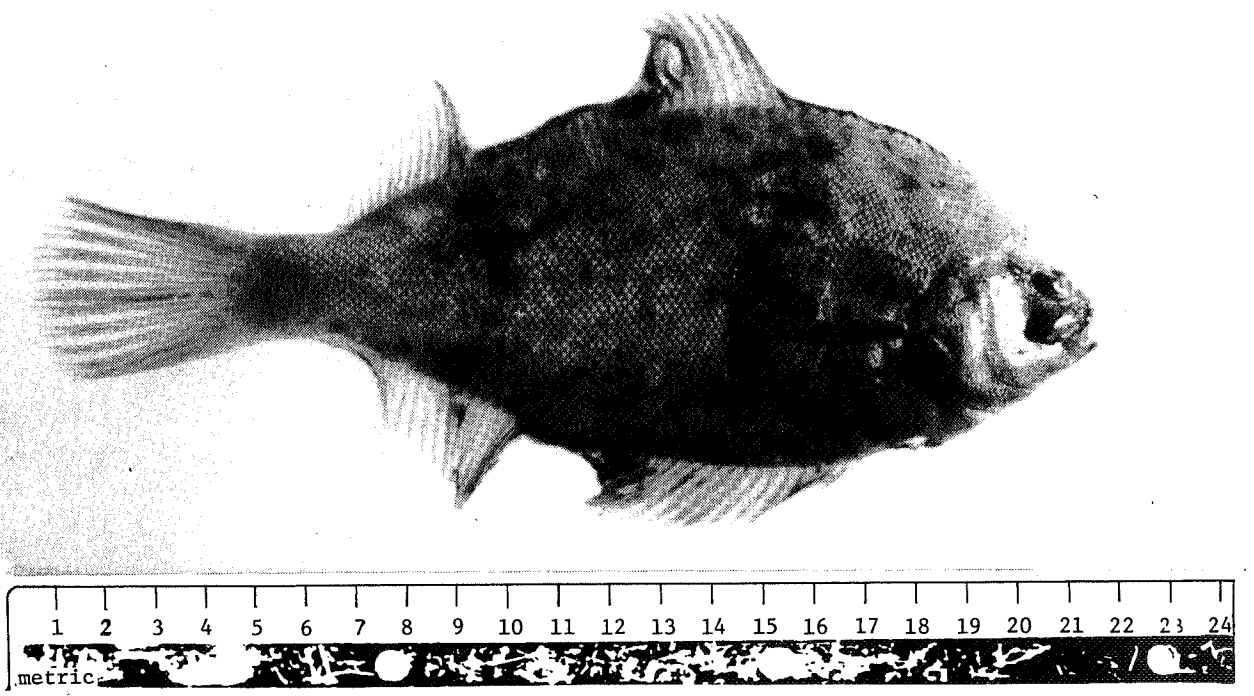

Figure 6. A flounder collected from the New York Bight showing severe fin erosion; such a syndrome is often common in fish taken from heavily contaminated waters.

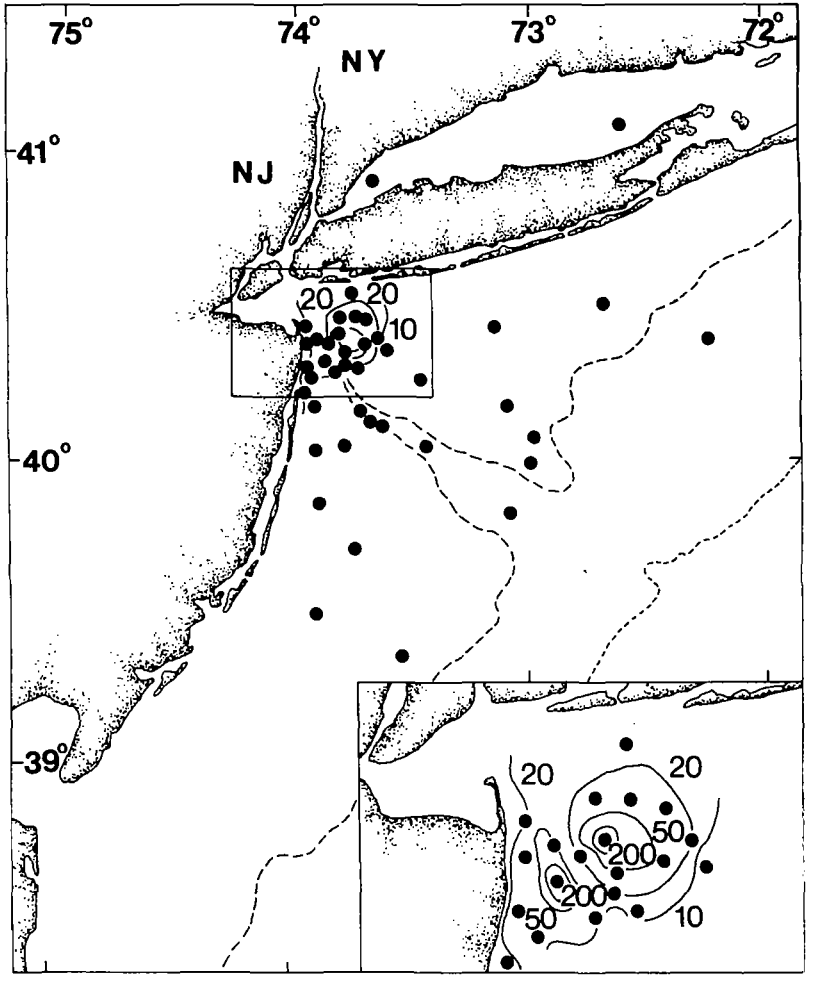

Figure 7. PCB concentration (PPB) in sediments of the New York Bight.

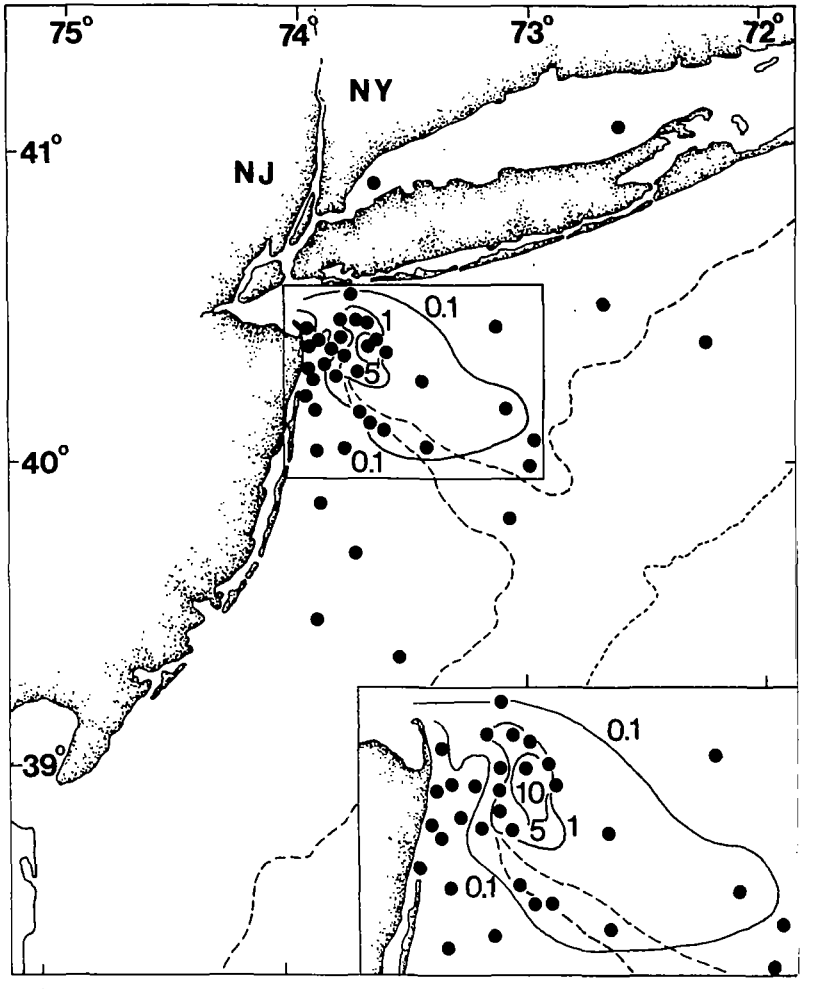

Figure 8. Coprostanol concentration (PPM) in sediments of the New York Bight.

SUPERFLUX I, II, AND III EXPERIMENT DESIGNS:

REMOTE SENSING ASPECTS

Janet W. Campbell, Wayne E. Esaias, and Warren D. Hypes
NASA Langley Research Center

INTRODUCTION

The Chesapeake Bay Plume Study, called Superflux, was initiated in January 1980 by a group of scientists, marine resource managers, and remote-sensing specialists with the conviction that their mutually complementary goals and interests could be served by a pooling of resources to conduct this study. The result was that the study was undertaken with a multi-faceted set of objectives:

(1) Process-oriented research: To understand the impact of estuarine outflows on continental shelf ecosystems

(2) Monitoring and assessment: To delineate the role of remote sensing in future monitoring and assessment programs

(3) Remote sensing research: To advance the state of the art in remote sensing systems as applied to sensing of the marine environment, thereby hastening the day when remote sensing can be used operationally for monitoring and assessment and for process-oriented research.

It is recognized that to study an estuarine plume and its impact on shelf ecosystems, the coupling of biological and physical processes must be understood. Time and space scales associated with these processes in a highly dynamic, tidally driven estuarine plume require the capability to sample an area on the order of 10^3 kilometers over time intervals much smaller than the tidal period. Figure 1 illustrates the respective sampling regimes associated with boats, aircraft, and satellites as compared to time and space domains of important processes in an estuary-ocean system. Because sampling via aircraft fills a critical gap, an underlying hypothesis of Superflux was the belief that airborne remote sensors, interacting with surface vessels collecting in situ data, could provide the synopticity required to study a highly dynamic estuarine plume. In fact, it is believed that any future monitoring program involving remote sensing would rely on some combination of boats, aircraft, and satellites.

Another premise underlying the Superflux experiments was that the transfer of technology from NASA to the National Marine Fisheries Service (NMFS) could be accomplished effectively and more quickly through highly interactive programs involving marine scientists and the remote sensing

technologists at NASA. This interaction would influence the development of remote sensing technology, increase its relevancy to the needs of the marine scientists, and accelerate its availability. At the same time, marine scientists would become familiar with the capabilities and limitations of present remote sensors, and the appropriate protocol for their utilization would evolve.

Because of the importance placed on involvement and interaction, the Superflux study was open to all who wanted to participate and, despite the paucity of funds to support their involvement, many institutions contributed to the project. A list of participating institutions is given in table 1.

DESIGN CONSIDERATIONS

As a first step in meeting Superflux objectives, the NASA remote sensing specialists saw the need to integrate state-of-the-art airborne remote sensors into one or more systems. The eight remote sensors used in Superflux are described in table 2. Prior to the Superflux experiments, these eight sensors were being developed as separate projects at three different centers within NASA. With few exceptions, they had been flown separately in flight missions designed to test the particular instrument under its ideal operating conditions. In the Superflux experiments, the sensors were being asked to provide a meaningful oceanographic data set for characterizing the Chesapeake Bay plume.

In designing the Superflux experiments, consideration had to be given to (1) the sensors operational constraints and their need for performance validation, and (2) the oceanographic sampling objectives. These considerations were not always mutually compatible and, therefore, compromises had to be made. A list of the various considerations is given in table 3, along with other considerations which, in general, added to the logistical complexity of the experiments.

Considerations relative to the sensors' operation and performance included constraints on aircraft altitudes and groundspeeds, solar elevation angles and Sun position relative to the direction of flight, and weather conditions (cloudiness or haze). Each sensor has its own operational envelope with respect to these conditions and these envelopes did not always overlap. Furthermore, good conditions for sensor operations did not always correspond to acceptable conditions for boats. For example, clear skies required for the high-altitude scanners were often accompanied by relatively high surface winds that inhibited boat operations.

Other important considerations were related to the need for remote sensor performance validation and calibration. These included the requirements for coincident sea truth data, the desire to maximize the range of water parameters being sensed, and the replication of measurements (e.g., repeated passes over the same area).

In some instances, the considerations relative to oceanographic objectives conflicted with the sensor-driven ones. For example, the need to have concurrent measurements of temperature, salinity, and chlorophyll a fluorescence required the simultaneous operation of sensors at altitudes and groundspeeds that were less than optimum. The importance of sampling at certain tidal phases sometimes conflicted with Sun angle constraints, and the need for good spatial coverage and appropriate grid densities precluded meticulous sensor validations (e.g., sea truth, replications, etc.).

THE EXPERIMENT DESIGNS

Three experiments were conducted in 1980. Superflux I coincided with high fresh water inflow to the Bay (March 17-20, 1980), Superflux II with moderate fresh water inflow (June 16-27, 1980), and Superflux III with unusually low fresh water inflow (October 15-22, 1980). Each experiment was preceded by a reconnaissance flight made with a VIMS aircraft to determine visually the general location and extent of the Bay plume. The primary experiments consisted of several missions flown by the NASA P-3 aircraft carrying remote sensors and supported by boats collecting water column sea truth data. A NASA Lear Jet also participated in Superflux III.

In most cases, the boats were collecting data along cruise tracks that spanned several hours or days. The sea truth data collections were, therefore, brief incidents in their overall missions. The boat missions are described in more detail in reference 1.

REMOTE-SENSING SYSTEMS

Of the seven remote sensors listed in table 2, six were flown on the P-3. Because of differences in operational constraints (envelopes), two systems of sensors emerged. A system, as defined here, is a group of sensors that could be flown on the same aircraft and operated simultaneously. These two systems are described in table 4.

The low-altitude system consisted of the two lidar fluorosensors (AOL and ALOPE), the infrared radiometer (PRT-5), and the microwave salinity mapper (L-Band). The 20-channel visible wavelength scanner (MOCS) was also operated but only nadir data (directly beneath the aircraft) were analyzed. This system provided one-dimensional nadir tracks of chlorophyll a fluorescence, turbidity, temperature, salinity, and indicators of phytoplankton species composition (or pigment classes) present. Collected from altitudes between 150 and 300 m (500-1000 feet) and at groundspeeds of approximately 100 m/sec (200 kts), the data have spatial resolutions between 10 and 100 m. While these data by themselves provide excellent relative measurements, absolute accuracies require calibration with sea truth, and

to obtain good sea truth data for this nadir-looking system, the aircraft has to pass directly over the boats (±50 m).

The high-altitude system provided 2-dimensional imagery from scanners and cameras at altitudes ranging from 1500 to 13 000 m (5000 to 43 000 ft), and groundspeeds between 150 and 200 m/sec (~ 300 to 400 kts). Correlation of the remote multispectral data (backscattered sunlight in narrow spectral bands) with water parameters is still highly empirical, particularly in coastal and estuarine waters which consist of complex mixtures of dissolved and particulate materials. Nevertheless, the qualitative information provided by the imagery is still quite valuable in delineating the spatial extent of the turbidity plume, the location of visible fronts, and other visible evidences of dynamic processes such as upwelling, eddies, horizontal shears, etc.

The missions flown in the Superflux I, II, and III experiments are summarized in table 5. Of the 17 missions flown, all but three were either shelf transects or mappings (see column 2 in table 5). The six shelf transect missions, two with the low-altitude system and four with the high-altitude system, gave high priority to the remote sensing testing and validation considerations discussed above. An example of the shelf transect mission flight track flown on June 20, 1980, is shown in figure 2. These missions generally consisted of a transect that began well inside the Chesapeake Bay or James River and proceeded out the mouth of the Bay and eastward beyond the shelf break. Sea truth vessels were concentrated along the transect and this transect, which maximized the range of water parameters sampled, was repeated several times.

Eight mapping missions, five low-altitude and three high-altitude, placed higher priority on the areal coverage of the plume and other oceanographic design considerations. Figure 3 shows a flight track of the June 23, 1980 low-altitude mapping mission and figure 4 shows a flight track of the June 24, 1980 high-altitude mapping mission. The mapping missions were aimed at delineating the plume with good spatial resolution and synopticity. Attention was given to the tidal phase and to the resolution of features within the plume and along the plume boundary.

In addition to the shelf-transect and mapping missions, missions were flown over the upper Chesapeake and Delaware Bays at the request of participants in those areas. These are also listed in table 5.

OTHER CONSIDERATIONS IN THE EXPERIMENT DESIGNS

Navigation and tracking were especially important for the low-altitude system and somewhat less critical for the high-altitude one. Navigation, referring to the ability to target the aircraft's position to pass directly over a boat, depended on the P-3 aircraft's inertial navigation system (INS) which directed the autopilot. This was found to be somewhat inaccurate and resulted in missed distances between aircraft and boat of

as much as a half kilometer on the earlier missions. Once the boat is in sight, the aircraft can maneuver to fly directly over it, but the resultant rolling and banking motions seriously degrade the remote sensing data. As more experience was gained, techniques were devised to allow interruptions in low-altitude flight legs to locate a boat and fly directly over it before resuming the flight pattern.

Tracking, i.e., recording the exact position of the aircraft as a function of time, was an especially successful aspect of the Superflux experiments. A newly-developed airborne Loran-C system mounted on the P-3 recorded longitude and latitude as a function of time at 9-second intervals.

Communications posed major problems at first, but by the time of Superflux III a satisfactory communications network had been worked out. This consisted of two ground stations: a primary station at Wallops with long-range transmitters and receivers for communicating with the P-3 and several of the boats, and a secondary base located at the central boat-docking facility in Virginia Beach. The latter, linked to Wallops via telephone, was manned for extended periods of time to serve as a centralized communications base for the boat investigations. Onboard the P-3 was a high-powered radio for communicating with Wallops and with several of the vessels that had been equipped with antennas borrowed from NASA. One boat served as the central communications link for all other vessels.

A third factor strongly influencing experiment designs was the need to fly through military-restricted air space. Strict procedures had to be followed to receive clearances to enter these areas. When clearances were not granted, or were withdrawn at the last minute, sampling designs had to be adjusted quickly and all participants had to be notified. This was a factor which influenced every mission design but was not one that could be controlled.

CONCLUSIONS

The purpose of this presentation was to give an overview of the experiment designs for the airborne remote sensing missions that were a part of the Superflux experiments. More specific details concerning the Superflux experiment designs are contained in reference 2. References 3 and 4 contain excellent summaries of state-of-the-art remote sensing technology.

The remote sensing instruments, many of which had previously only been test-flown, were here asked to provide meaningful data sets. The challenge was to combine these sensors into systems, i.e. to solve the problems related to sensor interfaces and coordinate the aircraft and boat interactions to accomplish experiment objectives. The Superflux experiments were successful in demonstrating that remote sensing can play an important role in sampling mesoscale oceanographic phenomena which cannot be addressed by any other means.

REFERENCES

1. Thomas, James P.: Superflux I, II, and III Experiment Designs: Water Sampling and Analyses. Chesapeake Bay Plume Study - Superflux 1980, NASA CP-2188, 1981 (Paper no. 5 of this compilation).

2. Annual NEMP Report on the Health of the Northeast Coastal Waters of the United States, 1980. Northeast Monitoring Program, National Oceanic and Atmospheric Administration, Sandy Hook Laboratory, Report no. SHL 80-24, 1981.

3. Curfman, H. J.; Oberholtzer, J. D.; and Schertler, R. J.: An Assessment of the Role of Remote Sensing in the Study of Inland and Coastal Waters. NASA TM-8188, 1980.

4. Esaias, Wayne E.: Remote Sensing of Oceanic Phytoplankton: Present and Future Goals. Primary Productivity in the Sea, P. Falkowski, ed., Environmental Science Research, vol. 19, Plenum Press, 1980.

TABLE 1. - SUPERFLUX PARTICIPANTS

Federal and State Organizations
NMFS/Northeast Fisheries Center (Sandy Hook and Oxford Labs)
NASA-Langley Research Center
NASA-Wallops Flight Center
NASA-Lewis Research Center
NOAA/National Environmental Satellite Service
NOAA/Atlantic Marine Center
U.S. Navy (Oceana and Little Creek)
U.S. Naval Academy
Environmental Protection Agency
U.S. Coast Guard
State of Maryland Department of Natural Resources
State and Private Universities
College of William and Mary (Virginia Institute of Marine Science)
Old Dominion University
Johns Hopkins University (Chesapeake Bay Institute and Applied Physics Laboratory)
University of Delaware College of Marine Studies
Anne Arundel Community College
University of Miami
Research Triangle Institute

TABLE 2. - AIRBORNE REMOTE SENSORS USED IN SUPERFLUX

Name	Type of Sensor	Characteristics	Measurements
AOL	Laser (Lidar) Fluorosensor	Uses single-wavelength laser to induce fluorescence; measures emission in 40 channels; has vertical profiling capability	Fluorescence of chlorophyll *a* and other pigments; light attenuation
ALOPE	Laser (Lidar) Fluorosensor	Uses two-frequency laser to induce fluorescence; measures single-channel chlorophyll *a* fluorescence	Chlorophyll *a* fluorescence; phytoplankton color group diversity
L-Band	Microwave Radiometer	Measures passive microwave radiation from water surface in single channel	Salinity (requires independent measurement of surface temp.)
PRT-5	Infrared Radiometer	Measures passive thermal radiation from water surface in single channel; commercially available	Surface temperature
MOCS	Multispectral Scanner	Measures backscattered sunlight in visible and near-infrared spectral range; has 20 bands, 15 nm wide	Chlorophyll *a*; suspended and dissolved matter that affects color
TBAMS	Multispectral Scanner	Has 8 bands in visible and near infrared spectral range plus one thermal channel; high sensitivity to water color variations	Two-dimensional imagery; maps of chlorophyll *a* and suspended sediments
OCS	Multispectral Scanner	Has 10 bands in visible and near infrared spectral range; forerunner of CZCS instrument on NIMBUS 7 satellite; flown on NASA Lear Jet	Two-dimensional high-altitude imagery; maps of chlorophyll *a* and suspended sediments

TABLE 3. - SUPERFLUX EXPERIMENT DESIGN CONSIDERATIONS

Considerations Relative to Sensor Operations and Performance:
(1) Aircraft altitude and groundspeed (2) Sun angles (3) Weather (4) Sea truth requirements (5) Range of water parameters (6) Repeatability of measurements
Considerations Relative to Producing Good Oceanographic Data Set:
(1) Simultaneous operation of sensors (2) Phase of tide (3) Spatial coverage and grid density
Other Considerations:
(1) Navigation and tracking (2) Communications (3) Restricted air and surface zones (clearances required)

TABLE 4. - TWO SENSOR SYSTEMS USED IN SUPERFLUX

	System	Platform	Nature of Data
Low-Altitude	AOL ALOPE L-Band PRT-5 MOCS	NASA P-3 aircraft at low altitudes (150 to 300 m (500 to 1000 ft))	1-dimensional nadir tracks (directly beneath aircraft)
High-Altitude	MOCS TBAMS Camera	NASA P-3 aircraft at high altitudes (1.5 to 7.5 km (5000 to 25 000 ft))	Digital imagery and photography; 2-dimensional mappings of parameters
	OCS	NASA Lear Jet (13 km (43 000 ft))	2-dimensional imagery and mappings of parameters

TABLE 5. - SUMMARY OF SUPERFLUX MISSIONS

	Date	Mission Type	System	Aircraft	No. Vessels
Superflux I	3/17/80	Shelf transect	Low-altitude	P-3	5
	3/19/80	Double mapping	Low-altitude	P-3	3
	3/19/80	Shelf transect	High-altitude	P-3	3
	4/2/80	Exploratory	High-altitude	P-3	0
Superflux II	6/17/80	Delaware Bay	Low-altitude	P-3	2
	6/19/80	Chesapeake and Delaware Bays	High-altitude	P-3	8
	6/20/80	Shelf transect	Low-altitude	P-3	4
	6/20/80	Shelf transect	High-altitude	P-3	4
	6/23/80	Mapping	Low-altitude	P-3	6
	6/24/80	Mapping	High-altitude	P-3	5
	6/25/80	Mapping	Low-altitude	P-3	6
	6/27/80	Mapping	Low-altitude	P-3	5
Superflux III	10/15/80	Mapping	High-altitude	Lear Jet	4
	10/20/80	Mapping	High-altitude	Lear Jet	1
	10/21/80	Shelf transect	High-altitude	P-3	3
	10/22/80	Shelf transect	High-altitude	P-3 Lear Jet	1

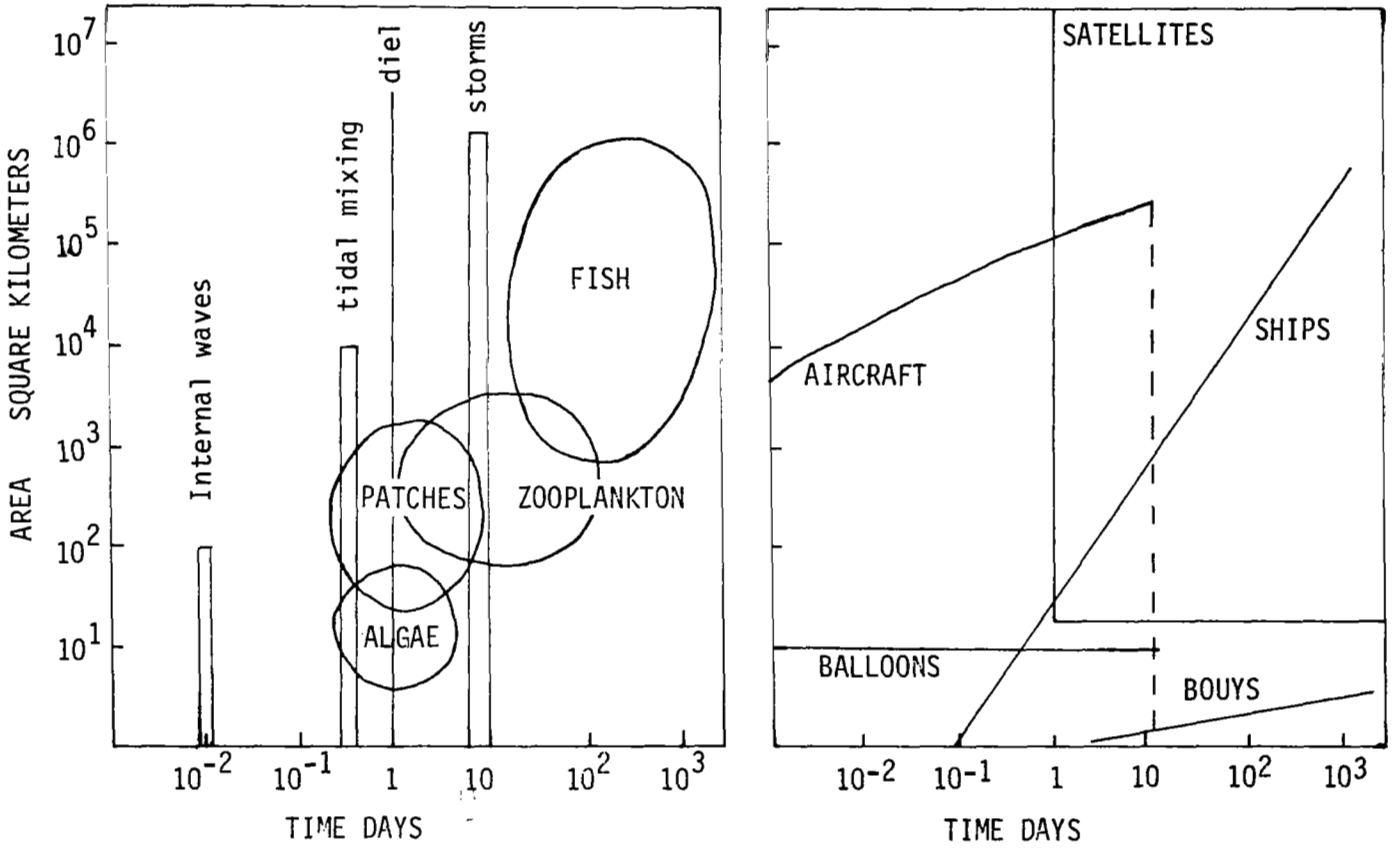

(a) Processes, indicating periods for physical forcings and excursion-generation times of some biological components.

(b) Sampling, indicating limits of coverage for various platforms.

Figure 1.- Time-space domains for oceanic phenomena (adapted from ref. 2).

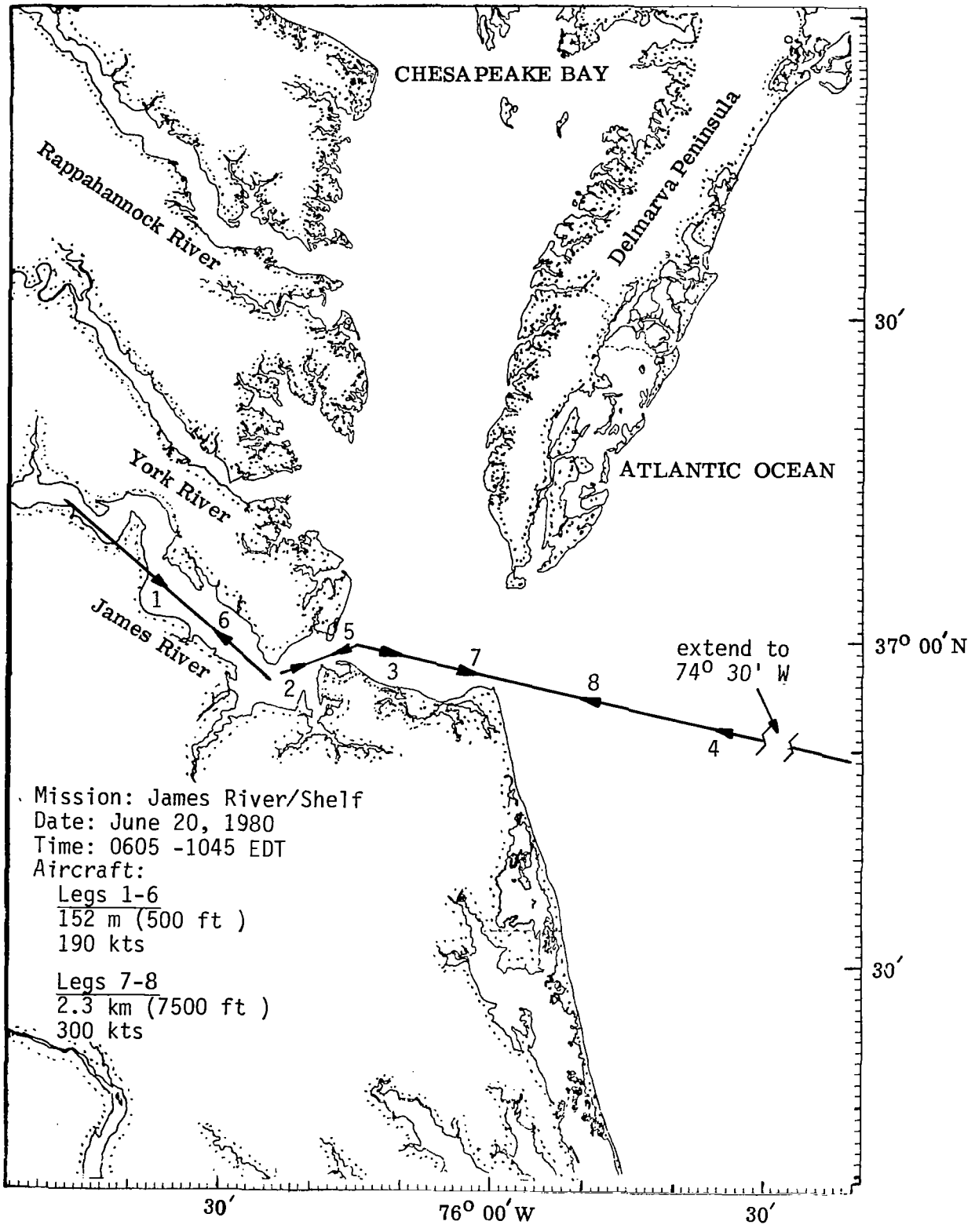

Figure 2.- Flight tracks of James River/shelf transect missions on June 20, 1980. Low-altitude system was flown between 0605 and 0745 EDT and high-altitude system between 0940 and 1045 EDT.

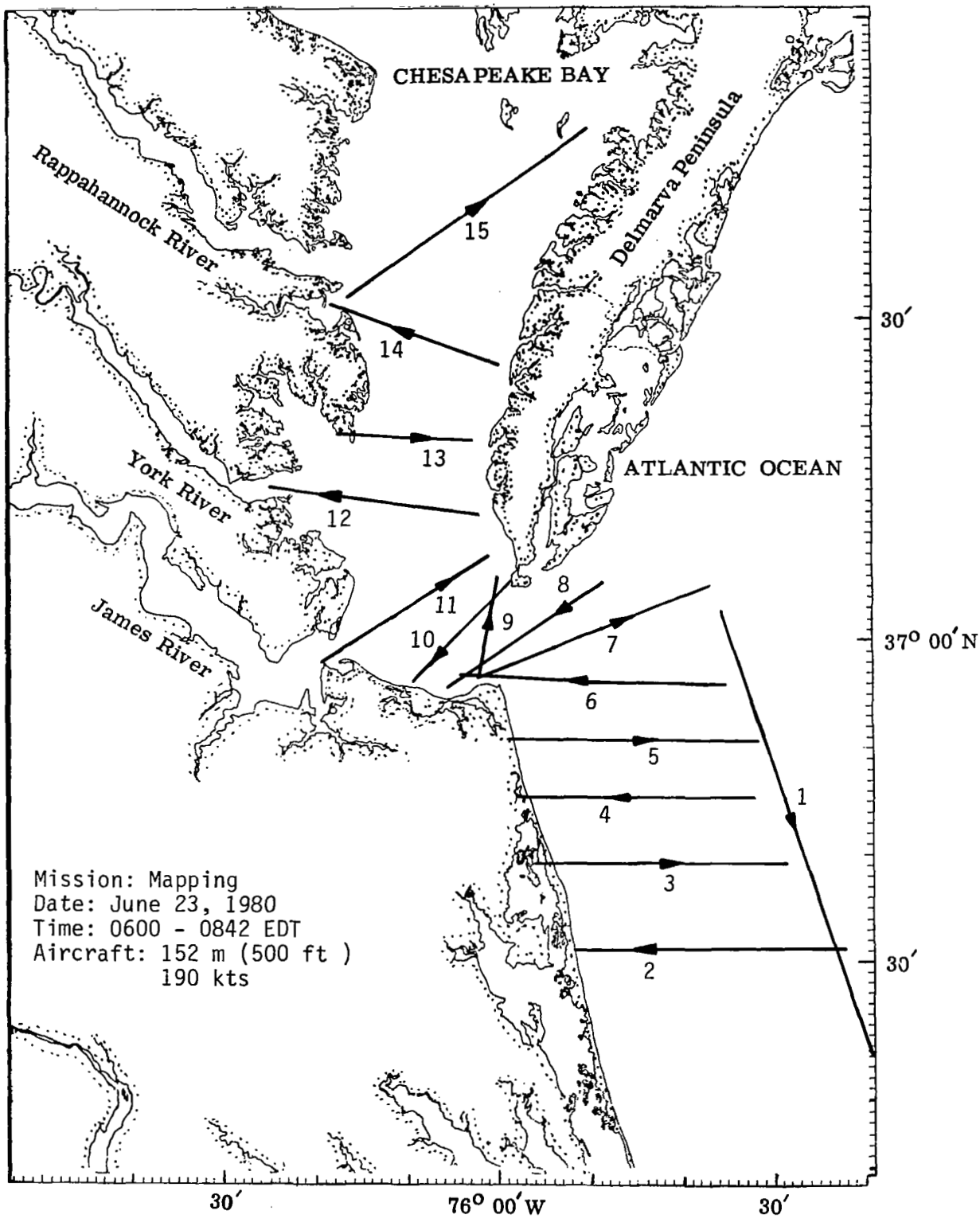

Figure 3.- Flight track of low-altitude mapping mission on June 23, 1980.

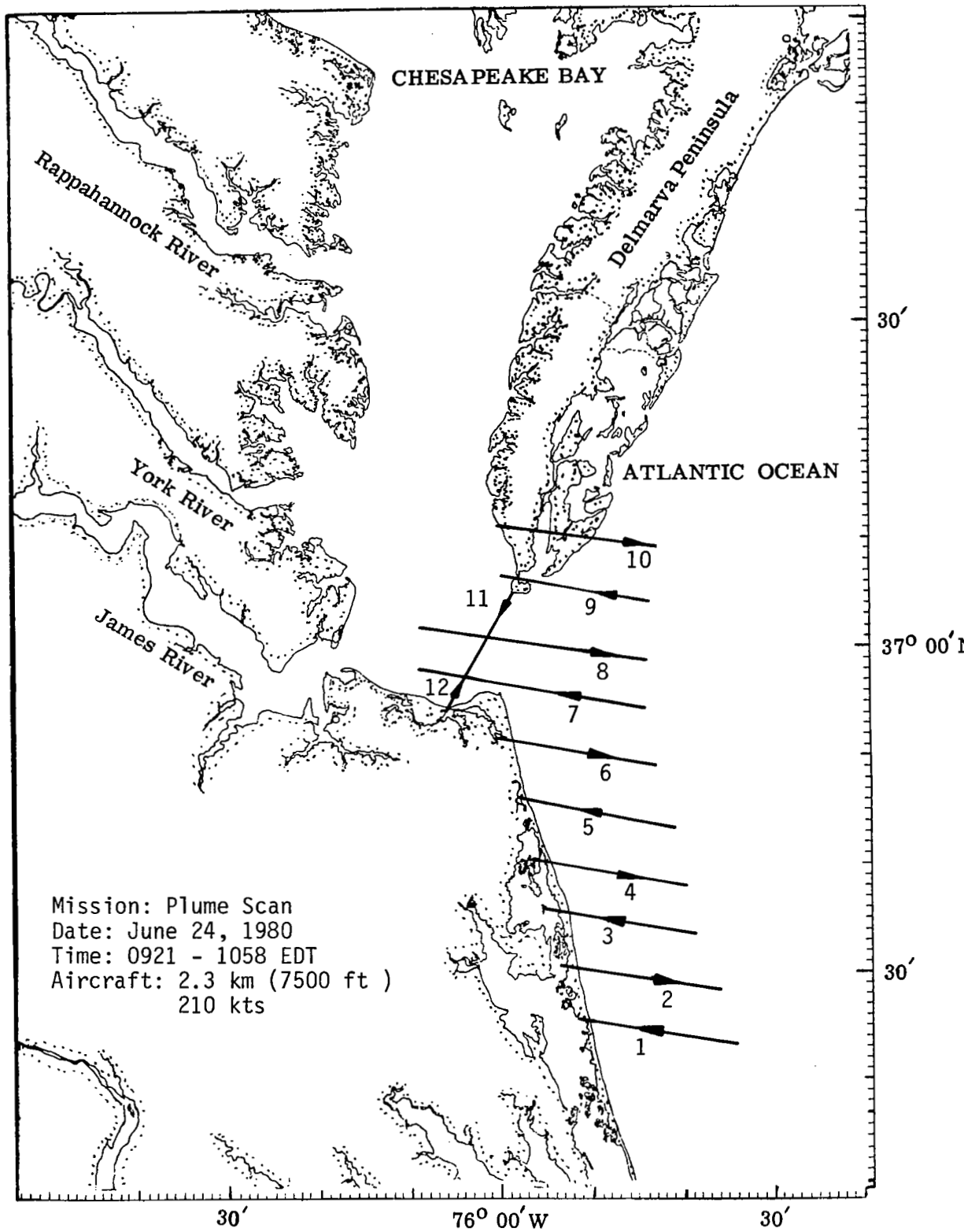

Figure 4.- Flight track of high-altitude plume scan mapping mission on June 24, 1980.

SUPERFLUX I, II, and III EXPERIMENT DESIGNS:

WATER SAMPLING AND ANALYSES

James P. Thomas
National Marine Fisheries Service
Northeast Fisheries Center
Sandy Hook Laboratory
Highlands, New Jersey

INTRODUCTION

Superflux, a joint National Oceanic and Atmospheric Administration (NOAA) and National Aeronautics and Space Administration (NASA) study, with state and academic participation, involves both airborne remote sensors and sea-going oceanographic research vessels. Its purposes are to: 1) advance the development and transfer of improved remote sensing systems and techniques for monitoring environmental quality and effects on living marine resources; 2) increase our understanding of the influence of estuarine "outwellings" (plumes) on contiguous shelf ecosystems; and 3) provide a synoptic, integrated and timely data base for application to problems of marine resources, and environmental quality. As such it is a study which requires a multi-disciplinary and, consequently, a multi-organizational approach.

Chesapeake Bay is the largest estuary in the United States and is under ever-increasing use and stress by man. The potential for studying effects of increasing stress on offshore environments, plus the potential for developing a coherent study with a number of investigators, each providing different yet relevant talents, led us to select the Chesapeake Bay mouth and offshore plume as a primary area for studying estuarine-shelf interactions in conjunction with remote sensing. The use of airborne remote sensors in concert with sea-going oceanographic research vessels offered the potential to understand a tidally dynamic area. The remote sensors could provide a synoptic picture of the surface distributions and abundances of selected variables (temperature, salinity, chlorophyll *a*, phytoplankton color groups, and total suspended matter). Surface ships provide the data required to calibrate the remote sensors (as sea truth) as well as the three-dimensional view of the water column required to interpret remote sensing imagery. Additionally, ships can collect data not directly relatable to that from remote sensors (certain contaminants and biostimulants, as well as biological effects data) yet of high interest in terms of environmental quality and resource management. Such measurements, it would be hoped, would be relatable to certain of the variables measured by remote sensors. In that way, remote sensing imagery could help solve the temporal-spatial problems encountered by ships in tidally dynamic areas by providing, in conjunction with shipboard data for interpretability, synoptic information relevant to the determination

of environmental quality and the management of resources. The goal of Superflux is to hasten the day when this would occur.

To date three experiments, timed to coincide with periods of high, medium, and low freshwater discharge, have taken place. These were 11-20 March 1980 (Superflux I), 17-27 June 1980 (Superflux II) and 13-22 October 1980 (Superflux III). Drought conditions existed during Superflux experiments II and III.

SUPERFLUX I

During the first experiment (11-20 March 1980), NASA flew four missions with airborne remote sensors. The missions were of two basic types: 1) plume mapping missions which overflew the Chesapeake Bay mouth and plume area, and 2) shelf transect missions which flew from the James River mouth east across the shelf to the continental slope/rise area. The low altitude missions across the shelf and over the plume collected data with two laser fluorosensors (Airborne Lidar Oceanographic Probing Experiment-ALOPE and an Airborne Oceanographic Lidar-AOL) for chlorophyll, phytoplankton color groups and total suspended matter, an L-band microwave radiometer for salinity, and a PRT-5 infrared radiometer for temperature. On the high altitude flights, a narrow swath width (nadir looking) Multichannel Ocean Color Scanner (MOCS) was used to sense chlorophyll and total suspended matter. The L-band microwave and PRT-5 infrared radiometers were also used.

The Northeast Fisheries Center (NEFC), National Marine Fisheries Service (NMFS), in conjunction with the NOAA, National Ocean Survey (NOS), the U. S. Coast Guard, Old Dominion University (ODU), and the Virginia Institute of Marine Science (VIMS), collected the required sea truth for these missions (figs. 1 and 2). As part of the experimental design, pre- and post-survey flights by a VIMS Beaver aircraft were made to provide visual information on the location and shape of the Chesapeake plume (figs. 3 and 4). The pre-survey flight information was used to establish station locations for a detailed cruise between the mouth of Chesapeake Bay and Oregon Inlet, North Carolina to define the three-dimensional structure of the plume in regard to temperature, salinity, dissolved oxygen, chlorophyll *a*, phaeopigments, and total plankton respiration (fig. 5). Additional independent studies (Bay Plex) were carried out in the bay mouth by Dr. George Oertel and colleagues, ODU, and in the plume for fine structure definition by Dr. John Ruzecki, VIMS.

SUPERFLUX II

The second experiment (17-27 June 1980), in terms of area flown, ships participating, sensors used, and oceanographic variables measured, was greatly expanded relative to the first operation. NASA flew seven missions which included four over the plume, one across the shelf, one over the Delaware Bay

mouth, and one up the full length of the Chesapeake Bay. The low altitude flights over the Chesapeake and Delaware plumes and across the shelf involved the use of two laser fluorosensors (ALOPE and AOL), the MOCS, the L-band microwave radiometer, and the PRT-5. The high altitude flights over Chesapeake and Delaware bays, across the shelf and over the Chesapeake plume, used the nadir looking MOCS, the L-band and PRT-5 radiometers, as well as a relatively wider swath width scanner (Test Bed Airborne Multichannel Scanner-TBAMS), which was felt might be more suitable for two-dimensional mapping of chlorophyll and total suspended matter.

In conjunction with a large number of institutions including NOS, NASA, U. S. Naval Academy, State of Maryland Department of Natural Resources, University of Delaware, Anne Arundel Community College, University of Miami, Chesapeake Bay Institute (CBI), ODU, and VIMS, NEFC participated in the experiment to provide sea truth and other measurements. A total of 14 vessels participated (fig. 6). Again, a VIMS Beaver aircraft made pre- and post-survey overflights to provide information on the location and shape of the Chesapeake plume (fig. 7). Based on this information, the NOAA ship *Delaware II* occupied 26 stations from the mouth of the Chesapeake Bay south to Oregon Inlet, North Carolina (fig. 8) to gather data throughout the water column in regard to temperature, salinity, dissolved oxygen, nutrients, chlorophyll a, phaeopigments, phytoplankton species composition, total suspended matter (TSM) and total plankton respiration. Additional work under contract was carried out aboard the *Delaware II* at the 14 northernmost stations closest to the bay mouth. Contracts were given to: 1) ODU (Drs. Terry Wade and George Oertel) to study hydrocarbons associated with total suspended matter; 2) VIMS (Dr. Richard Harris) to examine selected heavy metals associated with total suspended matter; and 3) VIMS (Drs. Howard Kator and Paul Zubkoff) to study bacterial biomass and heterotrophic potential associated with the Chesapeake plume. Other contract work to ODU, including nutrients (Dr. George Wong), phytoplankton species composition (Dr. Harold Marshall), and TSM (Dr. George Oertel), was initiated to see if we could use remote sensing to tell us something about contaminants, biostimulants, and biological effects in the plume area.

During this experiment, NEFC also collected continuous underway and discrete samples (every 10-15 minutes) across the shelf and along several transects of the plume for chlorophyll a and phaeopigment determinations, both in conjunction with remote sensing overflights and independent of them (fig. 9).

Additional studies were undertaken by VIMS (Dr. John Ruzecki) to examine the fine structure of the plume in regard to temperature, salinity, and chlorophyll. This was accomplished by collecting continuous underway data with periodic stations for conductivity, temperature and depth (CTD) casts. ODU (Dr. George Oertel and colleagues) again performed a comprehensive set of experiments called Bay Plex in the Bay mouth. These experiments were designed to provide information about the source of the various water masses coming out of the mouth of Chesapeake Bay. During this same time, CBI (Dr. Bill Boicourt) moored some 50 current meters in lower Chesapeake Bay and adjacent shelf area. Finally, the University of Miami (Dr. Mitch Roffer)

examined the distribution of certain fish in relation to sea surface temperature obtained via satellite and shipboard measurements.

SUPERFLUX III

During the third experiment (13-22 October 1980), NASA flew four missions, two of which were for plume mapping and two shelf transects; all were high altitude. Two aircraft, a NASA P-3 carrying a nadir looking MOCS and a NASA Lear Jet carrying a wide swath width Ocean Color Scanner (OCS), participated to examine total suspended matter and chlorophyll concentrations both in the plume and across the shelf.

The NEFC, with NASA, VIMS, and ODU, collected required sea truth for each of these missions. The experiment started on 13 October with a pre-survey flight by the VIMS Beaver Aircraft (fig. 10). The results of that flight plus pre-mission satellite imagery of the area were presented at a pre-cruise meeting by Dr. John Ruzecki (VIMS) and Dr. Fred Vukovich (Research Triangle Institute, North Carolina), respectively. Dr. John Munday (VIMS), also under contract, presented preliminary information in regard to Landsat images of the area. Based on this information the R/V *Kelez* carried out a plume survey (fig. 11). At the northernmost 14 stations (excluding stations 822 and 824), samples were collected throughout the water column for determination of hydrocarbons (ODU) and heavy metals (VIMS) associated with total suspended matter, as well as for bacterial biomass and heterotrophic potential (VIMS), dissolved and particulate organic carbon and nitrogen (NEFC/ Univ. Delaware), and algal bioassay (ODU). At 24 stations between the bay mouth and Oregon Inlet, North Carolina, samples were collected throughout the water column for temperature, salinity, dissolved oxygen, dissolved inorganic nutrients (ODU), chlorophyll a and phaeopigments, phytoplankton species composition (ODU), total suspended matter (ODU) and total plankton respiration.

Several new experimental approaches were initiated during this third experiment. The first of the three OCS overflights occurred on 15 October. For this overflight of the Chesapeake Bay plume, four research vessels were stationed along four transects perpendicular to the flow of the plume (fig. 12). The R/V *Langley* (NASA) collected data across the bay mouth, the R/V *Holton* (ODU) along a transect east northeast from Cape Henry, the R/V *John Smith* (VIMS) east from Rudee Inlet and the R/V *Kelez* (NOAA) east from the Dam Neck Firing Range. The object was to sample the plume - vertically and horizontally - with surface vessels during the same time interval as the OCS overflight, about two hours. This was accomplished successfully.

In addition, a 12 hour study was done along the plume transect running east northeast from Cape Henry to improve understanding of tidal influence on our data. Vertical casts using a CTD were made for temperature and salinity,and near high and at low tide at station 69 close to Cape Henry, samples were taken for dissolved oxygen, nutrients, chlorophyll a and phaeopigments, total plankton respiration, bacterial biomass and heterotrophic

potential, total suspended matter, hydrocarbons and heavy metals.

On October 21 (fig. 13), discrete surface bucket samples for chlorophyll a and phaeopigments were collected every 10-15 minutes across the shelf from the bay mouth to the continental slope to provide detailed information in preparation for the NASA cross-shelf transects which occurred later that day (MOCS) and the following day (MOCS and OCS). Of particular interest was the aircraft-directed shipboard sampling (fig. 14) to ensure definition of the major hydrographic (chlorophyll) regimes across the shelf. Particular emphasis was placed on defining the so-called "green river" (chlorophyll) offshore.

As with the March and June experiments, additional studies were accomplished in October by VIMS (fine structure of the plume) and by ODU (Bay Plex).

STANDARDIZATION

To standardize sampling and analytical methods, a division of responsibilities was instituted at the time of the first experiment wherein each participating group became responsible for the sampling protocol and processing of particular types of samples. For example, the NEFC was responsible for chlorophyll a and phaeopigments, Dr. Marshall (ODU) for phytoplankton and Dr. Kator (VIMS) for bacteria. This standardization applied particularly to samples being collected from several research vessels at the same time. The various protocols and sampling procedures are discussed as appropriate in the succeeding papers.

CONCLUDING REMARKS

We have heard from Dr, John Walsh that the outflow of waters and nutrients from Chesapeake Bay during the summer may be the dominant factor in sustaining primary production in shelf waters off the bay. Such an effect on the contiguous shelf ecosystem could be labelled as positive. Dr. Jack Pearce noted that estuaries were major sources of pollutants to the continental shelf, and that certain of the living marine resources showed above-expected contaminant levels at widely distributed locations away from the estuary. This could be labelled a negative influence. He talked further about the potential role remote sensors could play, particularly over large or especially dynamic areas (e.g. estuarine plumes), by providing the temporal-spatial frequency and synopticity required for application to problems of marine resource and environmental quality. Sampling of the planktonic component of the marine ecosystem through traditional approaches (ships) has been labor intensive and is less than desirable because of the lack of temporal-spatial frequency and synopticity. In response, Dr. Janet Campbell discussed sensor development and outlined possibilities for technology

transfer to help provide the required sampling "breakthrough". I mentioned the interaction between surface ships and remote sensors to enhance our ability to interpret the imagery in terms of the vertical water column and other variables not directly measureable via remote sensing.

Thus we may say that: estuarine outwellings influence contiguous continental shelf ecosystems both positively and negatively; the immediate area of influence is dynamic and therefore requires synoptic sampling for understanding; synopticity for the surface layer can be obtained using remote sensors; added capability for interpreting the imagery can be obtained by having surface vessels work in conjunction with the remote sensors; and this interaction aides further in the development of sensors and the transfer of technology to provide us with the "tools" we need to do our jobs.

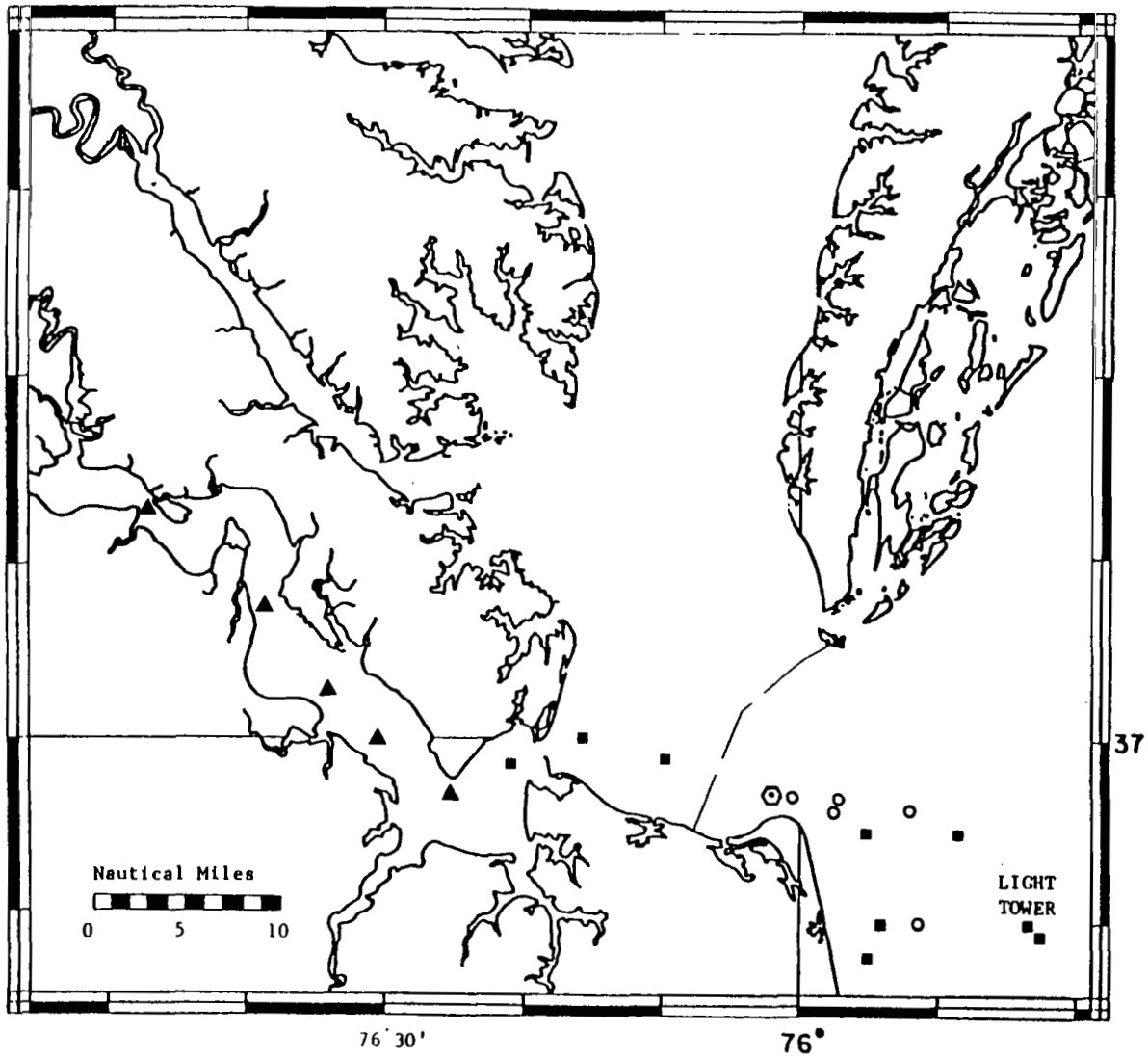

Figure 1.- Station locations for sea truth sampling during Superflux I, 11-20 March 1980. ▲ U. S. Coast Guard Launch; ■ NOAA-NOS Launch; ⊙ ODU R/V *Holton*; ○ VIMS R/V *John Smith*.

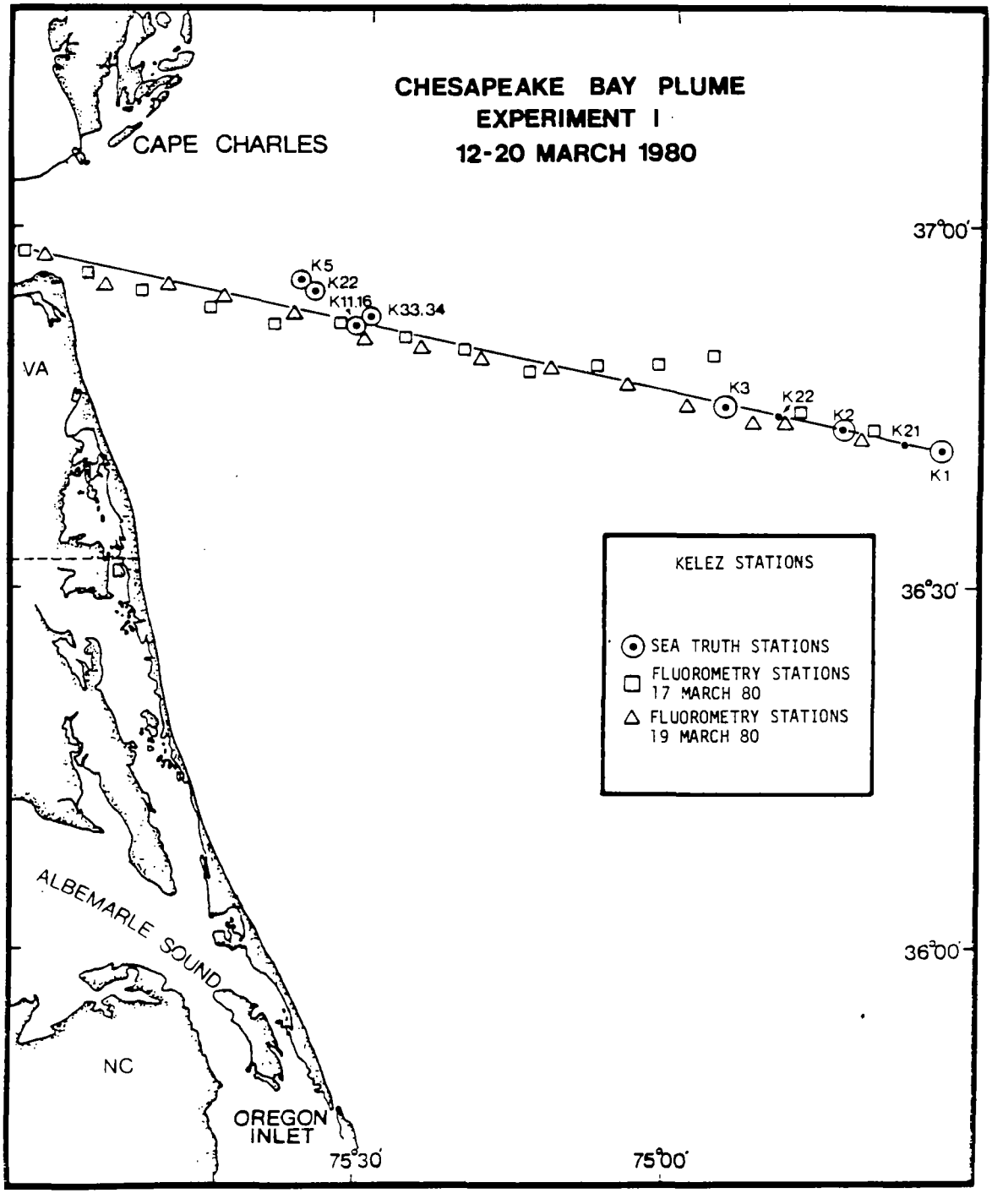

Figure 2.- Station locations sampled by NOAA Ship *Kelez* to provide sea truth for remote sensors.

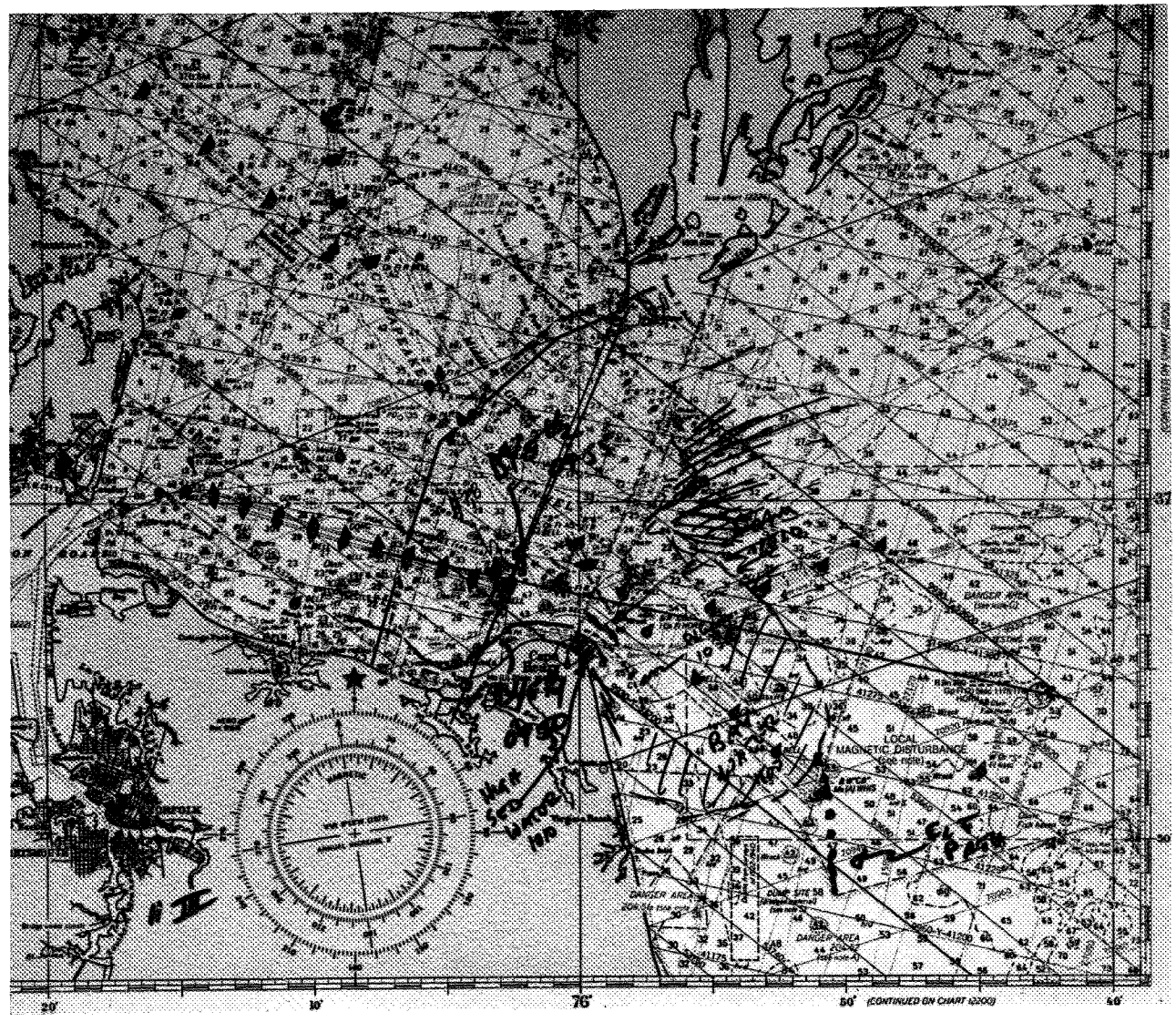

Figure 3.- Map showing locations and shape of Chesapeake Bay plume during pre-survey flight by a VIMS Beaver aircraft on 11 March 1980. Visual observations made by Dr. John Ruzecki, VIMS.

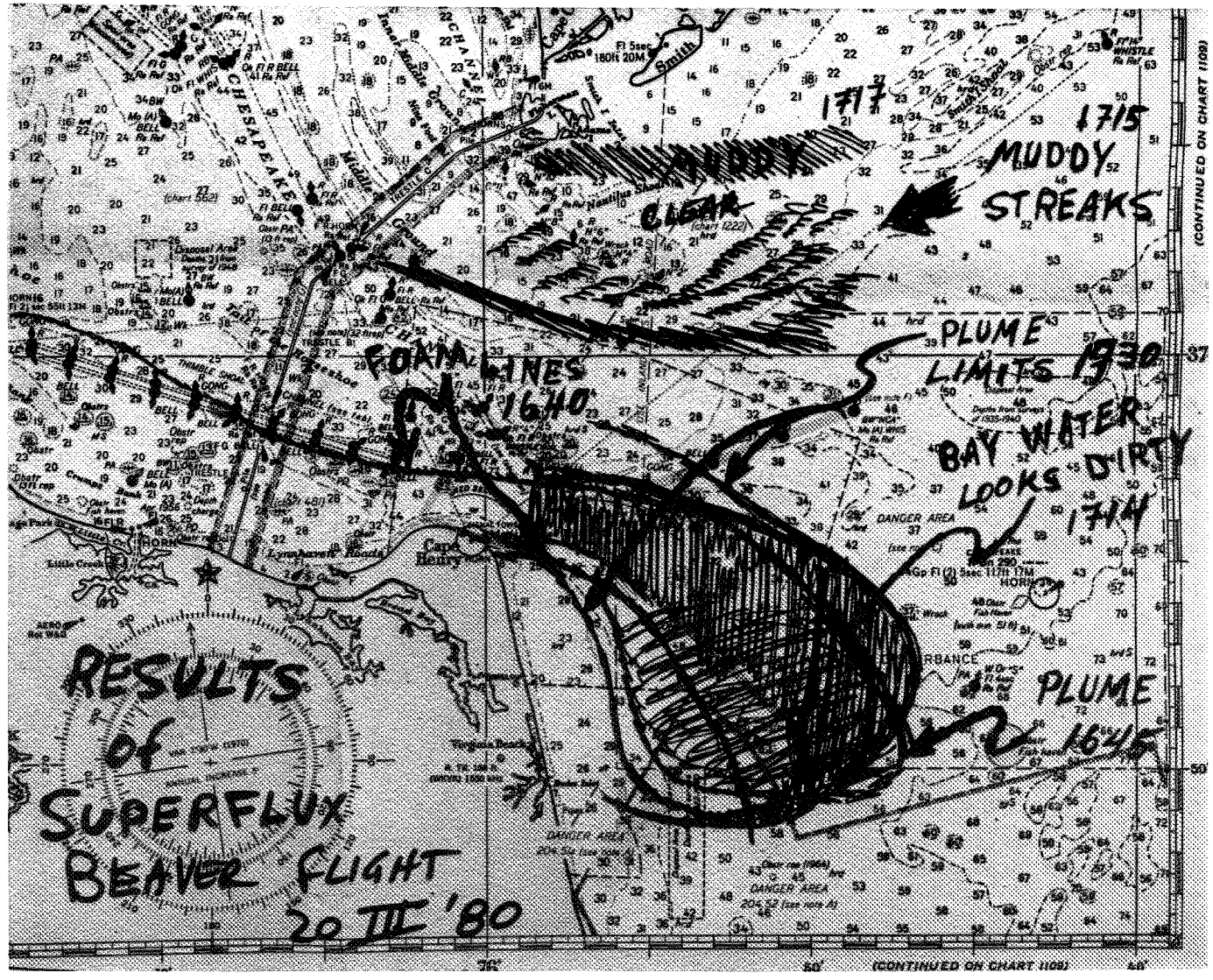

Figure 4.- Map showing location and shape of Chesapeake Bay plume during post-survey flight by a VIMS Beaver aircraft on 20 March 1980. Visual observations made by Dr. John Ruzecki, VIMS.

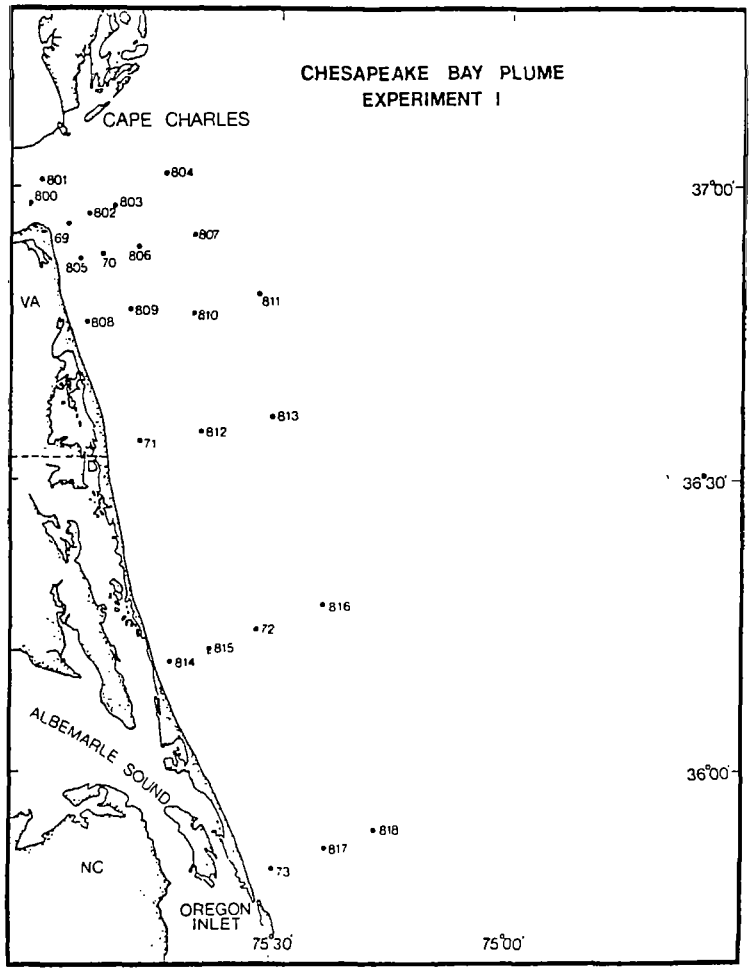

Figure 5.- Station locations sampled by NOAA Ship *Kelez* during detailed survey of Chesapeake Bay plume, 12-20 March 1980.

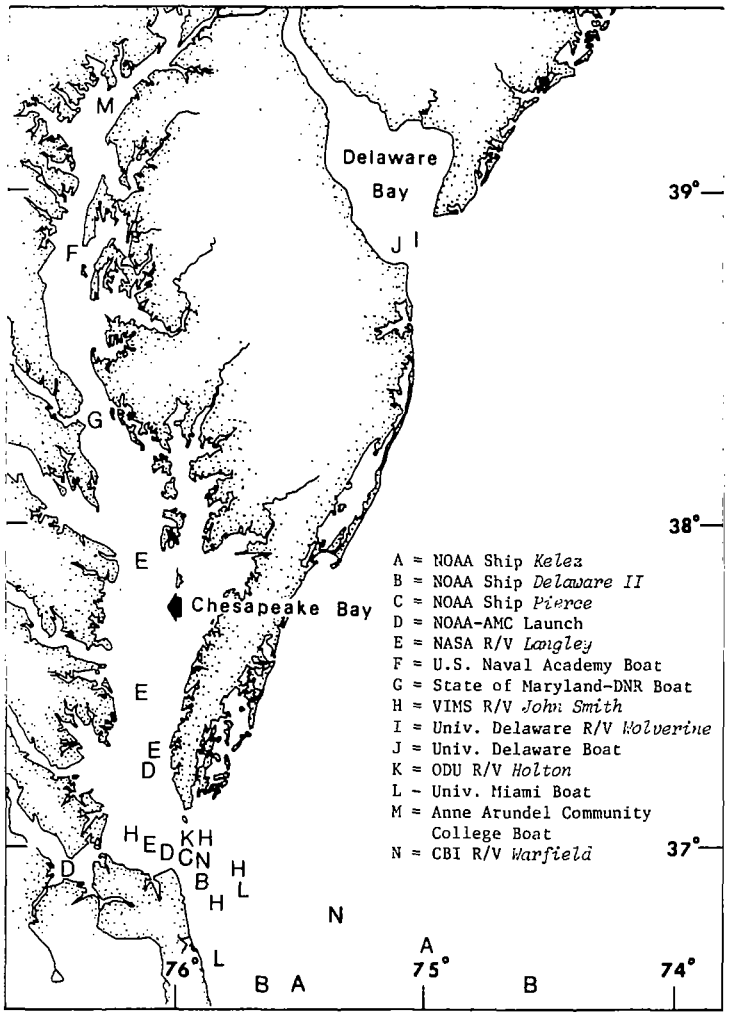

Figure 6.- Map showing locations of vessels participating in the collection of sea truth during Superflux II, 17-27 June 1980.

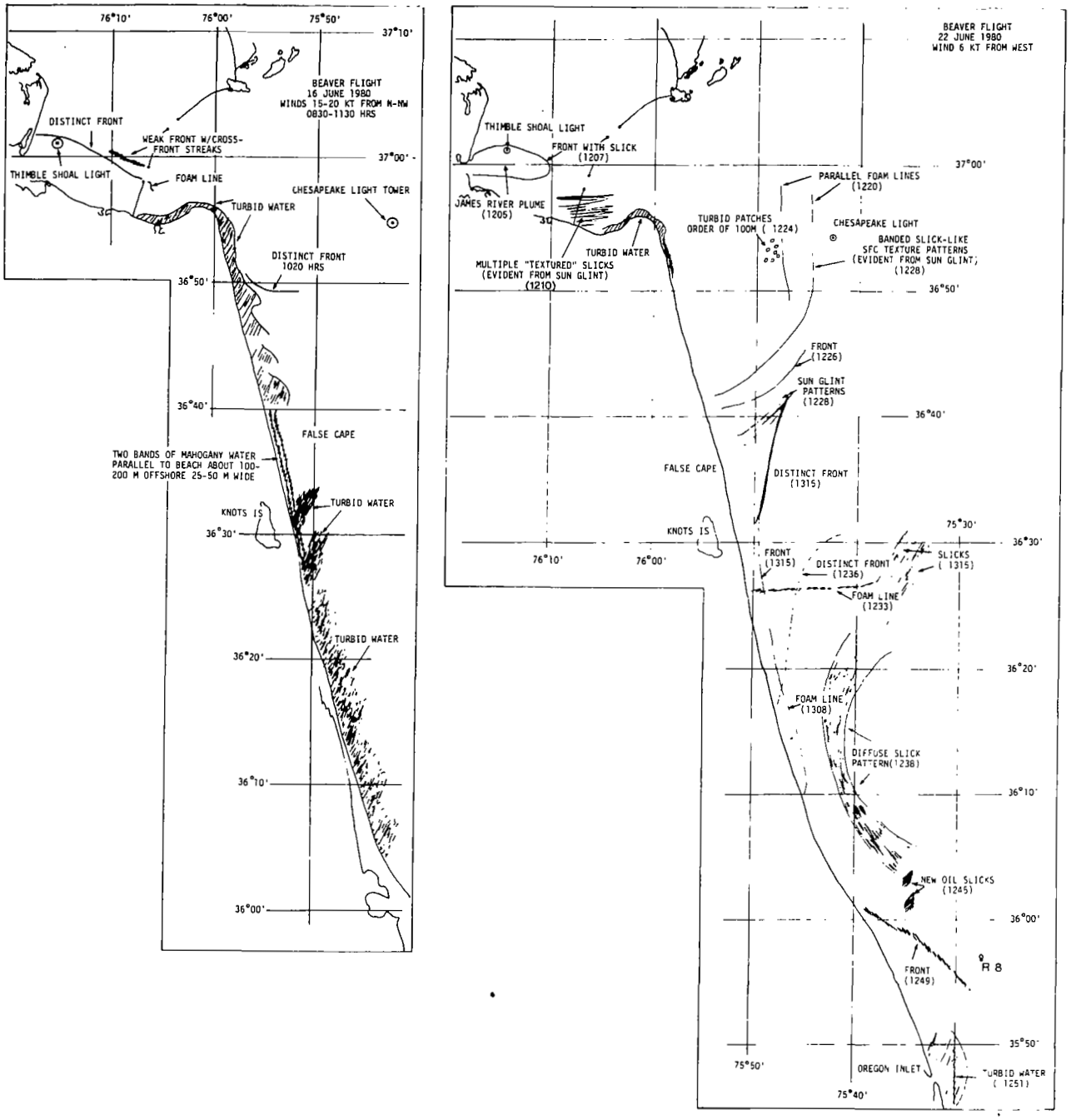

Figure 7.- Map showing location and shape of Chesapeake Bay plume during pre- and post-survey flights by a VIMS Beaver aircraft on 16 and 22 June 1980. Visual observations made by Dr. John Ruzecki, VIMS.

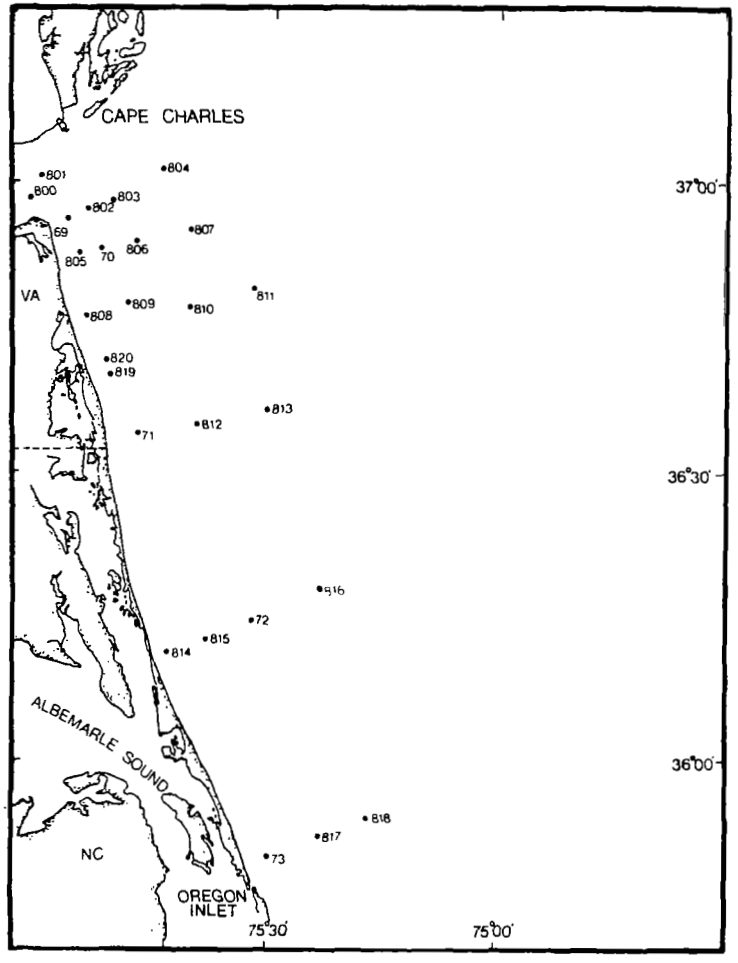

Figure 8.- Station locations sampled by NOAA Ship *Delaware II* during detailed survey of Chesapeake Bay plume, 17-27 June 1980.

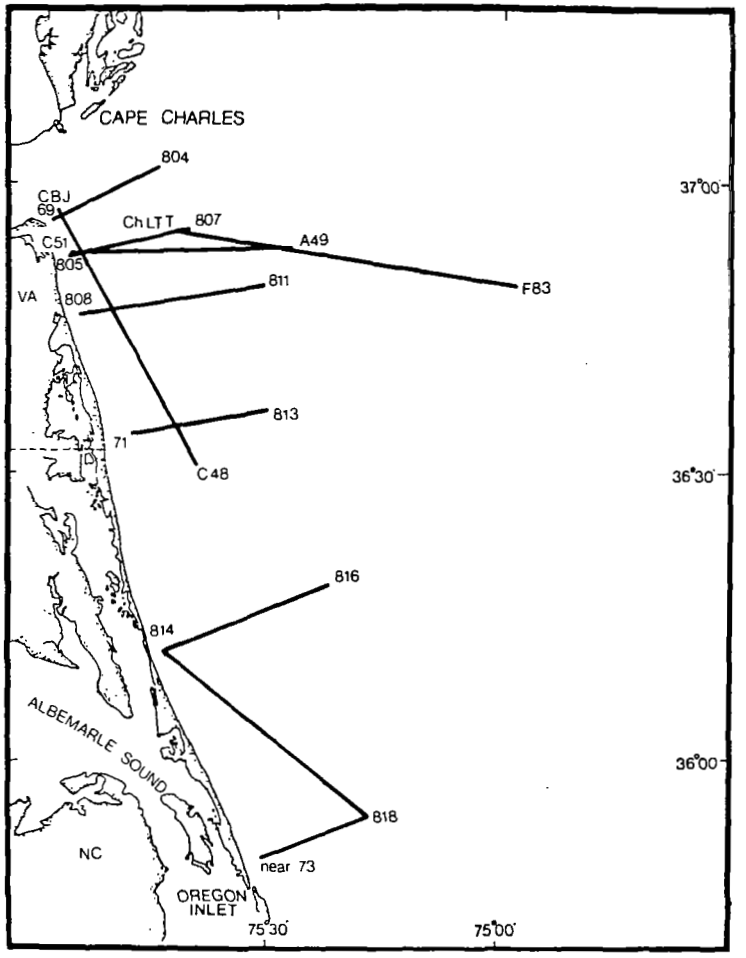

Figure 9.- Map showing locations of transects along which continuous and discrete underway chlorophyll a and phaeopigment samples were collected during Superflux II. All samples were collected from a depth of 3 meters.

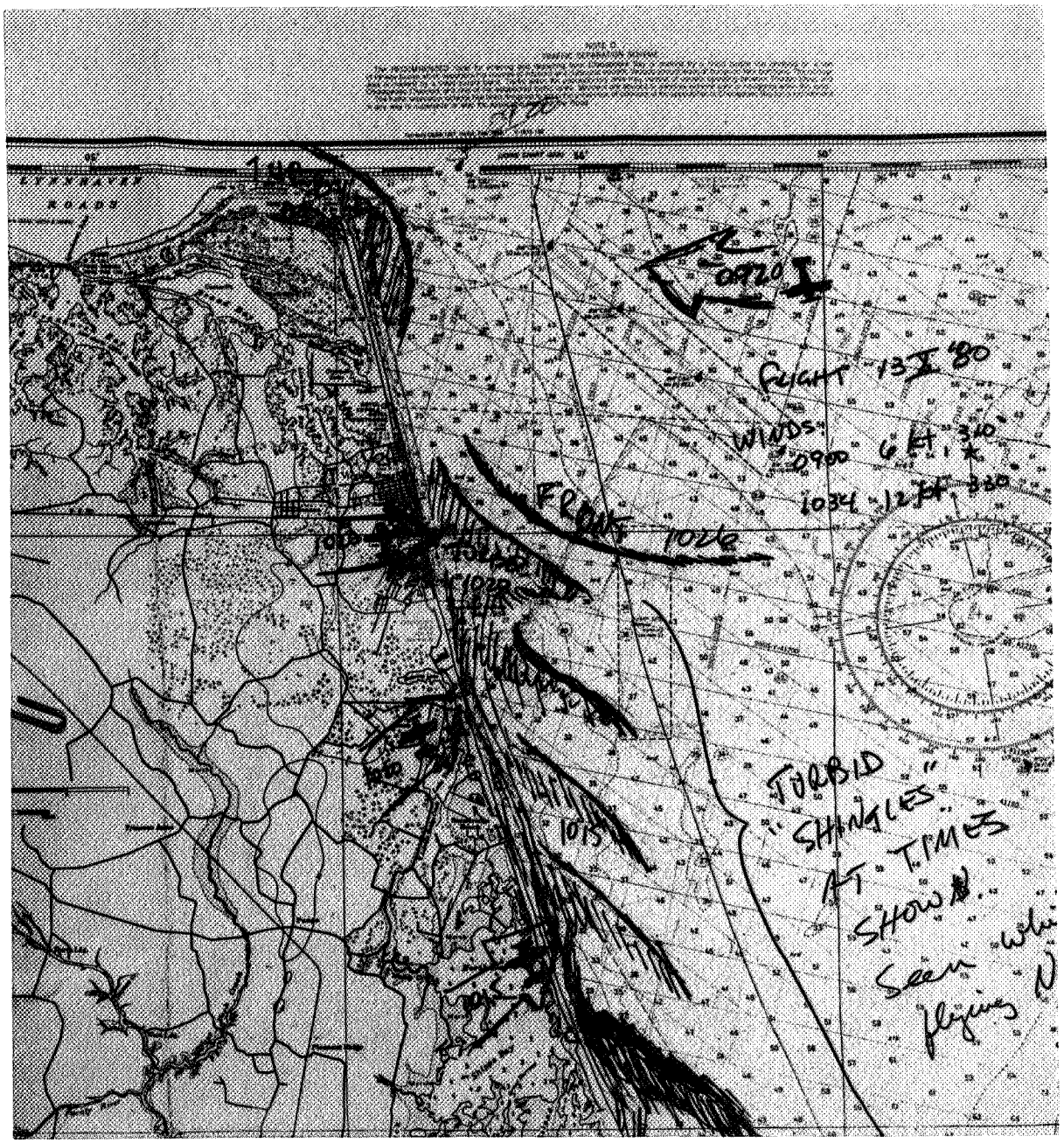

Figure 10.- Map showing location and shape of Chesapeake Bay plume during pre-survey flight by a VIMS Beaver aircraft on 13 October 1980. Visual observations made by Dr. John Ruzecki, VIMS.

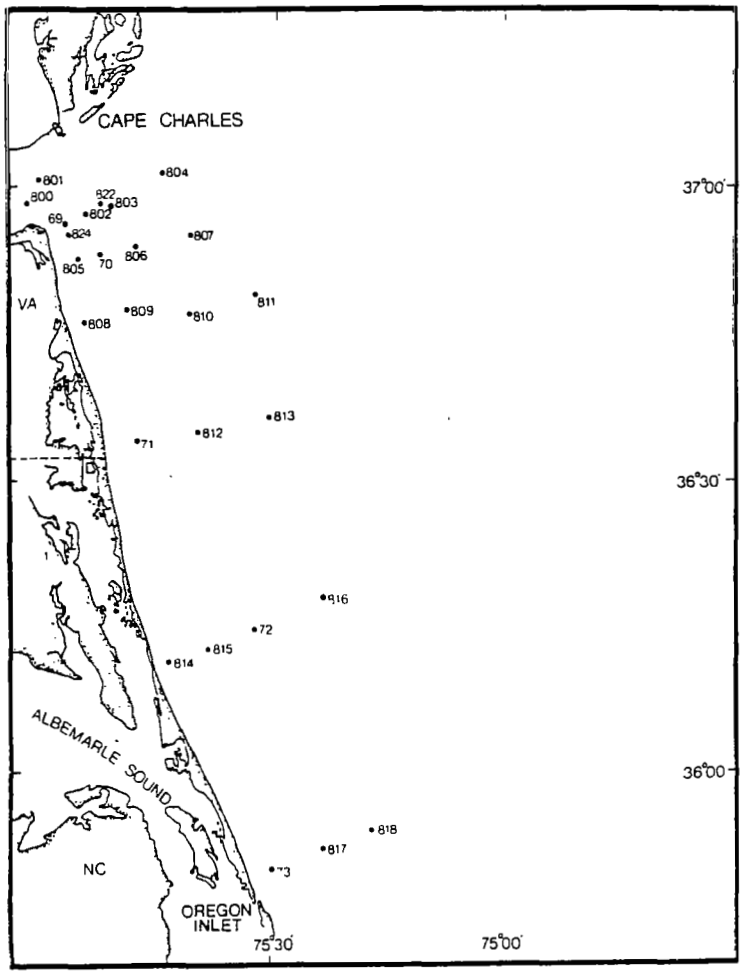

Figure 11.- Station locations sampled by NOAA Ship *Kelez* during detailed survey of Chesapeake Bay plume, 14-22 October 1980.

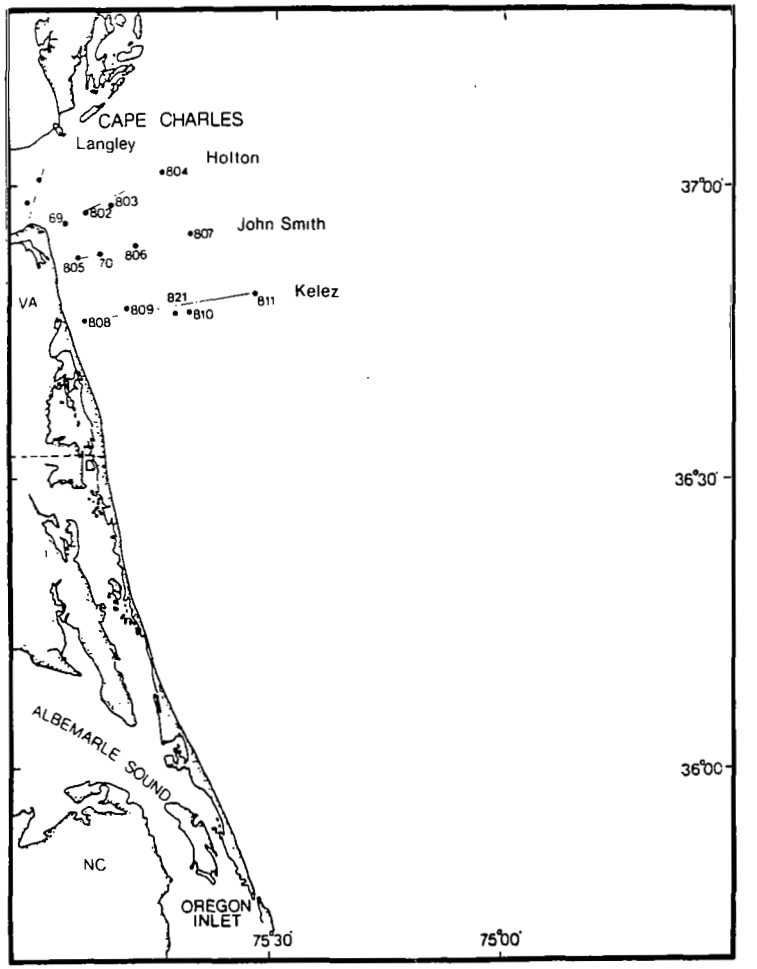

Figure 12.- Locations of transects and stations sampled concurrently with a two hour Ocean Color Scanner overflight on 15 October 1980.

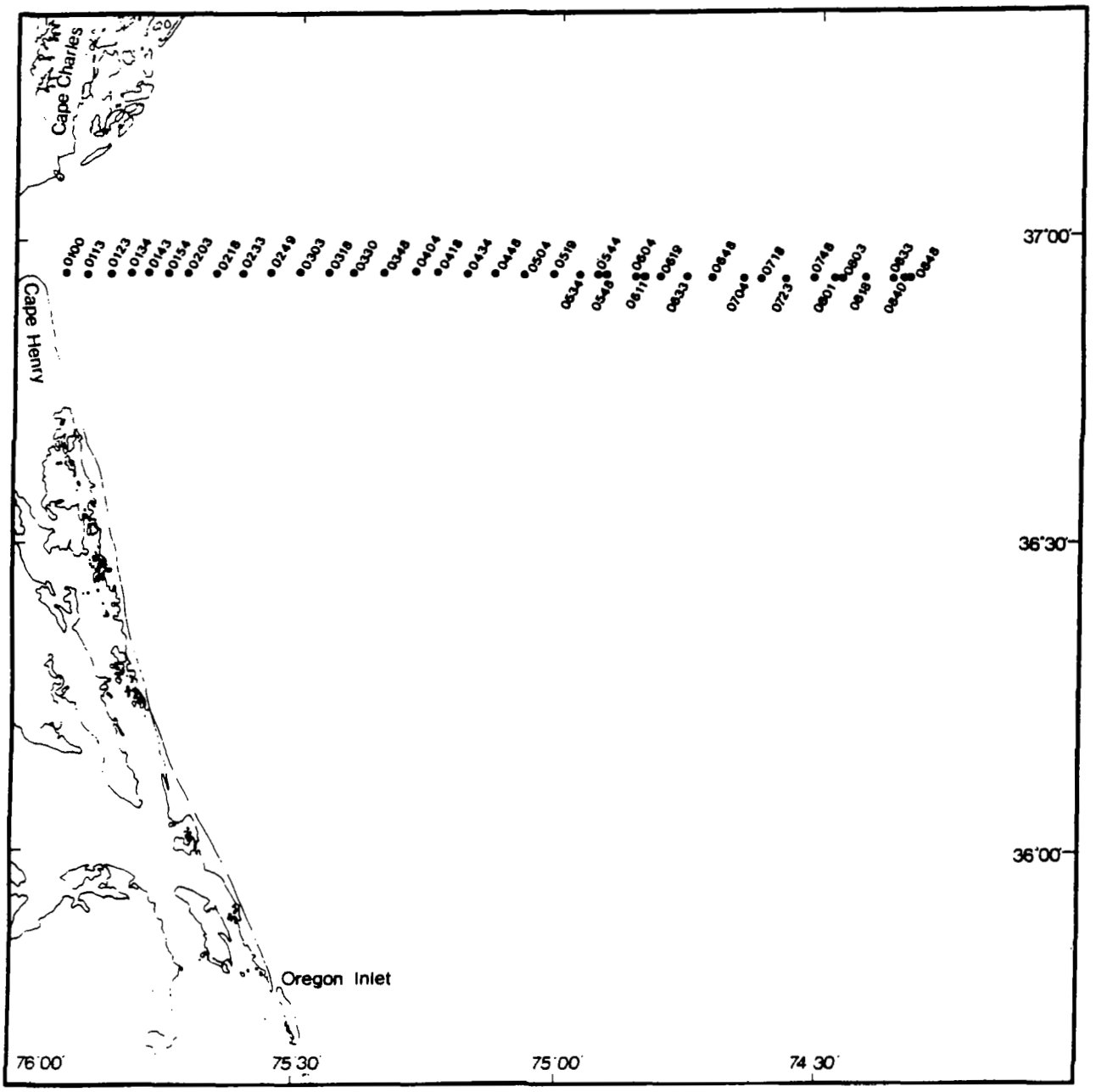

Figure 13.- Surface bucket stations sampled for chlorophyll a, phaeopigments, and temperature on 21 October 1980.

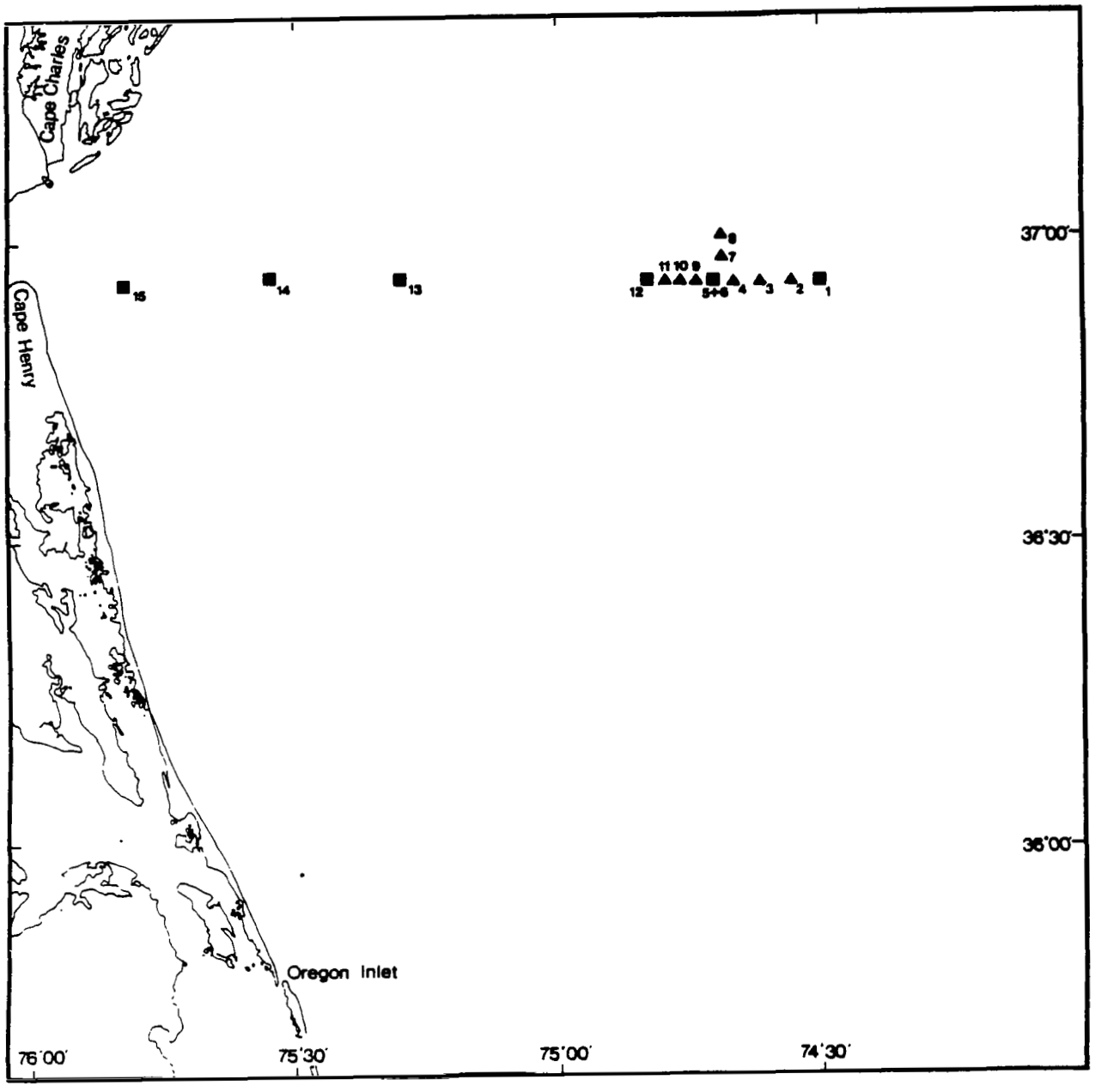

Figure 14.- Stations sampled by NOAA Ship *Kelez* during MOCS-OCS overflights on 22 October 1980. Squares indicate locations of hydrocast samples from 1 meter and 3 meters. Triangles indicate locations of surface bucket samples only.

CIRCULATION IN THE CHESAPEAKE BAY ENTRANCE REGION:

ESTUARY-SHELF INTERACTION

W. C. Boicourt
Chesapeake Bay Institute
The Johns Hopkins University

SUMMARY

Current meters and temperature-salinity recorders confirm that the upper layers of the continental shelf waters off Chesapeake Bay can be banded in summer, such that the coastal boundary layer (consisting of the Bay outflow) and the outer shelf flow southward while the inner shelf flows to the north, driven by the prevailing southerly winds. These measurements show that the estuary itself may also be banded in its lower reaches such that the inflow is confined primarily to the deep channel, while the upper layer outflow is split into two flow maxima on either side of this channel.

INTRODUCTION

As oceanographers began to study the water motion in the Chesapeake Bay mouth, only a few moored instruments were employed to measure the flow field. The reasons for this sparse sampling stemmed partly from the difficulty in mooring and processing records from the instrumentation available at the time, but also stemmed partly from a sense that these few measurements, when combined with a large amount of shipboard temperature and salinity data, were sufficient to delineate the patterns of motion. Over the years, as instrument and sampling arrays became more elaborate, the flow regime in the mouth region has seemed to defy the simple expectations of the oceanographers by showing progressively smaller space scales of variability and by its complex, highly three-dimensional current patterns which are controlled by the local topography.

A knowledge of where the Bay inflow originates, where the outflow goes, and how far offshore the influence of the estuarine circulation extends would aid many studies of the Chesapeake Bay and inner continental shelf. A knowledge of the flow regime and dynamics of the Bay entrance region is crucial, however, for the construction of numerical models of the estuarine circulation. Present efforts are limited by the lack of a proper formulation of boundary conditions on the seaward end of the model (either the mouth or inner shelf). Little information is available, for instance, to answer the question of how much recirculation of water discharged on an ebb tide occurs on the subsequent flood.

The recent studies by the Chesapeake Bay Institute in the Bay mouth region under the sponsorship of the National Science Foundation, the Environmental Protection Agency, the National Ocean Survey, and the Army Corps of Engineers

have provided an evolving description of the flow regime and the dynamics controlling estuary-shelf exchange. With the advent of the Superflux prospectus, an opportunity arose to enhance previously planned observational efforts by combining them with the remote sensing experiments. The following paper contains a report on the preliminary results of these measurements.

BACKGROUND

It has long been known that the classical estuarine circulation of Chesapeake Bay consists of a two-layer flow, with the upper layer discharging low-salinity water onto the continental shelf while the lower layer draws higher-salinity shelf water into the Bay (ref. 1). The inflow source and the fate of the outflow waters, however, have been revealed only recently. The drift-bottle and seabed drifter experiments of Bumpus (ref. 2) have provided some glimpses of possible water-parcel trajectories in the offing of Chesapeake Bay. These glimpses are of value, in spite of inherent biases and uncertainties in such drifter measurements, because they help formulate questions and sampling strategies for present studies. Bumpus' data suggest that, in the mean, the inflow to Chesapeake Bay occurs as a slow, broadly distributed flow from the north and east. Boicourt (ref. 3) showed that the source of the inflowing water depends on the wind direction and that the inflow is confined primarily to the deep Chesapeake Channel, near Cape Henry (fig. 1). He also showed that the Chesapeake Bay outflow turns to the south (fig. 2) and flows as a quasigeostrophic jet along the Virginia and North Carolina coast (fig. 3). The offshore boundary often occurs as a sharp salinity front and can be seen in the synthetic aperture radar images from the Seasat satellite. That this buoyant plume is affected by the Coriolis force is not surprising, although dynamical analysis has been somewhat murky. Takano's (ref. 4) well-known model of the movement of fresh water from a river into a stationary sea purports to show a cyclonic turn of the outflowing water after leaving the mouth of the river. Although the resultant predictions (illustrated in ref. 5) agree qualitatively with Boicourt's observations for the Chesapeake Bay outflow, Takano's equations contain an error in formulation such that the stream function is symmetrical on the continental shelf, and not skewed cyclonically as reported. The Coriolis acceleration should be important in the Chesapeake Bay outflow, both in the southward turn and in the narrow current formed along the coastal boundary south of Cape Henry. Even if a characteristic velocity U in the outflow were chosen as large as 50 cm/s, a Rossby number

$$R_o = \frac{U}{f\,L}$$

where a characteristic length L was taken as the width of the outflow (10^6 cm) and the Coriolis parameter f is 0.9×10^{-4} s^{-1} would be less than unity (of the order ½). Beardsley and Hart (ref. 6) provide a three-dimensional dynamical model of the flow of an estuary onto a continental shelf. This treatment is dynamically correct, but more refinement is necessary to enable a careful comparison of theory and observation.

The exchange between the Chesapeake Bay and the adjacent continental shelf waters does not necessarily occur as a steady, two-layer outflow and inflow. Boicourt (ref. 3) found that the wind can dominate this exchange, such that a northwest wind in November 1971 could drive an outflow surge that, over a two-day interval, lowered the water level of the Chesapeake Bay approximately 1 m. The net water discharged during this interval amounted to 10% of the mean volume of the Bay proper. Wang and Elliott (ref. 7) and Wang (ref. 8) show that the wind-driven exchange is not as simple as first thought. Consideration must be given to the response of the Bay to local winds, but also to the response of the continental shelf to both local and non-local winds for a proper accounting of the net exchange through the Virginia Capes. Strong winds can drive outflow surges over a two-day period, but over longer periods (5-10 days), the water level in the Bay can be controlled by the set-up and set-down on the continental shelf, a process which may counteract the level change driven on the shorter time scale.

Our previous studies have shown that the inner shelf of the Middle Atlantic Bight, away from the mouths of estuaries, is dominated by wind forcing (ref. 9). The reason for this dominance is twofold: 1) the mean longshore flow (not wind-driven) from Cape Cod toward Cape Hatteras *decreases* from a maximum near the shelf break toward the coast, and 2) the inner shelf is shallow and therefore prone to wind driving. These two reasons are related in that the shoreward decrease in the mean southward flow is probably the result of increased dominance of bottom friction as the depth decreases. The southward mean flow on the continental shelf has been well documented. Recent long-term measurements (ref. 10) suggest there is a greater variability about this mean in the waters off the Chesapeake Bay than in the New York Bight or New England shelf waters (figs. 4 and 5). An example of the dominance of wind-driven motion over this mean flow for the inner shelf region is shown in figures 6 and 7. Figure 6 contains vector time series of currents measured at four moorings at the cross-shelf section off Chesapeake Bay shown in figure 6 in the summer of 1974. The strong correlation of the wind stress record from Norfolk with the 10-m current record at the inner shelf station 408A indicates clearly that the wind is the primary driving force in the region. Offshore (stations 413A, 415A, and 416B) the wind-driven motion is seen as a modulation of the mean southward flow. The means of these records are shown in figure 7, where the dots are southward flow and the crosses are northward flow. Station 408A means reveal, as could be expected from a glance at figure 6, that the prevailing southerly winds can reverse the mean southward flow in the inner shelf. The winds in July 1974 were neither sufficiently strong nor persistent to reverse the mean southward flow on the outer shelf.

The Chesapeake Bay Institute planned an experiment in the Bay entrance region for January-February 1979. At the outset of this study, the expectation was that the influence of the Chesapeake Bay estuarine circulation could not be detected far offshore during this season. The reasoning was simple:

1) The magnitude of the estuarine circulation is at a minimum in winter.

2) The prevailing winds are northerly, adding a wind-driven component to the southward mean flow and restricting the

inflow and outflow of the estuary to a narrow band along the coast.

3) The water is unstratified--previous continental shelf observations show that the flow is nearly barotropic and parallel to isobaths during this season.

Earlier observations had also shown that the path of the deep inflowing water to Chesapeake Bay is strongly controlled by the topography. Whether the source of the inflowing shelf water is from the north or south of the entrance, the primary inflow is via the main channel near Cape Henry (fig. 8). If the source is from the north, the deeper water must move around the offshore extention of Middle Ground shoals before entering the Bay. Short-term current measurements indicate that there may be intermittent flow (with time scales of 4-8 days) *into* the Bay, throughout the water column on the north side of the Bay entrance, near Fisherman's Island. Temperature and salinity distributions help fuel this speculation because the stratification often appears weak or nonexistent in the North Channel area (refs. 2 and 9).

In January 1979, eleven vertical arrays of current meters and temperature-salinity recorders were moored in the Bay entrance and on the adjacent inner shelf (fig. 9). Sites were selected in an attempt to bring a balance to the conflicting requirements of spatial coverage and spatial resolution. On the inner shelf, space scales of the flow patterns were expected to be significantly greater than in the primary entrance channel, and therefore moorings MF1, MF2, MF3, and MF8 (fig. 9) have greater separations than in the entrance channel, where high resolution is desired. Mooring MF9 was located in the high-traffic area near Cape Henry. Measurements of the inflowing water at this site were deemed valuable, but a mooring would be highly vulnerable to ship collision. For this reason, the subsurface floatation was located at a depth below the keel of vessels operating in the entrance channel, and the mooring was attached to the bottom via an acoustic release.

In spite of high mooring losses due to ship collision, crab dredging, and Saudi Arabian minesweeping, the data return is sufficient to provide clues to the flow patterns. An interval of 240 common hours beginning 4 February 1979 was chosen as the most suitable for this purpose. The mean flows (fig. 10) at the four offshore moorings (MF1, MF2, MF3, MF8 in fig. 9) were remarkably consistent in both speed and direction during the 240-hour interval. The mean flows are of the order 10 cm/s to the south-southwest, parallel to local isobaths. An examination of the longer records from the offshore moorings indicates that this agreement held up for the two-month deployment of the instruments.

The measured inflow to the Bay at 10 m at mooring MF5 and 16.8 m at mooring MF9 provides more substantial indication of the flow field around Middle Ground ridge than the earlier estimates. The low mean outflow in the upper layer in the North Channel section (fig. 10; MF12 in fig. 9) is of particular interest. The question as to whether there are times when there is net density-driven inflow to the Bay throughout the water column in this area will have to await further analysis of the component of motion driven by the

prevailing northwesterly winds. The progressive vector diagram of the record from 3.7 m depth at station MF12 would suggest that, in spite of the low stratification shown on the northern half of the mouth cross-section, the vertical shear of the gravitational circulation is sufficient to ensure a net outflow in the upper layer. The mean outflow at 3.7 m depth at station MF11 (5 cm/s) is consistent with the estuarine circulation, but is not as strong as that expected at station MF10 in Thimble Shoals Channel, especially in winter with prevailing northwesterly winds. The outflow to the Bay occurs as a jet along the Virginia coast, with greatest thickness near the shore, with the halocline shoaling to a high-shear lateral front 8-15 km offshore. The southward mean flow at station MF6 reflects both the outflow and the component driven by the northerly winds.

With the arrival of summer, a substantial change occurs in both estuarine and continental shelf waters. First, the stratification is increased, in the estuary by the spring runoff, and on the shelf by the spring warming. The second difference between summer and winter is that the winds switch from prevailing northwesterly in winter to prevailing southwesterly. The increased stratification on the shelf serves to allow greater independence of upper and lower layer flows. The prevailing southwesterly winds can drive a northward mean flow on the inner shelf, and may even reverse the southward mean flow on the outer shelf, if they are sufficiently strong and persistent. The expectations, then, for summertime flow are: 1) that increased stratification allows a greater chance to decouple upper and lower layer flows and therefore allows the estuarine influence to extend further offshore and, 2) the prevailing southerly winds will drive northward flow on the inner shelf.

SUMMER 1980

SUPERFLUX

The 1980 Superflux experiment was timed so that many ongoing experiments in the Chesapeake Bay mouth region could be combined conveniently to take advantage of the additional coverage and resolution provided by the other studies, especially the remote sensing experiments. The Chesapeake Bay Institute was engaged in a large-scale study of the Bay circulation for the U. S. Environmental Protection Agency and the National Ocean Survey. The goals of the experiment were to 1) obtain calibration and verification data for a three-dimensional numerical model under construction, and 2) examine the three-dimensional flow structure in the lower Chesapeake Bay and inner continental shelf, where the influence of the Earth's rotation and topographical control by channels is especially pronounced. Twenty moorings (fig. 11) were placed thoughout the Bay in late June, 1980, from the mouth to Worton Point. Instrumental resources were concentrated in the southern reaches of the Bay to provide better resolution of the flow structure there. The relatively sparse array placement in the upper reaches was deemed acceptable because moorings were located at positions where previous high-density mooring arrays had provided three-dimensional flow details. Three additional moorings (MF2, MF14, and MF7) were placed on the inner shelf to examine the flows at the Army Corps of Engineers Norfolk dredged material disposal site (MF2) and to

examine the flow in the transition zone between estuary and continental shelf circulations (fig. 12).

The mean flows from the 38-day experiment show that the currents on the inner shelf were consistent with the expectations (fig. 13). The measured upper-layer currents at MF2 and MF14 were in tight agreement, with a north-northeast flow driven by the prevailing southwesterly winds. The flow at the inshore mooring MF7 shows a mean southward flow in the upper layer, *opposite to flow on the shelf immediately offshore*. Mooring MF7 is located just offshore of the expected maximum-velocity zone of the southward jet of low-salinity outflow from Chesapeake Bay. The position and strength of the velocity maximum, however, are highly variable in time, due to variations in the winds and in the Bay outflow transport. The lateral shear in the upper layer between the southward flow indicated at MF7 and the northward flow indicated at MF14 probably occurs over a much smaller lateral distance, at the lateral front (or series of fronts) along the outflowing plume.

These upper-layer flow measurements lend further credence to the earlier suggestion that the Middle Atlantic Bight shelf currents are ordered in a series of bands parallel to the coast. The outer shelf is moving south in the mean, while the inner shelf is at the mercy of the winds, such that the summer flow is typically to the north. The narrow (10-20 km) band along the coast can be affected by estuarine circulation such that, along the Virginia and North Carolina coasts, the flow is to the south. The strength and spatial extent of this influence depends primarily on the magnitude of the estuarine outflow.

Lower-layer mean currents (fig. 13) show that the estuarine inflow requirements affect the flow as far offshore as station MF2. While the speed of the lower-layer mean at MF2 is small, and therefore the direction of the mean is somewhat uncertain, the time record shows consistent flow to the southwest, broken only by a few wind-driven flow events. With only three offshore moorings and only two points in the vertical for resolving the profile, constructing a detailed flow pattern is difficult. The inflow pattern inferred from these few offshore measurements, however, is in agreement with the earlier measurements.

The measured upper-layer flows in the Bay entrance cross-section (fig. 13) *are not* consistent with expectations. The strong outflow on the southern side of the cross-section is expected, but both the rapid decrease to the north and the strong outflow in the North Channel (M5) are surprises. An examination of synthetic aperture radar imagery from Seasat shows that a pronounced lateral front, aligned with the Middle Ground shoals, occurs near station M3. The time records of currents at stations M3 and M4 show strong tidal flows, but the means are consistently less than 1 cm/s. The strong upper-layer currents at M5 are a surprise because the expectation was that the flow would be weak out of the estuary, or perhaps even directed into the estuary. This expectation was sufficiently well-embedded that a legitimate worry has arisen as to our ability to interpret Eulerian means in the presence of highly channelized flows. Large Stokes velocities are possible when a strong reversing tide interacts with a complex bottom topography.

The cross-sectional structure of the Bay entrance mean currents is shown in figure 14. The classical estuarine circulation is clearly in evidence in the deep channel near Cape Henry, with a surface outflow and a subsurface inflow jet. The mean currents at station M3 show that the low mean flows are consistent throughout the water column here. The two-layer entrance flow is again in evidence in the North Channel (station M5). Clues to the dynamics of the flows over the shoals and in the North Channel region are provided by the temperature-salinity recorders on the moored current meters. Low-frequency currents can be correlated with both the salinities and the stratification in the mouth cross-section to help unravel their interdependence. Perhaps the question as to the Eulerian measurements' suitability can be decided by a careful look at the correlations at tidal frequencies and below. The salinity variability signal, at both tidal and subtidal frequencies, is sufficiently large to suggest that this technique is a promising avenue toward deciphering the Bay-shelf exchange processes . Figures 15 and 16 contain two realizations of the salinity structure in the Bay mouth cross-section. One section (fig. 15) was measured during a Superflux overflight on 23 June 1980. The nearly horizontal pycnocline and the occurrence of the salinity minimum on the north side of the entrance are the result of southerly winds. A more typical situation occurs on 15 July (fig. 16), where the salinity structure in the southern half of the mouth section corresponds more closely to the mean current structure (fig. 13).

The salinity sections indicate that the current measurements probably miss a significant part of the upper layer outflow. Practical considerations prevent routine mooring of current meters much shallower than the 2.7-m depth of the uppermost instruments in the summer 1980 measurements. The salinity sections also suggest that the subsurface inflow may at times reach the surface near station M3 and not in the North Channel as previously had been expected. Current measurements from the Wolf Trap cross-section (WT1-WT5 in fig. 11) show that the lower layer can reach the surface in mid-estuary.

REFERENCES

1. Pritchard, D. W. (1955) Estuarine circulation patterns. *Proceedings of the American Society of Civil Engineers 81:* Separate No. 717, 11 pp.

2. Bumpus, D. F. (1973) A description of the circulation on the continental shelf of the east coast of the United States. *Progress in Oceanography 6:* 111-157.

3. Boicourt, W. C. (1973) The circulation of water on the continental shelf from Chesapeake Bay to Cape Hatteras. Ph.D. Thesis, The Johns Hopkins University, Baltimore, Maryland, 183 pp.

4. Takano, K. (1954) On the salinity and the velocity distribution off the mouth of a river. *Journal of the Oceanographic Society of Japan, 10:* 92-98.

5. Defant, A. (1961) *Physical Oceanography Vol I.* MacMillan and Co., New York, 729 pp.

6. Beardsley, R. C. and J. E. Hart (1978) A simple theoretical model of the flow of an estuary onto a continental shelf. *Journal of Geophysical Research 83 (C2):* 873-883.

7. Wang, D. P. and A. J. Elliott (1978) The effect of meteorological forcing on the Chesapeake Bay: The coupling between an estuarine system and its adjacent coastal waters. *In:* J. C. J. Nihoul (ed.), *Hydrodynamics of Estuaries and Fjords,* 127-145, Elsevier, Amsterdam.

8. Wang, D. P. (1979) Subtidal sea level variations in the Chesapeake Bay and relations to atmospheric forcing. *Journal of Physical Oceanography 9:* 564-572.

9. Boicourt, W. C. and P. W. Hacker (1976) Circulation on the Atlantic continental shelf of the United States, Cape May to Cape Hatteras. *Memoires de la Societe Royale des Sciences de Liege, Sixieme Serie 10:* 187-200.

10. Beardsley, R. C. and W. C. Boicourt (1980) On estuarine and continental shelf circulation in the Middle Atlantic Bight. In: *Evolution of Physical Oceanography,* B. A. Warren and C. Wunsch, eds. MIT Press, Cambridge, 623 pp.

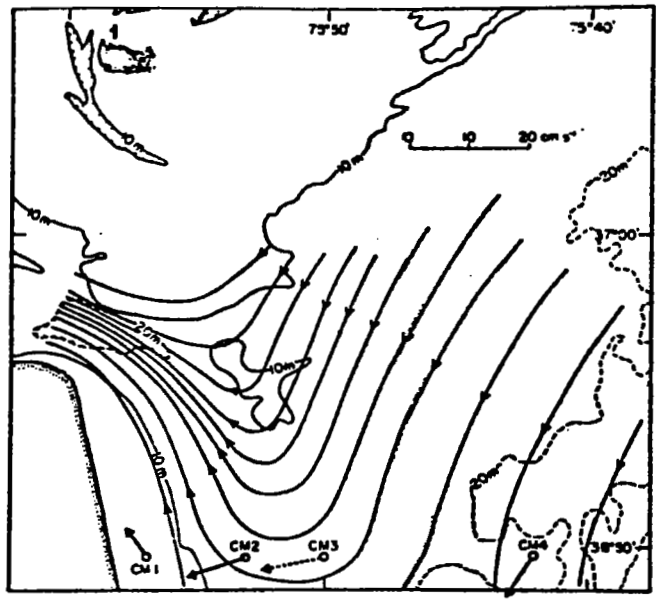

(a) Calm or northerly winds.

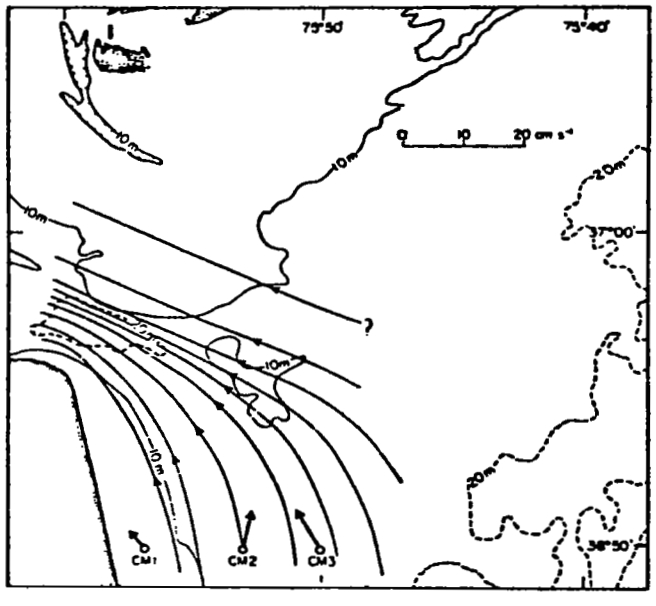

(b) Southerly winds.

Figure 1.- Inflow (lower layer) streamline pattern for periods of calm or northerly winds, and for periods of southerly winds.

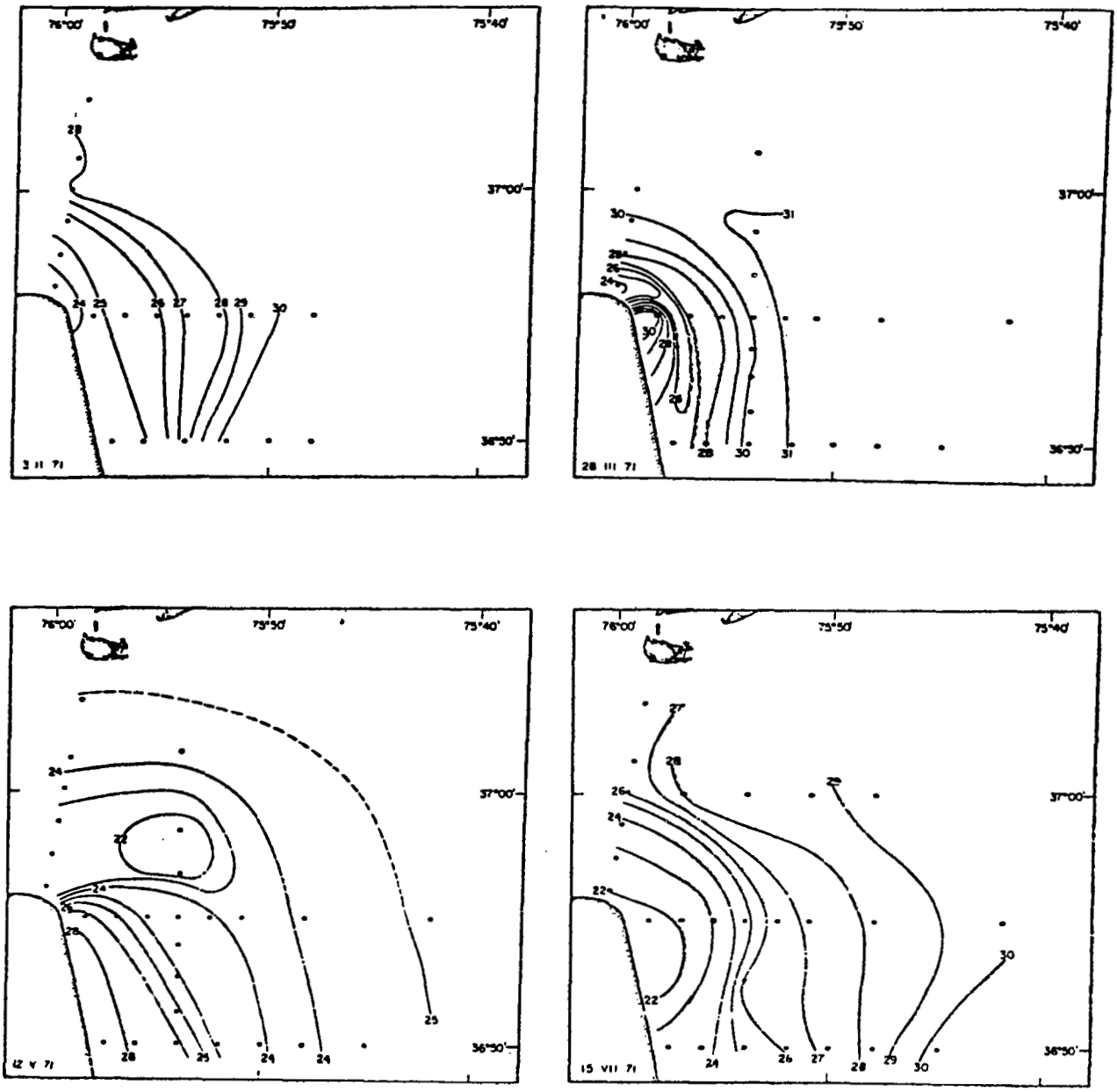

Figure 2.- Surface salinity distributions, Chesapeake Bay mouth region (from ref. 3).

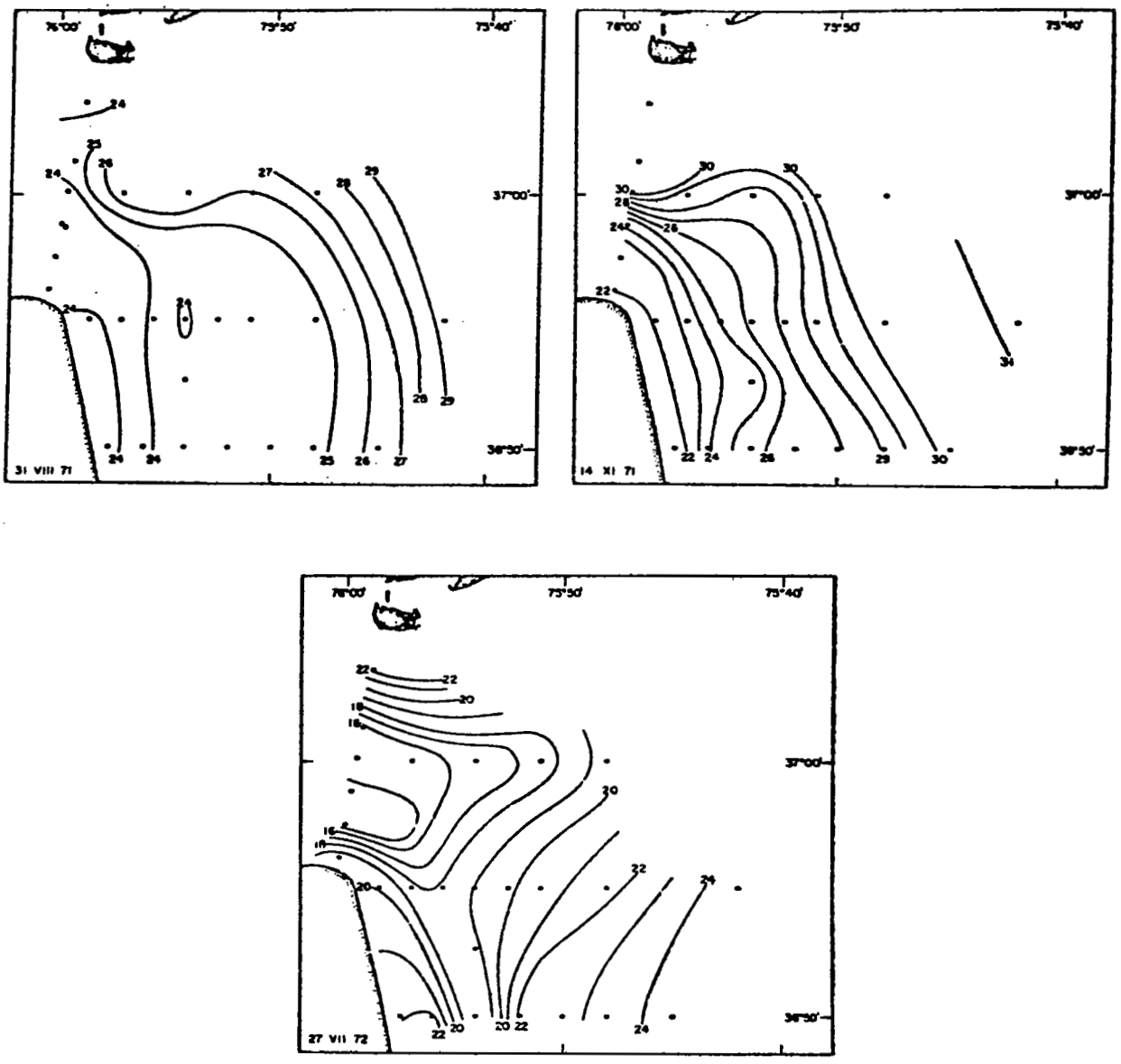

Figure 2.- Concluded.

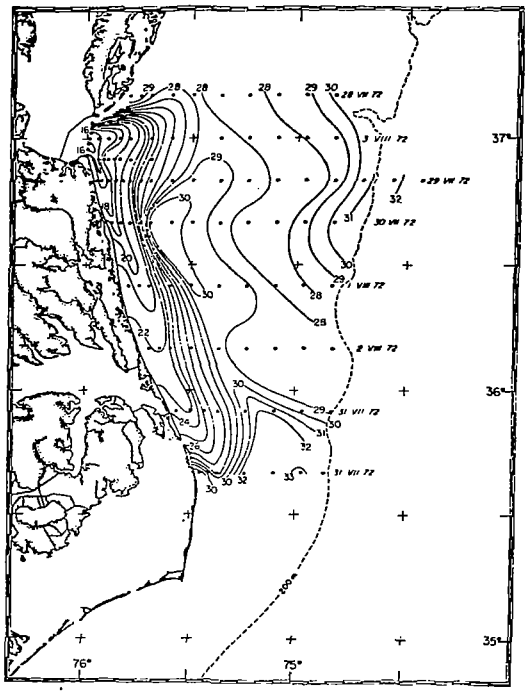

Figure 3.- Surface salinity distribution, July-August 1972 (from ref. 3).

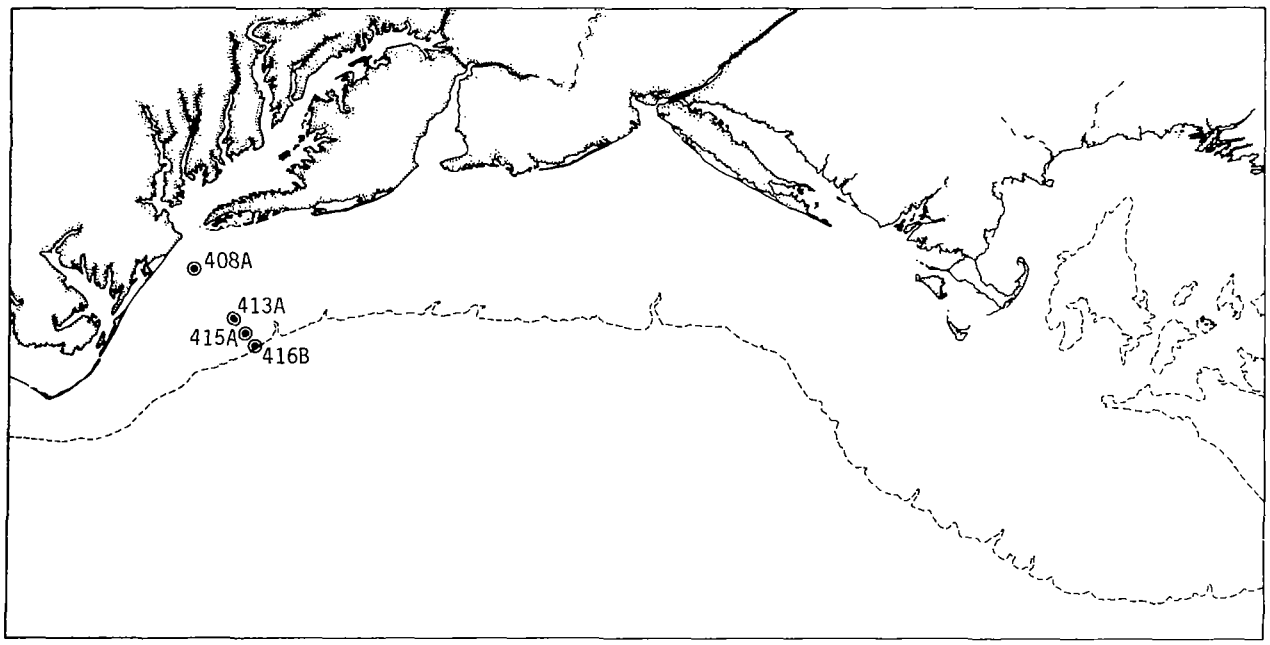

Figure 4.- Map of Middle Atlantic Bight showing current meter mooring positions for records in figure 3 (adapted from ref. 10).

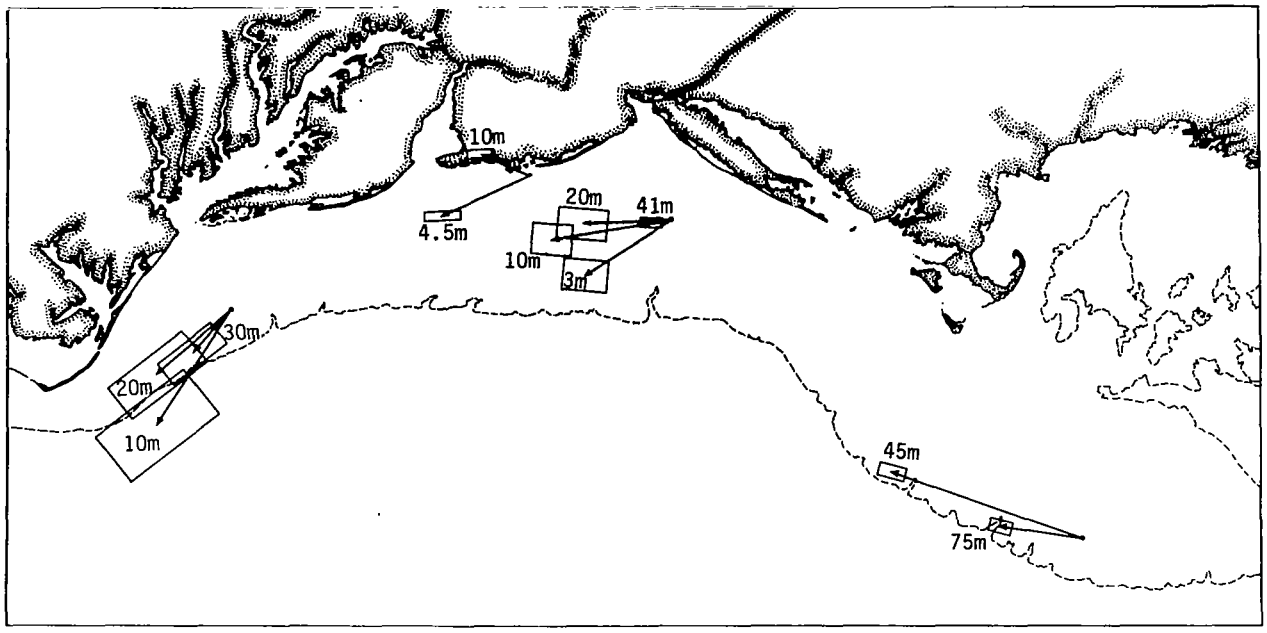

Figure 5.- Map of long-term currents computed from one year or longer current time series with moored current meters in the Middle Atlantic Bight and Georges Bank region (adapted from ref. 10). Standard error for each mean current computation is indicated by rectangle around head of current vector.

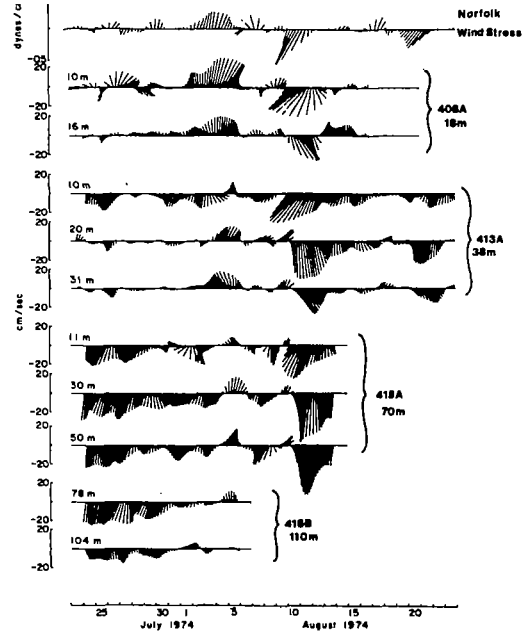

Figure 6.- Summer vector time series of Norfolk wind stress and subtidal currents measured at cross-shelf section off Chesapeake Bay shown in figure 1. Current measurement depths are shown to the left and mooring designations and local water depths shown to the right. North is upward, approximately parallel with the alongshelf direction.

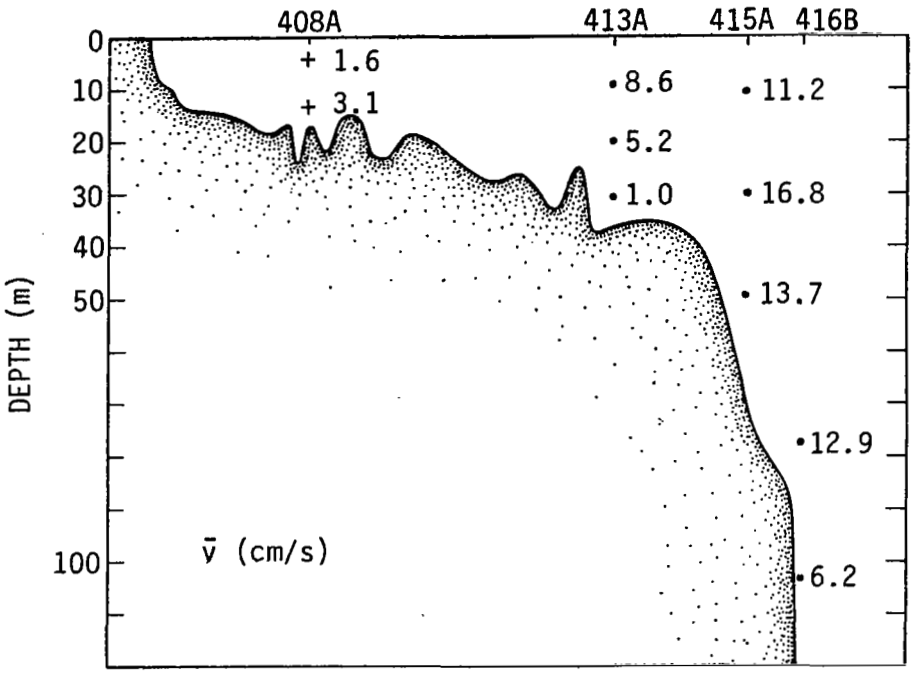

Figure 7.- Long-term mean longshore flow $\bar{v}$ for July and August 1974 (adapted from ref. 9).

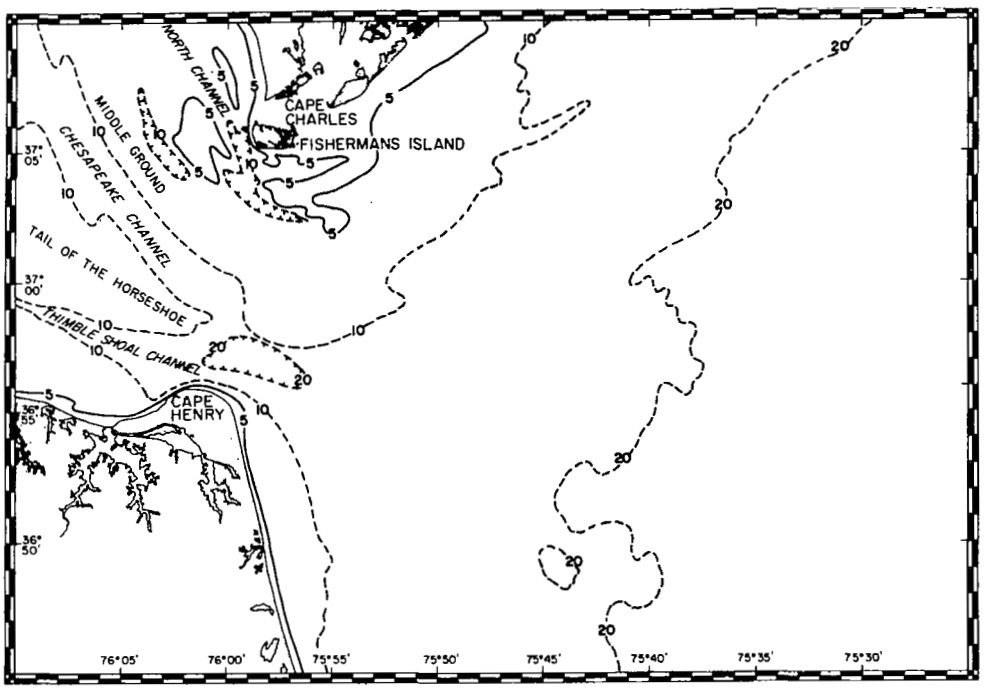

Figure 8.- Bathymetry of the Chesapeake Bay mouth region.

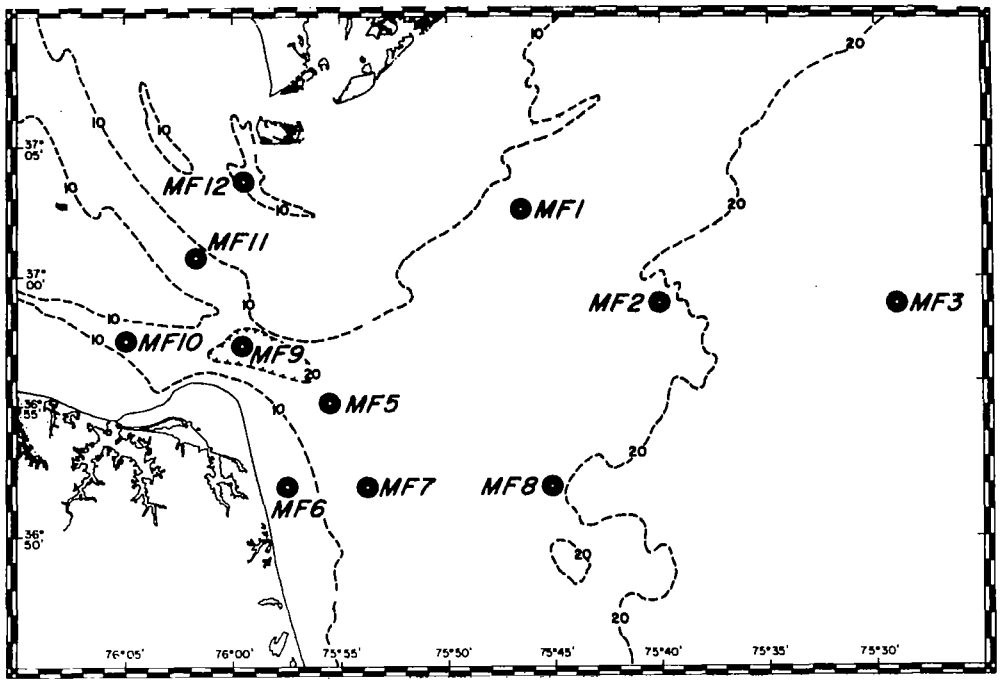

Figure 9.- Mooring positions for January-March 1979 experiment. Norfolk dredged material disposal site is located at station MF2.

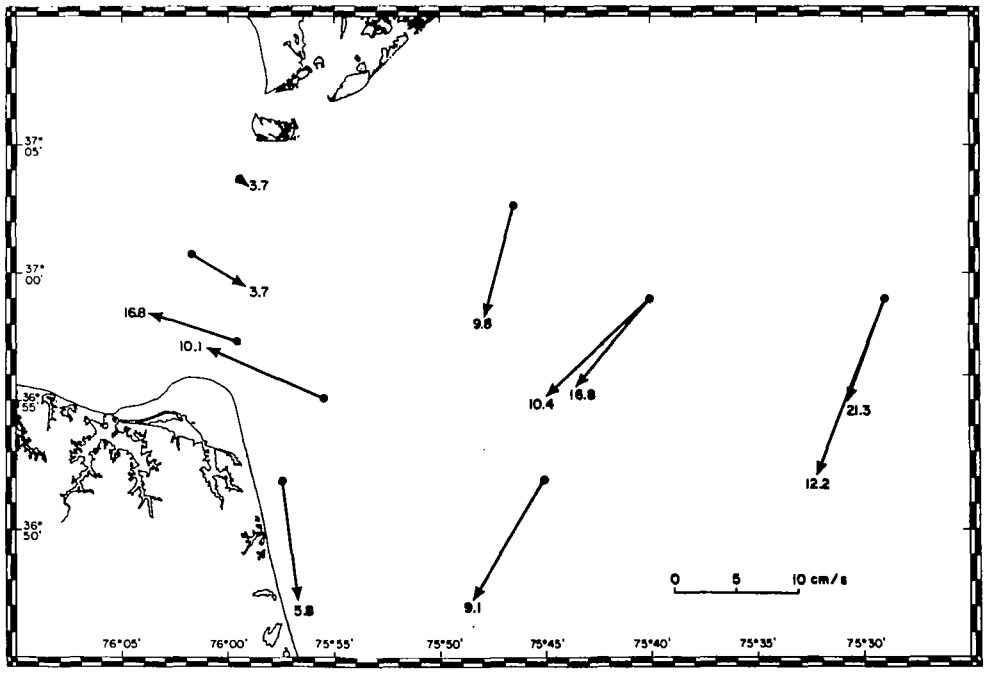

Figure 10.- Mean velocities for 240-hour interval beginning 0000 on 4 February 1979. Depths of measurements (m) are indicated at the head of the velocity arrows. Mooring position designations are shown in figure 9.

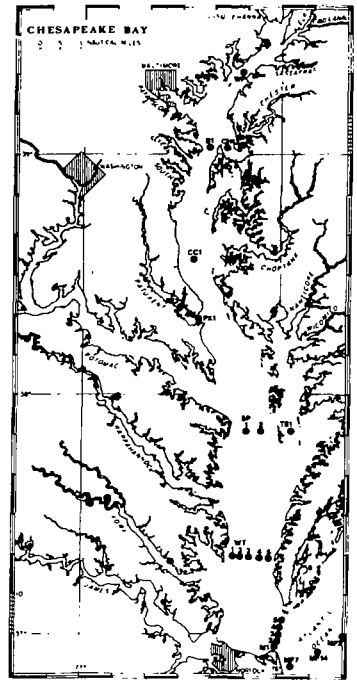

Figure 11.- Mooring locations for CRIMP80 measurement program. Chesapeake Bay and inner shelf were instrumented with 61 current meters on 23 moorings for 38 days beginning 23 June 1980.

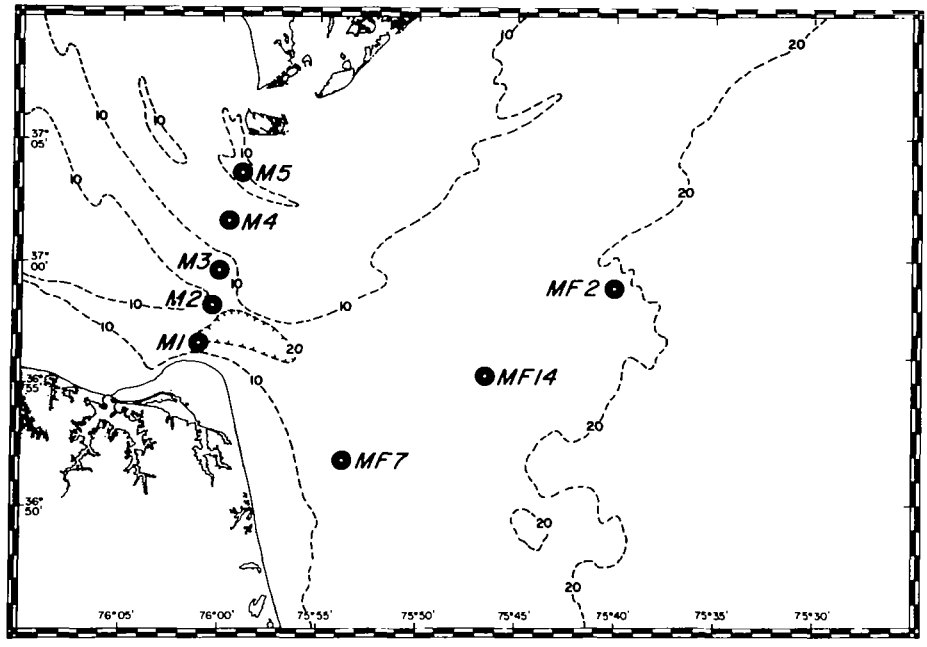

Figure 12.- Summer 1980 mooring positions.

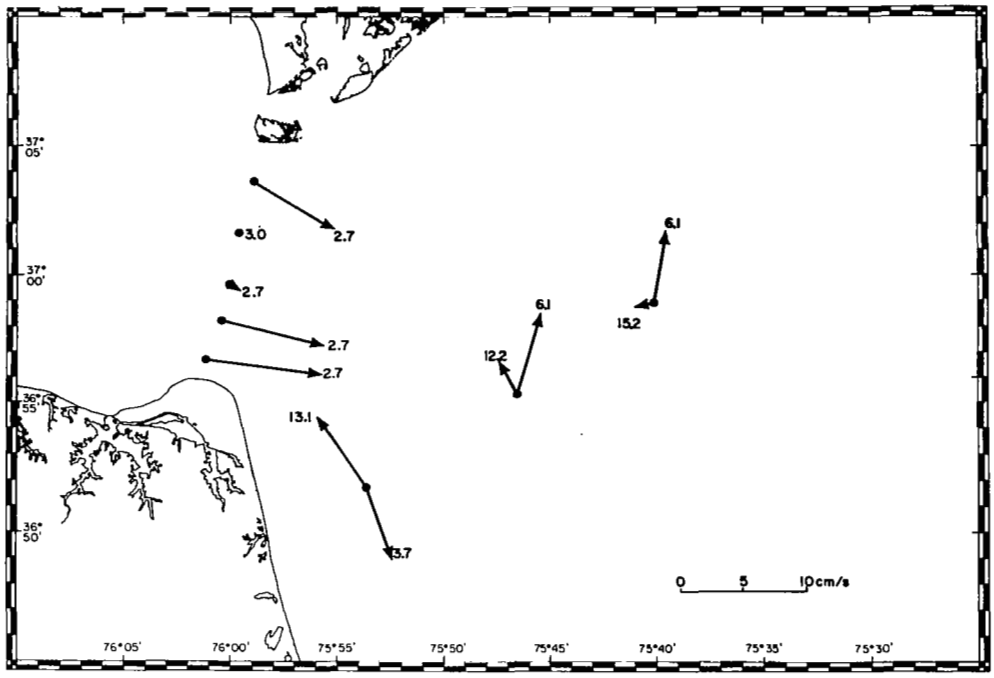

Figure 13.- Mean velocities for 38-day interval beginning 23 June 1980. Depths of measurements (m) are indicated near head of velocity arrows.

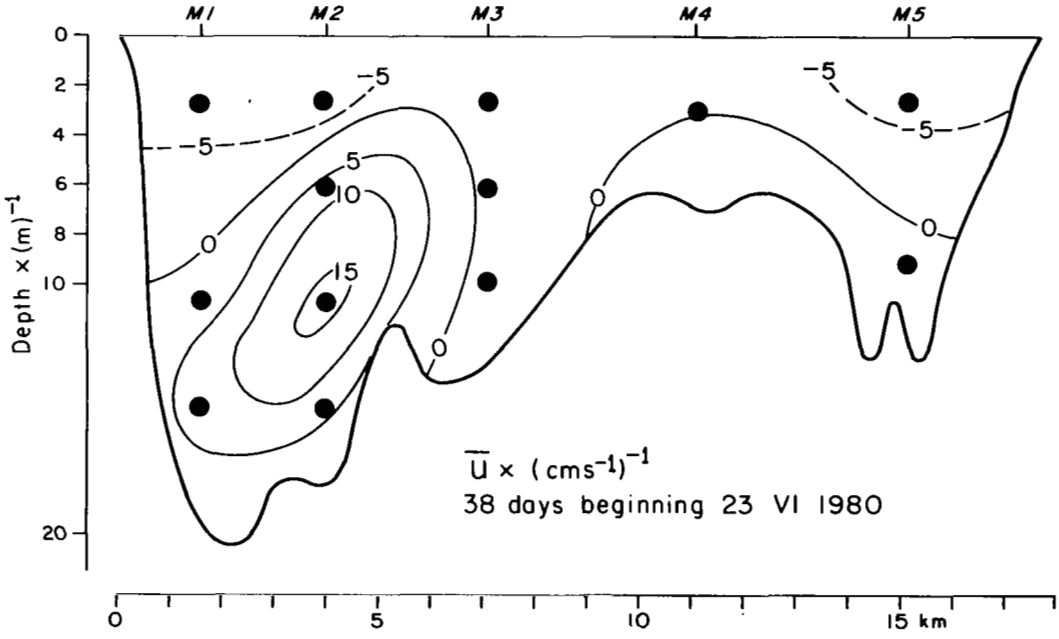

Figure 14.- Mean velocity through the Chesapeake Bay mouth for an interval of 38 days beginning 23 June 1980. Positive velocities are into the Bay. Current meter positions are indicated by the solid circles. Vertical exaggeration is 500:1.

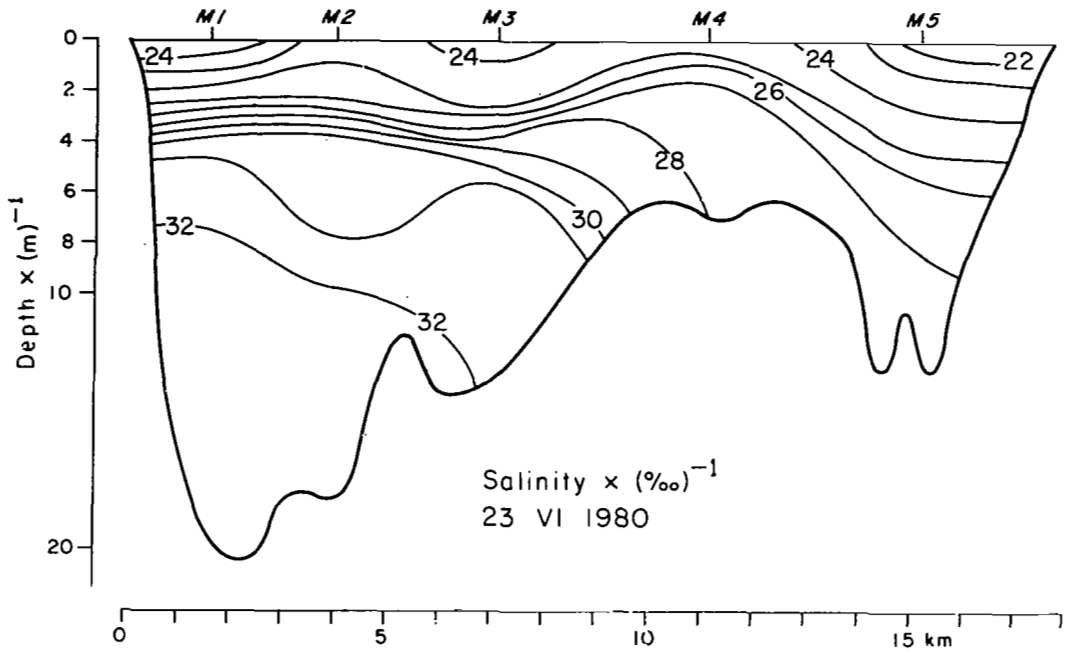

Figure 15.- Salinity distribution in the Chesapeake Bay mouth section for 23 June 1980. Vertical exaggeration is 500:1.

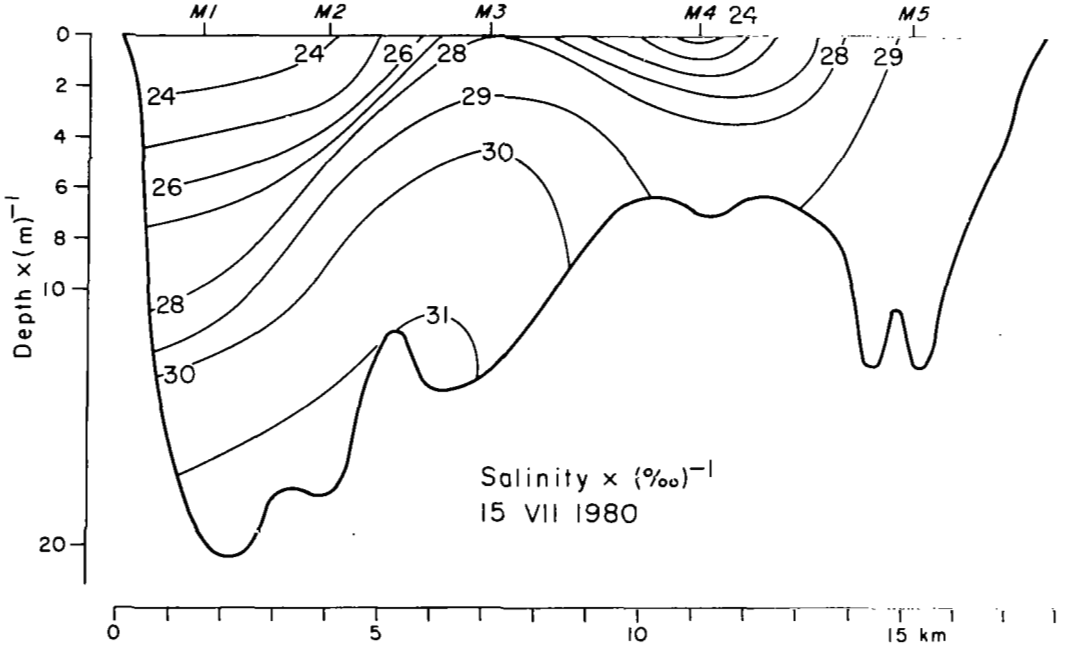

Figure 16.- Salinity distribution in the Chesapeake Bay mouth section for 15 July 1980. Vertical exaggeration is 500:1.

CHESAPEAKE BAY PLUME DYNAMICS FROM LANDSAT[1]

John C. Munday, Jr. and Michael S. Fedosh
Remote Sensing Center
School of Marine Science
College of William and Mary
Gloucester Point, Virginia

ABSTRACT

Examination of 81 dates of Landsat images with enhancement and density slicing has shown that the Chesapeake Bay plume usually frequents the Virginia coast south of the Bay mouth. Southwestern (compared to northern) winds spread the plume easterly over a large area. Ebb tide images (compared to flood tide images) show a more dispersed plume. Flooding waters produce high turbidity levels over the shallow northern portion of the Bay mouth.

INTRODUCTION

A central research question for the Atlantic marine fishery is the distribution of nutrients and pollutants outwelled from coastal bays and estuaries. Investigating the seaward flux of materials, both spatially and temporally, should be fruitful toward understanding fishery productivity and its fluctuations. The plume of the Chesapeake Bay, queen of the east coast estuaries, is attractive to study in this regard from several viewpoints (plume composition, volume discharge, Bay productivity, and Bay-shelf ecology), and has become the initial focus for flux studies coordinated by the NOAA National Marine Fisheries Service.

A leading phase of such study is to resolve the dynamics of the Chesapeake Bay plume. To do so by ship-based study alone would involve prohibitively large effort over long times; therefore, it is advantageous to use remote sensing technology provided by NASA to reduce the effort and provide repetitive synoptic views over large areas. The most striking view is provided by the NASA Landsat satellite, which since its first launch in 1972 has produced over eighty cloud-free images of the lower Chesapeake Bay region. The limitations of Landsat for Bay plume study are recognized -- the sensors primarily discriminate suspended sediment in the upper few metres of the water column, and the

[1] Supported by NOAA National Marine Fisheries Service through Grant NA-80-FA-C-00051.

images are only snapshots of continuous dynamic processes -- nevertheless, Landsat can provide an overview of the plume dynamics which is useful in guiding future aerial remote sensing and ship-based investigations.

In this study a large set of Landsat images has been examined using visual methods and image enhancement devices. The principal objective has been to determine what continental shelf regions are frequented by the Bay plume. A second objective has been to determine the effects of tidal phase and wind on plume dynamics.

METHODS

Eighty-one dates of cloud-free Landsat images of the southern Chesapeake Bay (path 15, row 34) were obtained from the USGS EROS Data Center, Sioux Falls, South Dakota. The overpass times span the phases of the diurnal tidal cycle as shown in Figure 1a; actual tide data were obtained for Sewells Point, Hampton Roads, which according to NOAA tidal tables experiences high and low tide 0:52 and 1:15 hours respectively after Cape Henry at the mouth of Chesapeake Bay. Tide data used in analysis of plume-tide relationships discussed later were adjusted for these differences. The distribution of dates over months of the year is shown in Figure 1b; surprisingly, there are no seasonal data gaps due to cloud cover. Seventy-five images are 18.5-cm (1:1,000,000) positive transparencies of MSS band 5; twenty dates (including six dates not studied in the large format images) were obtained in 70-mm-format (1:3,369,000) positive transparencies of MSS bands 4 to 7.

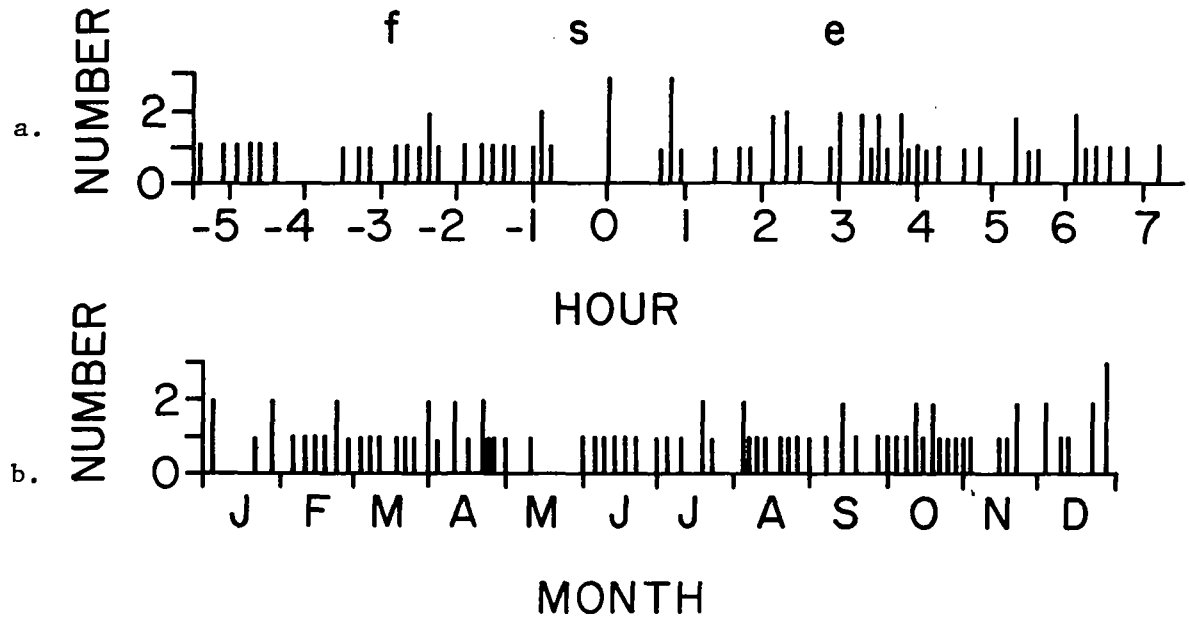

Figure 1. Tidal phases (1a:top) and seasonal distribution (1b:bottom) for Landsat overpasses of southern Chesapeake Bay. Tidal reference: high tide at Sewells Point, Hampton Roads.

Wind data were obtained from the Norfolk Regional Airport weather station covering the twelve hours preceding each overpass at 3-hour intervals. These data were vector-averaged for each pass; the composite wind regime for all passes is shown in Figure 2a, compared to the 1946-1970 record for Norfolk in Figure 2b. For use in image analysis the wind data of Figure 2a were grouped into the quadrants 0-89° (+0, 90, 180, and 270°) labeled 1, 2, 3, and 4.

The methods of image analysis included visual interpretation coupled with machine-assisted enhancement. Two interpreters analyzed each 18.5-cm image on a light table; the first interpreter traced turbidity boundaries manually based on visual inspection, and the second checked the tracing, making modifications as needed. The 70-mm images were enhanced with an International Imaging Systems (I^2S) color additive viewer, and the color enhancements were photographed on color slide (35-mm) film for projection during later analysis. Each 18.5-cm image was enhanced with an I^2S 32-channel optical density analyzer with a vidicon, digital processor, and color-coded television display. A black mask covering land areas was used during this analysis to focus attention on water patterns; that the mask had negligible effect on the density analysis was evidenced by the constancy of patterns when the image was rotated through 90°

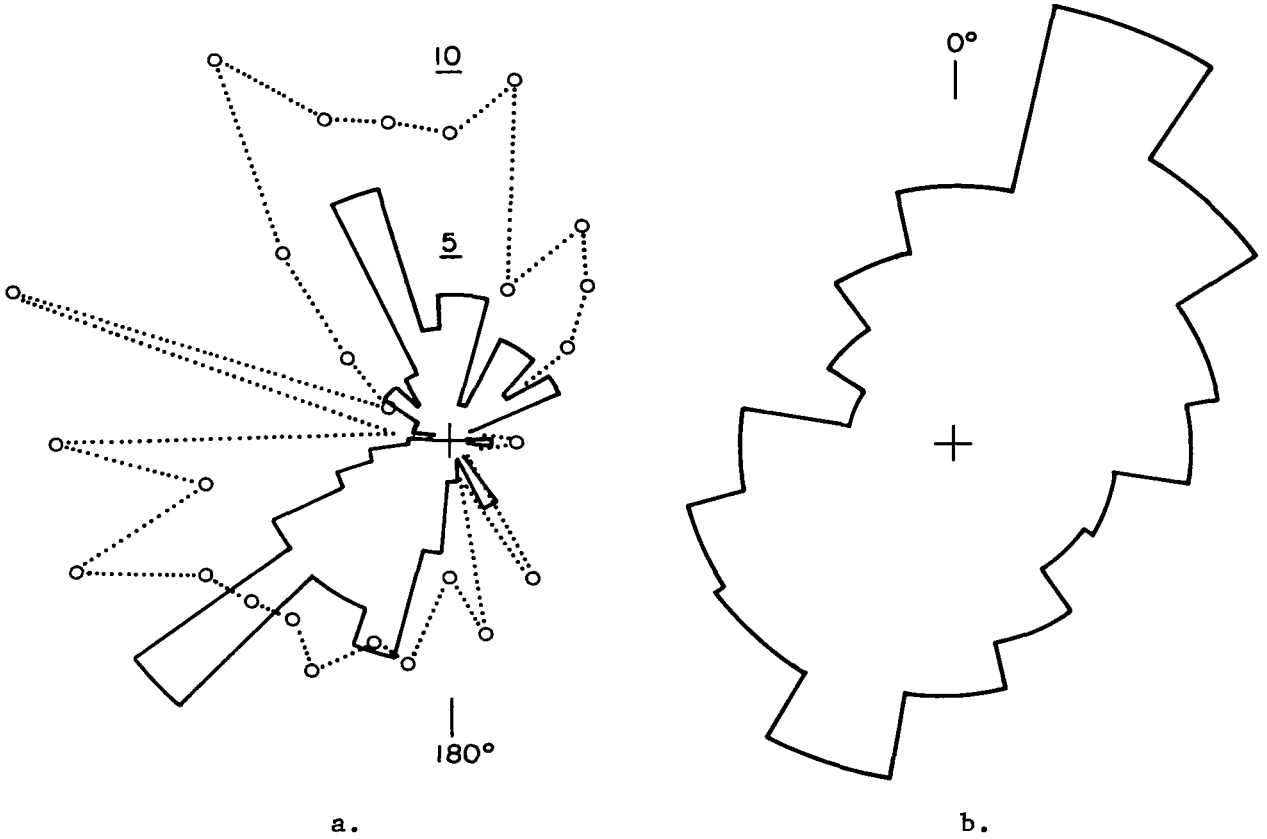

a. b.

Figure 2. Winds at Norfolk Regional Airport.
a. Landsat passes. Solid line: wind frequency. Dotted line: average wind speed in knots.
b. The record for 1946-1970. Wind frequency only.

(the danger is that electronic band width limitations during scanning across sharp brightness gradients will cause smearing in the color coded output). The display was photographed on color slide (35-mm) film for projection during later analysis. Also, a contour map of optical density was prepared from the display by placing an acetate sheet on the I^2S light table and manually drawing contours while viewing the display monitor; this procedure produced contour maps at the original image scale.

The above procedures produced two types of maps. The one consists of visually-discriminated turbidity boundaries extending sometimes over long distances, possibly through background turbidity gradients not noticeable visually. These background gradients would be weak, because the eye during the mapping process ignores weak gradients, but enhances sharp gradients and emphasizes the continuity of turbidity-marked hydrodynamic features over long distances. The second type of map is of photographic density contours which qualitatively picture the absolute turbidity levels. With appropriate calibration this type of map could become a map of absolute concentrations of suspended solids.

In the contour map, a plume with a turbidity gradient will be dissected by the density contouring and may fail to be noticed. On the other hand, the I^2S is more sensitive than the eye to weak density changes, revealing turbidity boundaries which would not be detected by visual analysis alone. It is emphasized that visual maps and density contour maps enhance different aspects of an image and should not be expected to be similar. Examples of the maps are shown in Figure 3; negative copies of several 18.5-cm MSS 5 images (with masking of the land areas) are shown in Figure 4.

Figure 3a. Visually discriminated turbidity boundaries for Landsat image of 8 July 1978.

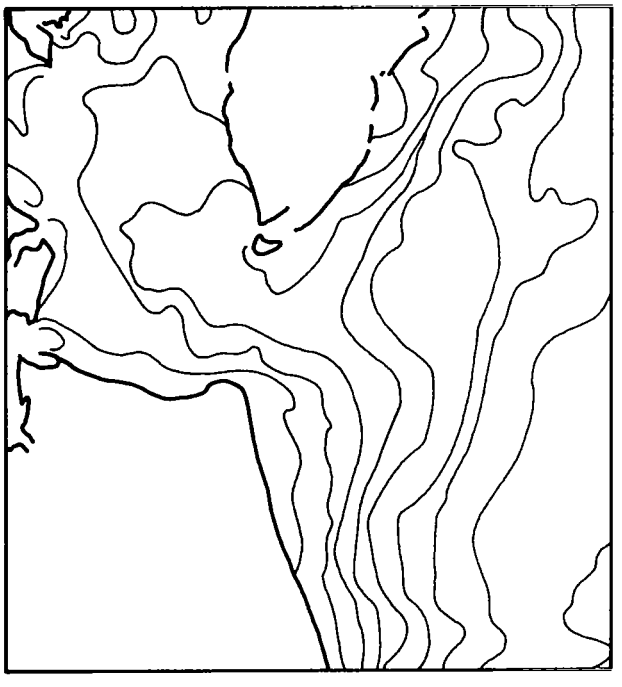

Figure 3b. Photographic density contours from density analyzer enhancement of same image.

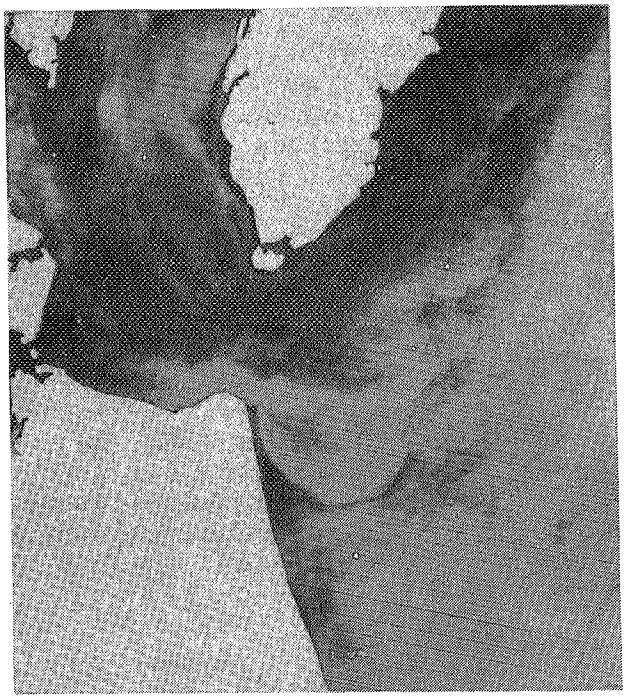

4a. 27 Jan 78. -1:52; 251°, 19.6 kn.

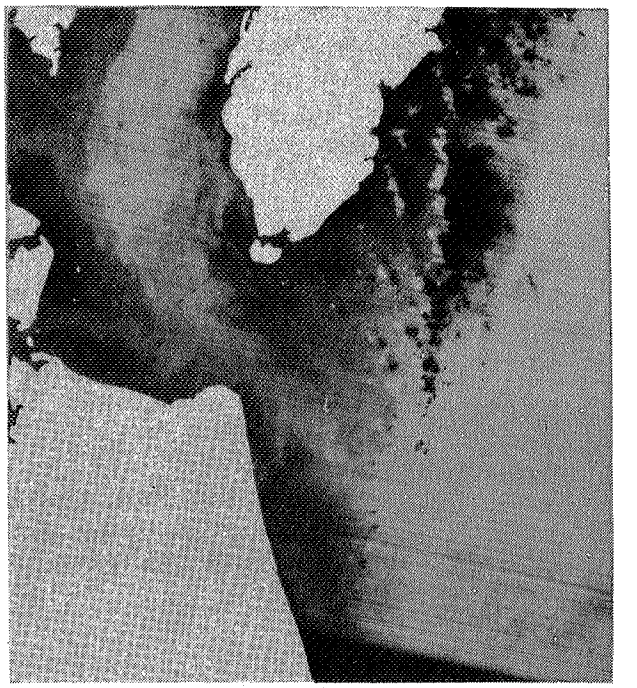

4b. 13 Feb 73. +5:08; 217°, 4.2 kn.

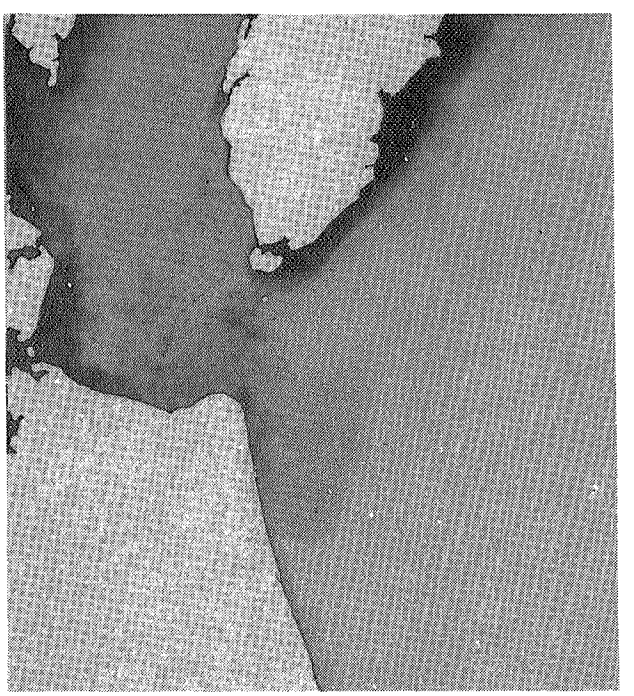

4c. 19 Oct 79. +3:07; 60°, 1.9 kn.

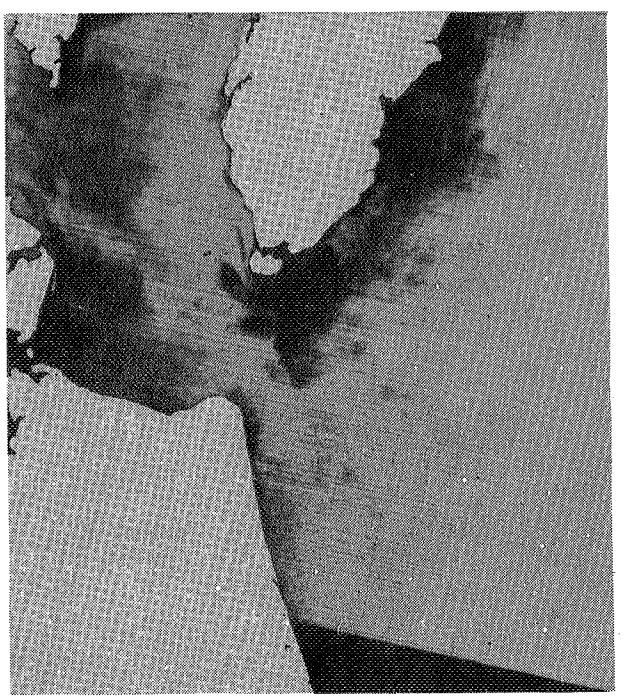

4d. 11 Sep 77. +2:17; 354°, 9.9 kn.

Figure 4. Landsat images of the Chesapeake Bay plume. MSS 5 negatives with masking of land areas. Top is north. Tides: hours before (-) or after (+) high tide at Cape Henry. Winds: 12-hour average from Norfolk. Scale 1:106.

Patterns on the original 18.5-cm images and on the several data reduction products were simultaneously compared during extraction of measurements. Measurements were based on a 1-mm grid overlay (graph paper) facilitating use of the image scale of 1 mm:1 km. The distance and direction of plume-related features were measured with respect to an origin at 37° N latitude/76° W longitude. Azimuthal sectors and 1-cm grid squares frequented by turbid boundaries associated with the plume were determined using the sector and grid map in Figure 5; when an edge of the "plume" (see below) was noticed at some radial distance and direction from the origin, sector/zone segments radially outward to this position were "counted" (as having been "visited"). Simple relationships were then sought between the spatial distribution of counts and several variables including wind direction by quadrants (from 12-hour average wind vectors), wind speeds, wind duration, tidal phase, bathymetry, passage of weather fronts, and fresh water inflow into the Bay.

To the present, it has been possible to complete only some spatial analysis and statistical analysis using single-variable statistics. Further work is needed using multi-variate methods.

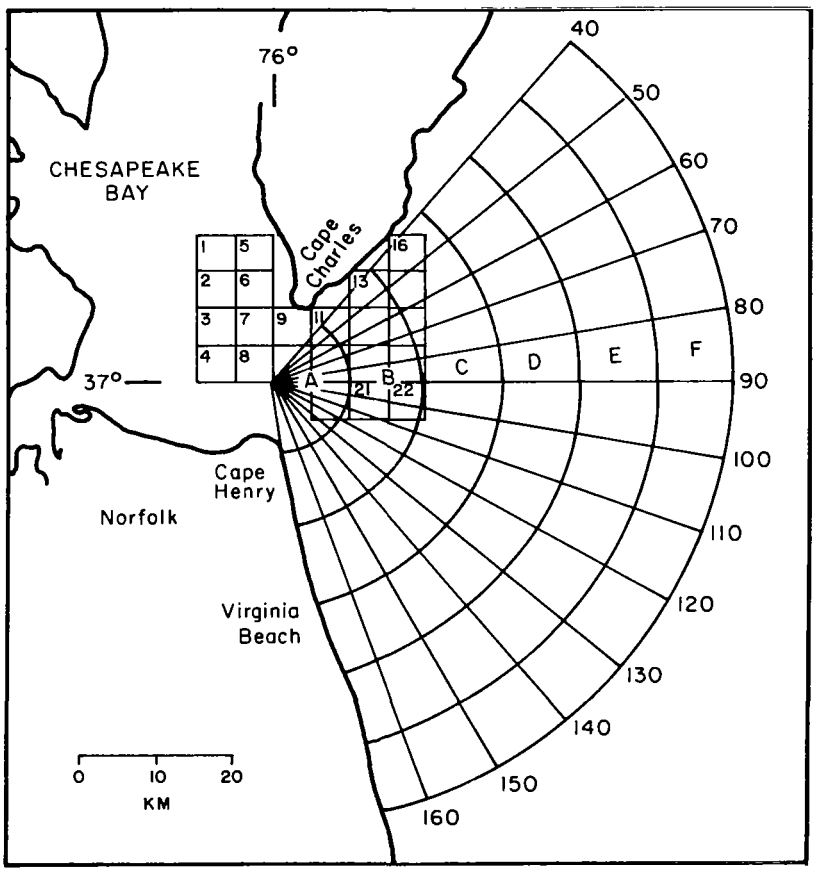

Figure 5. Sector and grid map for image data extraction.

DEFINITION OF THE "PLUME"

The counting of areas as "visited" was based only on the presence of turbidity discontinuities which appeared to be significant with respect to Chesapeake Bay plume dynamics. This counting policy was made deliberately wide and somewhat vague, because of the lack of historical data on plume dynamics. It gave the interpreters much freedom of choice. In subsequent studies, a more restrictive policy can be used based on the results obtained here.

There are several consequences of the above policy. First, some of the features of turbidity which were "counted" may be associated, not with the plume, but with along-shore currents. According to Bumpus (1973), there is generally a net non-tidal southerly current along the Eastern Shore and Virginia-North Carolina borders toward Cape Hatteras. This current could involve shear and turbidity gradients (some images give the impression of turbidity discontinuities parallel to shore at the 30-m isobath). Second, studies by Harrison et al. (1967), Johnson (1976), and Ruzecki et al. (1976) show that flow adjacent to Cape Henry is rotary, that the general southerly flow is sporadic rather than continuous, and that flow is wind-influenced in the alongshore direction. These findings should be considered in the interpretation of any observed features.

Third, it is probable that the collection of plume features on any one image is derived from several tidal cycles. In this regard, the distance of features from the mouth should be helpful in discriminating the different cycles. Drogue data published by Johnson (1976) and Ruzecki et al. (1976) suggest that the tidal excursion at the Bay mouth is only about 8 km, whereas at the Chesapeake Light Station (23 km east) the tidal excursion is negligible. Thus, features beyond 15-20 km almost certainly result from non-tidal flow and the net movement from several cycles of tidal flow.

However, apart from the distance factor, the features themselves do not suggest a distinction between features for the cycle in progress from those for preceding cycles. Distinguishing sequential plumes using multispectral satellite images was first described by Mairs and Clark (1973); their approach was not successful here because plumes are too faint on the small set of multispectral images on hand. Defining plumes more clearly using digital processing of Landsat CCT data should prove useful. In contrast, for the smaller plumes from the Eastern Shore inlets, the distinction of sequential tidal cycles is possible on single band images; the inlet plumes often have the appearance of a sequence of turbidity pulses.

Fourth, it should be noted that Landsat records upwelling radiance from only the surface layers. The depth of the observed turbidity varies inversely with its opacity, with the depth of observation for prevailing turbidities being perhaps 5 m. Thus, plume features at greater depth are not recorded. Also, higher turbidities are produced by scour and resuspension over shallow depths, with the consequence that turbidity levels become decoupled from plume waters per se. Generally, then, Landsat is not always recording plume water boundaries as defined by vertical profiles of temperature, salinity, nutrients and biological variables.

Composites of Observed Boundaries

Composites of the turbid boundaries seen on all the images divided into flood and ebb tide groups are shown in Figure 6. Viewed in the manner of a geologic fault map, the ebb tide composite shows most "lineaments" found between Cape Charles and Cape Henry are oriented toward 120°. The flood tide lineaments although more random are oriented similarly. In both cases, most lineaments beyond the mouth are found near the coast southward; only a few lineaments beyond the mouth are found toward 40° to 90°. An initial hypothesis was therefore that the plume usually frequents the southeasterly direction. Subsequent analysis was oriented toward testing this hypothesis.

Figure 6a. Composite of turbidity boundaries for flood tide.

Figure 6b. Composite of turbidity boundaries for ebb tide.

Sector/Zone Count Analyses

The map in Figure 7a shows sector/zone counts for all wind classes and tidal phases; zones A through E for sectors at $\theta \sim 150°$ are the most frequently visited. Sorting the pass dates by wind quadrant, Q_i, yields $Q_1 = 20$ images, $Q_2 = 3$, $Q_3 = 41$, $Q_4 = 17$. Maps for the wind quadrants are shown in Figures 7b-d (a map is omitted for Q_2 because of its low value). Q_4 produced the tightest pattern along the Virginia-North Carolina coast; Q_3 (southwest winds) produced the most dispersed pattern (notice especially the visits to zones D-F for $\theta \sim 90°$).

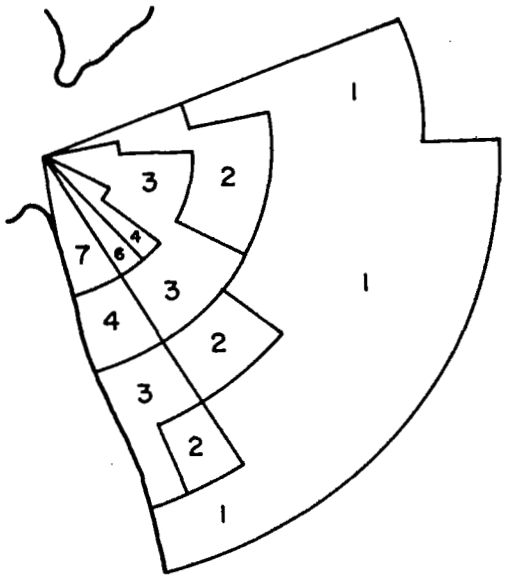

a. All wind quadrants.

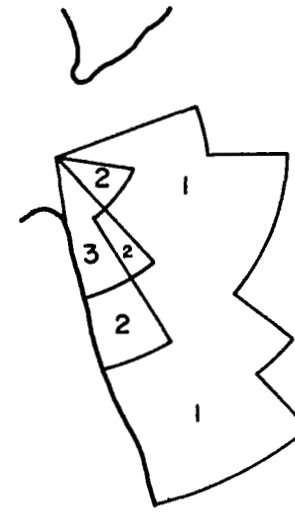

b. Winds from quadrant 1: 0°-90°.

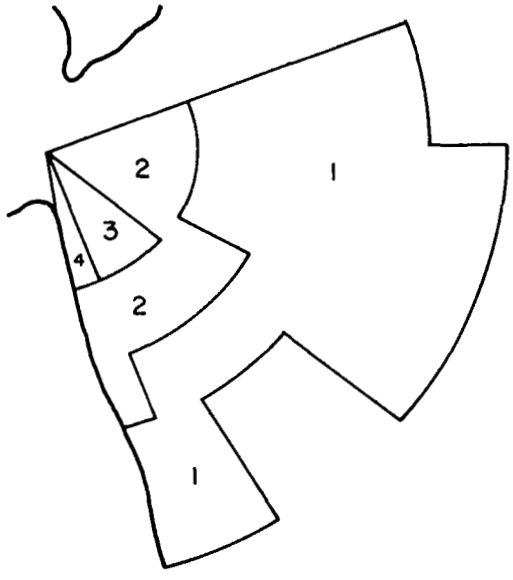

c. Winds from quadrant 3: 180°-270°.

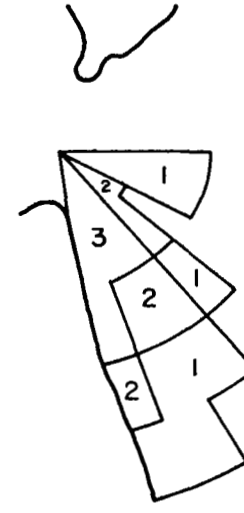

d. Winds from quadrant 4: 270°-360°.

Figure 7. Areas visited by the plume under different wind conditions. The numerals represent sector/zone counts as follows: 1: 0-5 counts; 2: 6-10; 3: 11-20; 4: 21-30; 5: 31-40; 6: 41-50; 7: >50.

To enhance the differences between results from different wind quadrants, ratios have been formed of sector/zone counts using the quadrants 3 over 1, and 4 over 1. Counts for each quadrant were adjusted upward by 1 count for each pass where no plume was discriminated (which in effect produces a contrast stretching of the ratios): the adjustment frequencies for each quadrant were 1, 1, 6, and 0 respectively. The ratios were then normalized for differences among the Q_i values. The resulting ratios R are shown in Tables 1 and 2. Numerical values of R near 1.0 indicate no difference in effects of wind direction for the two quadrants under consideration. Table 1 (quadrants 3 over 1) shows $R > 1$ for $\theta < 140^o$ (zones B-E), a clear demonstration that southwest (compared to northeast) winds disperse the plume over a larger area and swing its dominant direction away from the southeast toward the east. Table 2 (quadrants 4 over 1) demonstrates that northwest (compared to northeast) winds constrain the plume to the coastline toward the southeast.

TABLE 1

NORMALIZED RATIOS OF COUNTS

FOR WIND QUADRANT 3 OVER QUADRANT 1

Zone \ Sector	6*	7	8	9	10	11	12	13	14	15	16
A	1.46	1.46	1.46	1.27	0.91	0.98	1.12	0.92	0.77	0.83	0.84
B	∞	2.93	1.95	2.44	1.83	1.83	1.95	1.66	1.25	0.84	0.88
C	3.41	4.39	4.88	2.68	1.79	1.34	2.11	1.71	0.98	0.80	0.98
D	3.90	3.90	4.39	4.39	3.90	4.39	4.39	2.44	1.46	0.98	0.98
E	2.93	3.41	3.41	3.41	3.41	3.41	3.41	2.93	1.46	1.30	1.22

TABLE 2

NORMALIZED RATIOS OF COUNTS

FOR WIND QUADRANT 4 OVER QUADRANT 1

Zone \ Sector	6*	7	8	9	10	11	12	13	14	15	16
A	0	0	0	0.24	0.17	0.34	1.01	1.18	1.01	1.09	1.02
B		0	0	0.39	0.29	0.29	0	1.88	1.57	1.02	1.02
C				0	0	0	0	0.29	1.18	1.32	1.62
D								0	0.39	0.94	1.18
E									0	0.39	0.29

* 10^o interval from 60^o to 70^o; similarly for all sectors.

Sector-count maps for flood versus ebb tide in Figure 8 show somewhat more dispersion of plume features for ebb tide. A subset of the ebb tide data for southwest winds (Q3) higher than 8 knots included only five images; in these images a plume could not be discriminated. These results are further evidence that southwest winds disperse the plume on ebb tide.

In subsequent study, polar coordinates were determined for the most distant point on each plume. The results for flood and ebb tides and wind quadrants Q1, Q3, and Q4 are shown in Figure 9a through 9f. The results are similar to the earlier results. The results show that southwestern winds for passes during ebb tide are associated with the greatest dispersion and extension of the plume. For northern winds, plumes for all tidal phases are found close to Virginia Beach.

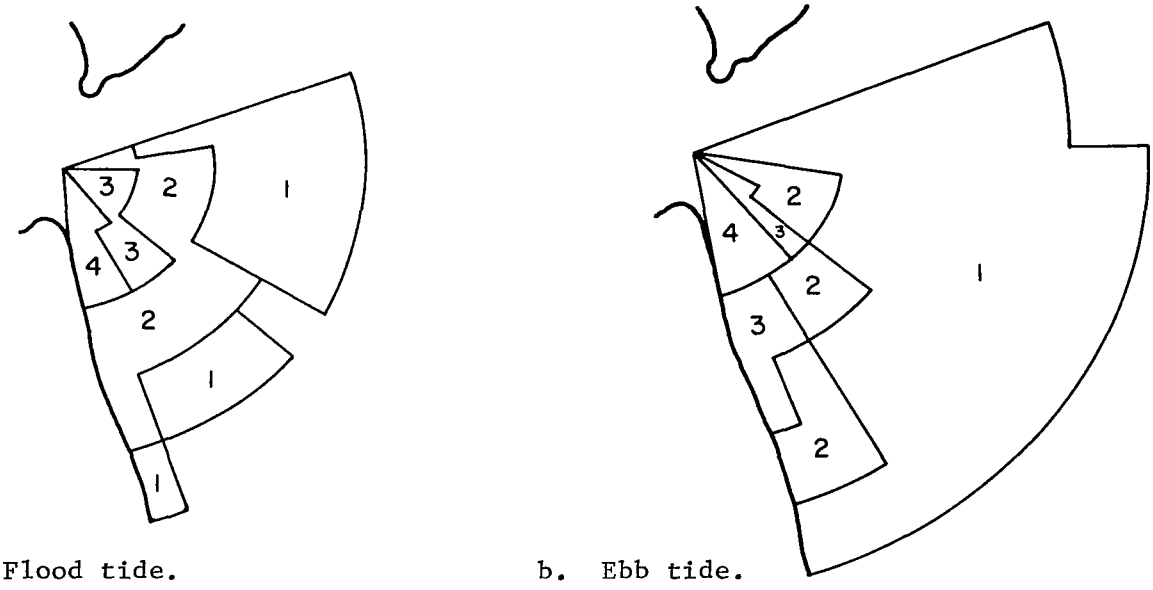

a. Flood tide.

b. Ebb tide.

Figure 8. Areas visited by the plume under different tidal phases. Same numerical symbols as in Figure 7.

Cape Charles Grid Analysis

Many images reveal turbidity in late-ebb/early-flood, located adjacent to Fisherman's Island (at the tip of Cape Charles) on the north side of the Bay mouth (Munday and Fedosh, 1980). The patterns suggest that early flood waters moving into the northern side of the Bay mouth carry residual suspended sediment from the Eastern Shore nearshore zone, and additional material resuspended in the shallow areas adjacent to Fisherman's Island. If true, turbidity on the western side of the mouth (compared to the eastern side) should be relatively more frequent during flood, as flooding waters traverse increasing areas of shallows.

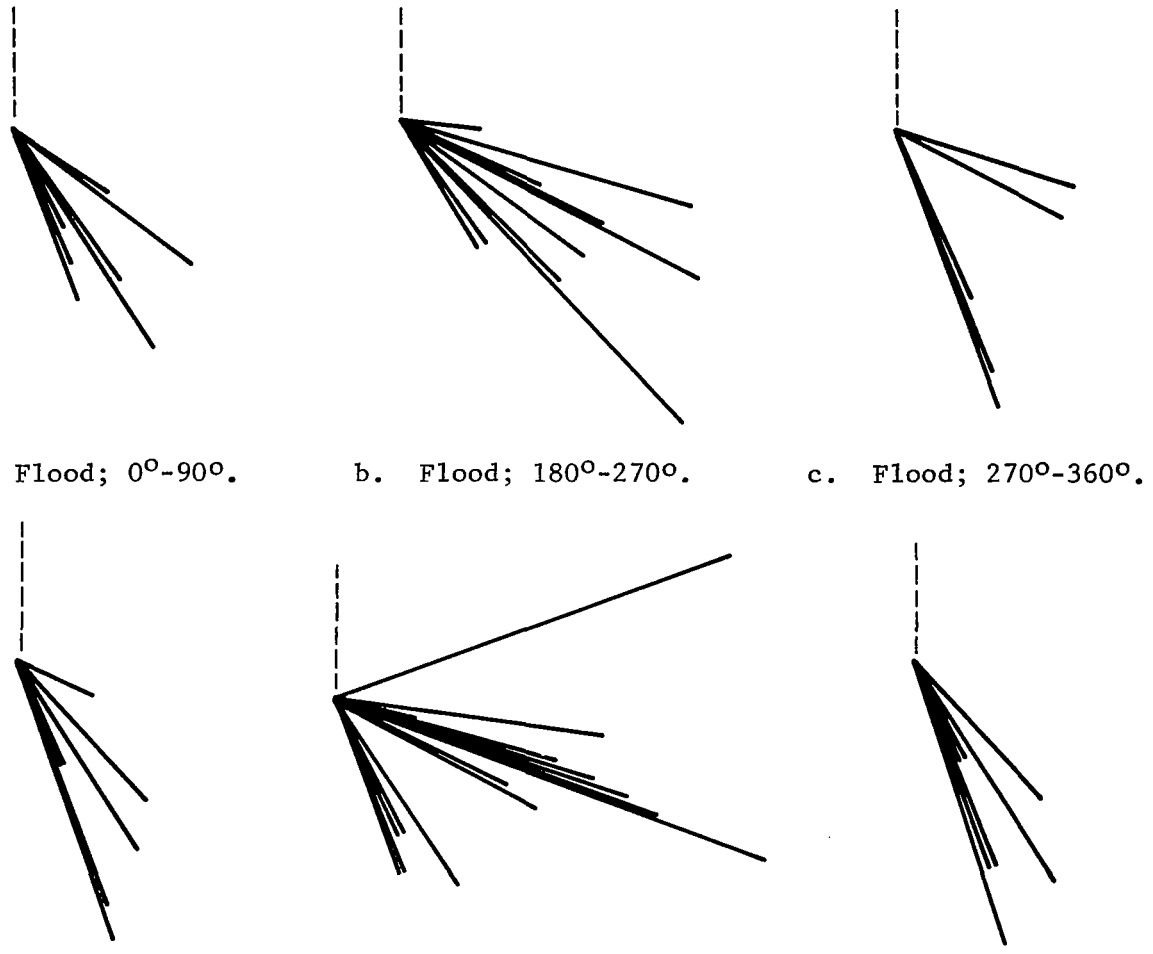

a. Flood; 0°-90°. b. Flood; 180°-270°. c. Flood; 270°-360°.

d. Ebb; 0°-90°. e. Ebb; 180°-270°. f. Ebb; 270°-360°.

Figure 9. Plume extension under different tidal and wind conditions. Radial lines for the most distant point on each plume. North shown as dotted line.

To test this hypothesis quantitatively using Landsat images, a counting procedure was employed based on the square grid shown in Figure 5. A cell was counted when turbidity in the cell was higher than background as judged visually. Counts were made for ebb and flood tide passes and subset into the four wind quadrants. Ratios of flood to ebb counts were formed and normalized for flood and ebb pass frequencies; the normalized ratios truncated to integers are shown in Figure 10a. Western cells are, as expected, relatively more frequented by turbidity than eastern cells during flood tide. Truncated normalized ratios for the wind quadrants are shown in Figure 10b for Q_1 over Q_3, and Figure 10c for Q_1 over Q_4 (Figure 10c numbers were multiplied by 2 before plotting). Figures 10b and 10c demonstrate that western (compared to northeastern) winds reduce western and increase eastern turbidities.

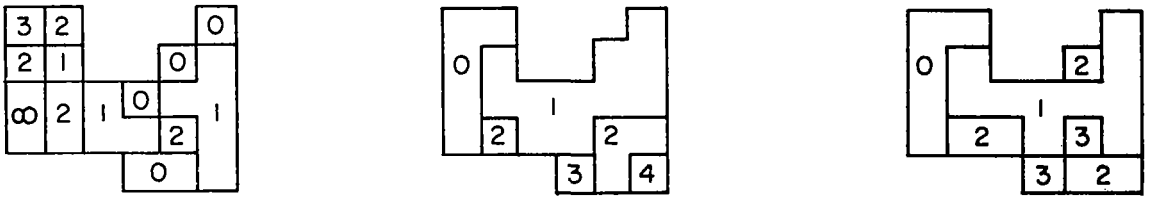

a. Flood/ebb ratios. b. Wind quadrants 1 to 3. c. Wind quadrants 1 to 4 (ratios x 2).

Figure 10. Relative turbidity near Cape Charles. Frequency ratio for each grid cell normalized and truncated.

Wind Duration and Wind Speed

Correlation and regression analyses have been performed on wind speed and wind duration versus plume extension, with tidal phase and wind quadrant as parameters. None of the analyses have yet produced statistically significant results. Multivariate statistical methods will be utilized for further analysis. Perhaps appropriate measures of the plume have yet to be discovered.

DISCUSSION

Image analysis has shown that the "plume" (as broadly defined here) usually frequents the southeasterly direction (120°-150° relative to the mouth). Passes during ebb (compared to flood) show a somewhat more dispersed plume. Southwestern winds are effective in dispersing and extending the plume, especially on ebb tide passes, while for northern winds plumes remain close to Virginia Beach.

These effects of winds have been shown using vector-averaged Norfolk wind data from the 12 hours preceding the Landsat overpass. Because the shelf water relaxation time from wind effects is probably greater than 12 hours, longer wind records should be studied. Also, Chesapeake Light Tower winds would perhaps be more appropriate than Norfolk winds for examining the effect of shelf water currents on the plume dynamics.

For flood tide, a striking feature of many images is a strong turbidity pattern on the shallow northern side of the Bay mouth adjacent to Fisherman's Island. The pattern suggests a predominance of the northern side during flood tide, due to the Coriolis force and southerly drift along the Eastern Shore. Analysis shows that the turbidity is relatively greater in flood tide and northeastern winds. No such patterns were observed for flood tide in the southern portion of the Bay mouth; in addition to the Coriolis deflection toward the north, the water in the southern portion is much deeper, reducing surface turbidities which originate in tidal scour.

For ebb tide, the plume for northerly winds is tongue-shaped, but the shape is difficult to characterize further. Little was observed which would suggest rotary motion off Cape Henry as observed by Harrison et al. (1967).

REFERENCES

Bumpus, D.F. 1973. A description of the circulation on the continental shelf of the east coast of the United States. Progress in Oceanography (Ed. B.F. Warren), 6:111-156. Pergamon Press, N.Y.

Harrison, W., J.J. Norcross, N.A. Pore, and E.M. Stanley. 1967. Circulation of shelf waters off the Chesapeake Bight. ESSA Prof. Paper No. 3, U.S. Dept. Commerce, Washington, D.C., 82 p.

Johnson, R.E. 1976. Circulation study near Cape Henry, Virginia, using Lagrangian techniques. Techn. Rep. No. 21, Inst. Oceanography, Old Dominion Univ., Norfolk, Virginia, 80 p. + app.

Mairs, R.L. and D.K. Clark. 1973. Remote sensing of estuarine circulation dynamics. Photogramm. Eng. 39(9):927-938.

Munday, J.C., Jr. and M.S. Fedosh. 1980. Southern Chesapeake Bay circulation and suspended sediment transport analyzed using Landsat imagery. Proc. Amer. Soc. Photogr. Fall Techn. Mtg., Niagara Falls, N.Y., p. RS3F:1-5.

Ruzecki, E.P., C. Welch, J. Usry, and J. Wallace. 1976. The use of the EOLE satellite system to observe continental shelf circulation. Eighth Ann. Offshore Techn. Conf., Houston, Texas, p. 697-708.

MONITORING THE CHESAPEAKE BAY

USING SATELLITE DATA

FOR SUPERFLUX III*

Fred M. Vukovich and Bobby W. Crissman
Research Triangle Institute
Research Triangle Park, North Carolina

SUMMARY

TIROS-N and NOAA-6, and GOES visible infrared satellite data were used to identify and locate surface oceanographic thermal fronts for the purpose of issuing daily and pre-mission advisory briefings in support of the Superflux III in situ and remote-sensing experiment in the Chesapeake Bay region. Satellite data were collected for the period 1 - 22 October 1980. A summary of that data is presented.

INTRODUCTION

The Research Triangle Institute participated in the Superflux III experiment by using data from TIROS-N, NOAA-6, and GOES to monitor ocean surface temperature discontinuities in the Chesapeake Bay region. Both infrared and visible satellite data were utilized for the monitoring. RTI also used these satellite data to prepare preoperational briefings of expected conditions for the Superflux field operations office during the operating period of Superflux III.

SATELLITE DATA

TIROS-N, NOAA-6, and GOES visible and infrared satellite data were used to monitor continuously the Chesapeake Bay region from 1 to 22 October 1980. Satellite data were collected by the satellite receiving station (RTI/SRS) located on the campus of RTI. This facility has the capability to interrogate the TIROS-N and NOAA-6 satellites in real time and to acquire quasi-real time (within 15 minutes of acquisition) GOES satellite data through a link with the Washington, D.C. GOES facility.

---

*Work performed for U. S. Department of Commerce , National Oceanic and Atmospheric Administration, National Marine Fisheries Service, the Northeast Region, under Contract No. NA-81-FA-C-00002.

The visible and infrared satellite data depict observed features in contrasting shades (or levels of gray). The visible imagery (0.55-0.9 μm for TIROS-N and NOAA-6 and 0.55-0.7 μm for GOES) can be used to delineate land, water, and cloud/fog fronts or boundaries. The infrared imagery (10.5-11.5 μm for TIROS-N and NOAA-6 and 10.5-12.6 μm for GOES) can be used to delineate surface oceanic thermal fronts associated with a variety of features characterized by contrasting temperatures. The primary effort in this project was to identify and locate thermal fronts in the Chesapeake Bay region.

In order to satisfy the objectives of this project, considerable satellite imagery was collected from the period 1 through 22 October 1980. The data for TIROS-N and NOAA-6 are outlined in Table 1 and the data for the GOES satellite are outlined in Table 2. The data represent those days when skies were sufficiently clear for the ocean surface in the Chesapeake Bay region to be observable.

The availability of NIMBUS 7 data from the coastal zone color scanner (CZCS) was examined. These data would complement the ocean color data collected by aircraft. Table 3 shows the potential data availability from the CZCS.

It was of interest to examine our data files to determine the data availability for Superflux I and Superflux II which were conducted prior to the initiation of this contract. Table 4 gives the dates for which clear-sky images are available from the NOAA-6 and TIROS-N satellites. We also contacted NASA's Goddard Space Flight Center to determine the availability of infrared data from the Heat Capacity Mapping Mission (HCMM) satellite. Data processing had not yet been completed for 1980 data. Therefore, no determinations could be made.

DATA ANALYSIS

Figures 1 through 7 yield examples of the TIROS-N and NOAA-6 infrared imagery for the period 8 October through 22 October 1980. In the imagery, black is warm and white is cold. The levels of gray treat intermediate values of temperature. These images are generally characterized by the same features. The Gulf Stream warm water region off the coast of the Carolinas and departing from the coastal region at around Cape Hatteras is the main current feature found off the southeast coast of the United States (see Figure 1). In the Chesapeake Bay region, there is a narrow zone (a darker shade of gray relative to the immediate surrounds, in Figure 1) of warm water oriented north-south found along the coast. East of that narrow zone of warm water is a larger mass of cold water also oriented in a north-south direction (the lighter shade of gray in Figure 1). East of that zone is a large mass of warm water which appears to be warmer than the near coastal warm water because it has a darker shade of gray and which has fingers of warm water protruding into the cold mass on the western side. Immediately south of the Chesapeake Bay mouth and stretching as far south as the Oregon Inlet in many cases, is a

narrow zone of cold water (the lighter shade of gray in Figure 1) trapped along the shoreline.

Figures 8 through 10 together with Figure 4 present the infrared imagery collected on 16 October 1980 through the period 0047 GMT to 2000 GMT. These data essentially give a temporal description of the water mass off the coast near the Chesapeake Bay mouth for that day. The imagery shows the same general features off the coast near the Chesapeake Bay previously discussed; i.e., the narrow zone of warm water stretching north-south along the coast, the colder water further east, the warmer water much further east, and the narrow zone of cold water trapped along the coast just south of the mouth of the Chesapeake Bay. Of interest in these images is the small zone of cold water developing off the coast due east of the Oregon Inlet. This feature is evident on the 0835 GMT and the 1305 GMT images, but is not evident at 0047 GMT or at 2000 GMT. It is believed that this is cold water outflow through the Oregon Inlet. We have not checked the tidal tables as yet to determine whether this outflow was produced by the tides. The images do indicate that the waters in the Pamlico Sound were cold relative to the waters immediately off the coast. This suggests that the water in the Chesapeake Bay may be cold and that the cold water trapped from the Chesapeake Bay mouth southward along the shoreline may be the outflow from the Chesapeake Bay. The other alternative explanation is upwelling along the coast. We hope that analysis of digital satellite data combined with in situ data collected during Superflux III will clarify this point.

Table 1. Hard-copy of TIROS-N and NOAA-6 satellite imagery collected.

Satellite: TIROS-N		
DATE	ORBIT	TIME (GMT)
10/08/80	10240	08:26
10/12/80	10304	20:47
10/13/80	10311	09:10
10/13/80	10318	20:36
10/14/80	10325	08:58
10/14/80	10332	20:25
10/15/80	10339	08:47
10/15/80	10346	20:12
10/16/80	10353	08:35
10/16/80	10360	20:00
10/17/80	10367	08:25
Satellite: NOAA-6		
DATE	ORBIT	TIME (GMT)
10/08/80	6666	12:42
10/10/80	6695	13:40
10/11/80	6709	13:17
10/13/80	6744	23:50
10/16/80	6773	00:47
10/16/80	6780	13:05
10/17/80	6787	00:25
10/17/80	6794	12:42
10/20/80	6837	13:17
10/21/80	6844	00:37
10/21/80	6851	12:53
10/22/80	6858	00:14
10/22/80	6865	12:31
10/22/80	6872	23:52

Table 2. Hard copy of GOES satellite imagery collected.

DATE	TIME (GMT)	DESCRIPTION
10/07/80	17:00	1
10/07/80	21:00	1
10/08/80	14:00	1
10/08/80	17:00	1
10/11/80	18:30	2
10/12/80	18:30	2
10/13/80	18:30	2
10/14/80	18:30	2
10/14/80	19:00	3
10/15/80	14:00	3
10/15/80	18:00	3
10/15/80	18:30	2
10/17/80	18:30	2
10/19/80	18:30	2
10/20/80	13:00	3
10/20/80	18:00	2
10/20/80	20:00	3
10/21/80	18:00	3
10/21/80	18:30	2
10/22/80	01:30	4
10/22/80	18:00	3
10/22/80	18:30	2

1- Enhanced 3.2-km resolution sector centered at 26° N, 90° W
2- Enhanced 1.6-km resolution sector centered at 37° N, 75°W
3- Enhanced 1.6-km resolution DA1 sector
4- Standard 3.2-km resolution DB5

Table 3. Ocean color data from NIMBUS 7 CZCS.

DATE	ORBIT NO.	TIME OVER AREA (EST)	EQUATOR CROSSING
10/15	9948	1140	77°W
10/16	9998	1159	81°W
10/17		PASS NOT GOOD	
10/18		PASS NOT GOOD	
10/19	10039	1111	71°W
10/20	10053	1130	75°W
10/21	10067	1149	80°W
10/22		PASS NOT GOOD	
10/23		PASS NOT GOOD	
10/24	10108	1120	72°W

Table 4. Satellite infrared data available for SUPERFLUX I and II from NOAA-6 and TIROS-N

SUPERFLUX I	SUPERFLUX II
(16 - 20 March 1980)	(18 -28 June 1980)
12 March 1980	11 June 1980
14 March 1980	12 June 1980
15 March 1980	13 June 1980
18 March 1980	16 June 1980
	17 June 1980
	20 June 1980
	27 June 1980
	1 July 1980

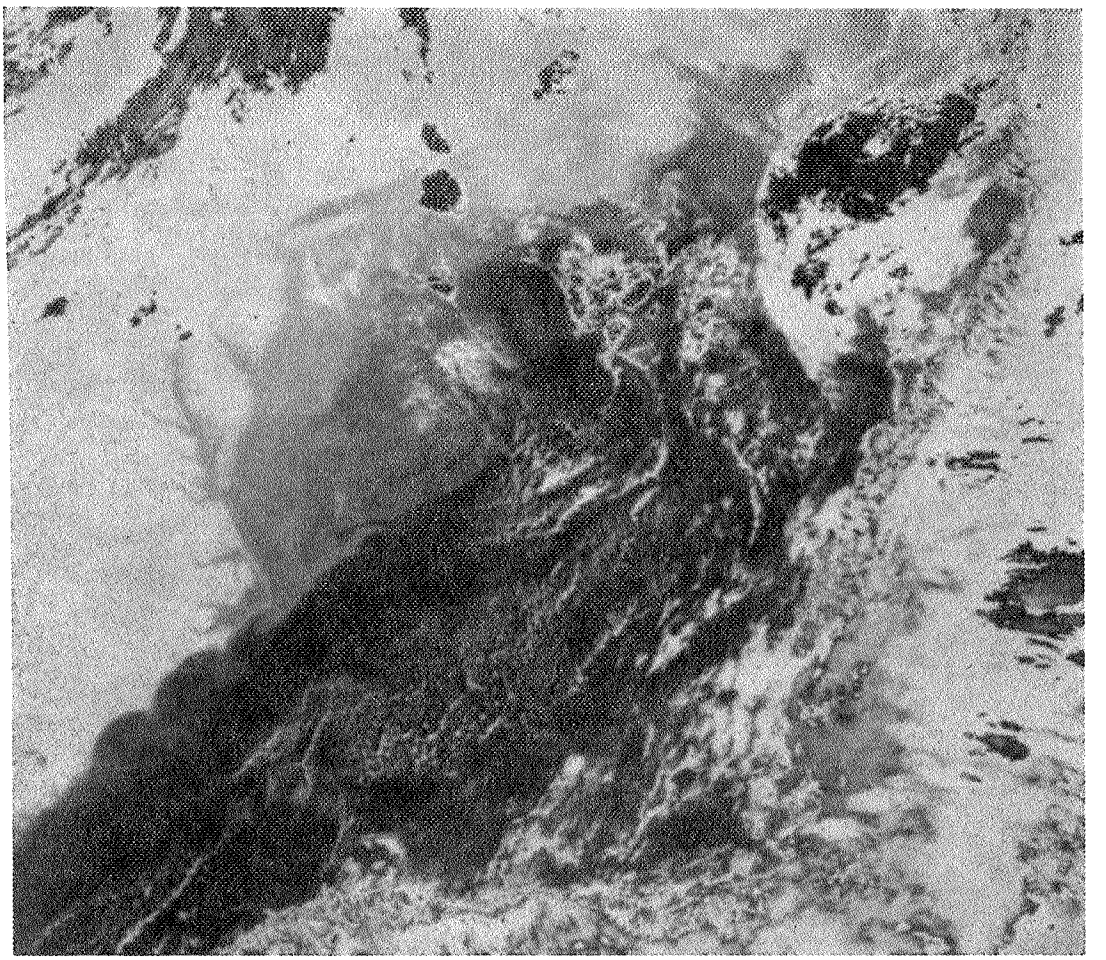

Figure 1. NOAA-6 infrared image for 8 October 1980, 12:42 GMT.

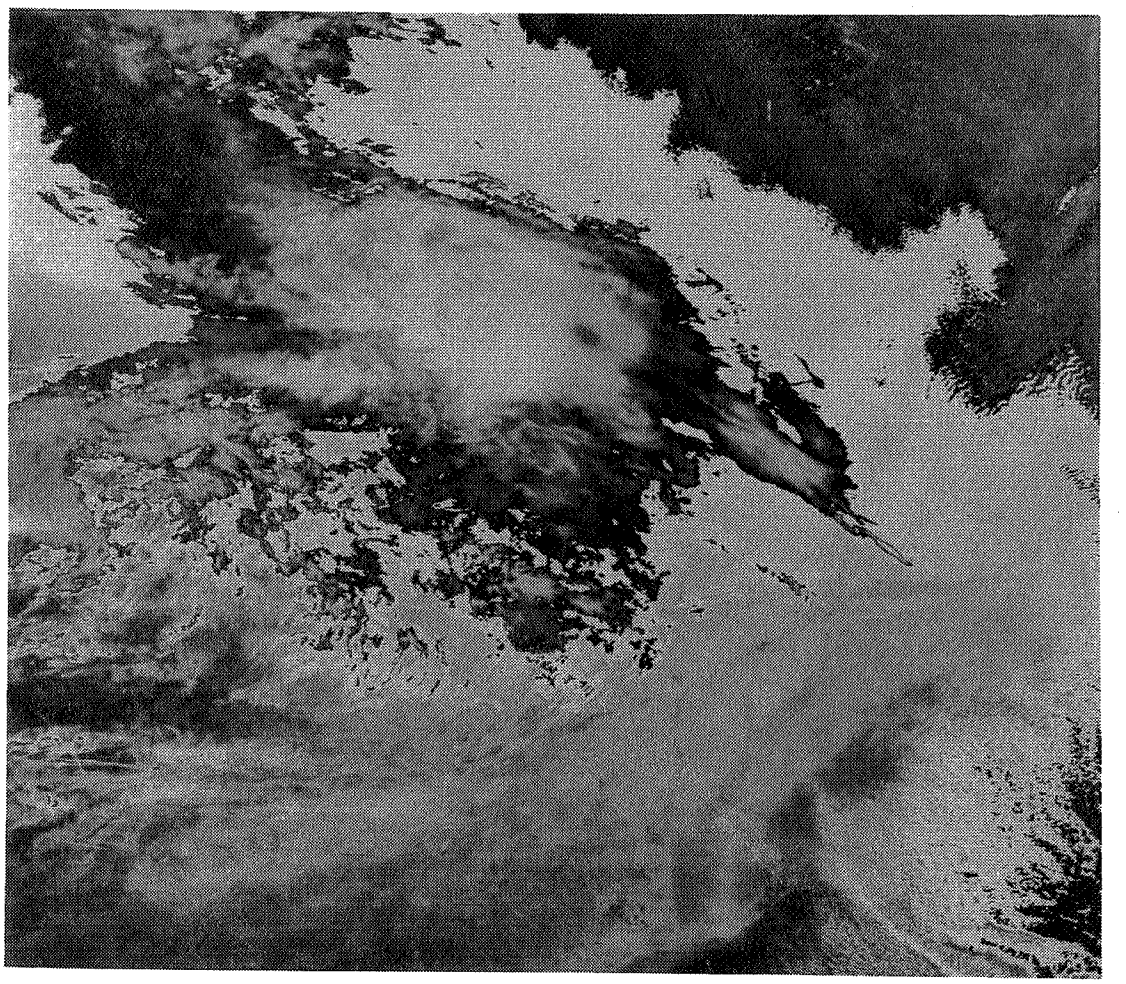

Figure 2. TIROS-N infrared image for 14 October 1980, 2025 GMT.

Figure 3. TIROS-N infrared image for 15 October 1980, 0847 GMT.

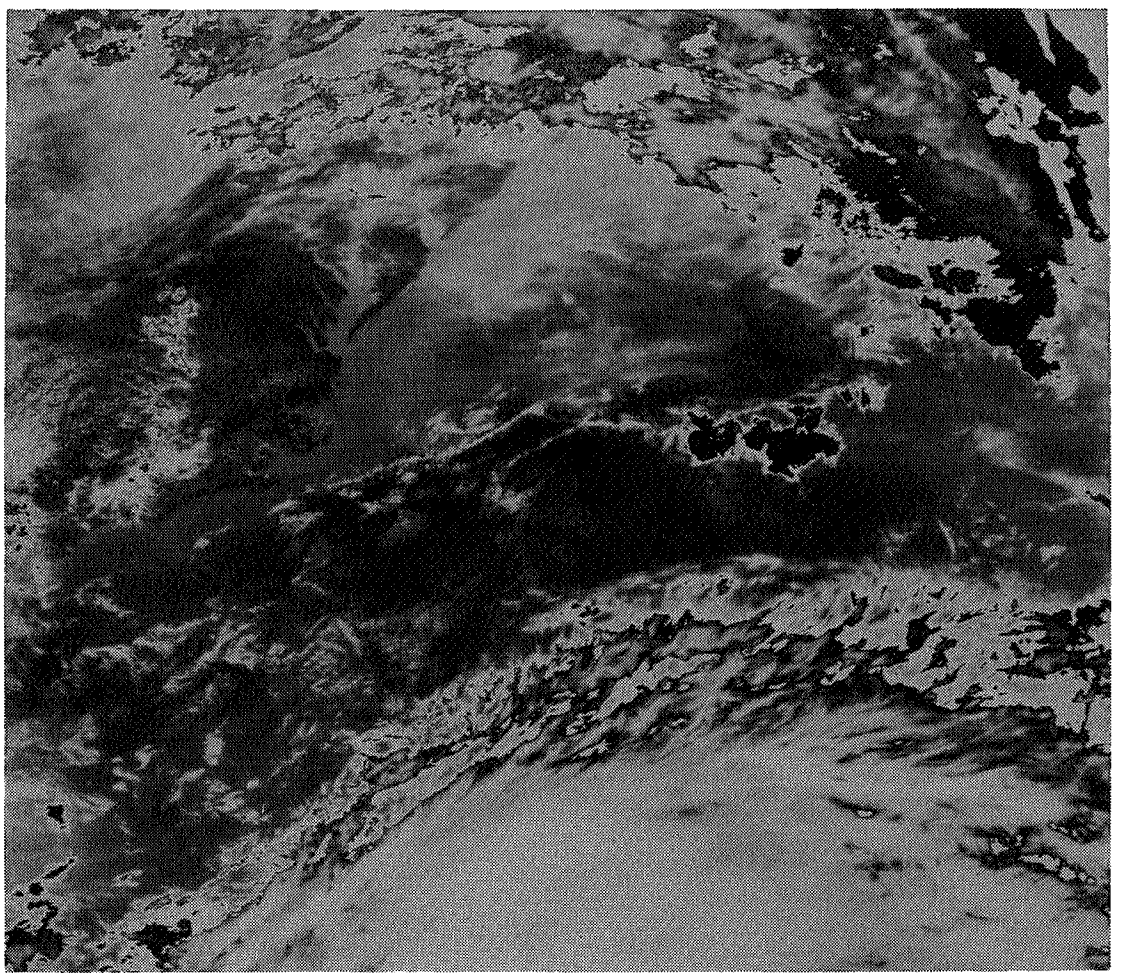

Figure 4. TIROS-N infrared image for 16 October 1980, 2000 GMT.

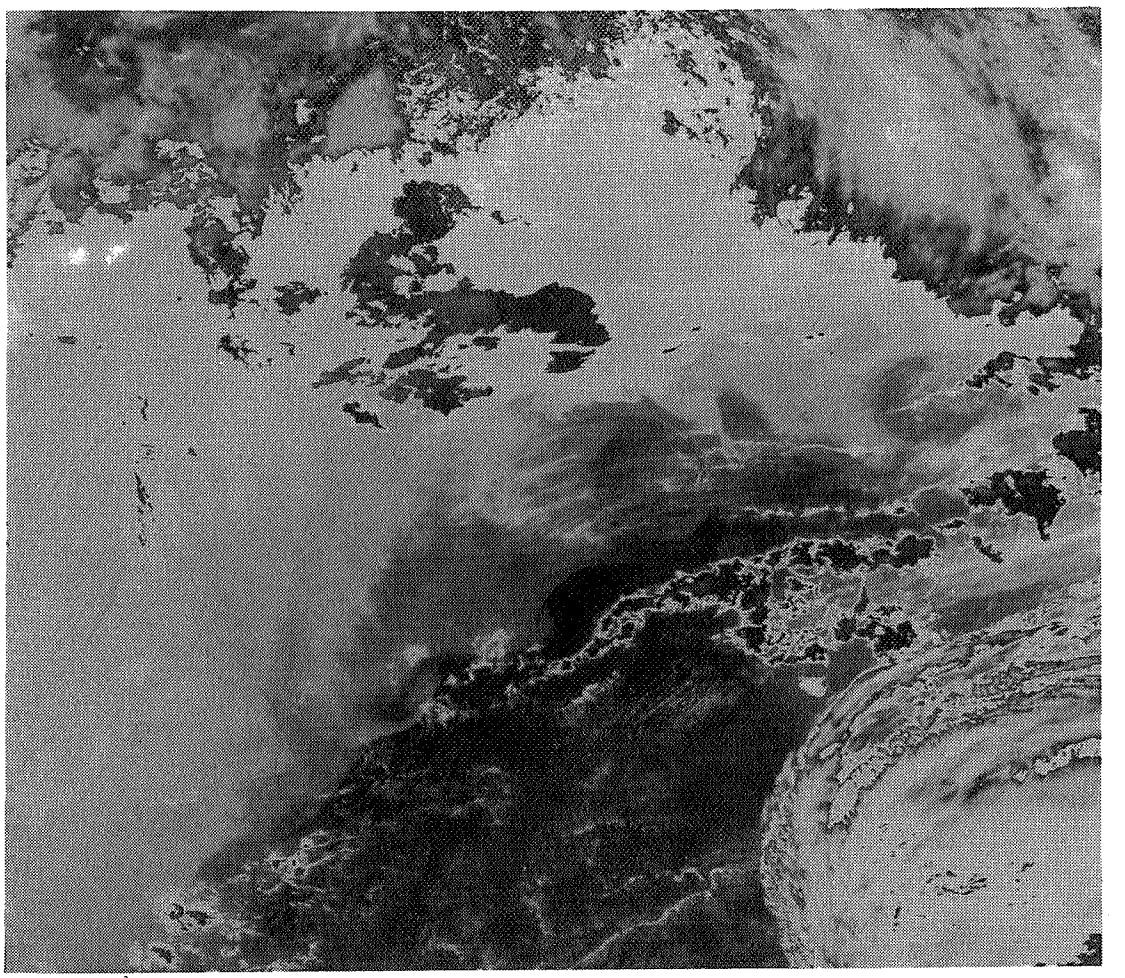

Figure 5. NOAA-6 infrared image for 17 October 1980, 1242 GMT.

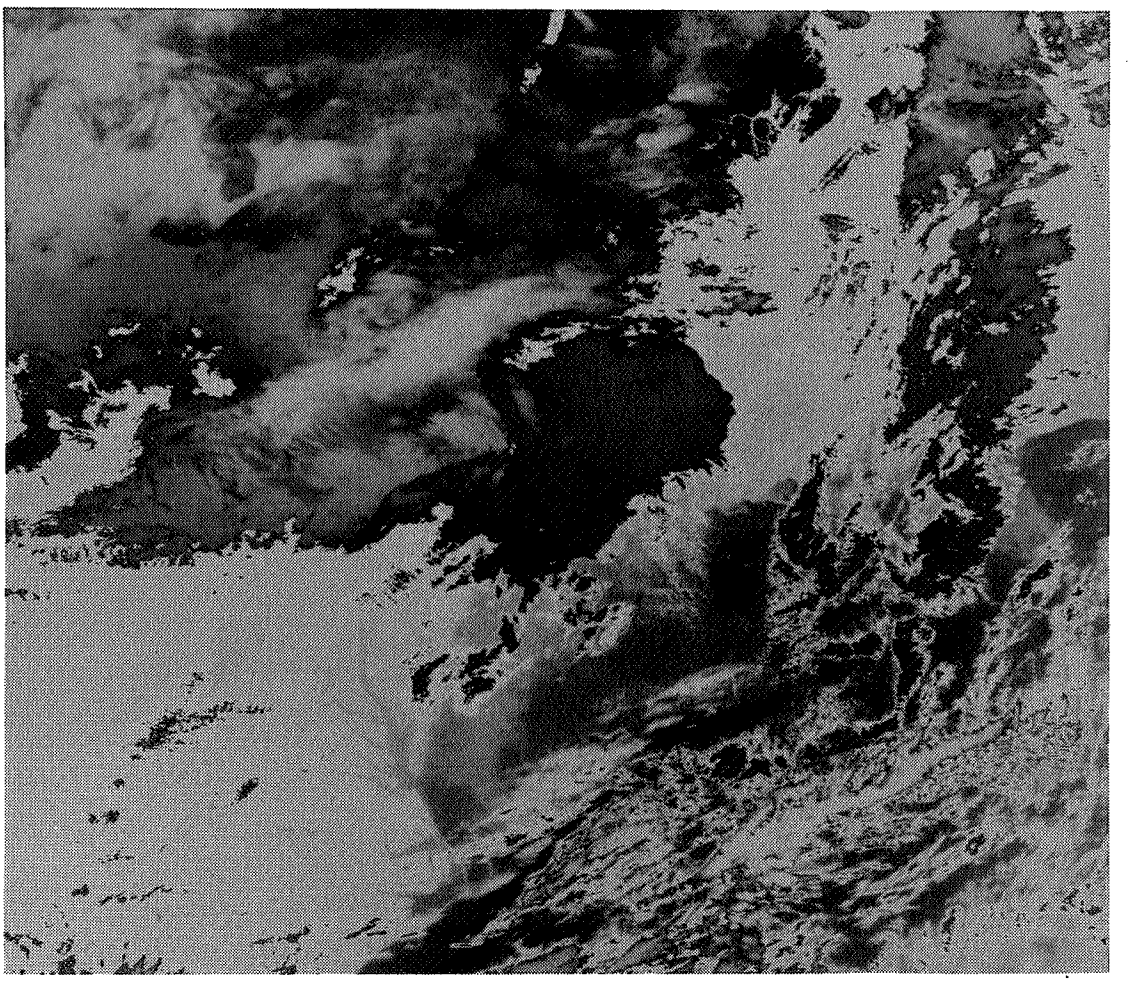

Figure 6. NOAA-6 infrared image for 21 October 1980, 1253 GMT.

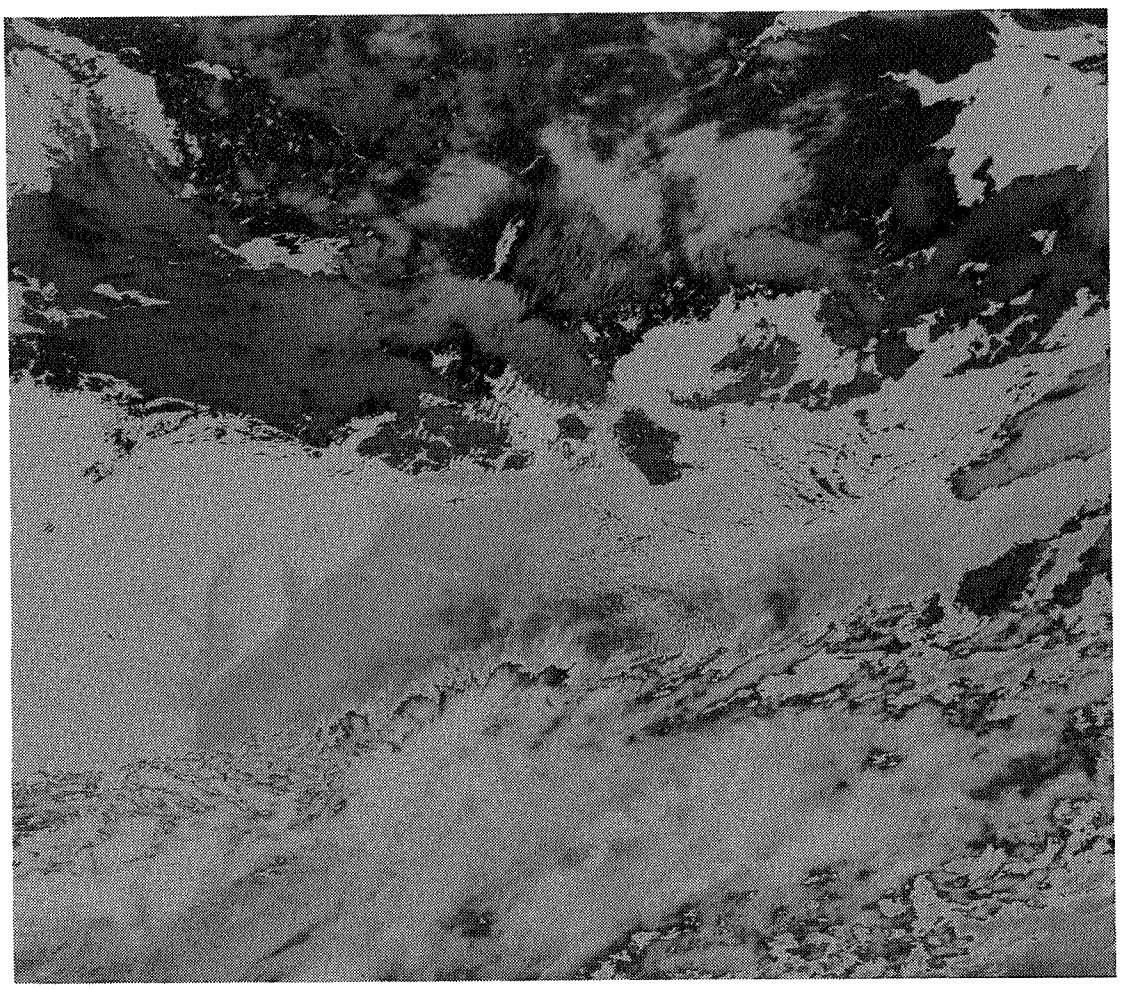

Figure 7. NOAA-6 infrared image for 22 October 1980, 2352 GMT.

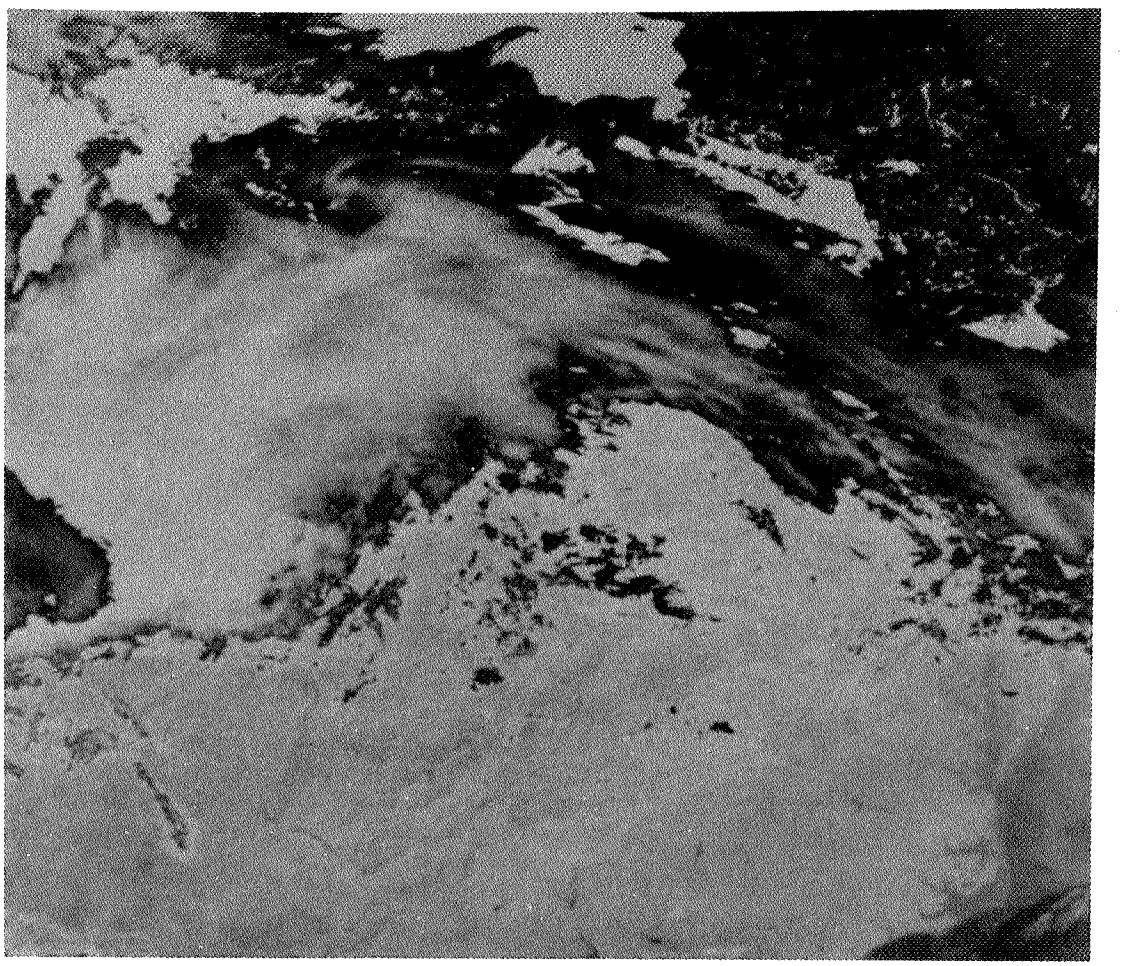

Figure 8. NOAA-6 infrared image for 16 October 1980, 0047 GMT.

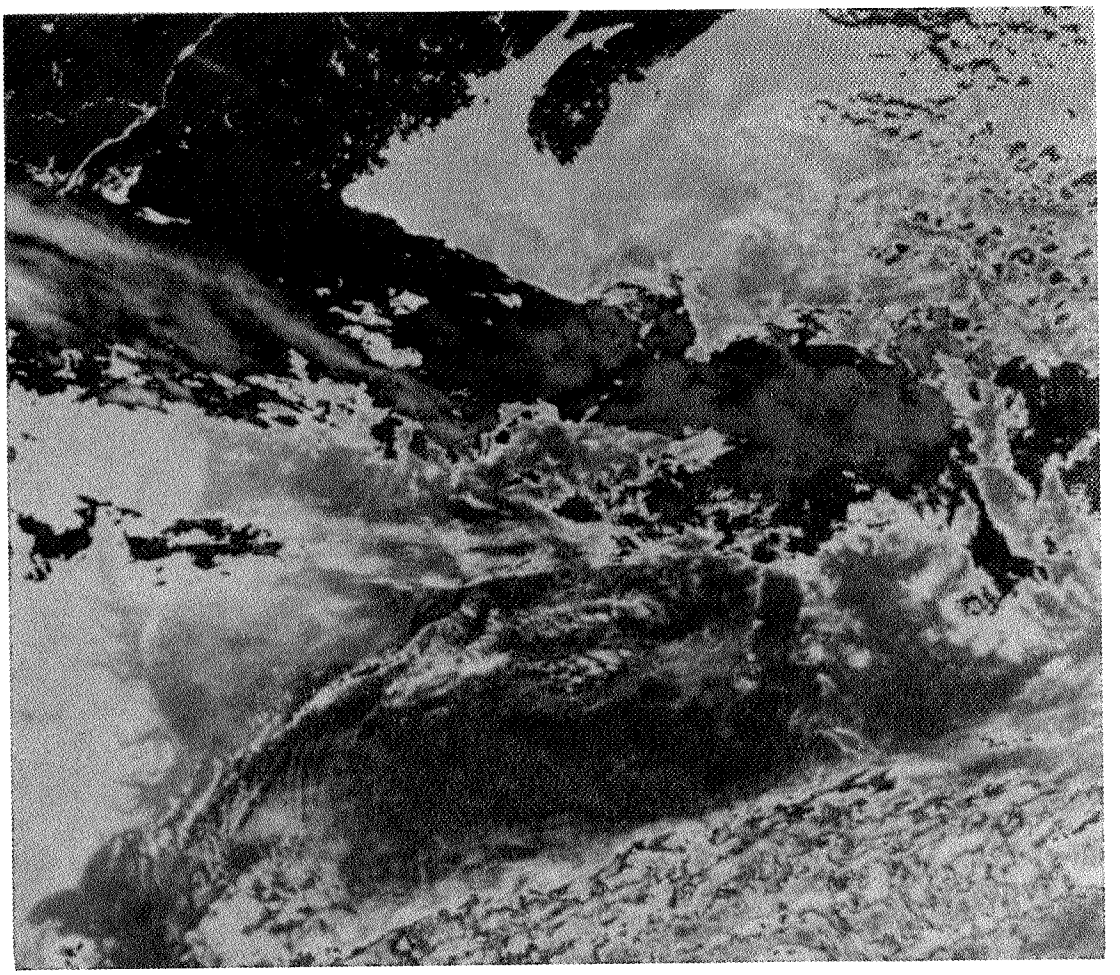

Figure 9. TIROS-N infrared image for 16 October 1980, 0835 GMT.

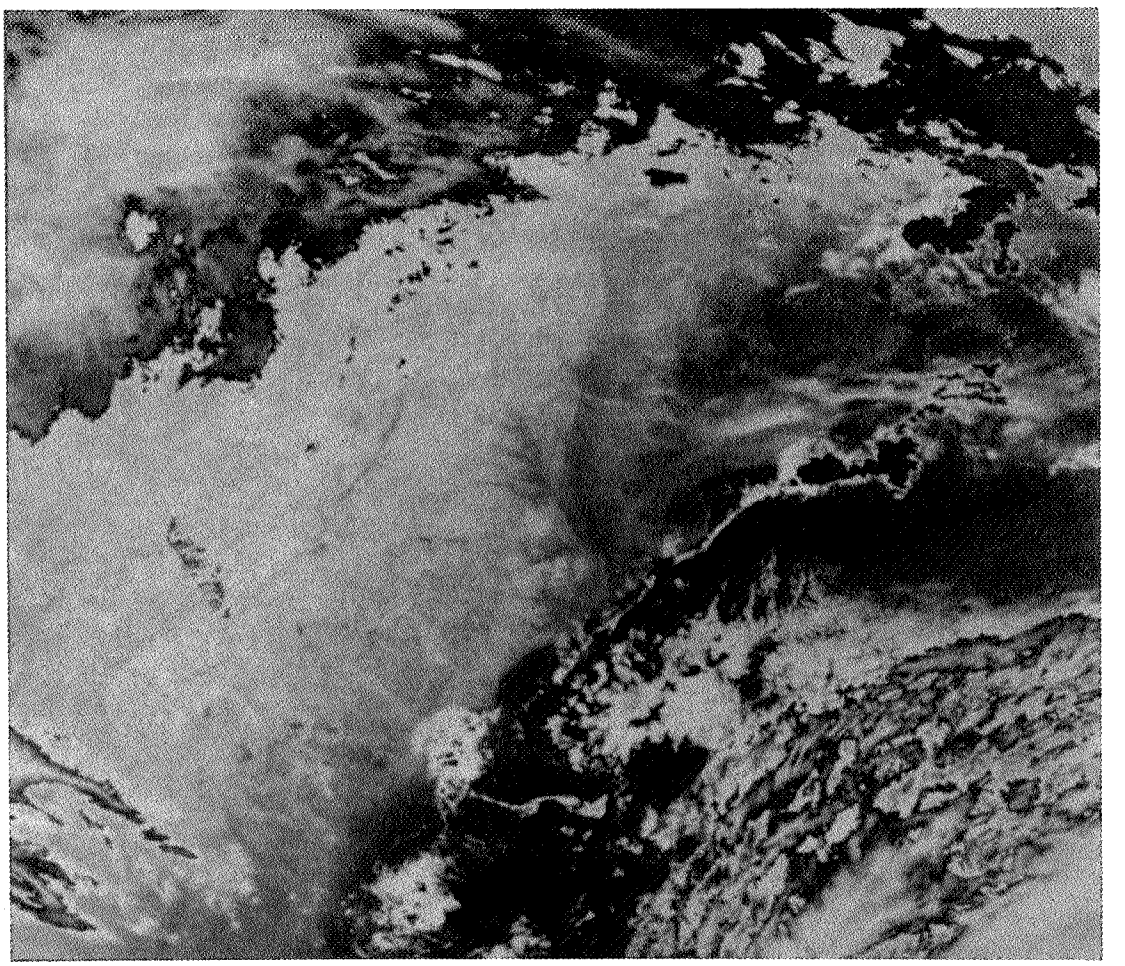

Figure 10. NOAA-6 infrared image for 16 October 1980, 1305 GMT.

TEMPORAL AND SPATIAL VARIATIONS OF THE CHESAPEAKE BAY PLUME*

Evon P. Ruzecki
Virginia Institute of Marine Science
College of William and Mary

SUMMARY

Historical records and data obtained during the Superflux experiments are used to describe the temporal and spatial variations of the effluent waters of Chesapeake Bay. The alongshore extent of the plume resulting from variations of freshwater discharge into the Bay and the effects of wind are illustrated. Variations of the cross-sectional configuration of the plume over portions of a tidal cycle and results of a rapid-underway water sampling system are discussed.

INTRODUCTION

Waters from Chesapeake Bay exit at the Virginia Capes and usually extend towards the south as a near-surface feature. Bay waters in the contiguous area of the continental shelf can be identified by a number of characteristics which are discussed in most of the contributions to this volume. Discussions in these companion papers refer to turbidity plumes, nutrient plumes, phytoplankton or chlorophyll plumes, freshened-water plumes, and others. Although they may be treated as separate features, each of these plumes represents Bay water as identified by the observed constituent. Inconsistencies in the shape or location of these plumes in shelf waters result from two factors, (1) the time scale over which individual sets of observations were made, and (2) the non-homogeneous character of the Bay effluent.

This paper examines the shape of the Bay plume as determined by vertical measurements of salinity under varying Bay discharges of fresh water and over time scales ranging from half a tidal cycle (6.2 hr) to several days. Results of salinity measurements made during the Superflux experiments and a rapid method of obtaining surface truth data are also presented and discussed.

CONFIGURATION OF BAY WATER ALONG THE COAST

Theoretical Basis

Movement of water through the mouth of Chesapeake Bay is dominated by tidal oscillations and strongly influenced by winds and the history of freshwater discharge into the Bay through its tributaries. In general, over a series of tidal cycles and as a result of estuarine circulation, freshened Bay water exits at the surface on the southern side of the Bay mouth (Cape Henry), is deflected to

*Support for this project was furnished by NASA Langley Research Center (contract LA471B), National Marine Fisheries Service, NOAA (contracts NA-80-FE-A0015 and NA-31-FA-C0005), and the Virginia Institute of Marine Science.

the right by the Earth's rotation and the general circulation of shelf waters (refs. 1 and 2), and then proceeds towards the south as part of the general shelf circulation. Estuarine-type circulation of Chesapeake Bay results in movement of shelf waters into the Bay predominantly along the bottom in deeper channels and on the northern (Cape Charles) side over the multi-tidal time frame.

During an individual tidal cycle, flooding and ebbing occur over the entire cross-section of the Bay mouth; however, phase differences and variations in the strength and duration of flood and ebb currents result in the general non-tidal water movements described above. The strength and duration of nontidal currents and the depression of Bay water salinities are affected by the recent (one- to two-month) history of freshwater addition to the Bay. Hence, both the salinity and alongshore extent of the Bay plume can be expected to change seasonally with fluctuations in runoff. The general position of the Bay plume is subject to change in response to wind conditions. In particular, winds from the southern sector will tend to impart an offshore (eastward) component to the plume as a result of Ekman circulation (ref. 3).

During the summer of 1962, Harrison et al. (ref. 4) measured currents in the vicinity of Cape Henry and Virginia Beach, Virginia. They inferred from their data that nontidal surface currents in this region result in an anti-cyclonic eddy located between Cape Henry and Rudee Inlet (36°56' N to 36°50' N) centered approximately 3 km from the beach, as shown in figure 1(a). This eddy could result from flood and ebb current patterns shown in figures 1(b) and 1(c) where ebbing (easterly and southerly) currents are strongest at Cape Henry and some distance seaward of Virginia Beach and flooding (northerly) currents south of the Bay mouth are strongest close to shore (ref. 5). Hydraulic model tests (ref. 6) and field studies indicate a surface-to-bottom phase difference in currents at the Bay mouth with more saline bottom water from the continental shelf starting to flood before fresher surface water and surface water ebbing occuring prior to ebbing of bottom water.

Based on these considerations, the effluent from Chesapeake Bay should appear, in shelf waters, as a lens of freshened water (with high concentrations of Bay water constituents) extending offshore and towards the south at the end of an ebbing tide. Half a tidal cycle later this effluent plume should show a partial retraction (back into the Bay) of its northernmost portion, with dilution and southerly transport of the southernmost portion. Previous extensions of the plume might be identifiable along the coast towards the south as they move with the general shelf circulation, but they would be diluted by mixing with ambient shelf water (ref. 7). The combined effects of wind and runoff would result in offshore displacement coupled with horizontal widening and vertical thinning of the plume in response to winds with a component from the south, onshore displacement coupled with horizontal narrowing and vertical thickening in response to winds with a component from the north, and fresher water (with higher concentrations of Bay constituents) extending further south in response to increased river flow. Tidal variations and freshwater discharge effects on the Bay effluent are evident from sets of data taken near the mouth of Chesapeake Bay and in contiguous shelf waters.

Historical Evidence

Several data sets (available from the VIMS data archives) can be used to describe the influence of tides and river flow on the Bay plume. On May 9 and 10, 1973 the Virginia Institute of Marine Science (VIMS) of the College of William and Mary and the Chesapeake Bay Institute (CBI) of the Johns Hopkins University conducted a joint cruise which occupied stations in the triangular area between Cape Charles, Cape Henry, and the Chesapeake Light Tower. Stations were 1.8 km (1 n. mi.) apart (fig. 2(a)) and were each occupied twice to coincide as closely as possible with flooding and ebbing tides. Results of salinity measurements at these stations during flood and ebb are shown in figures 2(b) and 2(c), respectively. Relationships between predicted tidal currents (at 36°58.8' N, 76°00.4' W) and ship arrival at locations A, B, and C are shown to the left of each figure. It is evident from figure 2(b) that a flooding tide compressed the core of the Bay plume towards the Virginia Beach/Cape Henry region (location C), and lower salinity water (less than 26 °/oo) extended as a veneer less than 5 m thick one-third of the way across the Bay mouth. During the ebbing tide (fig. 2(c)) the plume left Cape Henry and extended towards the south. It was centered approximately 10 km from the beach and remained in the upper 5 m of the water column. This response of the plume to tidal forcing agrees with the hypothetical circulation patterns shown in figures 1(b) and 1(c). Winds on May 10, 1973 averaged 3.8 m/sec (7.5 kt) from the north-northeast and appear to have had little effect on the plume.

Three other data sets provide information for comparisons of the Bay plume under differing conditions of freshwater inflow. Data from a temperature/salinity survey of shelf waters in March of 1967 show a high concentration of Bay water moving as a plume parallel to the Virginia coast approximately 15 km offshore as indicated in figure 3. Stations a through h were occupied in alphabetical order during a six-hour period covering the last part of ebb and the first part of the flooding tide on March 18. Stations i through m were occupied a day later during similar portions of the tidal cycle. Bay water in the shelf region is indicated by envelopes representing fractions of Bay water based on salinity measurements according to:

$$f = \frac{S_s - S_m}{S_s - S_b}$$

where S_s is the salinity of shelf water, S_b is the salinity of Bay water, and S_m is the measured salinity. The quantity S_s represented the ambient bottom salinity 30 km east of the Bay mouth (32.5 °/oo), while S_b was the lowest surface salinity at the Bay mouth (25.5 °/oo).

Average daily discharges of fresh water into Chesapeake Bay for January, February, and March 1967 were on the order of 1.3, 1.2, and 3.5×10^3 m^3/sec and represented between 50 and 78% of the average flows for these months for the period from 1929 to 1966 (2.3, 2.8, and 4.3×10^3 m^3/sec respectively) (ref. 8). Surface winds during the sampling period started at 0.8 m/sec (1.5 kt) from the north on March 18, increased and veered to blow from the south-southeast at 7.5 m/sec (15 kt) the night of March 18-19, and moderated slightly to 6 m/sec (12.5 kt) from the south-southeast the following night. Bay water configura-

tions shown in figure 3 are therefore a first approximation of the three-dimensional shape of the plume under conditions of below-average spring discharge and an ebbing tide but widely varying wind conditions. Stations a through h show the base of the plume (a-b) with a submerged parcel of mostly shelf water off Cape Henry (at b) and a thick parcel of mostly (>50%) Bay water off Rudee Inlet (at d). The latter may represent the most southerly extension of Bay water on this particular ebbing tide. Lower concentrations of Bay water found at stations e through h are assumed to be residual from the previous tide. The seaward extension of a thin layer of Bay water sampled at stations i through m was in response to the strong southerly winds. This offshore component of surface waters would have to be replaced by an onshore intrusion of bottom water, a secondary response to surface wind stress suggested at stations i and j where an intrusion of bottom shelf water was directed towards the Bay mouth from the east-southeast. With these allowances for the wind shift, figure 3 shows the general configuration of the Bay plume at the end of ebb tide under conditions of a depressed spring discharge.

An extreme event of high freshwater discharge into Chesapeake Bay occurred as a result of the passage of Tropical Storm Agnes at the end of June 1972. Results of VIMS shelf cruises on July 6-8 and August 3-4, 1972 (ref. 7) are presented as figures 4 and 5 and show the general plume configuration in response to this high discharge. (Tropical Storm Agnes increased discharge into Chesapeake Bay from 2.1×10^3 m^3/sec on June 20 to an average of 48.1×10^3 m^3/sec on June 23-24. Previous average June flows were 1.8×10^3 m^3/sec.) Figure 4 shows the plume fifteen days after peak discharges into the Bay (Bay salinity, S_b, was taken to be 18 °/oo and shelf salinity, S_s, 32.5 °/oo) with a higher concentration of Bay water extending towards the south in the same general configuration as the March 1967 plume (fig. 3) but closer to shore. Two weeks later (fig. 5) a much greater impact of the Agnes flooding was evident. Patches of Bay water were encountered as far south as Oregon Inlet, North Carolina, and the region normally subjected to 25% Bay water was covered with 100% Bay water (for fig. 5, S_b was taken to be 16 °/oo and S_s remained at 32.5 °/oo). The two patches of 60% Bay water located 78 and 133 km from the Bay mouth indicate nontidal shelf currents on the order of 1.5 m/sec, assuming they are residuals from previous ebb tides. Bay water concentrations of 40% covered an area in excess of 5.5×10^3 km^2 and remained in the upper 10 m of the water column. During both sampling periods (July 6-9 and August 3-4) winds were moderate (<4 m/sec) from the northeast. Wind effect on the plume would have been to confine it to the coast and possibly force it to be deep and narrow.

Configurations of the Bay plume as represented by figures 3, 4, and 5 are based on data collected over 2- to 3-day periods and therefore suffer from lack of simultaneity. They do, however, illustrate large variations in the extent of the plume which result from extremes in the addition of freshwater to Chesapeake Bay.

SUPERFLUX EXPERIMENTS

One of the objectives of the Superflux experiments was to determine the impact of effluents from large estuaries on waters of the continental shelf. To meet this objective, the extent of the plume from Chesapeake Bay was measured

using the best and most rapid techniques available. Information from aircraft-borne state-of-the-art remote sensors was augmented with shipboard surface-truth measurements and samples. The procedure allowed the measuring of surface features over a large area in a short time but provided only widely spaced vertical sampling at selected locations within the plume and the adjacent Bay and shelf areas. As expected, the remote sensing aspects of the Superflux experiments revealed the two-dimensional structure of the plume with respect to salinity, chlorophyll, suspended solids, and other constituents of surface waters in much greater detail than the traditional sampling used to estimate its three-dimensional character as shown in figures 3, 4, and 5. Additionally, the compressed sampling time (hours as opposed to days) provided better simultaneity to this synoptic coverage than had been available previously. Similar rapid coverage of only the plume area could have been accomplished in two to three hours using traditional sampling methods; however, such an experiment would have required seven fast (15-kt) ships each equipped with a fast CTD (conductivity, temperature, and depth instrument) and underway sampling equipment. It would have provided vertical as well as horizontal measurements, but ship, personnel, and equipment requirements would have been most difficult to satisfy.

In an attempt to obtain information on the cross-sectional configuration of the plume and on the horizontal distribution of temperature, salinity, and chlorophyll in the plume and adjacent waters using in situ sensors, VIMS conducted pilot studies between remote sensing flights during the Superflux experiments. Temperature/salinity measurements were made along a section of closely spaced stations extending seaward from the vicinity of Rudee Inlet, using a Brown CTD. Between stations, the CTD was incorporated into a flow-through system which pumped water from a depth of 1 m and passed it through a fluorometer to measure chlorophyll content. When the section was completed the system remained operative while the research vessel moved to the next Superflux station to obtain additional surface truth data. As the experiments progressed, two additional fluorometers were added to the flow-through system and, in final configuration, temperature, salinity, dissolved oxygen, two chlorophyll bands, and nephelometry were measured. All data were recorded on both strip charts and magnetic tape with a voice channel on the latter for time, position, and sample identification information. The flow-through system was mounted on the research vessel CAPT. JOHN SMITH as shown in figure 6.

Data Collection

Cross-plume sections of closely spaced (1 to 2 km) stations were occupied between overflights of remote sensing instrumentation during all three Superflux experiments. Whenever possible, the flow-through system was operated between stations. Cruise tracks and cross-plume section locations are shown in figures 7(a), 7(b), and 7(c) and are labeled to indicate the date each was run. Sections are shown as boxed regions and were located off Rudee Inlet on March 19 and June 24 and off Virginia Beach on October 15-16. An additional section was occupied across the Bay mouth on October 15-16 (fig. 7(c)). The section of Rudee Inlet was sampled once on March 19 and five times on June 24. The Bay mouth and Virginia Beach sections were each sampled three times on October 15 and four times on October 16 (these data were collected with the assistance of

C. S. Welch and the VIMS 1980 Introduction to Physical Oceanography class). Data on freshwater discharge into Chesapeake Bay for the period from January to October 1980 were obtained from the U.S. Geological Survey (ref. 9) and wind data for the five-day period prior to cruises were obtained from Norfolk Airport, 40 km west of the study area. Tidal current information was based on NOAA predictions in Tidal Current Tables 1980 (ref. 10).

Results and Discussion

Average streamflow data for January through October 1980 (fig. 8) along with multiannual average streamflow for the same months show that flows during February 1980 (prior to Superflux I) were less than half the normal February flows, and although April flows were higher than average, flows in June (during Superflux II) were below average as were those prior to Superflux III (August, September, and October). Thus, the seaward or alongshore extension of the Bay plume was probably not as great during the Superflux experiments as it would have been in more "normal" years. Winds measured at Norfolk for the five-day periods prior to each sampling of the plume cross-section are shown as stick plots in figure 9.

Cross-Plume Salinity Sections.- The cross-sectional configuration of the Bay plume is illustrated by positions of isohalines as functions of depth and distance offshore. During Superflux I, the section off Rudee Inlet was occupied just prior to noon on March 19 during the flooding portion of the tidal cycle and figure 10 shows that the core of Bay water, centered 2-3 km from the beach, was confined to the upper 8 m of the water column (as indicated by the 27 $^{o}/oo$ isohaline). From 5 to 12 km offshore, Bay water is confined to the upper 3 m of the water column. This seaward extension of surface plume water may have been caused by winds blowing offshore just prior to sampling.

This general configuration of the Bay plume off Rudee Inlet (nearshore core with an offshore surface extension) was again evident on June 24 (fig. 11). This short time series of sections shows the plume core initially 1 km offshore and migrating seaward as lower salinities reach the section sampled. The offshore extension of surface water is again evident but not as pronounced as in March, although winds were generally from the south prior to sampling. Sampling was conducted during the latter half of the ebbing tide and the southerly progression of Bay water is evident from the widening and deepening of the area covered by the 23 and 25 $^{o}/oo$ isohalines.

Results of salinity measurements made across the Bay mouth and off Virginia Beach on October 15-16 are shown in figures 12 and 13 (note the reversal of the time axis in these figures when compared to fig. 11). The dashed lines in these figures indicate secchi depth, Cape Henry is on the left in figures 12(a) and 13(a), and Virginia Beach is on the left in figures 12(b) and 13(b). At the Bay mouth, two parcels of freshened water were evident (off Cape Henry and in the centered portion of the Bay) during the first maximum ebb current sampling on October 15 (fig. 12(a)). Intrusions of high salinity water at the bottom and along the Cape Charles (northern) portion of the Bay mouth are evident during the flooding portion of the tidal cycle. During the following ebb (1600 to 2100 hr in fig. 12(a)) the salinity structure bore a closer resemblance to

flooding rather than ebbing conditions, a situation that is contrary to what is expected considering tide and wind conditions (see fig. 9). Off Virginia Beach during this same time (fig. 12(b)) a lens of freshened water was evident at the beginning of the flood portion of the tidal cycle and the seaward portion of the Bay plume was delineated by a strong frontal region 15 km offshore. The final Virginia Beach sections on October 15 show an offshore migration of the plume and an onshore extension and upward movement of higher salinity bottom water. Bay mouth conditions the following day (fig. 13(a)) show a somewhat well-defined plume base near Cape Henry; however, lowest surface salinities were measured during the predicted flooding portion of the tidal cycle. The core of high salinity bottom water remained within 5 km of Cape Henry but showed a northward migration during the flooding tide and a southerly migration during ebb. The parcel of low salinity surface water off Cape Charles on the first section (approximately 0900 on October 16) is most likely a remnant of the Bay plume from the previous tide. Winds on October 15-16 were from the south (fig. 9) and probably served to transport the Bay plume and other surface waters offshore and to the north. During the following flooding tide (0900 on October 16) Bay water returned from offshore and entered around Cape Charles. Support for this suggestion of recirculation of the Bay plume is available from salinity data collected off Virginia Beach on October 16 (fig. 13 (b)). Here, lowest salinities were found 15 km offshore during the start of the flood portion of the tidal cycle when a well-pronounced plume should have been evident close to shore.

Figures 10 through 13 therefore illustrate changes in the cross-sectional structure of the Bay plume that result from variations in freshwater additions to Chesapeake Bay (high springtime flows, moderate late spring flows and very low late summer flows) and local wind conditions (wind from the southerly and northerly sectors).

Flow-Through System Results.- An example of the raw output from the flow-through system (fig. 14) shows substantial fine-scale variation in the output signals from the Brown CTD (conductivity and temperature) and two Turner design fluorometers (fluorescence and nephelometry). Records of this sort have been processed for the triangular-shaped cruise track run on March 19, 1980 (see fig. 7(a)) to yield 30-second averages of temperature, salinity, and fluorescence. This cruise track is shown in greater detail in figure 15. In this figure "event" marks, where loran positions were taken, are shown as numbered x's and each dot along the cruise track is the approximate midpoint of a 30-second average. Superflux station locations, times, observed fronts, and the positions of stations along the Rudee Inlet section are also shown. Measurements of temperature, fluorescence, and computed salinity along this cruise track are shown in figure 16. As in figure 15, each 30-second average is represented by a data point. Frontal regions are clearly evident (events 14, 19, and 28-29) and show temperature, salinity, and fluorescence differences between the Bay plume and adjacent shelf waters.

When displayed on a T/S (temperature/salinity) correlation diagram (ref. 11), comparisons between salinity, temperature, and chlorophyll content (as fluorescence) can be made. To do this, each 30-second averaged value of fluorescence was identified with its associated T/S class (class width of 0.5°C and 0.5 °/oo). The sum of all fluorescence values in each T/S class was then

normalized against the grand total of all fluorescence values. The total number of temperature, salinity, and fluorescence samples for each T/S class was normalized in a similar way to determine sample distribution in T/S space. Plots of both results are shown as figures 17(a) and 17(b) with T/S classes which sum to 75% of all fluorescence or samples measured enclosed in a heavy line and classes which total 50% of all fluorescence or samples measured marked with a closed circle in the upper right corner. In both cases, the predominant modes representing most fluorescence and greatest number of measurements run from 6.5°, 22 °/oo to 4.5°, 28 °/oo. If fluorescence-producing material were uniformly distributed over the study area, figure 17(a) would be a duplicate of figure 17(b). The difference between figures 17(a) and 17(b) is presented as figure 17(c) and shows greater-than-uniform fluorescence in the modal classes between 22 and 24 °/oo and the classes between 25.5 and 28 °/oo with greatest elevations at 22 to 23 °/oo and 26.5 to 27.5 °/oo (classes in figure 17(c) with negative values have a large bar across the number). These two groups of classes represent 19.88 and 10.29% of total fluorescence and 15.29 and 7.48% of all samples, respectively. The fluorescence-depressed class within the 75% mode represents 19.83% of total fluorescence and 28.96% of all samples. This crude analysis suggests two populations of fluorescence-producing materials associated with lower (Bay) salinities and higher (shelf) salinities. A more thorough investigation of this condition can be accomplished by comparing results of remote sensors designed to measure fluorescence with those which measured salinity. Indeed, the next reasonable step to take in the Superflux program would be a thorough comparison of remotely sensed and in situ data.

CONCLUSIONS

Previously collected data show the response of the Chesapeake Bay plume to large fluctuations in freshwater discharge and variations over a tidal cycle. Rapid sampling of closely spaced stations during the Superflux experiments provided information on the vertical character of the Bay plume at selected locations and indicated fluctuations in width and depth of this feature over a tidal cycle. These measurements also showed that the surface wind stress can easily displace the plume in a short period of time. Data of this sort, when coupled with remotely sensed data, provide a third and fourth dimension to information on the spatial and temporal character of features such as the Chesapeake Bay plume. Comparison of remotely sensed data with in situ measurements is the next logical step in the Superflux program.

REFERENCES

1. Beardsley, R. C.; and Hart, J.: A Simple Theoretical Model for the Flow of an Estuary onto a Continental Shelf. J. Geophys. Res., vol. 83, pp. 873-883, 1978.

2. Bumpus, D. F.; and Lauzier, L. M.: Surface Circulation on the Continental Shelf off Eastern North America Between Newfoundland and Florida. Serial Atlas of the Marine Environment, Folio 7, American Geographical Society, 1965.

3. Ruzecki, E. P.; Welch, C. S.; Usry, J.; and Wallace, J. W.: The Use of the EOLE Satellite System to Observe Continental Shelf Circulation. Eighth Annual Offshore Technology Conference, vol. 2, paper no. 2592, pp. 697-708, 1976.

4. Harrison, W.; Brehmer, M. L.; and Stone, R. B.: Nearshore Tidal and Nontidal Currents, Virginia Beach, Virginia. U. S. Army Coastal Engineering Research Center, Technical Memorandum no. 5, 1964.

5. Stanley, E. M.: A Two-Dimensional Time-Dependent Numerical Model Investigation of the Coastal Sea Circulation Around the Chesapeake Bay Entrance. Ph. D. Dissertation, College of William and Mary, 1976.

6. Gulbrandsen, L. F.: Baltimore Harbor and Channels Deepening Study; Hydraulic Model Boundary Control and Data Presentation. Report on file at U. S. Army Engineer Waterways Experiment Station, CE, Vicksburg, Miss., and U. S. Army Engineer District, Baltimore, Md., 1979.

7. Kuo, A. Y., Ruzecki, E. P.; and Fang, C. S.: The Effects of the Agnes Flood on the Salinity Structure of the Lower Chesapeake Bay and Contiguous Waters. The Effects of Tropical Storm Agnes on the Chesapeake Bay Estuarine System, Chesapeake Research Consortium, Inc., CRC publication no. 54, The Johns Hopkins University Press, pp. 81-103, 1976.

8. Schubel, J. R., Carter, H. H.; and Cronin, W. B.: Effects of Agnes on the Distribution of Salinity Along the Main Axis of the Bay and in Contiguous Shelf Waters. The Effects of Tropical Storm Agnes on the Chesapeake Bay Estuarine System, Chesapeake Research Consortium, Inc., CRC publication no. 54, The Johns Hopkins University Press, pp. 33-65, 1976.

9. Cumulative Streamflow into Chesapeake Bay. Monthly Summary for November, 1980, U. S. Dept. of the Interior, 1980.

10. National Ocean Survey: Tidal Current Tables 1980. Atlantic Coast of North America. U. S. Dept. of Commerce, NOAA, 1979.

11. Montgomery, R. B.: Characteristics of Surface Water at Weather Ship J. Deep-Sea Res., suppl. to vol. 3, pp. 331-334, 1955.

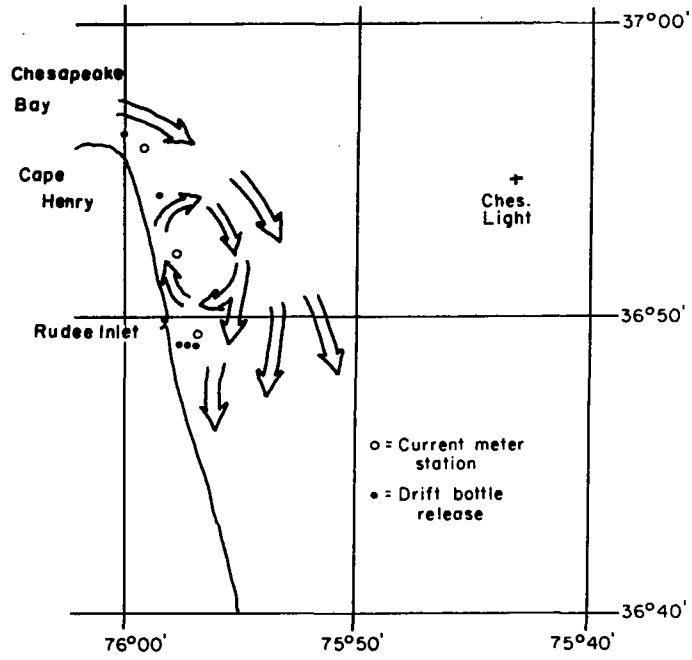

(a) Nontidal residual configuration.

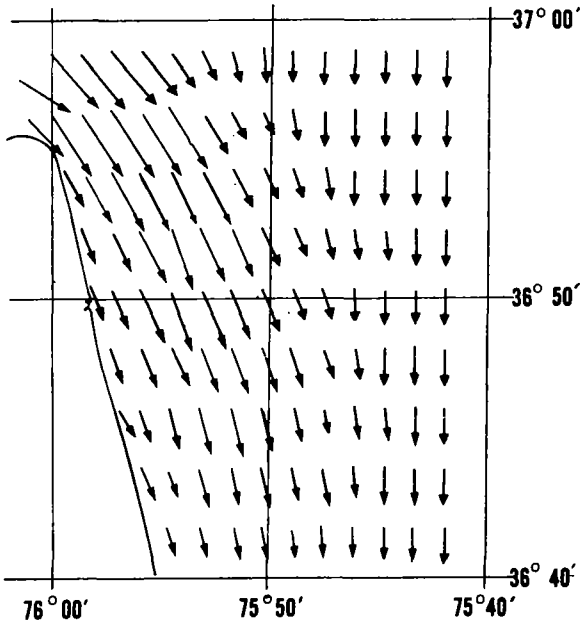

(b) Hypothesized ebb configuration.

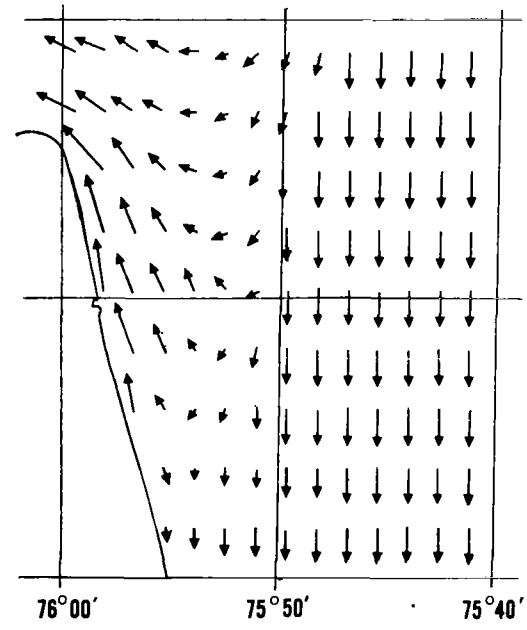

(c) Hypothesized flood configuration.

Figure 1.- Schematic representation of surface currents off Cape Henry and Virginia Beach, Va., showing nontidal residual and hypothesized ebb and flood configurations.

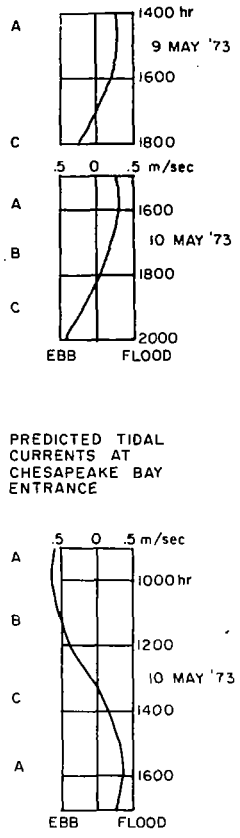

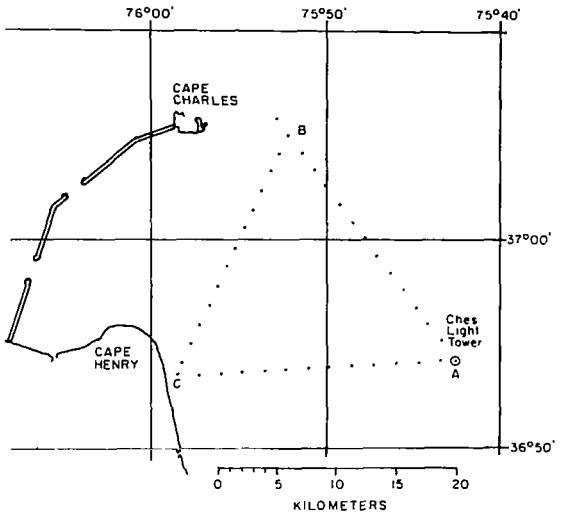

(a) Station locations.

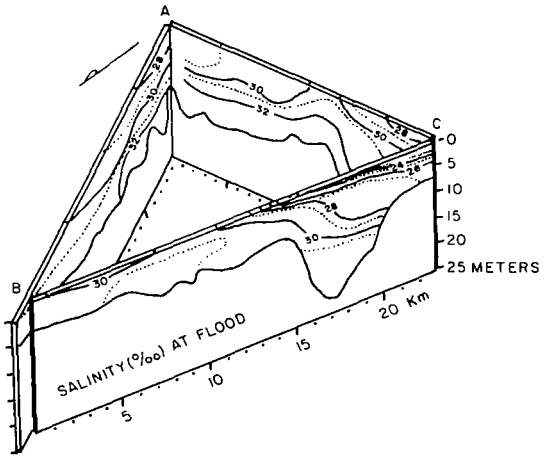

(b) Flood conditions.

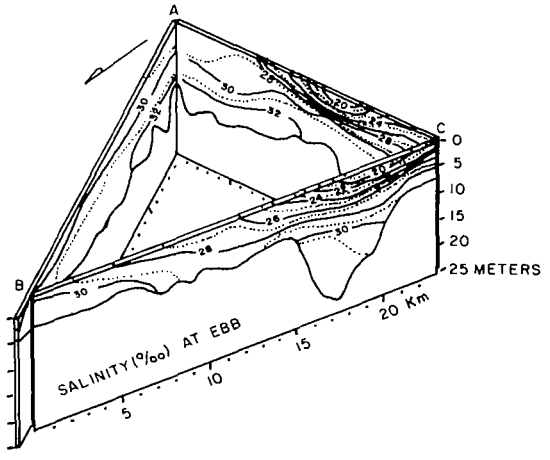

(c) Ebb conditions.

Figure 2.- Flood and ebb salinities at the mouth of Chesapeake Bay on May 9 and 10, 1973.

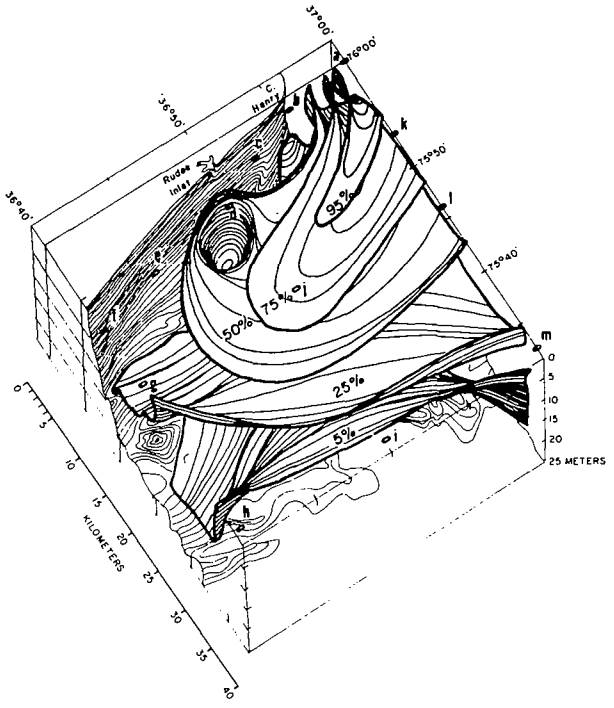

Figure 3.- Envelopes representing various fractions of Bay water on the continental shelf during March 18 and 19, 1967.

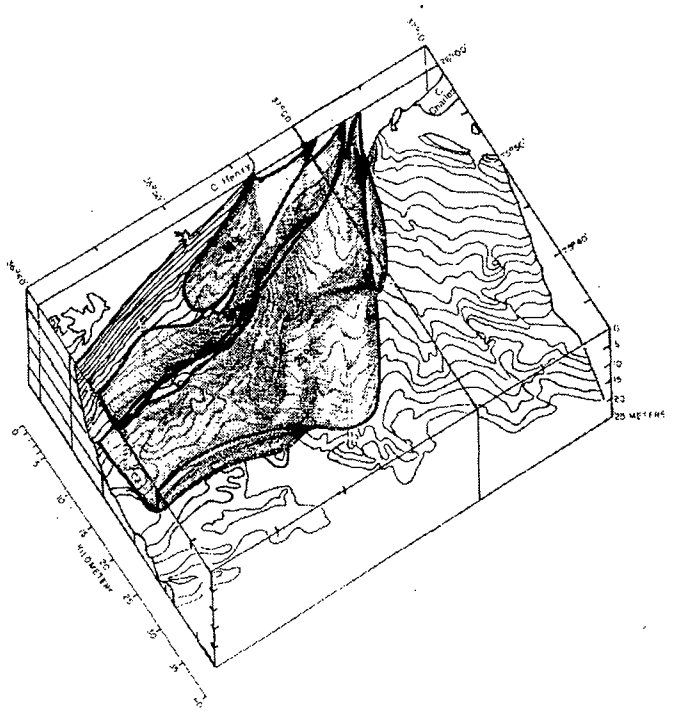

Figure 4.- Fractions of Bay water on the continental shelf on July 6-8, 1972, 15 days after peak flooding from Tropical Storm Agnes.

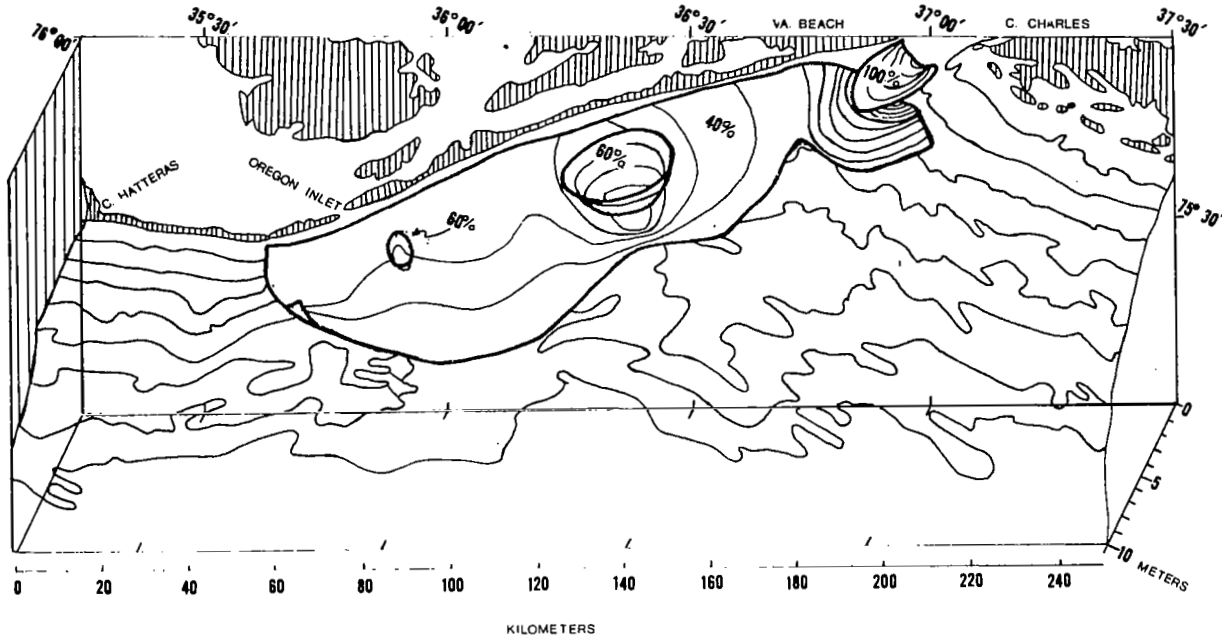

Figure 5.- Fractions of Bay water on the continental shelf on August 3 and 4, 1972, 41 days after peak flooding from Tropical Storm Agnes.

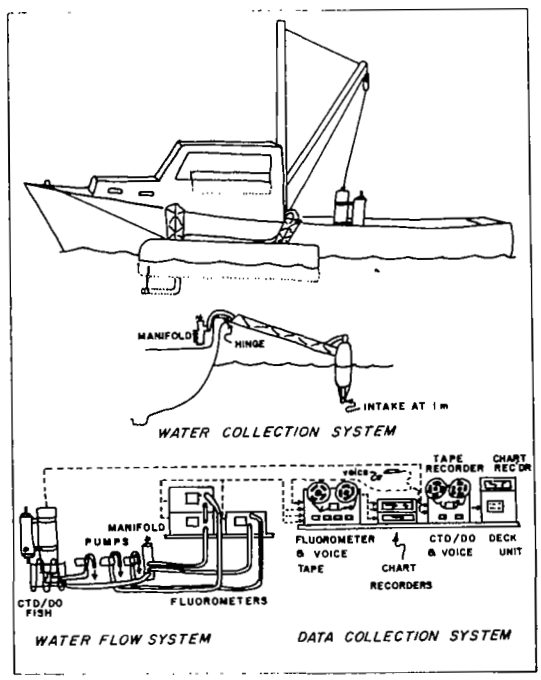

Figure 6.- Flow-through system used to collect temperature, salinity, D.O., chlorophyll, and nephelometry data from a depth of 1 m while cruising at 5 m/sec (10 kt).

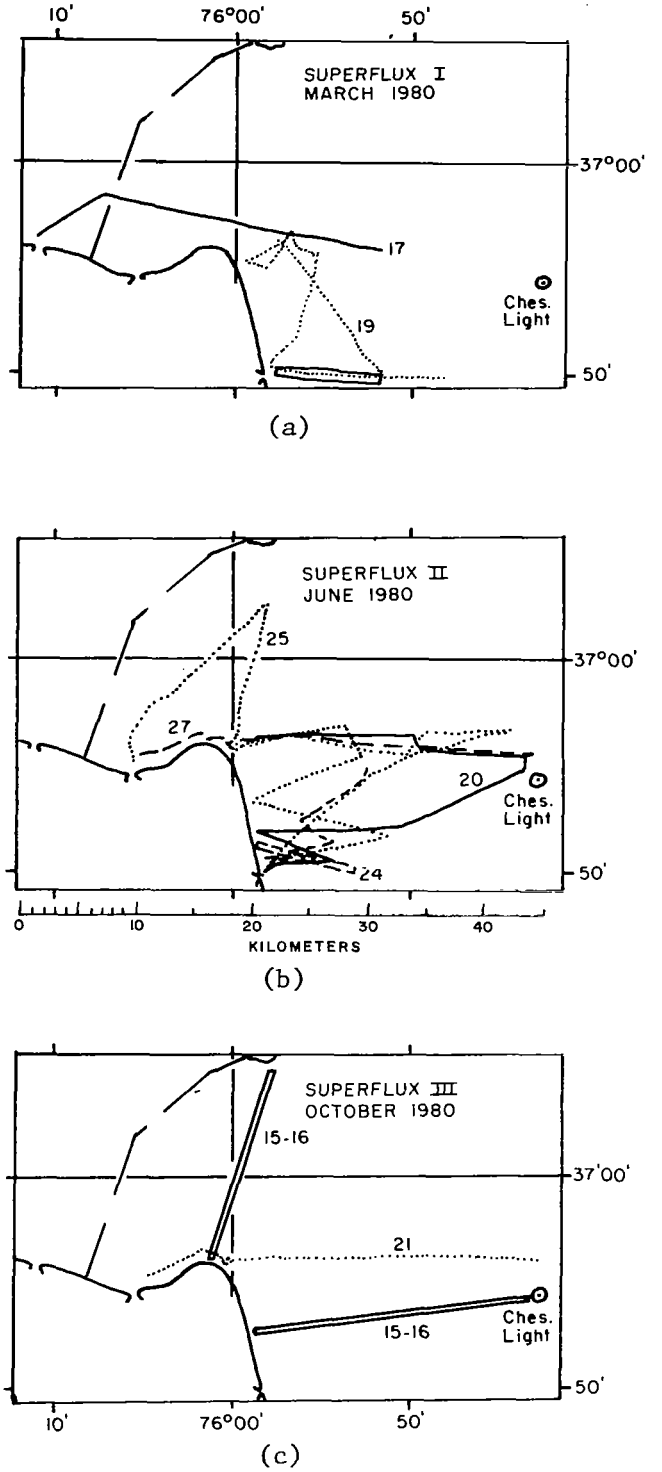

Figure 7.- Cruise tracks of R/V CAPT. JOHN SMITH during Superflux experiments. Sectional data were obtained from boxed regions on March 19, June 24, and October 15 and 16, 1980.

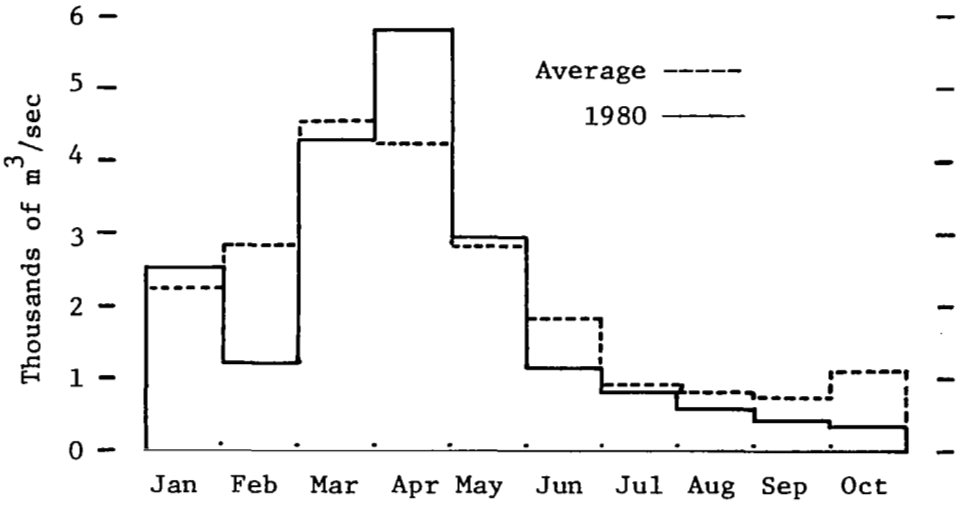

Figure 8.- Average monthly streamflow into Chesapeake Bay for the months January through October. Multiannual averages are dashed lines, 1980 averages are solid lines.

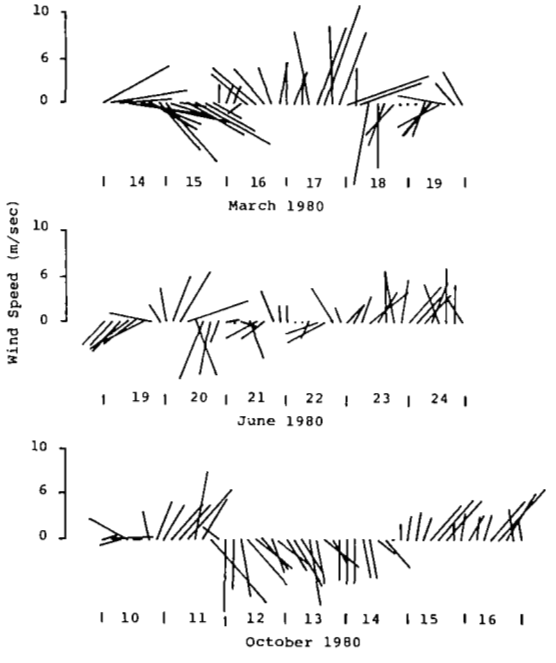

Figure 9.- Stick plots of winds at Norfolk, Va. for five-day periods prior to plume section sampling on March 19, June 24, and October 15 and 16, 1980. North is to the top of the page and sticks point in the direction the wind was blowing.

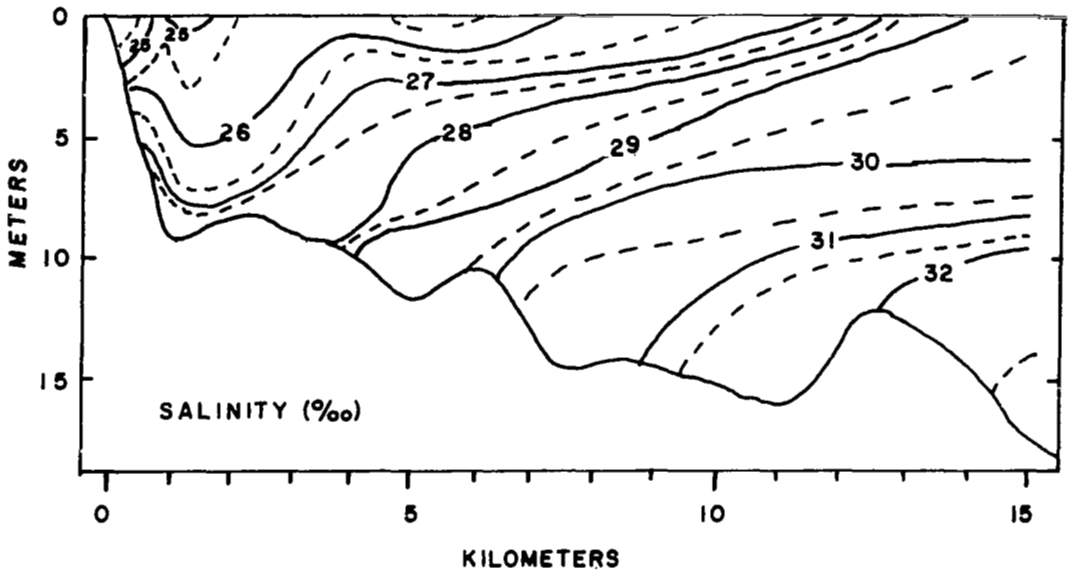

Figure 10.- Salinity distribution off Rudee Inlet on March 19, 1980.

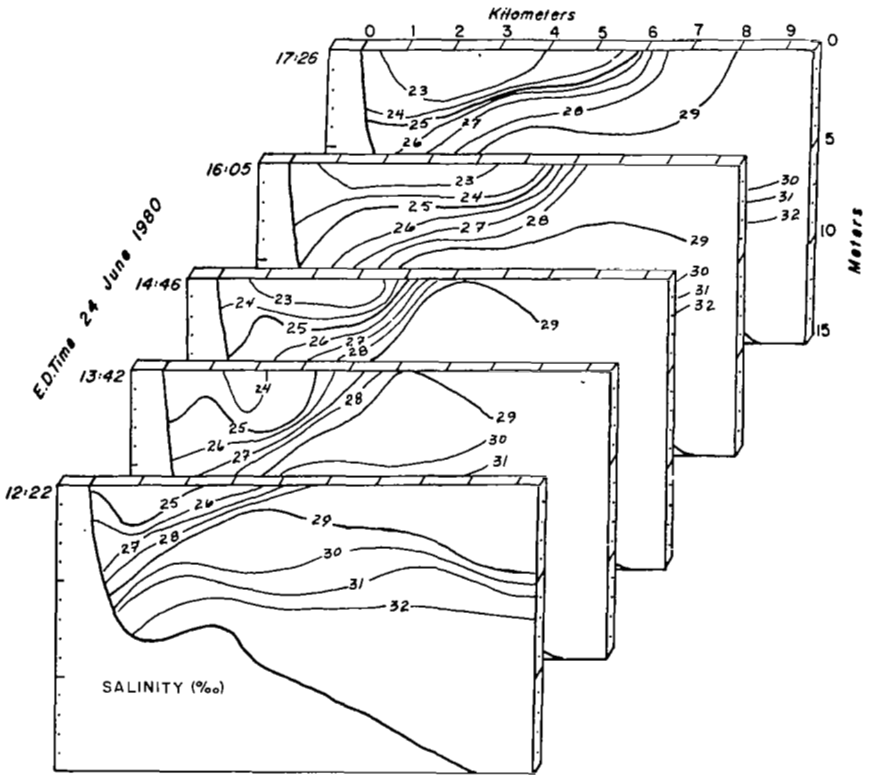

Figure 11.- Salinity distribution off Rudee Inlet on June 24, 1980.

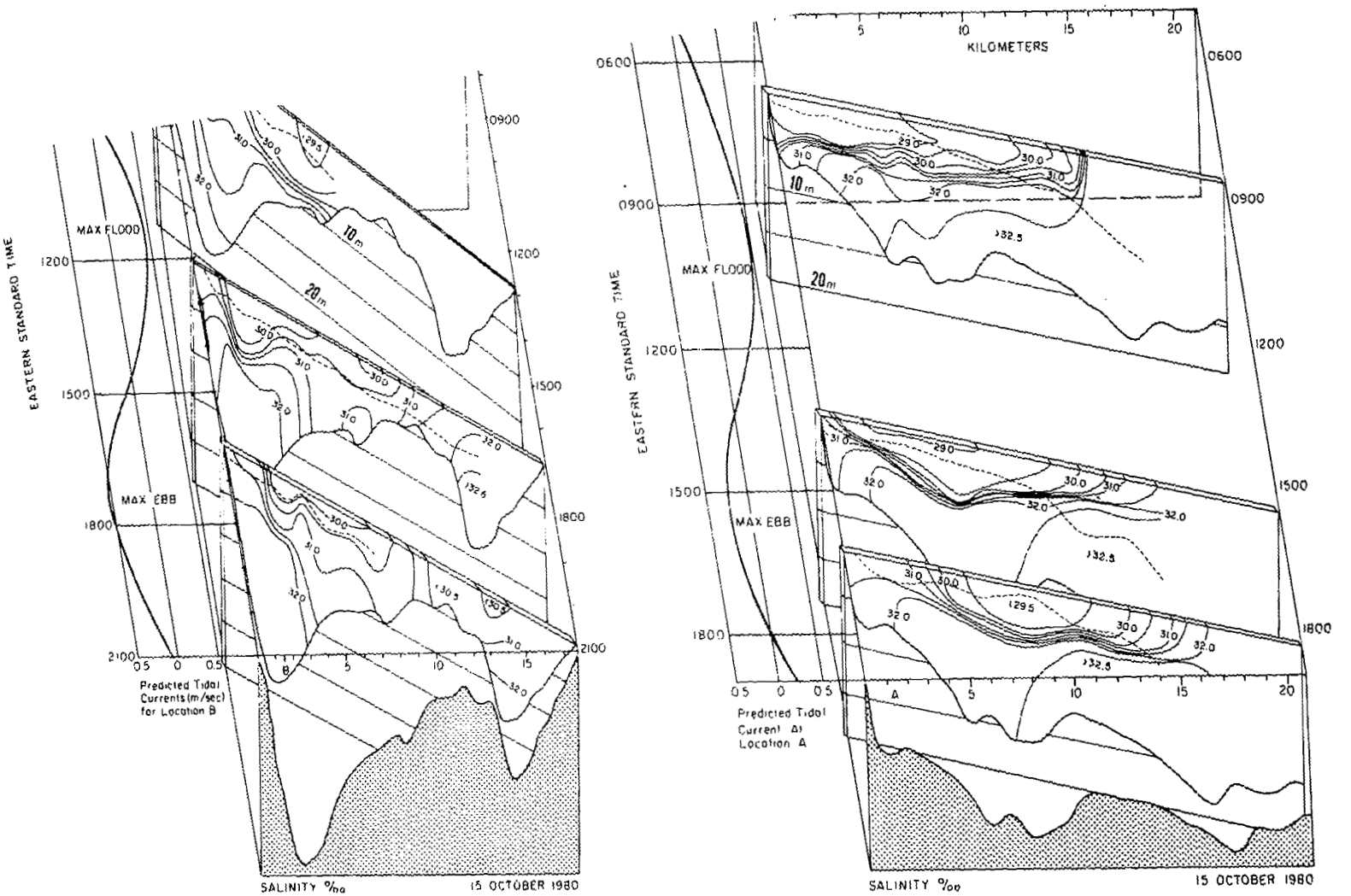

(a) Bay mouth.

(b) Virginia Beach.

Figure 12.- Salinity structure across the Bay mouth and off Virginia Beach on October 15, 1980. Rotation of each section with respect to the time axis indicates time elapsed during sampling. Dashed lines indicate secchi depth.

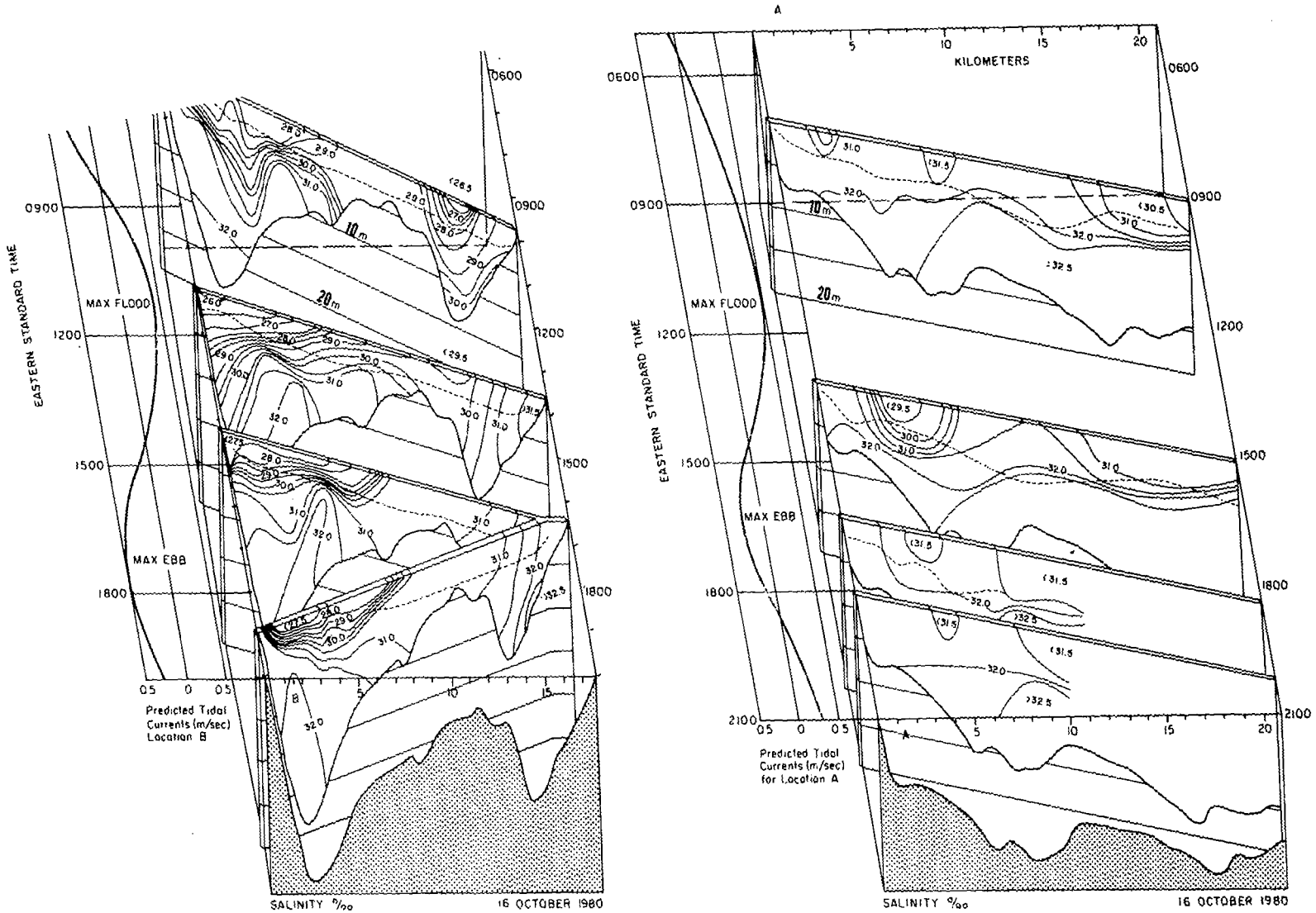

(a) Bay mouth.

(b) Virginia Beach.

Figure 13.- Salinity structure across Bay mouth and off Virginia Beach for October 16, 1980.

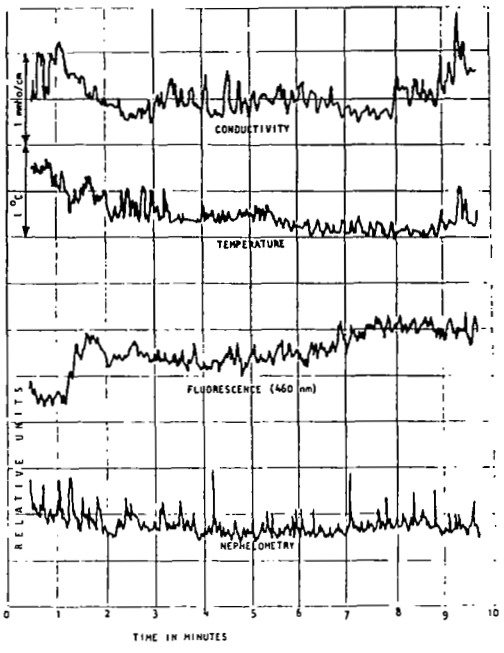

Figure 14.- Example of analog records of conductivity, temperature, fluorescence, and nephelometry obtained from the flow-through system (fig. 6) June 27, 1980.

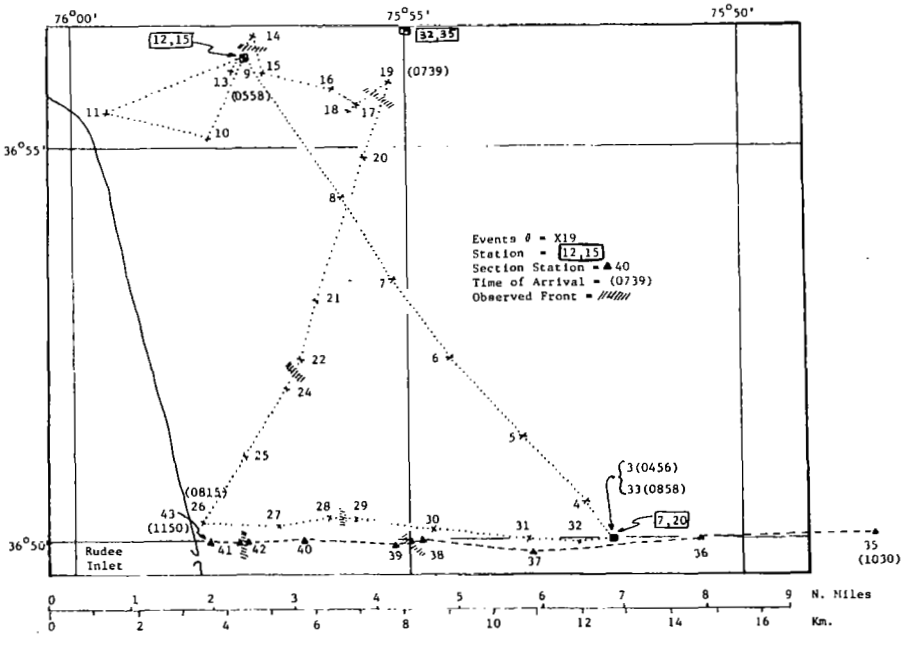

Figure 15.- Detailed cruise track of R/V CAPT. JOHN SMITH on March 19, 1980.

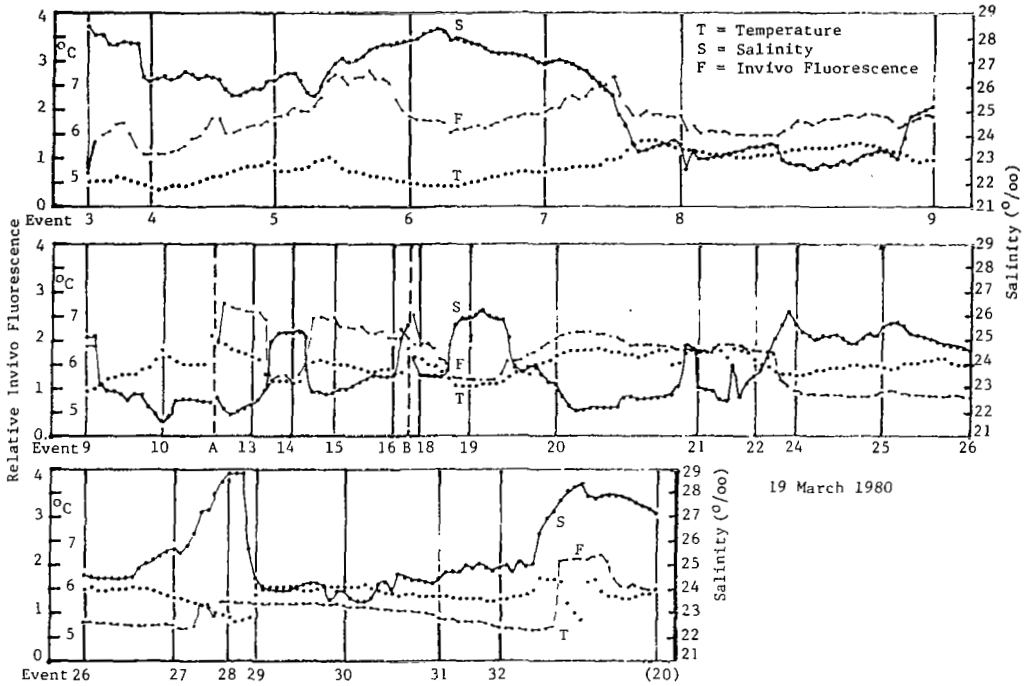

Figure 16.- Temperature, salinity, and fluorescence data obtained along cruise track shown in figure 15.

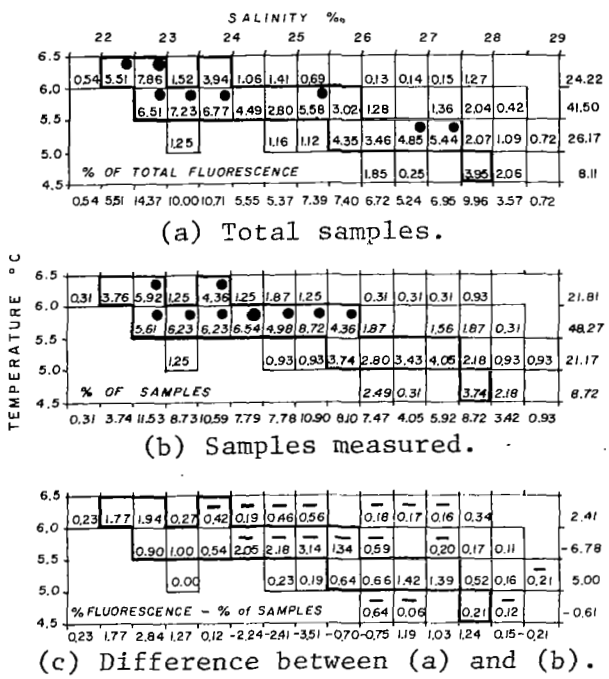

(a) Total samples.

(b) Samples measured.

(c) Difference between (a) and (b).

Figure 17.- Temperature/salinity correlation diagrams showing percent of total fluorescence, percent of samples measured, and their difference for temperature, salinity, and fluorescence data displayed in figure 16.

REMOTE SENSING OF THE CHESAPEAKE BAY PLUME SALINITY VIA MICROWAVE RADIOMETRY

Bruce M. Kendall
NASA Langley Research Center

SUMMARY

The NASA-Langley-developed L-Band microwave radiometer was used to remotely measure sea surface salinity during the March 1980 (Superflux I) and June 1980 (Superflux II) Chesapeake Bay Plume Studies. Obtained measurements of microwave brightness temperatures of the sea surface were combined with measurements of sea surface temperature obtained with an infrared radiometer and inverted to produce corresponding values of sea surface salinity. Results from the plume measurements, which indicate the southward extent of the plume along the Virginia-North Carolina coast, are presented and discussed. Additional measurements obtained for the Delaware Bay Mouth flight on June 17, 1980, and the James River-Shelf flight on June 20, 1980, are also discussed.

INTRODUCTION

The results of several aircraft programs have demonstrated that geophysical parameters such as temperatures, salinity, and thickness of oil spills can be derived from passive microwave measurements with an accuracy that satisfies most user applications (ref. 1). In particular, a technique was demonstrated to remotely measure sea-surface temperature and salinity with a dual-frequency microwave radiometer system (ref. 2). Accuracies in temperature of 1^{o} C and in salinity of 1 part per thousand ($^{0}/00$) for salinity greater than 5 $^{0}/00$ were attained after correcting for the influence of extraterrestrial background radiation, atmospheric radiation and attenuation, sea-surface roughness, and antenna beamwidth. The radiometers, operating at 1.43 and 2.65 GHz, comprise a third-generation system using null balancing and feedback noise injection. This dual-frequency microwave radiometer system was developed at the NASA Langley Research Center for the purpose of obtaining sea-surface temperature and salinity maps of coastal and estuarine areas. As the objectives of the joint NASA-NOAA (NMF) Chesapeake Bay Plume studies were to determine surface extent and concentration of various water quality parameters using synoptic data obtained by remote sensors which could be compared with in-situ-measured sea truth samples, the NASA-Langley microwave radiometer system was flown on-board the NASA-Wallops Flight Center P-3 aircraft during the March 1980 (Superflux I) and June 1980 (Superflux II) experiments to study the Chesapeake Bay Plume surface characteristics. Salinity mappings of the lower Bay area and southward along the Virginia and North Carolina coast were performed to measure the plume extent and movement. These measurements were performed using the L-Band (1.43 GHz)

radiometer to measure salinity and an infrared radiometer to measure sea surface temperature. The S-Band (2.65 GHz) radiometer was not used because of the increased amount of radio interference from coastal radar installations at its frequency.

This paper will describe the theory of the radiometric measurement of salinity and the results of the June 1980 measurements. The results of the March 1980 measurement are not available at this time as a data recording problem with the infrared radiometer precludes a timely reduction of that data.

THEORY AND DATA REDUCTION

The measurement technique is based on the principle that matter, when heated to an equilibrium temperature T, will emit electromagnetic radiation, whose spectral dependency is governed by the Planck radiation law.

It has long been known that Earth's atmosphere is essentially transparent to transmission of electromagnetic radiation at frequencies of 1 to 3 GHz. Extensive work over the years on microwave signal propagation through the atmosphere at centimeter wavelengths has indicated that the influence of clouds is small at these frequencies except under very severe storm conditions. An added factor for consideration is that the background galactic noise tends to decrease substantially as frequencies increase beyond about 1 GHz. Therefore, the frequency regime from 1 to 3 GHz is a well-suited choice for minimizing the effects of extraterrestrial background radiation and atmospheric interference.

Despite these advantages, accurate surface temperature measurement by airborne radiometers in this microwave region requires detailed knowledge of these effects for correcting the instrumental observations. The corrections to the measured brightness temperature of the ocean surface can still be on the order of a few kelvins and therefore, must be taken into account. The apparent temperature T_R (which may also be called the equivalent radiometric temperature of the complete set of received radiations) is calculated from the equation of radiative transfer by making use of the Rayleigh-Jeans approximation to the Planck law (as explained in ref. 2) for a measurement in nadir direction.

$$T_R = T_B[1 - \tau(h)] + (1 - e)[1 - \tau(h)][(T_{cos} + T_{gal})(1 - \tau_o) + T_{atm}] + \tau(h)\langle T\rangle + \Delta T_w + \Delta T_p \qquad (1)$$

The first term accounts for the attenuated $[1 - \tau(h)]$ emission (T_B) from the ocean surface. The second term in equation (1) comprises the temperature of the downward radiation of the extraterrestrial noise $(T_{cos} + T_{gal})$ attenuated $(1 - \tau_o)$ by the entire atmosphere, and the downward radiation T_{atm} of the atmosphere itself, reflected $(1 - e)$ by the ocean surface and in turn attenuated $[1 - \tau(h)]$ by the intervening atmosphere between the ocean and radiometer. The term $\langle T\rangle\ \tau(h)$ is the averaged physical temperature of the intervening atmosphere between the radiometer and the sea surface times the atmospheric opacity $\tau(h)$ for the instrument altitude H. The next term ΔT_w is the

apparent temperature contribution due to the sea surface roughness generated by shear forces of the surface winds. The last term ΔT_p is due to the antenna pattern deviating from the ideal "pencil" beam shape.

The brightness temperature T_B is related to the molecular temperature of a radiating surface via the emissivity of the surface. The emissivity of a dielectric surface at a particular wavelength is determined by its complex dielectric constant which for calm seawater is a function only of temperature and salinity. Therefore, the brightness temperature of the sea surface is given by

$$T_B(\lambda) = e_\lambda(T_s, S)T_s \tag{2}$$

where the emissivity e at the wavelength λ is expressed in terms of surface temperature T_s and salinity S. Plots of brightness temperature as a function of salinity and surface temperature at 1.43 GHz are given in figure 1. The inversion of microwave (L-Band) brightness temperature using the infrared radiometer measurement of surface temperature to salinity is shown graphically in figure 1 and is obtained using derived regression equations.

Although the demonstrated absolute accuracy of the radiometer system is 1 $^0/_{00}$ for salinity (>5 $^0/_{00}$) and 1° C for temperature, the relative accuracy within a given data set is better than 0.5 $^0/_{00}$ and 0.5° C. The spatial resolution of these measurements is given by the antenna beam "footprint" and is one-third of the measurement altitude.

The output data of both radiometers are converted to digital form by a data processor developed at the NASA Langley Research Center. The processor also conditions and formats the housekeeping data from other sources that are necessary for the reduction of the radiometric data, such as flight parameters, time, latitude, and longitude. The data processor is capable of adjusting measurement integration times independent of the radiometer settings. This capability provides an efficient way to adapt the overall integration time to the aircraft altitude and measurement spatial resolution (antenna half-power footprint size).

RESULTS

All the radiometer flight measurements during the June 1980 Superflux II program were made on-board the NASA-Wallops Flight Center P-3 aircraft at an altitude of 152 m and an aircraft speed of 190 knots. As the radiometer antenna footprint or surface resolution cell was 51 m (one-third of the measurement altitude), the resulting measurement time to advance one resolution cell was 0.5 seconds. However, the position data of latitude and longitude which was being recorded from the aircraft inertial navigation system (INS) was up-dated only once every 2 seconds. Therefore, the radiometer measurement data during these series of flights were only sampled and recorded every 2 seconds. The L-Band microwave radiometer had a one-second integration time for the measured data so that the output data was integrated over two

resolution cells. With a two-second sampling rate, only every other integrated measurement was sampled. This fact coupled with the wide spacing between flight lines dictated by flight time restraints resulted in a little less than desirable conditions for the radiometric salinity mapping of a geographical area. However, the obtained data did allow for contour mapping of the measured areas as discussed in the following sections of this paper. The experience obtained during these measurements led to the use of a 0.3-second sampling rate for a series of flight measurements which were later made over the fronts of the Chesapeake Bay Mouth area. This faster sampling rate allows for a much finer scale measurement of salinity which can be seen by using time plots of individual flight lines. This removes the restrictions of the up-date time of latitude and longitude from the data reduction. Although the parameters of latitude and longitude were recorded from the aircraft INS, the resulting long term drifts during the 3-hour flights were prohibitive for the accurate mapping of salinity. Errors as large as 2 nautical miles near the end of a particular flight were experienced. Therefore, the obtained salinity data positions were corrected using data as recorded from the on-board Loran-C system. The following is a discussion, in chronological order, of the radiometric flight measurements made during the June 1980 Superflux II missions.

On June 17, 1980, the radiometric measurement of salinity was performed on several flight lines across the mouth of the Delaware Bay between the hours of 6:37 and 7:40 EDT. Also a few lines were flown from the Bay mouth out over the open ocean. The results of these measurements are shown in figure 2 where salinity contours are shown as a function of latitude and longitude. While the amount of data obtained was limited in terms of geographic area size, the obtained contours are sufficient to show that the Bay mouth during this time period (mid flood tide cycle) has lower salinity waters at the southwestern end and higher salinity waters toward the northeastern end. Figure 2 also shows the gradual increase in salinity as you progress outward from the Bay mouth over the open ocean. Also indicated in figure 2 are the locations of several oil spills that were detected by the L-Band radiometer along the open ocean flight lines. These detections were indicated by a sharp step-function type decrease in the L-Band radiometer measured brightness temperature of several degrees Kelvin.

The next mission was flown on June 20, 1980, between 06:04 and 07:42 EDT which was near the end of the ebb tidal cycle. This flight consisted of a flight line down the James River, across the Chesapeake Bay mouth and out over the open ocean to the continental shelf break and return. The results of this mission are shown in figure 3 where representative salinity numbers are shown along the measurement flight line. This figure shows the general increase in salinity as you progress down the James River toward the saltier Bay waters; the salinity increasing across the Bay entrance toward the open ocean with some variations due to the mixing action of the Bay waters; and then the gradual further increase in salinity outward over the open ocean to the continental shelf break.

The overflight radiometer measurements for the Chesapeake Bay Plume were performed on June 23, 25, and 27, 1980. The approximate locations of the flight lines are shown in figure 4. The measurements of June 23, 1980, were performed

between the hours of 06:00 and 08:33 EDT which was at the middle of the ebb tidal cycle. The obtained salinity contour lines for this measurement are shown in figure 5. In constructing the salinity contours shown in figure 5 from the measured data some liberty had to be taken in contouring between the flight lines (fig. 4) due to their wide spacing. However, the amount of data obtained was sufficient to allow line-to-line contouring that was representative of the general changes in the surface water salinity and thus outline the Chesapeake Bay Plume extent. As seen in figure 5, the lower salinity Chesapeake Bay water flows out, during ebb tidal cycle, through the lower part of the Bay entrance and southward along the Virginia and North Carolina coast to its southernmost extreme. This body of lower salinity Bay water could be described as a salinity plume by the isohalines of figure 5. Also seen in figure 5 are the higher salinity ocean waters being swept into the Bay entrance at the northern end, due to Coriolis forces, but not extending very far up the inside of the Delmarva peninsula as had been previously measured (ref. 2) as the low salinity waters are seen to extend across the entire Bay mouth.

The measurements made on June 25, 1980 were performed between the hours of 05:53 and 08:51 EDT which occurred at the beginning of an ebb tidal cycle. The results of these measurements are shown in figure 6. The most obvious feature of the salinity contours in this figure is the compression of the lower salinity waters inward at the Chesapeake Bay mouth and the narrow width of the plume along the coast. Evidently this was the result of having just undergone a complete flood tidal cycle. This observation can be seen even more clearly if figure 6 is compared with figure 5 which shows the outflowing of the Bay waters during mid ebb tidal cycle.

The last flight measurement of this area was made on June 27, 1980 between 09:34 and 11:38 EDT which was at mid tidal cycle. This mission, however, did not cover the complete area shown in figure 4 as the most southern flight line for this day was line No. 5. The results of these measurements are shown in figure 7. Because of the shorter area of coverage, only the upper portion of the Bay plume is seen in figure 7 as the lower salinity waters exit the Bay entrance. The southern extent of the plume along the coast was beyond the area of measurement.

CONCLUDING REMARKS

The extent of the Chesapeake Bay Plume was mapped by remote measurement of its surface salinity using an L-Band microwave radiometer during the June 1980 Chesapeake Bay Plume Studies (Superflux II). The obtained measurements of microwave brightness temperature of the sea surface were combined with measurements of the sea surface temperature obtained with an infrared radiometer and inverted using a regression analysis to produce corresponding values of sea surface salinity. The results of these measurements demonstrate the utility of using surface salinity as a descriptive feature for the extent of the Chesapeake Bay Plume and one that can be timely measured by a remote sensor. While it would be desirable to have obtained many more measurements over several tidal

cycles and for the different seasons of the year to form a complete data bank of surface salinity measurements for the Chesapeake Bay Plume area, the results obtained, to date, are representative of the Plume and because of the "first time" nature thereby form a benchmark of information which other work or measurements can reference.

REFERENCES

1. Swift, C. T.: Passive Microwave Remote Sensing of the Ocean - A Review. Boundary-Layer Meteorology, vol. 18, 1980, pp. 25-54.

2. Blume, H-J. C.; Kendall, B. M.; and Fedors, J. C.: Sea-Surface Temperature and Salinity Mapping From Remote Microwave Radiometric Measurements of Brightness Temperature. NASA TP-1077, Dec. 1977.

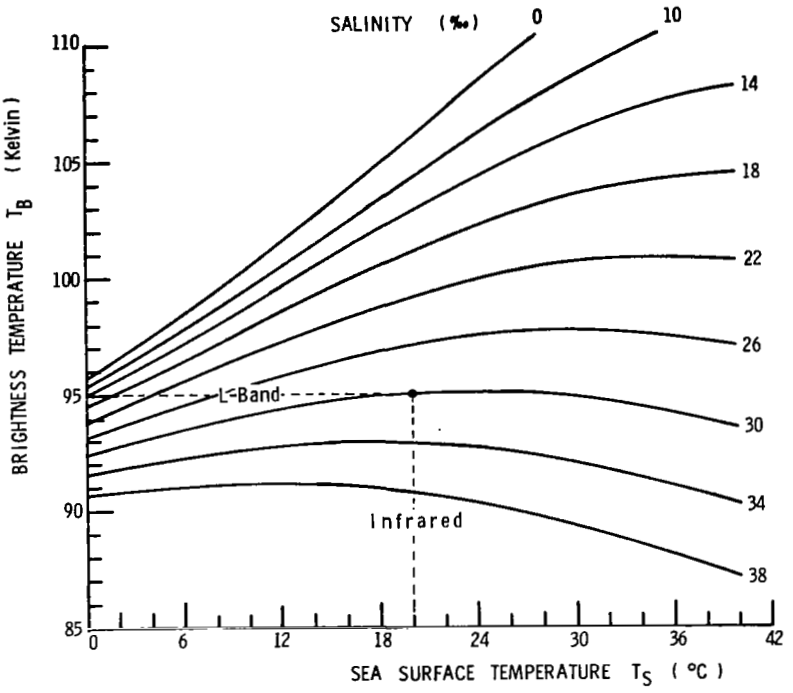

Figure 1.- Brightness temperature at normal incidence versus molecular sea-surface temperature for smooth sea at 1.43 GHz.

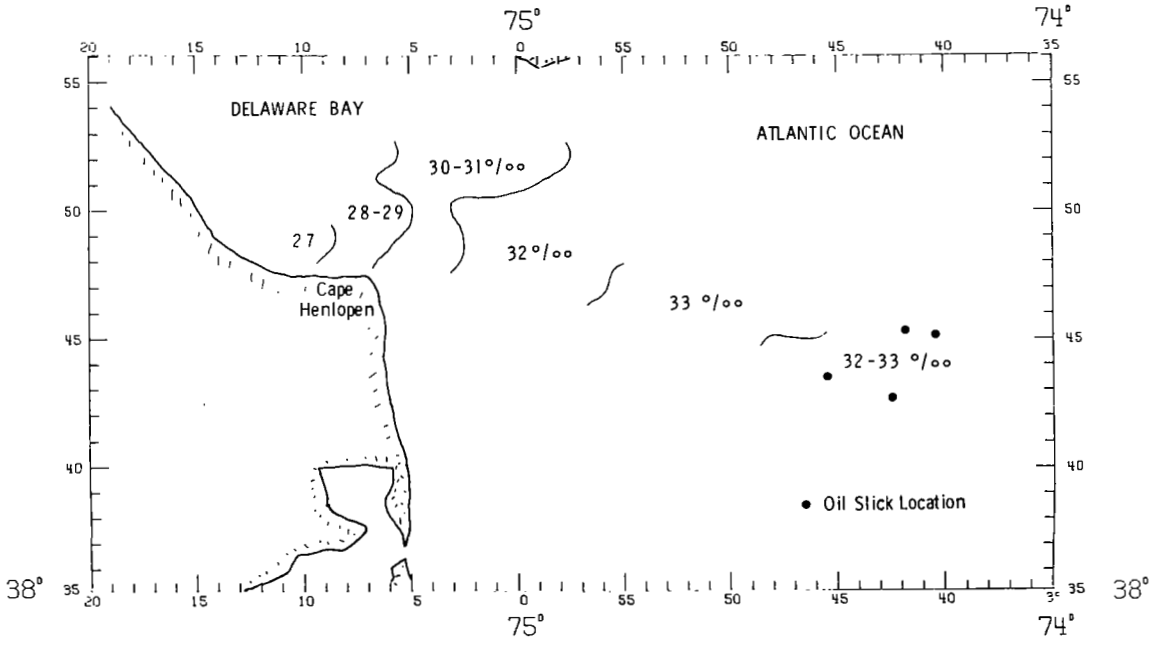

Figure 2.- Salinity map of Delaware Bay Mouth on June 17, 1980 (06:37-07:40 EDT).

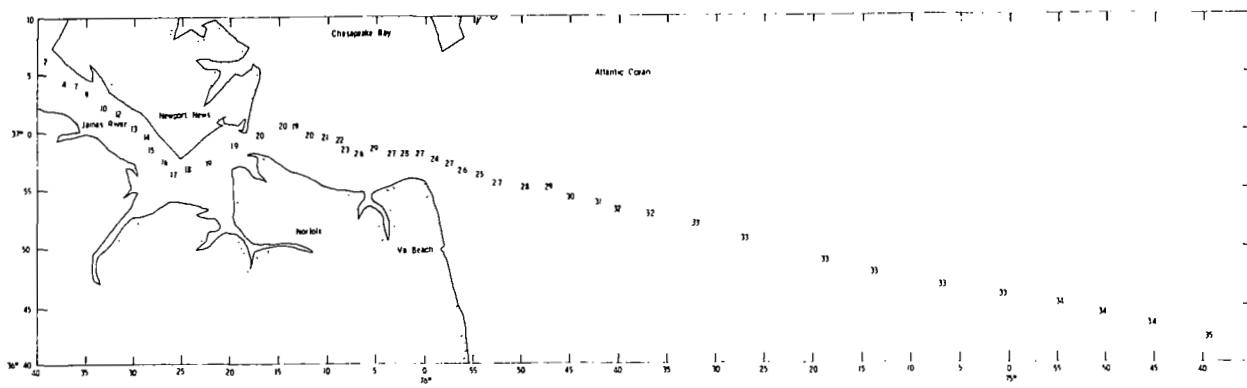

Figure 3.- Average salinity values ($^{0}/00$) for James River-Continental Shelf Break on June 20, 1980 (06:04-07:42 EDT).

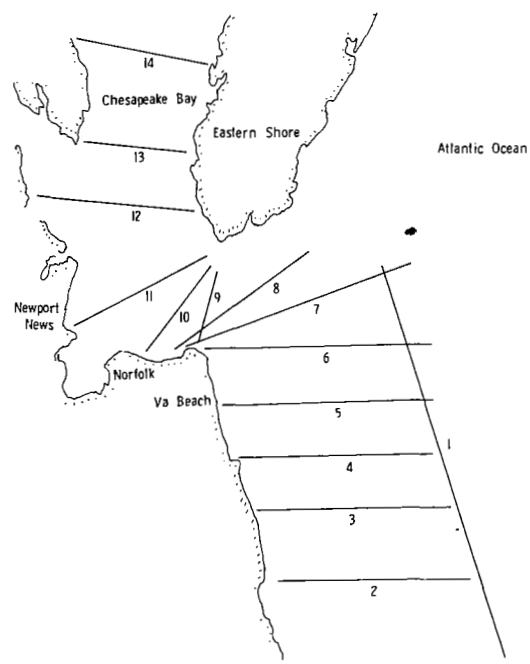

Figure 4.- Flight lines for June 1980 Chesapeake Bay Plume measurements.

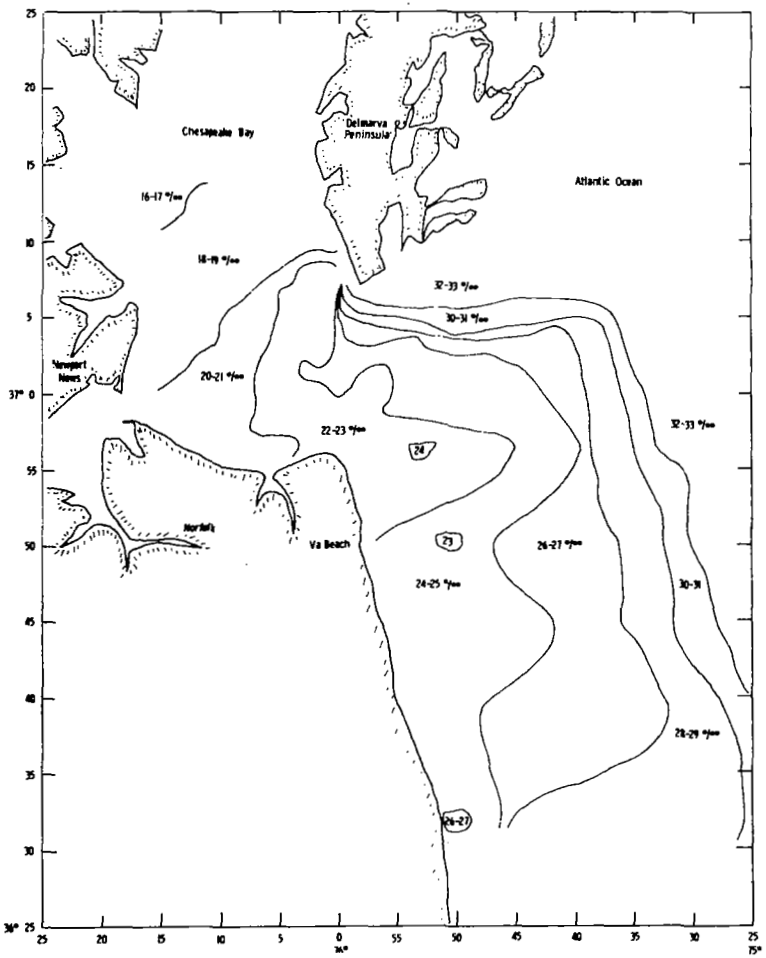

Figure 5.- Salinity map of Chesapeake Bay Plume on June 23, 1980 (06:66-08:33 EDT).

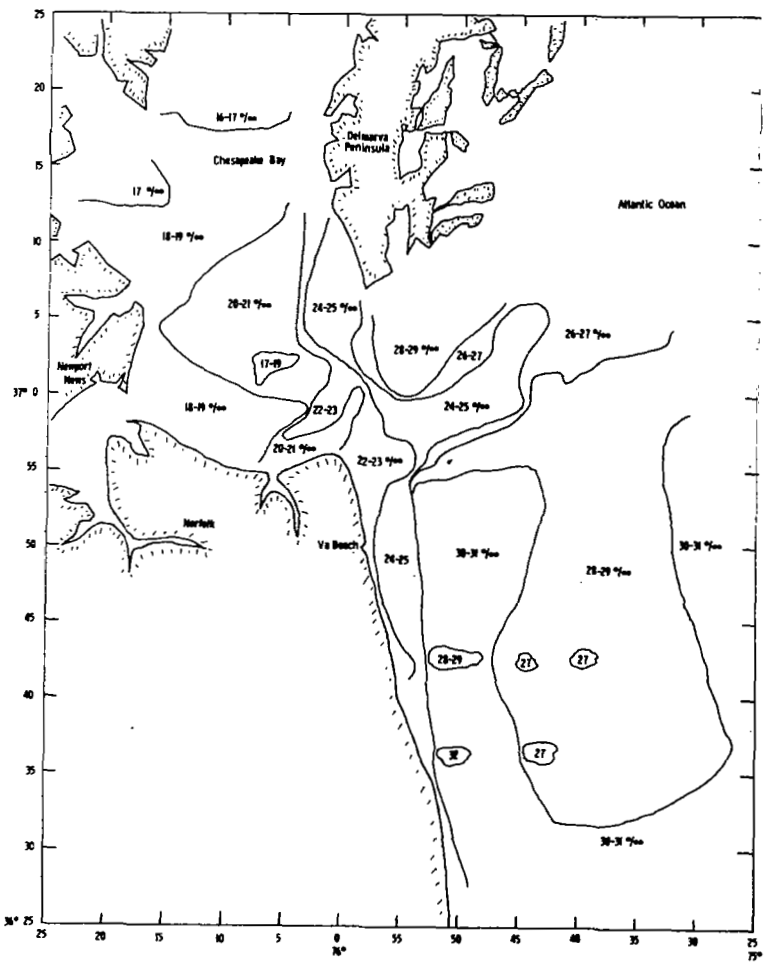

Figure 6.- Salinity map of Chesapeake Bay Plume on June 25, 1980 (05:53-08:51 EDT).

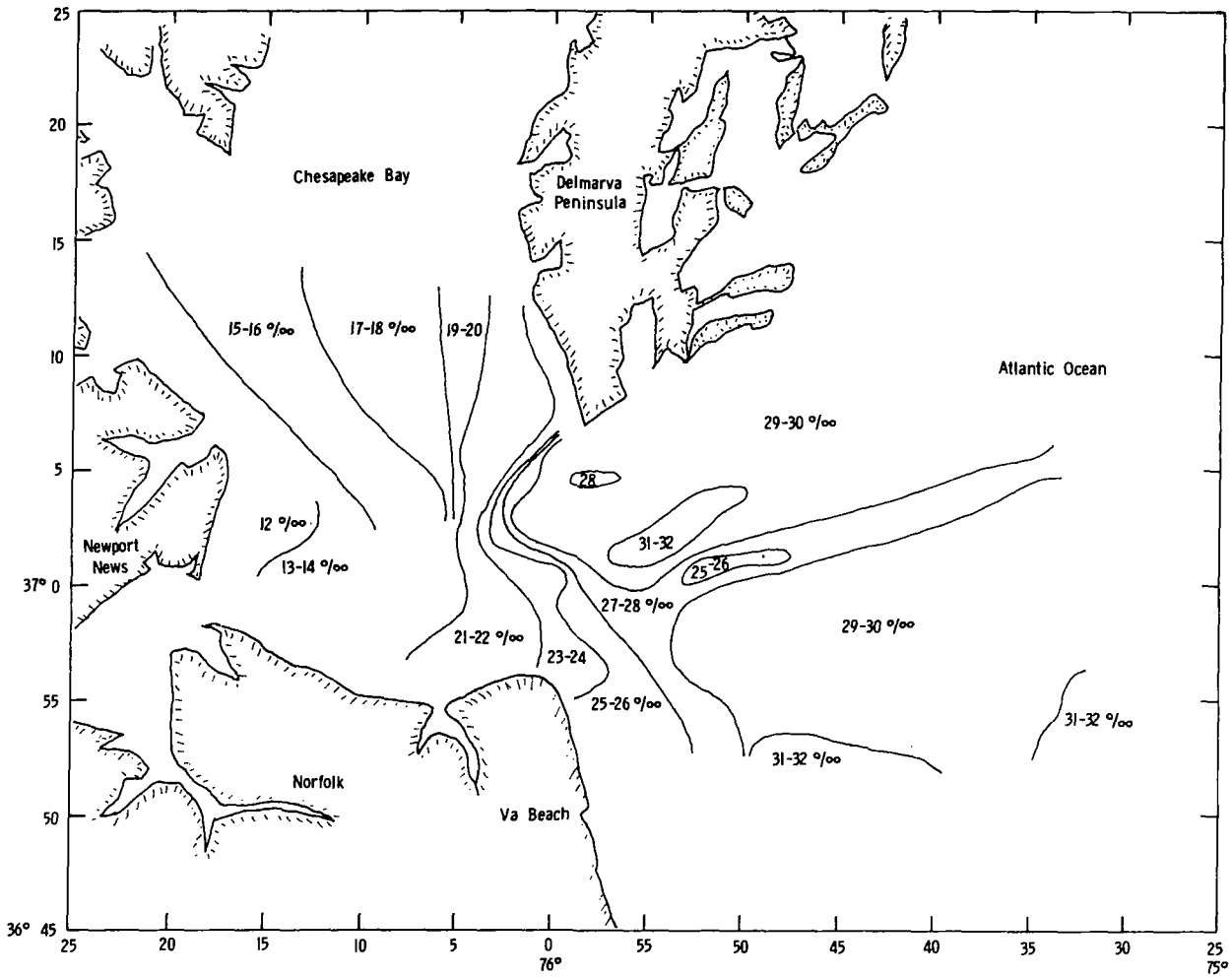

Figure 7.- Salinity map of Chesapeake Bay Plume on June 27, 1980 (09:34-11:38 EDT).

MAPPING WATERMASS BOUNDARIES USING FLUOROSENSING LIDAR[1]

Charles C. Sarabun, Jr.
The Johns Hopkins University
Applied Physics Laboratory
Laurel, Maryland

SUMMARY

An initial application of multispectral LIDAR data from the NASA Airborne Oceanographic Lidar (AOL) to the mapping of watermass boundaries is presented. The approach uses the multispectral lidar data from the fluorosensing mode in a cluster analysis to define water types. Individual data points are classified as to parent water type(s) and then plotted in plan view to show the watermass boundaries and mixing regions. The methodology was applied to the AOL data from the 23 and 25 June SUPERFLUX overflights. The results are compared to salinity-mapping radar results from the same region.

INTRODUCTION

The regions where two or more different watermasses meet are usually characterized by a high degree of spatial and temporal variability. They are often the sites of locally intense mixing and interacting smaller-scale phenomena such as intrusions and interleavings. Field studies of such regions are difficult because of the multiplicity of length and time scales present, and conventional shipborne hydrographic techniques often cannot provide adequate spatial resolution or data of a sufficiently synoptic character. Remote sensing systems have the capability to survey large areas on a nearly synoptic basis and many of these systems are capable of providing the needed spatial resolution. Since investigators have shown that watermasses with distinct physical origins and histories often have a distinct biochemical makeup as well, (refs. 1,2,3,4), remote sensing systems which measure biochemical parameters could be employed to characterize water types present in a survey region, and to map their horizontal structure. One such system is the Airborne Oceanographic Lidar (AOL) operated by NASA/ Wallops Flight Center. This system actively irradiates the water column with light at a fixed wavelength, and measures the intensity of the return signal. Operated in the fluorosensing mode, the system measures a wideband spectrum of laser-stimulated fluorescence from the biochemical constituents of the water, such as chlorophyll and other light-absorbing pigments.

[1]This work was partially supported under Navy Contract N00024-81-C-5301.

To use the fluorosensing AOL data for classifying water types, one would ideally like to use all of the information available in the return spectra simultaneously. A convenient technique for dealing with data vectors consisting of many measured parameters is cluster analysis. Cluster analysis is a method of dividing a total data set into groups, or clusters, using all of the measured parameters. In this paper we describe an initial application of such a technique to AOL fluorosensing data. The data were obtained on 23 and 25 June as part of an examination of the application of aircraft remote sensing to the study of the Chesapeake Bay outflow. The AOL operation and data set are described elsewhere in these proceedings (ref. 5).

The data sets used in the analysis consisted of discrete spectral samples in twenty bands, plus simultaneously recorded data from a thermal infrared scanner. A sample AOL spectrum is shown in Figure 1. The 23 June data set consisted of 4053 sample spectra taken along the flightlines shown in Figure 2a. The 25 June data set consisted of 5410 sample spectra along the flightlines shown in Figure 2b. The data were smoothed along each flightline and rescaled to the interval [-1, +1] so that subsequent processing would not be dominated by any single band.

ANALYSIS METHODOLOGY

Analysis of the AOL data proceeded in three stages, (1) empirical orthogonal function (EOF) decomposition to reduce the dimensionality of the sample spectra, (2) cluster analysis to define basic water types and (3) projection of each data point on the characteristic vectors of the water types to determine the spatial distribution of each water type. Each of these processing stages is discussed below.

EOF Analysis

Because many of the spectral peaks seen in Figure 1 cover several adjacent spectral bands, the AOL data were subjected to an EOF decomposition to define a new orthogonal basis for the spectrum. This new basis is computed from the covariance matrix formed by using the entire set of spectral samples to compute the covariance between bands. The eigenvectors of this matrix form the new basis, and the eigenvalues represent the amount of the total variance in the data accounted for by the associated eigenvector (ref. 6). In practice, the first several eigenvalues accounted for almost all of the variance in the data. This fact allowed the dimensionality of the problem to be reduced in subsequent analysis by retaining only major contributions to the variance in the transformed spectra. The reduced, transformed spectra were then used in the cluster analysis (in what follows, sample spectrum means the transformed, reduced spectrum).

Cluster Analysis

The cluster analysis provides a means for dividing the total set of sample spectra into subsets, called clusters, where the sample spectra in each cluster are somehow similar. These clusters are then assumed to represent characteristic water types present in the surveyed region. There exists a variety of similarity (and dis-similarity) measures which could be used to subdivide the data (refs. 7,8). The similarity criterion used in the examples presented in this paper is essentially a distance measure in a space whose axes are the spectral bands of the sample spectra. A distance measure was selected to facilitate the assignment of percentages in the final stage of processing.

The distance measure used here is the ℓ_∞ norm where the distance, d_{ik}, between any two points $\vec{x}_i$ and $\vec{x}_k$ is defined as

$$d_{ik} = \underset{j}{\text{Max}} |x_{ij} - x_{kj}| \tag{1}$$

where j denotes a spectral band. The data are then arbitrarily divided into a given number of clusters, say L, and the centroid $\vec{Y}_k$ of the kth cluster is computed as

$$Y_{kj} = \frac{1}{m_k} \sum_{i=1}^{m_k} x_{ij} \tag{2}$$

where m_k is the number of sample spectral in the kth cluster and j is the spectral bands. The sum of the distances, E_k, of each element of the kth cluster from the cluster centroid is then computed as

$$E_k = \sum_{i=1}^{m_k} \left[\underset{j}{\text{Max}} |x_{ij} - Y_{kj}| \right] \tag{3}$$

The sum, D, of the E_k forms the objective function tested by the clustering algorithm to determine the locally optimal subdivision of the data into the prespecified number of clusters.

In application, each data point is experimentally transferred from its parent cluster to every other cluster until D reaches a minimum for that cluster level. Note that D_{min} is monotonically decreasing for increasing numbers of clusters, until $D_{min}=0$ when every point defines a separate cluster. The number of clusters, and hence water types, selected must depend in part upon the shape of the D versus cluster number curve, and the

physical significance of the number of clusters.

Projection of the Sample Spectra on the Cluster Centroids

The ultimate goal of the analysis is to classify each sample spectrum as to the parent water type(s) which makes up its spectral shape. We therefore wish to compute the scalar coefficients, A_k, such that

$$\max_j \left| x_{ij} - \sum_{k=1}^{L} A_k Y_{kj} \right| \tag{4}$$

is a minimum subject to the constraints that

$$\sum_{k=1}^{L} A_k = 1$$
$$0 \leq A_k \leq 1 \; . \tag{5}$$

This can be cast as a straightforward linear programming problem (ref. 9) which yields the desired A_k. Note that the A_k represent the proportion of each basic water type making up a particular $\vec{x}_j$, and that the criteria for best fitting the A_k has the same distance measure as the clustering algorithm.

To this point in the processing, no spatial information has been employed (except to assist in selecting an appropriate cluster level). The method classifies each data point based entirely upon its spectral characteristics. The results of the classification are then plotted in physical space to show the distributions of the different water types.

APPLICATIONS TO AOL FIELD DATA

The analysis technique described above was applied only to those flightlines outside the Bay mouth to attempt to define the boundaries of the Chesapeake Bay outflow plume. An L-band salinity mapping radar was flown simultaneously with the AOL and provides a basis for comparison with the AOL results reported here (ref. 10).

June 23, 1980 Data Set

The first data set considered was obtained during early ebb on 23 June 1980. The subset of flightlines used contained 1994 sample spectra. The EOF analysis was performed on the rescaled data and the sample spectra were transformed using the new basis. Since the first four eigenvectors accounted for 97 percent of the variance (Table I) only the spectral bands corresponding to the first four eigenvectors were retained in the transformed spectra.

The transformed sample spectra were then subdivided into one, two, three, four, and five clusters. Figure 3 shows a plot of D_{min} versus cluster number. D_{min} is monotonically decreasing and each increase in cluster number results in a decreasing reduction the value of D_{min}. Figure 4 shows the results of the clustering at the two and three cluster level. Note that the plume structure remains essentially unchanged but that the offshore region contains more structure at the higher cluster level. We thus have a well-defined baywater plume and an offshore region which can be further subdivided into at least two different water types; therefore the percentage distribution of the three water types, plume and two offshore water types, was computed for this data set.

Figure 5 shows the percentage distributions of the three water types. For comparison, the L-Band salinity map is shown in Figure 6. Our results show the Bay plume, Figure 5a, extending southward along the coast with two distinct bulges. The northward bulge is clearly the emerging plume for the current tidal cycle (the tide stage is early ebb), while the second bulge may well represent a remnant plume from the previous tidal cycle. The other two water types are shelf waters which have been subdivided into two sets, shelf water from north of the Bay mouth, Figure 5b, and shelf water from southeast of the Bay entrance, Figure 5c. Evidence that the second bulge of the plume is from a previous tidal cycle is seen in Figure 5b where an isolated pocket of northern shelf water lies between the southeast shelf water and the Bay water. A new influx of northern shelf water is apparent at the top of Figure 5b.

A comparison of the structure mapped by the analysis techniques used here and the L-band salinity map shows good agreement between the two within the license taken in contouring provided by the wide flightline spacing. Notice, however, that the clustering approach has been able to distinguish between two types of shelf water, especially east of the Bay entrance, thus providing potentially useful information about the complex circulation in this region.

June 25, 1980 AOL Data Set

The 25 June data set analyzed consisted of 3109 sample spectra. The results of the EOF analysis are given in Table I, where 97 percent of the variance is accounted for by the first four eigenvectors. The transformed spectra were clustered in the same way as the 23 June set, and the D_{min} values versus cluster number are plotted in Figure 3. The variance is more distributed over the eigenvectors than for the 23 June case, and there is a more evident difference between clustering at the two- and three-cluster level, Figure 7. For comparison with the 23 June results the analysis of this data set continued at the three-cluster level.

The results of mapping water type percentages are shown in Figure 8. These plots are considerably different from the results presented in Figure 6. Here we see that despite being very near slack water after flood in the tidal cycle, the Bay water type covers the whole northern and western portion of the region near the Bay entrance, with a band of roughly uniform width extending southward along the coast. Notice that the bulges seen on 23 June are not in evidence here. The other two water types defined by the technique are not as clearly distinguishable as in the previous example. Type 2, Figure 8b, could be interpreted either as northern shelf water trapped from the previous ebb cycle as in the 23 June case, or as an intermediate type consisting of a mixture of shelf, Figure 8c, and plume water.

The L-Band salinity map also shows a high degree of variability (Figure 9). Notice that the plume boundary of Figure 8a closely parallels the dotted boundary overlaid in Figure 9. The cluster analysis does not show the higher salinity tongue just south of Cape Charles in Figure 9. Also in Figure 9, the high salinity band (30-31 ppt) southeast of Cape Henry corresponds well with the type 2 water defined by the cluster analysis. The complex structure seen in Figure 9, especially the high salinity band, and the eastern extent of the plume in the northeast as defined by the cluster analysis could well be the result of offshore wind driving the surface waters eastward. Such a situation would spread the Bay water eastward of the Bay entrance, and could also result in local upwelling at the location of the high salinity band of Figure 9.

SUMMARY AND CONCLUSIONS

The results presented above are only preliminary; however, the methodology described here is shown to effectively define water types based solely on the AOL spectrum and the thermal infrared scanner data. It is noteworthy that despite the fact that no spatial information was employed in the analysis, the method divides the data into spatially contiguous, physically plausible clusters. A comparison of the results of the cluster analysis with a very limited alternate data set shows good agreement in general, although differences are apparent in detail. The complexity of the spatial structure developed for 25 June (both salinity and water type mapping) precludes detailed interpretation without additional supporting information such as wind conditions and exact tide stage.

The 25 June water type mapping results, in contrast, show a smooth, realistic structure. The clear delineation of three basic water types and the spatial plots of their distribution are suggestive of the circulation pattern in the region. On ebb, the Bay water emerges and flows south along the coast while shelf water from along the Delaware Peninsula is transported southward and lies between the plume water and shelf water from southeast of the Bay entrance. South of Cape Henry, the three water types interact and mix. During flood, the tidal currents off Virginia Beach are

directed roughly northwest which results in the trapping during flood of plume water and northern shelf water in the inshore region south of Cape Henry. Early in each ebb cycle these trapped remnants are still in evidence. For the plume, this results in the double bulge seen in Figure 6a, and the scalloping of the plume seen in SEASAT-SAR imagery of the coast south of Cape Henry. Thus, to the extent that the analysis defines realistic water types, the results provide useful information about the distribution of those water types and the circulation patterns which can produce such distributions.

With respect to the analysis methodology a number of areas bear further investigation. In the results presented here three analysis steps were performed, the EOF analysis, the clustering, and the assignment of water type percentages. For the EOF analysis the data were rescaled to [-1, +1] so that no single spectral band would dominate the results. One would certainly like to investigate other scalings such as unit variance scaling, no scaling, or some weighted rescaling. Further, one should investigate including the L-band results in the analysis as an additional dimension of the data vectors since these data were obtained simultaneously with the AOL data. In clustering the data the ℓ_∞ norm was used since that distance measure was easily employed in the later assignment of water type percentages. However, other norms do exist such as the euclidean or ℓ_2 norm and the ℓ_1 norm,

$$\sum_j |x_{ij} - x_{kj}| \qquad (6)$$

The second measure can easily be accommodated by the linear programming approach used in the third stage of the processing. The euclidean norm could also be accommodated by casting the assignment problem as a quadratic programming problem (ref. 11). Finally, the selection of final cluster level is presently subjective in that no absolute objective criterion exists for choosing an optimal cluster level. In practice it may not be possible to develop such a criterion in view of the monoticity of D_{min} with cluster level, however it may be possible to refine the selection process by also considering the distributions of number of spectra in each cluster and the mean and variance of the distance of sample spectra from their cluster centroids.

Despite the fact that none of the above variations was included in the preliminary analysis reported here, the results are physically realistic and compare favorably with a limited comparative data set. Further refinements in the approach may well improve the overall quality and confidence of the final results.

REFERENCES

1. Sarabun, C. C.: Structure and Formation of Delaware Bay Fronts. PhD. Dissertation, College of Marine Studies, University of Delaware, 1980.

2. Sick, L. V.; Johnson, C. C.; and Engel, A.: Trace Metal Enhancement in the Biotic and Abiotic Components of an Estuarine Tidal Front. Journal of Geophysical Research 83(C9), 1978, pp. 4659-4667.

3. Tyler, M. A.; and Seliger, H. H.: Annual Subsurface Transport of a Red Tide Dinoflagellate to Its Bloom Area: Water Circulation Patterns and Organism Distributions in the Chesapeake Bay. Limnology and Oceanography, 23(2), 1978, pp. 227-246.

4. Wiebe, P. H.; Hulbert, E. M.; Carpenter, E. J.; Jahn, A. E.; Knapp, G. P., III; Boyd, S. H.; Ortner, P. B.; and Cox, J. L.: Gulf Stream Cold Core Rings: Large-scale Interaction Sites for Open Ocean Plankton Communities. Deep-Sea Research, 23, 1976, pp. 695-710.

5. Hoge, F.; and Swift, R. N.: Application of the NASA Airborne Oceanographic Lidar to the Mapping of Chlorophyll and Other Organic Pigments. Chesapeake Bay Plume Study - Superflux 1980, NASA CP-2188, 1981 (Paper no. 26 of this compilation).

6. Wallace, J. M.; and Dickinson, R. E.: Empirical Orthogonal Representation of Time Series in the Frequency Domain. Part I: Theoretical Considerations. Journal of Applied Meteorology, 11(6), 1972, pp. 887-892.

7. Sneath, P. H. A.; and Sokal, R. R.: Numerical Taxonomy: The Principles and Practice of Numerical Classification. W. H. Freeman and Company, San Francisco, 1973.

8. Spath, H.: Cluster Analysis Algorithms for Data Reduction and Classification of Objects. John Wiley and Sons, New York, 1980.

9. Sarabun, C. C.: System Identification in Nonlinear Differential Equations by Quasi-linearization and Linear Programming. Masters Thesis, Univ. North Dakota, 1973.

10. Kendall, Bruce M.: Remote Sensing of the Chesapeake Bay Plume Salinity Via Microwave Radiometry. Chesapeake Bay Plume Study - Superflux 1980, NASA CP-2188, 1981 (Paper no. 10 of this compilation).

11. Hadley, G.: Linear Programming. Addison - Wesley Publishing Company, Inc., Reading, Mass., 1962.

TABLE I

PERCENT VARIANCE ACCOUNTED FOR BY
FIRST FOUR EMPIRICAL ORTHOGONAL FUNCTIONS.

EOF	23 June	25 June
1	89.5	73.8
2	3.6	12.4
3	2.5	8.6
4	1.4	1.7
TOTAL	97.0	96.5

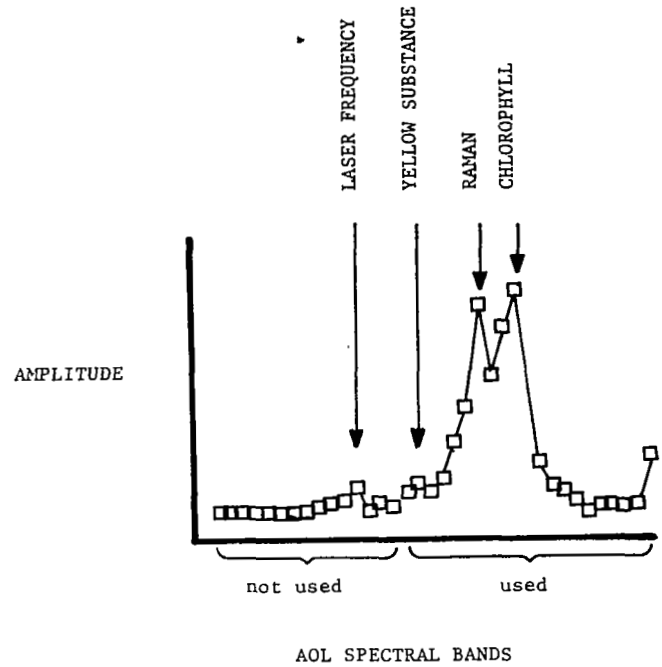

Figure 1.- AOL return spectrum. Only the leftmost 20 channels were used in the analysis. Major peaks are annotated. (Provided by F. Hoge and R. Swift, NASA/Wallops Flight Center.)

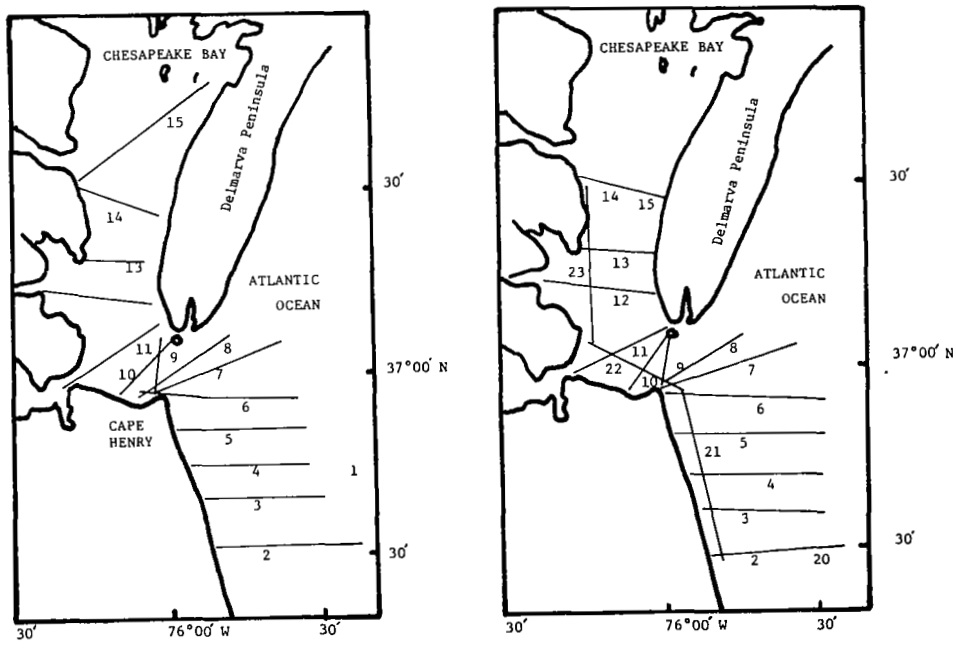

(a) June 23. (b) June 25.

Figure 2.- June 23 and 25 AOL flight lines.

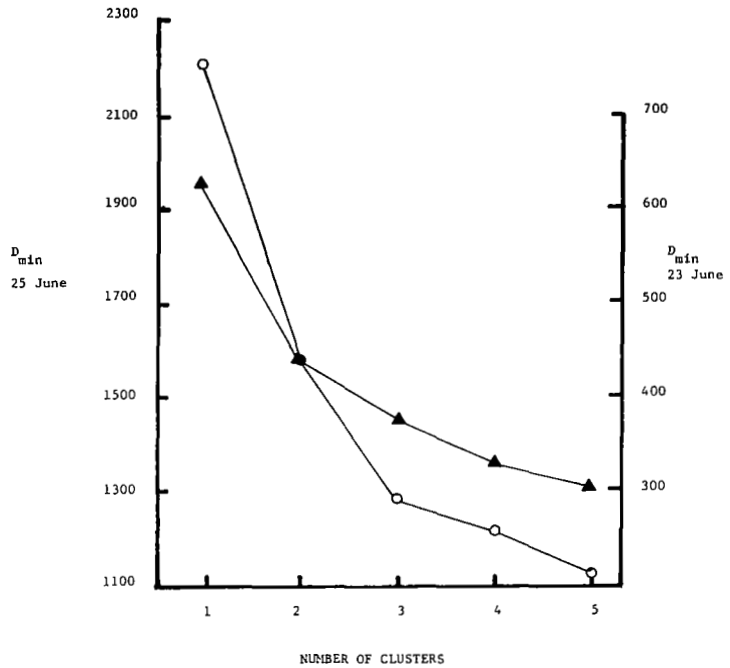

Figure 3.- D_{min} versus number of clusters for 23 June (▲) and 25 June (O).

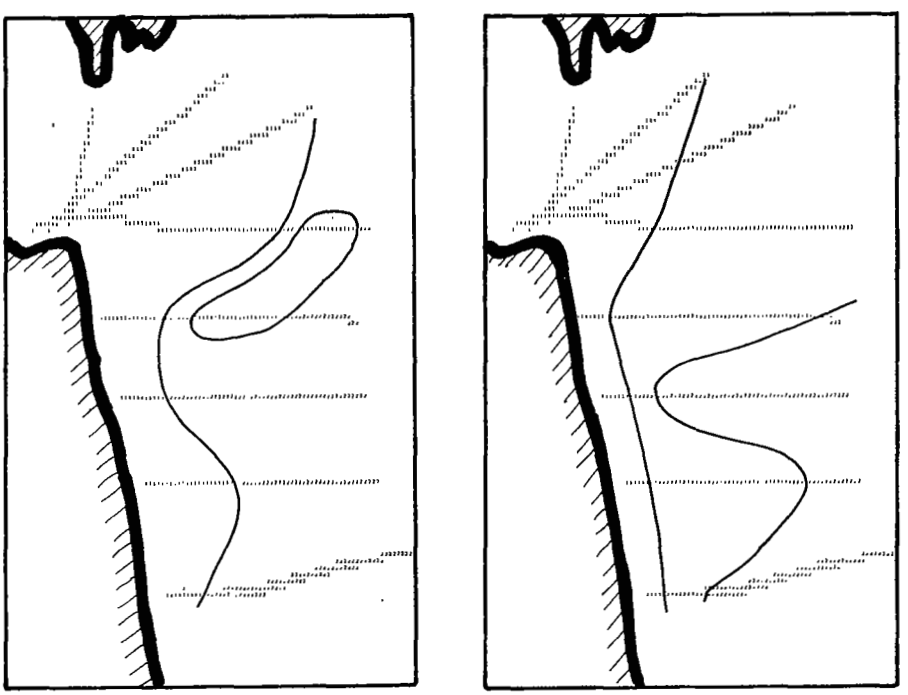

(a) Two clusters. (b) Three clusters.

Figure 4.- Spatial distribution of cluster assignments for June 23 for two and three clusters.

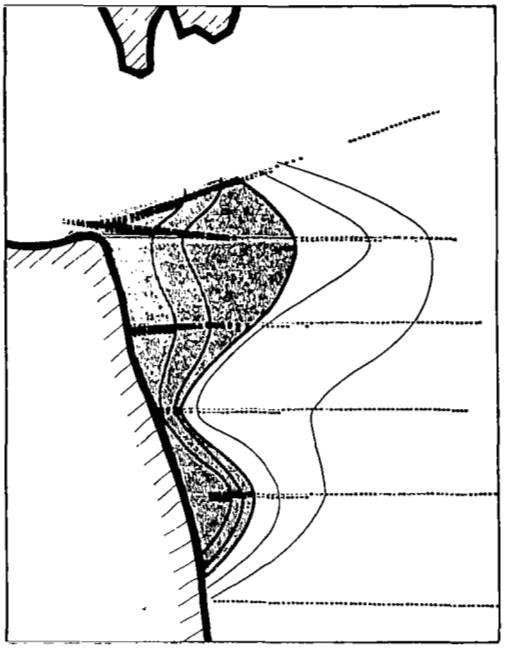

(a) Shaded areas indicate more than 50% water type 1.

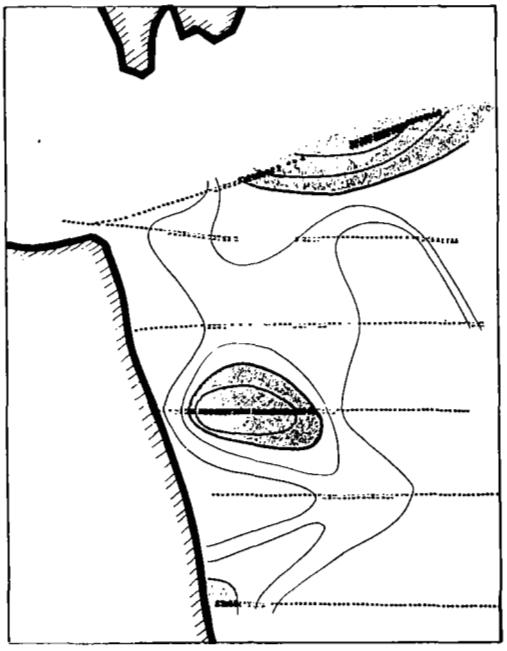

(b) Shaded areas indicate more than 50% water type 2.

Figure 5.- Spatial distribution of water types 1, 2, and 3 for June 23.

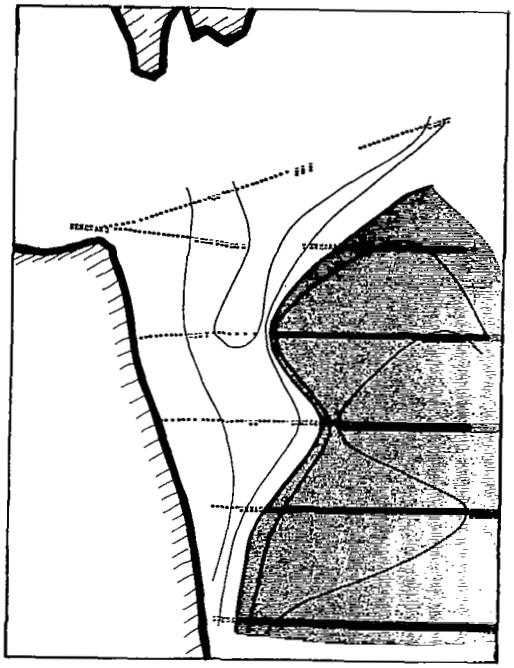

(c) Shaded areas indicate more than 50% water type 3.

Figure 5.- Concluded.

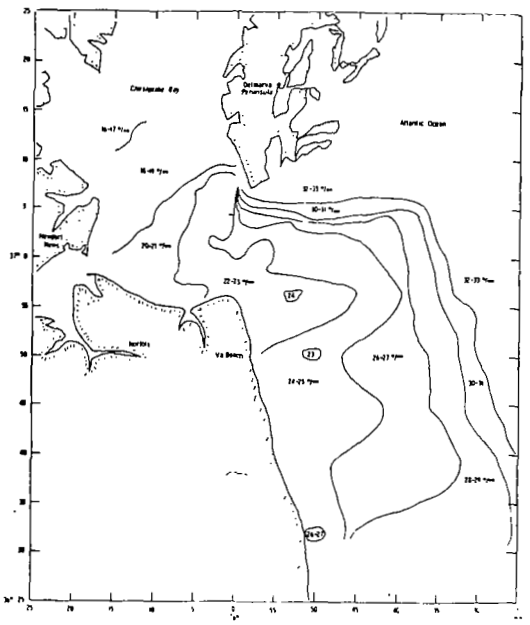

Figure 6.- L-band microwave radiometer salinity map (from ref. 10).

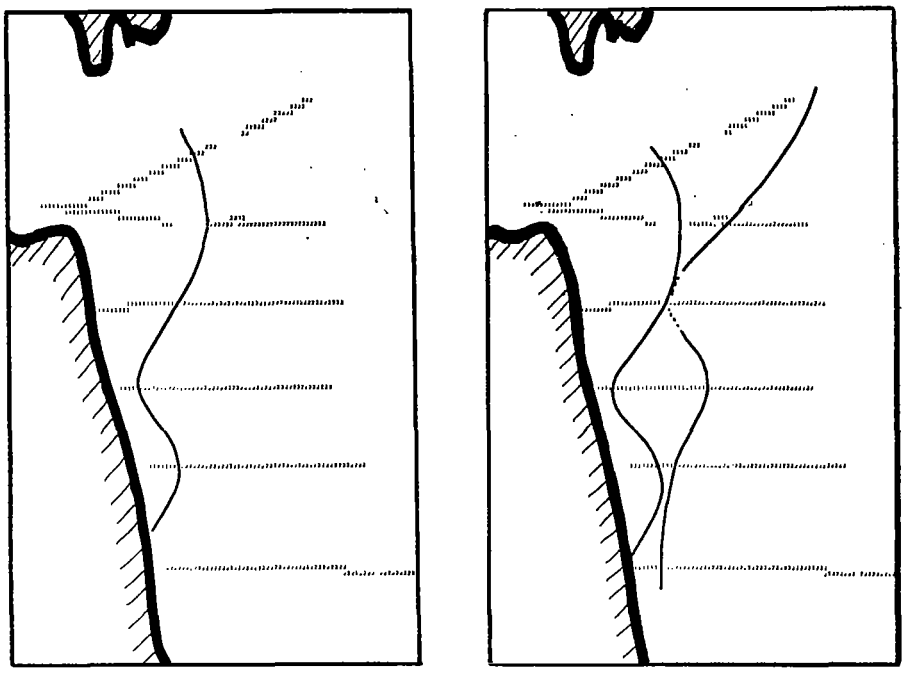

(a) Two clusters. (b) Three clusters.

Figure 7.- Spatial distribution of cluster assignments for June 25 for two and three clusters.

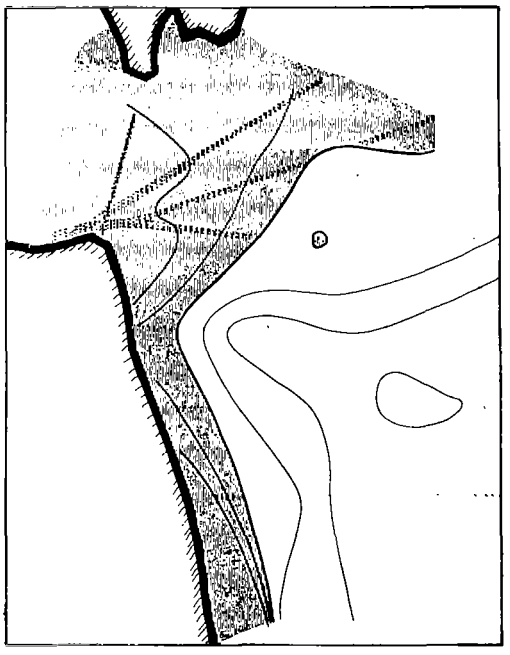

(a) Shaded areas indicate more than 50% water type 1.

Figure 8.- Spatial distribution of water types 1, 2, and 3 for June 25.

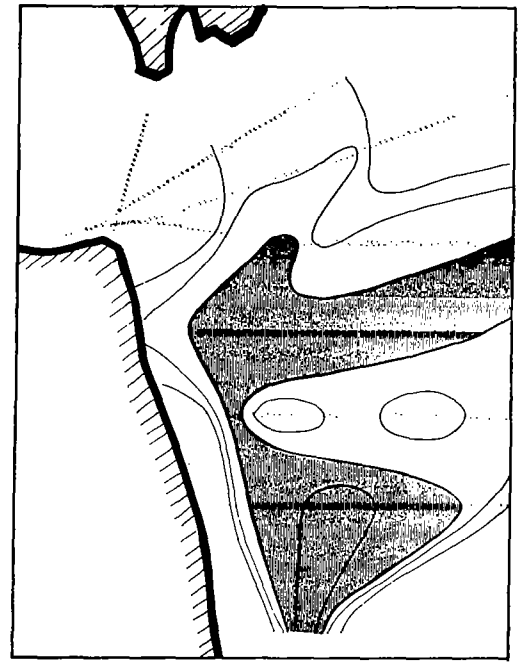

(b) Shaded areas indicate more than 50% water type 2.

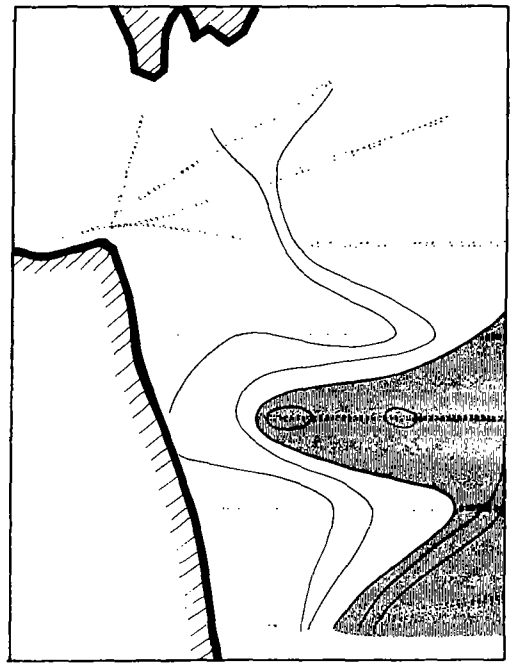

(c) Shaded areas indicate more than 50% water type 3.

Figure 8.- Concluded.

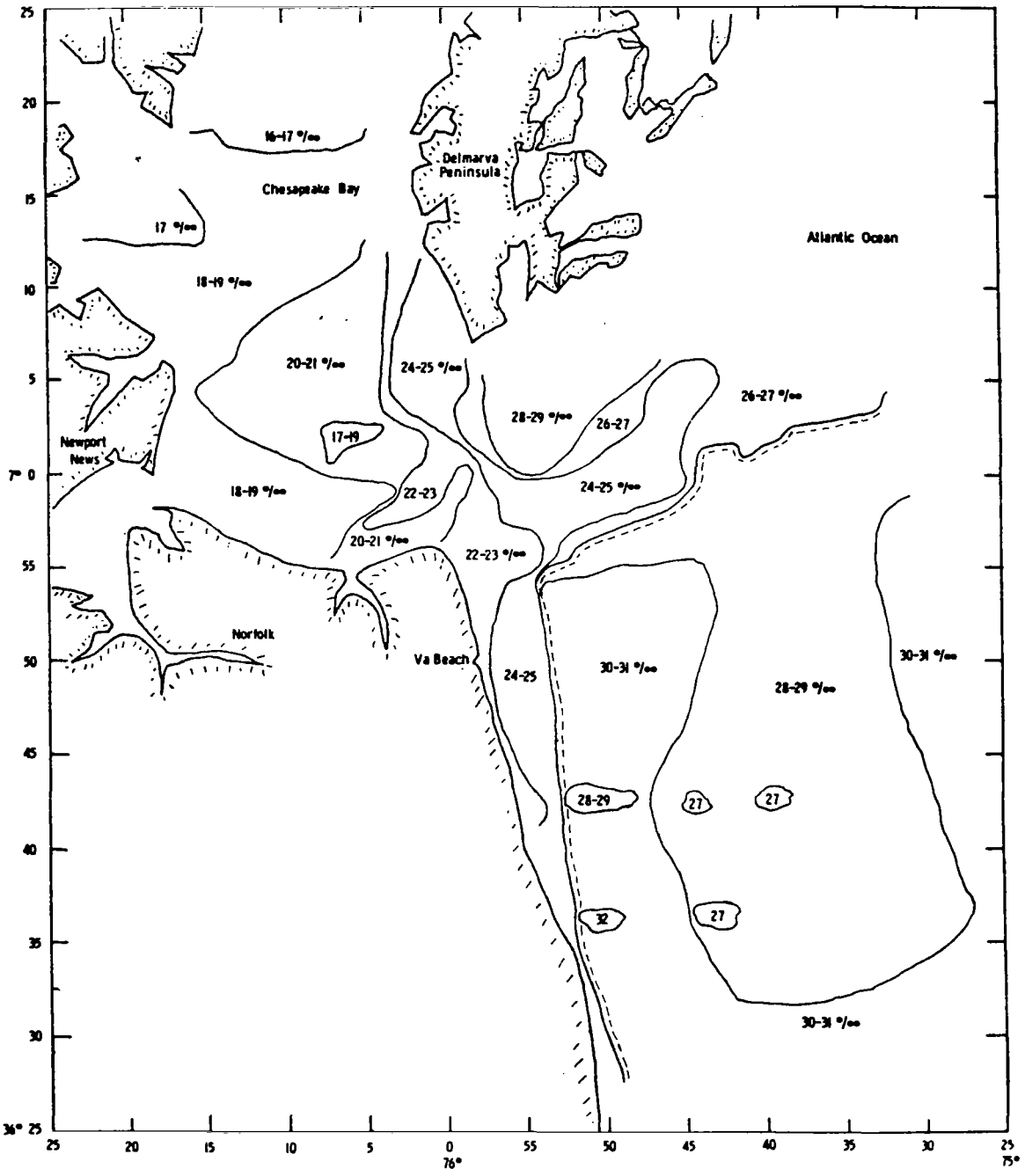

Figure 9.- L-band microwave radiometer salinity map (from ref. 10).

PRELIMINARY ANALYSIS OF OCEAN COLOR SCANNER DATA FROM SUPERFLUX III

Craig W. Ohlhorst
NASA Langley Research Center

SUMMARY

The Ocean Color Scanner collected data on October 15, 20, and 22, 1980, during Superflux III. Single channel gray scale data products generated 5 minutes after the scanner data were collected showed details of the Chesapeake Plume structure, suggesting that this quick-look capability could have potential use to experimenters in real time. The Chesapeake Bay Plume extended offshore about 5 nautical miles on October 15 and 7 nautical miles on October 20. The scanner data also show many other water features within the lower bay itself.

INTRODUCTION

In order to assess the possibility of relating high altitude remotely sensed spectral signatures to Chesapeake Bay plume features, an Ocean Color Scanner (OCS) was flown at an altitude of 12.5 kilometers (41 000 feet) during the Superflux III experiment on October 15, 20, and 22, 1980.

The OCS is a ten-band instrument covering the spectral range of 418 to 804 nanometers. Each channel has a bandwidth of 20 nanometers. The instantaneous field of view at nadir is 60 meters at the 12.5-kilometer altitude. The center wavelengths for the ten bands are listed on table I. An integral part of the OCS system is a set of instruments that allows for real time transmission of a single channel of scanner data. The image can be generated 5 minutes after the data is collected, giving investigators a real time look at the data. A film recorder is used to create the single-channel image. The recorded image is a gray scale film product with the shades of gray corresponding to the backscattered light intensity levels recorded in a particular channel. The single-channel images can be used to qualitatively indicate the location and distribution of suspended particulate matter.

EXPERIMENT

The OCS was flown on October 15, 20, and 22, 1980. There were six flight lines flown on October 15 (see fig. 1). Flight line 4 was flown twice, once in a southeast direction (line 4) and later, in a northwest direction (line 6). The arrows on the flight lines in figure 1 indicate the direction in which aircraft flew while the times listed are the start times

of each flight line. The tide times shown in figure 1 are for the Chesapeake entrance for October 15. A comparison of the flight times with the tide schedule indicates that the overflights bracketed slack after ebb tide which met one objective of the experiment (i.e., to view maximum plume expansion). The beginning and ending flight line coordinates, the starting times, aircraft heading, Sun azimuth, and Sun elevation are listed in table II.

On the 15th, five boats participated in sea truth collection; 18 data sets were collected. Five stations were sampled at the time of the first and third flight lines. Four stations were sampled during flight line 5. One station was sampled during flight line 6 and three stations were sampled about a half hour after the last flight ended. The positions of the 18 stations are shown in figure 2. Only 17 stations are shown since Station J was sampled at two different times. The time of each station collection and the boat position coordinates are listed in table III. On this day, the winds were out of the southwest at 10 knots.

On October 20, 1980, the OCS flew three flight lines, as shown in figure 3. The arrows indicate the direction the aircraft flew while the times represent the start time for each line. The October 20 tide times at the Chesapeake entrance are also shown on figure 3. The flight line times bracket the maximum ebb tide time. The beginning and ending flight line coordinates, the start time, aircraft heading, Sun azimuth, and Sun elevation are listed in table IV. Strong winds from the northwest of about 18 knots kept all the sea-truth collecting boats inshore, except the Kelez which collected seven sea-truth data points under flight line 1. The stations are located as shown on figure 4. The times and location coordinates of the stations are given in table V.

The OCS flew a third mission on October 22. The purpose of this mission was to fly at the same time as the Multichannel Ocean Color Sensor being flown on a P-3 aircraft at a lower altitude. Two parallel flight lines were flown (fig. 5). The first covered an area from the mouth of the Chesapeake Bay to as far west as $74^{o}40'$ west longitude. The second flight was flown 180^{o} to and about 3 nautical miles north of the first line. (See table VI).

SUMMARY AND DISCUSSION

The single-channel gray scale data products generated did show details of the Chesapeake Bay plume structure. Complete analysis of the multispectral scanner data requires three steps: (1) preprocessing of the digital data, (2) correlation of digital data with sea truth data, and (3) use of correlation to produce quantitative maps. At the time of this Symposium, the digital data were still being preprocessed. One of the preprocess steps that has been completed is a scan angle correction. The OCS has a scan angle of $\pm 45^{o}$. As the angle increases, the distance from the scanner to the water surface element being viewed increases and increasingly greater amounts of Sun and sky radiation scattered by the atmosphere reach the scanner and contribute to the total radiation sensed. At the same time, the longer path

length results in increased atmospheric attenuation of the radiation originating from the water. The scan angle correction normalizes the radiance at non-zero scan angles to that at nadir. For this work, the correction is made empirically. Figure 6 shows the shape of a typical algorithm used to correct the digitized data. The correction differs from channel to channel and can also differ in the same channel from flight line to flight line.

After the scan angle correction was applied, false color images were generated from Band 7 (664-684 nanometers) of the October 15 and 20 digitized data. Black and white copies of the color originals are shown in figures 7, 8, and 9. Figure 7 is a mosaic of flight lines 2, 3, and 4 collected on October 15. On this day, the winds were from the southwest at 10 knots and the scanner data was collected around slack after ebb tide. The radiance color code is shown under the 9:34 EST flight line. The shade of gray on the left represents the lowest radiance levels while those on the right represent the highest radiance levels. So within the bay, the chalk color represents a body of water with a lower radiance level than the surrounding dark gray color water. Areas with lighter shades of gray within the dark gray body of water represent radiance levels that are higher than the surrounding dark gray. A variety of features can be pointed out. There is a lower radiance level body of water that extends from the mouth of the York River to a line roughly parallel with the mouth of the Hampton Roads. From the Hampton Roads mouth to the mouth of the Chesapeake Bay, the water radiance level is higher, as indicated by the dark shade of gray color. Still higher radiance levels are seen hugging the coast around both Cape Henry and Cape Charles. Off of Virginia Beach, the water has a high radiance level. If it is assumed that the dark gray color water mass extending out of the bay mouth represents the Chesapeake plume, then the plume extended about 5 nautical miles offshore.

On the 15th, flight lines 1, 3, and 5 covered the mouth of the bay. Figure 8 shows the three lines. This figure gives a short time history of the water movement around the Bay mouth. The gray scale is the same as in figure 7. If the three flight lines are viewed in their time sequence, then the chalk colored water mass is seen to move south. The dark gray water mass also seems to move southeast out of the bay. These flight lines have not been normalized for Sun angle differences so the apparent movement of the dark gray water mass out of the Bay may be due, in part, to an increase in water radiance caused by an increase in Sun elevation.

Figure 9 presents a mosaic of flight lines 1 and 3 that was taken on October 20. On this day, the winds were out of the northwest at about 18 knots. The scanner data was collected around ebb tide. The gray scale color code is shown under the 12:10 EST flight line. A definite plume is seen coming out around Cape Henry flowing south. It extends farther south than the October 15 plume. There is a second outflow coming out the middle of the Bay mouth. There also seems to be a third outflow around Cape Charles. Water in both the Thimble Shoal Channel and the Chesapeake Channel has a lower radiance than the surrounding water. The Chesapeake plume seems to extend about 7 nautical miles offshore which is farther than it was on October 15.

FUTURE WORK

Correlation of the digital data with chlorophyll and suspended solids will be attempted. OCS and MOCS data will also be compared.

TABLE I. - OCEAN COLOR SCANNER INFORMATION

Flight Altitude 12.5 km (41000 feet)

Bands	Center Wavelength
1	428 nm
2	466
3	508
4	549
5	592
6	632
7	674
8	714
9	756
10	794

Bandwidth 20 nm Ground Resolution 60 m, (300 feet)

TABLE II. - OCTOBER 15, 1980 FLIGHT DATA

Flight Line	Coordinates Begin	Coordinates End	Start Time EST	Aircraft Heading	Sun Azimuth	Sun Elevation
1	36°45.1'N x 75°51.3'W	37°21.2'N x 76°21.9'W	9:19	328.9°	132°	30°
2	37°18.5'N x 76°29.2'	36°47.0' x 76°03.3'	9:34	146.5°	135°	32°
3	36°36.2' x 75°39.5'	37°23.6' x 76°21.1'	9:50	325.5°	140°	35°
4	37°14.8' x 75°57.3'	36°37.3' x 75°24.8'	10:06	145.2°	143°	36°
5	36°35.6' x 75°35.5'	37°17.2' x 76°11.6'	10:25	325.3°	149°	39°
6	(4 over again) 36°40.9' x 75°28.0'	37°15.0' x 75°57.5'	10:51	322.1°	155°	41°

TABLE III. - SEA TRUTH DATA COLLECTED UNDER OCS OCTOBER 15, 1980 FLIGHTS

	Kelez	John Smith	Judith Ann	RV Langley	Holton
FL-1					
Station	808	805	J	LY1	69
Time EST	9:14	9:19	9:30	9:20	9:19
Location	36°45.7'N	36°51.5'	36°59.3'	36°57.1'	36°55.0'
	75°54.67'W	75°55.4'	75°58.5'	76°02.2'	75°58.0'
FL-3					
Station	809	70	J-1	LY2	802
Time EST	9:50	9:58	9:48	9:58	9:50
Location	36°46.36'N	36°52.1'	36°59.5'	36°58.6'	36°56.0'
	75°48.77'W	75°52.6'	75°58.5'	76°00'	75°55.3'
FL-5					
Station	821	806		LY3	803
Time EST	10:28	10:32		10:40	10:33
Location	36°47.42'N	36°52.5'		37°01.5'	36°58.0'
	75°42.62'W	75°49.5'		75°56.2'	75°51.5'
FL-6					
Station	810				
Time EST	10:48				
Location	36°47.67'N				
	75°41.12'W				

TABLE III. - SEA TRUTH DATA COLLECTED UNDER OCS OCTOBER 15, 1980 FLIGHTS

(continued)

	Kelez	John Smith	Judith Ann	RV Langley	Holton
Station	811	807			804
Time EST	11:44	11:27			11:25
Location	36°48.73'N	36°54.2'			37°01.02'
	75°32.26'W	75°40.6'			75°44.2'

TABLE IV. - OCTOBER 20, 1980

Flight Line	Coordinates Begin	End	Start Time EST	Aircraft Heading	Sun Azimuth	Sun Elevation
1	36°46.4'N x 75°51.1'W	37°25.7'N x 75°57.4'W	11:31	352.8°	168°	43°
2	36°43.2' x 75°37.7'	37°19.5' x 75°42.4'	11:58	355.1°	178°	44°
3	37°19.9' x 76°10.9'	36°49.9' x 76°06.2'	12:10	172.7°	184°	43°

TABLE V. - SEA TRUTH DATA COLLECTED UNDER OCS OCTOBER 20, 1980 FLIGHTS

Station	Time EST	Location
KZ 1	11:30	$36^{o}56.03'N \times 75^{o}53.00'W$
KZ 2	11:35	$36^{o}56.58' \times 75^{o}52.95'$
KZ 3	11:40	$36^{o}57.16' \times 75^{o}52.90'$
KZ 4	11:45	$36^{o}57.72' \times 75^{o}52.81'$
KZ 5	11:50	$36^{o}58.41' \times 75^{o}52.94'$
KZ 6	11:55	$36^{o}59.07' \times 75^{o}53.01'$
KZ 7	12:00	$36^{o}59.72' \times 75^{o}53.12'$

TABLE VI. - OCTOBER 22, 1980

Flight Line	Coordinates Begin	End	Aircraft Heading
1	$36^{o}59.5'N \times 76^{o}20'$	$36^{o}59.5'N \times 74^{o}40'W$	90^{o}
2	$37^{o}02' \times 74^{o}40'$	$37^{o}02' \times 70^{o}10'$	270^{o}

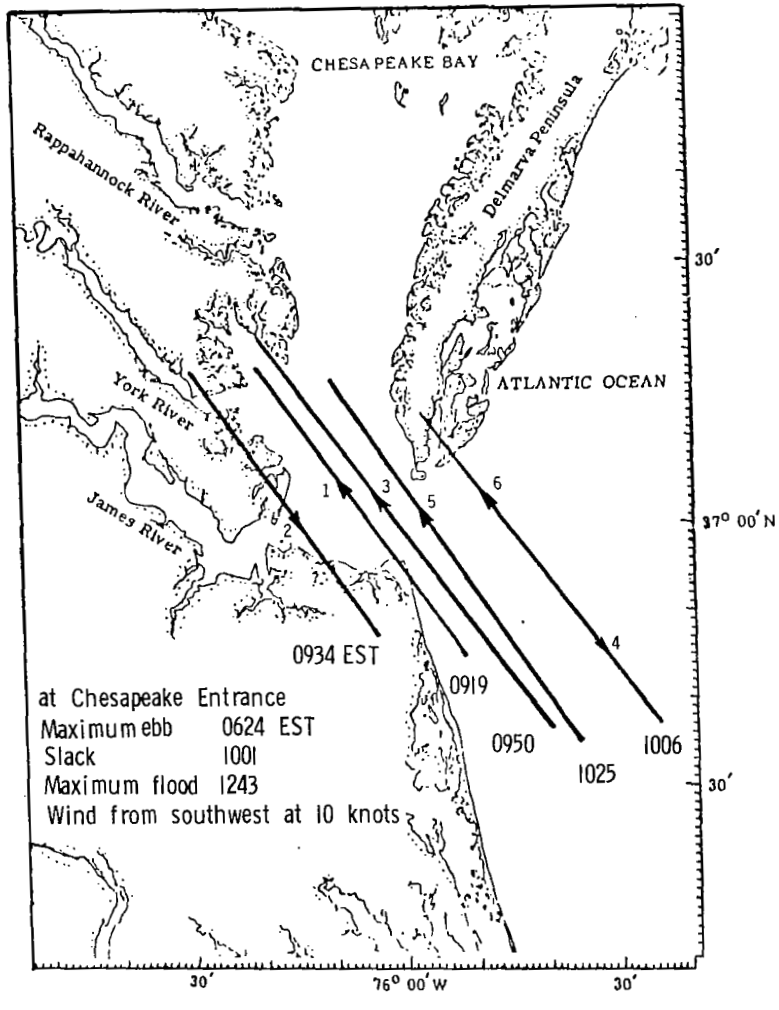

Figure 1.- Flight track of Lear Jet/OCS mapping mission on October 15, 1980.

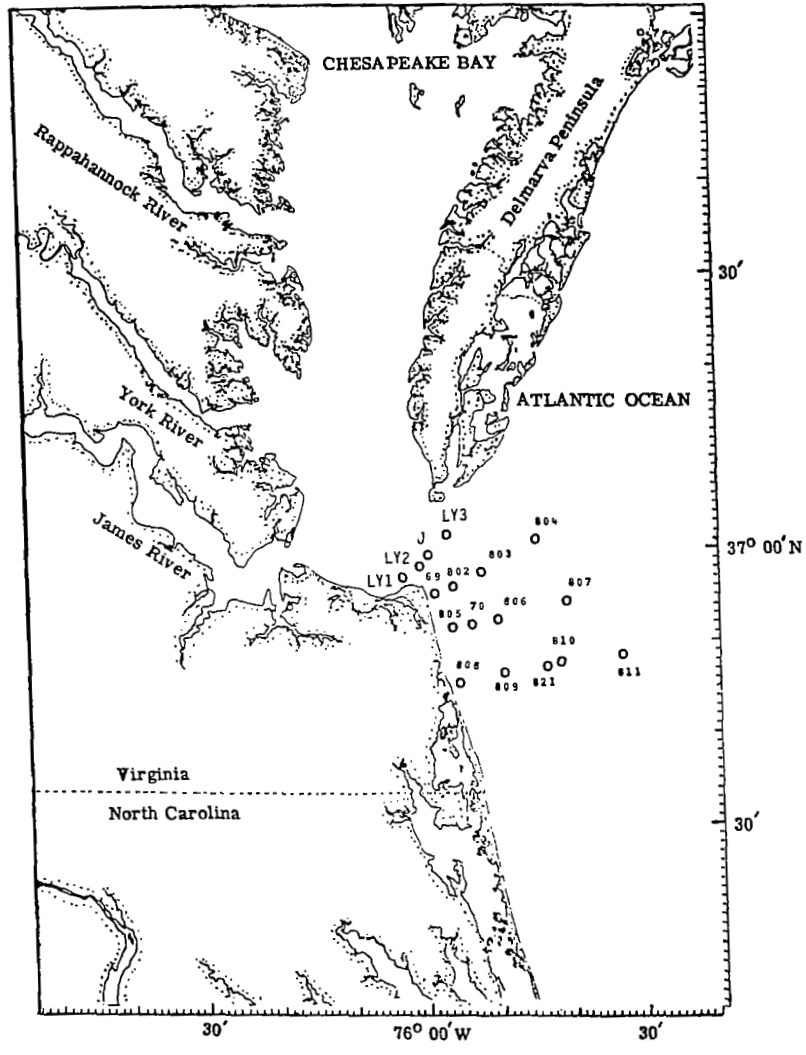

Figure 2.- Location of sea-truth stations on October 15, 1980.

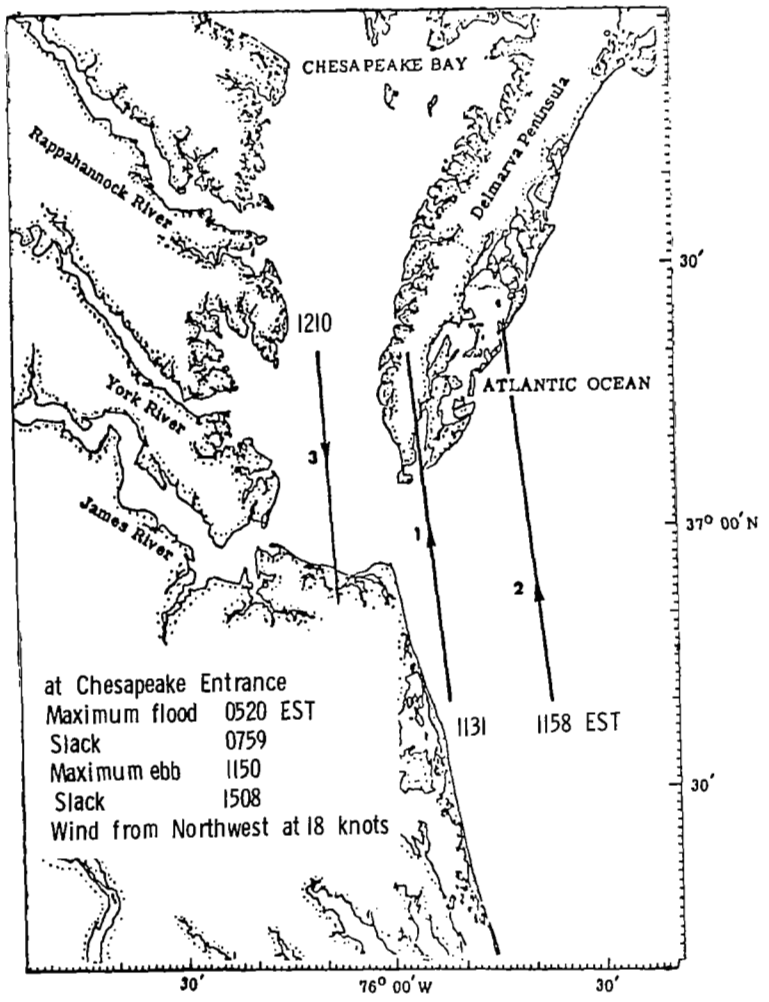

Figure 3.- Flight track of Lear Jet/OCS mapping mission on October 20, 1980.

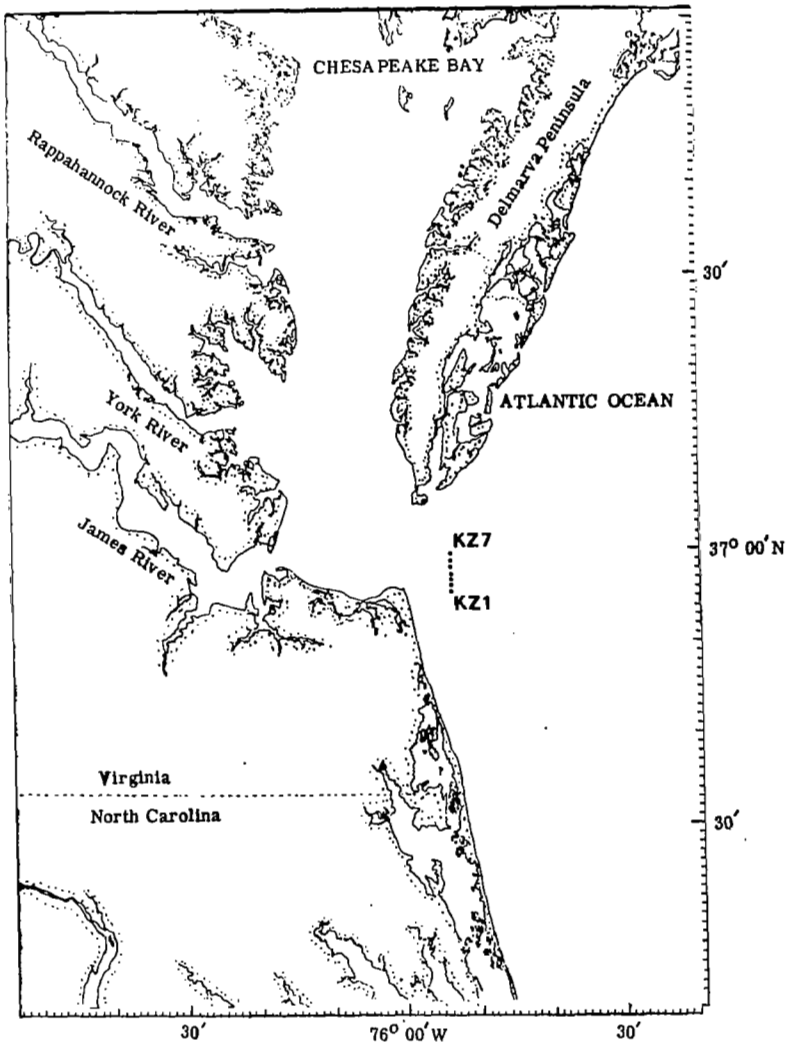

Figure 4.- Location of sea-truth stations on October 20, 1980.

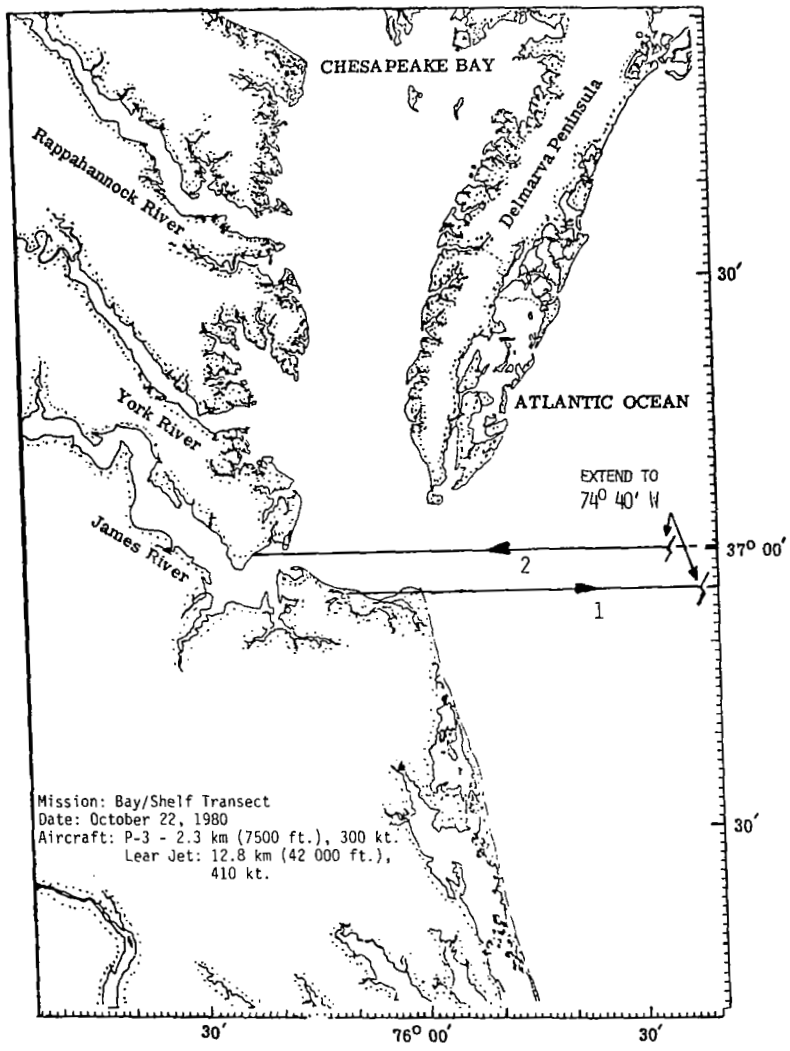

Figure 5.- Flight tracks of P-3/MOCS and Lear Jet/OCS missions on October 22, 1980.

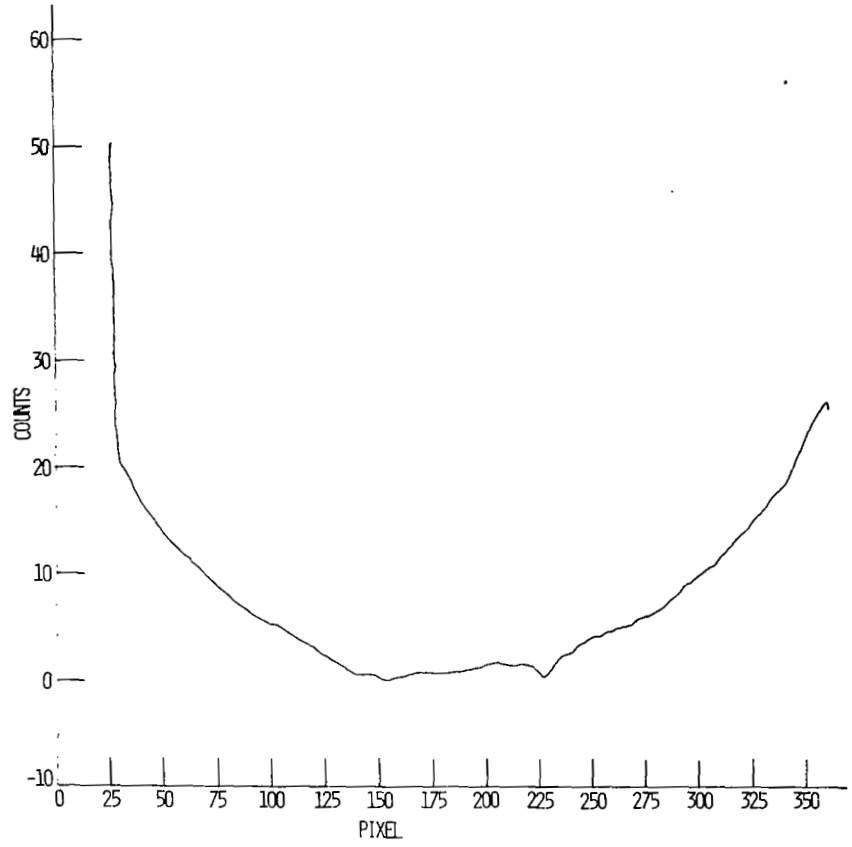

Figure 6.- Scan angle correction curve.

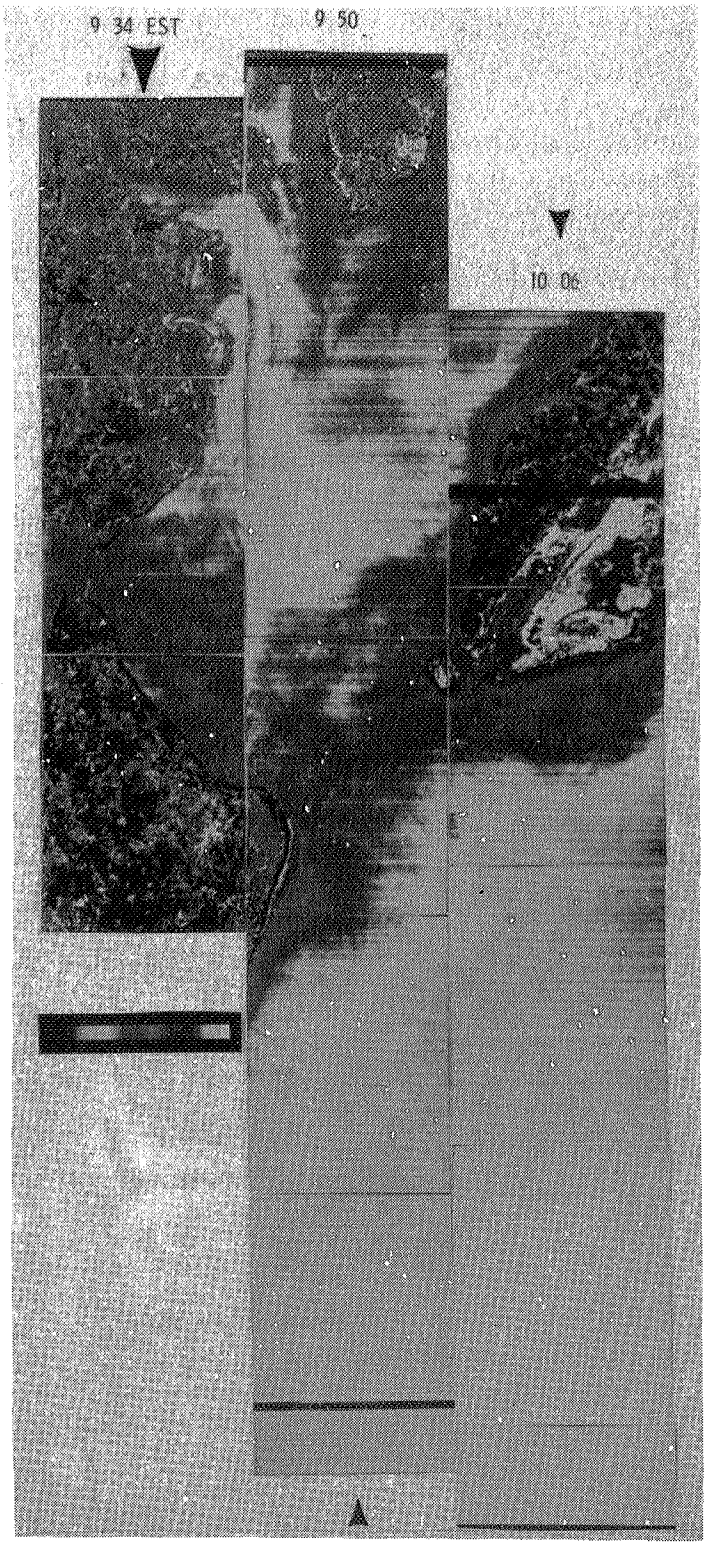

Figure 7.- Mosaic of flight lines 2, 3, and 4 taken on October 15, 1980.

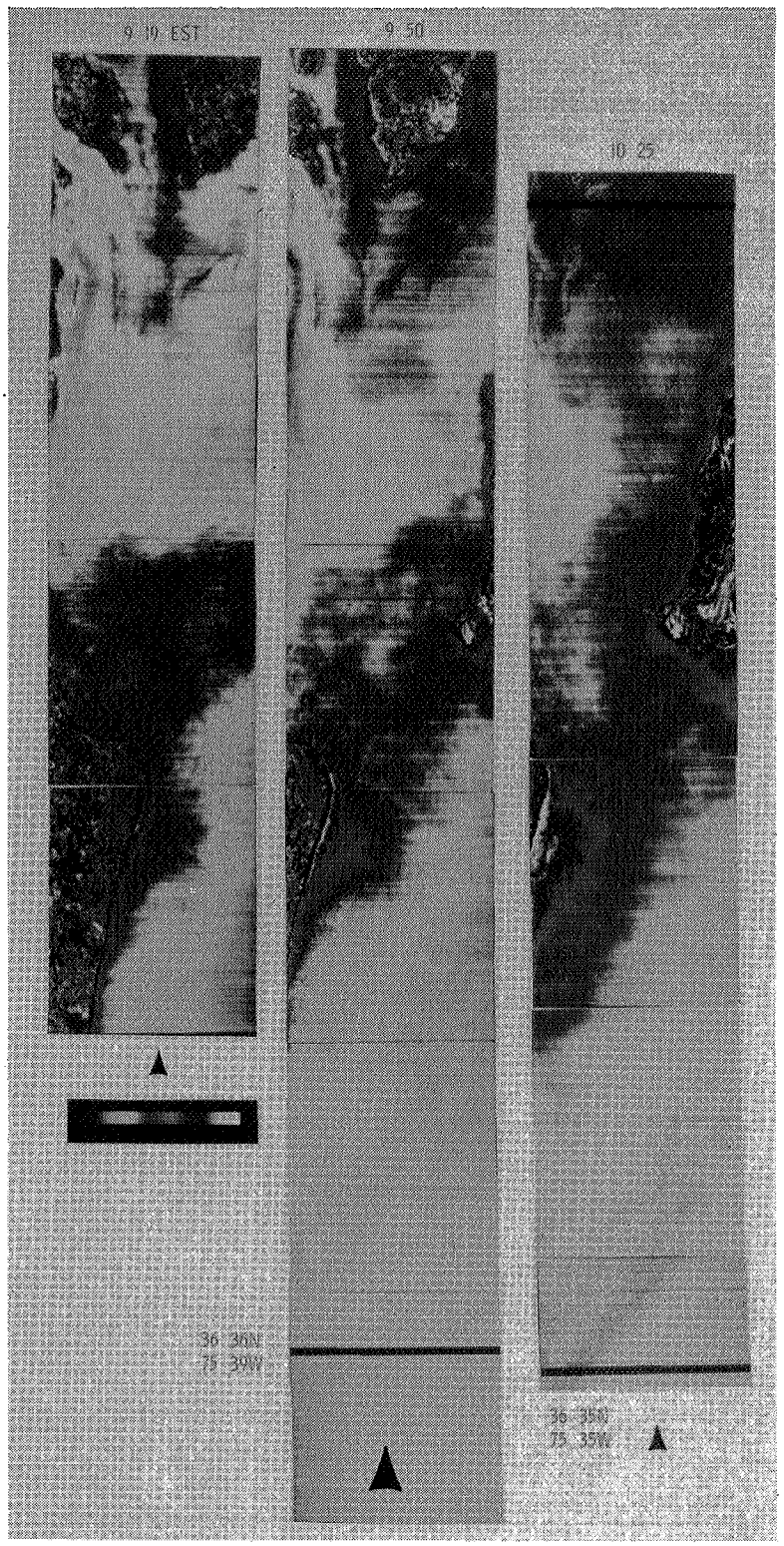

Figure 8.- Composite of flight lines 1, 3, and 5 taken on October 15, 1980.

Figure 9.- Mosaic of flight lines 1 and 3 taken on October 20, 1980.

LAGRANGIAN CIRCULATION STUDY

NEAR CAPE HENRY, VIRGINIA

Ronald E. Johnson
Old Dominion University

SUMMARY

A study of the circulation near Cape Henry, Virginia, has been made using surface and seabed drifters and radar-tracked surface buoys coupled to subsurface drag plates. Drifter releases were conducted on a line normal to the beach just south of Cape Henry. Surface drifter recoveries were few; wind effects were strongly noted. Seabed drifter recoveries all exhibited onshore motion into Chesapeake Bay. Strong winds also affected seabed recoveries, tending to move them farther before recovery. Buoy trajectories in the vicinity of Cape Henry appeared to be of an irrotational nature, showing a clockwise rotary tide motion. Nearest the cape, the buoy motion elongated to almost parallel depth contours around the cape. Buoy motion under the action of strong winds showed that currents to at least the depth of the drag plates substantially are altered from those of low wind conditions near the Bay mouth. Only partial evidence could be found to support the presence of a clockwise nontidal eddy at Virginia Beach, south of Cape Henry.

INTRODUCTION

This presentation is a summary review of a study funded by NASA/Langley Research Center (LaRC) (ref. 1) of the circulation along the coast in and just south of the entrance to Chesapeake Bay, Virginia. A net nontidal clockwise eddy inferred by previous investigators (ref. 2) was reinvestigated, in a limited way, by the use of surface and seabed drifters, by the use of radar-tracked floats with subsurface drag plates, and by cross-sections of the physical properties of temperature, salinity, and density. While table I lists all cruise days, locations, and the particular research method used, only the drogue data from August 8 - 9 and December 5 - 6, 1973, and the drifter data from June 22 - 23, 1974 will be discussed. (See reference 1 for the remainder of the cruise information).

REVIEW

Drogue Study

Previous investigations of the study area using current meters have primarily been associated with the Coast and Geodetic Survey (now National Ocean Survey) and have been mainly interested in tidal current predictions. Current meter stations were located at the Chesapeake Light Station,

in the entrance to the Bay, and near shore at the north and south ends of Virginia Beach. These positions were outside the present study area, except for the station near the north end of Virginia Beach, and were not useful in obtaining information about the circulation in the inferred eddy.

A search of the literature has produced only two other current studies in this area. The first and most recent current study was really a study of shelf circulation. Reference 3 tracked free drifting buoys using the French EOLE satellite in the western North Atlantic in the winter of 1973. The four buoys had drag plates at either 5 or 30 m. After initial deployment near the Chesapeake Light Tower they drifted southeasterly parallel to the coast. Upon reaching the vicinity of Cape Hatteras, the three remaining buoys were entrained in the Gulf Stream and drifted northeast. Reference 3 reports that the random error in position about the mean ranged from 1.4 to 2.3 km depending upon the transponder.

The second study, although 12 years old, did investigate the nearshore area of Cape Henry. Reference 2 made simultaneous measurements by both Eulerian and Lagrangian methods for up to 13 tidal cycles along the shore. Three Roberts Radio Current Meter Stations were occupied from Cape Henry to Rudee Inlet about 1.6 km (1 mi) offshore. A brief drogue study was conducted during one of the tidal cycles simultaneously with a dye and drifter release.

Reference 2 claims that the clockwise eddy movement is confirmed by the nontidal current values (isolated from the total current record). The station near Cape Henry shows easterly net current values at both surface and mid-depth locations (no bottom meter), while the central station, near 40th Street, indicates a net northerly current at surface, mid-depth, and bottom positions. The southern station, just south of Rudee Inlet, shows extremely small net current values (less than 2 cm/sec) in an easterly direction for surface, a southerly direction for mid-depth, and a northerly direction for the bottom meter position. The brief drogue study showed a clockwise loop of less than one nm width (normal to shore) and about three nm in length. The time of observation was slightly less than one tidal cycle. By itself, this loop could indeed be associated with the rotary tide. The results of the three current meter stations (which were averaged over 9 to 13 tidal cycles) offer the best evidence for this net motion, but do not completely cover the study area. The dye study was not conclusive in that the dye cloud was only monitored for six hours during an ebb flow situation.

Drifter Study

The earliest reported use of drifters to study circulation near the entrance to Chesapeake Bay suggested that the offshore shelf waters exhibited primarily southerly drift, but that the inshore waters just south of Cape Henry described a clockwise movement extending south to Rudee Inlet and to an unknown extent seaward (refs. 4 and 5).

Reference 2, besides the current meters mentioned in the previous chapter, deployed surface drift bottles from positions just south of Cape Henry and off Little Creek Harbor. While they experienced a recovery of 38.9 percent from the Cape Henry releases and 57.3 percent from the Little Creek releases, little can be learned of the inferred eddy from the recovery positions. These were mostly south of Rudee Inlet, a direct indication of the net nontidal surface outflow from the Bay and of the general southerly flow of the shelf waters.

A number of seabed drifters of the plastic umbrella-shaped variety (Woodhead-Bumpus seabed drifters) were released at a single point on a separate occasion in connection with a brief dye and current meter study at the tip of Cape Henry. These were released at slack water before ebb. A recovery of 80 percent of the drifters was made a few hours later up to 2.7 nm (5 km) south of the release point. Most of the seabed drifters were recovered at the south end of Virginia Beach and probably were carried by shelf current around the eddy area.

Reference 6 released vast numbers of seabed and surface drifters off the Chesapeake bight during 1963-1964. The recovery of large numbers of seabed drifters in or near Chesapeake Bay from releases to the north and east indicated net bottom inflow into the bay as well as the expected southerly drift. Apparently the inflow was related to changes in river discharge and seasonal prevailing winds. The general trend of the surface waters as determined by drift bottle recoveries was also southerly, but highly dependent upon the prevailing wind direction. Most recoveries were made during periods of onshore winds. No mention is made of the inferred clockwise eddy south of Cape Henry. However, reference 7 placed generalized flow pattern arrows on figure 15 of reference 6 which indicate a possible clockwise circulation of the bottom currents inferred from winter releases of seabed drifters. The size of the cell, however, is quite large in comparison to the Virginia Beach study area.

Brehmer (ref. 8) specifically studied the problem of nearshore bottom currents off Virginia Beach. His approach was to release seabed drifters along a transect parallel to and approximately 5.6 km (3.5 mi) offshore from Cape Henry to False Cape. His results indicated that during the fall and winter months recoveries suggest northerly nearshore nontidal bottom drift from Rudee Inlet to Cape Henry. South of Rudee Inlet the drift was southerly. During the summer months, however, the recoveries inferred that the nontidal drift patterns were primarily inshore and slightly northerly as far south as False Cape. No attempt was made to establish the seaward extent of the circulation, but Brehmer states that his data "appear to confirm the presence of the clockwise eddy in the Atlantic Ocean south of Cape Henry."

METHODS

Drogue Study

The buoy-tracking phase of this study utilized up to 4 surface buoys with drag plates centered at 6.1 m (20 ft). The steel plates are crosses, 0.9 m (3 ft) high by 1.5 m (5 ft) wide. S-band radar was used to interrogate each buoy in turn, taking approximately 5 to 20 min to locate and position all 4 buoys. The radar operates in the 2700 to 2900 MHz range and is limited to line-of-sight operation. Each buoy is "told" to turn on and become an active target for the radar by a double pulse from the radar unit. The pulse widths vary from 2 to 12 msec. Each buoy receives on the same frequency but "senses" from the width of the time delay between pulses when it is its turn to be interrogated.

The MPS-19 S-band radar was housed in a mobile tracking van provided and operated by personnel from Wallops Station, NASA, located at Wallops Island, Virginia. The four buoys were provided by the Sensor Development Section (SDS), NASA/LaRC. In addition, the SDS also provided the rechargeable batteries for the floats (up to 40 hr transmitting life) and the small trailer used to record and plot the buoy trajectories. Ship communication was through portable FM units supplied by the Wallops Station crew. The Department of Oceanography, Old Dominion University (ODU), provided the R/V *Linwood Holton* for release and recovery of the buoy/drogue plate combinations and personnel for data recording and plotting. Power for the shore operation of the radar van and data-recording trailer was obtained from a Wallops-Station-supplied 50-kW diesel-powered generator.

In the attached figures, the initial position of each buoy is indicated by "S," the final position at pickup by "F." The numbers and associated tick marks indicate the sequence number and location of tidal current reversal. Appendix A, tables A1 through A4 of reference 1, contains the tabulated data for each buoy and each day of tracking. The tables contain sequential data point number, local time, range from radar vans, and azimuth. The individual buoy's initial and final position latitude and longitude are given, as well as the position of the radar van. The position fixes are accurate to within 5 m (5.5 yd) to a distance of 28 km (15 nmi). The position error of the location of the radar van must be added to the buoy position error. Horizontal sextant angles are used to determine van position. The accuracy depends upon chart position of the sextant targets, distance to the targets, sextant error, and operator error. These errors have been estimated to be ±9 m (±10 yd).

Drifter Study

The drifter program used both surface and seabed drifters. The surface drifters were made of weighted heat-sealed plastic pouches containing sand to allow the bags to float with a minimum of surface area above the water. The sand forced the bag into a near vertical position so that the water motion effect on the bags of the surface of "skin" layer would be minimized. Each

pouch contained a red postcard with identifying information and requested the finder to give the data and time found as well as the actual location. Return information could be provided as to when and where released if the finder so desired.

The seabed drifters were of the Woodhead-Bumpus type. These were slightly negatively buoyant, plastic, umbrella-shaped floats. Each had a plasticized postcard attached under the umbrella with the same request for information.

The surface drifter envelopes were thrown individually into the water at each station. The number thrown varied from 7 to 10, depending upon availability for that particular cruise. All stations during a cruise had the same number released, however.

The seabed drifters had to be weighted so that sinking time to the bottom would be as short as possible, otherwise the drifters would behave partially as surface and intermediate layer drifters as well as seabed. Salt spools of 76-cm (3-in.) diameter about 2.5 cm (1 in.) thick, were used for the weight. Each cluster of 5 to 10 seabed umbrellas was fastened to a salt spool with a small rubber band. The spool and rubber band were attached in such a way that when the spool dissolved the rubber band released the drifters. The sinking and release of the drifters was observed to take about 45 min to 1 hr in 15 m (50 ft) of water. Water temperature was near 15.6° C (60° F).

The groups of drifters, both surface and seabed, were assembled and identified prior to each cruise. Before throwing them overboard all numbers were checked as to release date, time, and location. Upon recovery, the shortest distance between release and recovery was used to determine travel distance and speed, and direction was then calculated. All data for surface and seabed drifters are tabulated in Appendix B of reference 1.

DISCUSSION

Drogue Study

August 8-9, 1973.— The buoy-tracking runs of August 8-9 were an attempt to look at the flow around the "corner" of Cape Henry. Permission was obtained from the U.S. Army to allow placement of the radar tracking van within Fort Story. This position, near the tip of Cape Henry, allows line-of-sight tracking for several miles within the bay as well as along the coastline of Virginia Beach.

Figure 1 shows the radar van position as well as the trajectories of each of the buoys. Only three buoys were deployed during this tracking operation. Buoy 3 was in a nonoperating condition at the time scheduled. Unfortunately, the strong net seaward flow during this tracking operation caused the buoys to be carried from the line of sight much sooner than expected; only intermittant fixes were obtained after data point 73 (buoy 1), data point 76 (buoy 2), and data point 69 (buoy 4). Final positions were obtained from the R/V *Linwood Holton* at time of recovery: data points

76, 77, and 71 for buoys 1, 2, and 4, respectively. No information was obtained concerning flow reversals between the last radar position and ship recovery position. In addition, a malfunction in the automatic range determination unit required manual determination of range from 1233 to 1717 EDT on August 8. Several ranges prior to this are in possible error due to malfunction prior to 1233 EDT. Both sets of observations have been marked and footnoted (see ref. 1, Appendix A).

The clockwise motion of the three buoys is evident, but the proximity to the Cape Henry "corner" causes the buoy tracks to become more elliptical in shape. Except for the reversal, this pattern is quite similar to standard frictionless flow around a corner, or one side of flow from an orifice. Notice that each buoy system moves parallel to the 9-m (30-ft) depth contour during the strength of the ebb and flood cycles and moves approximately perpendicular to the contour during the slack times. The rotary nature of the tidal currents on the shelf prevents a pure reversal in direction.

Speeds for the buoy's drag plate stems exceeded 1.4 m/sec (2.7 kn) during the ebb cycle in the channel just north of Cape Henry and exceeded 0.7 m/sec (1.4 kn) during the next ebb off Virginia Beach. The flood strength was only 0.3 m/sec (0.5 kn).

December 5-6, 1973.— An attempt was made to restudy the flow around the top of Cape Henry by moving the radar tracking van "around the corner." This would result in improved line-of-sight fixes. The new position is shown in figure 2 along with the tracks of the two operational buoy-drogue systems.

Shortly after deployment of the two buoys, the wind increased from under 5 m/sec (10 kn) from the south to over 12.9 m/sec (25 kn) from the southeast (average wind December 5 was 20 kn). This caused a rather sudden change in surface currents to occur. The initial effect was to cause ocean water to be moved into the Bay on a flood cycle lasting nearly 12 hr, starting at approximately 0900 EST and terminating at about 1900 EST on the fifth. The duration of flooding predicted by the U.S. National Ocean Survey (1972) was for only 2.5 hr (approximately 1400 to 1630 EST). The maximum flood current was computed to be approximately 1.0 m/sec (1.9 kn) compared to the predicted maximum of 0.4 m/sec (0.7 kn).

The net drift was northeasterly during the day of December 5 and started to show signs of returning to a southwesterly direction on December 6, the winds having shifted around to the north with an average speed of 5.7 m/sec 11 kn) on December 6. The net drift, computed from the track of buoy 3, was approximately 20.4 km (11 nmi) for an average speed of 0.2 m/sec (0.4 kn). The Ekman wind-driven current speed was obtained from figure 5 of reference 9 as 0.10 m/sec for an average depth of 9 m (30 ft) and wind speed of 12.8 m/sec (25 kn). This large contribution to the net motion reinforces the need for continual observation of wind conditions during all circulation studies. No calculation of wind wave currents was made, but these were probably less than 25 percent of the direct wind-driven current during the time.

Drifter Study

The stage of the tide could not be observed to have any influence on the recovery of drifters for the previous four drifter releases (ref. 1). This was, at least in part, due to the one-time release of drifters along the line of stations. An attempt was made during the cruise of June 22, 1974 to investigate this effect by the release of drifters along the line of stations four times over a tidal cycle.

The nearest tidal current prediction station is number 4475, Virginia Beach, north end, 36°52'N and 75°58'W. This is about 1.9 km (1 nmi) south and shoreward of station one. The times of release for the four sets at station one corresponded well with the predicted tidal current information as follows (U.S. National Ocean Survey, 1973):

Station One Release Time	Tidal Condition
1. 1038 EDT	Maximum Flood
2. 1423 EDT	Slack Before Ebb
3. 1700 EDT	Maximum Ebb
4. 1932 EDT	Slack Before Flood

It must be noted here that the tide at stations seaward of number one does not behave as it does at the predictor station.

The winds during the two days prior to and during the day of release were generally from the south at less than 7.7 m/sec (15 kn) average; however, for the next week, winds were northerly, averaging just under 7.7 m/sec (15 kn).

The recovery positions for the seabed drifters are presented in figures 3 through 6 and for surface drifters in figures 7 through 10. Table II presents a summary of recovery information for the four release runs.

An inspection of the seabed drifter information from table II and figures 3 through 6 does not show any obvious connection to stage of tidal current near station one. Over 56.4 percent of all released seabed drifters were recovered, mostly north of the release line, indicating onshore northerly (into the Bay) flow. Further inspection suggests that the more easterly station releases were recovered to the south. The surface drifter information is even more widely scattered. It appears that the northerly wind affected the seaward released drifters more than the shoreward only for the first release set. Returns were either from near Cape Henry or from North Carolina. Only 31.0 percent of all surface drifters were recovered, indicative of either seaward surface flow or pouches that leaked and sank. Hence visual inspection of the data is not conclusive.

A statistical study of drifter returns was then implemented by Mr. Richard Philips, Ph.D. student within the ODU Department of Oceanography. Unfortunately, the data were not analyzed comparing each run, but only as to significance of north or south recovery positions for each station. This resulted because of insufficient data in adding the four additional classifications and also because less than nine percent of the drifters were recovered within two days. Drifters in circulation for more than two or three semidiurnal cycles tend to lose their original tidal identity.

The surface and bottom data were analyzed separately. The surface circulation is quite different from that near bottom due to the presence of the Bay mouth and wind effects. The data were analyzed using the one-way analysis of variance approach and with a modified Duncan multiple-range test. All analyses were performed at the 95 percent confidence level.

The bottom drifter data results suggest the presence of the inferred eddy. Stations one through four all had net northerly drift, while stations five through seven all had southerly drift. The surface study was inconclusive; no trends appeared to indicate northerly flow, only southerly flow: a consequence of wind shift part way through the drift? Again, it was noted that a bimodal distribution existed with one group clustered in North Carolina and the other group centered near the release position. This possibly can be explained by the relative densities of people along the beaches. The two major recovery areas are prime resort areas and could account for the few recoveries between them.

SUMMARY AND CONCLUSIONS

The investigation of the nearshore circulation in the vicinity of Cape Henry was undertaken to extend the current knowledge of the inferred net nontidal eddy reported in the literature. Establishment of this feature, of course, would greatly aid the understanding of the circulation along Virginia Beach and, hence, the erosive problem faced by that city.

Lagrangian methods were employed. The seabed and surface drifters duplicated, but also extended, earlier work. Release transects across the inferred eddy center of rotation were made. Radar-tracked drogues were used for the first time. Four separate cruises were made, lasting from 8 to over 30 hr of tracking time. A combination of factors, including weather, ship and manpower availability, and insufficient subsurface tidal information, prevented the deployment and tracking of the buoys exactly in or near the inferred eddy location. The size and scope of the original grant also precluded making more data collection runs.

The drogue studies support the concept of onshore and clockwise motion during at least part of a tidal cycle. The individual buoy/drag plate assembly motion seemed to follow an irrotational pattern, however, rather than the rotational one expected from motion associated with an eddy.

The drogue study of August 8-9, 1973 was slightly north of the inferred eddy, located at the entrance to the bay. This series was partially interrupted by loss of line-of-sight contact with the surface buoy; however, the described trajectories closely resemble the flow pattern found around theoretical, frictionless corners. The path closely followed the bottom contours, again turning in a clockwise fashion through flood, ebb, etc. The orbit was reduced to almost linear proportions on the buoy closest to shore. All three buoy tracks appeared to be merging to the same flow line after 10 hr or so.

The study of December 5-6, 1973 was affected by a rather intense south to southwest wind shortly after buoy deployment that quickly altered the long-term surface current on the shelf. The buoy paths, while retaining tidal characteristics, showed a northeasterly trend counter to that previously noted. This, of course, suggests that any nontidal eddy located along Virginia Beach near Cape Henry could be hidden or "washed out" for long periods at a time.

The summer drifter release of June 22, 1974 was an attempt to study the stage of the tide vs. time of drifter release. This could not be done due to insufficient returns. One result that did emerge, however, showed that the seabed drifters from stations one through four had a net northerly drift, while those from stations five through seven had a net southerly drift. The surface study was inconclusive.

As yet no positive determination of the presence of a nontidal clockwise eddy has been shown. The present data collection more clearly shows the response of the nearshore regime under the action of wind. However, not enough long-term studies have been made to subtract the wind and other currents from the record, leaving the residual. This sort of analysis requires the use of 30-day or longer drogue studies, anchored current meters, or both.

REFERENCES

1. Johnson, Ronald E.: Circulation Study near Cape Henry, Virginia, Using Lagrangian Techniques. Progress Report for NASA Master Contract Agreement NAS1-11707, Task Authorization Nos. 14 and 24, Sept. 1976. (Also Tech. Rpt. No. 21, Institute of Oceanography, Old Dominion Univ., Norfolk, VA)

2. Harrison, W.; Brehmer, M.L.; and Stone, R.B.: Nearshore Tidal and Nontidal Currents, Virginia Beach, Virginia. Tech. Memo No. 5, U.S. Army Corps of Engineers, Coastal Engineering Research Center (Washington, D.C.), 1964.

3. Wallace, J.W.; and Usry, J.W.: Data Report of Four Free-Drifting Buoys Tracked by the EOLE Satellite in the Western North Atlantic Ocean in the Winter of 1973. NASA TM X-72768, 1975.

4. Joseph, E.B.; Massmann, W.H.; and Norcross, J.J.: Investigations of Inner Continental Shelf Waters off Lower Chesapeake Bay, Part I. General Introduction and Hydrography. Chesapeake Science, Vol. 1, 1960, pp. 155-163.

5. Norcross, J.J.; Massmann, W.H.; and Joseph, E.B.: Data on Coastal Currents off Chesapeake Bay. Special Scientific Report No. 31, Virginia Institute of Marine Science (Gloucester Point, VA), 1962.

6. Harrison, W.; Norcross, J.J., Pore, N.A.; and Stanley, E.M.: Circulation of Shelf Waters off the Chesapeake Bight. Surface and Bottom Drift of Continental Shelf Waters Between Cape Henlopen, Delaware, and Cape Hatteras, North Carolina, June 1963 - December 1964. ESSA Professional Paper No. 3, U.S. Dept. of Commerce, 1967.

7. Beauchamp. R.G. (Ed.): Marine Environmental Planning Guide for the Hampton Roads/Norfolk Naval Operating Area. Spec. Pub. 250, U.S. Naval Oceanographic Office, 1974.

8. Brehmer, M.L.: Nearshore Bottom Currents off Virginia Beach, Virginia. Special Scientific Rept. No. 18. Virginia Institute of Marine Science (Gloucester Point, VA), 1971.

9. Whitlock, C.H.; and Talay, T.A.: The Influence of Surface Waves on Water Circulation in a Mid-Atlantic Continental-Shelf Region. NASA TN D-7771, 1974.

TABLE I.-DATA ACQUISITION INFORMATION

Cruise Date	Location	Methods
3 Apr 1973	Virginia Beach	Drifter
10 May 1973	Virginia Beach	Drogue
11 May 1973	Virginia Beach	Drogue
22-23 May 1973	Thimble Shoal Channel	Drogue
8 Jun 1973	Virginia Beach	Drifter
26 Jul 1973	Virginia Beach	Drifter
8-9 Aug 1973	Cape Henry	Drogue
5-6 Dec 1973	Cape Henry	Drifter/Drogue
22-23 Jun 1974	Virginia Beach	Drifter/Thermohaline

TABLE II.-DRIFTER RECOVERY SUMMARY FOR JUNE 22, 1974

Time EDT	Drifter	Drifter Release per Station	Recovery per Station							Recovered
			Station							
			1	2	3	4	5	6	7	
1038-1117	Seabed	5	4	5	4	5	2	1	0	60.0
	Surface	9	6	2	0	5	7	3	4	42.9
1473-1500	Seabed	5	4	4	4	2	2	2	4	62.9
	Surface	9	2	2	1	3	3	1	3	23.8
1700-1733	Seabed	5	4	3	3	5	0	1	2	51.4
	Surface	9	2	3	7	1	1	2	4	31.8
1932-2014	Seabed	5	4	4	3	3	2	2	0	51.4
	Surface	9	3	1	2	1	3	2	4	25.4

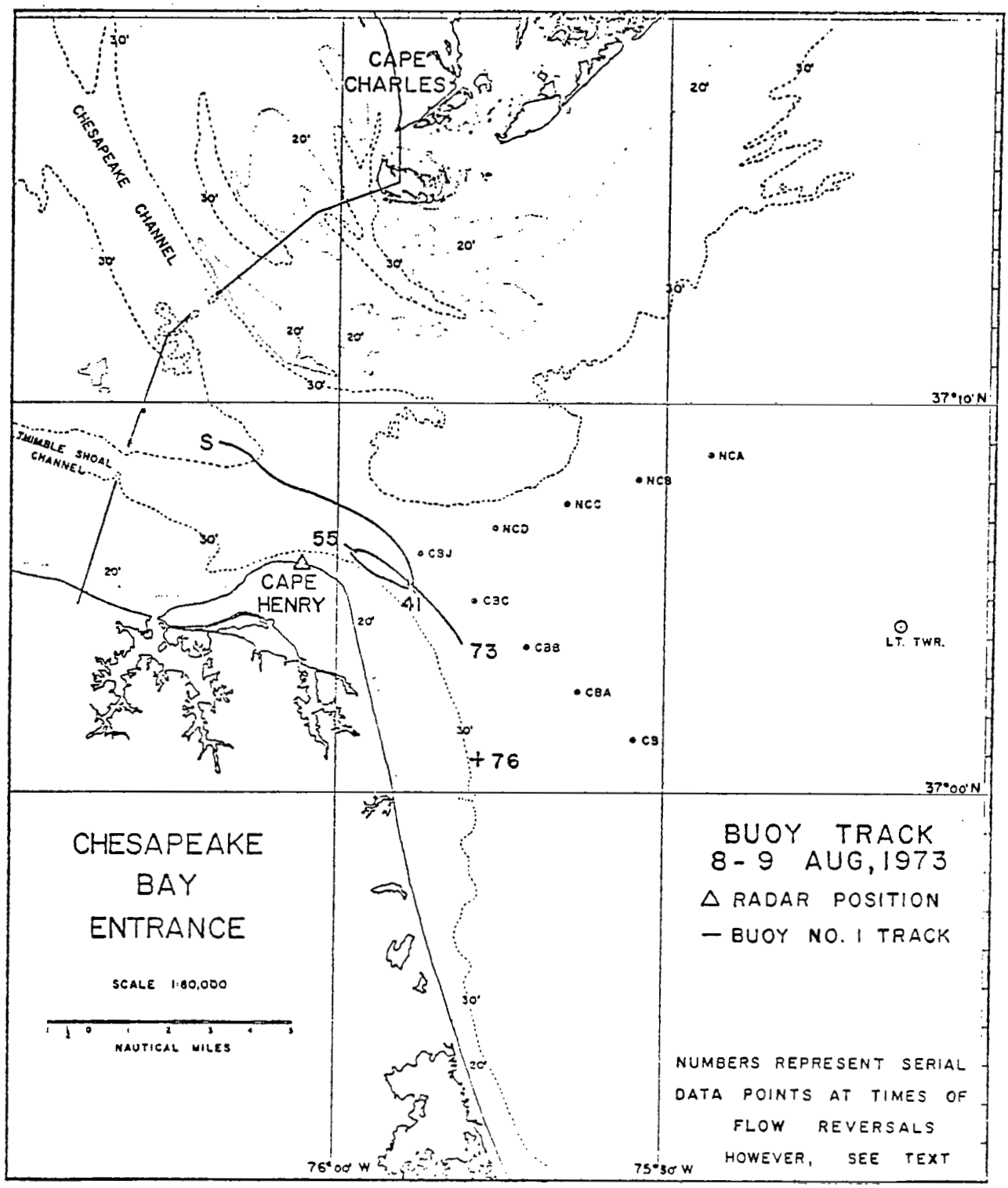

Figure 1.- Trajectories of radar-tracked buoys for 24 hours on August 8-9, 1973.

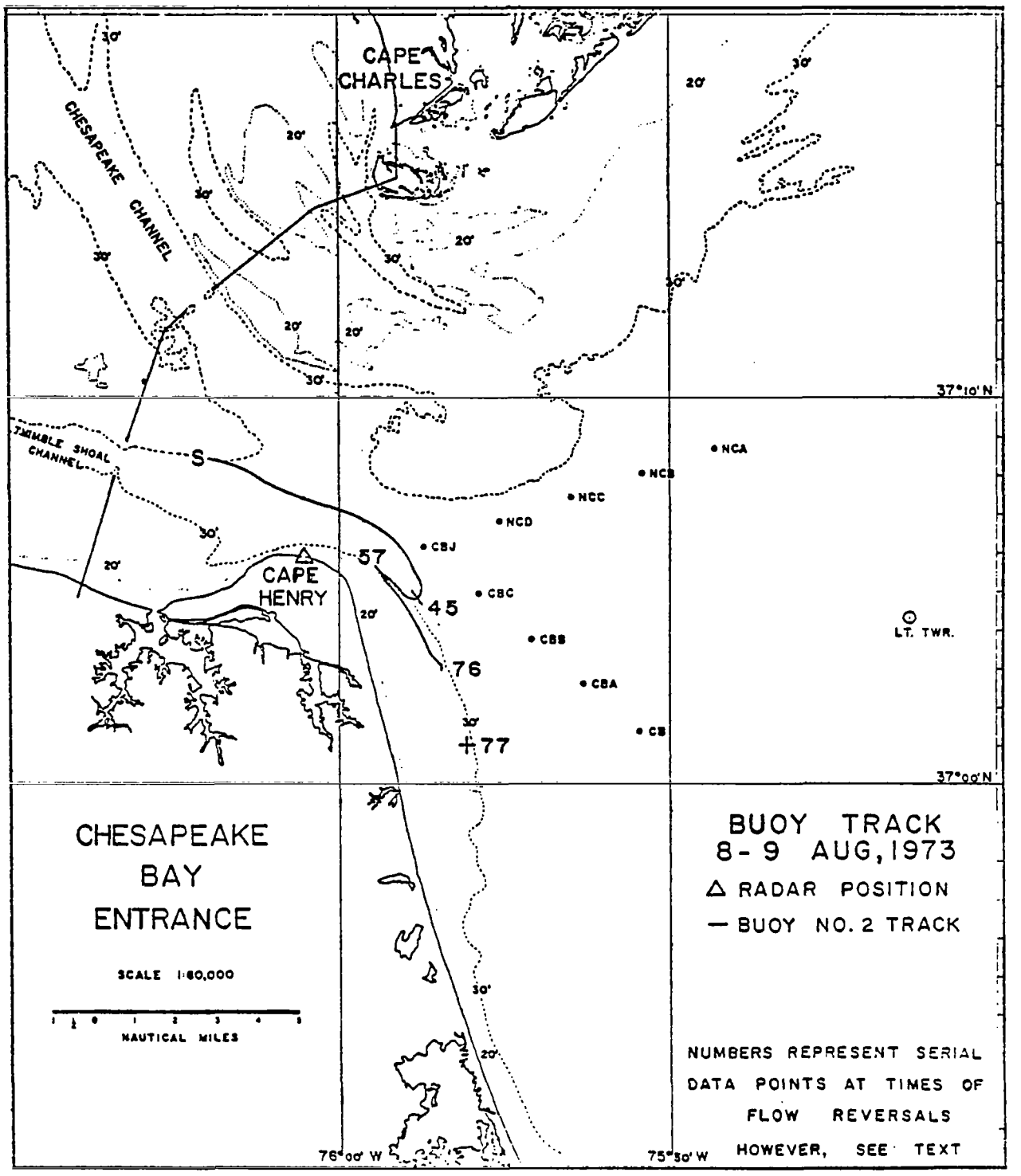

Figure 1.- Continued.

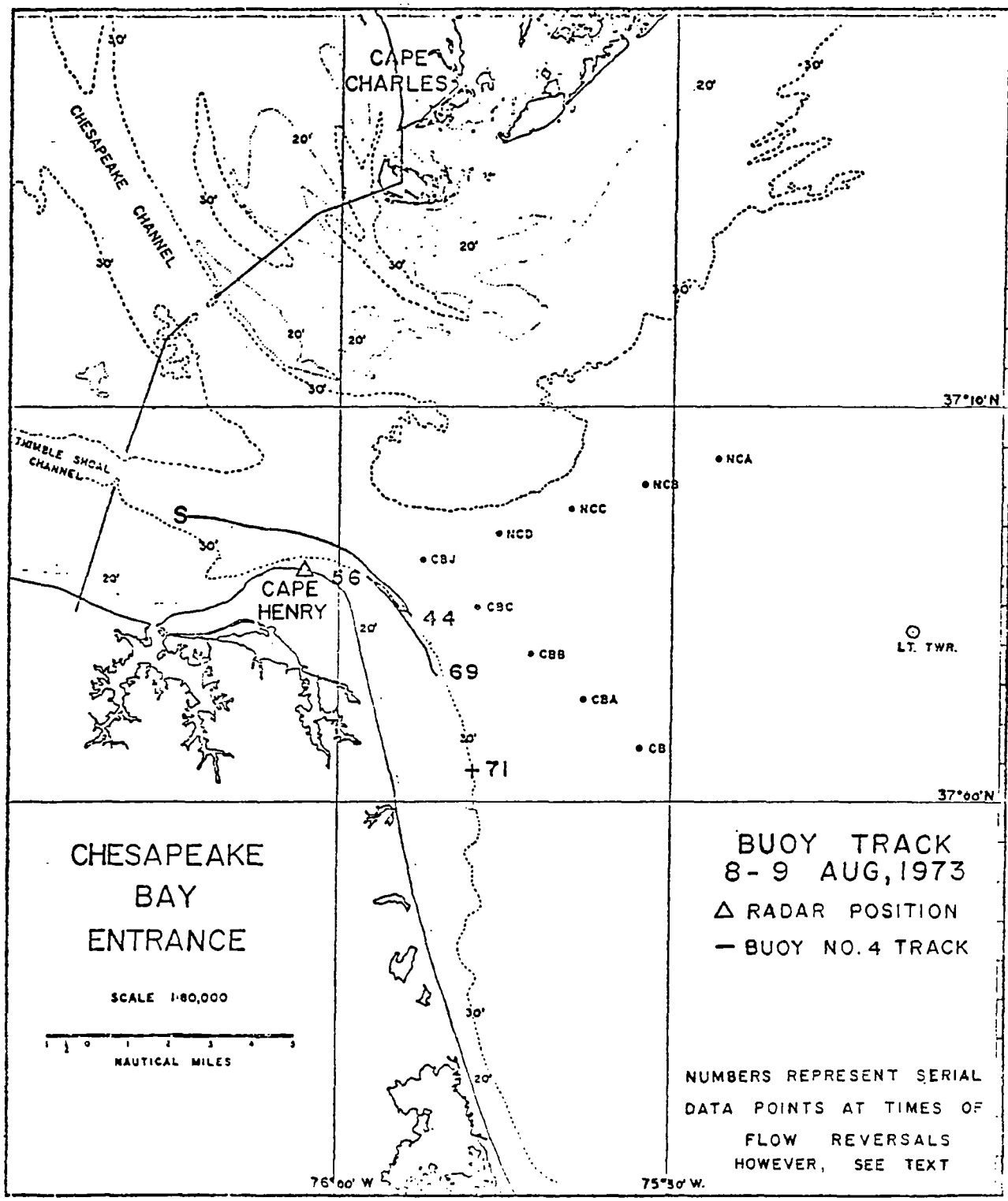

Figure 1.- Concluded.

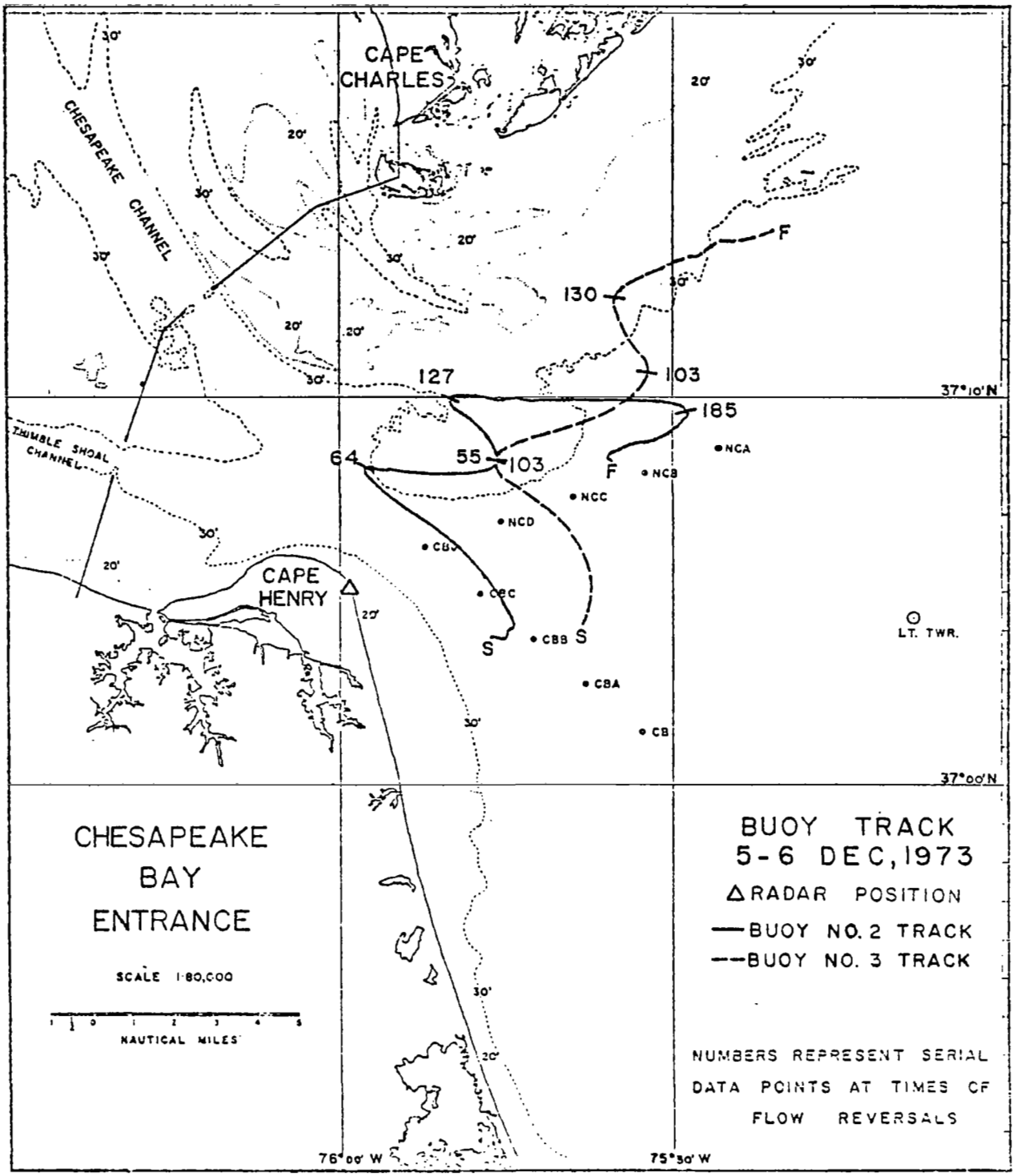

Figure 2.- Trajectories of radar-tracked buoys for 34 hours on December 5-6, 1973.

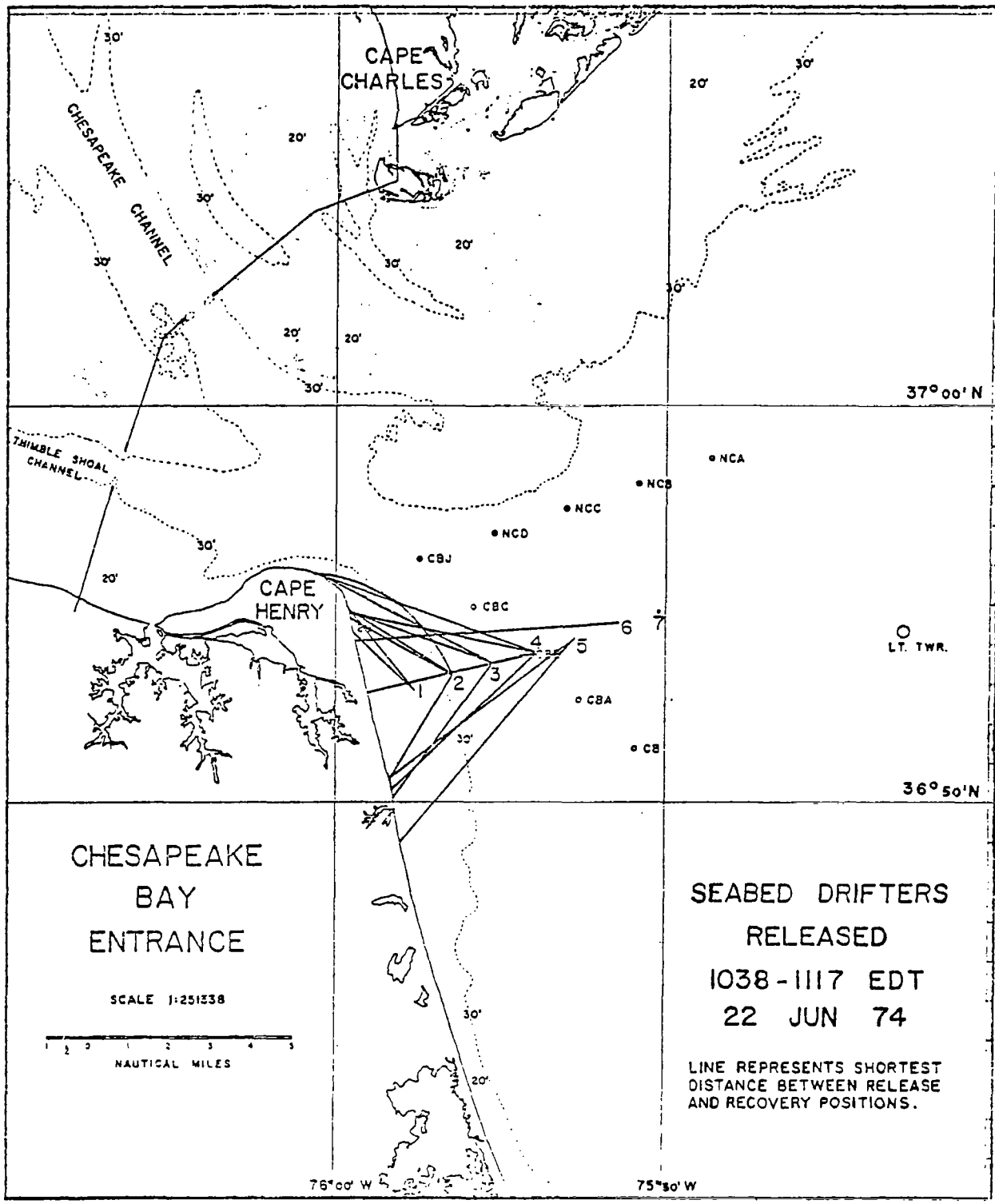

Figure 3.- Recovery positions for seabed drifters released 1038-1117 EDT, June 22, 1974.

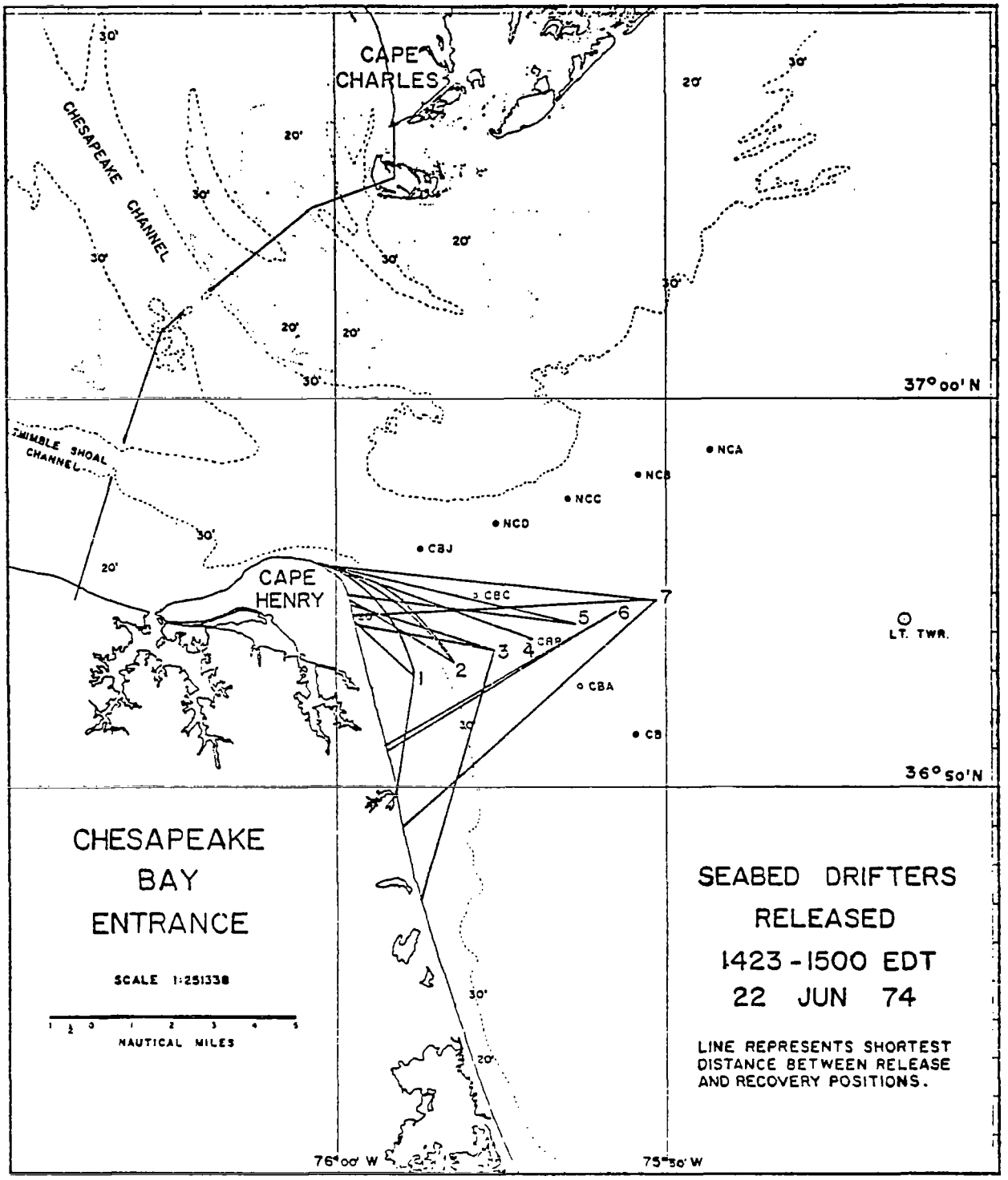

Figure 4.- Recovery positions for seabed drifters released 1423-1500 EDT, June 22, 1974.

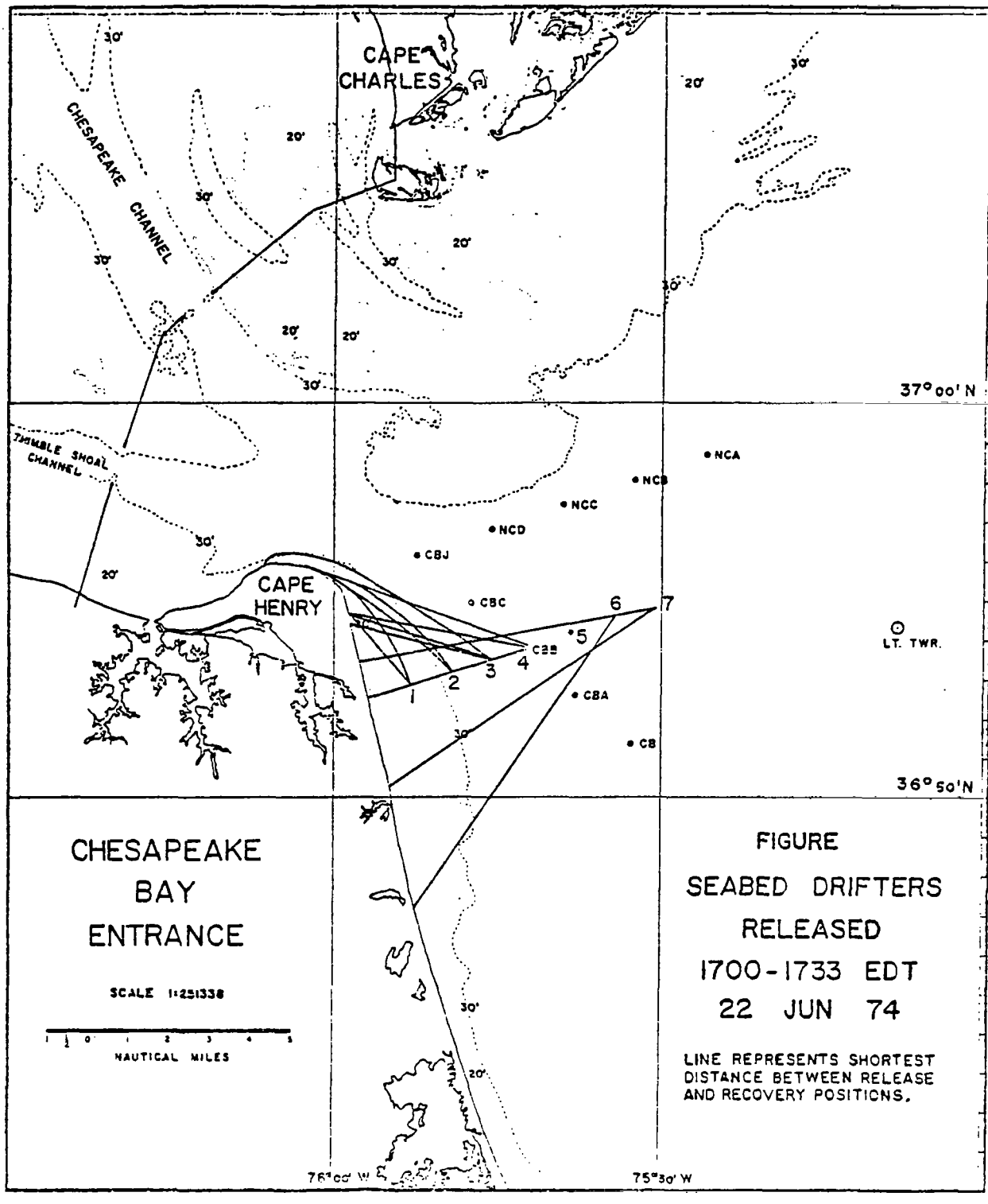

Figure 5.- Recovery positions for seabed drifters released 1700-1733 EDT, June 22, 1974.

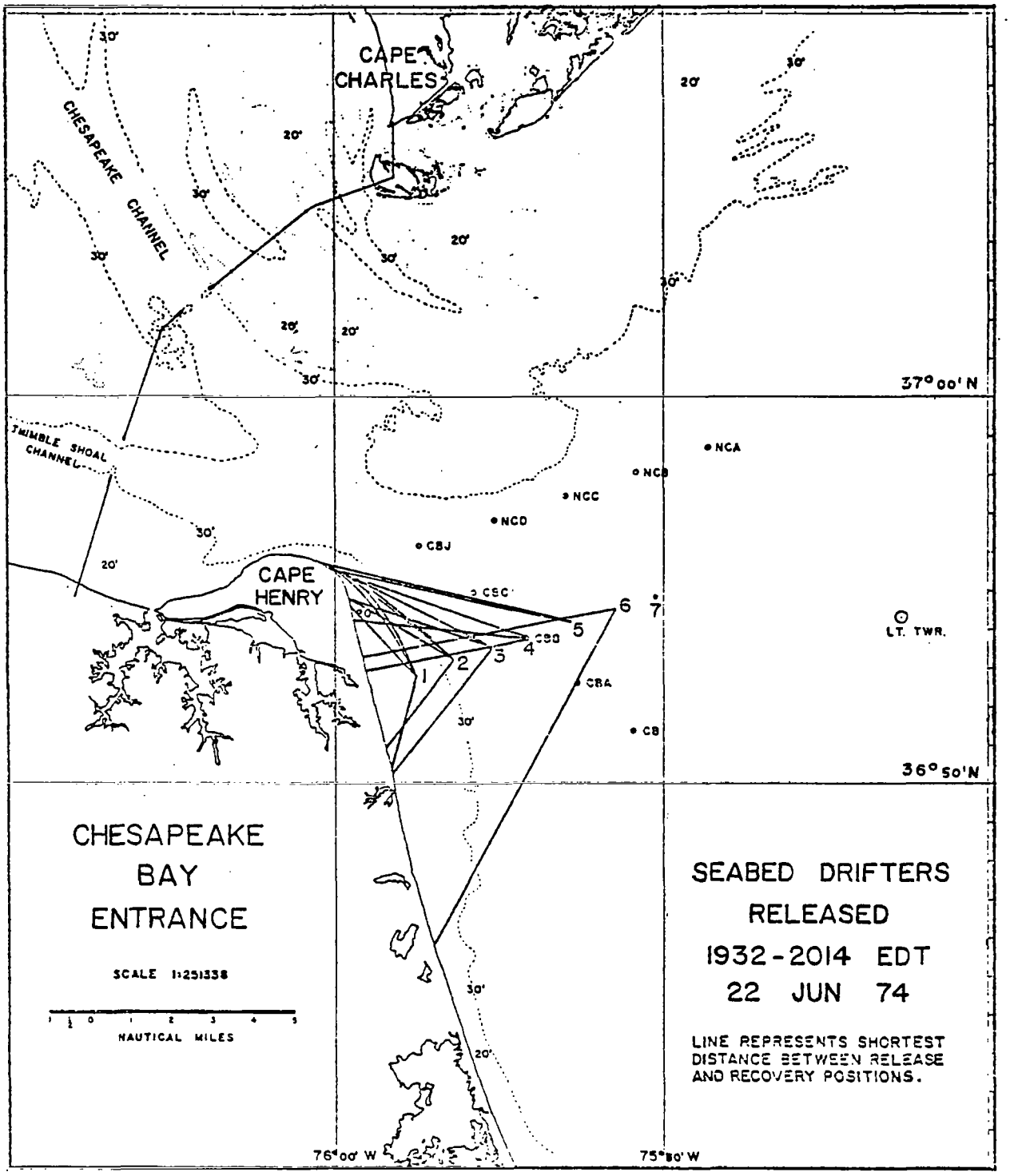

Figure 6.- Recovery positions for seabed drifters released 1932-2014 EDT, June 22, 1974.

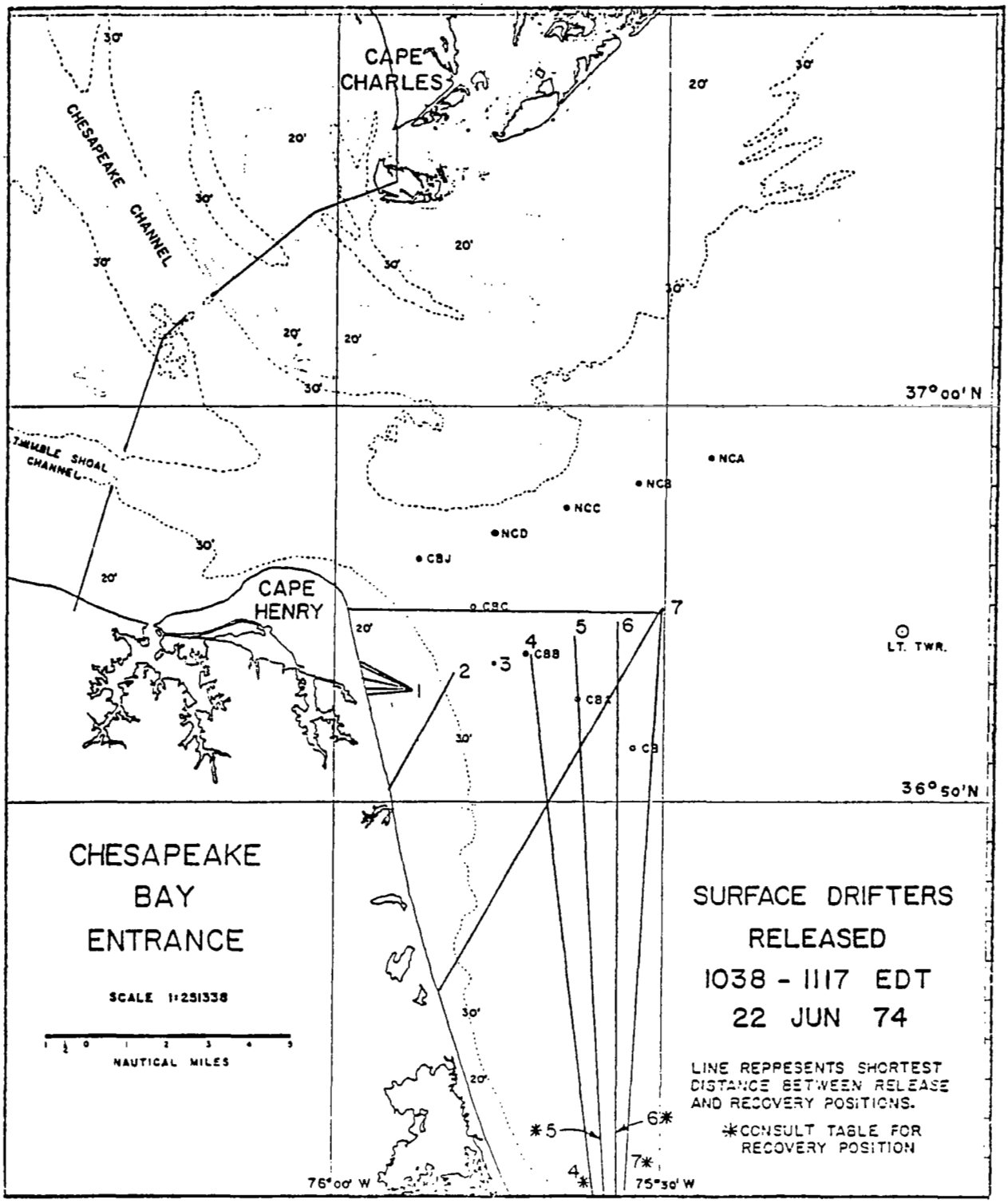

Figure 7.- Recovery positions for surface drifters released 1038-1117 EDT, June 22, 1974.

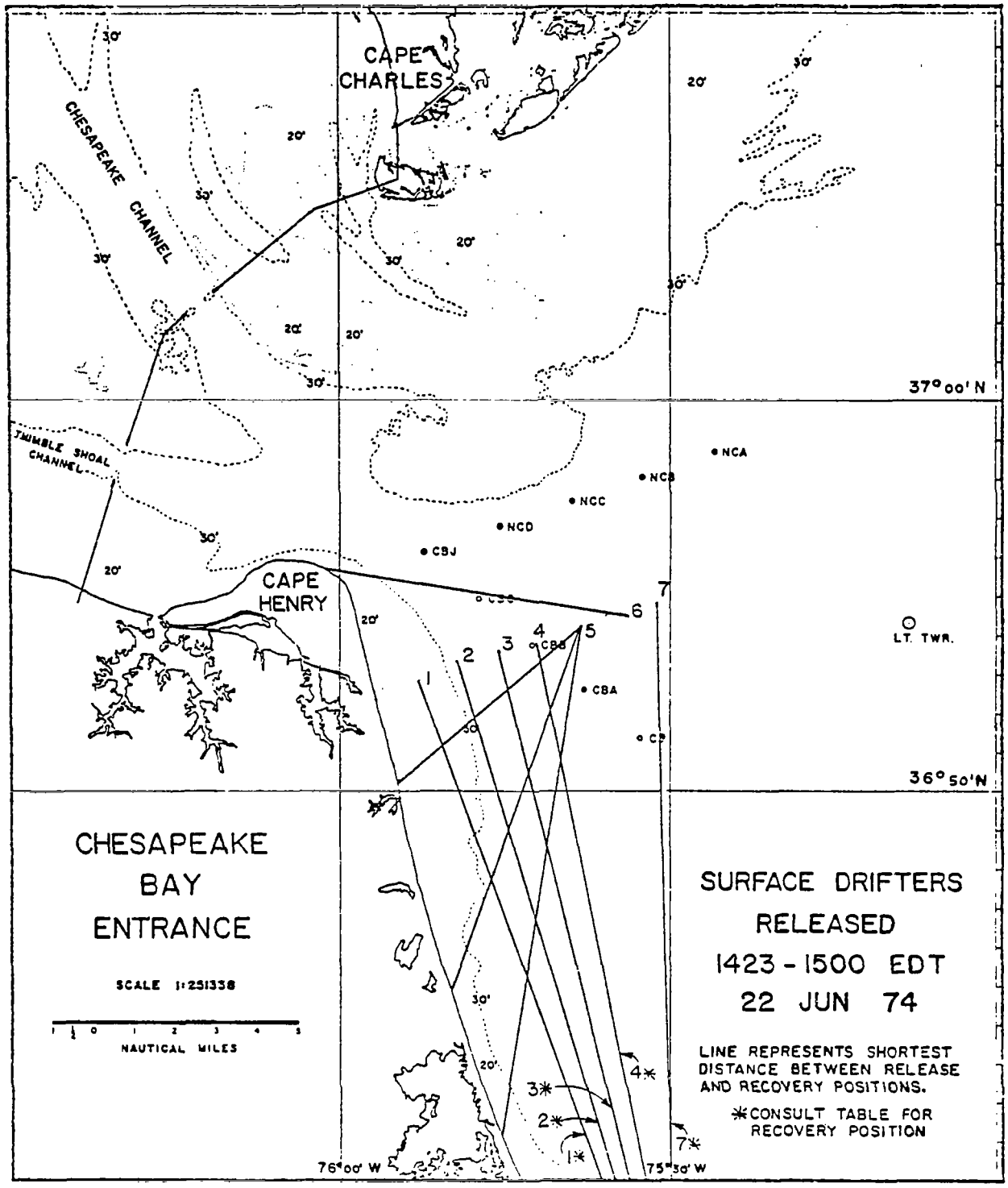

Figure 8.- Recovery positions for surface drifters released 1423-1500 EDT, June 22, 1974.

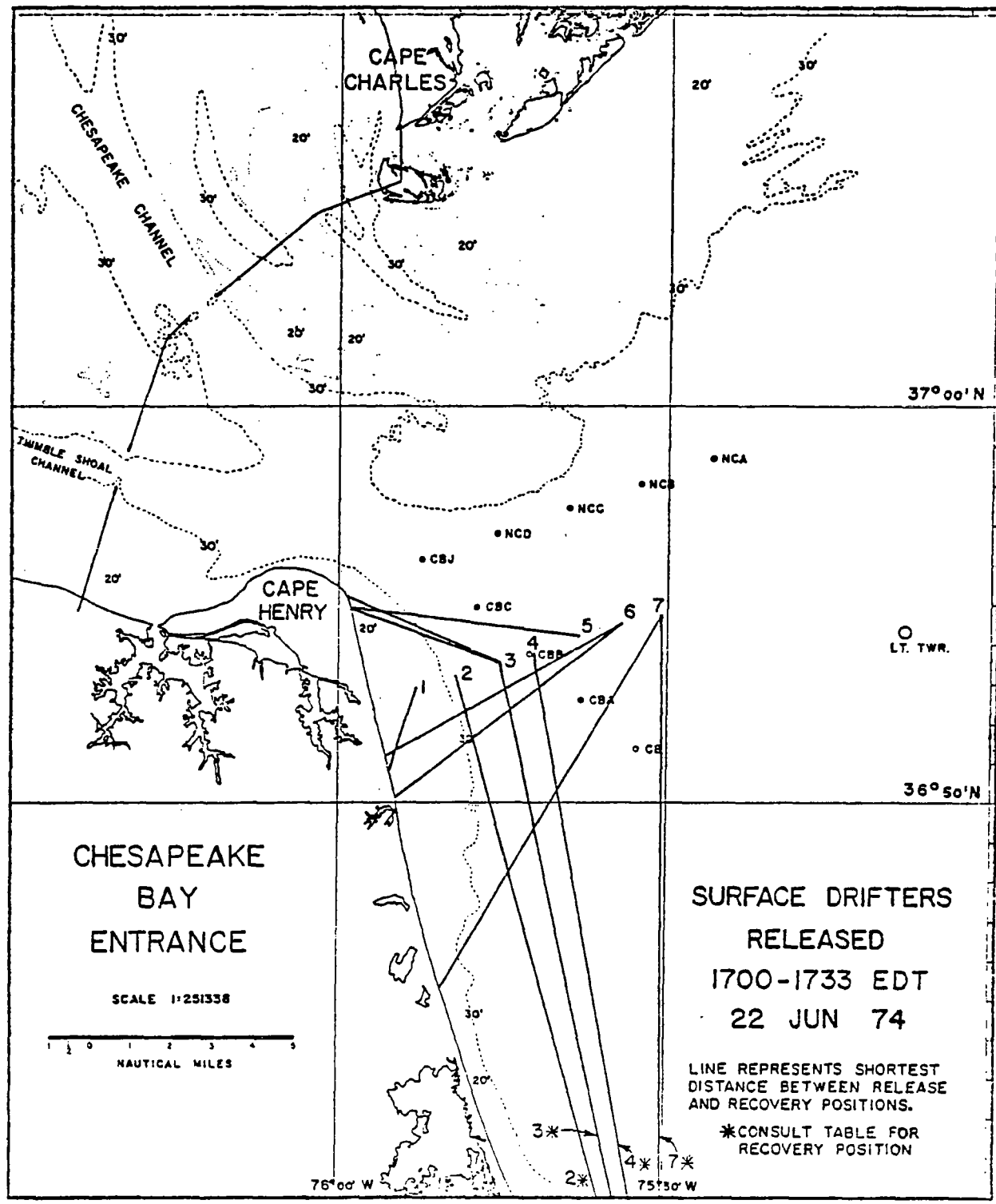

Figure 9.- Recovery positions for surface drifters released 1700-1733 EDT, June 22, 1974.

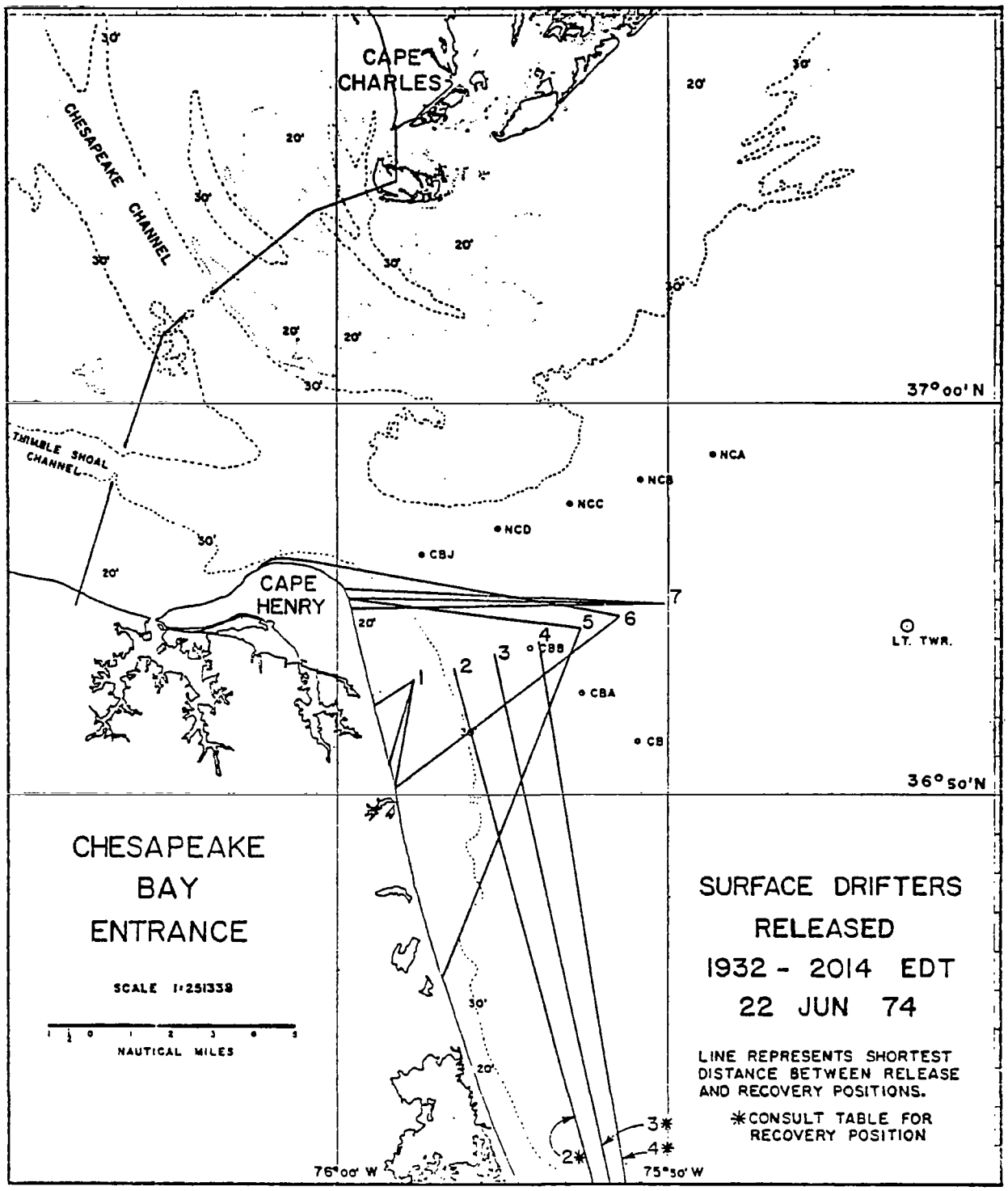

Figure 10.- Recovery positions for surface drifters released 1932-2014 EDT, June 22, 1974.

SUSPENDED PARTICULATE MATTER IN THE CHESAPEAKE BAY ENTRANCE AND ADJACENT SHELF WATERS

Kathryn J. Gingerich and George F. Oertel
Old Dominion University

INTRODUCTION

The Department of Oceanography, Old Dominion University, participated in a 1980 NASA/NOAA Superflux program. To support the scientific objectives of the program, water samples were collected and analyzed for hydrocarbons, chlorophyll, nutrients, and suspended solid concentrations and size distributions. The program consisted of three experimental study periods (March, Superflux I, June, Superflux II, and October, Superflux III) in 1980 to study the plume of Chesapeake Bay under various seasonal conditions.

This report utilized the data collected during the Superflux II mission to describe the distribution of several component characteristics of suspended solids that may have influenced the Chesapeake Bay entrance and adjacent shelf waters.

Superflux II was conducted between the 18th and the 27th of June, 1980. The NOAA ships Delaware II and George B. Kelez and the R/V Linwood Holton collected water from 50 stations adjacent to the entrance of Chesapeake Bay (figs. 1(a) and 1(b)). Samples were collected at standard Superflux stations (along four shelf transects) and at six BAPLEX stations. BAPLEX is a program at the Department of Oceanography to study bay plumes. Station locations and sequences of sampling were determined by Dr. James P. Thomas, Superflux work unit monitor (tables 1 to 3).

Approximately 400 samples were collected for the various analyses, including 138 for suspended solids. Characteristics of suspended solids that were analyzed included: total suspended matter (TSM), total suspended inorganics (TSI), total suspended organics (TSO), percent organics, particle size distribution (PSD) and presence or absence of 11 of the most prominent particle types.

METHODS

Optimal vertical representation of the water column was obtained by sampling four depths at each station. Surface samples were taken with buckets and 8-liter Niskin bottles were used to obtain water samples from two mid-depths and 1 m above the bottom. Samples to be analyzed for suspended solids were withdrawn first, followed by the biological and chemical samples. Approximately one liter was collected for determination of TSM and 500 milliliters were

collected for PSD analysis. Temperature and salinity measurements were also taken at each station with an RS-5 inductive salinometer.

The suspended solids were filtered onboard ship immediately following sample collection using Gelman type A/E glass fiber filters that had been prewashed, preignited and preweighed. Filters were weighed on a Mettler Balance with an accuracy of 0.1 mg.

Initially, a microscopic overview of the filters revealed Ceratium sp., Peridinium sp., a variety of centric diatoms, Biddulphia sp., tintinnids, lamillebranch larvae, pennate diatoms, a variety of zooplankton, fecal pellets, inorganic/organic fibers and quartz grains as the most prominent particle types present in the samples. More thorough microscopic analysis of each filter was performed to determine the presence, absence, or abundance of each particle type.

Concentrations of TSO and TSI were determined by weight loss after ignition of the filters for 2 hours at 400° C. The filters were equilibrated for 1 hour before being weighed.

OBSERVATIONS AND DISCUSSION OF RESULTS

The three major parameters of suspended solids, total suspended matter, total suspended inorganics and total suspended organics, were plotted in cross-section and areally for the three depth intervals. Since precipitation on the watersheds of the Chesapeake Bay was abnormally low in June, low concentrations of total particulates were expected. The average concentration of the 138 samples analyzed for TSM was 3.2 mg/ℓ (table 4).

The distribution of surface concentrations illustrated that the concentrations of total suspended matter were lower at the shelf stations and higher adjacent to the Bay entrance (fig. 2). The highest surface concentrations were found adjacent to Cape Henry, Virginia. The concentrations were relatively constant (2.1 to 2.5 mg/ℓ) across the Bay entrance in a northeast direction and in a southerly direction along the Virginia coastline.

The areal distributions of concentrations at the mid-depth interval (3 to 6 m) and at 1 m above the bottom showed the same general trend (figs. 3 and 4). The highest concentrations were near Cape Henry, and concentrations decreased in an offshore direction and south of False Cape.

The cross-sectional diagrams of the five transects (fig. 5) were constructed as an alternate method of viewing the data. The BAPLEX transect (profile A) indicated a minor increase in total suspended matter with depth, with higher values at the margins of the entrance adjacent to Cape Henry and Fishermans Island. Approximately 9.2 km to the south of profile A (profile B), the concentration of total suspended matter decreased in an offshore direction and increased with depth. Data from profiles C, D and E exhibited similar trends with increasingly lower concentrations away from Cape Henry.

Surface distribution of organic matter showed very little variation in concentration (fig. 6). Concentrations were generally low and values ranged from 0.4 to 1.4 mg/ℓ with a mean of 1.1 mg/ℓ. It was anticipated that organics would comprise the major portion of total suspended particulates due to the extremely low runoff, but it was found that organic material accounted for only 30 to 50 percent of TSM in the majority of the samples. The organic percentage of TSM increased slightly in an offshore direction. Relatively high inorganic percentages of total suspended matter may be due to three potential sources: (1) resuspension within the Bay, (2) resuspension over shoals in the Bay mouth area, and/or (3) runoff. Since the concentration of organic matter was relatively constant, variations in concentrations of inorganic matter controlled variations in the concentrations of total suspended matter. Spatial distributions of total suspended inorganics at the three depth intervals showed trends identical to those for TSM (figs. 7 to 9).

Inspection of the microscopic components of the suspended solids data revealed several general trends that complimented the trends observed for concentrations of organic and inorganic suspended matter (appendix).

Centric diatoms, fecal pellets and quartz grains appeared to have sources within the Bay, whereas zooplankton were found in patches outside the Bay entrance. Centric diatoms were present at all depths at the stations across the Bay mouth (profile A) and in surface and mid-depth nearshore waters. Stations further offshore did not contain these species at any depth (stations 803, 804, 807, 810, and 813). Quartz grains were observed in samples from all depths in the Bay entrance and from nearshore stations for transects B, C and D (stations 69, 802, 803, 805, 819 and 820). Tintinnids showed a similar pattern; they were observed at all depths at the Bay mouth stations (profile A) and stations 819 and 820. Fecal pellet distribution in bottom waters appeared to be limited to the Bay entrance area and nearshore waters adjacent to Cape Henry and Virginia Beach (stations 69, 802, 805, 808, 820, 819 and 71). Inorganic/organic fibers were present in surface waters for all BAPLEX stations and at depth at stations adjacent to Thimble Shoal Channel (stations 3 and 800). Surface waters off False Cape, Virginia, also contained some of this material.

The distribution of concentrations of total suspended matter as depicted by contouring procedures has obvious limitations since the sample collection was spaced over a 10-day period. It was also difficult to create a synoptic view of the area, but the Superflux II observations did not seem to illustrate the presence of a surface or near-surface turbidity plume emerging from the mouth of Chesapeake Bay. Trends observed were characteristic of June conditions only and cannot be used to predict patterns and concentrations during different seasons and under different runoff conditions.

Partial analysis of the October 15, 1980 portion of the Superflux III data did illustrate the presence of a surface or near-surface turbidity plume associated with Chesapeake Channel waters. The October 15 experiment involved a sampling scheme that was more appropriate to local dynamics, therefore aiding in the creation of a synoptic view of the region. Four ships were employed to collect samples simultaneously along four transects (fig. 1b). Similar procedures were followed for suspended solids analysis of total

suspended matter, total suspended inorganics and total suspended organics. Concentrations were plotted in cross-section to determine whether a pattern was evident (fig. 10).

The contours drawn for the Bay entrance (profile A) were speculative because bottom samples were not collected at those three stations. However, concentrations along profile A illustrated higher concentrations at the surface adjacent to Chesapeake Channel. Insufficient data collection from the Bay margins prevents any speculation on concentration variability that may have been produced by the North Channel or the James River.

Profile B illustrated relatively high surface concentrations adjacent to Virginia Beach and decreasing values in an offshore direction. The central part of profile C showed the strongest influence of Chesapeake Channel waters and the possible existence of a turbidity plume.

Twenty-two km south of Cape Henry there was still evidence of relatively high surface concentrations through the central part of the profile.

CONCLUSION

Analyses of water samples collected during the Superflux II mission indicated several turbid regions associated with resuspended material, although there seemed to be no semblance of a surface or near-surface turbidity plume emerging from the Chesapeake Bay mouth. This was probably related to drought conditions prior to and during the time of the experiment. Superflux III size distribution data (ref. 1) and total suspended matter calculations did illustrate the possible existence of a near-surface turbidity plume in the Bay entrance area. Completion of the analyses for the Superflux III data, including the determination of TSO and TSI, will provide more information about the contents and presence of a surface or near-surface turbidity plume in the area of the Chesapeake Bay entrance.

REFERENCE

1. Byrnes, Mark R,; and Oertel, George F.: Particle Size Distribution of Suspended Solids in the Chesapeake Bay Entrance and Adjacent Shelf Waters. Chesapeake Bay Plume Study - Superflux 1980, NASA CP-2188, 1981 (Paper no. 16 of this compilation).

STATION DEPTH	DATE TIME DEPTH(M)	TOTAL CONCENTRATION (mg/ℓ)	INORGANIC CONCENTRATION (mg/ℓ)	ORGANIC CONCENTRATION (mg/ℓ)	PERCENT ORGANICS	Ceratium sp.	Peridinium sp.	Centric diatoms	fecal pellets	Lamelli-branch larvae	Zooplankton	Pennate diatoms	quartz grains	Biddulphia sp.	Inorganic/organic fibers	Tintinnids
Delaware II																
800-1	6-17	2.29	1.35	0.93	40.9	X			X	X						
800-5	2100	2.96	2.04	0.92	31.0	X			X	X						
800-7	15	3.90	2.16	0.93	30.0	X		X	X					X		X
801-1	6-18	2.73	1.72	1.01	37.0	X	X	X								X
801-5	1210	2.10	1.10	1.00	47.6	X	X		X	X		X				
801-10	15	3.90	3.20	0.70	18.0	X		X	X				X			X
801-13		4.50	3.50	1.00	22.2	X	X		X				X	X		X
69-1	6-18	3.49	2.35	1.14	32.7	X	X	X					X			
69-5	1445	4.65	3.33	1.31	28.3	X	X	X		X			X			
69-10	11	10.60	9.30	1.30	12.3	X	X	X	X				X	X		X
802-1	6-18	2.68	1.75	1.03	38.5	X	X	X		X			X			
802-5	1700	0.61	0.00	0.61	100.0	a	X			X	X					
802-10	18	2.37	1.34	1.03	43.5	X	X		X			X	X			
802-15		7.94	7.11	0.82	10.4	X		X	X				X			X
803-1	6-18	3.10	2.20	0.90	29.0	X	X			X	X			X		
803-5	2030	2.20	1.40	0.80	36.4	a	X						X			
803-10	11	2.22	1.31	0.91	40.9	X	X				X	X	X			
804-1	6-18	2.35	1.33	1.02	43.5	X	X			X						
804-5	2330	2.00	1.00	1.00	50.0	a	X			X						
804-10	14.6	1.72	0.91	0.81	47.1	a	X			X	X					
804-15		3.06	2.24	0.82	26.7	X			X							X

STATION DEPTH	DATE TIME DEPTH(M)	TOTAL CONCENTRATION (mg/ℓ)	INORGANIC CONCENTRATION (mg/ℓ)	ORGANIC CONCENTRATION (mg/ℓ)	PERCENT ORGANICS	Ceratium sp.	Peridinium sp.	Centric diatoms	fecal pellets	Lamelli-branch larvae	zooplankton	Pennate diatoms	quartz grains	Biddulphia sp.	inorganic/organic fibers	Tintinnids
1A-1	6-19 0952 20.1	2.60	1.70	0.90	34.6	X		X		X			X			
2A-1	6-19 1018 20.1	4.90	3.50	1.40	28.6	X	X			X	X					
3A-1	6-19 1036 9	5.50	4.30	1.20	21.8	X		X	X				X			X
805-1	6-19	2.60	1.60	0.80	30.8	X	X			X			X			X
805-5	1200	2.80	1.80	1.00	35.7	X	X									X
805-10	10	9.80	8.30	1.50	18.1	X		X	X	X			X			
70-1	6-19	1.90	0.90	1.00	52.6	X	X			X			X			
70-5	1720	1.50	0.70	0.80	53.3	X	X			X						X
70-10	13	2.60	1.50	1.10	42.3	a	X	X		X	X		X			
70-13		1.90	1.00	0.90	47.4	a		X			X			X		
806-1	6-19	1.20	0.60	0.60	50.0	X				X	X					
806-5	1940	1.00	0.30	0.70	70.0	X										
806-10	15	1.50	0.60	0.90	60.0	X	X			X	X					
806-15		3.23	1.92	1.31	40.6	X		X	X	X		X		X		

STATION DEPTH	DATE TIME DEPTH (M)	TOTAL CONCENTRATION (mg/ℓ)	INORGANIC CONCENTRATION (mg/ℓ)	ORGANIC CONCENTRATION (mg/ℓ)	PERCENT ORGANICS	Ceratium sp.	Peridinium sp.	Centric diatoms	fecal pellets	Lamellibranch larvae	zooplankton	Pennate diatoms	quartz grains	Biddulphia sp.	Inorganic/organic fibers	Tintinnids
807-1	6-19	1.46	0.73	0.73	50.0	X					X					
807-5	2150	1.32	0.66	0.66	50.0	X					X					
807-10	16.5	1.18	0.65	0.52	44.4	X	X				X					
807-15		2.04	1.22	0.82	40.0	a			X			X		X		
66-1	6-20 0535 1280	1.46	1.06	0.40	27.3	X										
67-1	6-20 0635 914	1.24	0.83	0.41	33.3	X	X									
68-1	6-20 0735 93	1.09	0.61	0.48	43.8						X					
81-1	6-20 0845 48	0.86	0.33	0.53	61.5	X										
82-1	6-20 0945 35	1.07	0.53	0.53	50.0	X										
83-1	6-20 1100 33	1.13	0.73	0.40	35.3											

STATION DEPTH	DATE TIME DEPTH (M)	TOTAL CONCENTRATION (mg/ℓ)	INORGANIC CONCENTRATION (mg/ℓ)	ORGANIC CONCENTRATION (mg/ℓ)	PERCENT ORGANICS	Ceratium sp.	Peridinium sp.	Centric diatoms	fecal pellets	Lamelli-branch larvae	zooplankton	Pennate diatoms	quartz grains	Bidduiphia sp.	inorganic/ organic fibers	Tintinnids
808-1	6-20	1.92	1.32	0.60	31.0	X	X	a						X		
808-5	1750	2.30	1.51	0.79	34.3	X	X	X	X	X						
808-10	10	4.40	3.10	1.30	29.6	X		X	X					X		
809-1	6-20	1.48	0.60	0.87	59.1	X	X	X	X	X			X			
809-5	2000	1.28	0.61	0.68	52.6	X	X			X						
809-10	15	2.38	1.29	1.09	45.7	a	X	X		X	X					
809-15		2.27	1.47	0.80	35.3	X		a			X			X		
810-1	6-20	1.54	0.81	0.74	47.8	X					X					
810-6	2235	0.97	0.48	0.48	50.0	X				X	X					
810-12	17	1.61	0.74	0.87	54.2	a	X			X				X		
810-18		2.27	1.33	0.93	41.2	X	X					X				
811-1	6-21	0.74	0.20	0.54	72.7	X					X					
811-7	0835	2.04	1.43	0.61	30.0	X					X					
811-14	20	1.39	0.90	0.49	35.0	X	X									
811-21		2.01	1.21	0.81	40.0	a	X									
813-1	6-21	0.88	0.47	0.41	46.2	X					X					
813-6	1105	1.22	0.68	0.54	44.4	X				X	X					
813-12	18	1.43	0.88	0.54	38.1	a	X									
813-18		2.08	1.34	0.74	35.5	a	X				X	X				

STATION DEPTH	DATE TIME DEPTH (M)	TOTAL CONCENTRATION (mg/ℓ)	INORGANIC CONCENTRATION (mg/ℓ)	ORGANIC CONCENTRATION (mg/ℓ)	PERCENT ORGANICS	Ceratium sp.	Peridinium sp.	Centric diatoms	fecal pellets	Lamelli-branch larvae	zooplankton	Pennate diatoms	quartz grains	Biddulphia sp.	inorganic/organic fibers	Tintinnids
812-1	6-21	1.22	0.74	0.47	38.9	a	X			X	X					
812-10	1410	1.20	0.67	0.53	44.4	X	X			X	X					
812-15	20	1.19	0.66	0.53	44.4	X	X				X					
812-20		1.62	0.88	0.74	45.8	a	X				X					
71-1	6-21	1.37	0.75	0.62	45.0	X					X					
71-6	1755	1.60	0.83	0.76	47.8	a	X	X		X	X					
71-12	14	1.69	1.01	0.68	40.0	X	X	X	X	X						
Kelez																
800-1	6-24	4.80	3.50	1.30	27.1	X	X	X	X			X	X	X	X	
800-5	2152	35.10	27.60	7.50	21.4	X		X	X		X	X		X	X	
800-10	12.8	5.40	4.20	1.20	22.2											
800-15		12.90	11.10	1.90	14.7	X		X	X			X	X	X	X	
46-1	6-25	1.10	0.60	0.50	45.5	X									X	
46-3	0703	1.40	0.60	0.80	57.1	X									X	
	24															
47-1	6-25	1.27	0.80	0.47	36.8	X						X			X	
47-3	0808	1.71	1.23	0.48	28.0	X						X			X	
	15.8															
48-1	6-25	2.46	1.87	0.60	24.2	X	X					X			X	
48-3	0857	-	-	-	-	X	X				X					
	24															

STATION DEPTH	DATE TIME DEPTH (M)	TOTAL CONCENTRATION (mg/ℓ)	INORGANIC CONCENTRATION (mg/ℓ)	ORGANIC CONCENTRATION (mg/ℓ)	PERCENT ORGANICS	Ceratium sp.	Peridinium sp.	Centric diatoms	fecal pellets	Lamelli-branch larva	zooplankton	Pennate diatoms	quartz grains	Biddulphia sp.	inorganic/ organic fibers	Tintinnids
805-1	6-25	2.20	1.10	1.10	50.0	X	X	X	X	X			X			
805-5	1236	2.50	2.50	0.00	0.00	X	X	X	X	X					X	X
805-10	9.8	4.00	2.90	1.10	2.75	X		X	X	X			X	X	X	
70-1	6-25	2.80	1.70	1.10	39.3	X	X	X		X			X		X	X
70-5	1433	2.00	1.00	1.00	50.0	X	X	X		X			X			
70-10	15.5	3.60	2.30	1.30	36.1	X	X	X					X		X	
70-15		4.40	1.90	1.50	34.1	X	X	X	X	X			X	X	X	
819-1	6-26	2.50	1.50	1.00	40.0	X	X	X		X					X	X
819-5	1015	2.50	1.50	1.00	40.0	X	X	X		X					X	
819-10	11.0	11.90	9.40	2.50	2.10	X	X	X	X	X			X	X	X	
820-1	6-26	2.58	1.44	1.13	44.0	a	X						X		X	
820-6	1045	2.80	1.80	1.00	35.7	X	X	X		X					X	
820-12	11.9	25.50	22.00	3.50	13.7	X	X	X	X	X		X	X	X	X	
49-1	6-27	3.30	2.50	0.80	24.2	X			X				X		X	X
49-3	0825 27.4	2.11	1.37	0.74	35.0	X	X						X			
50-1	6-27	6.70	12.80	3.90	23.4	X					X		X			X
50-3	0940 22.0	0.80	0.00	0.80	100.0	X	X			X	X					X
51-1	6-27	2.70	1.50	1.20	44.4	X	X	X		X	X				X	
51-3	1054 12.2	14.65	11.41	3.23	22.1	X	X	X	X	X			X			

STATION DEPTH	DATE TIME DEPTH (M)	TOTAL CONCENTRATION (mg/ℓ)	INORGANIC CONCENTRATION (mg/ℓ)	ORGANIC CONCENTRATION (mg/ℓ)	PERCENT ORGANICS	Ceratium sp.	Peridinium sp.	Centric diatoms	fecal pellets	Lamelli-branch larval	zooplankton	Pennate diatoms	quartz grains	Biddulphia sp.	inorganic/ organic fibers	Tintinnids
Holton																
00-Surface	6-18	3.87	2.10	1.77	45.7											
00-1	0755	4.75	3.38	1.38	28.9	NO COMPONENT PARTICLE ANALYSIS										
	9.1															
0-1	6-18	1.75	0.98	0.77	43.8											
0-3	0855	2.65	1.77	0.88	33.3											
	12.8															
0.5-Surface	6-18	2.42	0.99	1.43	59.1											
0.5-1	0920	1.89	1.11	0.78	41.2											
0.5-3	7.0	1.77	0.99	0.77	43.8											
1-1	6-18	1.98	0.77	1.21	61.1											
1-3	1030	5.72	0.87	1.85	68.0											
	8.0															
2-1	6-18	2.33	1.22	1.11	47.6											
2-3	1100	2.72	1.57	1.15	42.3											
	17.0															
3-1	6-18	2.55	1.28	1.28	50.0											
3-3	1130	1.73	0.86	0.86	50.0											
	13.1															
4-1	6-18	3.77	2.62	1.15	30.6											
4-3	1245	3.47	2.21	1.26	36.4											
	11.0															

STATION DEPTH	DATE TIME DEPTH (M)	TOTAL CONCENTRATION (mg/ℓ)	INORGANIC CONCENTRATION (mg/ℓ)	ORGANIC CONCENTRATION (mg/ℓ)	PERCENT ORGANICS	Ceratium sp.	Peridinium sp.	Centric diatoms	fecal pellets	Lamelli-branch larvae	zooplankton	Pennate diatoms	quartz grains	Biddulphia sp.	inorganic/organic fibers	Tintinnids
00-Surface	6-24	2.10	1.20	0.90	42.9	a		X		X			X	X	X	a
00-1	0800	1.90	1.00	0.90	47.4	a	X			X			X	X		a
00-3	10.7	1.70	0.80	0.90	52.9	X				X			X	X		X
00-Bottom		2.59	1.69	0.80	30.7	X			X	X			X	X		X
0-Surface	6-24	2.29	1.19	1.09	47.8	X	X			X	X		X		X	X
0-1	0830	2.20	1.50	0.70	31.8	X		X		X			X			X
0-3	12.2	2.53	1.82	0.71	28.0	X	X	X	X	X			X	X		X
0-Bottom		3.63	2.75	0.88	24.3	X		X	X	X			X	X	X	X
1-Surface	6-24	2.50	1.00	1.50	60.0	X				X			X	X	a	X
1-1	0905	1.59	0.80	0.80	50.0	X	X	X	X	X			X	X		X
1-3	8.2	1.90	1.10	0.80	42.1	X	X	X		X			X	X		X
1-Bottom		2.09	1.00	1.09	52.4	X		X	X	X			X	X		X
2-Surface	6-24	2.20	0.80	1.40	63.6	X		X		X			X		a	X
2-1	1025	2.00	0.90	1.10	55.0	X		X		X			X		X	X
2-3	15.5	1.69	0.70	1.00	58.8	a	X	X		X					X	X
2-Bottom		1.99	1.19	0.80	40.0	X		X	X	X		X	X	X		X
3-Surface	6-24	2.09	1.00	1.09	52.4	X		X		X			X		X	X
3-1	1105	1.70	0.80	0.90	52.9	X	X	X		X			X		X	X
3-3	13.1	1.90	0.70	1.20	63.2	X	X	X		X					X	X
3-Bottom		3.58	2.69	0.90	25.0	X		X	X	X			X		X	X

STATION DEPTH	DATE TIME DEPTH (M)	TOTAL CONCENTRATION (mg/ℓ)	INORGANIC CONCENTRATION (mg/ℓ)	ORGANIC CONCENTRATION (mg/ℓ)	PERCENT ORGANICS	Ceratium sp.	Peridinium sp.	Centric diatoms	fecal pellets	Lamellibranch larval	zooplankton	Pennate diatoms	quartz grains	Biddulphia sp.	inorganic/organic fibers	Tintinnids
4-Surface	6-24	2.10	0.90	1.20	57.1	X		X		X		X		X	X	
4-1	1140	1.80	0.70	1.10	61.1	X		X		X		X		X		
4-3	10.1	2.21	1.01	1.21	54.6	X		X		X		X	X	X		
4-Bottom		4.90	3.90	1.00	20.4	X	X	X	X			X	X		X	

KEY:

X = present

a = abundant

TABLE 1.- SAMPLE STATION DATA:

NOAA Delaware II Cruise, JUNE 17-23, 1980

Station no.	Date	Time	Latitude	Longitude	Depth (m)
801	6/17	2100	36° 57.3 N	76° 02.9 W	15
801	6/18	1210	36° 59.2 N	76° 00.6 W	15
69	6/18	1445	36° 55.0 N	75° 58.0 W	11
802	6/18	1700	36° 56.0 N	75° 55.0 W	18
803	6/18	2030	36° 58.0 N	75° 51.5 W	11
804	6/18	2330	37° 00.6 N	75° 44.4 W	14.6
1A	6/19	0952	36° 57.6 N	75° 59.0 W	20.1
2A	6/19	1018	36° 56.6 N	75° 58.9 W	20.1
3A	6/19	1036	36° 55.6 N	75° 59.0 W	9
805	6/19	1200	36° 52.0 N	75° 56.0 W	10
70	6/19	1720	36° 52.4 N	75° 53.5 W	13
806	6/19	1940	36° 53.2 N	75° 48.6 W	15
807	6/19	2150	36° 54.4 N	75° 41.8 W	16.5
66	6/20	0535	36° 40.2 N	74° 30.0 W	1280
67	6/20	0635	36° 41.6 N	74° 36.4 N	914
68	6/20	0735	36° 42.9 N	74° 42.6 W	93
81	6/20	0845	36° 43.9 N	74° 49.2 W	48
82	6/20	0945	36° 45.3 N	74° 56.5 W	35
82	6/20	NS	36° 45.3 N	74° 56.5 W	35
83	6/20	1100	36° 46.5 N	75° 02.6 W	33
808	6/20	1750	36° 45.5 N	75° 54.7 W	10

TABLE 1.- Concluded

Station no.	Date	Time	Latitude	Longitude	Depth (m)
809	6/20	2000	36° 46.4 N	75° 49.0 W	15
810	6/20	2235	36° 37.6 N	75° 41.2 W	17
811	6/21	0835	36° 48.7 N	75° 32.6 W	20
813	6/21	1105	36° 35.9 N	75° 31.2 W	18
812	6/21	1410	36° 34.5 N	74° 40.2 W	20
71	6/21	1755	36° 33.7 N	75° 48.1 W	14

TABLE 2.- SAMPLE STATION DATA:

NOAA KELEZ CRUISE, JUNE 24-27, 1980

Station no.	Date	Time	Latitude	Longitude	Depth (m)
800	6/24	2152	36° 57.14 N	76° 02.63 W	12.8
46	6/25	0703	36° 29.5 N	75° 22.7 W	24.0
47	6/25	0808	36° 29.8 N	75° 32.0 W	15.8
48	6/25	0857	36° 29.8 N	75° 39.8 W	24.0
805	6/25	1236	36° 52.0 N	75° 56.1 W	9.8
70	6/25	1433	36° 52.3 N	75° 53.6 W	15.5
819	6/26	1015	36° 40.0 N	75° tw.8 W	11.0
820	6/26	1045	36° 42.4 N	75° 53.9 W	11.9
49	6/27	0825	36° 31.0 N	75° 52.0 W	27.4
50	6/27	0940	36° 52.0 N	75° 43.0 W	22.0
51	6/27	1054	36° 52.0 N	75° 55.6 W	12.2

TABLE 3.- SAMPLE STATION DATA:

R/V LINWOOD HOLTON CRUISE, JUNE 18, 1980, AND JUNE 24, 1980

Station no.	Date	Time	Latitude	Longitude	Depth (m)
00	6/18	0755	37° 04.31' N	75° 56.44' W	9.1
0	6/18	0855	37° 04.20' N	75° 59.10' W	12.8
0.5	6/18	0920	37° 03.30' N	75° 59.60' W	7.0
1	6/18	1030	37° 02.50' N	76° 00.00' W	8.0
2	6/18	1100	36° 59.90' N	76° 01.45' W	17.0
3	6/18	1130	36° 57.75' N	76° 02.65' W	13.1
4	6/18	1245	36° 55.60' N	76° 03.80' W	11.0
00	6/24	0800	37° 04.31' N	75° 57.44' W	10.7
0	6/24	0830	37° 04.20' N	75° 59.10' W	12.2
1	6/24	0905	37° 02.50' N	76° 00.00' W	8.2
2	6/24	1025	36° 59.90' N	76° 01.45' W	15.5
3	6/24	1105	36° 57.75' N	76° 02.65' W	13.1
4	6/24	1140	36° 55.60' N	76° 03.80' W	10.1

TABLE 4.- MEAN AND STANDARD DEVIATION FOR BAPLEX-SUPERFLUX SAMPLES

		TSM (mg/ℓ)		TSO (mg/ℓ)		TSI (mg/ℓ)	
	No.	$\bar{X}$	σ	$\bar{X}$	σ	$\bar{X}$	σ
Surface (S-1 m)	58	2.33	1.19	.97	.51	1.49	1.73
Mid-Depth (3-8 m)	39	3.26	5.67	1.10	1.16	2.14	4.54
Near Bottom (>10 m)	41	4.16	4.49	1.05	.55	3.11	4.01

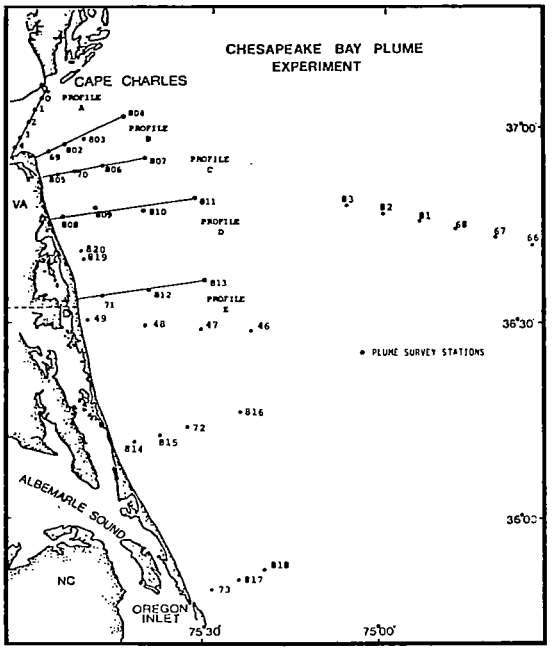

(a) Superflux station locations.

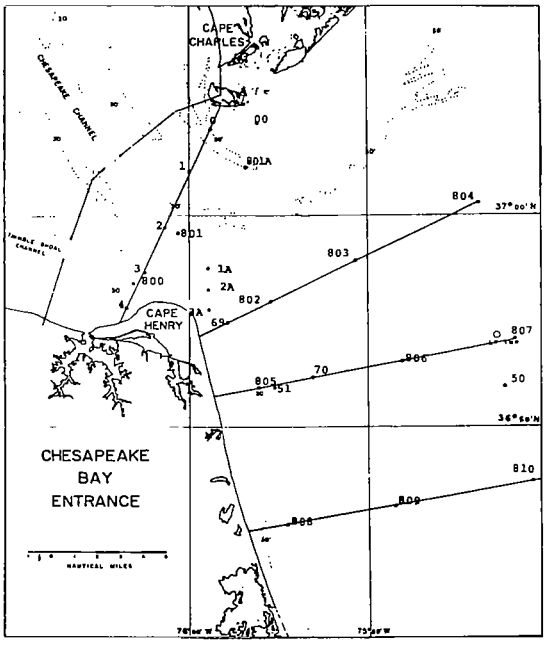

(b) Chesapeake Bay entrance station locations.

Figure 1.- Map showing station locations.

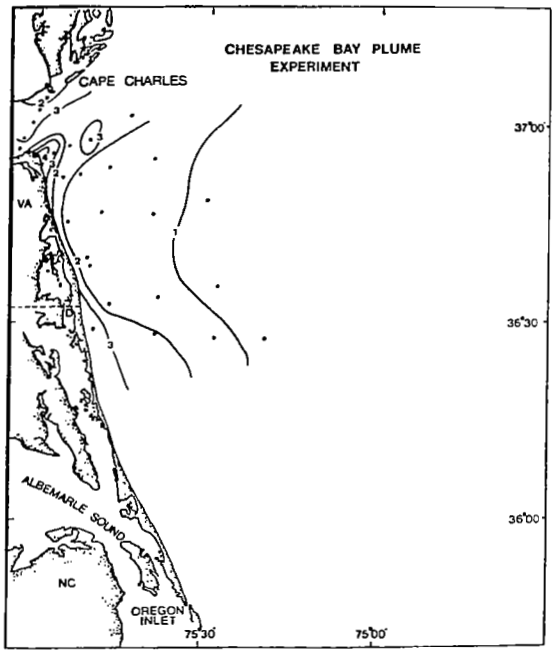

Figure 2.- Map illustrating concentration of total suspended matter (mg/ℓ) in surface water adjacent to Chesapeake Bay entrance.

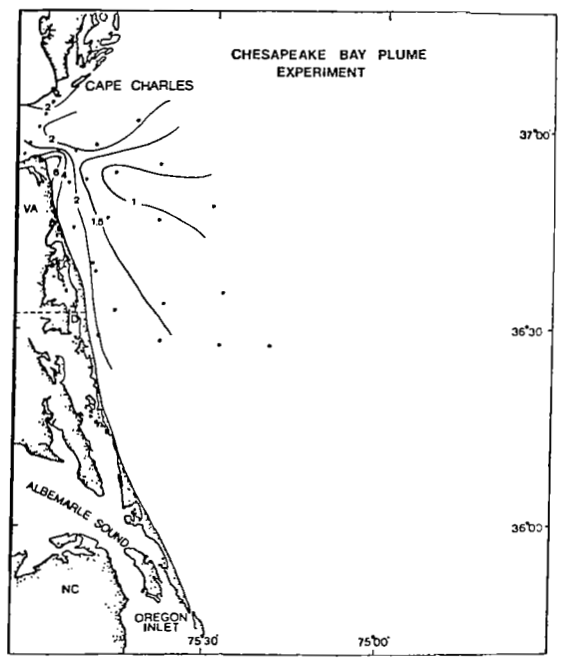

Figure 3.- Map illustrating concentration of total suspended matter (mg/ℓ) at intermediate depths.

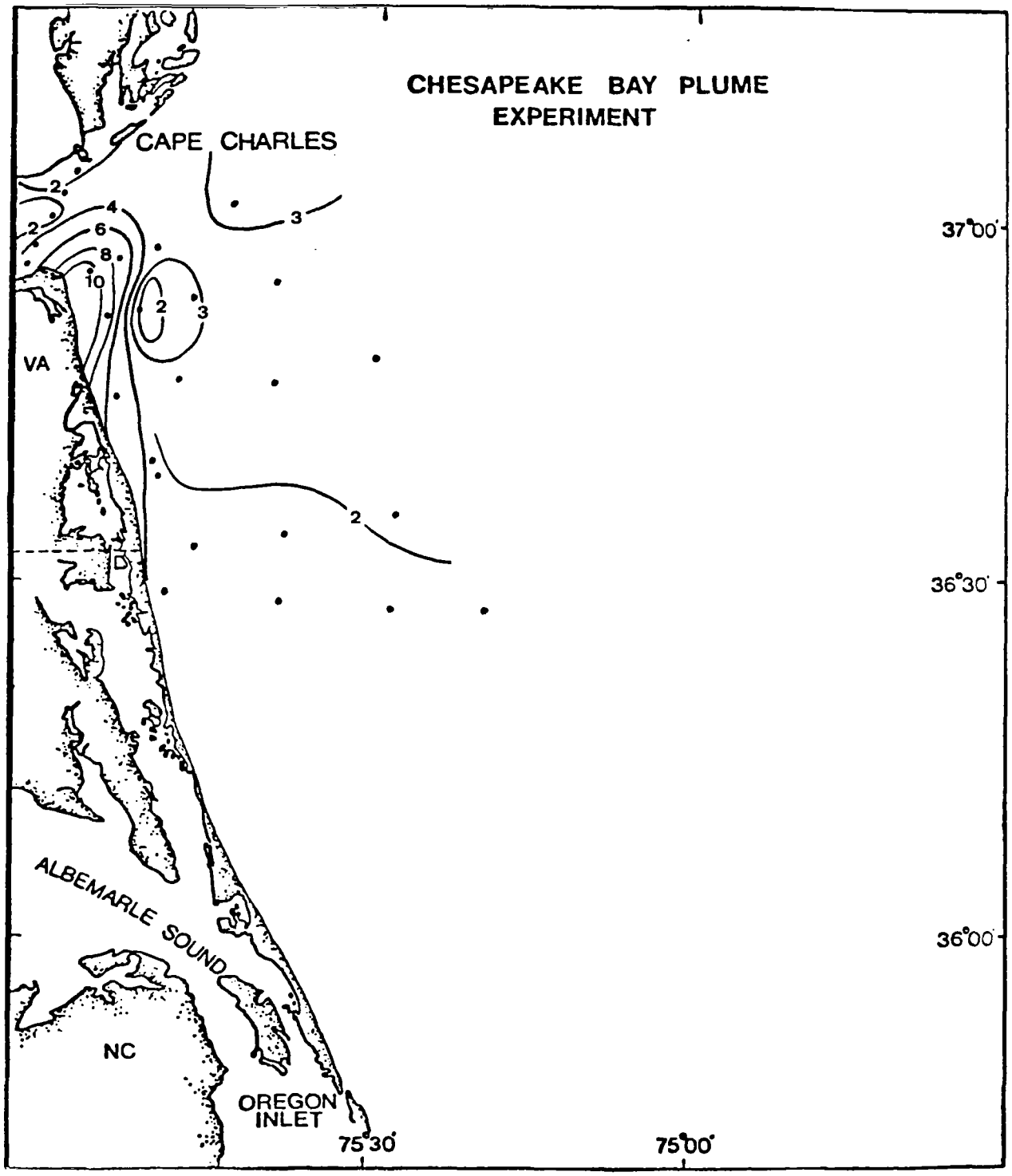

Figure 4. Map illustrating the near-bottom concentration of total suspended matter (mg/ℓ).

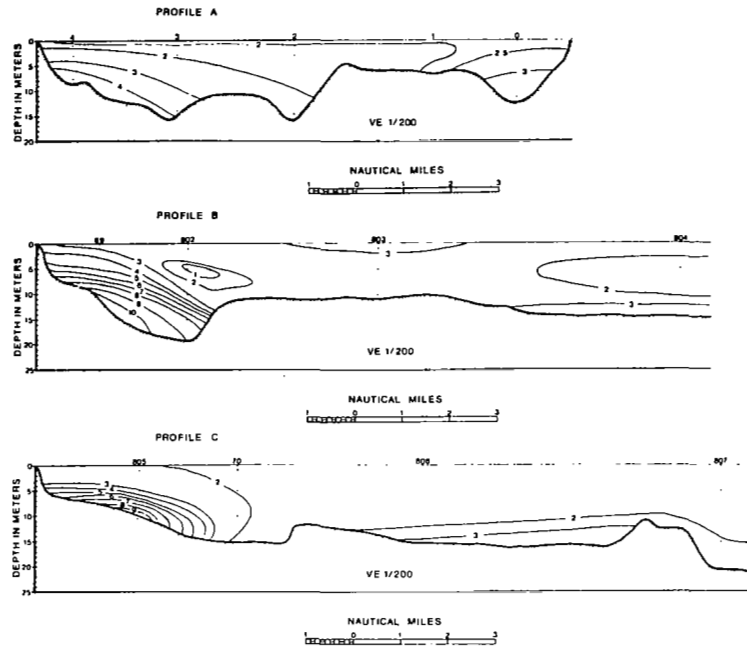

(a) Transects A, B, and C.

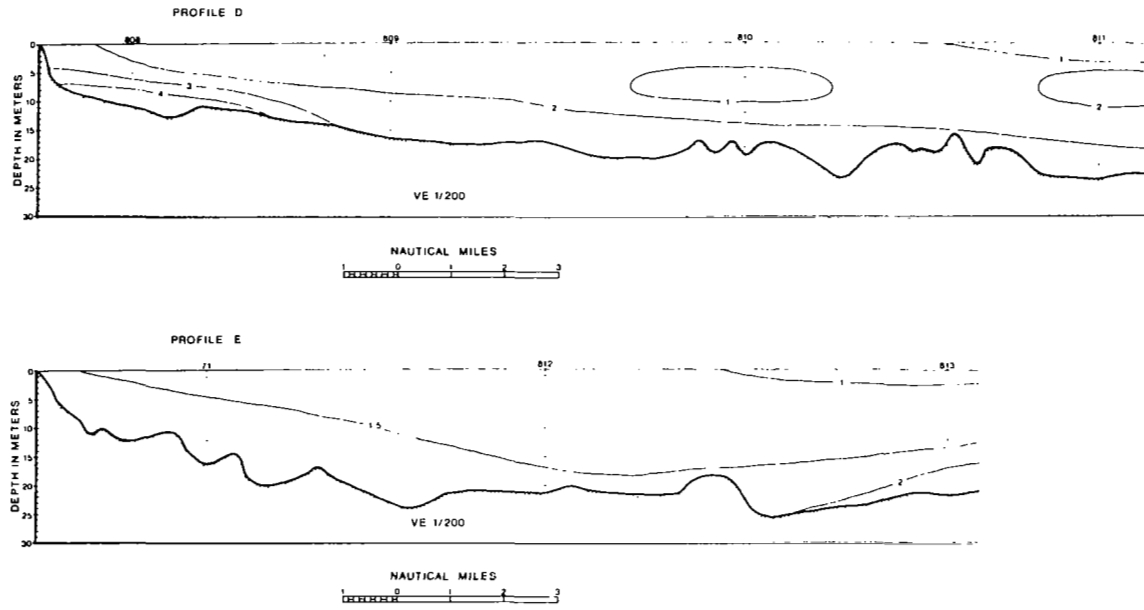

(b) Transects D and E.

Figure 5.- Profile of transects illustrating total suspended matter concentrations (mg/ℓ).

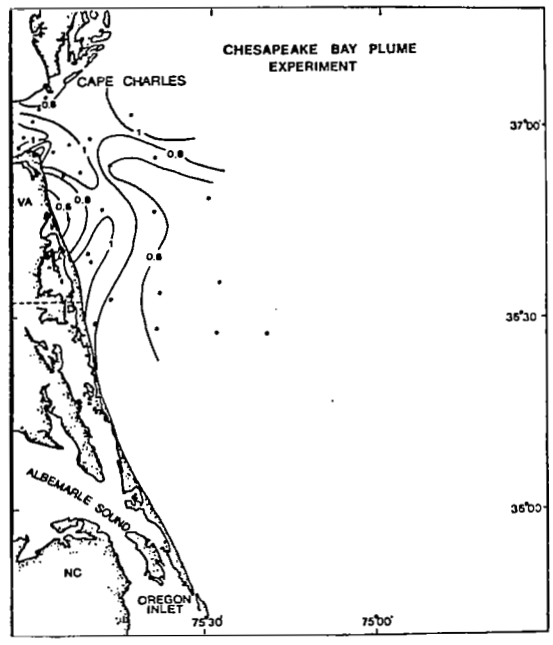

Figure 6.- Map illustrating concentration of total suspended organic matter (mg/ℓ) in surface water.

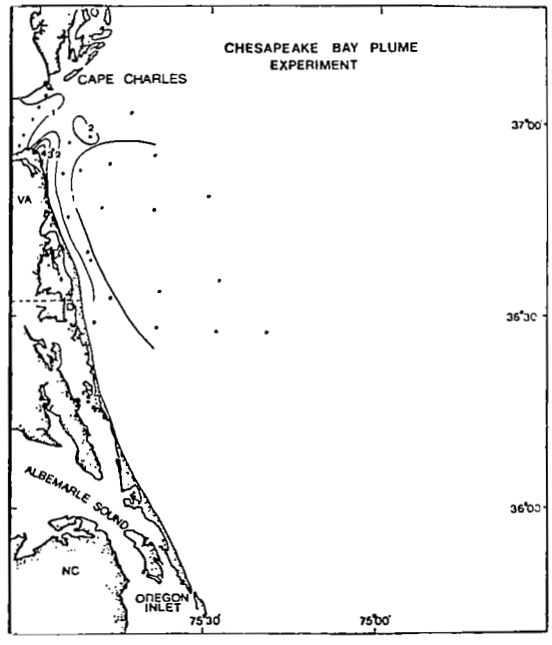

Figure 7.- Map illustrating concentration of total suspended inorganic matter (mg/ℓ) in surface water.

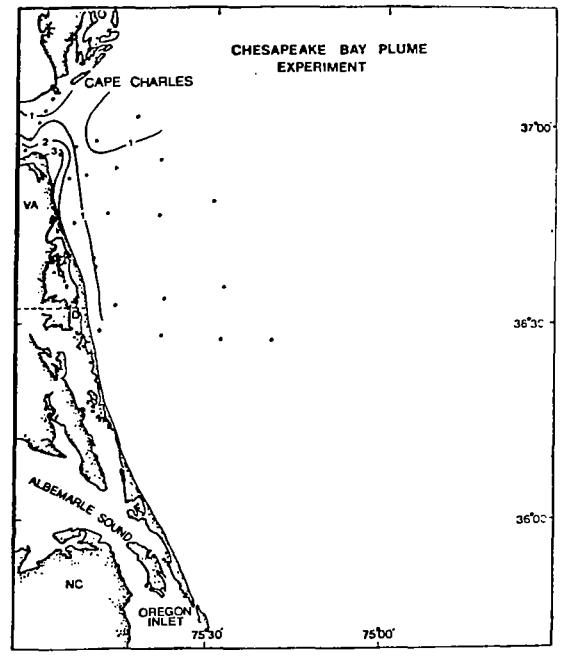

Figure 8.- Map illustrating concentration of total suspended inorganic matter (mg/ℓ) at intermediate depths.

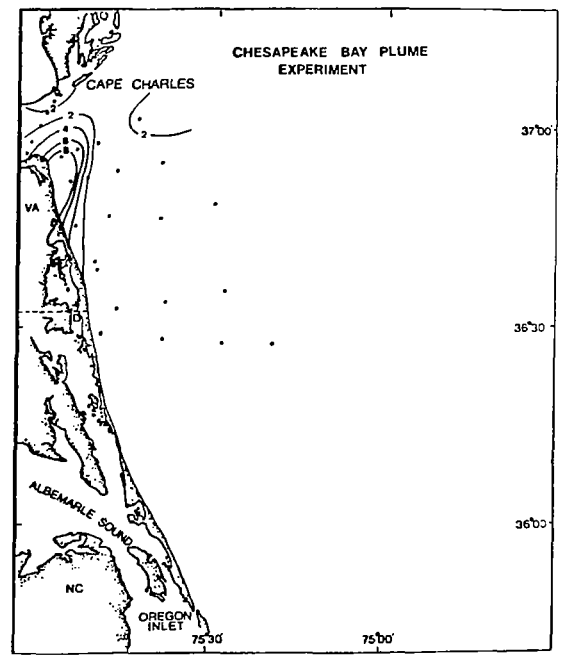

Figure 9.- Map illustrating near-bottom concentration of total suspended inorganic matter (mg/ℓ).

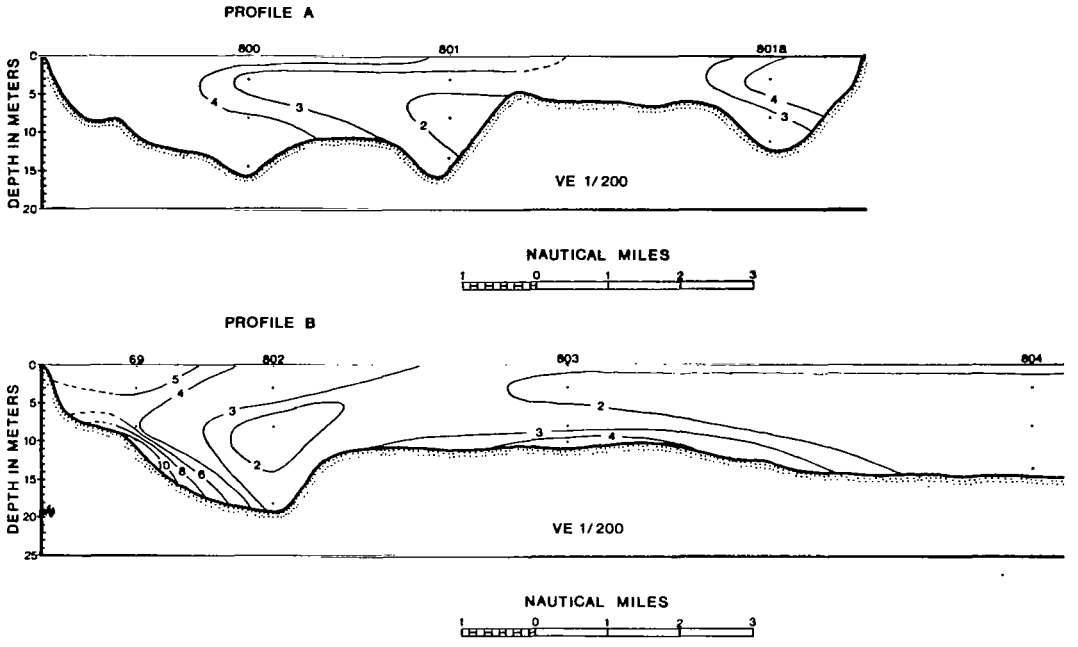

(a) Transects A and B.

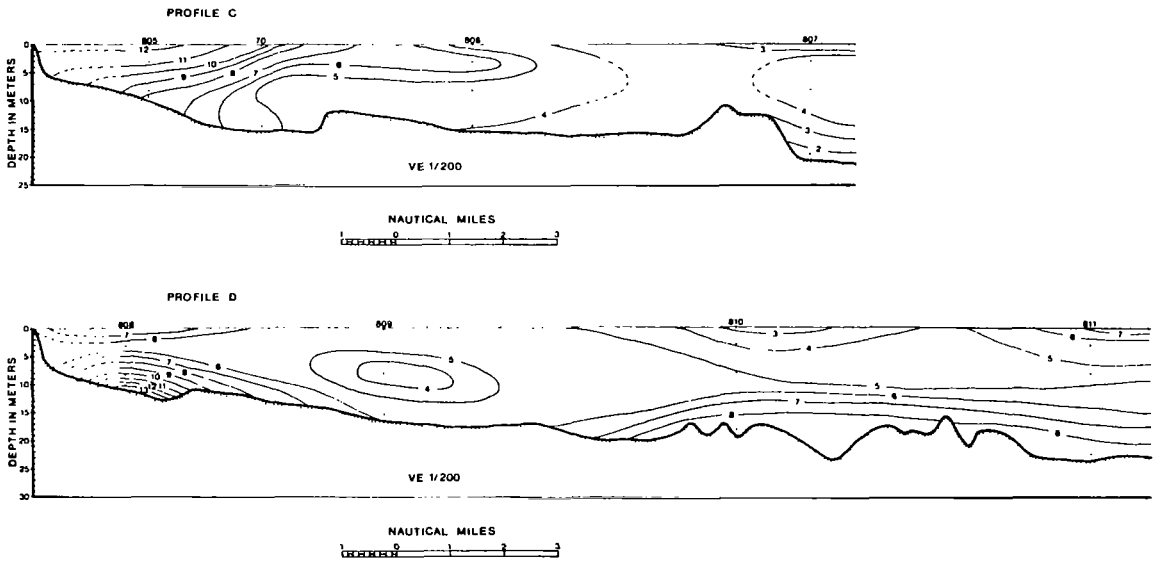

(b) Transects C and D.

Figure 10.- Profiles of Superflux III transects illustrating total suspended matter concentrations (mg/ℓ).

PARTICLE SIZE DISTRIBUTION OF SUSPENDED SOLIDS IN THE CHESAPEAKE BAY ENTRANCE AND ADJACENT SHELF WATERS

Mark R. Byrnes and George F. Oertel
Old Dominion University

INTRODUCTION

Characteristics of suspended solids, including total suspended matter (TSM), total suspended inorganics (TSI), total suspended organics (TSO), particle size distribution (PSD), and the presence of the 10 most prominent particle types were determined in cooperation with a NOAA/NASA program entitled Superflux. Superflux cruises were made in March, June and October, 1980.

The data set described below was determined from samples taken in October during a portion of Superflux III known as the racetrack mission. The R/V Langley (NASA), R/V Linwood Holton (ODU), R/V John Smith (VIMS), and NOAA Ship Kelez simultaneously collected samples along four transects (fig. 1). Samples were collected within a 2-hour period that coincided with the maximum ebb penetration of Chesapeake Bay outwelling (table 1). The objective of this portion of the study was to determine the particle size characteristics and contents of the Chesapeake Bay outwelling and adjacent shelf waters.

METHODS

Sixty-one samples were collected at sixteen stations during the October 15 racetrack mission. Samples were taken at the surface, -3 m, -8 m, and 1 m above the bottom to obtain maximum vertical representation of the water column. Equipment limitations did not permit sampling of the 1 m above bottom samples at stations 800, 801, and 801A. Five-hundred-milliliter samples were taken from 8 liter Niskin bottles and refrigerated to inhibit growth fluctuations of organisms in the sample. Particle size analysis was done within 24 hours of collection using a Model TA-II Coulter Counter. Instrument calibration was performed prior to analysis using an azide-free ISOTON II electrolyte solution and following standard procedures.

Each sample was analyzed for 150 s using a 400-μm aperture tube that provided a size range of 5 to 200 μm. Each analysis produced a size-distribution histogram, a total count of particles and a percent volume of the total population for each of 16 different size classes. Primary and secondary size modes of the total size frequency distribution were used to determine the areal and vertical continuity of size modes in waters in and adjacent to the entrance to Chesapeake Bay (table 2).

OBSERVATIONS AND RESULTS

Discussion

Total counts ranged from 30,000 to 500,000 particles per 150-s time interval. The three predominant size modes that reoccurred in samples were 8 to 10 μm, 20 to 25 μm and 64 to 80 μm. The two smaller size ranges apparently corresponded to inorganic particles, such as clay and silt, and to flocs of these particles. The largest size mode apparently had an offshore source that consisted of a variety of large diatom species, many of which were centric diatoms. Invariably, samples with larger total counts corresponded to those populations with smaller dominant size modes, whereas the samples with lower counts corresponded to the larger modes.

Sheldon and Parsons (ref. 1) discussed the relationship between particle diameter and concentration of suspended matter in an estuary and in coastal water for temperate latitudes. Particle size distribution for estuarine silt consisted largely of flocculated masses of very small inorganic particles, the principal constituent being quartz (fig. 2). Peak concentrations were in the 10 μm size range. Sheldon and Parsons also illustrated that the size distribution of particles in quiescent coastal waters had larger particles but the concentration of material in suspension was lower (fig. 3). The particle distribution showed modes at 20 μm, 50 μm, and 100 μm with the latter corresponding to the highest concentration. The dominant size class throughout the Superflux III study area was the 20 to 25 μm diameter range. The 20 to 25 μm size mode apparently had a polygenetic origin. When it was associated with the 8 to 10 μm mode, the population was apparently composed of inorganic material forming larger aggregates. In the presence of larger size modes, the 20 to 25 μm mode was probably produced by a variety of diatom species that fall in this range. Areal patterns of the primary and secondary size classes illustrated distinct areas characterized by specific modes (figs. 4 to 7).

Areal Patterns

Surface water.- The extent of the 8 to 10 μm size range at the water surface indicates a potential source associated with both Chesapeake and Thimble Shoal Channels (fig. 4). Since the 8 to 10 μm range is considered mostly inorganic, the distribution of this size range may illustrate a tidally driven turbidity plume. Another trend was that associated with station 800, where the only mode present was the 8 to 10 μm class. This anomaly may be related to turbidity associated with James River runoff or resuspension caused by high speed currents in the area. Samples from the outer part of the sample grid apparently had particles more characteristic of shelf waters. The 64 to 80 μm size mode was the predominant size class for the waters.

Intermediate water (-3 m).- The pattern of size mode distribution at intermediate depths was similar to the pattern illustrated for surface water (fig. 5). The extent of water containing the 8 to 10 μm size mode was smaller and closer to the coast than the respective distribution for surface water. The apparent influence of Chesapeake Channel water was still evident. The

20 to 25 μm class in the northern portion of the Bay mouth was influenced by the turbid runoff of the North Channel and possibly by resuspension of particles over shoals at the distal end of the channel. The 64 to 80 μm size mode that was characteristic of shelf water had a similar distribution as described above for surface water; however, it was closer to shore at intermediate depths.

Deep water (-8 m).- At 8 m the distribution of the 8 to 10 μm size mode was confined to the Chesapeake Channel area (fig. 6). The source for this material may have been from resuspension in the upper Bay or from resuspension in the immediate area. Samples containing 64 to 80 μm size particles were much closer to the Bay entrance. If this larger size class of particles was associated with shelf water, then it appears that a near-surface plume (containing the 8 to 10 μm size class) had partially overridden the deeper shelf water. The 20 to 25 μm size mode was present in most samples everywhere.

Near-bottom water (1 m above the seabed).- Near-bottom water characterized by the 64 to 80 μm class extended toward the axis of the Bay mouth (fig. 7). While particle size data in the Bay entrance were not collected, it is believed that shelf water with 64 to 80 μm particles migrated up the axis of Chesapeake Channel. The 8 to 10 μm size mode was absent as a primary or secondary mode in the samples collected and the 20 to 25 μm size mode was present in most samples.

Cross-sectional plots of size frequency data were made for each of the four transects to illustrate vertical changes (fig. 8). Profile A shows a "tongue" of mostly inorganic, fine-grained material that corresponded to the axis of Chesapeake Channel. The water mass with these fine-grained characteristics was traceable down the coast for about 22 km. South of profile C, the 8 to 10 μm size mode was a minor percent of the sample population. Beyond profile C, the particle size characteristics of shelf waters dominated the water column.

CONCLUSIONS

The distribution of primary and secondary particle size modes indicated the presence of a surface or near-surface plume, possibly associated with three sources: (1) runoff, (2) resuspension of material within the Bay, and/or (3) resuspension of material in the area of shoals at the Bay mouth. Additional supportive evidence for this conclusion was illustrated with Ocean Color Scanner (OCS) data (ref. 2). The OCS data showed an obvious increase in water turbidity associated with Chesapeake Channel and in water adjacent to Cape Henry, Virginia. This corresponded with the particle size data presented above. Initially, it was speculated that turbid water "outwelling" from the Bay had an upper Bay source; however, OCS data showed that the upper Bay was not a plausible source. The most likely source was resuspension due to wave and current action. This explanation would have been expected due to drought conditions that had existed for several months prior to the survey.

REFERENCES

1. Sheldon, R. W.; and Parsons, T. R.: A Practical Manual on the Use of the Coulter Counter in Marine Research. Fisheries Research Board of Canada, Pacific Oceanographic Group, 65 pp, 1967.

2. Ohlhorst, C.: Preliminary Analysis of Ocean Color Scanner Data From Superflux III. Chesapeake Bay Plume Study - Superflux 1980, NASA CP-2188, 1981 (Paper no. 12 of this compilation).

TABLE 1.- SAMPLE STATION DATA, OCTOBER 15, 1980

Vessel name	Station no.	Time	Latitude	Longitude	Depth (m)
R/V Langley	800	1018	36° 57.30' N	76° 02.90' W	--
	801	1058	36° 59.20' N	76° 00.60' W	--
	801A	1140	37° 02.10' N	75° 56.80' W	--
R/V Holton	69	1020	36° 55.00' N	75° 58.00' W	11
	802	1105	36° 55.00' N	75° 55.30' W	13
	803	1133	36° 58.00' N	75° 51.50' W	11
	804	1225	37° 01.02' N	75° 44.20' W	15
R/V John Smith	805	1017	36° 52.00' N	75° 56.00' W	11
	70	1047	36° 52.40' N	75° 53.50' W	15
	806	1127	36° 53.20' N	75° 48.60' W	15
	807	1148	36° 54.38' N	75° 41.07' W	21
NOAA Ship Kelez	808	1010	36° 45.50' N	75° 54.70' W	10
	809	1050	36° 46.40' N	75° 49.00' W	17
	821	1125	36° 47.42' N	75° 42.52' W	19
	810	1148	36° 47.67' N	75° 41.12' W	19
	811	1244	36° 48.73' N	75° 32.26' W	25

TABLE 2.- PRIMARY AND SECONDARY SIZE MODES

Station	Depth (m)	Primary mode (μm)	Secondary mode (μm)
800	Surface	8-10	--
	3	20-25	--
	8	20-25	--
801	Surface	20-25	8-10
	3	8-10	20-25
	8	20-25	8-10
801A	Surface	20-25	--
	3	8-10	--
	8	20-25	--
69	Surface	20-25	8-10
	3	20-25	8-10
	8	20-25	--
	Bottom	20-25	--
802	Surface	20-25	8-10
	3	20-25	8-10
	8	20-25	--
	Bottom	20-25	50-64
803	Surface	20-25	64-80
	3	20-25	--
	8	20-25	--
	Bottom	20-25	--
804	Surface	20-25	--
	3	20-25	80-100
	8	20-25	64-80
	Bottom	20-25	--

TABLE 2.- CONTINUED

Station	Depth (m)	Primary mode (μm)	Secondary mode (μm)
805	Surface	20-25	8-10
	3	20-25	8-10
	8	16-20	64-80
	Bottom	20-25	--
70	Surface	20-25	8-10
	3	20-25	8-10
	8	16-20	64-80
	Bottom	20-25	--
806	Surface	8-10	20-25
	3	20-25	64-80
	8	16-25	--
	Bottom	20-25	80-100
807	Surface	20-25	64-80
	3	16-25	--
	8	16-25	64-80
	Bottom	20-25	--
808	Surface	20-25	64-80
	3	20-25	64-80
	8	20-25	--
	Bottom	16-25	--
809	Surface	20-25	64-80
	3	20-25	--
	8	80-100	20-25
	Bottom	50-64	20-25

TABLE 2.- CONCLUDED

Station	Depth (m)	Primary mode (μm)	Secondary mode (μm)
821	Surface	80-100	--
	3	25-32	64-80
	8	80-100	--
	Bottom	64-100	--
810	Surface	80-100	20-25
	3	80-100	--
	8	64-80	--
	Bottom	64-80	25-32
811	Surface	80-100	20-25
	3	64-80	16-20
	8	80-100	20-25
	Bottom	20-25	80-100

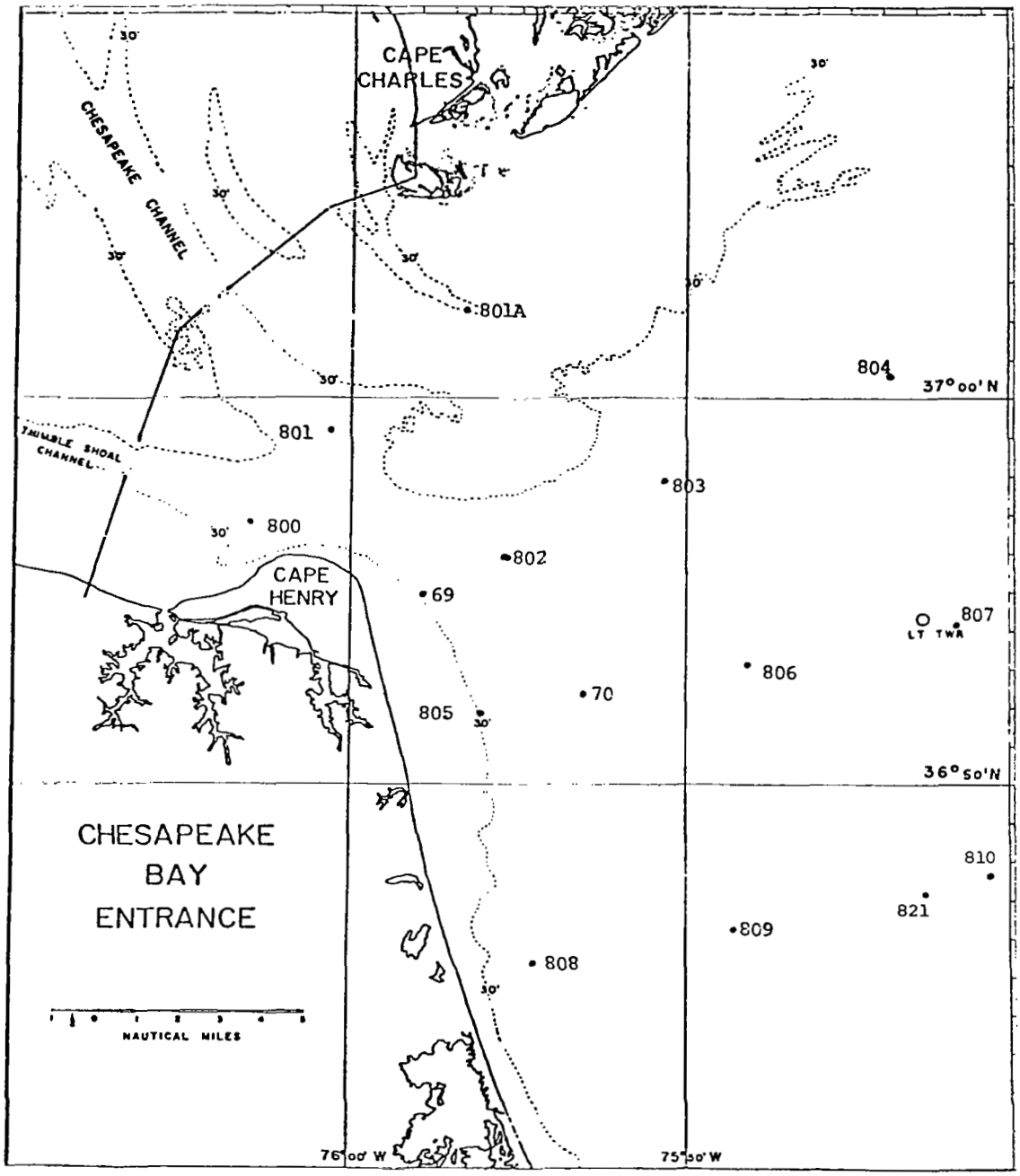

Figure 1.- Map showing station locations.

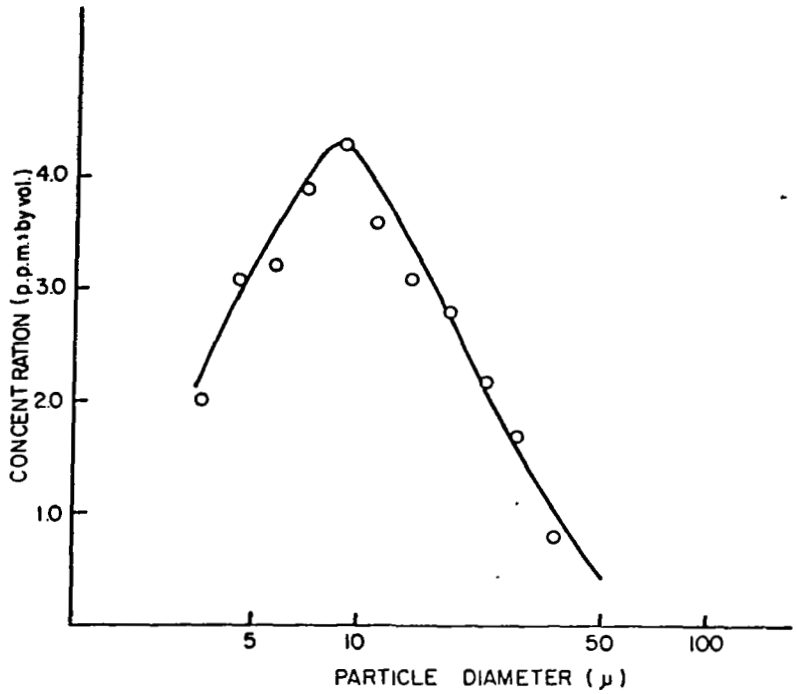

Figure 2.- Particle size distribution for estuarine silt. The material consisted largely of flocculated masses of very small inorganic particles, the principal constituent being quartz (from ref. 1).

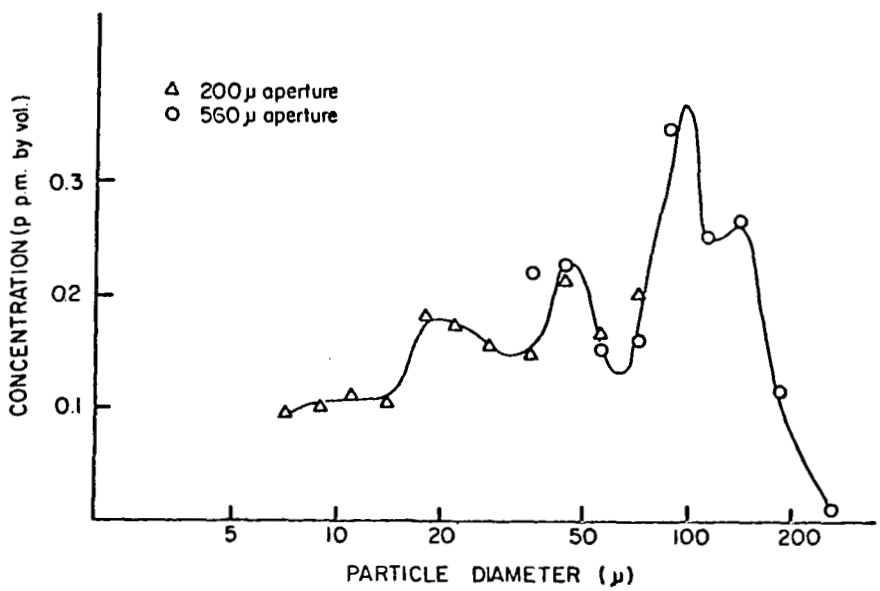

Figure 3.- Particle size distribution for coastal waters where a predominance of organisms is evident (from ref. 1).

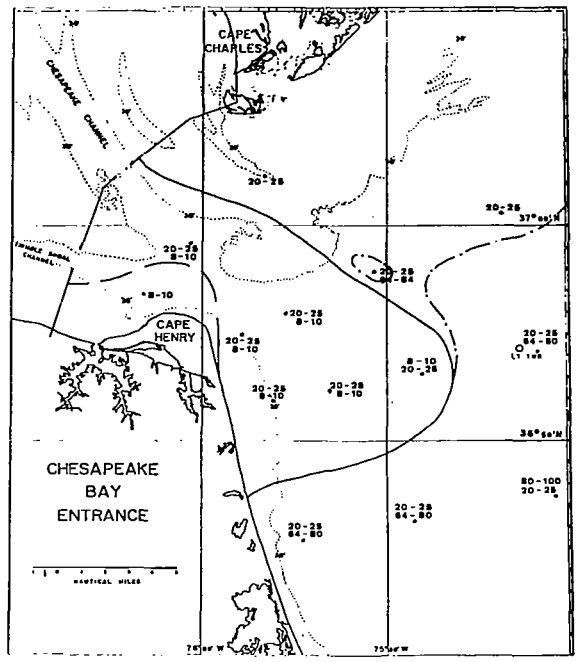

Figure 4.- Surface distribution of primary and secondary size modes. The numbers assocaited with each station represent the primary and secondary size modes for the sample population based on the percent volume of the sample population.

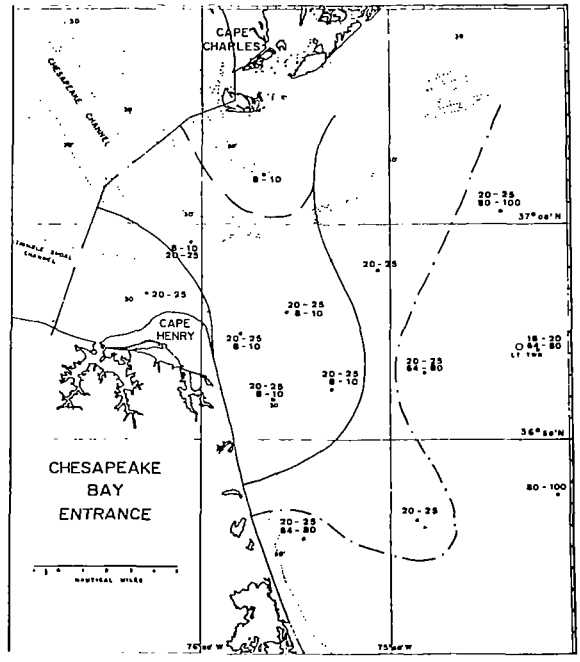

Figure 5.- Distribution of primary and secondary size modes at a depth of 3 m.

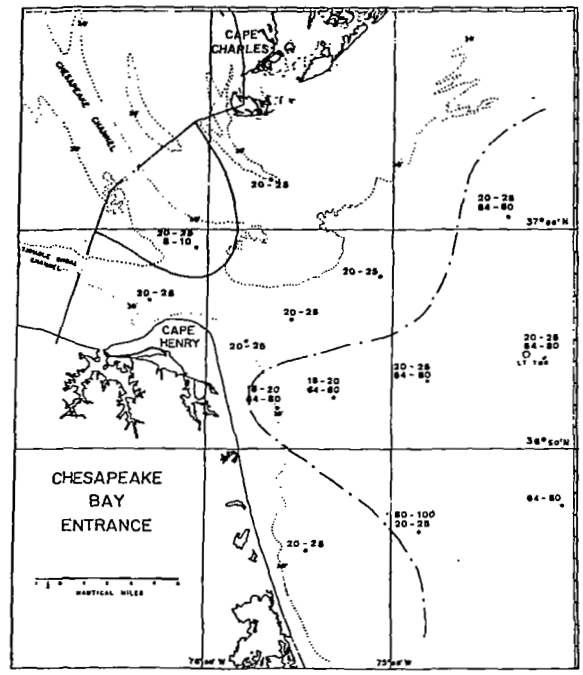

Figure 6.- Distribution of primary and secondary size modes at a depth of 8 m.

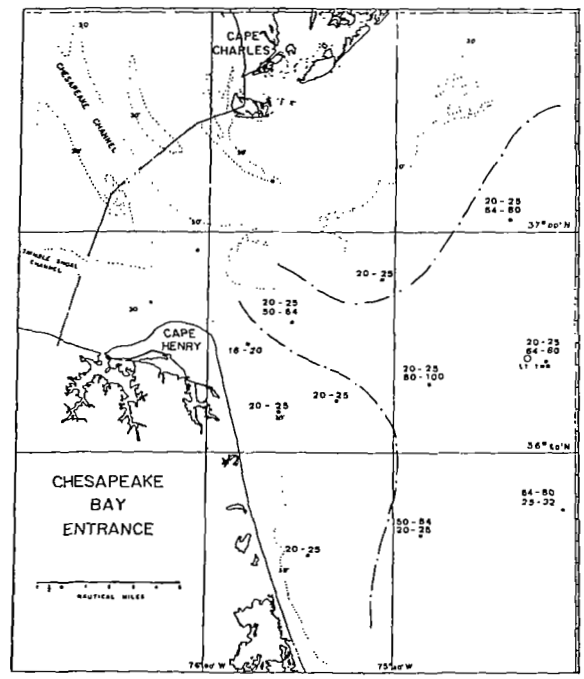

Figure 7.- Near-bottom distribution of primary and secondary size modes.

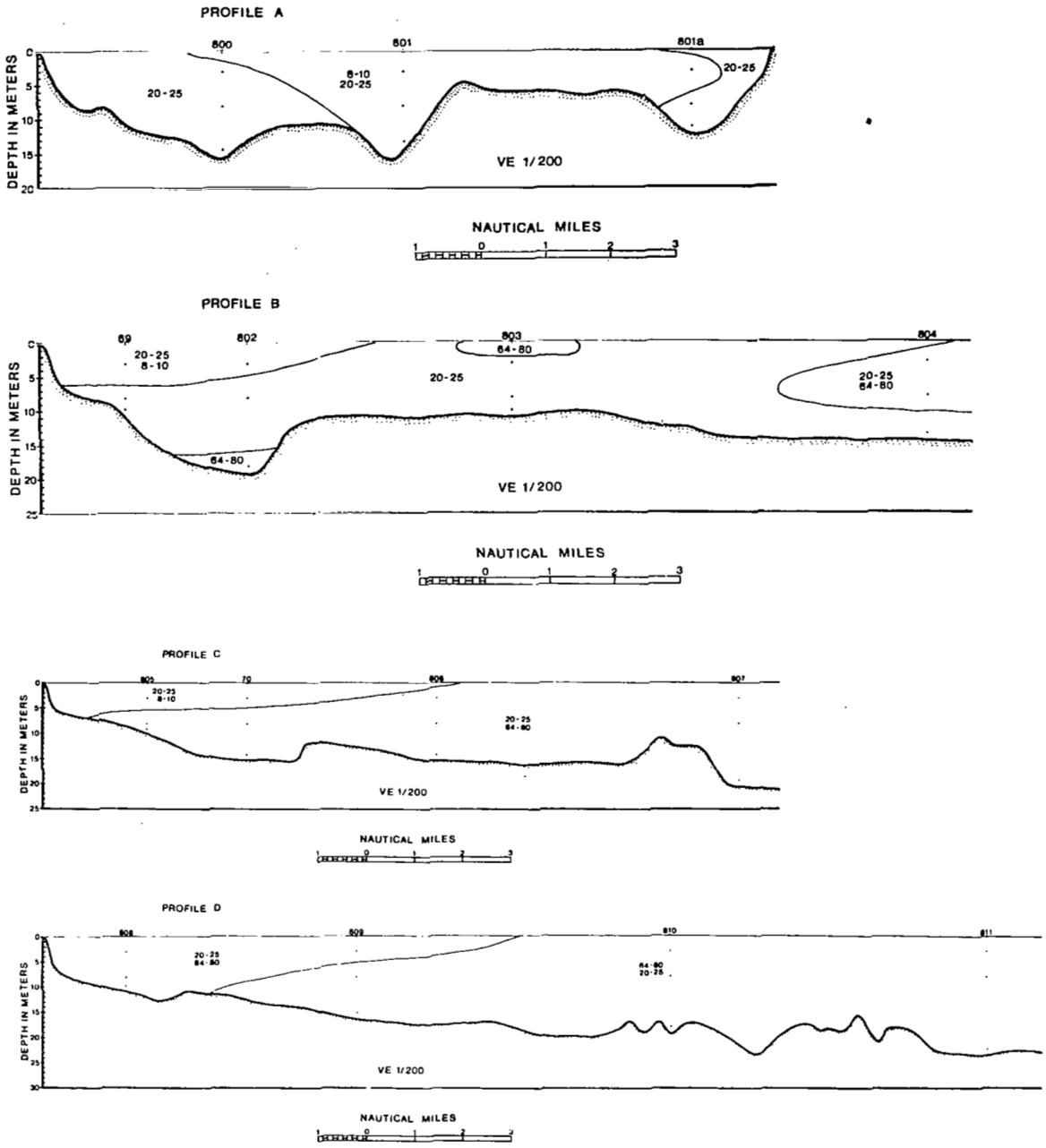

Figure 8.- Profiles of transects A, B, C, and D illustrating the distribution of primary and secondary size modes

CONCENTRATION OF HYDROCARBONS ASSOCIATED WITH PARTICLES IN THE SHELF WATERS ADJACENT TO THE ENTRANCE OF CHESAPEAKE BAY

Terry L. Wade and George F. Oertel
Old Dominion University

SUMMARY

Particulate hydrocarbon concentrations were measured in 94 water samples from the 1980 Superflux II and BAPLEX cruises. The concentrations ranged from below the detection limit (>0.7 μg/ℓ) to 32 μg/ℓ. The mean for all samples was 5.6 μg/ℓ. Particulate hydrocarbon concentrations are higher in the Bay mouth and lower in the shelf waters adjacent to the entrance of Chesapeake Bay. No coherent particulate hydrocarbon distribution is seen with depth in the water column. The Bay is postulated as one of the possible chronic sources of particulate hydrocarbons for the adjacent shelf waters. Additional research on the sources of particulate hydrocarbons and the processes affecting their temporal and spatial distribution is needed in order to further evaluate this postulation.

INTRODUCTION

The objective of this preliminary study was to measure concentrations of particulate hydrocarbons at selected stations adjacent to the entrance of the Chesapeake Bay. This work supports the NOAA-NASA program entitled Superflux. The objectives of Superflux are to determine the characteristics of plumes and contents of plumes influencing living resources in shelf waters and to determine the extent to which these characteristics and influences can be sensed remotely. The particulate hydrocarbon concentration of plumes was measured. An attempt was made to determine if the outwelling of Chesapeake Bay contains hydrocarbons which may adversely influence the living resources in shelf waters.

Petroleum hydrocarbons are entering the marine environment at a rate of approximately 6 million metric tons annually (MTA) (ref. 1). The most publicized inputs come from tanker accidents, but this source accounts for only 4.9 percent of the total input (ref. 1). A significant portion of the annual input (13 percent) is added directly to the coastal environment from sewage treatment plants, coastal refineries, and coastal industries. Another substantial portion of the annual input (31 percent) is from river and urban runoff, which may eventually reach the marine environment (ref. 1).

Detailed examination of wastewater treatment plants shows that these facilities may contribute a quantity of hydrocarbons equal to that entering from direct oil spills (ref. 2). Hydrocarbons discharged from wastewater treatment plants are predominantly (95 percent) associated with suspended

material and about half of this input is removed to the sediment in the vicinity of the discharge; the other half is transported away from the discharge site (ref. 2).

The association of petroleum hydrocarbons and sediment appears to be related to grain size characteristics. Particles smaller than 44 μm adsorb more hydrocarbons on a weight basis than do sediment particles larger than 44 μm (refs. 3 and 4). The interaction of petroleum hydrocarbons with very fine-grained sediment may form neutrally buoyant aggregates. Both of these processes favor dispersal over sedimentation of hydrocarbons.

Chesapeake Bay experienced numerous chronic inputs of anthropogenic hydrocarbons similar to those outlined above. These hydrocarbons may be deposited near their source of input, or may be adsorbed to suspended materials and transported to the open ocean. These hydrocarbons may adversely affect the open ocean ecosystem.

MATERIALS AND METHODS

This research required collection and analyses of water samples for particulate hydrocarbon concentrations. A total of 92 samples were collected during Superflux II cruises aboard the NOAA ships Delaware II (June 17 to June 23, 1980) and Kelez (June 24 to June 27, 1980) for hydrocarbon analyses. Bay Plume Experiment, or BAPLEX, is an ongoing program involving several researchers in the Department of Oceanography at Old Dominion University. BAPLEX data are included in this paper to provide additional information regarding the characteristics of water masses at the mouth of Chesapeake Bay. A total of seven samples were collected during BAPLEX cruises aboard the R/V Holton (June 19 and June 24, 1980).

The hydrocarbon analyses were performed using accepted methods and included analyses of procedural blanks and standards. The analytical techniques have been described in detail elsewhere (refs. 4 and 5). Samples consisting of approximately 16 ℓ of seawater were filtered through preignited Gelman A/E glass fiber filters and are therefore operationally defined as particulates. The filter, along with the retained material, was saponified/extracted under reflux. The hydrocarbons in the saponification mixture were partitioned into the organic phase by addition of dichloromethane. After removing the dichloromethane the residue was eluted through an alumina-silic acid column to separate the hydrocarbons from other organics. The hydrocarbon fraction was then analyzed on a Hewlett Packard 5830 gas chromatograph (GC) equipped with a 25 M methylsilicone, fused silica, WCOT, capillary column. Analyses were done by temperature programming from 80° to 270° C at 10° C min. The areas of the resolved peaks and unresolved complex mixture were measured by planimetry. Comparison of the areas of the resolved and unresolved peaks and unresolved complex mixture to the area of the internal standards allowed for quantitative measurement of the amount of hydrocarbon present.

RESULTS AND DISCUSSION

Sampling dates and locations for Superflux II and BAPLEX cruises are shown in reference 6. The Superflux II samples were collected over a 10-day period (June 17 to June 27, 1980) and at random stages during the tidal cycle. BAPLEX samples provide relatively synoptic data as all samples except one were collected within a 2-hour window during ebbing tide.

Procedural blanks were analyzed periodically to determine background levels of hydrocarbons. All sample concentrations reported here have been corrected for the concentrations found in the procedural blanks. A standard n-alkane mixture was injected daily to insure that the GC was operating properly. Analyses of the ships' fuel oils indicated that they are not a major source of hydrocarbons found in these samples.

When oil enters the environment it can undergo many complex reactions collectively called weathering. Weathering reactions, including evaporation, dissolution, photochemical oxidation, microbial degradation, and adsorption. The extent of weathering reactions depends upon the environmental conditions that the oil encounters, such as temperature, wind speed, current velocity, microbes present and type and site of particles present (ref. 1). The overall result of weathering is preferential loss of specific hydrocarbons (ref. 1). Samples from Superflux II and BAPLEX cruises show GC patterns characteristic of weathered oils, indicating that they have been in the marine environment for a few days or longer.

Particulate hydrocarbon concentrations were measured in 87 Superflux II and 7 BAPLEX samples. The results are summarized in table 1. Total particulate hydrocarbon concentrations for Superflux II samples ranged from below the detection limit, <0.7 μg/ℓ to 32 μg/ℓ, with a mean of 5 μg/ℓ. Total particulate hydrocarbon concentrations for the BAPLEX samples ranged from 4 to 20 μg/ℓ with a mean of 13 μg/ℓ. The nine surface samples collected at stations in the Bay mouth (BAPLEX stations 0, 1, 2, 3 and 4 and Superflux II stations 800 and 801) had a mean hydrocarbon concentration of 15 μg/ℓ, or approximately double the mean for all surface stations (7 μg/ℓ). Therefore, in June 1980 the mean surface concentration of particulate hydrocarbons was highest in the Bay mouth and lower in the shelf waters adjacent to the entrance of the Chesapeake Bay.

Superflux II station 800 1-m depth particulate hydrocarbon concentrations measured on June 17 and 24, 1980, were 32 and 7 μg/ℓ, respectively. These samples were taken 1 week apart and at different stages of the tidal cycle. No consistent trend of hydrocarbon concentration was seen with depth in the water column. These findings indicate that the processes effecting the transport, concentration and/or dispersal of hydrocarbons with depth are very complex. Interpretation of the data is complicated by the long time period (10 days) and random tidal stages during which these samples were collected.

Literature values for particulate hydrocarbon concentrations range from 1.3 to 4 μg/ℓ in the Gulf of St. Lawrence (ref. 7), 16 to 40 μg/ℓ near a spill

in Chedabucto Bay (ref. 8) and 0 to 4 µg/ℓ 1 year after that spill (ref. 9). Thus, the range of particulate hydrocarbon concentrations found during this study (<0.7 to 32 µg/ℓ) was of the same order of magnitude as samples collected for other coastal areas.

Total hydrocarbon concentrations of surface water samples collected in October 1973 from shelf waters adjacent to Chesapeake Bay ranged from 39 to 56 µg/ℓ (ref. 10). Hydrocarbons were also present in samples collected on Superflux II cruises in June 1980. Other data from the Superflux II cruise suggest that particulate materials originating in Chesapeake Bay are transported to the adjacent shelf waters (ref. 11). This evidence suggests that the outwelling of Chesapeake Bay may provide a chronic input of anthropogenic hydrocarbons to the adjacent shelf waters.

REFERENCES

1. National Academy of Sciences: Petroleum in the Marine Environment, National Academy of Sciences, Washington, DC, p. 107, 1975.

2. Van Vleet, E. S.; and Quinn, J. G.: Input and Fate of Petroleum Hydrocarbons Entering the Providence River and Upper Narragansett Bay from Wastewater Effluents, Environ. Sci. and Tech., 11, pp. 1086-1092, 1977.

3. Meyers, P. A.; and Quinn, J. G.: Association of Hydrocarbons and Mineral Particles in Saline Solution, Nature, 244, pp. 23-24, 1973.

4. Wade, T. L.; and Quinn, J. G.: Geochemical Distribution of Hydrocarbons in Sediments from Mid-Narragansett Bay, Rhode Island, Organic Geochem., 1, pp. 157-167, 1979.

5. Wade, T. L.; and Quinn, J. G.: Hydrocarbons in the Sangasso Sea Surface Microlayer. Marine Pollution Bulletin, 6, pp. 54-47, 1975.

6. Gingerich, K. J.; and Oertel, G. F.: Suspended Particulate Matter in the Chesapeake Bay Entrance and Adjacent Shelf Waters. Chesapeake Bay Plume Study - Superflux 1980, NASA CP-2188, 1981 (Paper no. 15 of this compilation).

7. Zsolnay, A.: Preliminary Study of the Dissolved Hydrocarbons and Hydrocarbons on Particulate Material in the Gotland Deep of the Baltic, Kieler Meeresforsch, 27, pp. 129-134, 1971.

7. Levy, E. M.: The Presence of Petroleum Residues Off the East Coast of Nova Scotia, in the Gulf of St. Lawrence River. Water Research, 5, pp. 723-733, 1971.

8. Gordon, D. C., Jr.; and Michalik, P. A.: Concentrations of Bunker C Fuel Oil in the Waters of Chedabucto Bay, Journal of the Fisheries Research Board of Canada, 28, 1912-1914, 1971.

9. Wade, T. L.: Measurements of Hydrocarbons, Phthalic Acid and Phthalic Acid Ester Concentrations in Environmental Samples from the North Atlantic, M.S. Thesis, University of Rhode Island, 1974.

10. Brown, R. C.; and Wade, T. L.: Coprostanol as a Potential Tracer of Particulate Sewage Effluent to Shelf Waters Adjacent to the Chesapeake Bay. Chesapeake Bay Plume Study - Superflux 1980, NASA CP-2188, 1981 (Paper no. 18 of this compilation).

TABLE 1.- HYDROCARBON CONCENTRATIONS

Samples	Number	Concentration (µg/ℓ) Range	Mean
Superflux II	87	>0.7 to 32	5.0
BAPLEX	7	4.1 to 20	13.4
Surface[a]	43	>0.7 to 32	6.6
Surface-bay entrance[b]	9	4.1 to 32	15.0

a = All surface (>1 m) samples collected from Superflux II or BAPLEX

b = Surface samples for Chesapeake Bay entrance (see text)

COPROSTANOL AS A POTENTIAL TRACER OF PARTICULATE SEWAGE EFFLUENT TO SHELF WATERS ADJACENT TO THE CHESAPEAKE BAY

Robert C. Brown and Terry L. Wade
Old Dominion University

SUMMARY

Samples were collected in the Chesapeake Bay entrance and contiguous shelf waters and were subsequently analyzed for particulate coprostanol and cholesterol concentrations. Surface coprostanol concentrations were fairly uniform, with a slight increase with depth. This increase with depth may be due to sewage-associated particulates settling as they leave the Bay, or the resuspension of contaminated sediment. Preliminary findings indicate sewage-associated materials are being transported from the Chesapeake Bay to shelf waters, where they may have a detrimental affect on living marine resources.

INTRODUCTION

Man is continuously discharging sewage effluent into the marine environment. Sewer systems, generally, not only service individual homes, but also service various industries and most often storm drainage systems. Therefore, the influent to sewage treatment plants contains many constituents, including pathogenic bacteria and viruses, heavy metals, pesticides, and petroleum hydrocarbons, in addition to domestic sewage (refs. 1 to 4). Unfortunately, even secondary sewage treatment does not remove all of these contaminants (refs. 2 to 5). In a recent study, Van Vleet et al. (ref. 3) suggested that the amount of oil discharged into the U.S. coastal waters via wastewater effluents can be nearly as important as the amount released to coastal waters by direct spills. Sewage effluents, thus, contain materials that may adversely affect water quality, which in turn, may reduce the value of the marine resources impacted.

The enumeration of fecal coliform bacteria is routinely used as an indicator of fecal contamination (refs. 2, 6 and 7). Recent studies (refs. 5, 8 and 9) describe the limitations of the coliform test as an indicator of sewage contamination in the marine environment. The inadequacy of coliform enumeration has lead researchers to investigate other parameters that may be more accurate indicators of fecal pollution. One promising alternative is coprostanol.

Coprostanol (5β-cholestan-3β-ol) is thought to be formed exclusively by the enteric bacterial reduction of cholesterol in man and higher animals (refs. 10 to 13). Unlike cholesterol, coprostanol is not a naturally occurring sterol in the marine environment; therefore, the detection of coprostanol

would indicate fecal contamination from either domestic wastes or runoff from pastures and barnyards (ref. 13). Coprostanol has also been found to be resistant to microbial degradation (refs. 5, 14, 15 and 16). Hatcher and McGillivary (ref. 16) found coprostanol throughout a new bight core that spanned a 26-year period, therefore providing a historical measure of the degree of sewage contamination. Coprostanol has also been shown to be a reliable indicator of fecal pollution even when the effluent was chlorinated for the purpose of bacterial reduction (refs. 6 and 8). Although this disinfection procedure reduced the bacterial population, there was no detectable change in coprostanol structural configuration or concentration. Coprostanol has been shown to be an indicator of fecal contamination and there may be a direct relationship between coprostanol concentrations and the degree of water pollution (refs. 5, 6 and 13).

Coprostanol is found to associate with particulate matter. Sediments near effluent discharges have a much higher concentration of coprostanol than the overlying waters, indicating that much of the coprostanol is removed to the sediment near the sewage outfall (ref. 8). Van Vleet et al. (ref. 3) noticed a similar trend for petroleum hydrocarbons discharged from a sewage treatment plant. They reported that half of the hydrocarbons were deposited near the outfall and the other half were removed from the area. Although much of the coprostanol may be deposited near sewage outfalls, it has been detected in seawater far removed from any fecal input sites (ref. 5). Therefore, coprostanol isolation and identification may serve as a viable indicator of the fate of fecal pollution and associated toxic materials resulting from the discharge of sewage effluents into natural waters.

The NOAA/NASA Superflux program provided a unique opportunity to more thoroughly investigate the transport of sewage-associated materials, utilizing coprostanol, from the Chesapeake Bay system (i.e., rivers and tributaries) to adjacent continental shelf waters. Furthermore, data of this nature may enable us to better understand the fate of sewage-associated material in the Chesapeake Bay and contiguous waters.

MATERIALS AND METHODS

Water samples were collected from the entrance to Chesapeake Bay and adjacent shelf waters and analyzed for particulate coprostanol and cholesterol concentrations. A total of 59 samples, taken aboard the NOAA vessels Delaware II (June 17-23, 1980) and George B. Kelez (June 24-27, 1980) during the Superflux II cruise, were analyzed. Seven samples were also taken from the R/V Linwood Holton (June 19 and 24, 1980), which was participating in a program conducted by the Department of Oceanography at Old Dominion University called BAPLEX.

The water samples, approximately 16 liters, were collected at various depths and were filtered on shipboard, as soon after collection as possible, through a preignited Gelman A/E glass fiber filter. The filters were wrapped in aluminum foil and kept frozen until they were analyzed back at the laboratory. An internal standard, nonadecanol, was added to the filter which was then

saponified/extracted under reflux for 2 hours with 100 ml of 0.5 N methanolic/KOH and 10 ml of toluene. The extract was filtered and the filtrate was placed in a separatory funnel containing 100 ml of 10 percent NaCl solution (adjusted to a pH of less than 2 with HCl). Seventy milliliters of dichloromethane (CH_2Cl_2) were added to the separatory funnel, the contents shaken, and the organic phase removed. The aqueous fraction was extracted two more times with 70 ml CH_2Cl_2 each time. The combined CH_2Cl_2 extracts were evaporated to dryness, and the residue was eluted through an alumina-silica gel column to separate alcohols and sterols from other organics. This fraction was then analyzed on a Hewlett-Packard 5830 gas chromatograph (GC), equipped with a 25-m methylsilicone, fused silica, WCOT, capillary column. The analysis was done by temperature programming from 80° to 270° C at 10° C/min. The eluting materials were detected with a flame ionization detector, the response of which was recorded and integrated with a Hewlett-Packard model 18850A reporting integrator. Concentrations of coprostanol and cholesterol were calculated with respect to the internal standard. Procedural blanks and standards were run systematically in association with all analyses to determine background levels of coprostanol and also to insure that the GC was operating properly. The presence of coprostanol was confirmed by coinjection with authenic coprostanol and by formation and GC analyses of TMS-derivatives.

RESULTS AND DISCUSSION

Particulate coprostanol and cholesterol concentrations were measured in 59 samples collected on the Superflux II cruises and 7 samples collected on the BAPLEX cruises. The BAPLEX samples provide more synoptic data because all of the samples, except one, were taken within a 2-hour window. The Superflux II samples, on the other hand, were taken over a 10-day period.

Various Superflux II and BAPLEX station locations are shown in figure 1. In figure 2, surface coprostanol concentrations at these stations are shown. The coprostanol concentrations of the BAPLEX samples are fairly consistent with a slightly elevated concentration near Cape Henry. This high concentration at BAPLEX station 4 may be caused by influence from Lynnhaven Inlet, or by direct discharge from ships. It is important to note that during the time of sampling there were numerous coal colliers moored in the Chesapeake Bay entrance. The discharge from these colliers and the heavy shipping traffic may explain this and other highly localized coprostanol concentrations. The particulate coprostanol concentration for the Superflux II samples varied considerably. Superflux II station 800 was sampled twice, on June 17 and 24. The difference between the coprostanol concentrations in these samples taken 1 week apart and at different stages in the tidal cycle illustrates the complexity of the transport system of particulates in the Chesapeake Bay entrance. The interpretation of data obtained over such a time interval in a complex system becomes very difficult.

A summary of coprostanol and cholesterol concentrations for Superflux II and BAPLEX samples is given in table 1A. The average coprostanol concentration for the BAPLEX samples is 0.190 µg/ℓ. For Superflux II samples,

the average coprostanol concentration is 0.250 μg/ℓ. Since only surface samples were collected at the BAPLEX stations, the Superflux II samples were broken down into surface (-1 m) samples and samples at depth (>-3 m). The average coprostanol concentrations for the surface and depth samples are 0.200 μg/ℓ and 0.278 μg/ℓ, respectively. The average coprostanol concentration for the BAPLEX surface samples is approximately the same as for the Superflux II samples taken at a depth of 1 m, indicating that on an average, the coprostanol concentration in surface waters of the Chesapeake Bay entrance and contiguous waters is fairly uniform. The average coprostanol concentration with depth is somewhat higher than that found in the surface waters. This increase with depth may come from either sewage-associated particles settling out as they leave the Bay, or the resuspension of contaminated sediment. The average cholesterol concentration determined in these samples is approximately five times higher than the coprostanol concentrations. The higher concentration of cholesterol is probably due to naturally occurring cholesterol in the marine environment. Coprostanol and cholesterol concentrations found in this study agree well with those reported in the literature (see table 1B and refs. 17 and 18). The Chesapeake Bay entrance is such a dynamic system that we cannot be certain which processes are dominant without more detailed study.

CONCLUSION

Particulate-associated coprostanol detected in the Chesapeake Bay entrance may originate from the discharge of sewage treatment plant effluent, runoff from nearby lands, or direct discharge from ships in the area. The coprostanol concentration in the surface water of the Chesapeake Bay entrance and contiguous waters is fairly uniform. An increase in concentration is found with depth, indicating the sewage-associated particulates are settling as they exit the Bay or contaminated sediment is being resuspended. The extended and somewhat random sampling scheme of this complex area makes the interpretation of the data difficult. However, we may conclude from this preliminary study that sewage-associated materials are being transported from the Chesapeake Bay to adjacent shelf waters where they may have adverse effects on living marine resources.

REFERENCES

1. Geldreich, E. E.: IN: Water Pollution Microbiology, R. Mitchell (Ed.), Wiley-Interscience, New York, NY, 1972, pp. 207-241.

2. Metcalf and Eddy, Inc.: Wastewater Engineering: Treatment Disposal Reuse, 2nd ed., McGraw-Hill Book Co., New York, NY, 1979, pp. 56-118.

3. Van Vleet, E. S.; and Quinn, J. G.: Input and Fate of Petroleum Hydrocarbons Entering the Providence River and Upper Narragansett Bay from Wastewater Effluents, Environmental Science and Technology, Vol. 11, 1977, pp. 1086-1092.

4. Burlingame, A. L.; Kimble, B. J.; Scott, E. S.; Walls, F. C.; De Leeuw, J. W.; De Lappe, B. W.; and Risebrough, R. W.: The Molecular Nature and Extreme Complexity of Trace Organic Constituents in Southern California Municipal Wastewater Effluents, IN: Identification and Analysis of Organic Pollutants in Water, L. H. Keith (Ed.). Ann Arbor Science Publishers, Inc., Ann Arbor, Michigan, 1972, pp. 557-585.

5. Dutka, B. J., Chau, A. S. Y.; and Coburn, J.: Relationship Between Bacterial Indicators of Water Pollution and Fecal Sterols, Water Res., Vol. 8, 1974, pp. 1047-1055.

6. Tabak, H. H.; Bloomhuff, R. N.; and Bunch, R. L.: Coprostanol: A Positive Tracer of Fecal Pollution, Develop. Ind. Microbiol., 13, 1972, pp. 296-307.

7. Smith, L. L.; and Gouron, R. E.: Sterol Metabolism-VI. Detection of 5B-Cholestan-3B-ol in Polluted Waters, Water Res., 3, 1969, pp. 141-148.

8. Goodfellow, R. M.; Cardoso, J.; Eliginton, G.; Dawson, J. P.; and Best, G. A.: A Fecal Sterol Survey in the Clyde Estuary, Marine Pollut. Bull., 8 (12), 1977, pp. 272-276.

9. Loh, P. C.; Fujioka, R. S.; and Lau, S.: Recovery, Survival and Dissemination of Human Enteric Viruses in Ocean Waters Receiving Sewage in Hawaii, Water, Air and Soil Bull., 12, 1979, pp. 197-217.

10. Rosenfield, R. S.; Fukushima, D. K.; Hellman, L.; and Gallagher, T. F.: The Transformation of Cholesterol to Coprostanol, J. Biol. Chem., 211, 1954, pp. 301-311.

11. Rosenfield, R. S.; and Gallagher, T. F.: Further Studies of the Biotransformation of Cholesterol to Coprostanol, Steroids, 4, 1964, pp. 515-520.

12. Techima, S.; and Kanazawa, A.: Occurrence of Coprostanol, 24 Ethylcoprostanol and 5α-Stanols in Marine Sediments, J. of the Oceanogr. Soc. of Japan, 34, 1978, pp. 85-92.

13. Murtaugh, J. J.; and Bunch, R. L.: Sterols as a Measure of Fecal Pollution, J. of Water Pollut. Control Fed., 39, 1967, pp. 404-409.

14. Nishimura, M.; and Koyama, T.: The Occurrence of Stanols in Various Living Organisms and the Behavior of Sterols in Contemporary Sediments, Geochim. et Cosmochim. Acta, 41, 1977, pp. 379-385.

15. Hatcher, P. G.; Keister, L. E.; and McGillivary, P. A.: Steriods as Sewage Specific Indicators in New York Bight Sediments, Bull. of Environ. Contam. and Toxicol, 14 (4), 1977, pp. 491-498.

16. Hatcher, P. G.; and McGillivary, P. A.: Sewage Contamination in the New York Bight. Coprostanol as an Indicator, Environ, Sci. and Technol., 13 (10), 1979, pp. 1225-1229.

17. Kanazawa, A.; and Teshima, S.: The Occurrence of Coprostanol, An Indicator of Fecal Pollution, IN: Seawater and Sediments, Oceanol. Acta, 1 (1), 1978, pp. 39-44.

18. Oquara, K.: Steroids of Coastal Waters and Sediments, Tokyo Bay, Sagami Bay, and Suruga Bay. The Spring Meeting of the Oceanographical Society of Japan, 1972, 112 pp.

TABLE 1A.- SUPERFLUX II AND BAPLEX RESULTS (µg/ℓ)

Source	Samples	Avg. coprostanol	Range	Avg. cholesterol	Range
BAPLEX (surf)	7	0.190	0.111-0.400	1.144	0.490-1.950
Superflux (all)	59	0.250	0.072-1.042	1.056	0.215-5.267
Superflux (-1 m)	21	0.200	0.072-1.042	0.956	0.215-5.267
Superflux (-3 m)	28	0.278	0.077-1.014	1.111	0.435-5.065

TABLE 1B.- COMPARISON OF COPROSTANOL AND CHOLESTEROL CONCENTRATIONS

Source	Coprostanol (µg/ℓ)	Cholesterol (µg/ℓ)	Reference
Superflux II	0.072-1.042	0.215-5.267	Present study
Clyde estuary	0.1-47.5	--	(8)
Ariake Sea	0.06-1.1	2.0-6.3	(17)
Tokyo Bay	0.2-6.6	2.2-8.6	(18)

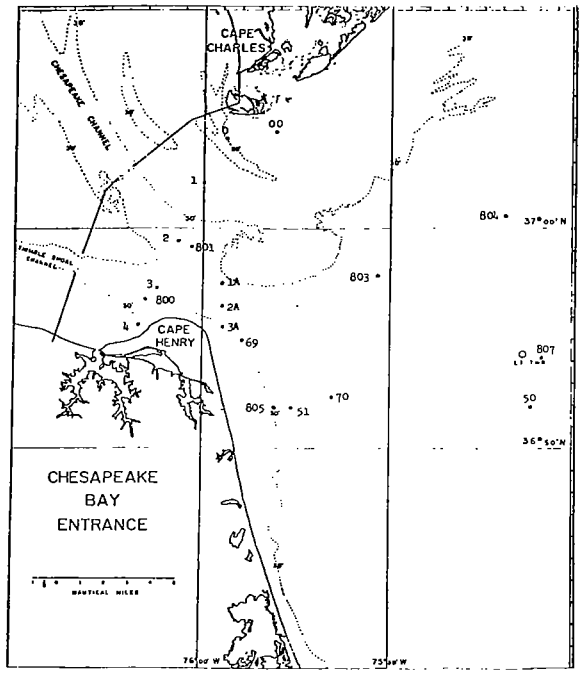

Figure 1.- Superflux II and BAPLEX sampling locations.

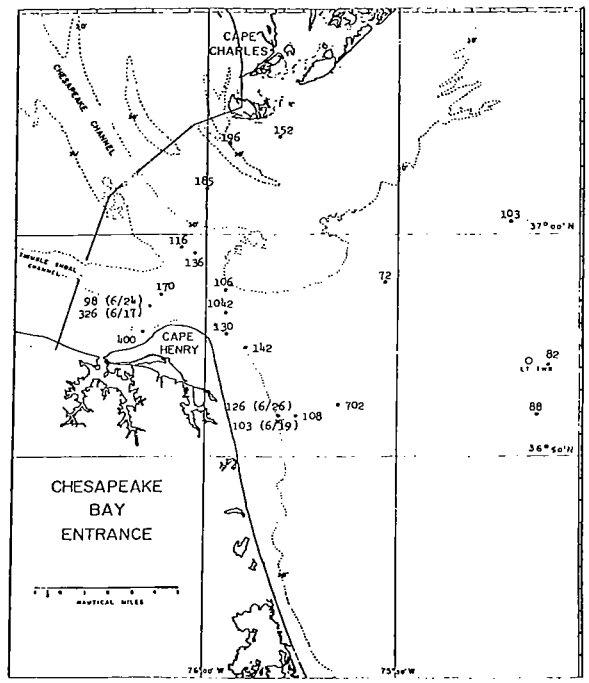

Figure 2.- Surface particulate coprostanol concentrations (µg/ℓ).

CHARACTERISTICS OF TOTAL SUSPENDED MATTER AND ASSOCIATED HYDROCARBON CONCENTRATIONS ADJACENT TO THE CHESAPEAKE BAY ENTRANCE

George F. Oertel and Terry L. Wade
Old Dominion University

INTRODUCTION

Purpose

The Department of Oceanography, Old Dominion University, participated in three series of experiments within the NOAA/NASA Superflux study. The initial oceanographic objective of the experiments was to characterize the quality of Chesapeake Bay outwelling onto the contiguous continental shelf. The long-term objective of the experiments was to assess the impact of the natural and anthropogenic effluents of the Bay on the living resources of the continental shelf. Hydrocarbons and suspended particulates have natural and anthropogenic sources; however, concentrations of these substances are a major concern in water quality assessment. An extensive survey of hydrocarbon and suspended solid concentration was designed for the lower Bay and contiguous shelf. Superflux missions were conducted in March, June, and October, 1980, to evaluate (1) a high runoff period associated with a spring phytoplankton bloom, (2) a low runoff period without a phytoplankton bloom, and (3) a low runoff period corresponding with a fall phytoplankton bloom. While all missions have been completed only the results from the June 1980 experiment are presented in this report.

In support of the oceanographic objectives of Superflux, there were also some remote sensing objectives. The overall remote sensing objective was to determine the feasibility of using a variety of remote sensors to generate a synoptic data set of various water quality parameters. This required carefully coordinating experimental design between remote sensing overflights and oceanographic measurements.

The purpose of this study was to determine concentrations of hydrocarbons and associated suspended particulates at stations in and adjacent to the entrance to the Chesapeake Bay and to determine if hydrocarbon concentrations could be estimated from remotely sensed concentrations of suspended matter. Sampling was accomplished from the R/V Linwood Holton and the NOAA ships George B. Kelez and Delaware II. Four remote sensing instruments flown during the Superflux II mission had potential value for sensing turbidity variations generated by changes in suspended solid concentration; they are passive sensors (Multichannel Ocean Color Scanner, MOCS; Test Bed Airborne Multispectral Scanner, TBAMS), and active laser systems (Airborne Lidar Oceanographic Probing Experiment, ALOPE and Airborne Oceanographic Lidar, AOL). The airborne oceanographic laser induces emission spectra from Raman backscatter. The water Raman backscattered signal essentially defined the volume of water fluorescent by the laser pulse.

Thus, as the concentration of suspended solids is increased, fewer water molecules are accessed.

The passive sensors scanned the water surface from elevations ranging from 3 to 7.5 km, whereas the laser sensors were flown in a profiling mode at 152 m. Passive and active remote sensing data were acquired in conjunction with sea truth data collection.

Experimental Design and Techniques

Ninety-two samples were collected from Superflux II mission station locations (fig. 1). These stations were primarily located above the continental shelf south of the entrance to the Chesapeake Bay. Only two stations were located in the Bay entrance and no stations were located in continental shelf water north of the Bay. To supplement these data, the ODU-BAPLEX program collected a data set at six stations across the Chesapeake Bay entrance. Samples were analyzed for hydrocarbon concentration, total suspended matter, total organic and inorganic matter, and particulate size frequency distribution following techniques described by Wade and Oertel (ref. 1), Gingerich and Oertel (ref. 2), and Byrnes and Oertel (ref. 3). Data were collected during an 11-day period between the 17th of June and the 27th of June, 1980. Four samples were collected at evenly spaced depths of the water column at each station. Temperature and salinity measurements were also made at each station in order to illustrate thermohaline gradients that are useful in determining Chesapeake Bay outwelling patterns.

OBSERVATIONS AND DISCUSSION OF RESULTS

The relatively long duration (8 days) over which the majority of the Superflux II samples were collected limited the interpretation of process events. During the 8-day period, it was obvious that some amount of variability in the data could be explained by the natural dispersion of water by tides and coastal currents. The comparison of data among stations of a specific transect (all taken on the same day) are more reliable than comparisons between adjacent transects (taken one or more days apart).

Analysis of total hydrocarbon concentration by gas chromatography provided data in values of micrograms hydrocarbon per liter (μg/ℓ) of water. However, laboratory studies (ref. 4) have illustrated that greater than 90 percent of hydrocarbon material in seawater samples is generally associated with suspended particulate matter. Thus, hydrocarbon concentrations are expressed as micrograms hydrocarbon per milligrams of total suspended sediment (μg/mg).

The areal distribution of hydrocarbon concentrations (μg/mg) illustrated relatively high surface concentrations in the Bay entrance (6 to 7 μg/mg). Two areas of relatively high surface concentrations extend seaward from the Bay entrance (fig. 2c). One area was contiguous with the shore of Virginia Beach and extended approximately 10 n. mi. south of Cape Henry. The second and

more prominent high concentration extended seaward from just north of Cape Henry along an azimuth of 150° (true) for approximately 15 n. mi. The axis of the second area of high concentration was approximately 7.5 n. mi. offshore and parallel to Virginia Beach. An areal plot of the total suspended matter illustrated that the nearshore high in hydrocarbon concentration corresponded with the position of a high concentration of total suspended matter, whereas the offshore increase in hydrocarbon concentration was not associated with an increase in total weight of suspended matter concentration (fig. 2a). In a "gross" sense, low-salinity water can be used as a tracer of the outwelling from Chesapeake Bay (fig. 2b). In an attempt to associate hydrocarbon and suspended matter concentrated with the outwelling of the Chesapeake Bay, the surveys of the distribution of low salinity water (<29 o/oo) were compared with hydrocarbon and total suspended matter concentration. The axis of the low salinity water was almost exactly between the two areas of relatively high hydrocarbon concentration. It is tempting to suggest that the effluent from the Chesapeake Bay is depleted in hydrocarbons, however, it is more appropriate to speculate on the mechanics of boundary conditions that may have caused the two anomalously high concentrations in those areas.

Vertical sections of data for transect lines B, C, and D illustrate that the concentration of hydrocarbons and suspended solids increased with depth in the nearshore zone but was apparently a surface phenomenon in the offshore area (figs. 3 and 4). Increases in concentration with depth may result from two different processes. The first and most plausible explanation is that re-suspension of fine grains from the seabed was the major source of suspended matter in the water column. After particulates with associated hydrocarbons were elevated into the water column, they were apparently transported southward in a hyperpycnal flow of higher salinity (28 to 32 percent) bottom water adjacent to Virginia Beach. The second explanation for the anomalously high nearshore concentration of hydrocarbons and particles is that the anomaly was associated with a hypopycnal (surface) flow and that the particulate fraction had partially settled through the water column. This would account for the increase in concentration of suspended particulates (by weight) with depth. There is no doubt that both of these processes have, in part, contributed to the distribution of hydrocarbon and suspended solid concentrations in the nearshore area.

At transect B, it is extremely difficult to distinguish between the nearshore and offshore hydrocarbon anomalies. However, it is apparent from profiles of the particulate data that the axis of the inner area was between standard stations 69 and 802 (fig. 5). The axis of the offshore anomaly was apparently located just seaward of standard stations 802, 806, and 810 at transects B, C, and D, respectively. This places the axis of the offshore anomaly along the vertical and areal boundary of the prominent low salinity outwellings of the Chesapeake Bay. Studies of other water mass boundary conditions in the Bay entrance have illustrated an increase in the concentration of buoyant materials (including hydrocarbons) at frontal interfaces.

In an attempt to correlate hydrocarbon concentration with total suspended solids, a correlation coefficient for all data was calculated. The correlation

coefficient of 0.2 illustrated that a very poor correlation existed for all data. This was anticipated since there was a diversity of sources and processes that had different influences on the concentration and dilution of hydrocarbons and suspended particles. The correlations between hydrocarbon and suspended particulate concentrations showed an increased correlation of 0.59.

While the offshore hydrocarbon anomaly was very well defined, that area was very poorly correlated with the weight concentration of suspended particulate matter. Two potential reasons for this poor correlation relate to sources and processes influencing the total concentration. The easiest explanation for the low correlation coefficient is that there were two independent and different sources of suspended solids and hydrocarbons for this zone. The second possibility is that the sorting characteristics of particles comprising the suspended solids of the nearshore and offshore anomalies were independently altered with time, and therefore the adsorption rates of hydrocarbons were variable. Microscopic analysis of filters illustrated that the particulate fraction was composed of approximately 25 types of particles, and that different proportions of these particles were present in the nearshore and offshore zones. While specific studies of surface area characteristics have not been completed, a wide variety of particle shapes was observed by microscopic inspection.

In general, particles with irregular shapes provided more surface area and sites for hydrocarbon adsorption than the more regular spherical particles. On a per-weight basis the smaller particles provide greater surface areas than larger particles. Thus a water sample having a relatively low concentration (mg/ℓ) because it is primarily composed of very fine-grained particles may have more surface area for hydrocarbon adsorption than a sample having a relatively high concentration (mg/ℓ) but composed of a fewer number of large particles. The offshore hydrocarbon anomaly had a relatively low weight concentration of suspended matter but had a relatively large surface area availability for hydrocarbon adsorption since the particles were very fine grained (table 1). This relationship was well illustrated in sample 71-6, where the volume percentage in the smaller mode (12.7 to 16.0 μm) was one-third of the volume present in the larger mode (80.6 to 101.6 μm mode); however, the smaller size mode had approximately twice the available surface area of the larger mode (fig. 5). Since larger and heavier particles settle more rapidly than smaller ones, the settlement of larger particles should have been more complete in the offshore zone than in the nearshore zone. Therefore, reduction in the relative weight concentration of suspended matter may have resulted in only a minor reduction in surface area available for adsorption of pollutants. A simpler explanation would be that the offshore area had a finer-grained source to begin with. Table 1 illustrates variations in the characteristics of particulate matter at four distinct areas: the Bay entrance, the nearshore hydrocarbon anomaly, the offshore hydrocarbon anomaly, and shelf water. In an attempt to determine the relative surface area available, the volume-percents of fine and coarse-grained particles were determined for the four areas described above. It was apparent from these data that samples with a high percentage (greater than 75 percent) of material less than 32 μm in diameter also had high concentrations of hydrocarbons. Samples with a low percentage

of the less than 32 μm material had no measurable hydrocarbons. Samples comprised of a moderate volume percent (25 to 50 percent) of small grains (less than 32 μm) had traces of hydrocarbons (1.8 to 2.5 micrograins per liter).

The weight concentration (mg/ℓ) of particles, the volume percent of large particles, and the absence or presence of quartz grains in the 70 to 120 μm size range provided additional data on the source of suspended particulates and hydrocarbons. The presence of suspended quartz grains in the 70 to 120 μm size range required a very close proximity to the source of the inorganic fraction, otherwise the large grains would have settled to the bottom. Raman data (ref. 5) for the Bay entrance illustrated a turbidity maximum across the Bay entrance with no apparent up-Bay or down-Bay source. The presence of relatively large quartz grains at the Bay entrance and along Virginia Beach (BAPLEX stations 1-s and 2-s, and Superflux II stations 69-s and 805-s) illustrated that high turbidity was apparently produced by local resuspension. At the offshore hydrocarbon anomaly, large quartz grains were not found in the water. While the volume percent of coarse and small particles was approximately equal, the fine fraction had greater than twice the surface area as the coarse, apparently planktonic fraction. On a weight basis the larger particles (both organic and inorganic) had the more significant influence on the total suspended matter (TSM) concentration, whereas the smaller inorganic particles (because of increased number and surface area) apparently had a greater influence on the relative amount of hydrocarbons that adsorbed to the suspended particles measured on a weight basis.

It is apparent from the above discussion that further attempts to correlate hydrocarbons with suspended particulates should consider relative surface area and grain shape characteristics.

CONCLUSIONS

While there was generally good correlation between anomalies of high hydrocarbon and suspended matter concentration, no linear correlation between concentrations could be established. Failure to determine a linear correlation was apparently due to the fact that the concentration of suspended matter was determined on a weight basis and adsorption characteristics of hydrocarbons are apparently dependent on a variety of other characteristics of suspended matter, including shape, surface, area, etc.

High concentrations of total suspended matter were associated with the shoals in the Bay entrance and its margins. Variations in concentrations of total suspended matter were generally produced by changes in the inorganic concentrations since organic concentrations remained relatively constant. Adjacent to Virginia Beach, local resuspension of bottom sediment was suspected because of the presence of suspended quartz particles in the 70 to 120 μm size range. The nearshore area of high suspended solid concentration and relatively high hydrocarbon concentration was landward of the inner boundary of the low salinity outwelling from Chesapeake Bay.

High concentrations of hydrocarbons were also measured along the seaward boundary of the low salinity outwelling from Chesapeake Bay. A combination of frontal boundary mechanics and particle surface area availability may have influenced the formation of this offshore hydrocarbon anomaly.

REFERENCES

1. Wade, Terry L.; and Oertel, George F.: Concentration of Hydrocarbons Associated with Particles in the Shelf Waters Adjacent to the Entrance of Chesapeake Bay. Chesapeake Bay Plume Study - Superflux 1980, NASA CP-2188, 1981 (Paper no. 17 of this compilation).

2. Gingerich, Kathryn J.; and Oertel, George F.: Suspended Particulate Matter in the Chesapeake Bay Entrance and Adjacent Shelf Waters. Chesapeake Bay Plume Study - Superflux 1980, NASA CP-2188, 1981 (Paper no. 15 of this compilation).

3. Byrnes, Mark R.; and Oertel, George F.: Particle Size Distribution of Suspended Solids in the Chesapeake Bay Entrance and Adjacent Shelf Waters. Chesapeake Bay Plume Study - Superflux 1980, NASA CP-2188, 1981 (Paper no. 16 of this compilation).

4. Meyers, P. A.; and Quinn, J. G.: Association of Hydrocarbons and Mineral Particles in Saline Solution. Nature, vol. 224, 1973, pp. 23-24.

5. Hoge, F. E.; and Swift, R. N.: Application of the NASA Airborne Oceanographic Lidar to the Mapping of Chlorophyll and Other Organic Pigments. Chesapeake Bay Plume Study - Superflux 1980, NASA CP-2188, 1981 (Paper no. 26 of this compilation).

TABLE 1.- CHARACTERISTICS OF SUSPENDED PARTICULATE MATERIAL AT THE BAY ENTRANCE, NEARSHORE, OFFSHORE, AND INNER SHELF

Location	Sample no.	Date	Percent <32 μm particles	Percent 50-80 μm particles	Presence of 70-120 μm quartz	Weight hydrocarbon μg/ℓ
Bay entrance	1-S	6-24	80.0	10.5	yes	18.0
	2-S	6-24	80.0	9.3	yes	14.0
Nearshore anomaly	69-S	6-18	N.D.	N.D.	yes	4.2
	805-S	6-19	N.D.	N.D.	yes	5.1
	71-6	6-21	24.0	24.3	no	2.5
Offshore anomaly	806-S	6-19	N.D.	N.D.	no	2.7
	810-S	6-20	N.D.	N.D.	no	10.0
	812-S	6-21	45.0	24.1	no	1.8
Shelf	811-S	6-21	9.4	34.4	no	0.0
	813-S	6-21	8.6	41.5	no	0.0

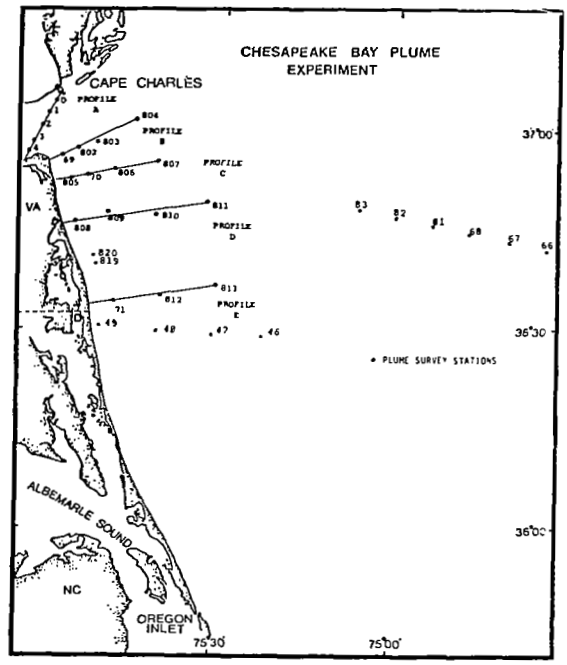

Figure 1.- Map showing station location for water samples.

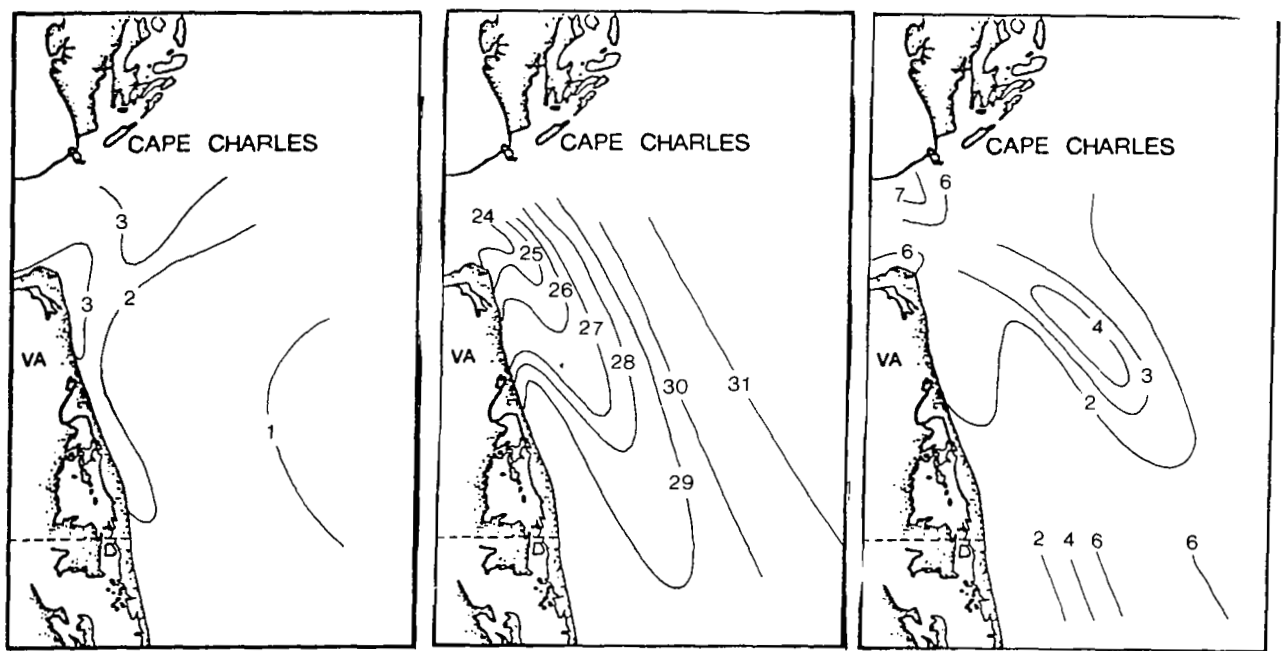

(a) Total suspended matter. (b) Salinity. (c) Hydrocarbon concentrations.

Figure 2.- Map illustrating concentration of total suspended matter (mg/ℓ), salinity ($^{o}/_{oo}$), and hydrocarbon μg/mg) in surface water adjacent to the Chesapeake Bay entrance.

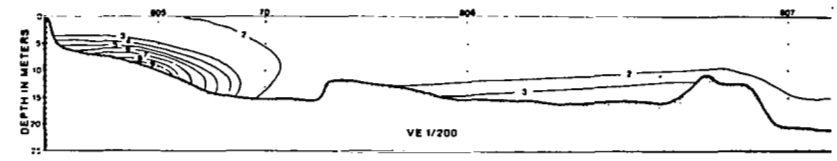

(a) Total suspended matter.

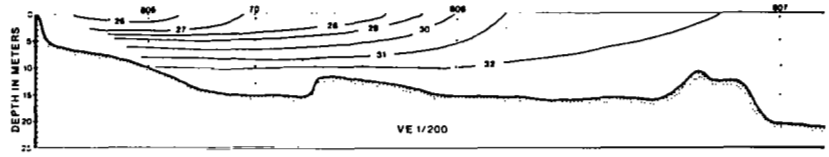

(b) Salinity.

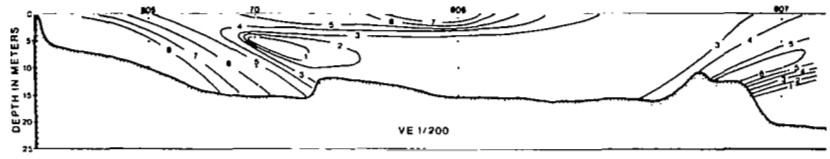

(c) Hydrocarbons.

Figure 3.- Profile of transect C illustrating total suspended matter concentration (mg/ℓ), salinity (°/oo), and hydrocarbon concentration (μg/ℓ).

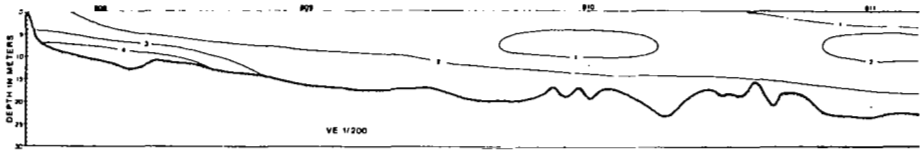

(a) Total suspended matter.

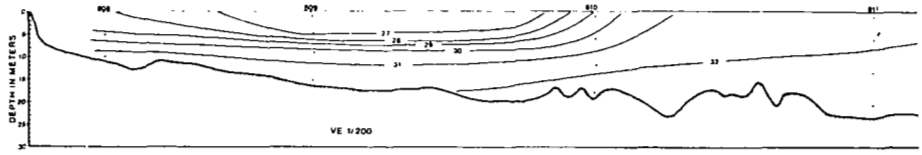

(b) Salinity.

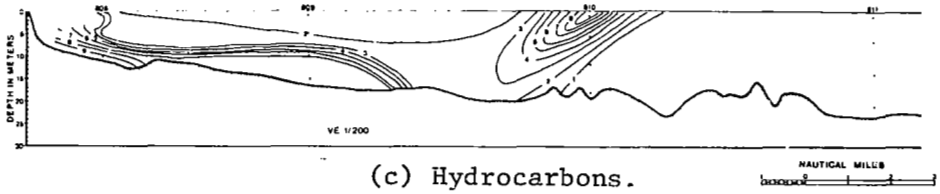

(c) Hydrocarbons.

Figure 4.- Profile of transect D illustrating total suspended matter concentration (mg/ℓ), salinity (°/oo), and hydrocarbon concentration (μg/ℓ).

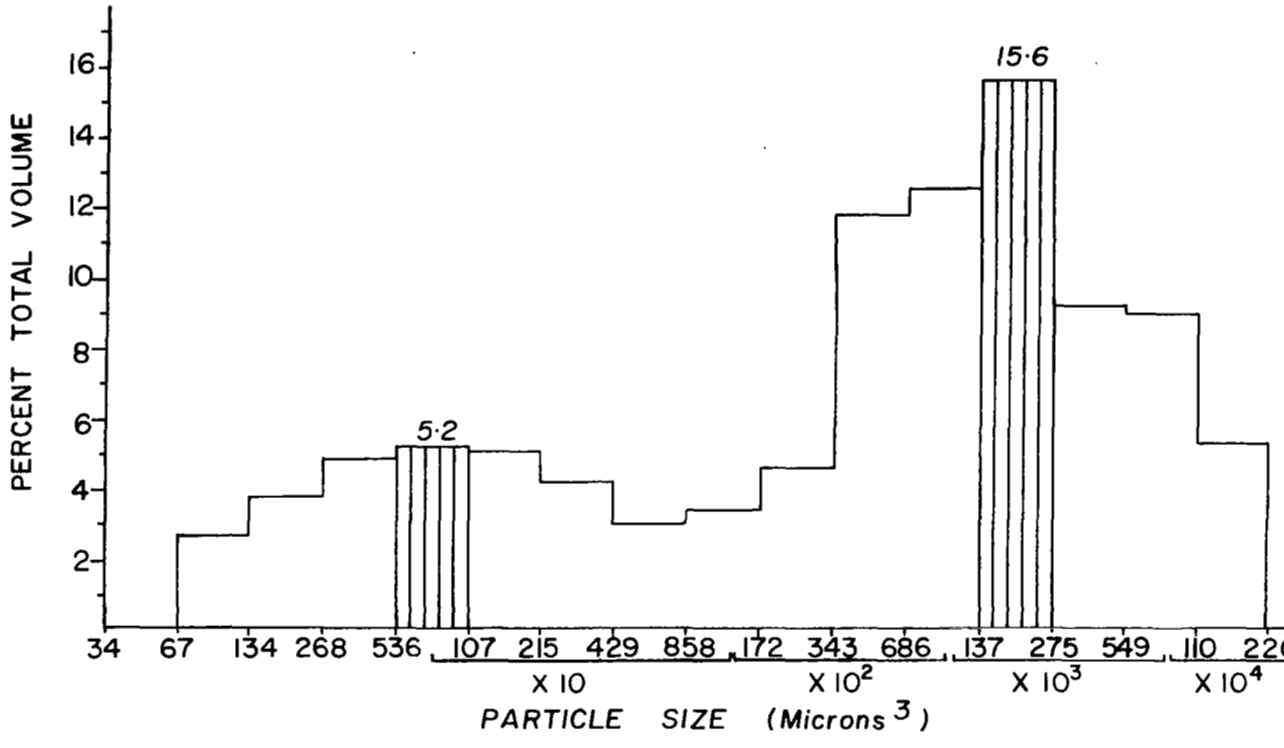

Figure 5.- Histogram of size frequency distribution of particles for sample 71-6.

NUTRIENTS IN WATERS ON THE INNER SHELF BETWEEN CAPE CHARLES AND CAPE HATTERAS*

George T. F. Wong and James F. Todd
Department of Oceanography
Old Dominion University

INTRODUCTION

High productivity has been observed in many areas of the oceans adjacent to land (ref. 1). A significant portion of the living resources from the seas is derived from these regions. This increased productivity may be caused by nutrients, trace metals or organic growth-promoting factors originating from land (ref. 2). The major route for the transport of materials from land to the coastal oceans is via rivers. In its pristine state, the composition of river waters is controlled by weathering processes. However, with increasing population and industrial activities in coastal regions and along river banks, anthropogenic inputs such as domestic sewage effluents and industrial wastes may have a significant direct or indirect influence on the composition of rivers, estuaries, and coastal oceans. Goldberg (ref. 3) suggested that river water may affect primary productivity in coastal water in several ways:

(a) By bringing in, diluting or removing (by sedimentation) plant nutrients
(b) By bringing in suspended material or dissolved colored substances and thus altering the depth to which sufficient light can penetrate to support photosynthesis
(c) By establishing the stability of the water column with a low density surface layer. The increased stability of the water column may increase production by reducing the tendency of cells to be carried below the critical depth for photosynthesis.

The primary objective of the project Superflux is to assess the influence of the outflow of water from the Chesapeake Bay on the adjacent shelf waters of the southern tip of the Middle Atlantic Bight. We shall discuss the distribution of nutrients in this region during three cruises in the summer and fall of 1980.

THE SOUTHERN MIDDLE ATLANTIC BIGHT

Our study area is considered to be the part of the shelf bound by Virginia and North Carolina to the west, the 100-m isobath to the east, and the imaginary lines extending due east from Cape Hatteras, North Carolina to the

*This work was supported by contract NA-80-FA-D-00007 from the National Oceanic and Atmospheric Administration.

south and Cape Charles, Virginia to the north. It is part of the Middle Atlantic Bight which extends from Cape Cod (Massachusetts) to Cape Hatteras. A large scale systematic study of the oceanography of the northern Middle Atlantic Bight (the New York Bight) which stretches from Cape Cod to Cape May (New Jersey) has been completed and the results were reported in a special Symposium volume (ref. 4). However, the southern Middle Atlantic Bight was much less extensively studied.

The annual outflow of freshwater from the Chesapeake Bay to the Atlantic Ocean estimated from the inflow of water into the Chesapeake Bay is about 60 km^3/yr (ref. 5). This constitutes over 50% of the freshwater inflow to the Middle Atlantic Bight (ref. 6) and virtually the total freshwater inflow to the study area. The Chesapeake Bay is the largest estuary in the United States. It has a drainage basin of 1.66×10^5 km^2. The population in the drainage basin is projected to be 30 million by the year 2020 (ref. 7). Land use in the drainage basin is highly diversified. There are urban, industrialized as well as agricultural areas. Significant amounts of anthropogenic materials are introduced directly or indirectly via the tributaries into the Bay. These inputs will affect the composition of the outflow that reaches the study area.

The major input of water to the study area is the alongshore transport over the shelf, which is estimated to be 8000 km^3/yr (ref. 6). Thus, the total freshwater input from the Chesapeake Bay is less than 1% of this alongshore flow. The cross-shelf exchange of shelf water with slope water has not been quantified. The volume of water in the study area is estimated to be about 3×10^2 km^3. Therefore, the maximum residence time of the water is about 0.5 month.

EXPERIMENTAL

A grid of stations was established for the Superflux cruises as shown in figure 1. In June, 1980 (Superflux II) 30 stations were occupied between June 17 and 23 by R/V Delaware II and 11 stations were occupied between June 24 and 27 by R/V Kelez. Between October 14 and 22, 1980 (Superflux III) 26 stations were occupied by the R/V Kelez. Samples were collected with Niskin bottles and analyzed for phosphate, nitrate, ammonia, and silicate. Nitrite was determined in the samples from Superflux II only. (Salinity was measured by investigators from the Northeast Fisheries Center, Sandy Hook Laboratory of the National Oceanic and Atmospheric Administration, and the data were made available to all participants in the Superflux program). Stations were occupied usually along east-west transects. No special attention was given to tidal conditions. It was not uncommon that the first and last stations of a transect were occupied more than a tidal cycle apart.

Dissolved reactive phosphate was determined by the method of Murphy and Riley (ref. 8) by the reduction of the phosphomolybdate complex with ascorbic acid. Nitrate was first reduced to nitrite by passing the samples through a Cd-Cu column and then measured as nitrite (ref. 9). Nitrite was

diazotized with sulfanilamide and the concentration of the azo dye formed was determined by spectrophotometry (ref. 10). Ammonia was measured by the indophenol blue method of Solorzano (ref. 11). Dissolved silicate was measured by spectrophotometry after the silicomolybdate complex had been reduced with metol (ref. 12). The precision of these methods for the determination of nutrients was about ±5%. The detection limits were about 0.03, 0.01, 0.05, 0.1, and 0.1 μmole/ℓ for phosphate, nitrite, nitrate, ammonia, and silicate, respectively (ref. 13). About half of the samples were analyzed onboard ship. The remaining ones were filtered, frozen and returned to shore-based lab for analyses.

RESULTS AND DISCUSSION

Distribution at 1 m

In June, a tongue of water with lower salinities (<29 o/oo) extending southward from the southern portion of the mouth of Chesapeake Bay (~37°N) to about 36°20' can be readily identified from the data obtained between June 17 and 23 (figure 2a). This water mass, which represented the influence of the outflow of freshwater from the Chesapeake Bay to the Atlantic Ocean, hugged the coast initially and turned eastward offshore as it spread southward. This distribution of salinity is in accord with the first order description of the circulation at the mouth of the Bay (ref. 14) since seawater enters the Bay through the northern portion of the mouth and freshwater leaves the Bay via the southern portion. Wong (ref. 15) also reported similar but less extensive data on the distribution of salinity at the mouth and within the southern part of the Bay. A closer examination of the distribution of salinity indicates that salinity did not increase monotonically away from the mouth of the Chesapeake Bay. Patches of water with salinities significantly higher than the surrounding waters were observed. Moreover, when the same station was occupied a week later, different salinities were observed (table 1). This patchiness and the short-term temporal variation in salinity are expected as a result of the tidal influence on the outflow of waters from the Chesapeake Bay and they clearly demonstrate the limitations of non-synoptic data for studying a non-steady-state phenomenon.

In October, the distribution of salinity was significantly different (figure 2). Waters with salinities below 31 o/oo were confined to the immediate vicinity of the mouth of the Chesapeake Bay. This longer term variation in salinity (table 1) is probably caused by the seasonal variations in the outflow of fresh water from the Chesapeake Bay. It should be noted that the summer and fall of 1980 were exceptionally dry. Thus, the influence of Chesapeake Bay water on the adjacent Atlantic water decreased as the drought continued.

The distributions of phosphate, nitrate, ammonia and silicate during the first cruise in June are shown in figures 3a - 3d. The distribution of nitrite is not presented because the concentrations rarely exceeded the detection limit. In the case of nitrate, phosphate, and silicate, with the exception of

station 800 at the southern side of the mouth of the Chesapeake Bay, the concentrations were also frequently at or close to the detection limits. Significant quantities of ammonia were detected at many stations although the distribution was patchy. In general, the concentrations of the nutrients decreased southward and seaward away from the mouth of the Bay (table 2 and ref. 16). The elevated concentrations of the nutrients at the mouth of the Bay suggest that the outflow of waters from the Chesapeake Bay may be a source of nutrients for the adjacent Atlantic waters. As expected, the patterns of the distributions of the nutrients were not similar to that of salinity since they do not have the same sources and sinks. The elevated concentrations of nutrients did not extend noticeably offshore or southward suggesting that they are not conservative and may be utilized and exhausted rapidly by organisms.

Ammonia was frequently the most abundant form of combined inorganic nitrogen. The concentrations were at times an order of magnitude higher than the sum of nitrate and nitrite. In marine waters, the common limiting nutrient is nitrogen (ref. 17). An N/P atomic ratio lower than 15:1 implies that the availability of inorganic nitrogen limits the phytoplankton production. At the mouth of the Bay as at station 800, nitrogen limitation was apparently observed as the ratio of N/P in both June and October was below 15 (table 2). However, at other stations such as station 816, phosphate was exhausted while significant amounts of ammonia remained. The N/P ratio greatly exceeded 15. In these cases, phosphate may be the limiting nutrient. The complex and patchy distribution of ammonia in comparison with that of the other nutrients reflects the higher degree of complexity of the chemistry of the nitrogen system. During the photosynthetic uptake and remineralization process of phytoplankton, in addition to the removal or replenishment of combined inorganic nitrogen in the water column, the speciation can also be modified by processes such as assimilatory nitrate reduction, preferential uptake of ammonia, and nitrification (refs. 18 and 19). The concentration of ammonia is further affected by the excretions of higher organisms such as zooplankton.

As in the case of salinity, the concentrations of the nutrients at a single station displayed short-term temporal variations. Significantly different concentrations were observed during the two cruises in June (table 2). These short-term variations render a precise estimation of the fluxes of material from the Bay to the adjacent Atlantic waters difficult, even if the outflow of water can be accurately measured. An intensive sampling program is clearly essential if such quantifications are to be made.

The distributions of phosphate, nitrate, ammonia, and silicate during October are shown in figures 4a - 4d. Again, a decrease of concentration from the mouth of the Chesapeake Bay seaward and southward was observed (table 2). A pocket of water with higher concentrations of nutrients was observed in the immediate vicinity of the Bay mouth. However, other pockets of nutrient-rich waters were found in some cases further south and further east. The distribution of ammonia was again more patchy than the other nutrients. Between June and October, the salinity at the Bay mouth (station 800) increased significantly (table 2). The nutrient concentrations had

increased also. However, the magnitudes of the changes in concentrations were similar to the short-term variations observed in a period of a week in June. Thus, real seasonal variations in the concentrations of the nutrients cannot yet be established.

East-West Transects

The distributions of salinity, phosphate, nitrate, ammonia, and silicate along a northern transect (stations 69, 802, 803, and 804) and a southern transect (stations 814, 815, 72, and 816) in June and October are shown in figures 5 to 8. In each east-west transect, salinity increased with depth and seaward. During each cruise, salinity increased southward. In June, a water mass with salinities below 30 o/oo was clearly defined in both transects. In October, waters with salinities below 30 o/oo were confined to the immediate vicinity of the mouth of the Chesapeake Bay and at depths of less than 2 m. In the southern transect, salinities were all above 32 o/oo. These distributions of salinities suggest a decreasing outflow of freshwater from Chesapeake Bay from June to October.

In June, in the northern transect, the concentrations of phosphate decreased seaward and increased towards the bottom at some stations. In the southern transect, with the exception of two samples, the concentrations were uniformly low, being less than 0.1 μM. In October, a decrease in concentration seaward was observed in both transects and an increase in concentrations towards the bottom was again observed at some stations. Similar concentrations and distributions of phosphate have been reported in the New York Bight (ref. 20). In the northern transects, the elevated concentrations in the top few meters of water close to the mouth of Chesapeake Bay may be related to the outflow of Chesapeake Bay water. The increase in the concentration of phosphate towards the bottom may be caused by a diffusive flux of phosphate from the sediments. Nutrients, including phosphate, are regenerated by the decomposition of organic matter in the sediments and elevated concentrations of phosphate in the interstitial waters relative to the bottom waters have been reported in coastal sediments (ref. 21). The resulting concentration gradient leads to a diffusive flux of phosphate to the water column. The elevated concentrations of phosphate in the bottom may also be explained by an advective mass of bottom water with high phosphate concentrations from areas north of the study area. Indeed, bottom waters with similar concentrations of phosphate were observed in the New York Bight (ref. 20). Thus, there are at least three possible sources of phosphate to the study area: (1) outflow from Chesapeake Bay; (2) diffusive flux of phosphate from the sediments; and (3) advection of nutrient-rich water from areas north of the study area. Thus, although water from the Chesapeake Bay is a potential source of phosphate to the study area, its contribution cannot yet be isolated from those of the other sources.

During June, the concentration of nitrate was uniformly low in both transects, being mostly less than 0.5 μmole/ℓ. In October, in the northern transect, significantly higher concentrations were observed at the mouth of the Chesapeake Bay. In the southern transect, no definite pattern similar to the

distribution of salinity was observed. The concentrations of nitrate at the stations close to shore were below 0.5 μM. The bottom water at the seaward stations had somewhat elevated concentrations. These distributions and seasonal variations were similar to those observed in the New York Bight (ref. 20). The distribution of ammonia was patchy although definite patterns were observed in each transect. As discussed previously, this patchiness might be caused by the higher level of complexity of the chemistry of the nitrogen system. Again, as in the case of phosphate, elevated concentrations were observed at some stations in the bottom waters and similar mechanisms can be proposed to explain these observations. The concentrations and depth profile of ammonia are not unlike those observed in the New York Bight (ref. 22). Thus, an advective flux of ammonia cannot be ruled out. Ammonia is also one of the initial products in the decomposition of organic matter in sediments. In coastal sediments, which are likely to have a thin oxidizing zone, ammonia is not further oxidized to nitrite or nitrate in such a reducing environment (ref. 23). Consequently, in the interstitial waters, concentrations of ammonia that are orders of magnitude higher than those in the bottom water have been observed (ref. 21) resulting in a diffusive flux of ammonia to the water column.

In June, the concentrations of silicate were uniformly low, being mostly less than 1 μmole/ℓ. In October, the concentrations of silicate decreased seaward and increased towards the bottom. The elevated concentrations in the bottom water may again be caused by an advective flux from the north or a diffusive flux from the sediments. The concentration gradient of dissolved silicon in the interstitial water can be maintained by the dissolution of solid phases such as skeletal parts of siliceous organisms (ref. 24) and such a concentration gradient has been observed in coastal sediments (ref. 21).

CONCLUSION

The outflow of freshwater from Chesapeake Bay is a potential source of nutrients to the adjacent shelf waters. However, a quantitative estimation of its importance cannot yet be made because (a) there are other sources of nutrients to the study area and these sources cannot yet be quantified and (b) the concentrations of nutrients in the outflow from Chesapeake Bay exhibit significant short-term and long-term temporal variabilities.

REFERENCES

1. Koblentz-Mishke, O.J., V.V. Volkovinsky and J.C. Kabanova (1970). Plankton primary production of the world ocean. IN: Scientific Exploration of the South Pacific. W.S. Wooster, editor. National Academy of Sciences, Washington, D.C. pp. 183-193.

2. Riley, J.P. and R. Chester (1971). Introduction to Marine Chemistry. Academic Press, New York.

3. Goldberg, E.D. (1971). River-ocean interactions. IN: Fertility of the Sea. J.D. Costlow, Jr., editor. Gordon and Breach, New York. pp. 143-156.

4. Gross, M.G., editor (1976). Middle Atlantic Continental Shelf and the New York Bight. Amer. Soc. Limnol. Oceanogr. Spec. Symp. Vol. 2. Allen Press, Lawrence, Kansas. 441 pp.

5. Schubel, J.R. (1972). The physical and chemical conditions of Chesapeake Bay, an evaluation. Chesapeake Bay Institute Special Report 21.

6. Beardsley, R.C., W.C. Boicourt and D.V. Hansen (1976). Physical Oceanography of the Middle Atlantic Bight. Amer. Soc. Limnol. Oceanogr. Spec. Symp. Vol. 2. Allen Press, Lawrence, Kansas. pp. 20-34.

7. Pelczar, M.J., Jr. (1972). The current status of the Chesapeake Bay. Opening remarks. J. Washington Acad. Sci. 62, pp. 54-55.

8. Murphy, J. and J.P. Riley (1962). A modified single solution method for the determination of phosphate in natural waters. Anal. Chim. Acta, 27, 31-36.

9. Wood, E.D., F.A.J. Armstrong and F.A. Richards (1967). Determination of nitrate in seawater by cadmium-copper reduction to nitrite. J. Mar. Biol. Assoc. U.K., 47, 23-31.

10. Benschneider, K. and R.J. Robinson (1952). A new spectrophotometric determination of nitrite in seawater. J. Mar. Res., 11, 87-96.

11. Solorzano, L. (1969). Determination of ammonia in natural waters by phenol hypochlorite method. Limnol. Oceanogr., 14, 799-801.

12. Mullin, J.B. and J.P. Riley (1955). The colorimetric determination of silicate with special reference to sea and natural waters. Anal. Chim. Acta., 12, 162-176.

13. Strickland, J.D.H. and T.R. Parsons (1972). A Practical Handbook of Seawater Analysis. Fisheries Research Board of Canada, Ottawa, Canada.

14. Pritchard, D.W. (1962). Salinity distribution and circulation in the Chesapeake Bay estuarine system. J. Mar. Res., 11, 106-123.

15. Wong, G.T.F. (1979). Alkalinity and pH in the southern Chesapeake Bay and the James River estuary. Limnol. Oceanogr., 24, 970-977.

16. Bainbridge, A.E. Geochemical Ocean Sections Study. GEOSECS Atlantic Final Hydrographic Data Report. 21 July 1972 to 31 May 1973. R/V Knorr. National Science Foundation-International Decade of Ocean Exploration, Washington, D.C.

17. Ryther, J.H. and W.M. Dunstan (1971). Nitrogen, phosphorus, and eutrophication in the coastal marine environment. Science, 171, 1008-1013.

18. Spencer, C.P. (1975). The micronutrient elements. IN: Chemical Oceanography. 2nd edition, Vol. 2. J.P. Riley and G. Skirrow, editors. Academic Press, New York, pp. 245-300.

19. Vaccaro, R.F. (1965). Inorganic nitrogen in seawater. IN: Chemical Oceanography. 1st edition, Vol. 1. J.P. Riley and G. Skirrow, editors. Academic Press, New York, pp. 365-408.

20. Segar, D.A. and G.A. Berberian (1976). Oxygen depletion in the New York Bight apex: causes and consequences. Amer. Soc. Limnol. Oceanogr. Spec. Symp. Vol. 2, Allen Press, Lawrence, Kansas, pp. 220-239.

21. Sholkovitz, E. (1973). Interstitial water chemistry of the Santa Barbara Basin sediments. Geochim. Cosmochim. Acta, 37, 2043-2073.

22. Duedall, I.W., M.J. Bowman and H.B. O'Connors, Jr. (1975). Sewage sludge and ammonium concentrations in the New York Bight apex. Est. Coast Mar. Sci., 3, 457-463.

23. Presley, B.J. and J.H. Trefry (1980). Sediment-water interactions and the geochemistry of interstitial waters. IN: Chemistry and Biogeochemistry of Estuaries. E. Olausson and I. Cato, editors. Wiley, New York, pp. 187-232.

24. Wong, G.T.F. and C.E. Grosch (1978). A mathematical model for the distribution of dissolved silicon in interstitial waters-analytical approach. J. Mar. Res., 36, 735-750.

Table 1. Time variability of salinity at two stations

STATION	DEPTH m	SALINITY (o/oo)* A	B	C
70	1	26.55	29.02	31.65
	5	27.16	30.87	31.72
	10	31.69	31.36	32.26
805	1	25.97	25.07	31.98
	5	28.06	27.74	31.82
	10	33.97	31.97	32.14

*Samples were collected on June 19 (A), June 25 (B), and October 17 (C), 1980.

Table 2. Nutrients and salinity at 1 m at the Bay mouth and in offshore waters.

	Bay Mouth			Innershelf		Open Ocean* (Gulf stream)
Station No.	800	800	800	816	816	212
Sampling date	6/17/80	6/24/80	10/14/80	6/22/80	10/19/80	3/30/73
Salinity (o/oo)	21.63	N.D.	27.09	31.50	32.72	36.430
Phosphate (μM)	0.38	0.52	0.56	0.01	0.06	0.05
Nitrate and Nitrite (μM)	2.7	0.4	1.5	UD	0.51	0.07
Nitrite (μM)	UD	0.04	ND	UD	ND	
Ammonia (μM)	ND	1.1	4.7	2.38	0.96	ND
Silicate (μM)	0.2	6.6	8.4	0.15	0.25	0.9
N/P	--	3	11	234	25	14

*Geochemical Ocean Sections Study at 3m at 35^{o} 59.4'N, 67^{o} 59.0'W (Ref. 16).

UD - Undetected

ND - No data

N/P - Atomic ratio of inorganic nitrogen to phosphate

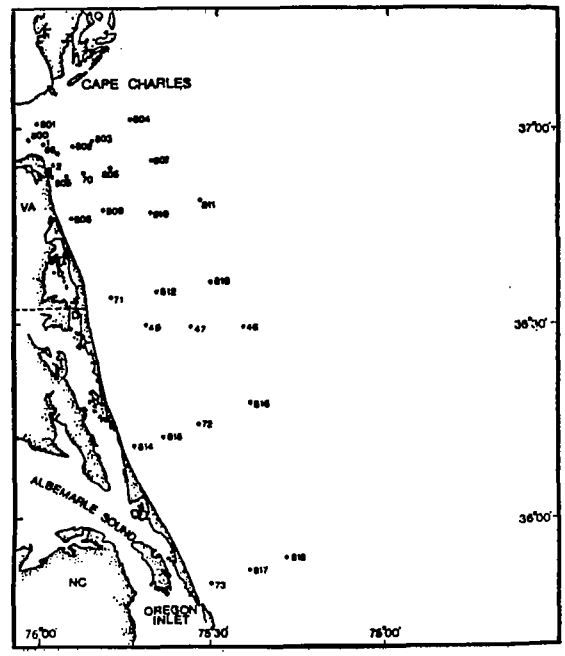

Figure 1.- Location of the stations of the Superflux cruises.

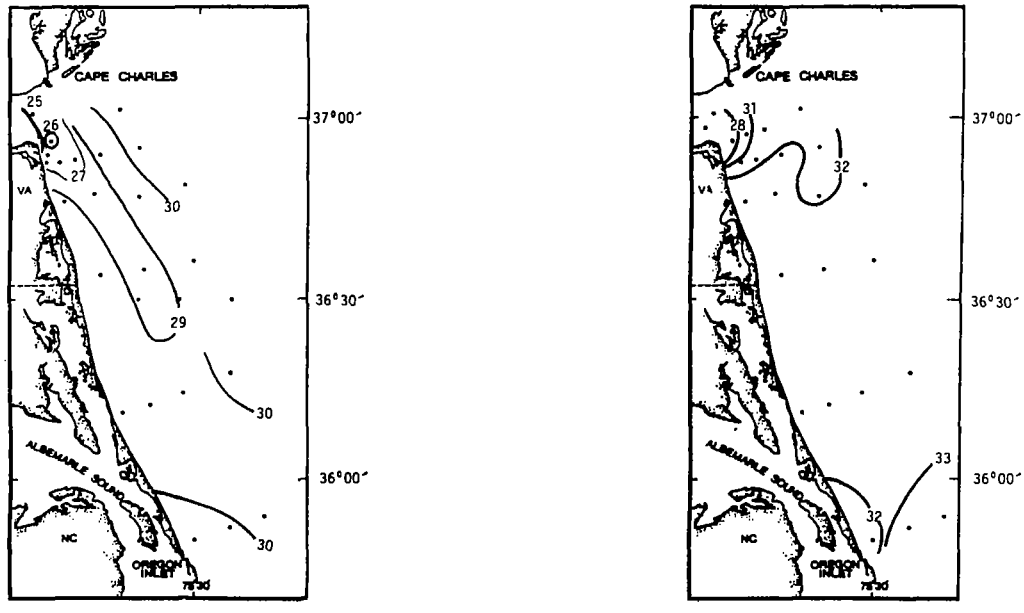

(a) June 1980.

(b) October 1980.

Figure 2.- Distribution of salinity in $^{o}/oo$ at 1 m in June and October 1980.

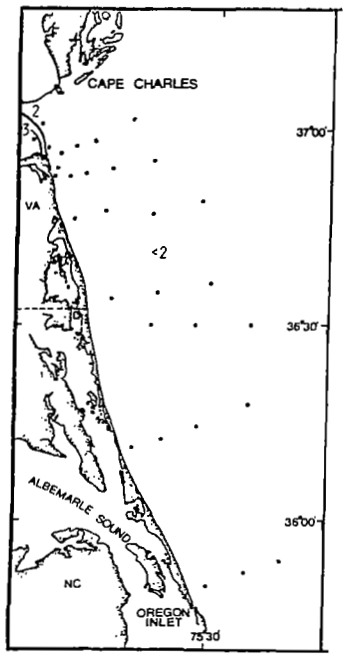

(a) Phosphate (μM).

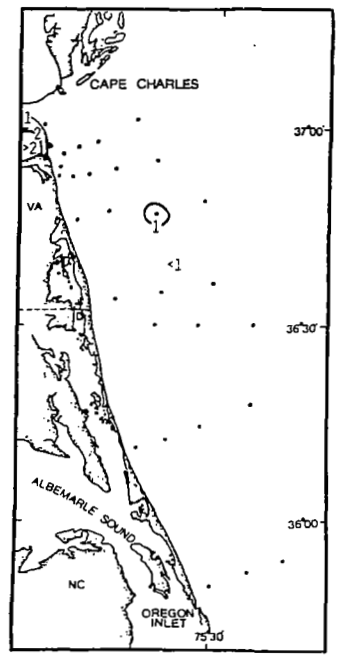

(b) Nitrate (μM).

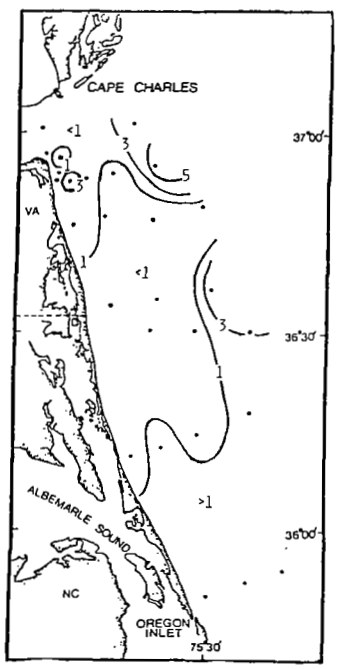

(c) Ammonia (μM).

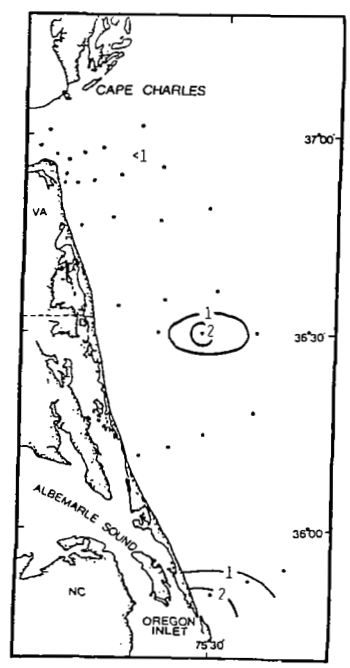

(d) Silicate (μM).

Figure 3.- Distribution of phosphate, nitrate, ammonia, and silicate at 1 m in June, 1980.

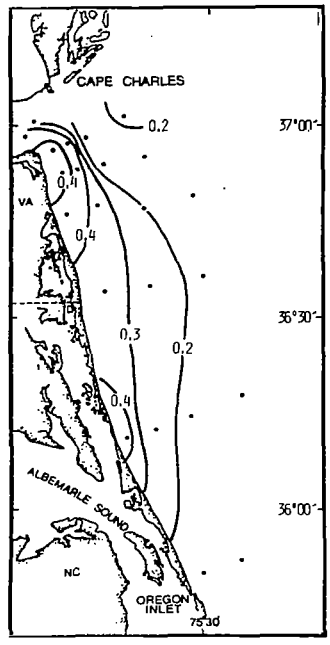

(a) Phosphate (µM).

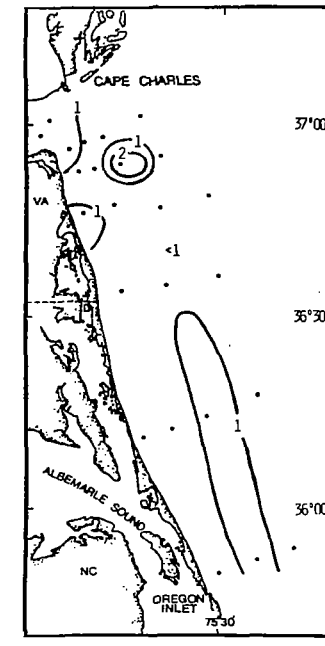

(b) Nitrate (µM).

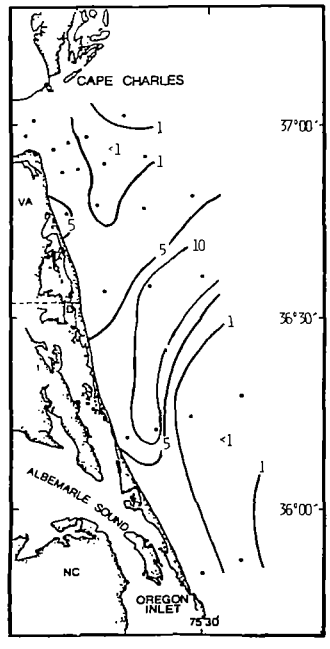

(c) Ammonia (µM).

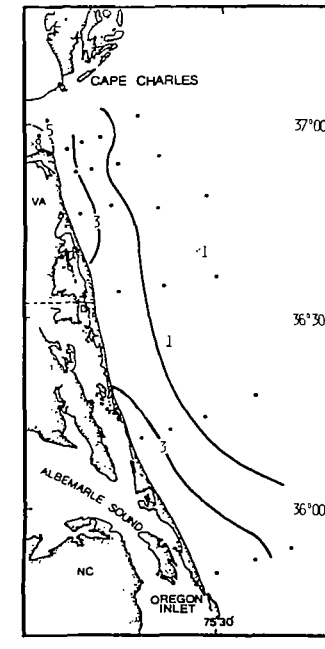

(d) Silicate (µM).

Figure 4.- Distribution of phosphate, nitrate, ammonia, and silicate at 1 m in October, 1980.

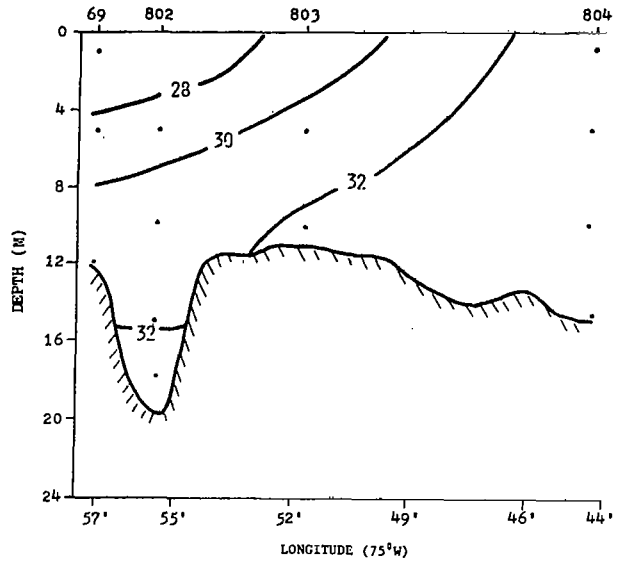

(a) Salinity (°/oo).

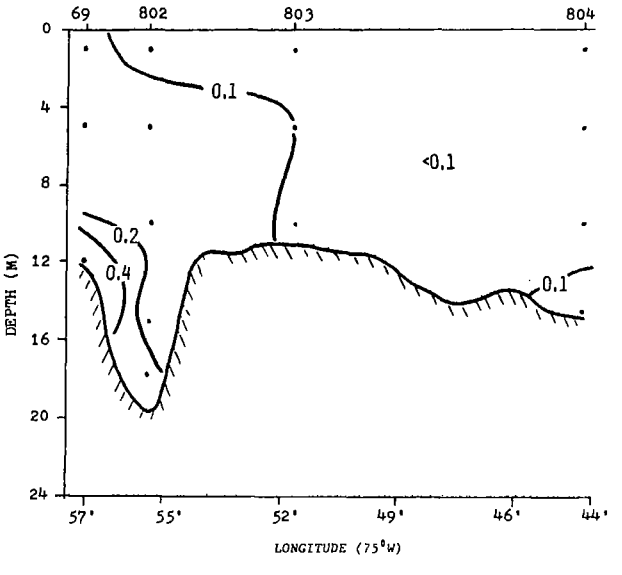

(b) Phosphate (μM).

Figure 5.- Distribution of salinity, phosphate, nitrate, ammonia, and silicate in a transect across the northern part of the study area in June, 1980.

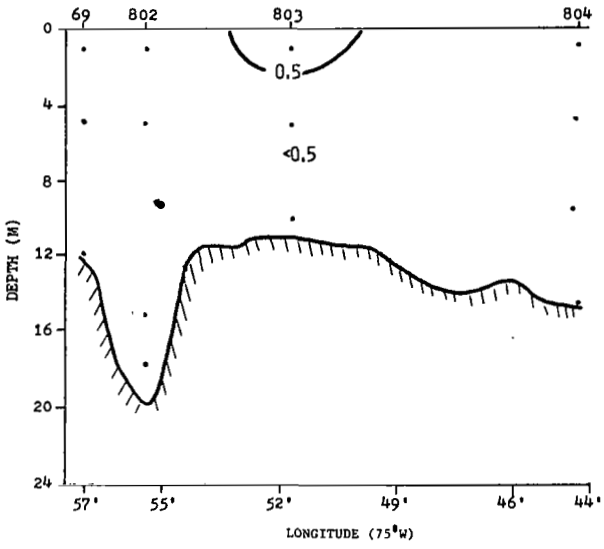

(c) Nitrate (μM).

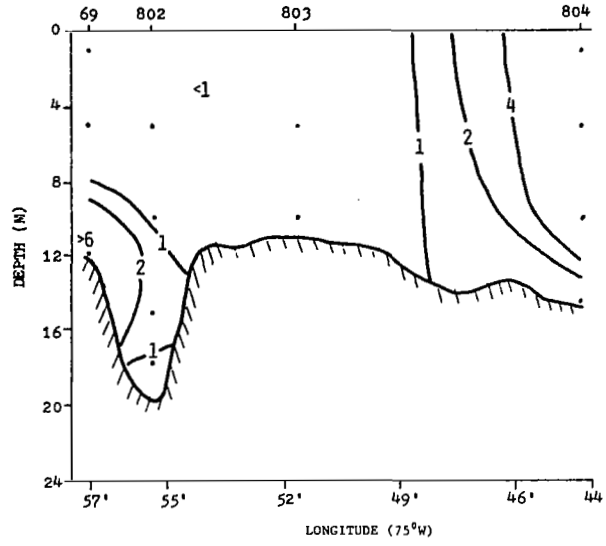

(d) Ammonia (μM).

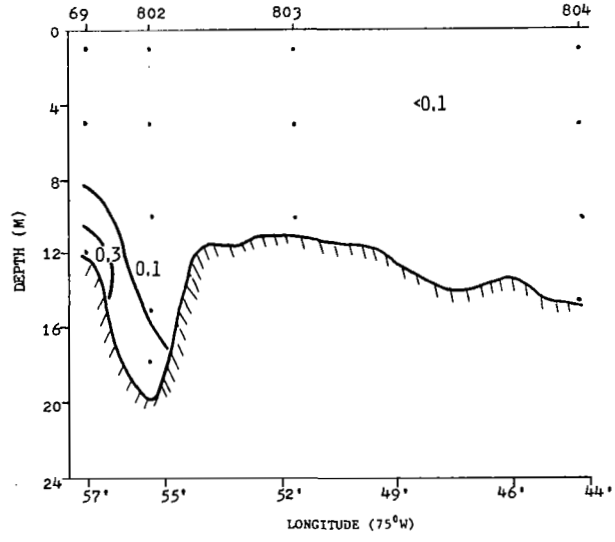

(e) Silicate (μM).

Figure 5.- Concluded.

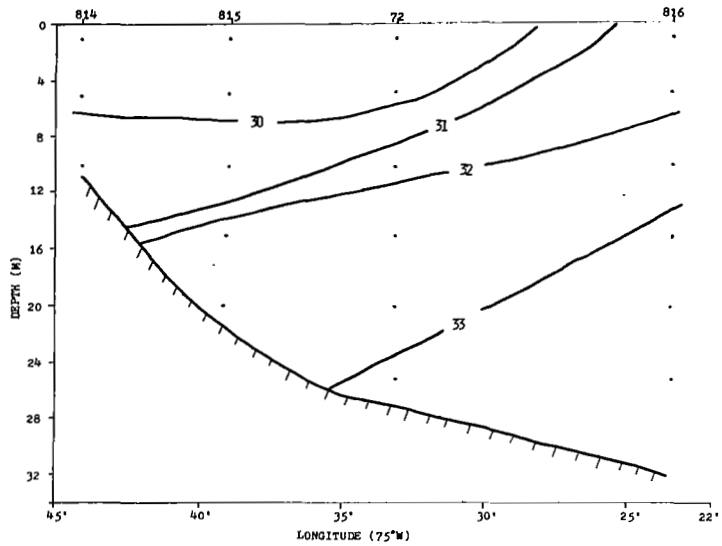

(a) Salinity (°/oo).

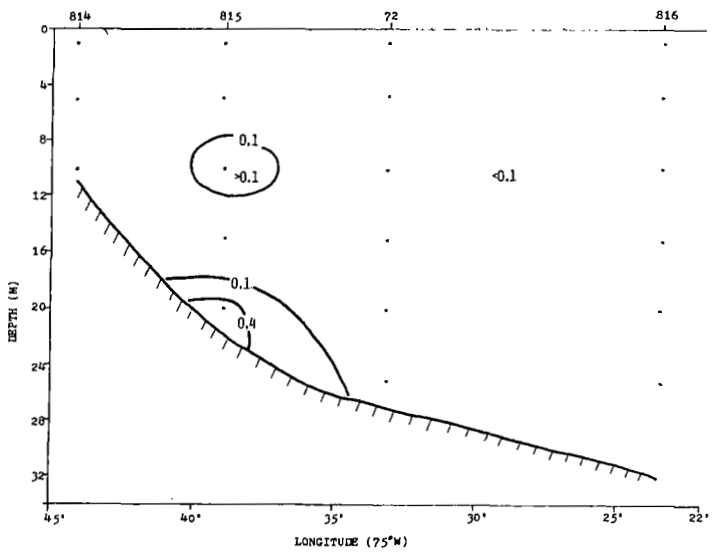

(b) Phosphate (μM).

Figure 6.- Distribution of salinity, phosphate, nitrate, ammonia, and silicate in a transect across the southern part of the study area in June, 1980.

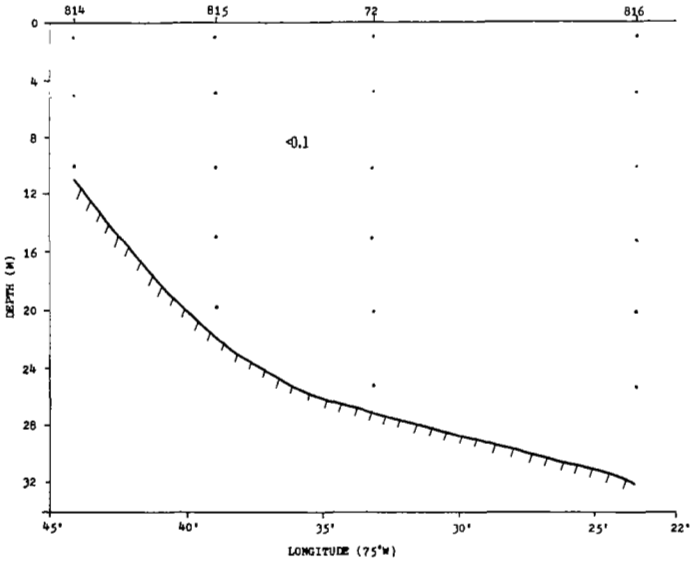

(c) Nitrate (µM).

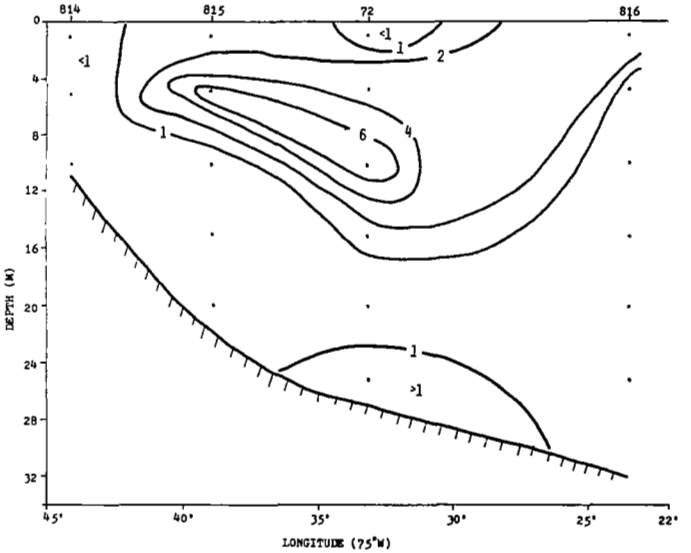

(d) Ammonia (µM).

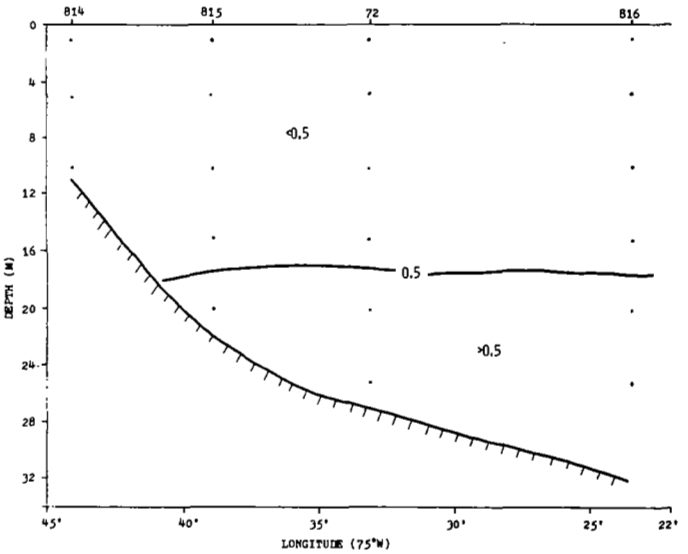

(e) Silicate (µM).

Figure 6.- Concluded.

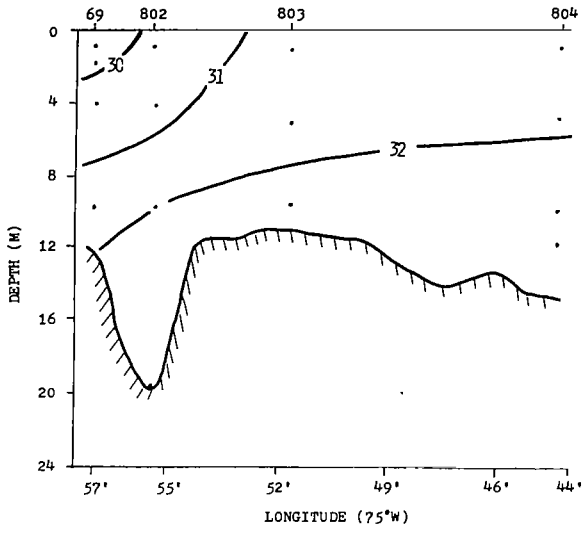

(a) Salinity (^{o}/oo).

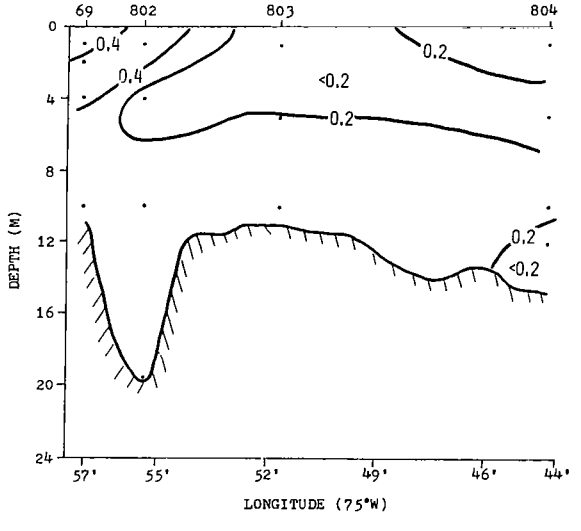

(b) Phosphate (μM).

Figure 7.- Distribution of salinity, phosphate, nitrate, ammonia, and silicate in a transect across the northern part of the study area in October, 1980.

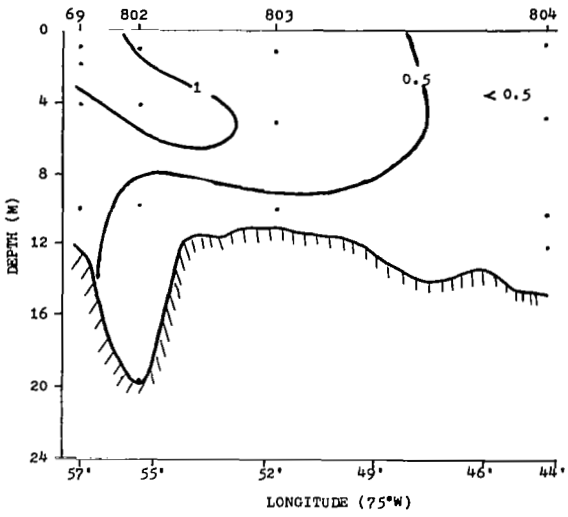

(c) Nitrate (μM).

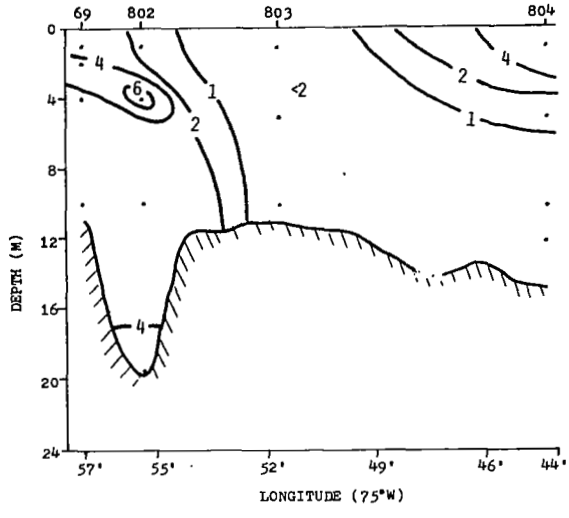

(d) Ammonia (μM).

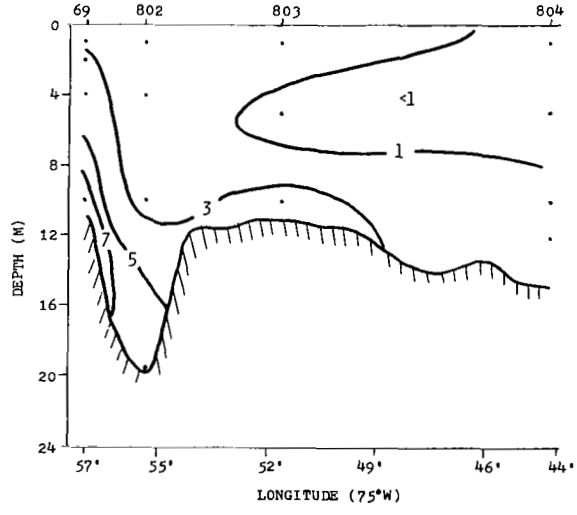

(e) Silicate (μM).

Figure 7.- Concluded.

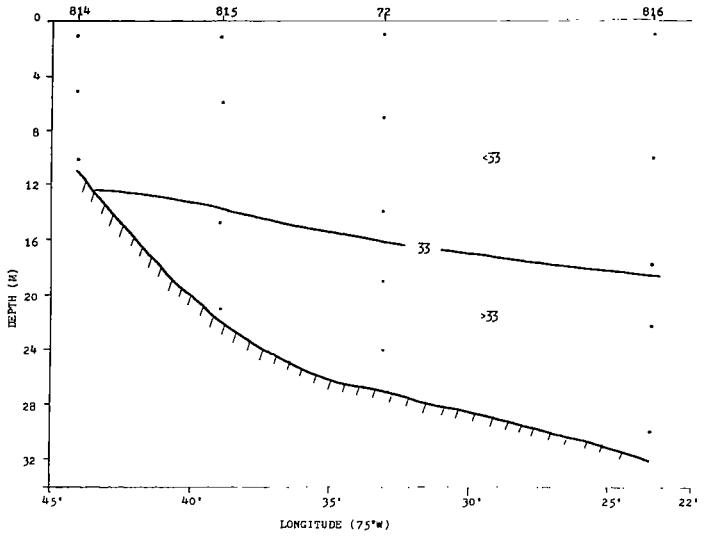

(a) Salinity (^{o}/oo).

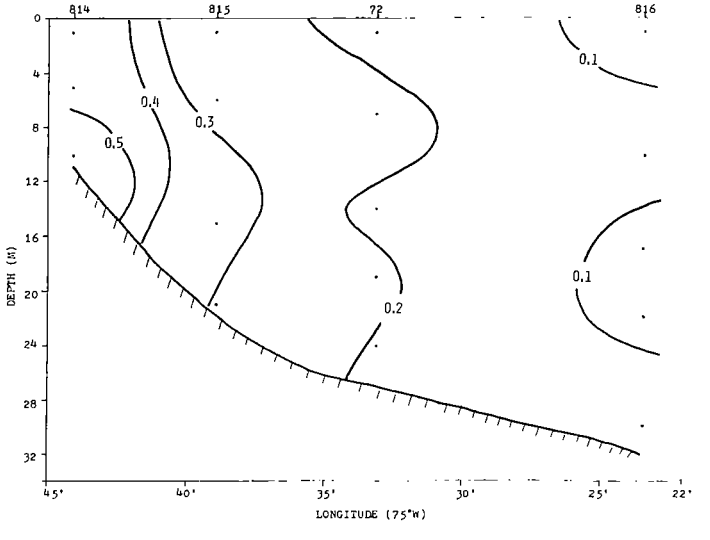

(b) Phosphate (μM).

Figure 8.- Distribution of salinity, phosphate, nitrate, ammonia, and silicate in a transect across the southern part of the study area in October, 1980.

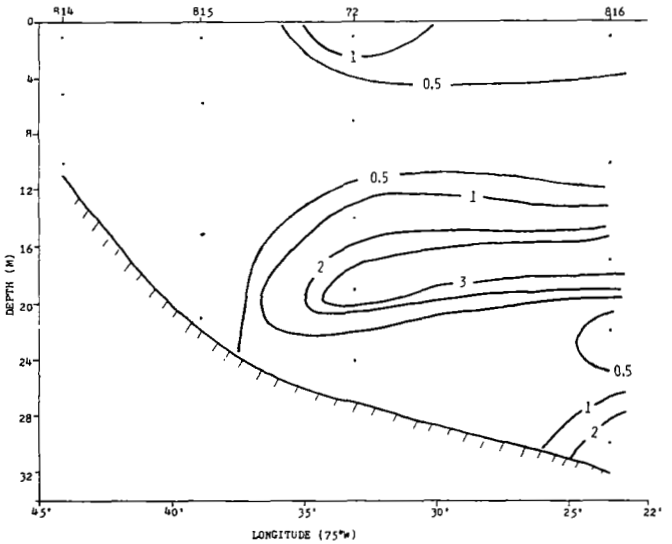

(c) Nitrate (μM).

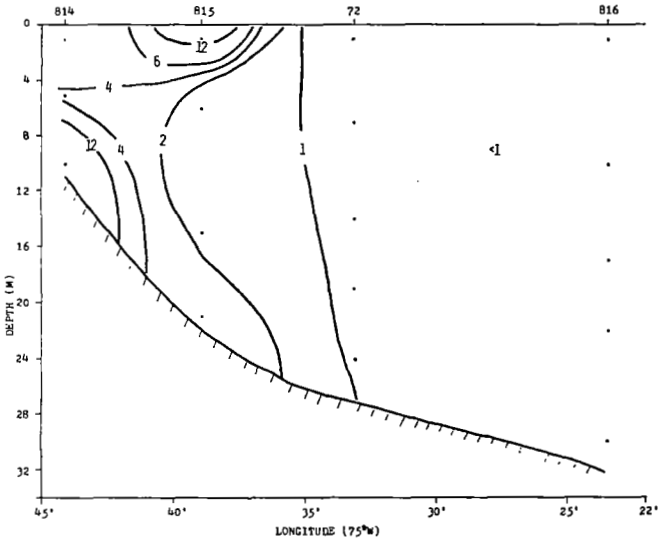

(d) Ammonia (μM).

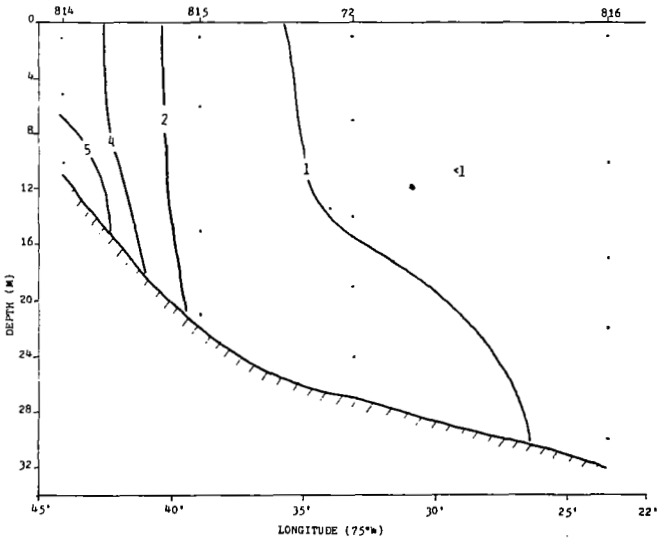

(e) Silicate (μM).

Figure 8.- Concluded.

REMOTE SENSING OF OPTICALLY SHALLOW, VERTICALLY INHOMOGENEOUS WATERS: A MATHEMATICAL MODEL *

W. D. Philpot and S. G. Ackleson
College of Marine Studies
University of Delaware

SUMMARY

A multiple-layer radiative transfer model of a vertically inhomogeneous, optically shallow water mass is briefly described. This model is directed toward use in remote sensing of water properties. Some preliminary results and qualitative predictions are presented.

INTRODUCTION

In most applications of remote sensing involving water quality the assumption is made that the water is vertically homogeneous. Usually the water is also assumed to be optically deep, i.e. absorption and reflection by the bottom are taken to be negligible. These assumptions are frequently adequate, as evidenced by the wide-ranging success in using remote sensing for observation of water properties. However, some concern has been voiced with respect to the general validity of the standard assumptions (ref. 1) and, in at least one case, a changing vertical distribution of material in water has been linked to variation in remote observations (ref. 2). It is the underlying thesis of the work presented here that vertically inhomogeneous and/or optically shallow waters are fairly common, that the inhomogeneity will affect the remotely sensed upwelling radiance and, therefore, that there is need for a mathematical model applicable to these situations and useful for remote sensing applications.

In the following pages a multiple-layer radiative transfer model of an optically shallow water mass is briefly described. In order for this model to be directly useful in remote sensing applications it must be invertible. This requirement necessitates several simplifying assumptions which will inevitably limit the accuracy of the model in at least some situations. Hopefully the advantages to be gained by having an easily manipulated model of a rather complex system should outweigh the loss in accuracy. Initially it is intended only that the model give a good qualitative description of the system, although care has been taken to formulate the model in such a way as to facilitate using the model to make quantitative predictions.

*This work was supported in part by Sea Grant contract # NA 80 AA-D-00106.

DESCRIPTION OF THE MODEL

Assumptions and Definitions

Radiative transfer models tend to be extraordinarily complex and utterly resistant to inversion. Much of the complexity arises because of the difficulty in describing anisotropic light fields. While the anisotropy is an important part of the interaction of light with water, it need not be described in minute detail. Characterization of the light field in general terms should provide the simplification necessary for deriving a model capable of describing a vertically inhomogeneous system but still susceptible to inversion.

The basic assumption is that the underwater light field may be effectively characterized by the apparent optical properties: the diffuse attenuation coefficients for upwelling and downwelling irradiance, the irradiance reflectance, and the radiance reflectance. The diffuse attenuation coefficient for downwelling irradiance is defined as

$$k_d(z) = \frac{-1}{E_d(z)} \frac{dE_d(z)}{dz} \tag{1}$$

where $E_d(z)$ is the downwelling irradiance at depth z. Likewise, the diffuse attenuation coefficient for upwelling irradiance is defined as

$$k_u(z) = \frac{-1}{E_d(z)} \frac{E_u(z)}{dz} \tag{2}$$

The diffuse attenuation coefficient will be dependent to some extent on the radiance distribution. However, evidence is growing that the underwater radiance distribution does not vary in a way that strongly affects the diffuse attenuation. In fact, observations by Baker and Smith (ref. 3) indicate that the diffuse attenuation coefficient for downwelling irradiance is remarkably insensitive to the radiance distribution, whether due to changes in sun angle or depth.

The irradiance reflectance, R(z), is defined as

$$R(z) = \frac{E_u(z)}{E_d(z)} \tag{3}$$

The term R(z), which has become a fairly standard measure of water color, is seemingly independent of illumination conditions (refs. 4 and 5). We may also define a radiance reflectance:

$$R_L(z,\theta) = \frac{L_u(z,\theta')}{E_d(z)} \tag{4}$$

where $L_u(z,\theta')$ is the upwelling radiance at depth z and in direction θ'.

In addition to the above standard properties we define two other parameters: the irradiance scattering function for downwelling light, $B_d(z)$, and a single-scattering irradiance attenuation coefficient for upwelling light, $k'(z)$. $B_d(z)$ is defined as the irradiance $dE_w(z)$ scattered upward at depth z from a horizontal slab of thickness dz when illuminated by the downwelling irradiance, $E_d(z)$:

$$B_d(z) = \frac{dE_w(z)}{E_d(z)dz} \tag{5}$$

The scattered irradiance, $E_w(z)$, is attenuated as it proceeds toward the water surface. However, the irradiance attenuation coefficient for upwelling light, $k_u(z)$, is not appropriate since it implicitly includes the backscattering of downwelling light already described by $B_d(z)$. To adjust for this we define a single-scattering irradiance attenuation coefficient, $k'(z)$, such that:

$$k'(z) = k_u(z) - B_d(z) \tag{6}$$

Like the other apparent properties, $B_d(z)$ and $k'(z)$ will be assumed to be quasi-inherent optical properties since they are dependent on the radiance distribution in essentially the same way as k_d, R_L, and R.

Model Geometry and Final Equations

This model treats the water as a plane-parallel medium of arbitrary depth in which the optical properties, depth and thickness of each layer, as well as the depth of the water and the bottom reflectance, may be specified independently. Figure 1 illustrates the model geometry for the relatively simple situation of one layer of turbid water in an otherwise homogeneous water column. The attenuation coefficients of pure water are k_w and k'_w, while the irradiance scattering function for pure water is B'_w. The corresponding optical properties of homogeneously distributed substances in the water are $n_s k_s$, $n_s k'_s$ and $n_s B'_s$ where n_s is a concentration parameter which may vary

between 0 and 1. For $n_s = 0$ the concentration of the material is zero. For $n_s = 1$ the concentration of the material is a maximum, i.e., the water has been replaced entirely by the substance.

An intermediate layer is shown in figure 1. This layer contains material which is optically distinct from the surrounding water. The optical properties of the material present in the layer are $n_\ell k_\ell$, $n_\ell k'_\ell$ and $n_\ell B'_\ell$, in complete analogy to the homogeneously distributed material.

A portion of the irradiance above the water surface, E_o, is reflected at the air water interface, $(S_a E_d)$. The remainder is transmitted $([1-S_a]E_d)$. The irradiance is attenuated as it passes down through the water column. At depth z, a portion of the downwelling irradiance is scattered back toward the water surface. This scattered irradiance is further attenuated as it travels to the surface and across the air-water interface.

A portion of the downwelling irradiance reaches the bottom (z = d) and is diffusely reflected there (A_d). The reflected portion is attenuated as it travels upward through the water column. The irradiance is affected by the local optical properties at each depth which are assumed to be constant within each layer.

The irradiance reflectance immediately below the water surface is given by

$$R(0-) = \frac{B_o}{k_o} \sum_{j=0}^{m} e^{-\sum_{i=0}^{j}(K_i-K_o)\Delta z_i} \left[e^{-K_o(h_j+\Delta z_j)} - e^{-K_o h_{j+1}} \right]$$

$$+ \sum_{j=1}^{m} \frac{B_i}{K_j} e^{-\sum_{i=0}^{j-1}(K_i-K_o)\Delta z_i} e^{-K_o h_i} \left[1-e^{-K_j \Delta z_j} \right] \qquad (7)$$

$$+ A_d e^{-K_o d} e^{-\sum_{i=0}^{m}(K_i-K_o)\Delta z_i}$$

where: $k_o = (1-n_s)(k_w + k'_w) + n_s\ (k_s + k'_s)$

$B_o = (1-n_s)B_w + n_s\ B_s \quad = B_d(z)$ for homogeneous regions

m = number of intermediate layers

h_i = depth to the top of layer i

Δz_i = thickness of layer i

$K_j = (1-n_s-n_i)\ (k_w+k'_w) + n_s\ (k_s+k'_s) + n_i\ (k_i+k'_i)$

$B_j = B_d(z) \quad$ for $h_i<z<h_i+\Delta z$

k_i = downwelling irradiance attenuation coefficient for layer i

k'_i = upwelling irradiance attenuation coefficient for layer i

n_i = concentration parameter for layer i

and where $\Delta z_o = h_o = 0$ and $h_{m+1} = d$. The first term on the right hand side of equation (7) describes the portion of $R_L(\theta')$ due to scattering from all the areas in which only the homogeneously distributed material is present; the second term describes the return from each of the layers; the third term accounts for the bottom reflectance. In deriving equation (7) it was assumed that none of the layers overlapped.

The irradiance reflectance is related to the observations immediately above the water surface by:

$$R = \frac{L_u(\theta) - \rho_a(\theta)\ L_k(\theta)}{(1 - S_a)E_d + E_r} \cdot \frac{Q(\theta')\ n_w^2}{1-\rho_w(\theta')} \qquad (8)$$

where: $L_u(\theta)$ = upwelling radiance above the water surface in direction θ

$L_k(\theta)$ = downwelling sky irradiance in direction θ

$\rho_a(\theta)$ = specular reflection at the water surface in air

$\rho_w(\theta')$ = specular reflection at the water surface

S_a = diffuse reflectance of the air-water surface

n_w = index of refraction of water

E_d = downwelling irradiance above the water surface

E_r = portion of the upwelling irradiance internally reflected in the water

$Q(\theta')$ = conversion factor relating radiance and irradiance reflectance

The above equations were derived in analogy to single-scattering radiative transfer models and as such will be called a single-scattering irradiance model (SSI). The primary distinction between the (SSI) model and two flow theory is that the downward scattering of upwelling light is ignored. This simplification causes results for strongly scattering waters to be inaccurate. In spite of its appearance, equation (7) is a relatively crude representation of the reflectance characteristics of an optically shallow, vertically inhomogeneous water body. The simplifying assumptions used in deriving equation (7) will limit the absolute accuracy of the model; however, it should provide a good qualitative description of variations in ocean color. Moreover, this model may be accurate enough in some situations to yield moderately accurate quantitative predictions.

APPLICATION OF THE RADIANCE MODEL TO AN OPTICALLY SHALLOW, HOMOGENEOUSLY ABSORBING WATER COLUMN

Upon formulation of the radiative transfer model for the case of an optically shallow, homogeneously absorbing water column, measurements of volume reflectance were conducted under the controlled conditions of a water tank. In an attempt to maintain a simple and inexpensive experimental design, sunlight was utilized as the illumination source. Variations in the absorptive capacity of the water as well as in column depth were considered.

Model Formulation

In applying the radiance model to the case of an optically shallow, homogeneously absorbing water column, a number of simplifications may be applied to equation (7). Each simplification is based upon one or more of the following assumptions:

1) the water column contains no intermediate layers possessing unique optical properties ($\Delta z = 0$)

2) the concentration of any particulate scattering material suspended throughout the water column is very small

3) the bottom is highly reflective and closely resembles a completely diffuse reflector

4) internally reflected irradiance, E_r, is negligible

5) observations are made in the nadir direction $\theta = 0$

Combining equations (7) and (8) and applying the above assumptions results in the relationship

$$\frac{L_u}{E_d} = \frac{(1-\rho_w)\ (1-S_a)}{Q\ n_w^2}\ A_d e^{-k_1 d} + \rho_k L_k \qquad (9)$$

Experimental Apparatus

Experiments were conducted using the cubic meter tank illustrated in figure 2. The sides of the tank were painted with a low-reflectance, ultra-flat black paint; the floor of the tank was coated with a high reflectance, flat white paint in order to optimize the return signal. Shadows from the sides of the tank were avoided by conducting all the measurements at a time when the sun was highest. At no time was the solar zenith angle greater than 35^o.

Radiance measurements were made using a United Detector Technology Spectral Radiometer designed to continuously scan the visible and near infrared portion of the light spectrum from 400nm to 1100nm. As shown in figure 2, the radiometer was positioned directly over the center of the tank so as to record upwelling radiance in the zenith direction. In this configuration the radiometer shaded the water surface directly underneath from downwelling sky radiance. Therefore, the reflectance term ($\rho_k L_k$) on the right side of equation (9) may be neglected.

The total downwelling solar irradiance was measured with the use of a panel coated with a standard reflectance medium, barium sulphate. Such a coating is noted for its high reflectance and close resemblance to a Lambertian reflector.

Experimental Procedure

Prior to filling the tank with any water the bottom albedo, A_d, was measured directly. The wavelength range considered for this measurement, as well as all others to be presented, was from 400nm to 700nm in increments of 20nm. After measuring A_d, several water types varying in absorptive capacity were added to the tank one at a time. The absorptance of each water type was controlled by adding known quantities of rhodamine dye.

Table 1 is a summary of the physical characteristics associated with each water type considered. In each case, volume reflectance was calculated by normalizing the recorded upwelling radiance from the tank to that reflected from the barium sulphate panel. Thus,

$$R = \frac{L_u}{E_d} = \frac{0.79\ L_u}{\pi L_{RP}} \qquad (10)$$

where 0.79 is the reflectance of the barium sulphate panel.

The only variable within equation (9) not directly measured was K_1. Values were calculated by simultaneously solving equation (9) for two different depths of each water type which yields

$$K_1 = \frac{\ln(R_1/R_2)}{d_2 - d_1} \tag{11}$$

Values chosen for the constant terms in equation (9) are as follows: $S_a = 0.06$, $\rho_w = 0.02$, $Q = \pi$, and $n_w = 1.33\text{-}1.39$. The latter range of values reflects the dependence of n_w upon the wavelength considered.

Results and Conclusions

Figure 3 is a plot of K_1 versus wavelength for each of the water types considered. With the addition of 2.7 ppm rhodamine dye to the tap water the value of K_1 increase sharply in the high absorption region between 480nm and 580nm. A maximum value occurs at 560nm. From 580nm to 700nm, K_1 drops to near that of clear tap water. The same trend, only more exaggerated, occurs for tap water with the addition of 10.8ppm rhodamine dye; the width of the absorption band increases to include 460nm and 580nm, and the absorption peak occurs at 540nm rather than 560nm.

In each water type with dye added, similar values of K_1 occur between 600nm and 700nm. It is interesting to note that such values are lower than those representing clear tap water with no dye added. Clearly, the dye is transparent for longer wavelengths which accounts for its characteristic red tinge. Yet, intuitively, this window should not be any more transparent than the clear water to which the dye was added. If indeed equation (10) accurately describes K_1, then the differing values in the longer wavelengths could be a result of the varying quality of the tap water used in the preparation of each water type. It was noted in the case of the clear tap water that the water used appeared to have a slight green tinge about it. As such, an associated absorption band in the red portion of the spectrum could account for the shape of the clear water curve. The tinge was not noticed in preparing either of the solutions containing rhodamine dye.

According to equation (11), the total attenuation coefficient may be calculated in terms of the change in upwelling radiance with respect to the change in water depth. The calculated values of K_1 are thus independent of bottom albedo. Rewriting equation (9) in terms of the bottom albedo with $Q = \pi$ and ignoring the reflectance term yields the relationship

$$A_d = \frac{\pi L_u n_w^2}{E_d(1-S_a)(1-\rho_w)} e^{K_1 d} \tag{12}$$

Utilizing equation (12), model predictions for A_d were derived in terms of the calculated values of K_1. As a comparison to the direct measurements of A_d, the calculated values of A_d as well as those directly measured were plotted with respect to wavelength and are presented in figure 4.

Model predictions for A_d were found to be quite similar to the directly measured values. A statistical correlation coefficient, r, was calculated as a measure of the similarity between the two curves. The comparison of measured to predicted values of A_d resulted in r equivalent to 0.957, a significant correlation.

The measured values of A_d as well as the calculated values of K_1 were used in conjunction with equation (9) to calculate model predictions for the upwelling radiance from the tank. Several depths for each water type were considered. Figure 5 represents both predicted and measured values of radiance reflectance (above the water surface) from clear tap water for three different water depths. The predicted values were found to correlate well with the measured values. Correlation coefficients of 0.974, 0.964, and 0.994 were calculated for the curves representing water depths of 3.81cm, 22.86cm, and 76.52cm respectively.

Comparable results were obtained for tap water with the additions of 2.7ppm and 10.8ppm rhodamine dye and are shown in figures 6 and 7 respectively. Again, predicted values were quite close to the measured values. For the tap water with 2.7ppm rhodamine dye added, values for r ranged from 0.963 to 0.983. In the case of tap water with the addition 10.8ppm rhodamine dye, values ranged from 0.959 to 0.979.

QUALITATIVE PREDICTIONS

We are now in a position to make some qualitative predictions concerning the way the reflectance of the water changes when the water is stratified. As an example, we will consider a situation which might well occur at a frontal boundary, such as at the outer edge of the Chesapeake Bay plume. The situation is illustrated in figure 8 which shows two adjacent water masses differing in color. A tongue of green water overlies a portion of the blue-green water.

Each water mass was characterized optically using measurements published in reference 6. Station 4, in Apalachee Bay where the river effluent contains significant qualitites of dissolved organic material from the large inland swamp regions, was taken as characteristic of the green water. Station 6b, in blue-green water near the mouth of the Mississippi, was chosen to represent the other water type. The irradiance reflectances and diffuse attenuation coefficients for these two stations are shown in figure 9. For this situation equation (7) becomes

$$R = R_{bg} e^{-K_g \Delta z} + R_g (1 - e^{-K_g \Delta z}) \qquad (13)$$

where R is the irradiance reflectance. The subscripts bg and g refer to blue-green (Sta. 6b) and green (Sta. 4) waters respectively. We have neglected the affects of bottom reflectance ($d \to \infty$). Since, for the purpose of modeling, the layers were assumed to be of optically infinite horizontal extent, the boundary between the two water masses is approximated in figure 8 by distinct levels.

Results are shown in figure 10 where R(0-) is plotted vs. wavelength for several thicknesses of the upper layer. When $\Delta z=0$ the reflectance is that of the blue-green water alone. As the thickness of the upper layer increases, the reflectance approaches that of optically deep green water. Note that at $\Delta=10$m, the reflectance of the two-layer system is essentially indistinguishable from that of optically deep green water. At this depth in these waters, a highly reflective bottom would be easily visible; the blue-green water has little effect due to its low reflectivity. The effective penetration depth for these waters, for the purposes of remote sensing, is only $\sim$10m although a reflective bottom might be detectable at 2 or 3 times this depth.

There are several points worth noting in comparing these curves.

(1) The change in color is quite rapid; most occur for a layer thickness of 2 attenuation lengths or less. This agrees with the conclusions of Gordon and McCluney (ref. 7).

(2) The most obvious point about figure 10 is the existence of a nodal point at 480nm. At this particular wavelength the reflectance of both water types is the same even though the optical properties may differ significantly (see figure 9). It is not possible to distinguish between the two water types by their reflectance at this nodal wave length. On the other hand, a nodal wave-length, when it exists, will provide an ideal point of reference when observing a two-component, stratified system.

(3) Less obvious, but at least as important, is the fact that the rate of change in reflectance is wavelength dependent. As can be seen from an examination of equation (13) the rate of change is entirely dependent on the spectral diffuse attenuation characteristics of the top layer which is the green water in this case.

CONCLUDING REMARKS

A relatively simple mathematical model of radiative transfer in a vertically inhomogeneous water mass has been presented. The model is quite simple in concept and is primarily designed to illustrate the ways in which water color may vary in situations which are difficult to model exactly. The preliminary experimental results presented above are

remarkably accurate, indicating that the model is faithful to reality in at least these simple situations.

Also presented were some qualitative predictions relating to a situation which might well arise in highly dynamic estuarine regions such as the Chesapeake Bay Mouth. These predictions suggest that, when the water column is stratified, considerable variation in color might occur if the top layer is variable in thickness within two attenuation lengths of the surface.

REFERENCES

1. Duntley, S. Q.; Austin, R. W.; Wilson, W. H.; Edgerton, C. F.; and Moran, S. E.: Ocean Color Analysis. Scripps Inst. of Oceanography (S.I.O.), Reference 74-10, 1974.

2. Philpot, W. D.; and Klemas, V.: Remote Detection of Ocean Waste. Ocean Optics VI, Proceedings of the Society of Photo-Optical Instrumentation Engineers, (SPIE), vol. 208, 1979, pp. 189-197.

3. Baker, K; and Smith, R. C.: Quasi-Inherent Characteristics of the Diffuse Attenuation Coefficient For Irradiance. Ocean Optics VI, Proceedings of the Society of Photo-Optical Instrumentation Engineers (SPIE), vol. 208, 1979, pp. 60-63.

4. Tyler, J.; and Smith, R. C.: Measurements of Spectral Irradiance Underwater. Gordon and Breach (New York), 1980.

5. Højerslev, N. K.: Water Color and Its Relation to Primary Production. Boundary-Layer Meteorology, vol. 18, 1980, pp. 203-220.

6. Austin, R. W.: Gulf of Mexico Ocean-Color Surface Truth Measurements. Boundary-Layer Meteorology, vol. 18, 1980, pp. 269-285.

7. Gordon, H. R.; and McCluney, W. R.: Estimation of the Depth of Sunlight Penetration in the Sea For Remote Sensing. Applied Optics, vol. 14, 1975, pp. 413-416.

Table 1

Physical Parameters of Water Tank

WATER TYPE	TRIAL	TIME	WATER DEPTH	BOTTOM TYPE
False Bottom	1	1202	0.00 cm	Flat white
Tap Water	1	1213	3.81	Flat white
	2	1232	22.86	
	3	1255	49.85	
	4	1314	76.53	
Tap Water	1	1322	74.93	Flat white
With 2.7 ppm	2	1333	50.83	
Rhodamine Dye	3	1343	25.40	
Added	4	1350	11.43	
Tap Water	1	1429	76.20	Flat white
With 10.8 ppm	2	1442	50.80	
Rhodamine Dye	3	1451	26.04	
Added	4	1458	12.70	

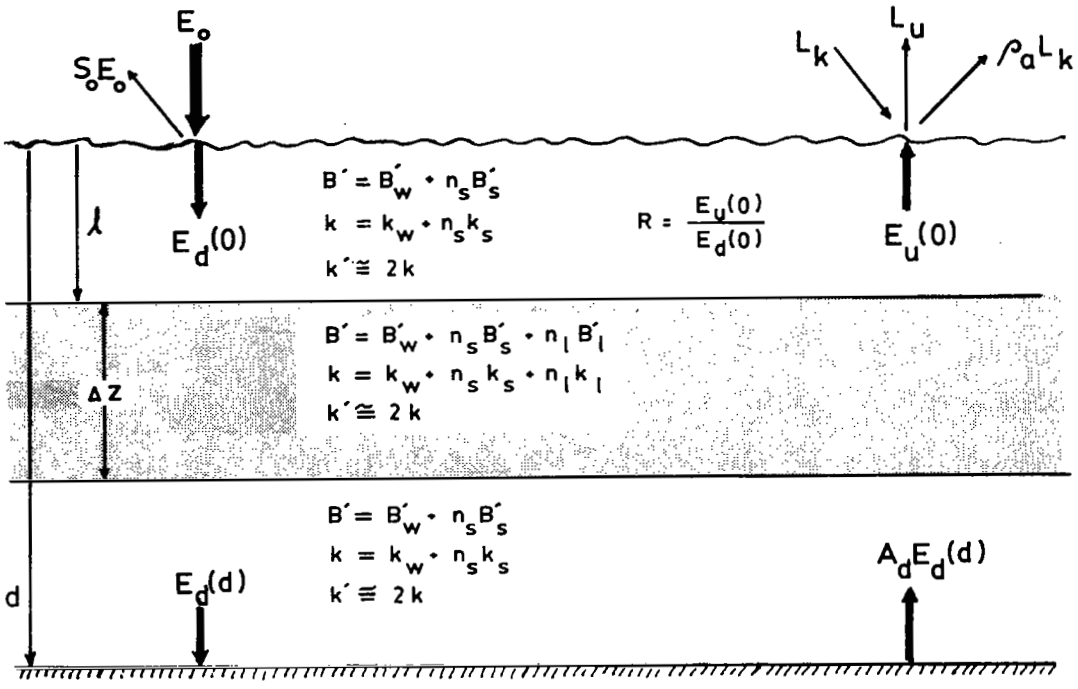

Figure 1.- Basic geometry of the multiple-layer model.

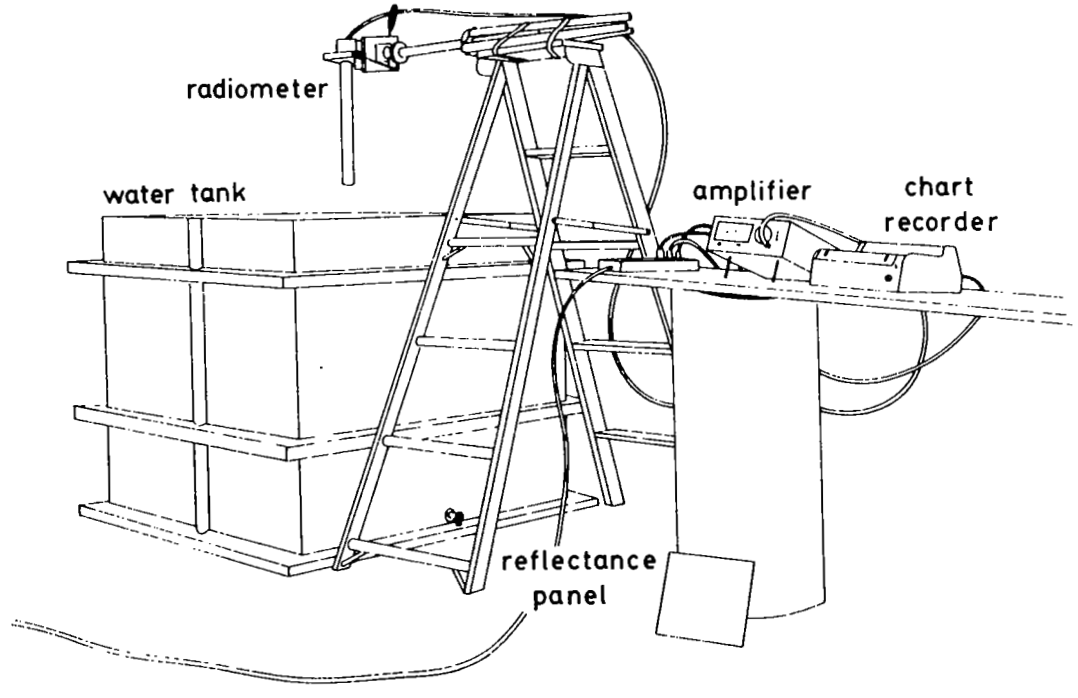

Figure 2.- Apparatus configuration to verify the multiple-layer radiance model for the case of a single homogeneously absorbing water column.

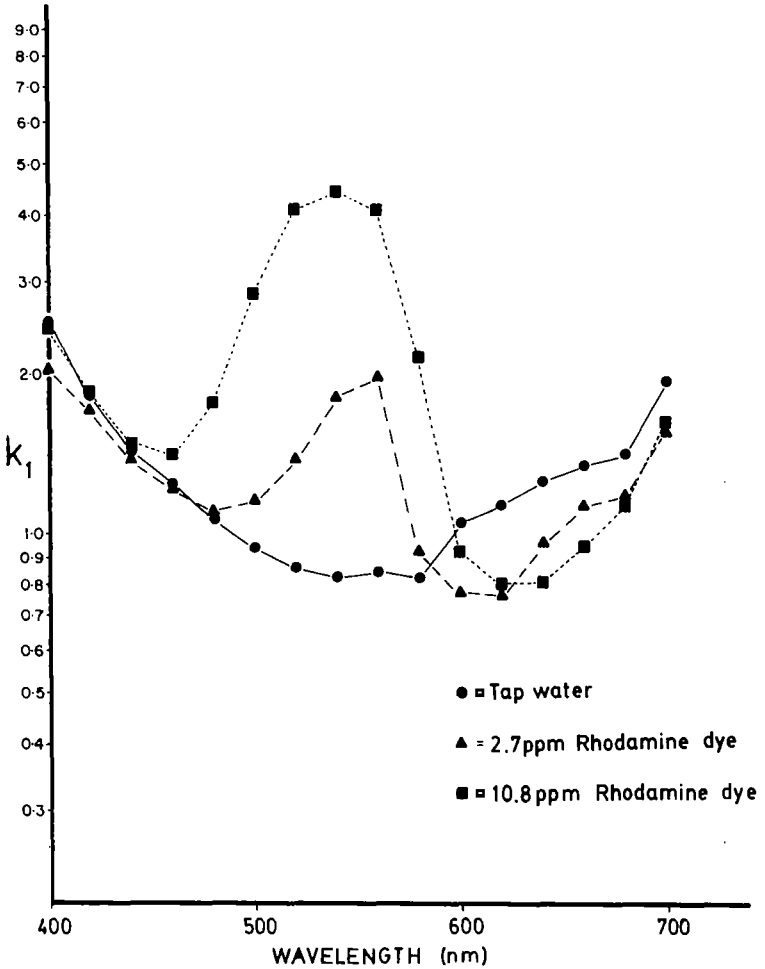

Figure 3.- Plot of the two-way attenuation coefficient versus wavelength for each water type where k_1 is equivalent to the sum of equations (1) and (2).

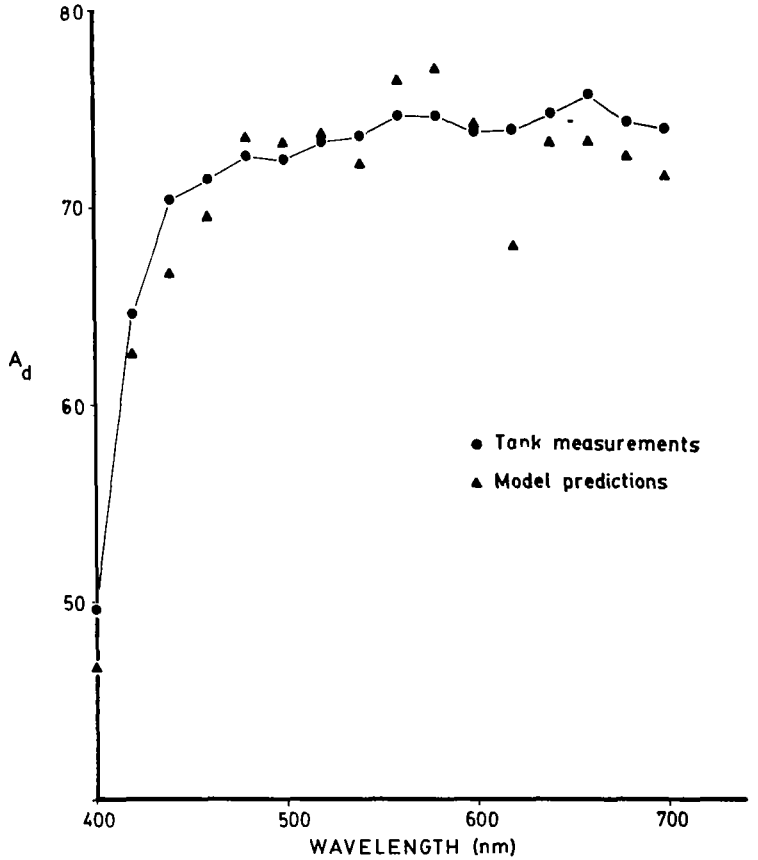

Figure 4.- Plot of direct measurements and model predictions of A_d, the reflectance of the tank bottom versus wavelength.

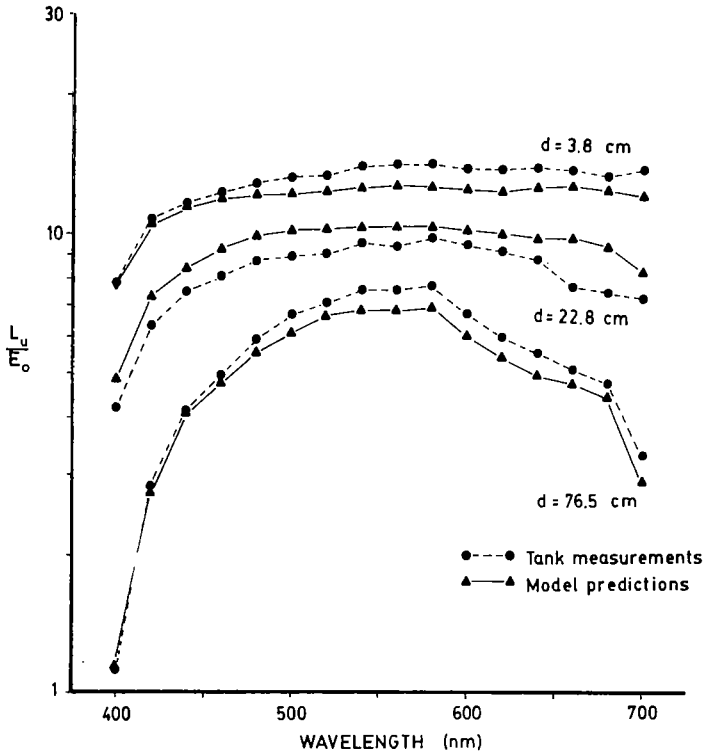

Figure 5.- Plot of measured and predicted values of volume reflectance versus wavelength for the case of clear tap water.

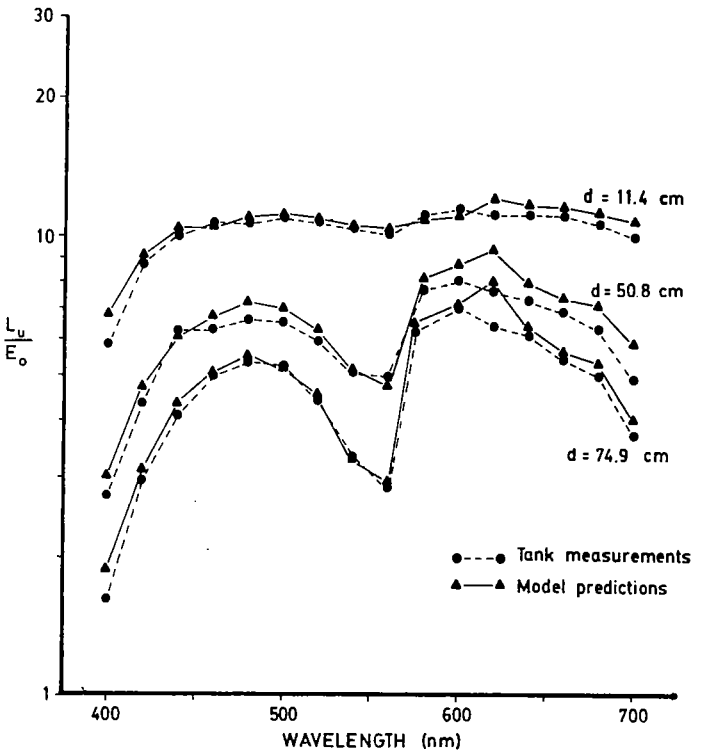

Figure 6.- Plot of measured and predicted values of volume reflectance versus wavelength for the case of clear water + 2.7 ppm Rhodamine dye.

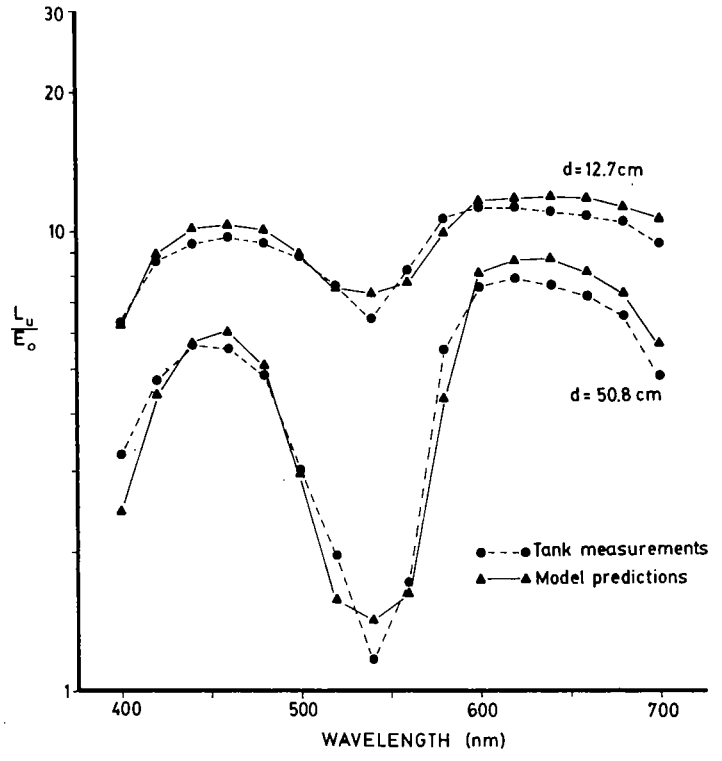

Figure 7.- Plot of measured and predicted values of volume reflectance versus wavelength for the case of clear water + 10.8 ppm Rhodamine dye.

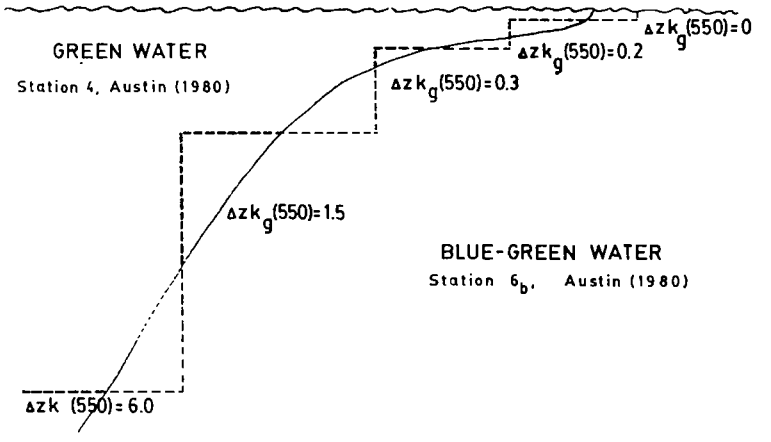

Figure 8.- Boundary between two water types. Green water overlies blue-green water. The depth is scaled to the diffuse attenuation length for the green water at 550 nm.

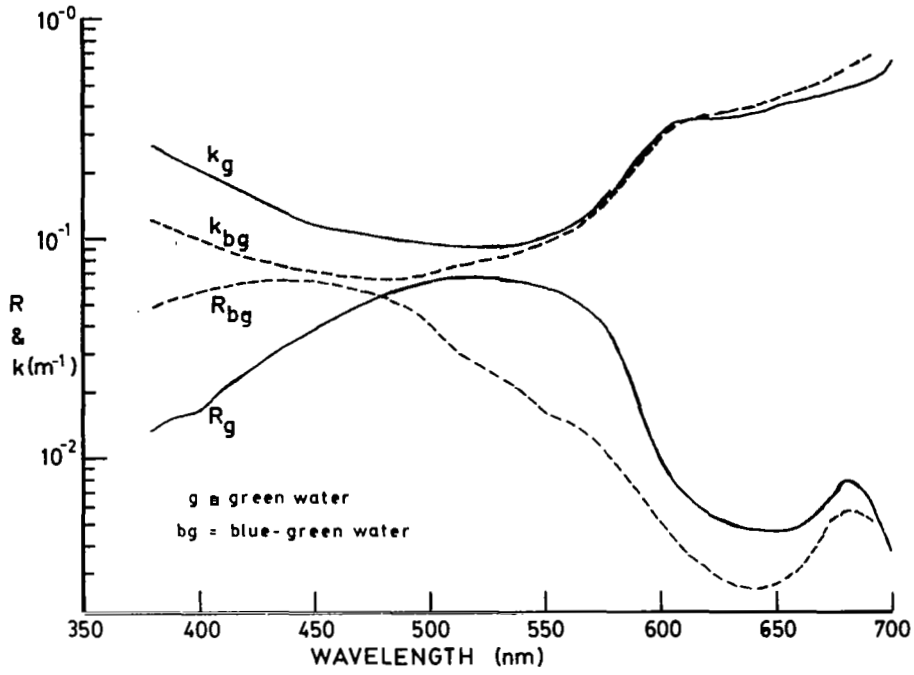

Figure 9.- Optical properties of green and blue-green waters.

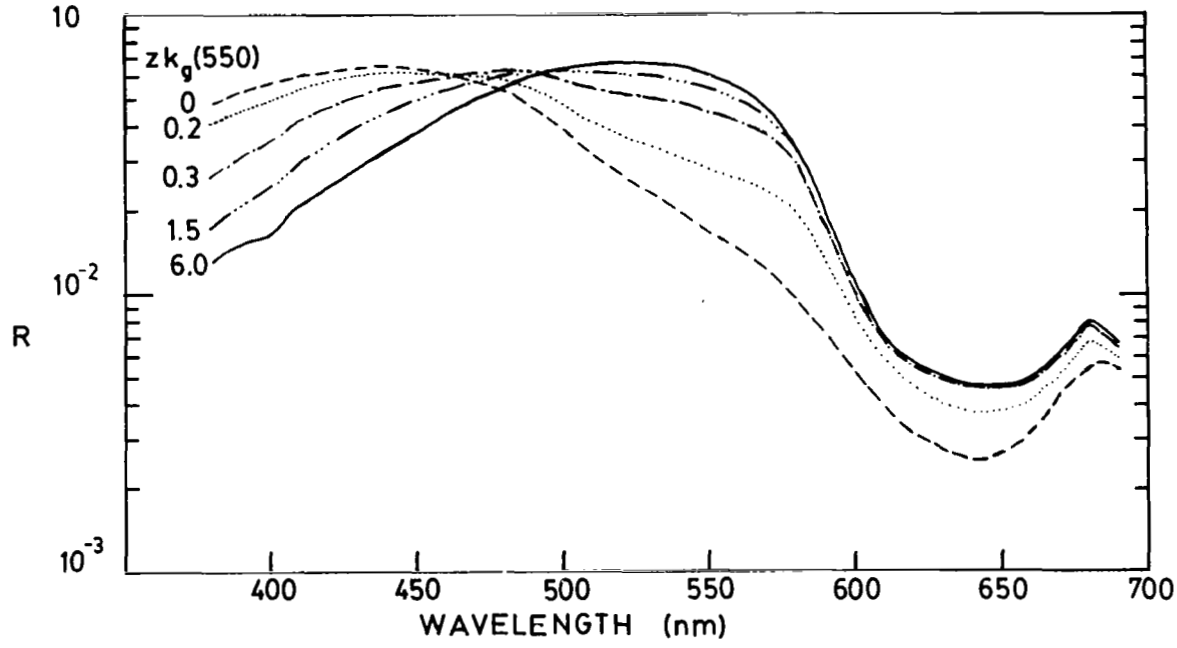

Figure 10.- Predicted irradiance reflectance for a two-layer water mass; green water overlays blue-green water.

REAL-TIME TEST OF MOCS ALGORITHM

DURING SUPERFLUX 1980

Gary W. Grew
NASA Langley Research Center

SUMMARY

During the October Superflux experiments a remote sensing experiment was conducted in which success depended upon the real-time use of a new algorithm, generated from MOCS (Multichannel Ocean Color Sensor) data onboard the NASA P-3 aircraft, to direct the NOAA ship Kelez to oceanic stations where vitally needed sea truth could be collected. Remote data sets collected on 2 consecutive days of the mission were consistent with the sea truth for low concentrations of chlorophyll a. Two oceanic regions of special interest were located and are being analyzed.

INTRODUCTION

As plans for the Superflux experiments were taking shape, a new ocean color algorithm for remotely monitoring suspended solids was under investigation. The algorithm is the outcome of analyses of remote data collected over a 6-year period with MOCS (Multichannel Ocean Color Sensor). Most of the MOCS data were collected in nearshore regions over plumes consisting of complex mixtures of suspended solids. To verify the potential of the algorithm, data was needed from offshore regions away from the high turbidity waters in the coastal zone. In particular, data was needed over deep water where chlorophyll a concentrations vary between 0.1 to 10 μg/ℓ. The expected participation in the Superflux experiments of the NOAA ship Kelez, with its capability of collecting sea truth data offshore and analyzing water samples onboard, offered an excellent opportunity for obtaining the vitally needed data to verify the algorithm.

The Superflux experiments also presented an opportunity for demonstrating the potential of the MOCS-aircraft real-time ocean color analyzer system. This system was developed for directing ships to positions where sea truth could be collected during the overflights. On past missions in which there was little or no foreknowledge of the compositions and concentrations of the suspended solids in the region of study, sea truth data were generally collected at evenly spaced points along flight tracks. The degree of success in obtaining the needed sea truth by this hit or miss technique has not been high. One purpose of this paper is to show that mission success can be greatly improved with the MOCS real-time system, which relies on the new algorithm for interpreting the color of the ocean.

MOCS-AIRCRAFT REAL TIME OCEAN COLOR ANALYZER (MARTOCA)

There are two basic parts to the MARTOCA system: the MOCS itself and the data processing subsystem. MOCS is a visible imaging spectroradiometer which performs multispectral scanning electronically by means of an image dissector (ref. 1). It covers the visible region of the spectrum, 400 to 700 nanometers, in 20 adjacent bands (tables 1 and 2). As shown in figure 1, the output from MOCS is fed into an A/D converter; all the data is stored serially on an analog tape recorder.

By means of the data selector in the real-time subsystem, samples of the data, usually center-of-track data, are processed and stored in a microprocessor; this data can be stored in and recalled from a digital tape recorder. During flight, or in the laboratory, a thumb wheel algorithm selector is used to display on an x-y oscilloscope cross plots of the algorithm or plots of the algorithm versus distance along the flight track. An example of the x-y display is presented in this paper.

In a much improved version of the real-time system currently under development, Loran C data will be fed into a minicomputer along with MOCS data. With this system latitude and longitude positions of special oceanic features can be determined rapidly and accurately.

ALGORITHM

Background

The algorithm is an outcome of the investigation of MOCS data by means of characteristic vector analysis (ref. 2). The data collected over Chesapeake Bay plumes reveal specific eigenvectors associated with specific regions on both sides of major plume boundaries. These eigenvectors have characteristic features which consistently appear, but their relative magnitudes vary due to interfering environmental factors, such as solar elevation, cloud cover, and sea state. One often-neglected variable is ocean surface reflection which can vary significantly across boundaries separating different water masses. MOCS data in conjunction with sea truth demonstrate that magnitude variations in the upwelling light due to such environmental changes can be much larger than the signal variations resulting from different algae concentrations. To show the effects of the environmental factors on spectral features and to simplify the discussion of the basis for the algorithm, comparisons between two pairs of MOCS spectra are presented.

In figure 2 the first pair of raw MOCS data was collected 2 nautical miles apart across a Chesapeake Bay plume boundary. Most of the signal variation between the two spectra seems to be due to algae concentration. If so, the plot in figure 3 of the differences in percent of these spectra shows features associated with the absorption and scattering properties of algae. For example, the chlorophyll a absorption band in the red region of the spectrum (675 nm) is evident about band 19. If no other factors influenced the upwelling

light, such difference spectra could be used to identify and map algae. Finding such pairs of spectra, however, is the exception rather than the rule.

A more typical case can be demonstrated with the spectra in figure 4 collected on different days under different environments for low and high concentrations of chlorophyll a. The large magnitude differences in the two spectra in figure 4(a) are a result of environmental factors, not the algae. The two spectra are shown normalized in figure 4(b) to illustrate, as in figure 3, the small differences in the spectral shapes. In figure 5, the difference spectra for this pair have features similar to those in figure 3 but distorted by environmental factors. Analyses of other MOCS data have shown that environmental parameters distort spectral signatures of suspended solids unequally across the visible spectrum, the variation being greater in the red region of the spectrum than in the blue. Since these variations will cause simple ratios of spectral bands, as well as single band data, to vary with environmental changes, it is difficult, if not impossible, to use these ratios to remotely quantify suspended matter in the ocean without extensive sea truth. An algorithm is needed which monitors only the significant information in each spectrum, e.g., for one particular region, the information within the envelope defined by the spectral differences in figure 3.

Equation

The consistency of spectral features, such as those in figure 3, in conjunction with the problems associated with the environmental factors led the author to investigate the algorithm

$$G_{j,m,n} = \frac{(S_j)^2}{S_{(j-m)} \cdot S_{(j+n)}} \tag{1}$$

where S_j is the MOCS signal for band j and m and n are constants. This algorithm, which amplifies and monitors changes in the spectral features, has been labeled "inflection ratio algorithm."

The rationale for this algorithm is based on the principle that at least three points are required to define a spectral feature. Consider the chlorophyll a absorption band in figure 3 that can be defined by bands 17, 19, and 20. A number of algorithms using three bands are, of course, possible, but such algorithms as

$$S_{17}+S_{19}+S_{20}$$

and

$$S_{17} \cdot S_{19} \cdot S_{20}$$

vary with the environment. Analyses of MOCS data have shown that, while simple ratios such as

$$\frac{S_{19}}{S_{17}} \quad \text{and} \quad \frac{S_{20}}{S_{19}}$$

vary with the environment, the ratio of the two ratios varies significantly less. Thus,

$$\frac{\frac{S_{19}}{S_{17}}}{\frac{S_{20}}{S_{19}}} = \frac{S_{19}}{S_{17}} \cdot \frac{S_{19}}{S_{20}} \tag{2}$$

$$= \frac{(S_{19})^2}{S_{17} \cdot S_{20}} \tag{3}$$

which by equation (1) is equal to $G_{19,2,1}$

As a first step toward simplifying the analyses, the author investigated all forms of the $G_{j,m,n}$ algorithm in which m equals n or

$$G_{j,m} = \frac{(S_j)^2}{S_{j-m} \cdot S_{j+m}} \tag{4}$$

Subsequently, as a further simplification, all possible values of this algorithm for m = 2, or

$$G_{j,2} = \frac{(S_j)^2}{S_{j-2} \cdot S_{j+2}} \qquad j = 3\text{-}18 \tag{5}$$

were investigated because (1) the smaller the value of m the less the influence of the environment on the algorithm, and (2) the spectral features have half-widths of about 30 nanometers or greater.

Inflection ratio spectra for $m = 2$ derived from MOCS spectra collected over relatively clear water on various missions are shown in figure 6. The atmospheric and sea conditions varied from mission to mission and the solar elevation angle during each overflight varied widely, as indicated in the figure. Since these curves are very consistent, one can be selected as a standard for examining the relative changes in the inflection ratio spectra for different water masses through the equation

$$H_{j,2} = \left(\frac{G_{j,2}}{G_{j,2(\text{standard})}} - 1 \right) 100 \qquad j = 3\text{-}18 \tag{6}$$

Plots of $H_{j,2}$ for the two MOCS spectra in figure 4 are shown in figure 7. By comparing figure 7 with figure 5 (or fig. 3) features in the inflection ratio spectrum of high chlorophyll *a* concentration can be associated with the spectral features of algae. This inflection ratio spectrum consistently can be generated from MOCS data collected over strong algae plumes. While the corresponding difference spectra, as in figure 5, could vary drastically for data collected over the same algae concentrations but under different environments, the inflection ratio spectra appear to remain relatively constant.

A second type of inflection ratio spectrum, often appearing but not clearly identified, is shown in figure 8. Indirect evidence, however, prior to the Superflux experiments suggested this spectrum may be associated with organic detritus. Evidence supporting this possibility is presented in later paragraphs.

OCTOBER MISSION

Operations

Because of several factors, the weather in particular, the goal of the MOCS experiment of collecting deep ocean data along with adequate sea truth was not met during the spring and summer Superflux experiments. Thus, for the October mission a plan was formulated for increasing the probability of mission success and at the same time for demonstrating the real time capability of the MOCS system.

The basic plan consisted of 2 consecutive days of MOCS data collection missions from an aircraft altitude of 2.3 km. An exploratory mission would be conducted on the first day with or without sea truth collection. The P-3 aircraft would be directed to fly out to and along the shelf break in search of a region where, based on the MOCS algorithm, a definite chlorophyll *a* concentration gradient existed across a boundary separating two different water

masses. If such a region were located, the NOAA ship Kelez would be directed to collect sea truth data in that region during the overflights on the second day.

Due to airway restrictions during the experiment the P-3 flights were confined to a narrow corridor between latitudes 36°55' N and 37°2' N. Fortunately our first flight track along latitude 36°56' N resulted in data collection over several different water masses including the desired chlorophyll a gradient. In addition, the experiment was fortunate enough to have the Kelez available to collect sea truth on both days.

The mission began at 1:00 a.m. on October 21, 1980, when the Kelez collected the first of a series of water bucket samples as it steamed toward the end of the track, shown in figure 9, to await the P-3 overflights. By 8:53 a.m. when the P-3 began its overflight along the same track, the Kelez was stationed at 36°56' N, 74°20' W. Using the MOCS algorithm a well-defined boundary was located near longitude 74°40'. No visible boundary was observed at the time by either the P-3 or the Kelez, nor was it observable later on aerial photography. Based on this boundary the Kelez was directed to collect additional sea truth data along the same track between 74°20' and 74°50' and then to remain in the region for the P-3 overflights the next day.

On the second day the Kelez again collected sea truth between the same coordinates during the P-3 overflights. In addition, the Kelez was directed to collect data at three specific locations on its return transit to port. Based on the MOCS algorithm each of these locations was in a different water mass.

Prediction

One of the x-y oscilloscope displays used in the real time analysis of ocean color is the cross plot of $G_{7,2}$ and $G_{12,2}$ for data along the center of the track. Figure 10 shows data collected from an altitude of 2.3 km on the first overflight (fig. 9) on October 21, 1980. Each point in the figure is equivalent to one data sample with a spacial resolution of 50 meters collected about every 300 meters along the track. Patterns similar to the one in the figure have been obtained on other missions. The same unnormalized scales are always used. Based on the large number of similar plots and their corresponding sea truth, this plot was interpreted in real time as stated below.

There appeared to be four basic oceanic regions, as labeled in figure 11, corresponding to four different types of water masses. Region 1, located east of the shelf break, consisted of very clear water with chlorophyll a concentrations less than 1 µg/l. Region 2 west of the shelf break had higher chlorophyll a than Region 1 but the average concentration was probably less than 2 µg/l. This is verified by examining the plot of the change in the inflection ratio spectra between Regions 1 and 2, as shown in figure 12. Spectra are shown for both days of the mission, as well as for a similar condition observed during the June mission. The prominent feature in the blue region of the spectrum was caused by a change in the absorption of light by phytoplankton across the shelf break, clearly indicating a phytoplankton gradient existed there.

Region 3 indicated that the average chlorophyll a was lower than in Region 2 but the turbidity was higher. The inflection ratio spectra between Regions 2 and 3 are shown for both days in figure 13. The shapes of these curves are characteristic of spectra from regions suspected of consisting of organic detritus (compare fig. 8 and fig. 13). It is possible that Region 3 could be an organic detritus plume.

Region 4 was considered to be the Chesapeake Bay plume. In this paper only regions outside the plume will be discussed, that is, Regions 1 to 3.

It was this real time analysis that led to directing the Kelez to collect sea truth data across the shelf break and in Region 3 on its return to port.

Sea Truth

Sea truth measurements from 37 bucket samples collected by the Kelez on a transit out to the shelf break on October 21, 1980, are shown in figure 14. Chlorophyll a concentration and F_o/F_a are plotted versus longitude position along latitude 36°56'. The F_o/F_a index is a linear function of the ratio of pheopigment to chlorophyll plus pheopigment in which a value of 1.1 indicates mainly pheopigment and 2.0 indicates mainly chlorophyll (ref. 3). Since by figure 12 $G_{7,2}$ is the most responsive algorithm to the data in Regions 1 and 2, it is used in figure 14 for comparison with the sea truth; $G'_{7,2}$, the inverse of $G_{7,2}$, is actually plotted to show a positive correlation with the sea truth.

In agreement with $G'_{7,2}$ four fairly distinct regions are evident by the chlorophyll a data--assuming that the transitions between regions are not considered to be regions. By visual inspection $G'_{7,2}$ and chlorophyll a appear to correlate well in Regions 1 and 2. In Region 3 $G'_{7,2}$ seems to correlate better with F_o/F_a.

Chlorophyll a

The cross plot of $G_{7,2}$ and chlorophyll a in figure 15 indicates a nonlinear relationship exists between the two parameters. A curve similar to Duntley's plot in figure 16 of reflectance for $\lambda = 450$ nm versus chlorophyll a was in fact expected. The scatter in the data for Regions 3 and 4 may be due partly to the time difference of 6 to 8 hours between water bucket collection and the overflight. However, the shape differences in the plots (fig. 14) for Region 3 suggest that the apparent scatter may be caused by the mixture of suspended substances in that region.

Figure 17 shows consistent chlorophyll a data in Regions 1 and 2 for both days of the experiment. This data set is the first good set from MOCS to be used in establishing a data base for remote sensing of low chlorophyll a concentrations. In figure 18 the author has taken the liberty of adding to the data set the average of the four data points for Region 4 and using it to draw a dashed curve similar to Duntley's plot (fig. 16). There is evidence, however, to suggest that the curve would not level off as quickly for high concentrations of chlorophyll a away from turbid coastal waters. Future missions being planned or proposed will be directed toward establishing the correct curve.

F_o/F_a Ratio

An investigation is being conducted to determine the significance of the similarities in the shapes of the curves for $G'_{7,2}$ and F_o/F_a in Region 3 (fig. 14). The cross plot of these two parameters in figure 19 shows that, while possible linear curves could be drawn between subsets of points, a complex pattern exists for the whole data set. This plot demonstrates, as should be expected, that different mixtures of suspended solids will influence an algorithm differently.

A variation of the $G_{7,2}$ algorithm was found that correlates fairly well with F_o/F_a for the three regions on the shelf (Regions 2 to 4). This algorithm is given by

$$G_{7,3,2} = \frac{S_7^2}{S_4 \circ S_9} \tag{7}$$

where band 5 has been replaced with band 4. Figure 20 shows two plots of this algorithm, one for each day of the mission. Even though the sea truth was collected 24 to 36 hours before the MOCS data for the second day, a linear relationship is evident in both cases. The data loop in the upper left corner of the figure indicates that the MOCS data and sea truth are out of phase; in other words the "plume" had shifted from one day to the next. To show this more clearly, the algorithm and the inverse of F_o/F_a are plotted versus sea truth station in figure 21. Based on this algorithm the plume shifted eastward. The relative magnitudes of the "plume" for the 2 days are uncertain because of a shift in the algorithm, and one of the two data points collected by the Kelez near this region on its return to port does not seem to agree with this shift. Further analysis may clear up this uncertainty.

This "plume" is interesting from several aspects. The F_o/F_a ratio has been used by marine biologists as an indicator of grazing regions of zooplankton. These tiny animals eat phytoplankton converting chlorophyll a into

pheopigments. Thus, low values of F_o/F_a such as in Region 3 (fig. 14), may indicate a depletion of algae by ingestion.

It is also possible the region is associated with either an old algae plume from the Chesapeake Bay or with resuspended solids high in organic matter. In these cases low values of F_o/F_a may indicate the presence of organic detritus. It is reasonable to expect the F_o/F_a index, the color of the ocean and, therefore, the inflection ratio spectrum to vary with the percentage of live and dead algae in the ocean. There is evidence suggesting that similar regions existed beyond the Chesapeake Bay plumes during both the spring and summer Superflux experiments, but the sea truth data analyzed thus far has not been sufficient for understanding this region.

One fact is quite clear, however: the inflection ratio spectra (fig. 13) from this region are distinctly different from those of algae (fig. 7). A dedicated experiment is needed to remotely locate this region and then to collect water samples for thorough analyses of the constituents in the water.

CONCLUDING REMARKS

The October mission was the most successful MOCS experiment conducted to date, primarily because of the real-time connection between the remote sensor on the aircraft and the sea truth ship. Predictions based on the real-time analysis of the MOCS algorithm were used to direct the Kelez to specific sea truth stations. The goal of locating a prime region of interest was achieved along with the successful collection of in situ data in that region. The data sets consisting of remote and in situ data for both days were consistent. It is anticipated that this data will play an important role in testing algorithmic consistency of future data sets of low concentrations of chlorophyll a. Real time predictions during the mission based on the algorithm were, as a whole, confirmed by the sea truth data.

The mission was also successful in that an additional oceanic region was located which may be of fundamental interest to marine biologists. Although the sea truth data presently available is not adequate to "explain" this region (Region 3 in fig. 14), discovery of it and its remote sensing signature may have set the stage for future experiments concerning its nature.

Analysis of the MOCS data with the sea truth, in addition to confirming predictions and demonstrating data consistency, reaffirmed the author's conviction concerning a fundamental point: no one j value of the MOCS algorithm or of any other simple algorithm is likely to be found that can be used alone to quantify different kinds of suspended matter. As supported by the plots in figures 15 and 19, different mixes influence the color of the ocean differently. In low turbidity water offshore $G_{7,2}$ (or $G_{7,3,2}$) and $G_{12,2}$ may be adequate, but MOCS data from other experiments suggest that perhaps as many as eight j values of $G_{j,2}$ may be required to identify and accurately quantify nearshore plumes.

REFERENCES

1. White, P. G.; Jenkin, K. R.; Ramsey, R. C.; and Sorkin, M.: Development and Flight Test of the Multichannel Ocean Color Sensor (MOCS). NASA CR-2311, 1973.

2. Grew, G. W.: Characteristic Vector Analysis as a Technique for Signature Extraction of Remote Ocean Color Data. Remote Sensing of Earth Resources, vol. VI, F. Shahrokhi, ed., The University of Tennessee Space Institute (Tullahoma), 1977, pp. 109-144.

3. Walsh, J. J.; Whitledge, T. S.; Barvenick, F. W.; Wirick, C. D.; Howe, S. D.; Esais, W. E.; and Scott, J. T.: Wind Events and Food Chain Dynamics Within the New York Bight. Limnology and Oceanography, vol. 23, no. 4, 1978, pp. 659-683.

4. Duntley, S. Q.: Detection of Ocean Chlorophyll From Earth Orbit. Fourth Annual Earth Resources Program Review, vol. IV, MSC-05937, 1972.

TABLE 1.- MOCS SPECIFICATIONS

Sensor:	Image Dissector
Scan Rate:	3.51 Scans/sec.
Number of Spectra:	150 Spectra/Scan
Spectral Range:	400-700 nm (Table 2)
Spectral Resolution:	15 nm
Field-of-View:	17.1°
Spacial Resolution:	4 x 2 millirad.

TABLE 2.- MOCS SPECTRAL BANDS

Band	Center Wavelength (nanometers)	Band	Center Wavelength (nanometers)
1	400	11	552
2	415	12	568
3	430	13	584
4	445	14	601
5	460	15	616
6	475	16	631
7	490	17	647
8	506	18	663
9	521	19	678
10	537	20	694

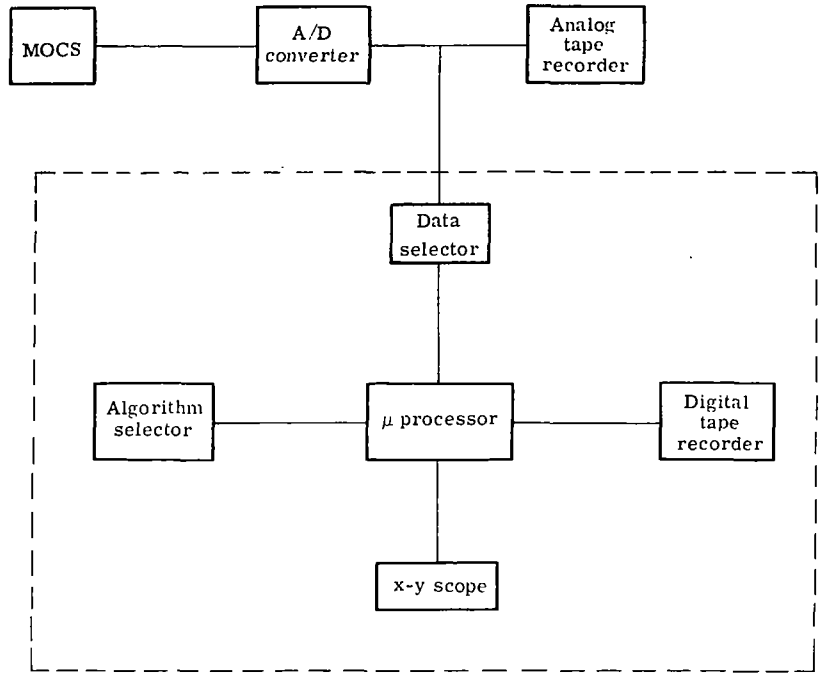

Figure 1.- MOCS aircraft real-time ocean color analyzer.

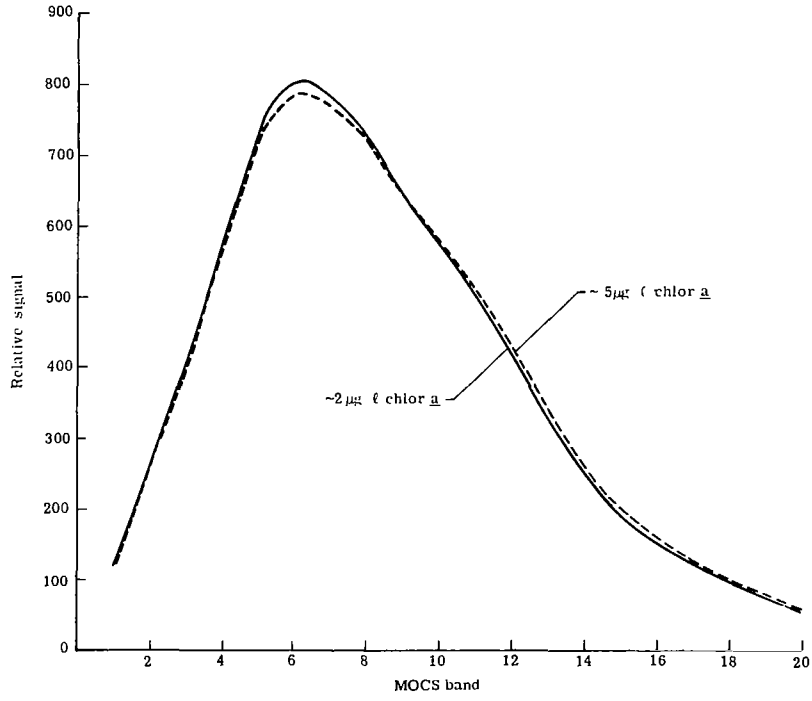

Figure 2.- Raw MOCS spectra collected on April 7, 1976 from 5.3 km altitude near Chesapeake Bay entrance.

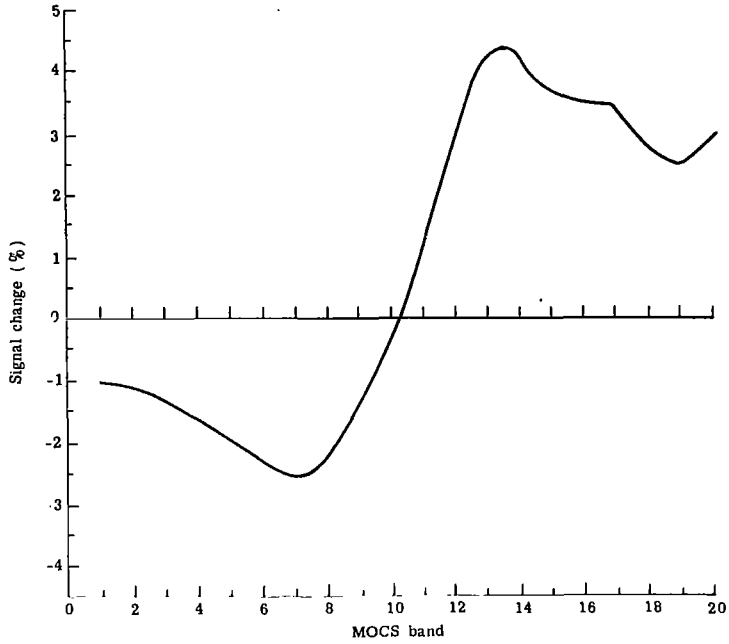

Figure 3.- Difference spectra of 2-5 μg/ℓ chlorophyll a from figure 2.

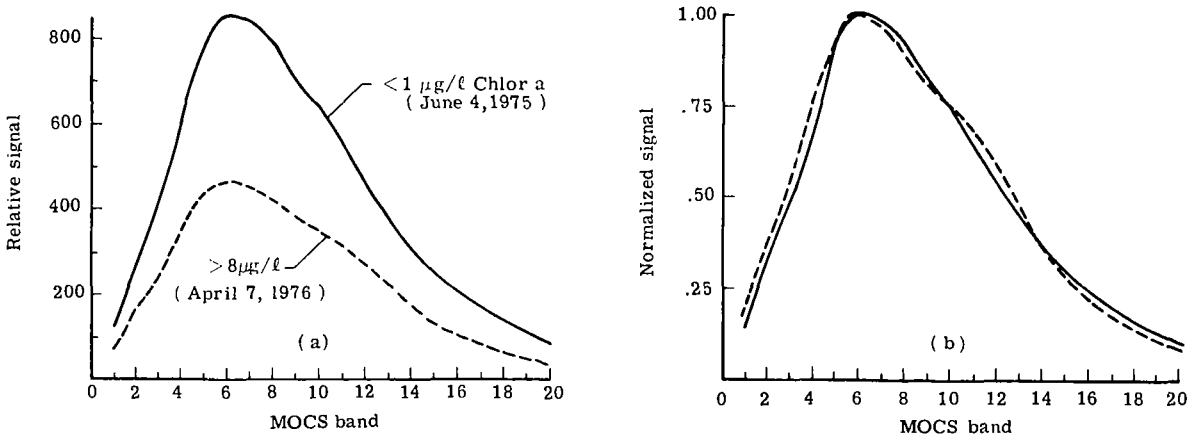

Figure 4.- Raw MOCS spectra (normalized in (b)) collected from 5.3 km altitude near Chesapeake Bay entrance.

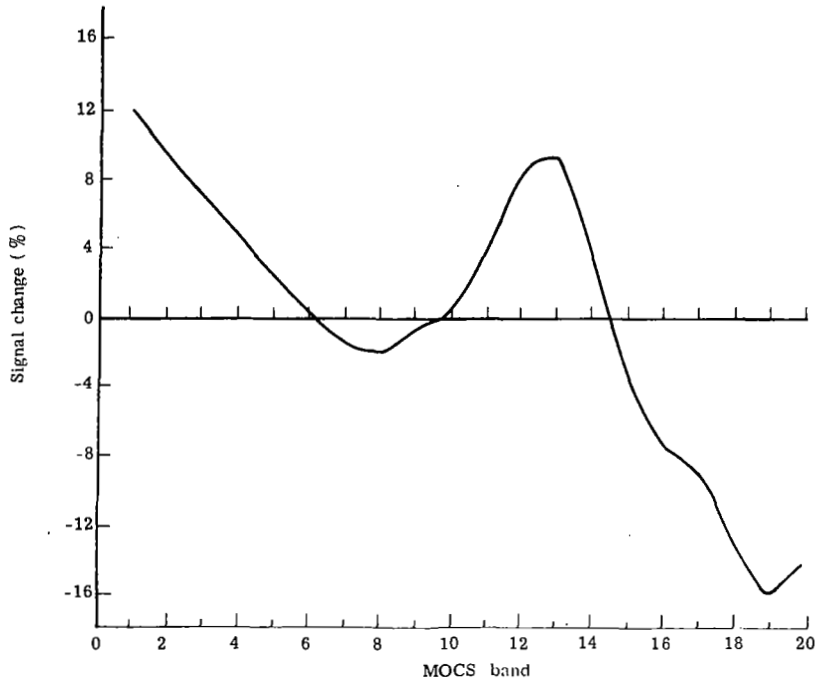

Figure 5.- Difference spectra for data in figure 4 (b).

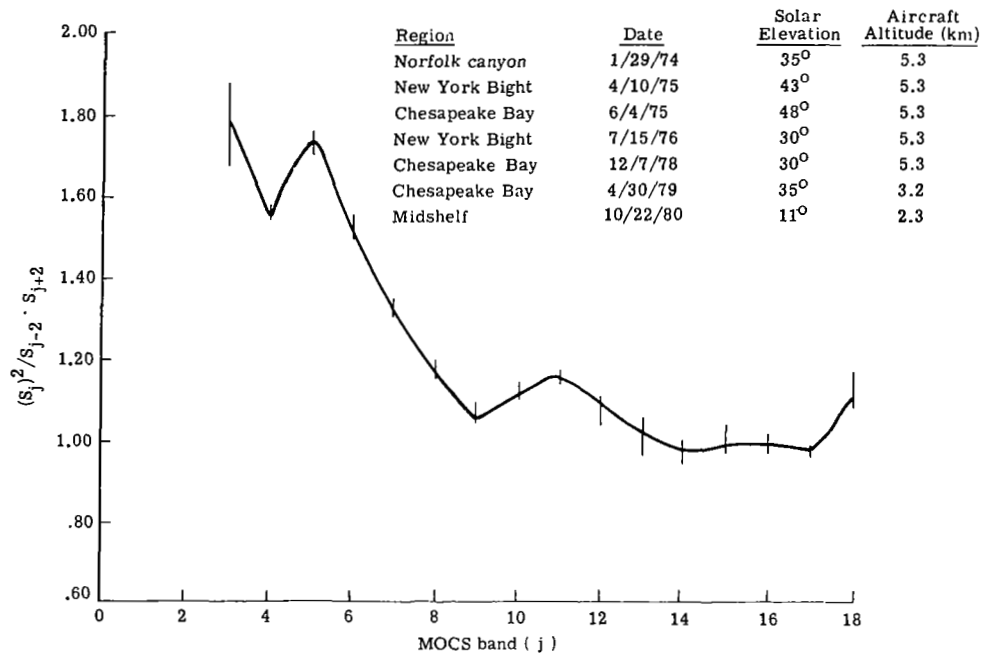

Figure 6.- MOCS inflection ratio spectra for clear water; vertical lines indicate range for samples from listed missions.

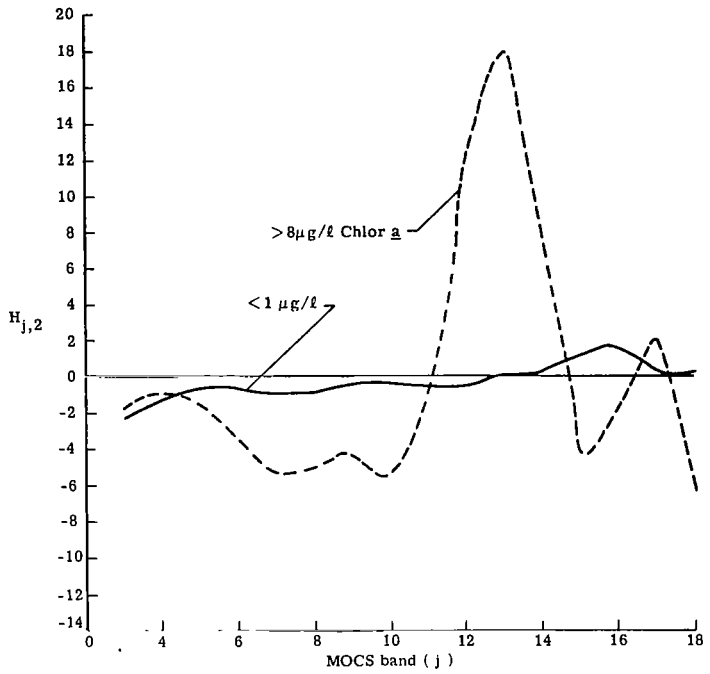

Figure 7.- Inflection ratio spectra for MOCS data in figure 4.

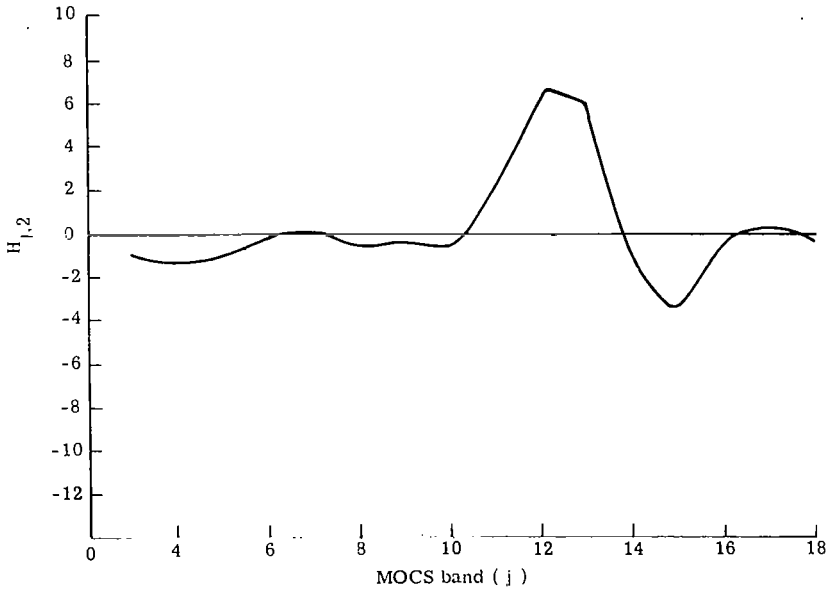

Figure 8.- MOCS inflection ratio spectrum for data collected near Chesapeake Bay entrance on March 27, 1979.

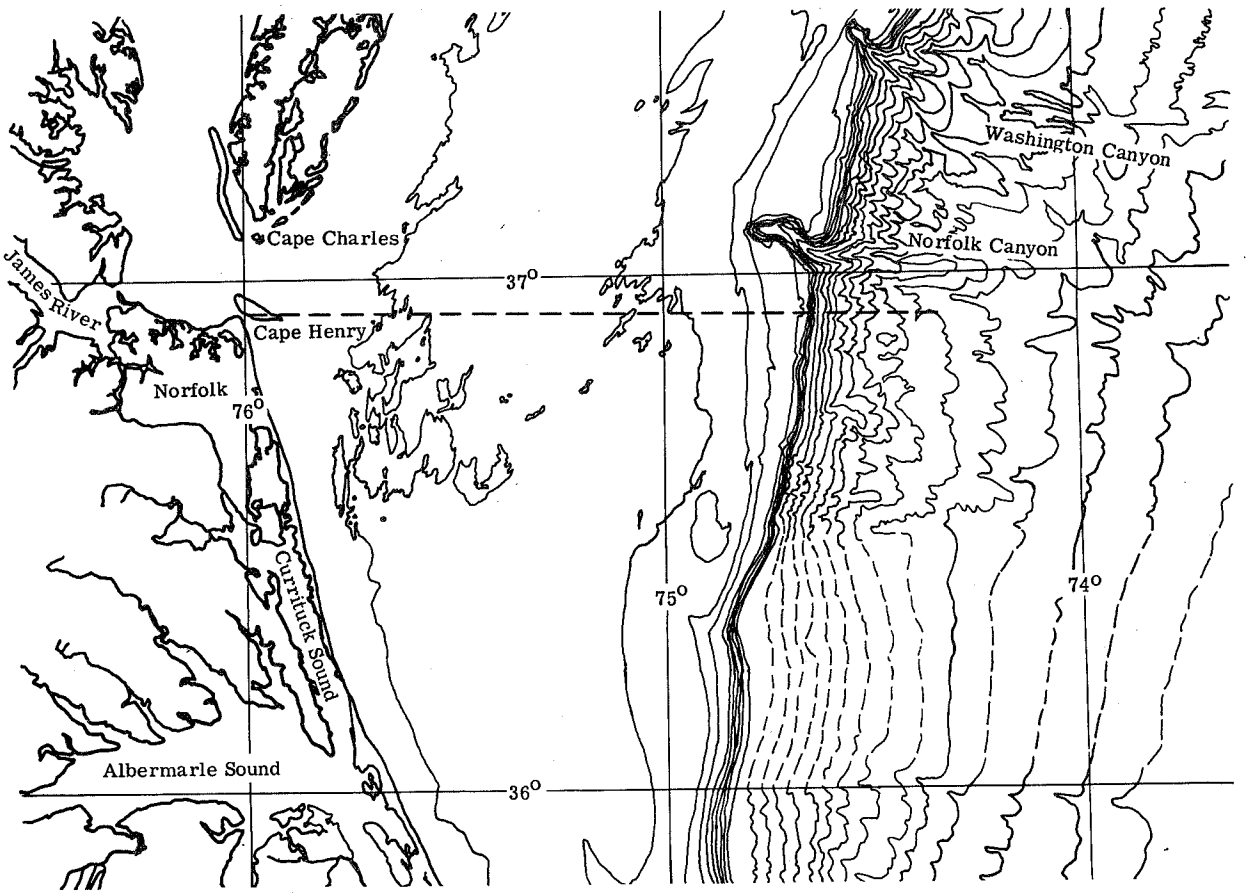

Figure 9.- Track of the Kelez and NASA P-3 on October 21, 1980.

$G_{7,2}$

$G_{12,2}$

Figure 10.- Cross plot of $G_{7,2}$ and $G_{12,2}$ for MOCS data collected on October 21, 1980.

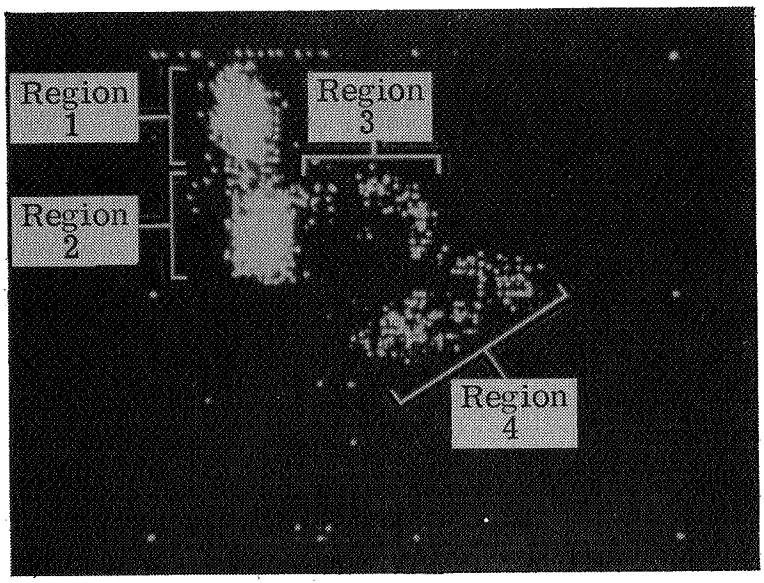

Figure 11.- Same as figure 10 with oceanic regions labeled.

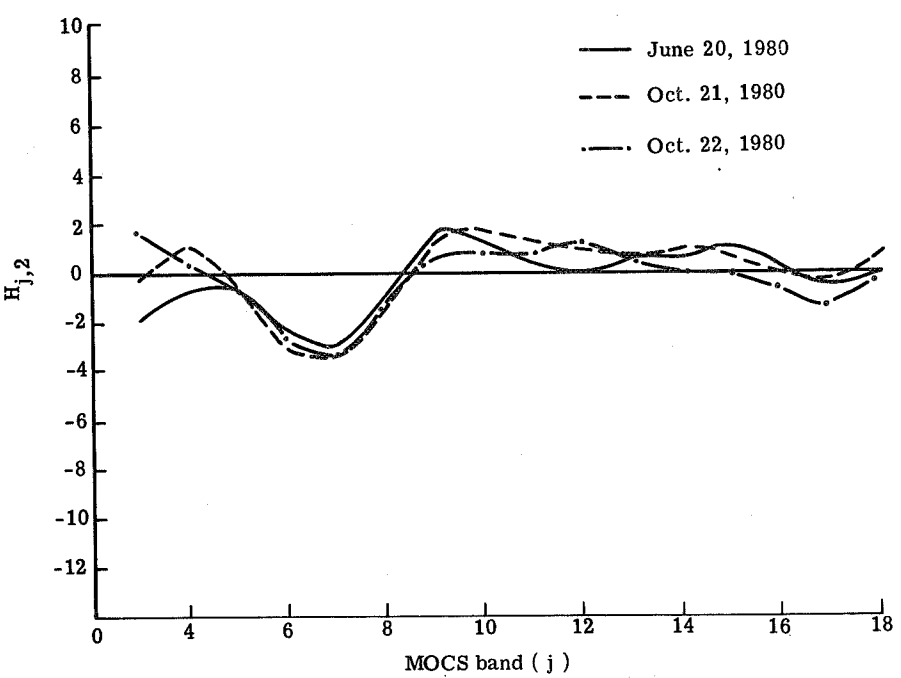

Figure 12.- Inflection ratio spectra for chlorophyll a (0-2 μg/ℓ) across shelf break.

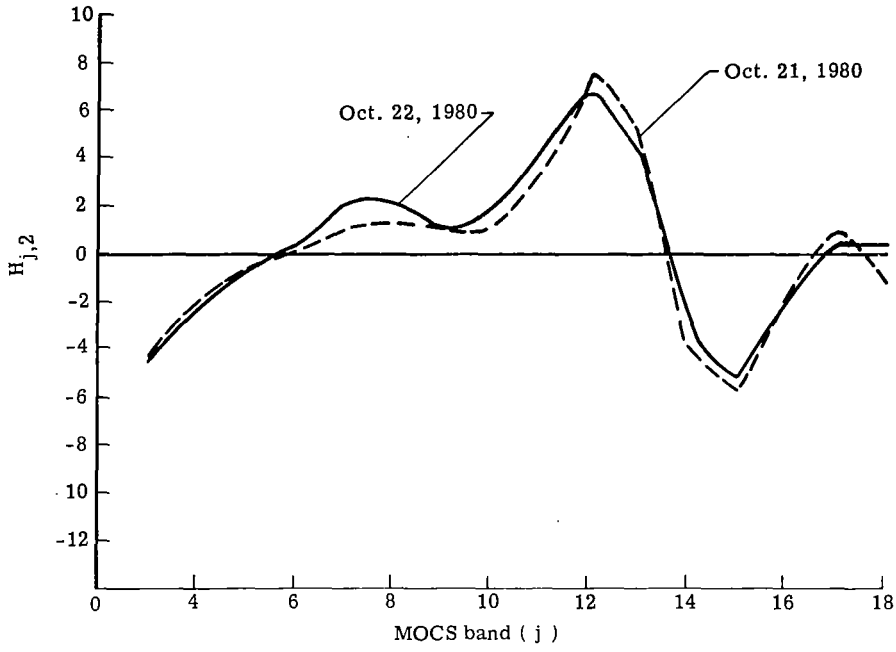

Figure 13.- Inflection ratio spectra between regions 2 and 3.

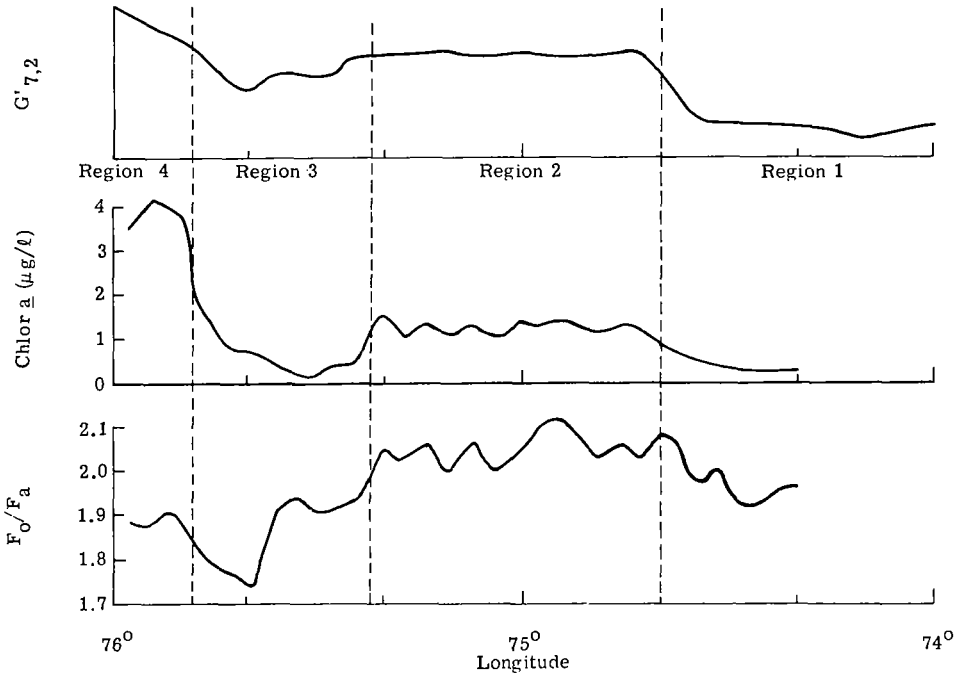

Figure 14.- Sketches of sea truth data and $G_{7,2}$ along flight track on October 21, 1980.

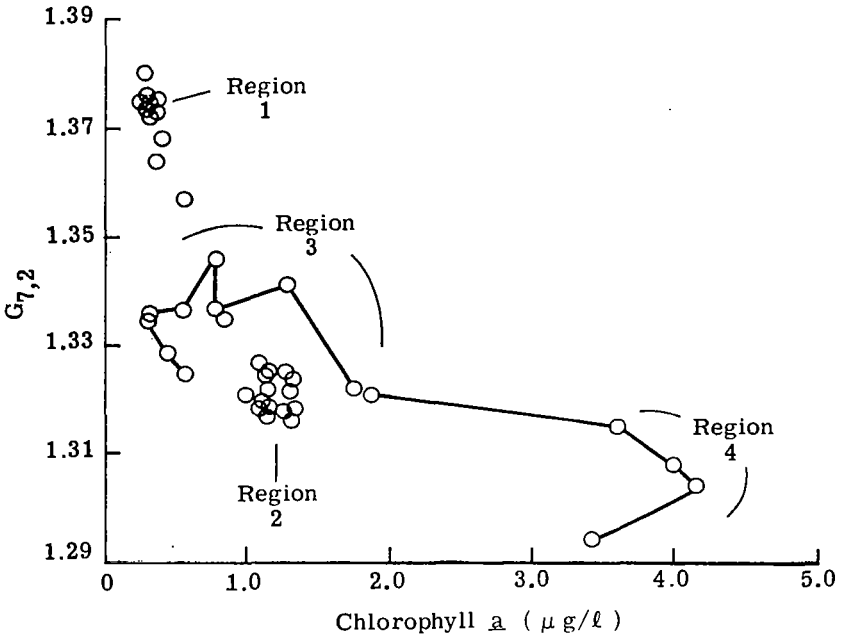

Figure 15.- $G_{7,2}$ versus chlorophyll a for data collected on October 21, 1980. (Lines connect consecutive stations in regions 3 and 4.)

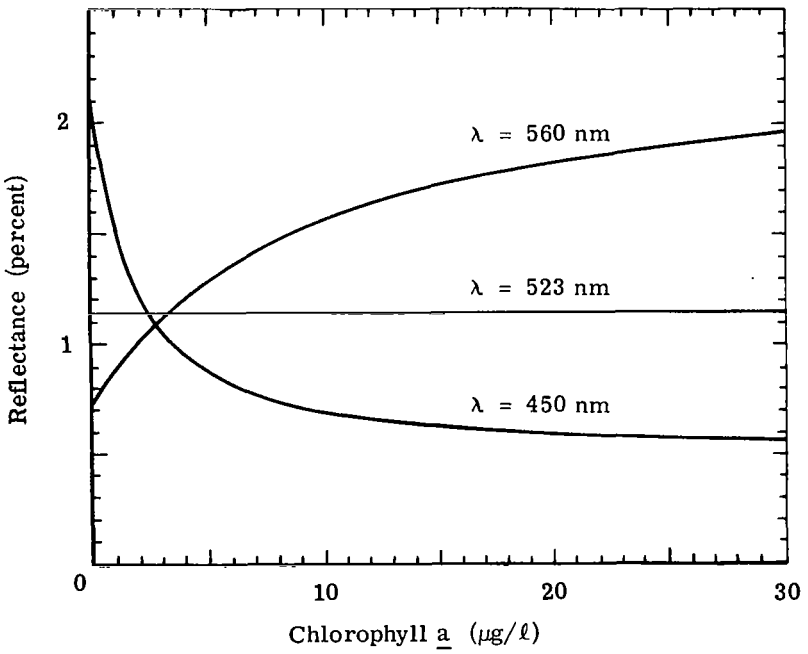

Figure 16.- Reflectance versus chlorophyll a. (From ref. 4).

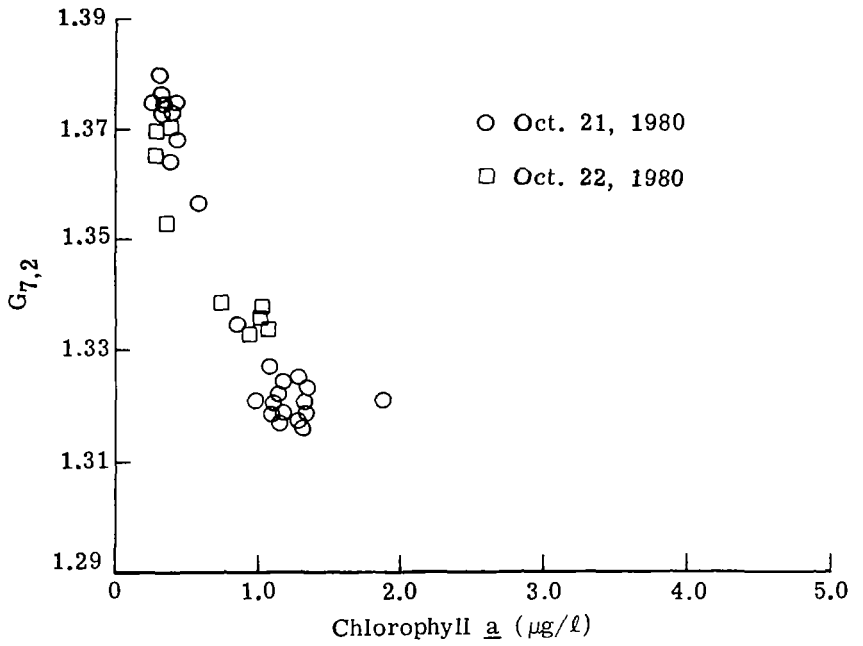

Figure 17.- $G_{7,2}$ versus chlorophyll a for regions 1 and 2.

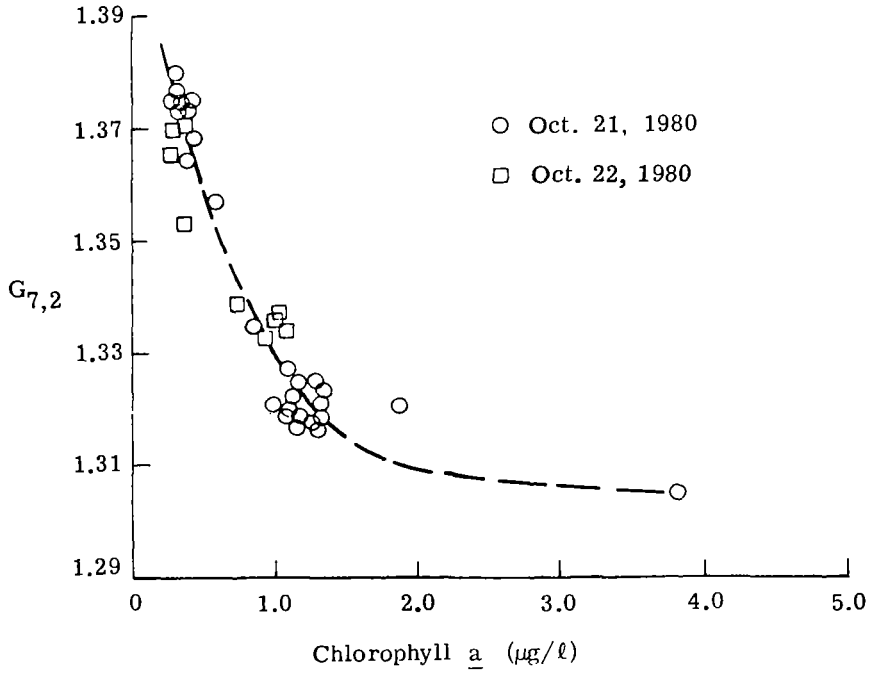

Figure 18.- Same as figure 17 with hypothetical curve added.

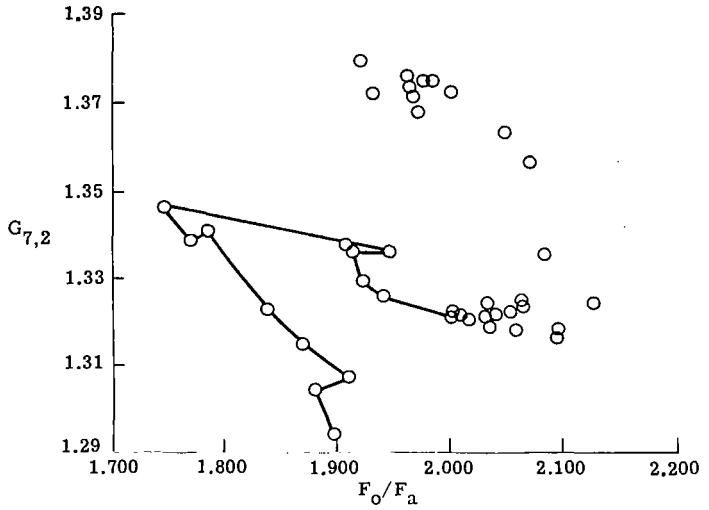

Figure 19.- $G_{7,2}$ versus F_o/F_a for data collected on October 21, 1980.

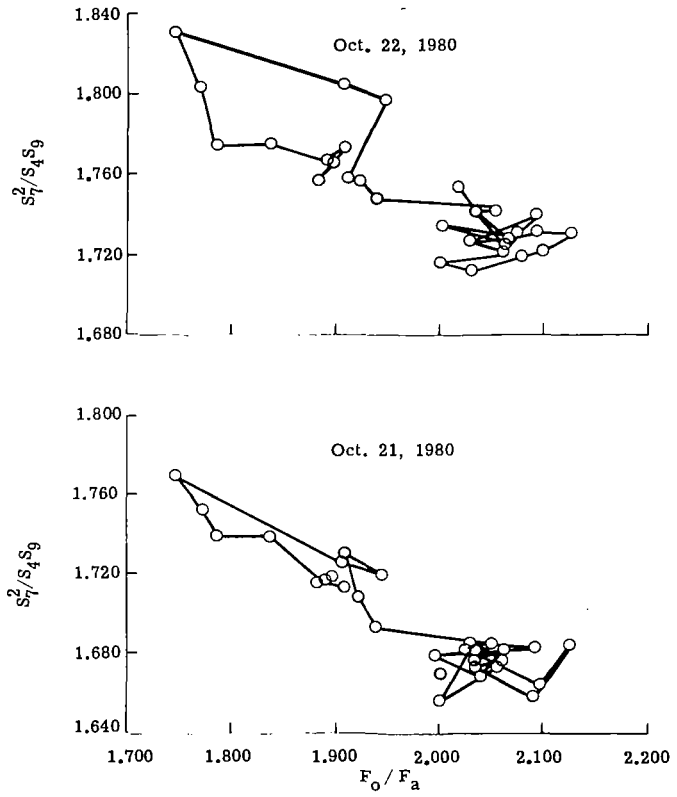

Figure 20.- $G_{7,3,2}$ versus F_o/F_a in regions 2, 3, and 4.

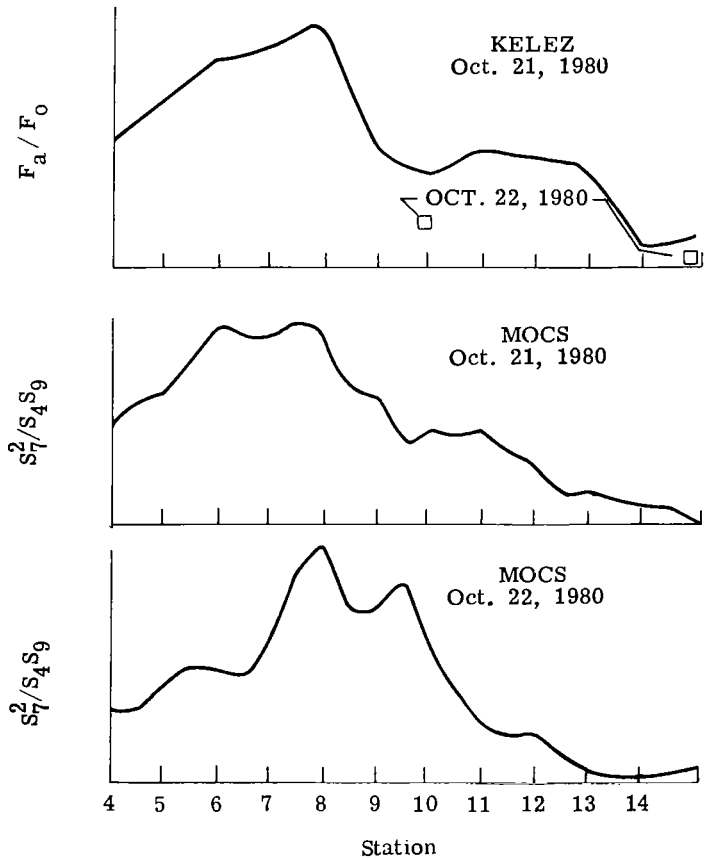

Figure 21.- Sketches of F_a/F_o and $G_{7,3,2}$ versus sea truth station in region 3.

ANALYSIS OF TESTBED AIRBORNE MULTISPECTRAL SCANNER DATA FROM SUPERFLUX II

David E. Bowker, Charles A. Hardesty, and Daniel J. Jobson
NASA Langley Research Center

Gilbert S. Bahn
Kentron International, Inc.

SUMMARY

The Langley Test Bed Aircraft Multispectral Scanner (TBAMS) was flown during the James Shelf, Plume Scan, and Chesapeake Bay missions as part of the Superflux II Experiment. Excellent correlations were obtained between water sample measurements of chlorophyll and sediment and TBAMS radiance data. The three-band algorithms used were insensitive to aircraft altitude and varying atmospheric conditions. This was particularly fortunate due to the hazy conditions during most of the experiments. A contour map of sediment, and also chlorophyll, was derived for the Chesapeake Bay plume along the southern Virginia-Carolina coastline. A sediment maximum occurs about 5 nautical miles off the Virginia Beach coast with a chlorophyll maximum slightly shoreward of this. During the James Shelf mission, a thermal anomaly (or front) was encountered about 50 miles from the coast. There was a minor variation in chlorophyll and sediment across the boundary. During the Chesapeake Bay mission, the Sun elevation increased from 50 degrees to over 70 degrees, interfering with the generation of data products.

INTRODUCTION

The Langley Testbed Airborne Multispectral Scanner, abbreviated TBAMS, was flown on three missions during the Superflux II experiment in June of 1980. TBAMS is a conventional rotating mirror scanner designed to be flexible with respect to spectral band location and sensitivity. For the Superflux II experiment, eight visible/near-IR bands, each 20 nanometers wide, were selected as given in figure 1. A thermal IR channel was also available. The two curves in figure 1 represent the normalized spectral response of TBAMS for two different water masses with the sediment and chlorophyll concentrations shown. In general, all of the bands respond to an increase in sediment. However, they also respond to an increase in haze, clouds, and other atmospheric parameters. To minimize this interference, spectral bands can be ratioed. The best ratio for sediment is Band 7/Band 8. This ratio is still sensitive to atmospheric variations, however. A better algorithm for minimizing the atmospheric contribution is the three-band ratio, $(\text{Band } 7)^2/(\text{Band } 6 \times \text{Band } 8)$. This algorithm is equivalent to

measuring the angular variation of the normalized response curve about Band 7. For the sediment variations shown, this angular change is about 4^{o}. In a similar manner, the three-band algorithm centered at Band 4 can be used to monitor low levels of chlorophyll.

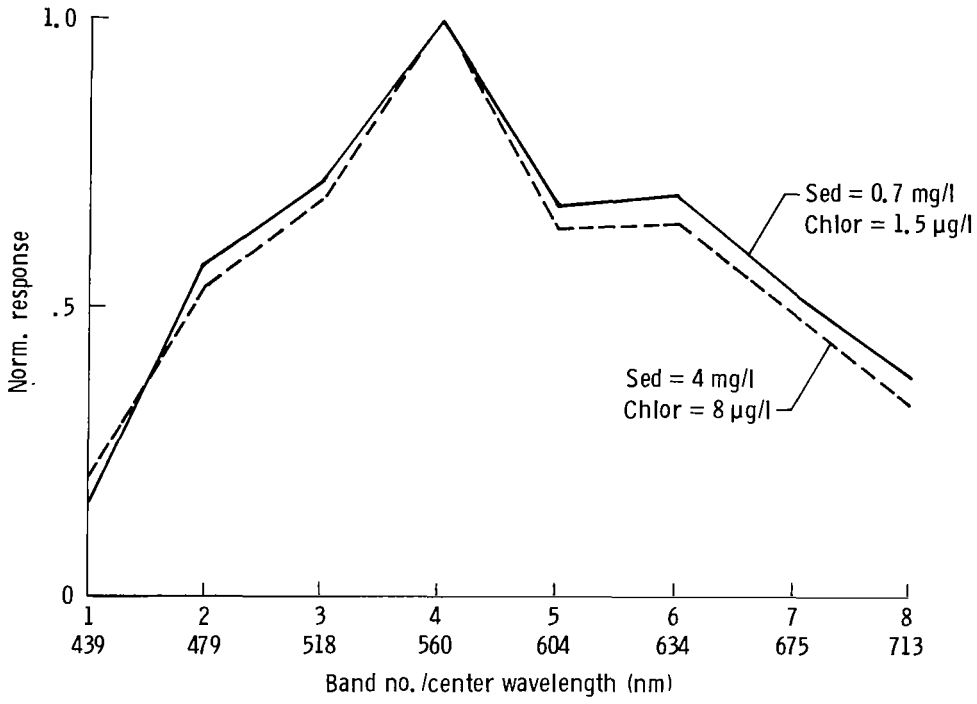

Figure 1. - Normalized response of TBAMS channels.

An indication of the three-band algorithm effectiveness in correcting for atmospheric, or what is more properly termed off-nadir, radiance variations is shown in figure 2. Several scanlines from the end of baseline 4 of the Plume Scan Mission have been averaged to minimize noise and minor variations in the water mass. The radiance variations along each scanline for the three bands shown display the characteristic increase at each end, due primarily to the increased path length from the surface to the sensor. It can be seen that the radiance variation is greatest for Band 6 and least for Band 8. When the three bands are ratioed, the off-nadir variation has essentially been removed while the sediment information has been retained.

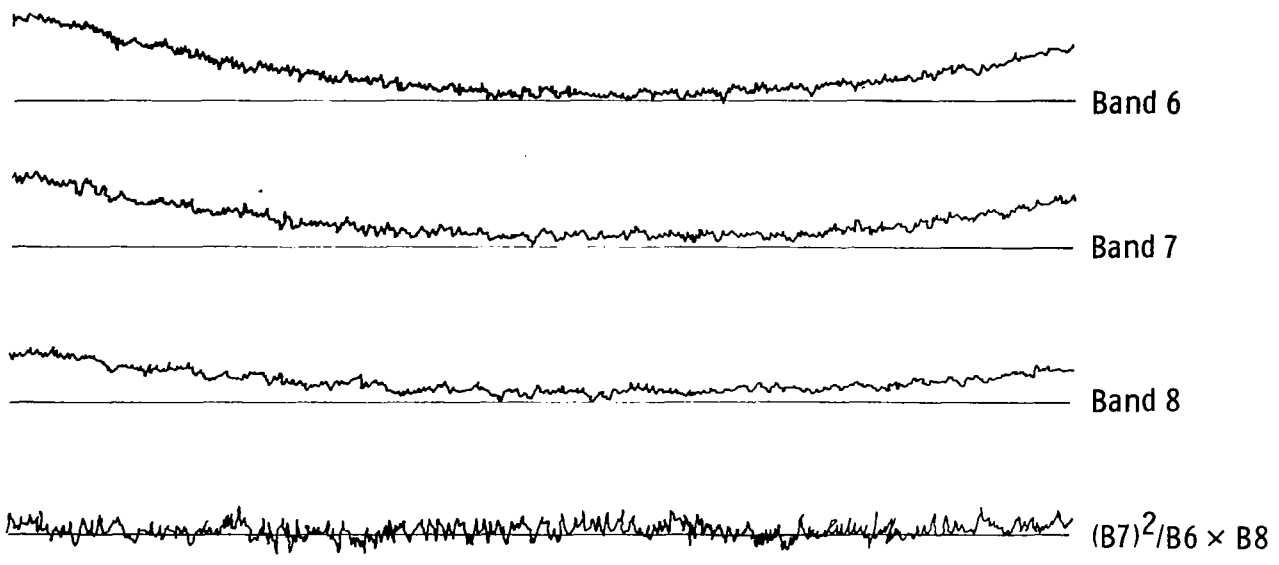

Figure 2. - Relative radiance variation along scan lines.

EXPERIMENT RESULTS

Plume Scan Mission

In order to convert the radiance variations at the sensor into sediment variations within the water column, a calibration curve was established. Ten ship stations located near the Chesapeake Bay entrance were overflown on either June 20 (James Shelf Mission) or June 24 (Plume Scan Mission).

Figure 3 is a plot of the $(\text{Band } 7)^2/(\text{Band } 6 \times \text{Band } 8)$ radiance ratio versus sediment concentration for these stations. Where samples were analyzed from 1m and 3m depths, the two values were averaged to give one value. The aircraft altitude during the overpass of the John Smith on June 20 was 5.3 km, while the altitude for the other stations was 2.3 km. Considering the variations in flight altitude, day of sampling, and haze conditions, this is a good correlation of data for such a small spread in sediment. (On similar experiments in this area during March of 1979, the sediment varied from 1 to 20 mg/1).

Flight lines for the Plume Scan Mission are plotted in figure 4. Originally, the mission was to have been flown at 7 km altitude with the baselines oriented parallel to the coast, but haze forced the aircraft down to 2.3 km and the baselines were oriented essentially perpendicular to the coast whereby the Bay Plume could be contoured. This orientation put the Sun line perpendicular to the scanner direction such that sunglint would

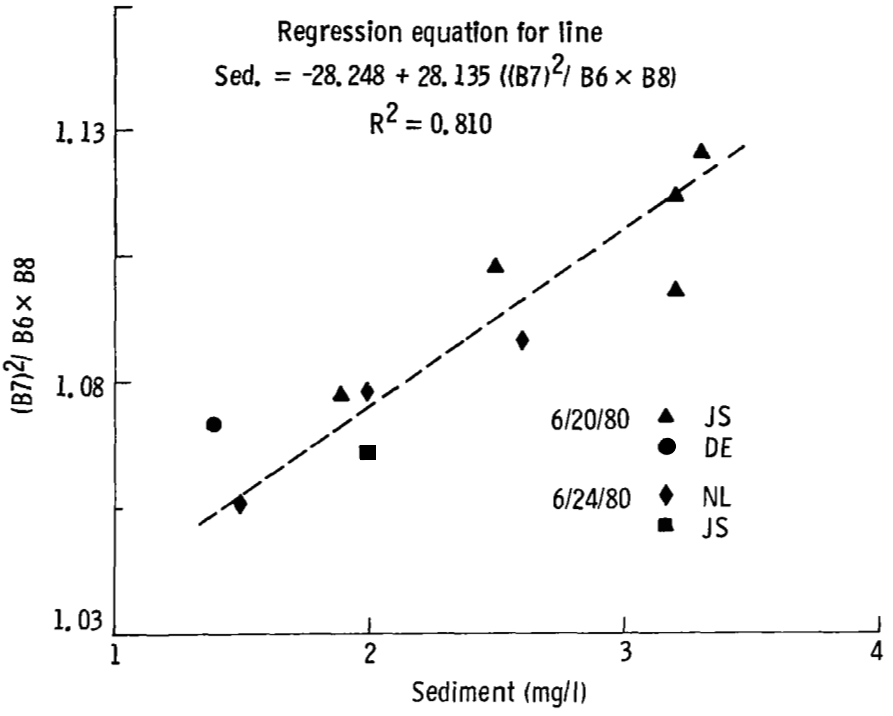

Figure 3. - Regression plot of sediment vs. band 7 algorithm.

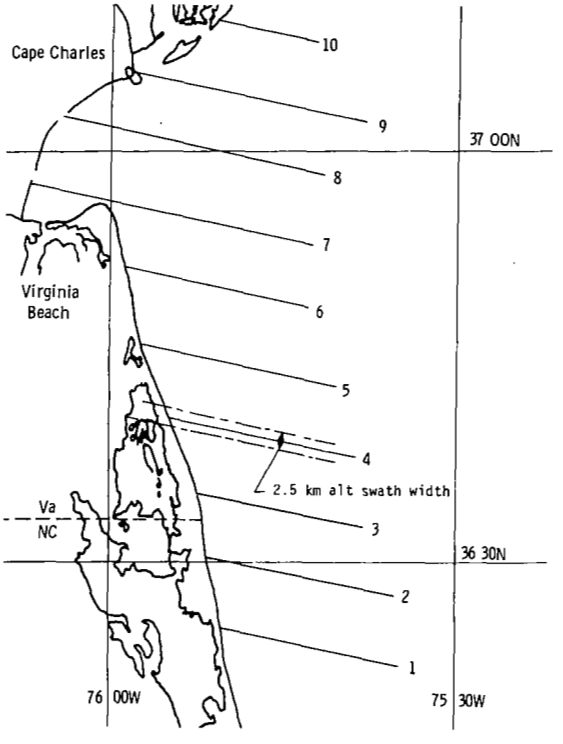

Figure 4. - Plume scan mission flight lines for 6/24/80.

be minimized. At this altitude, the swath width of the scanner is only 1.4 nmi. and two dimensional data products would not be very useful.

Sediment profiles along each baseline were generated using the calibration data from figure 3. Only the 25 scanner pixels at nadir were used in the initial product and then this was smoothed to eliminate the usual electronic and scene noise inherent in high resolution scanner data. The profiles for baselines 6 and 3 are shown in figure 5. In general, there is a high sediment area near the coast and a more pronounced plume reaching a maximum around 6 to 10 nmi. offshore.

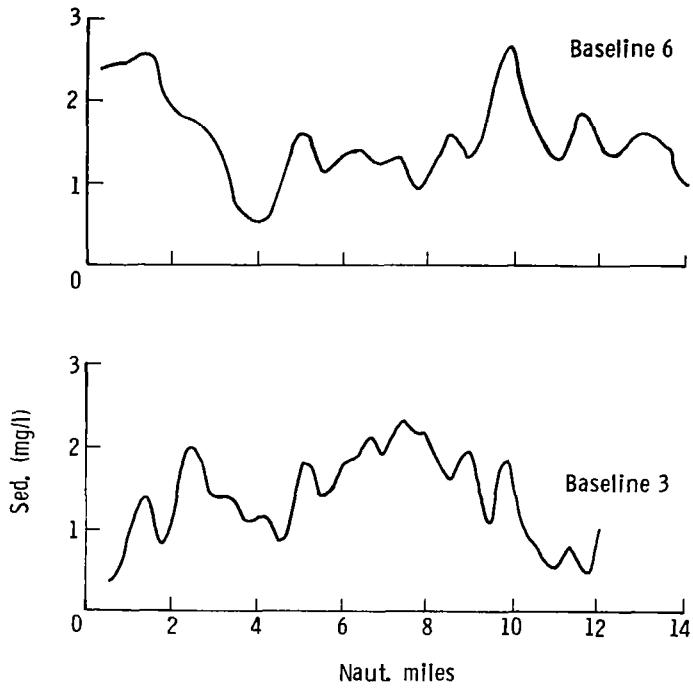

Figure 5. - Plume scan sediment profiles from baselines 3 and 6.

The sediment profiles from the ten baselines were used to construct the contour map presented in figure 6. Only the boundaries of the plume are shown; there were many oscillations about the 2 mg/l contour within the plume, but it was considered distracting to show all of the details on such a small plot. The main feature of the southern portion of the plume is the sediment maximum about 6 nmi. off the Virginia Beach coast. There is a similar maximum northeast of the Bay mouth.

The only ship stations within the scanner field of view are those shown in figure 6. The Warfield, which measured 18 mg/l sediment, was positioned between baselines 6 and 7. To explain this anomaly, we must look at the photography from the high altitude mission on June 20. Figure 7 is a T-11

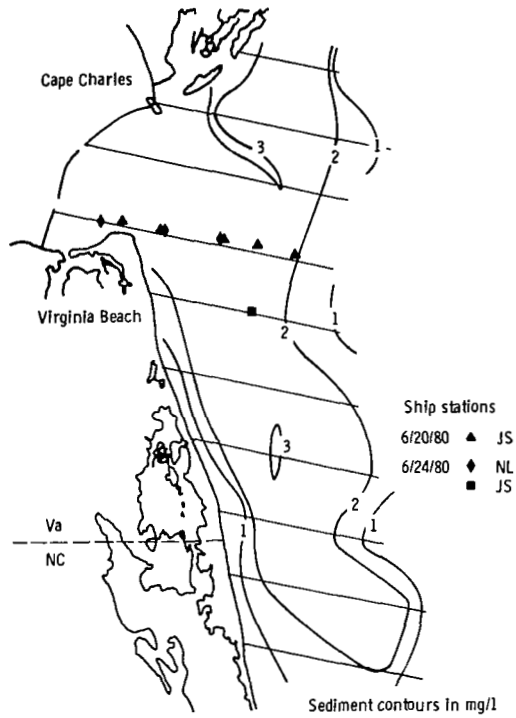

Figure 6. - Chesapeake Bay plume sediment contours for 6/24/80.

		1	2	3	4	5	6
1.	Ch a	1.000					
2.	Ph a	.992	1.000				
3.	Ch + Ph	.999	.990	1.000			
4.	N. Vol.	.024	-.065	.000	1.000		
5.	Vol.	-.380	-.538	-.424	.776	1.000	
6.	Tot. Sed.	.153	.152	.153	.935	.949	1.000

Table 1. - Correlation of ship data from Superflux II.

Figure 7.- Photo of Cape Henry area taken on 6/20/80 showing sediment plume.

image taken at 7 km over the Cape Henry area. A sediment plume is seen to follow the coast around Cape Henry and then spread into a front that curves from the Virginia Beach coast toward the northeast. A similar feature was probably present on June 24, in which case the baselines were not optimally located to monitor this important portion of the plume.

Chlorophyll also correlated with TBAMS radiance data, but it is necessary to investigate the relation between chlorophyll and total sediment to determine their degree of independence in the regression data. Table 1 gives the correlation between Ch a, Ph a, non-volatile, and volatile sediment components for the ship data used in the Superflux II data analysis. There were 24 chlorophyll and 17 sediment analyses and 4 volatile/non-volatile separations. The Ch a and Ph a measurements correlate well with each other and with their sum. Since both components influence the upwelled radiance spectra, the sum will be used in the correlation analysis, and where samples were taken at both 1m and 3m depths, an average of the two measurements was made. The low correlations in Table 1 between total sediment and the chlorophyll parameters are somewhat unusual in that these two parameters have generally been found to vary together in this same area. This is fortunate, however, since a regression between chlorophyll and radiances will be independent of sediment variations.

The three-band algorithm centered on Band 4 has been used in the chlorophyll regression analysis. The data are plotted in figure 8 where it is seen that there is an excellent correlation ($R^2 = 0.94$). Again, it should be noted that the radiance data were collected on two different days at two different altitudes; thus, the algorithm has done an excellent job of normalizing the atmospheric influence.

Chlorophyll profiles were generated along each baseline using the relation given in figure 8. A contour plot of this data is shown in figure 9. In the Bay mouth region, there is a minor extension of the contours seaward, but along the coast, the chlorophyll concentration falls off more rapidly. There is a major anomaly on baseline 4, similar to the sediment anomaly, but it is displaced toward the coast about 1.5 km or more. The Chesapeake Bay plume is therefore evident in the sediment map, but not in the chlorophyll distribution.

James Shelf Mission

The flight lines for the James Shelf Mission and the Chesapeake Bay Mission are shown in figure 10. Baseline 7 of the James Shelf Mission was initially flown at an altitude of 5.3 km, but clouds were encountered just beyond the Chesapeake Bay tower and the aircraft had to drop to 2.3 km. The return flight along baseline 8 began about 60 nmi. at sea at 2.3 km altitude. The temperature, sediment, and chlorophyll profiles from baseline 8 are shown in figure 11. Only the initial 25 nmi. of data are given, plotted in a west to east direction. The profiles represent nadir data smoothed in the same way as the previous data. The temperature plot indicates a major anomaly of approximately 1.4^{o} C. which might be the Gulf

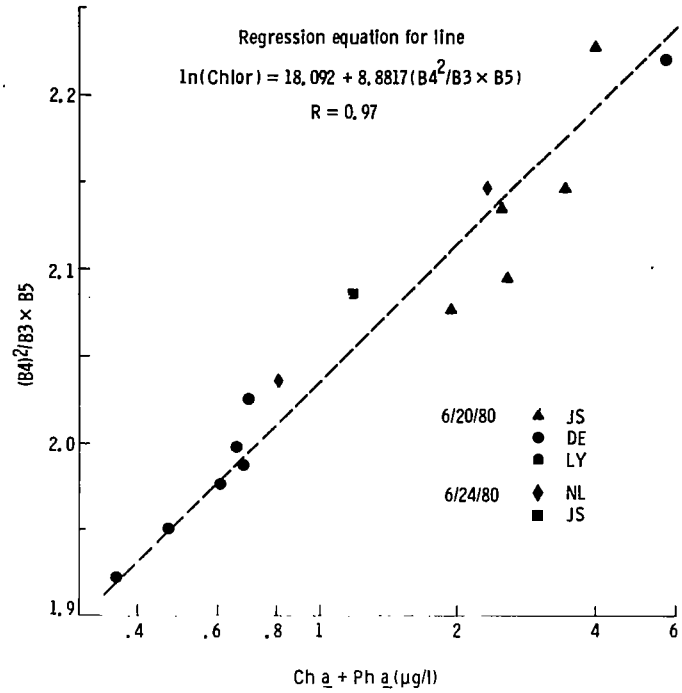

Figure 8. - Regression plot of Ch a + Ph a vs. band 4 algorithm.

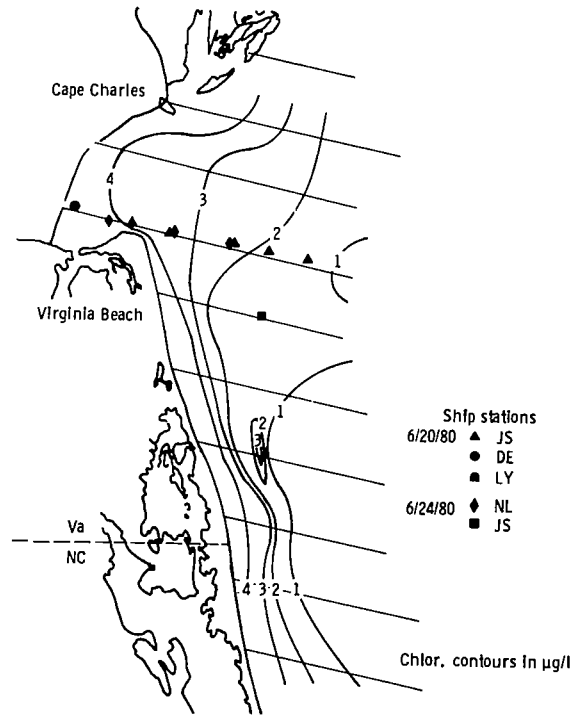

Figure 9. - Chesapeake Bay plume Ch a + Ph a contours for 6/24/80.

Figure 10. - Chesapeake Bay and James-shelf flight lines for 6/19/80 and 6/20/80.

Stream boundary. The sediment and chlorophyll data show only minor variations across this boundary; the data smoothing process would tend to minimize such effects. Baseline 7 profiles for sediment and chlorophyll shown in figure 12 are similar to those taken 4 days later during the plume scan mission.

Chesapeake Bay Mission

The calibration data for the Chesapeake Bay Mission are given in figure 13. There was not sufficient variation in the chlorophyll measurements to establish an adequate calibration. Note that the three-band algorithm centered on Band 5 has been used due to the higher values. The decrease in the radiance values with increasing chlorophyll at the lower end of the scale is real; this algorithm goes negative while the Band 4 algorithm goes positive below 8 to 10 μg/l. Another factor influencing the calibration was sunglint. The flight lines for this mission were basically oriented perpendicular to the Sun direction whereby the scanner looked into the Sun's reflection as it scanned off nadir. This may account for the negative shift in calibration for both parameters.

Figure 14 is a T-11 camera image taken from baseline 3 near Annapolis, Maryland. The vertical line indicates the flight direction, with north at the top. The horizontal line is what the scanner senses when it sweeps from right to left. Although the Sun's orientation is not exactly perpendicular to the flight line, it is evident that sunglint is dominating the scanner data in the right half of the scene. To illustrate this effect, the first

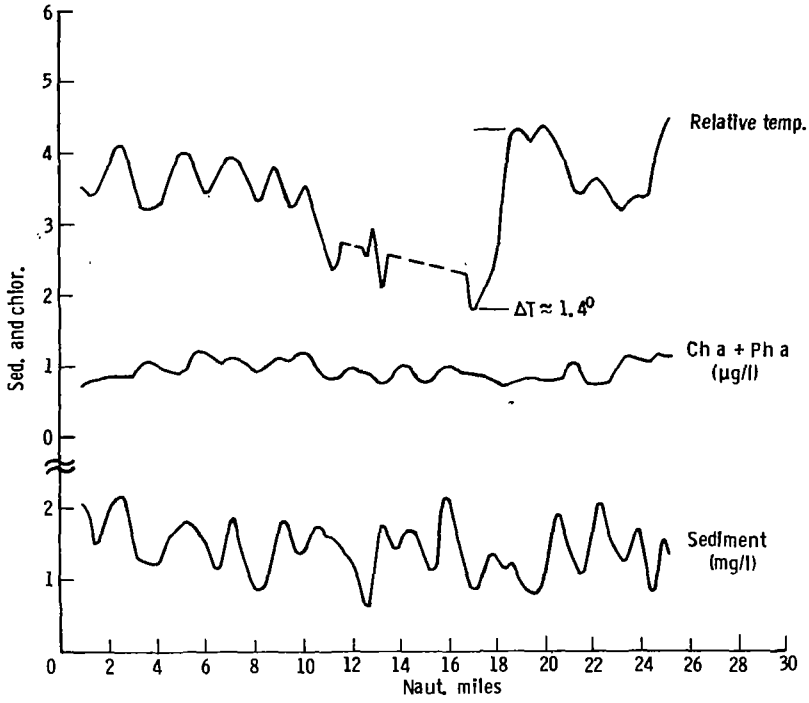

Figure 11. - James - shelf mission baseline 8 profiles.

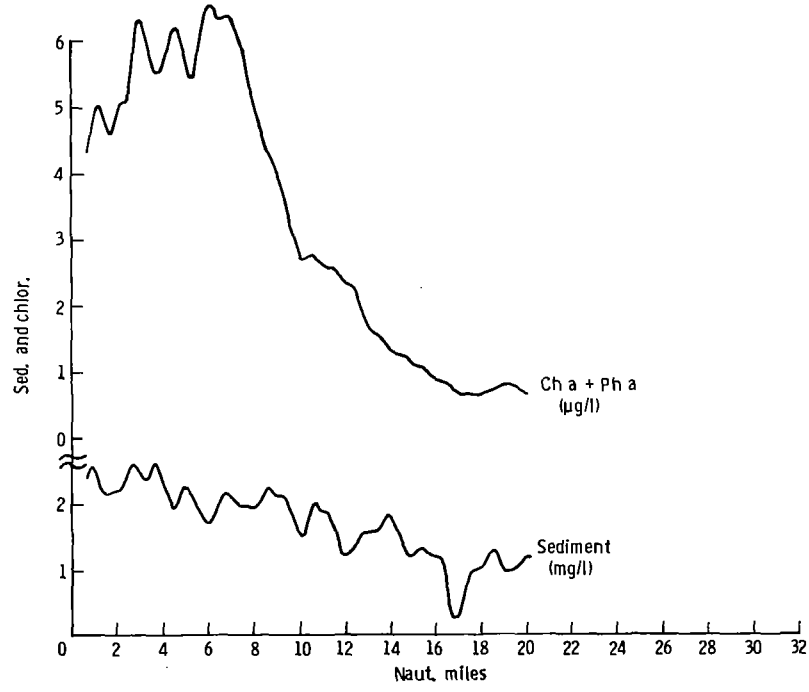

Figure 12. - James - shelf mission baseline 7 profiles.

1,000 scan lines from baseline 3, which contain no land data, were averaged to minimize the influence of sediment variations within the scene. The radiance variation in Band 4, along with the relative variations of the two sediment algorithms, is plotted in figure 15. The large spike in Band 4 is, of course, due to sunglint. The three-band sediment algorithm, which is a ten times enhancement about the value one, indicates a sediment variation from about 1.5 mg/l to 2.5 mg/l, according to the calibration curve in figure 13. By comparison, the Band 7/Band 8 algorithm seems to be more strongly influenced by the sunglint.

Although the three-band algorithm centered on Band 7 appears to normalize the sunglint within the data, it is apparent that the algorithm is not responding solely to subsurface sediment variations. The minimum value in the Band 4 scan has been displaced from nadir, which is at pixel number 350, to beyond pixel 450. Thus, sunglint is dominating most of the data and making it less useful for subsurface information. Surface effects are very pronounced, however, as is evident from figure 14, and operating the scanner in this mode could be beneficial for investigating parameters such as oil slicks.

The Sun elevation was about 50^{o} when the mission started at baseline 1 and by the time the aircraft reached the Delaware Bay, the Sun was over 70^{o}. The image in figure 16 is from baseline 6 near the mouth of the Bay. The aircraft was flying into the Sun and sunglint is evident at the center of the photo. Without subsurface calibration samples for this area, the TBAMS radiance data, which was taken along the vertical line in the photo, would not be effective for generating end products, such as contour maps.

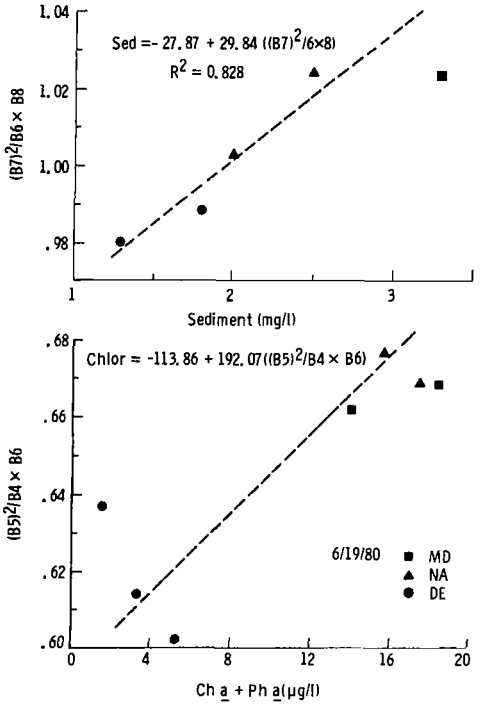

Figure 13. - Regression plots for sediment and chlorophyll from Chesapeake Bay mission.

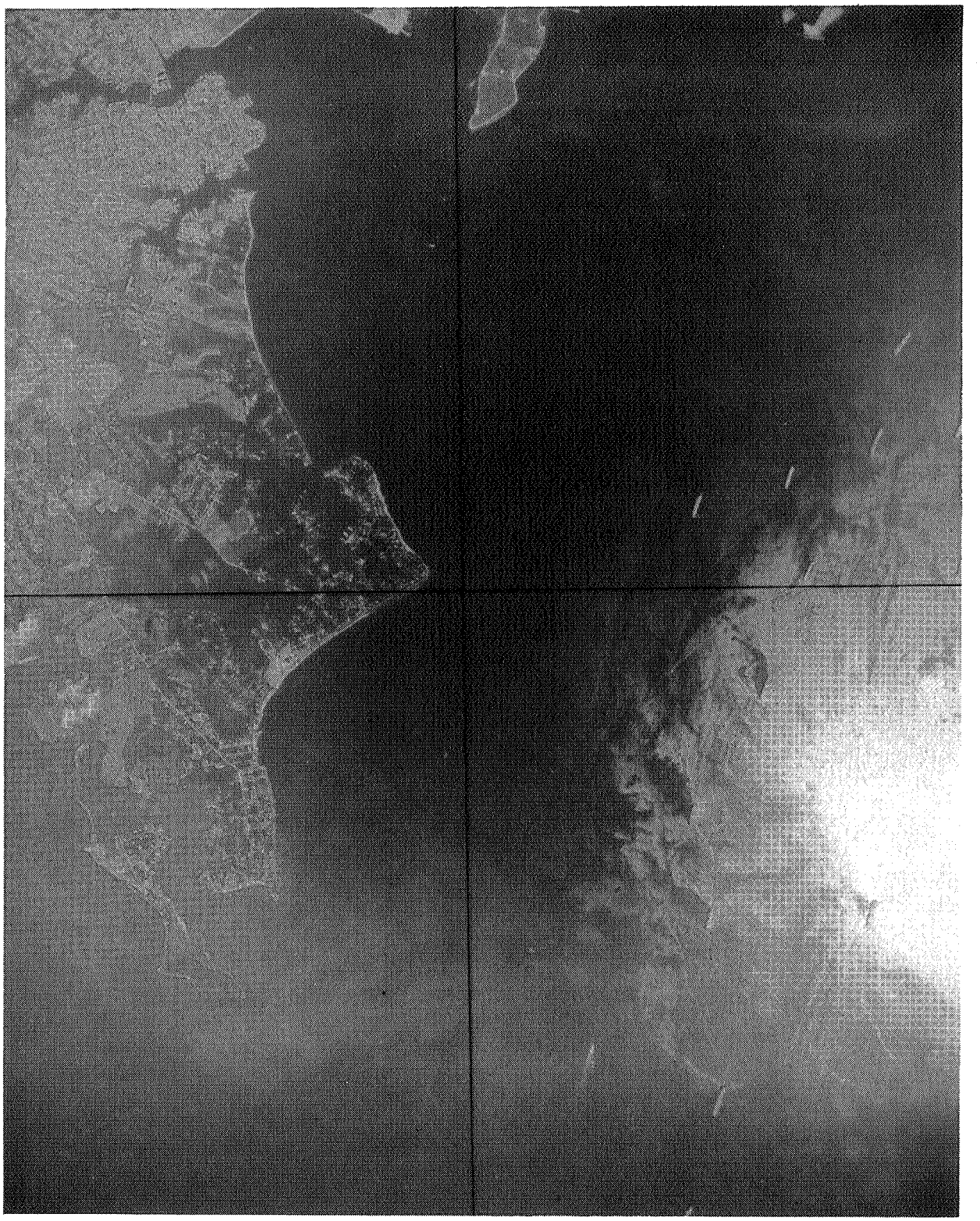

Figure 14.- Photo of Annapolis, MD area taken on 6/19/80.

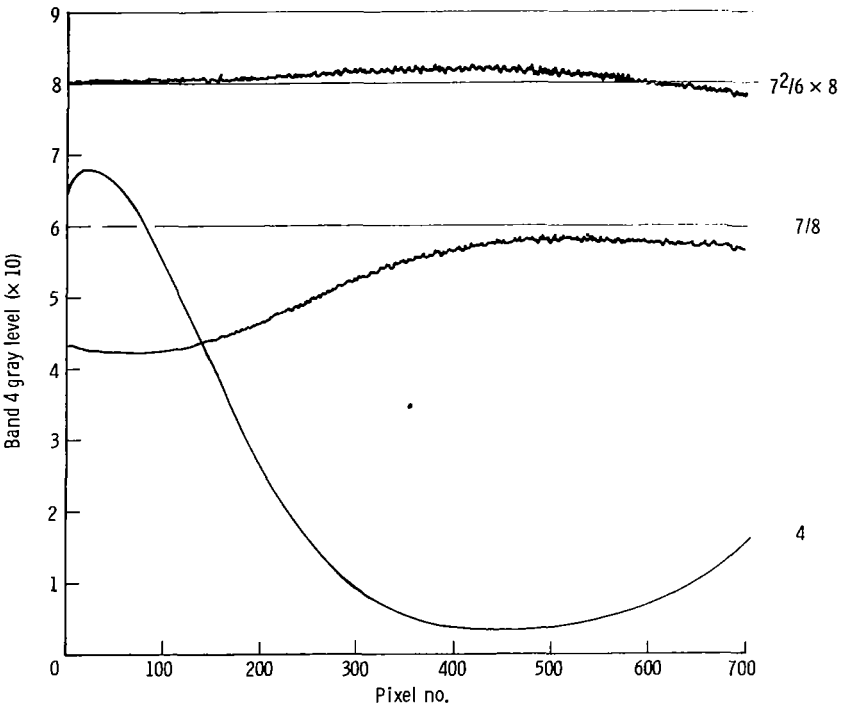

Figure 15. - Radiances from average of 1,000 scanlines beginning of baseline 3 Chesapeake Bay mission.

CONCLUSION

In summary, TBAMS has been successful in fulfilling its objectives during the Superflux II experiment. In particular, three highlights of the missions should be mentioned. First, an algorithm was demonstrated that monitored sediment and chlorophyll and was essentially insensitive to off-nadir radiance variations. Second, the Chesapeake Bay plume was successfully mapped when the sediment and chlorophyll variations were probably at a historic low. And third, it was found that sunglint did not interfere with the mapping mission, although it meant that the sensor was responding to surface reflections and not subsurface upwelling.

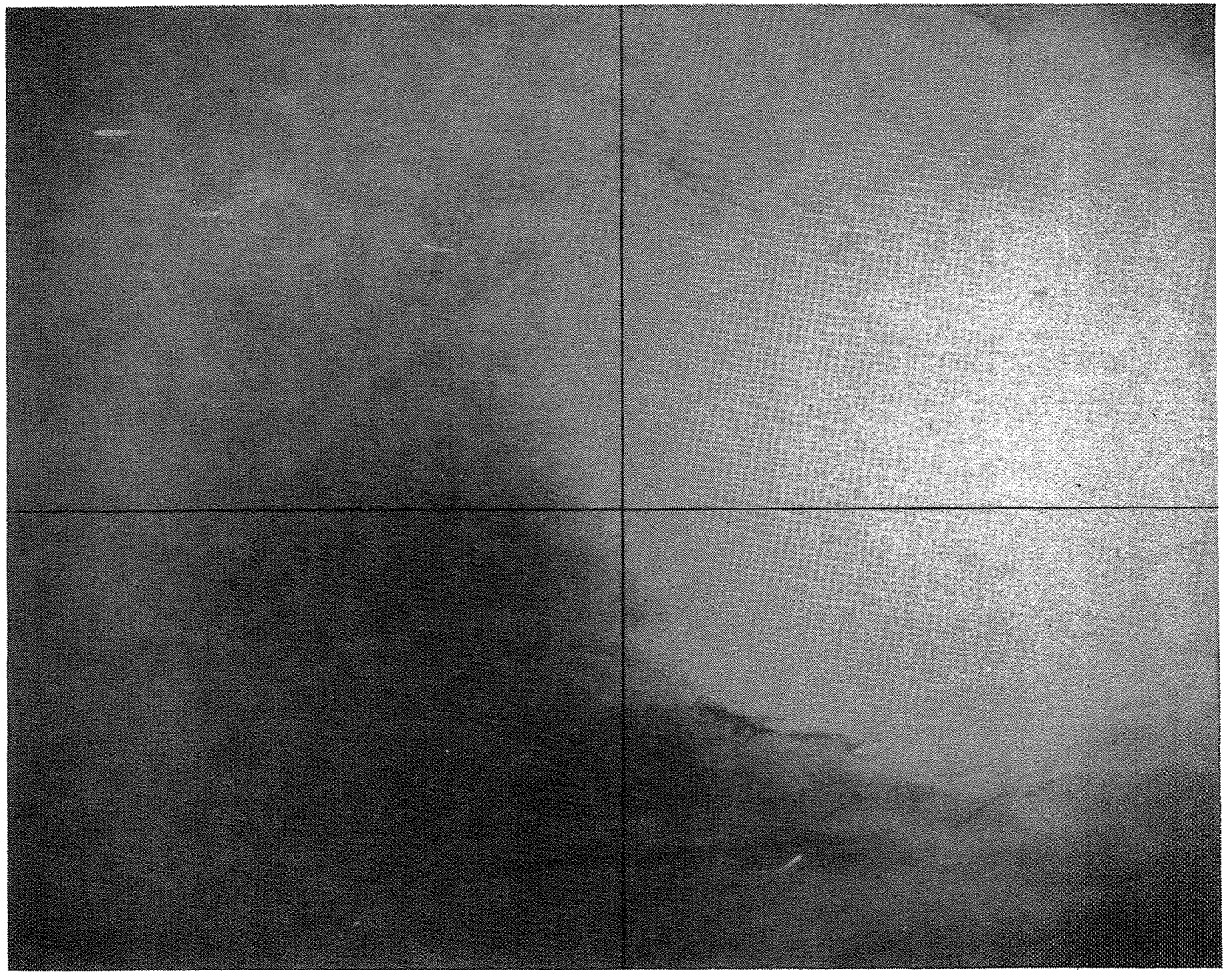

Figure 16.- Photo of Delaware Bay area taken on 6/20/80.

LASER REMOTE SENSING OF MARINE SEDIMENT LOAD AND ALGAL PIGMENTS: LABORATORY EXPERIMENTS

R. J. Exton and W. M. Houghton
NASA Langley Research Center

The fluorescence spectrum for natural waters contains several features which may be used for remote sensing of dissolved and suspended materials. Figure 1 shows the fluorescence emission spectrum for an estuarine water sample excited by an argon laser at 514.5 nm. The features of interest are: (1) scattering at the laser wavelength by particulates (Mie), (2) fluorescence from the pigments chlorophyl a and phycoerythrin, (3) Raman scattering by water, and (4) fluorescence by dissolved organic matter. These intensities increase with the concentration of the corresponding material and decrease with attenuation. Note that since the concentration of water is constant the Raman intensity provides a direct measure of attenuation.

The optical models relating intensities and concentrations are shown in figure 2. The first expression is the general case for laser backscatter assuming single scattering. The high altitude approximation, altitude >> remote sensing depth, allows the simple form shown rather than a nonintegrable integral form. Neither assumption significantly affects the relation between intensity and concentration. The symbols used are:

- P_o - laser output power
- A_c - area of collecting telescope
- n - refractive index of water
- h - altitude
- N - concentration
- σ^* - cross-section for backscatter
- γ - effective attenuation coefficient
- K - constant
- α - beam attenuation coefficient
- a - absorption coefficient
- b - scattering coefficient

The expression for the Mie and Raman intensities results directly from inserting the appropriate subscripts. In the Mie case the change in intensity with increasing concentration is not simple since both $N\sigma$ and γ increase. In general we expect a near linear relation at low turbidity changing to saturated condition at high turbidity. The Raman intensity varies inversely with attenuation only, since $N\sigma$ is constant for water. The final two expressions, Mie/Raman and fluor/Raman, use the Raman-attenuation relationship to remove the attenuation effect. The ratio of attenuation coefficients at the various wavelengths is approximately constant or at worst slowly varying, so that we expect the Raman intensity to indicate attenuation, Mie-to-Raman to indicate suspended sediment (total suspended solids), and fluorescence-to-Raman to indicate the concentration of the fluorescing material.

Laboratory experiments have been conducted to compare intensities and concentrations as indicated above. The apparatus shown in figure 3 was designed to provide a reasonable simulation of the remote sensing situation with natural samples brought back to the lab. Spectra are recorded with an Optical Multichannel Analyzer (OMA) which allows rapid recording on magnetic discs and subsequent algebraic manipulation. The detector is a silicon-intensified target vidicon tube preceded by an image intensifier. Spectral resolution is 2.5 nm. In our sampling procedure we emphasize returning the samples within 4 to 6 hours of collection and treating them so as to minimize biochemical stress. Samples for chemical and optical analysis are taken from the measuring tank immediately following the fluorescence measurement.

Figure 4 shows a typical recorded spectrum and the problem of overlapping peaks. The OMA allows subtracting the fluorescence due to Dissolved Organic Matter (DOM) and then integration of the remaining peaks to obtain true intensities. Figure 5 shows how the DOM spectrum is obtained by analysis of a filtered sample. The OMA normalizes this DOM curve in the region between 514.5 and 550 nm, judged to be free of Mie and phycoerythrin signal, and subtracts to produce the DOM corrected curve. This also determines the DOM intensity. Figure 6 shows the same procedure applied to a river sample containing a high level of DOM and no phycoerythrin.

Prior to studying natural samples, validation experiments were performed to check the expected behavior of the optical models. Figure 7 shows the results of a test in which a clay was added to distilled water and the intensities compared to attenuation. The various relations are as expected.

As a more rigorous test using natural samples a 1-day experiment was performed during September 1980. A wide variety of water types was included from fresh water in the James River to high salinity coastal water at the mouth of the Chesapeake Bay. Figure 8 shows the location of the sample sites. In addition, a few samples were made up by mixing ocean and river water. Figures 9 through 13 show the results of the intensities and chemical/optical comparisons. Inverse Raman intensity vs. attenuation gives excellent agreement--this is the most consistent and noise-free of all the comparisons. The Mie/Raman vs. TSS and chlorophyl/Raman vs. chlorophyl concentrations are also good. The DOM/RAM vs. DOC shows the worst comparison. This is probably caused by a nonfluorescing contribution to DOC. From our experience DOM fluorescence is due to humic material in land runoff. This is illustrated by the much better comparison of DOM/RAM vs. DOM absorption.

For one of the samples fluorescence was recorded using two different excitation wavelengths, shown in figure 14. This illustrates two considerations in choosing the exciting wavelength: (1) the variation of the chlorophyl excitation cross section with wavelength and (2) the overlap of spectral peaks. DOM and chlorophyl intensities are difficult to obtain using 532-nm excitation because of shift in the Mie and Raman peaks relative to the fixed fluorescence spectra of chlorophyl and phycoerythrin. Similarly for an excitation wavelength much below 510 nm the Raman and phycoerythrin peaks will begin to overlap. A wavelength of about 520 nm is optimum for good resolution of all features.

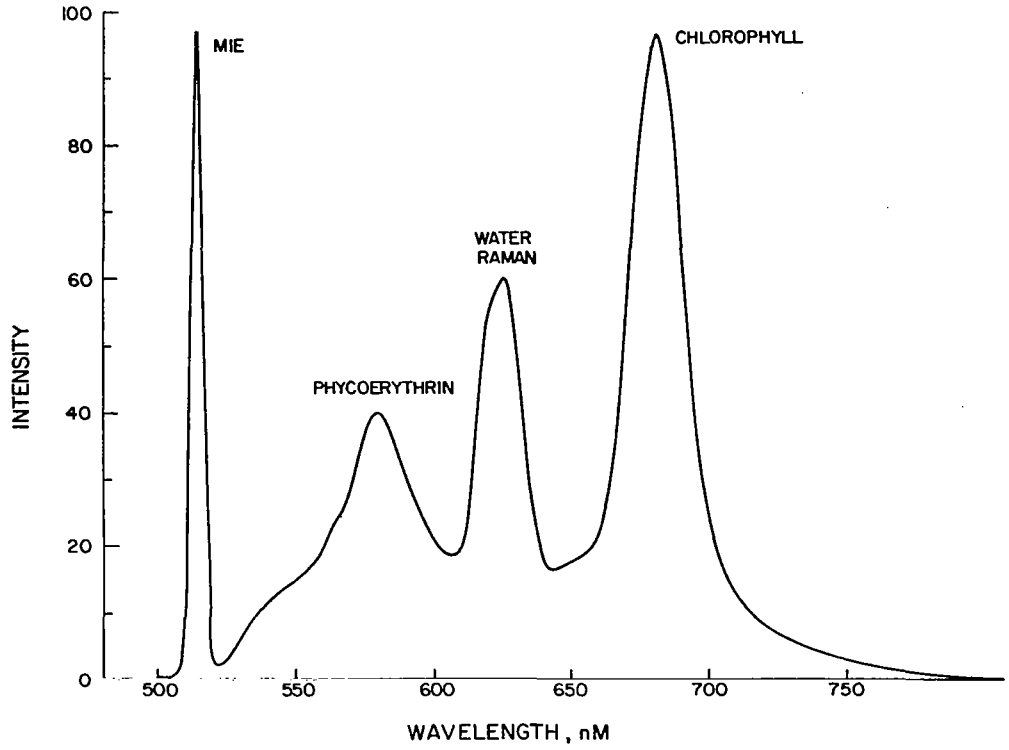

Figure 1

OPTICAL MODELS FOR LASER FLUOROSENSOR

SINGLE SCATTERING HIGH ALTITUDE

$$I = \frac{P_0 A_c}{n^2 h^2} \times \frac{N\sigma^*}{\gamma_1 + \gamma_2}$$

MIE

$$I = K \times \frac{N\sigma_M^*}{\gamma_M}$$

RAMAN

$$I = K \times \frac{N_R \sigma_R^*}{\gamma_R}$$

MIE / RAMAN

$$I = \frac{\gamma_M + \gamma_R}{\gamma_M} \times \frac{N_M \sigma_M^*}{N_R \sigma_R^*}$$

FLUOR. / RAMAN

$$I = \frac{\gamma_M + \gamma_R}{\gamma_M + \gamma_F} \times \frac{N_F \sigma_F^*}{N_R \sigma_R^*}$$

$\alpha = a + b$

$\gamma = a + K'b$

$\sigma^* = \sigma_{back}$

Figure 2

Figure 3

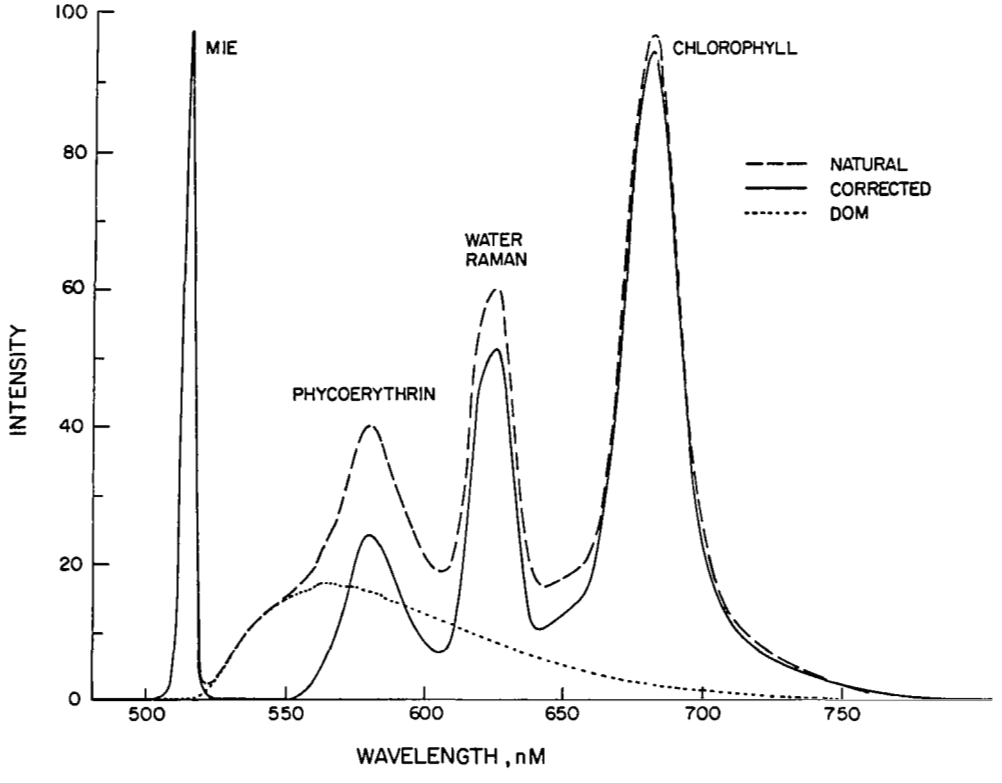

Figure 4

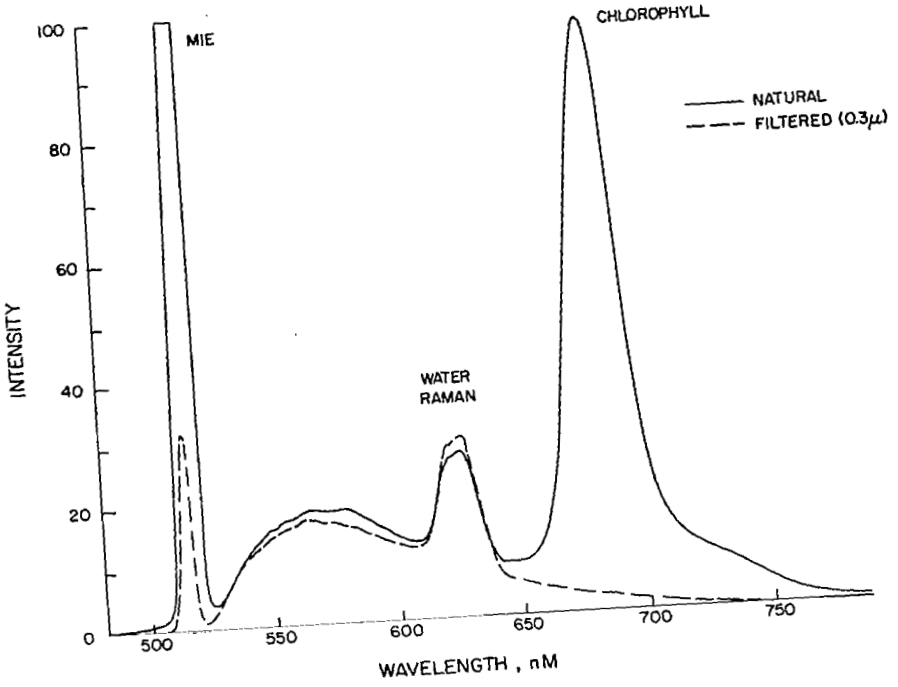

Figure 5

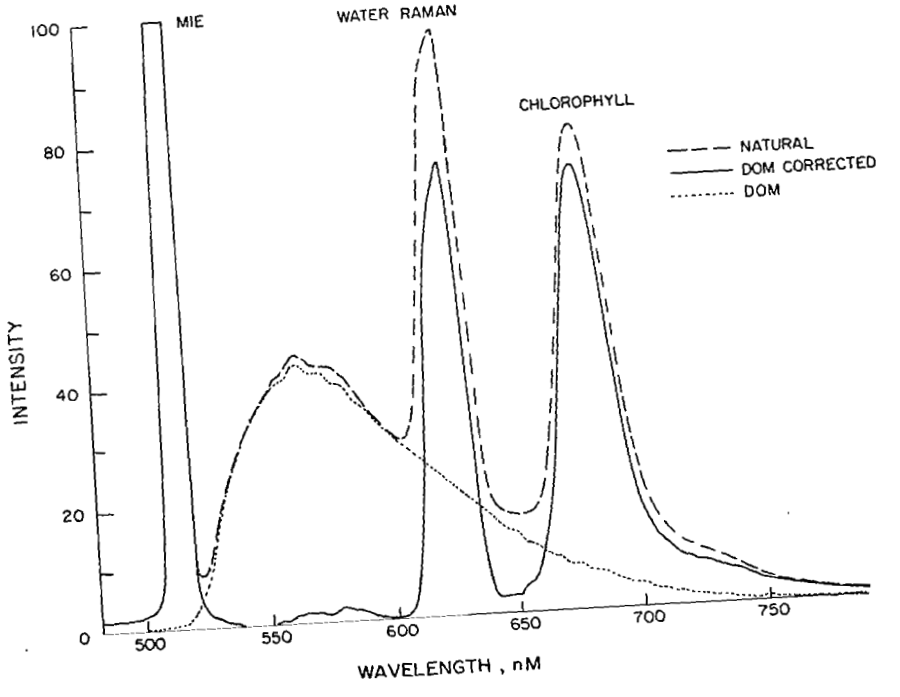

Figure 6

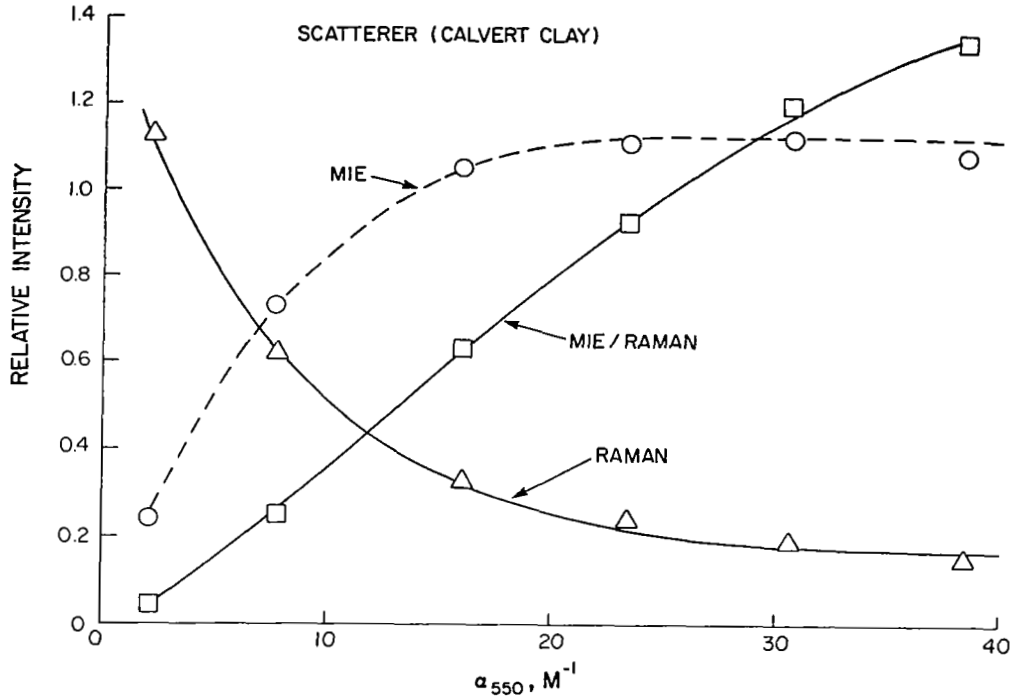

Figure 7

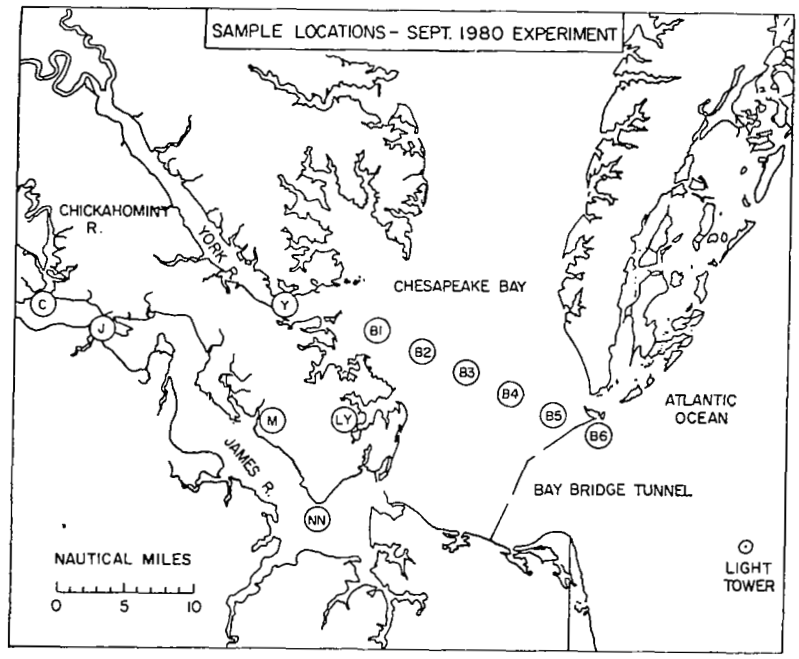

Figure 8

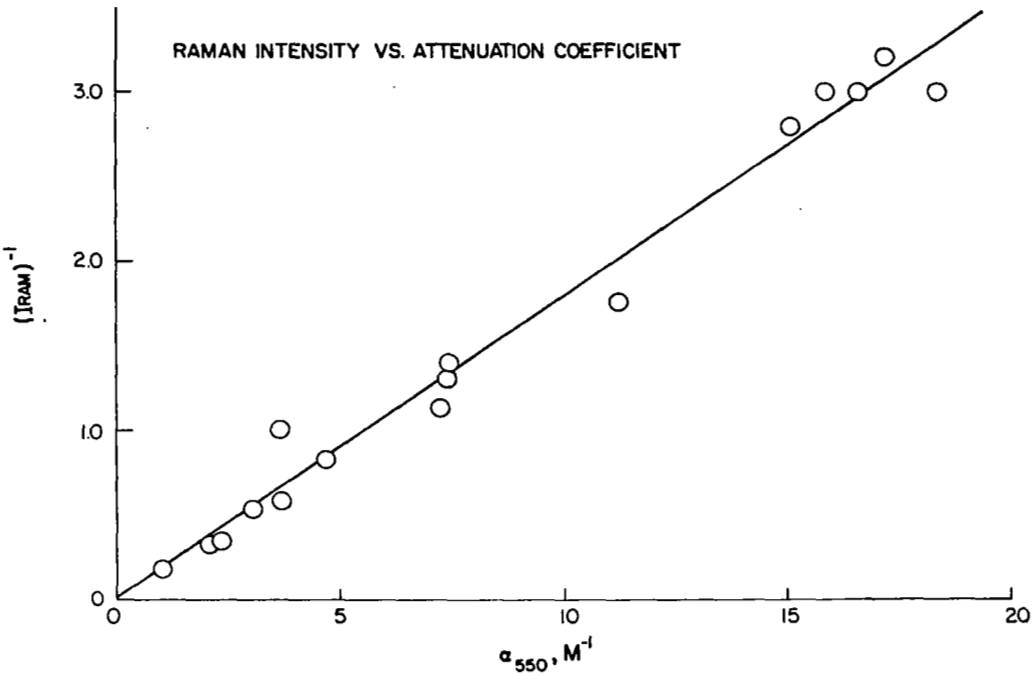

Figure 9

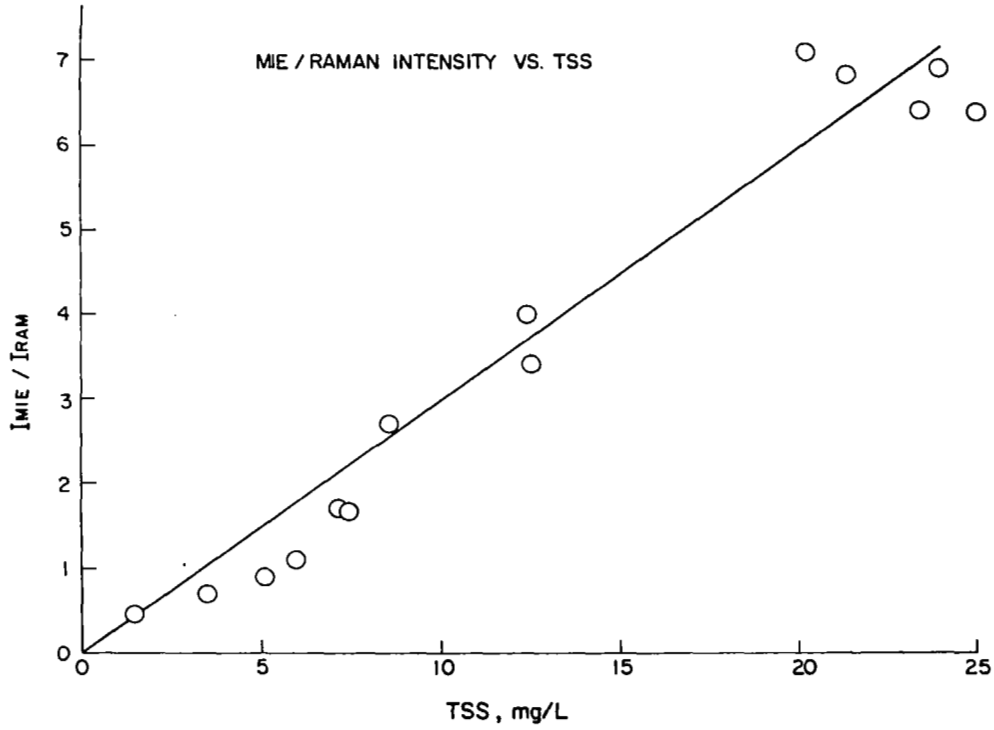

Figure 10

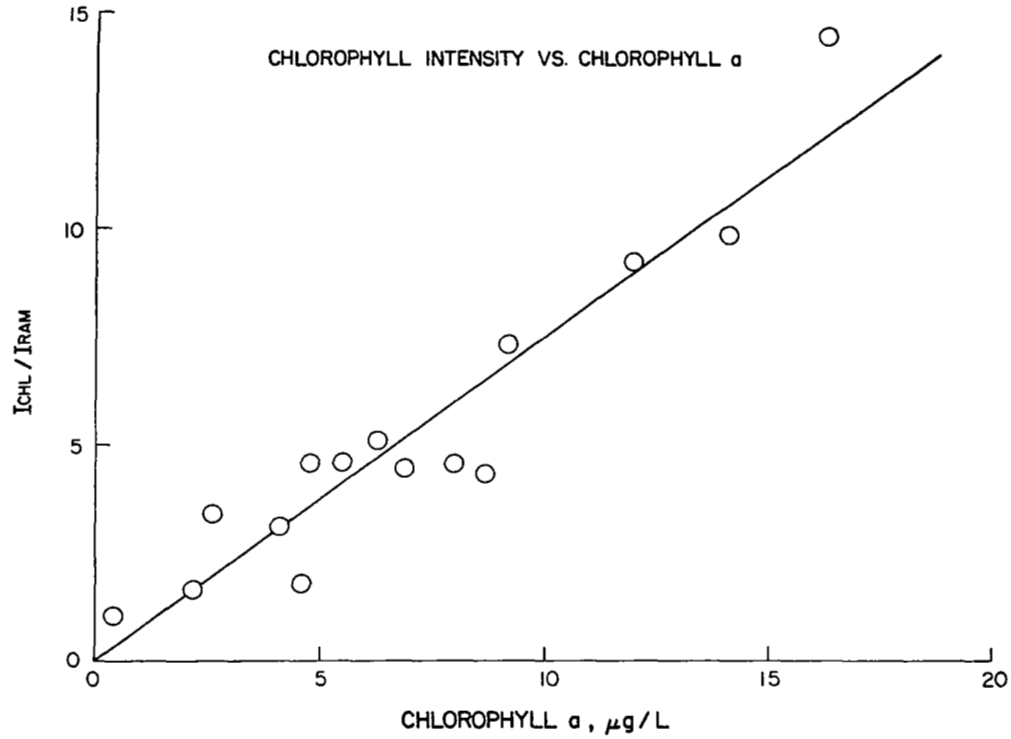

Figure 11

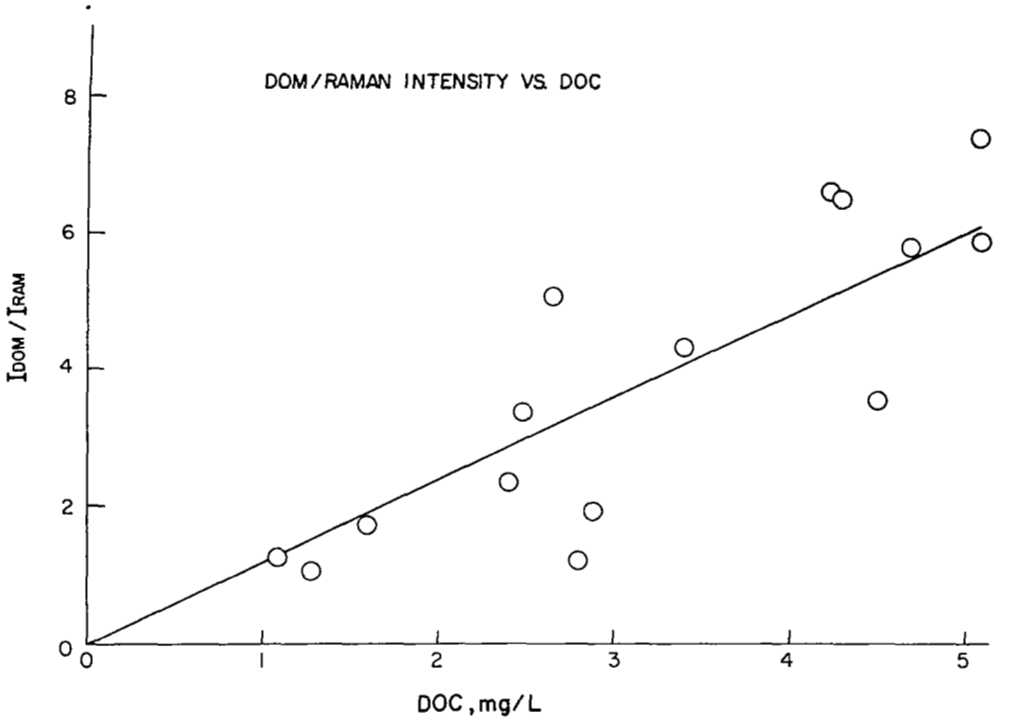

Figure 12

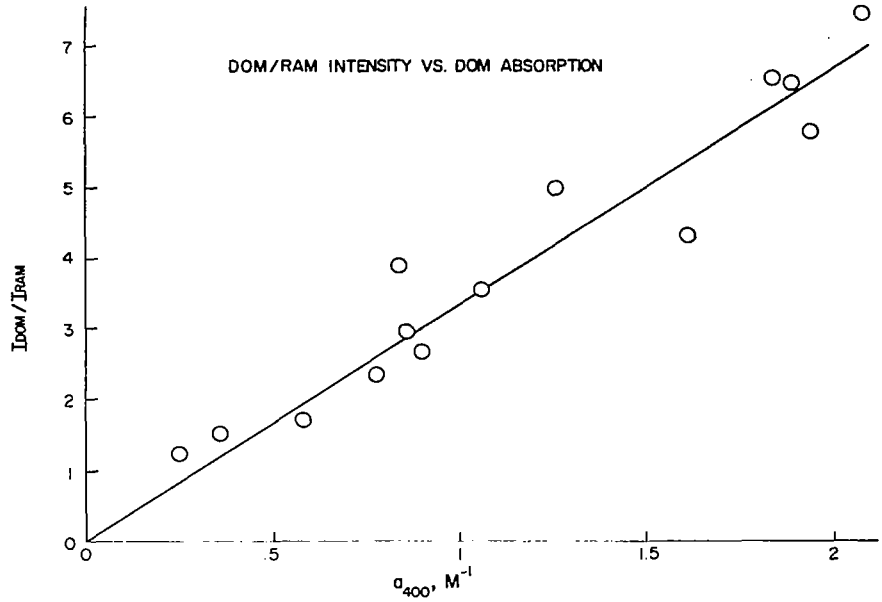

Figure 13

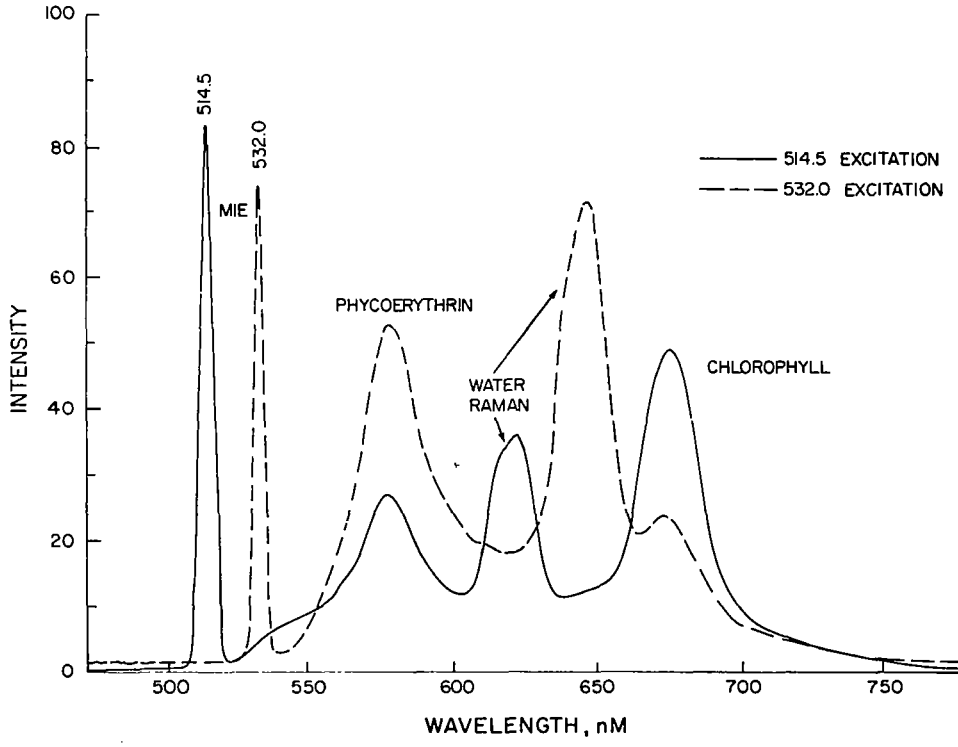

Figure 14

APPLICATION OF THE NASA AIRBORNE OCEANOGRAPHIC LIDAR TO THE MAPPING OF CHLOROPHYLL AND OTHER ORGANIC PIGMENTS

F. E. Hoge
NASA Wallops Flight Center
Wallops Island, Virginia

R. N. Swift
EG&G Washington Analytical Services Center, Inc.
Pocomoke City, Maryland

SUMMARY

This paper is intended to review laser fluorosensing techniques used for the airborne measurement of chlorophyll *a* and other naturally occurring waterborne pigments. Previous experiments demonstrating the utility of the Airborne Oceanographic Lidar (AOL) for assessment of various marine parameters are briefly discussed. The configuration of the AOL during the NOAA/NASA Superflux Experiments is described. The participation of the AOL in these experiments is presented and the preliminary results are discussed. This discussion centers on the importance of multispectral receiving capability in a laser fluorosensing system for providing reproducible measurements over wide areas having spatial variations in water column transmittance properties. This capability minimizes the number of truthing points required and is usable even in shallow estaurine areas where resuspension of bottom sediment is common. Finally, problems encountered on the Superflux missions and the resulting limitations on the AOL data sets are addressed and feasible solutions to these problems are provided.

INTRODUCTION

The NASA Wallops Flight Center (WFC) Airborne Oceanographic Lidar (AOL) participated in two series of field experiments conducted within the joint NOAA/NASA Superflux Study. During these experiments the AOL was flown onboard the WFC P-3A aircraft together with the Langley Research Center (LaRC) Multichannel Ocean Color Scanner (MOCS), L-band microwave radiometer, Test Bed Airborne Multispectral Scanner (TBAMS), and Airborne Lidar Oceanographic Probing Experiment (ALOPE) systems. The first series of Superflux missions was flown between March 17 and 19, 1980, while the second series was flown between June 20 and 27, 1980. Although all data sets have been reduced and have received preliminary analysis only those results from the June experiments are reported here and are hereafter labeled as WFC AOL Mission numbers 30, 31, 32 and 33.

These sensor systems formed a reasonably complementary group. The MOCS and TBAMS are passive multispectral scanners which can be directly analyzed with the active AOL multispectral system and can possibly be used to extend the utility of the lidar results which were acquired in a profiling mode. However, both of the passive sensors are ideally operated at a much higher altitude than 150 m and most of the passive data were obtained on separate missions. The L-band radiometer is a passive microwave sensor capable of determining the salinity of the surface water layer. The salinity information from the L-band radiometer together with thermal data from a Precision Radiometric Thermometer Model PRT-5 infrared sensor (recorded independently by the AOL and ALOPE systems) can be utilized to establish the physical framework necessary for ultimately interpreting the results of the optical sensors. The ALOPE, like the AOL, is a laser fluorosensing system but differs in that it utilizes two (and potentially four) laser wavelengths for excitation and has only a single channel receiver capability. The dual wavelength stimulation of the ALOPE system makes the recovery of relative concentrations of various phytoplankton color groups possible while the multispectral receiver capability of the AOL allows correction for spatial variations in water transmissivity properties through normalization with the 3400 cm^{-1} water Raman backscatter signal.

One of the most important objectives of the Superflux missions was to present an opportunity for testing various NASA remote sensing systems to meet NOAA/NMFS data acquisition requirements related to providing an initial baseline data set and future monitoring of Atlantic coastal waters. Further, these missions afforded NASA an opportunity to test its remote sensors in experiments where a number of surface truthing vessels were available and coordinated. Key to the joint program is the recognition by all that oceanic data acquisition requirements cannot be achieved using conventional techniques alone. Assessment goals can only be reached through extensive use of remote sensors (both airborne and spaceborne) and the prudent application of expensive conventional techniques to extend the reliable coverage of these remote sensors. The Superflux program seeks not only to determine the feasibility of remote sensing parameters of interest that can be directly measured by the sensors themselves, but also to evaluate the degree to which associated parameters (that are not directly measured by these sensors) can be reliably determined or inferred. Since the AOL has numerous potential applications beyond those demonstrated on the Superflux missions but which are likewise pertinent to the future NMFS assessment program, we have included a brief review of these capabilities as part of this paper.

The use of laser-induced water Raman backscatter for oil film detection and thickness measurement was demonstrated with the AOL over EPA-approved oil slicks in a series of experiments conducted in 1978. A 337.1-nm nitrogen laser was used to excite the 3400-cm^{-1} OH stretch band of natural ocean water beneath the oil slicks from an altitude of 150 m.[1] The signal strength of the 381-nm water Raman backscatter was always observed to decrease when the oil was encountered and then return to its original value after complete aircraft traversal of the floating slick. After removal of background and oil fluorescence contributions the ratio of the depressed-to-undepressed airborne

water Raman signal intensities, together with laboratory-measured oil extinction coefficients, was used to calculate the oil film thickness. In addition, analytical work currently ongoing at WFC indicates that thickness may also be recovered from airborne laser-induced fluorescence from the oil. Oil spill type classification or fingerprinting data analytical efforts are in progress using absolute oil fluorescence conversion efficiency techniques.

The measurement of the concentration of a fluorescent dye deployed in open ocean water was demonstrated with the AOL using similar techniques.[2] Since the amplitude of the Raman signal is directly proportional to the volume of water being accessed by the laser pulse, the amplitude of the fluorescence return varies directly as the number of dye molecules in that volume. In turbid waters only the very surface may be sampled and hence only high concentrations can be detected; whereas lower concentrations can be observed in clear water with significantly deeper beam penetration. Concentrations of Rhodamine WT dye (frequently used as a tag during circulation experiments) were measured to 2 ppb during field tests conducted in 1978.

The simultaneous measurement of Raman backscatter, chlorophyll *a*, and other naturally occurring pigments was demonstrated using the AOL in 1979 during experiments conducted in the German Bight and in estuarine waters in the vicinity of WFC.[3] These field experiments utilized essentially the same instrument configuration and technology reviewed in this paper, however the operation of the fluorosensor was improved and available surface truthing support was much better during the Superflux experiments, potentially allowing the Superflux results to be of greater analytical utility to marine scientists.

The feasibility of performing bathymetric measurements to depths of up to 10 m with an airborne lidar system was demonstrated using the AOL in a joint NASA/NOAA/NORDA program conducted in 1977.[4] The potential importance of this work to the future NMFS program would be the application of this previously developed depth resolution capability to resolving the vertical distribution of various fluorescent parameters such as chlorophyll *a*.[2,3]

INSTRUMENT DESCRIPTION

The Airborne Oceanographic Lidar (AOL) is a state-of-the-art scanning laser radar system having a multispectral time-gated receiving capability. The system is designed to allow adjustment in most transmitter and receiver settings. This built-in flexibility gives the AOL system potential application in many oceanographic areas. Portions of the hardware and software capabilities of the AOL have been briefly discussed elsewhere[1-5] but will be summarized and expanded as needed to illustrate the important aspects of the fluorosensing mode of the instrument as utilized during the Superflux experiments. Figures 1 and 2 should be consulted during this hardware description. Figure 2 is a detailed portion of the AOL spectrometer whose location in the system is given within Figure 1.

The AOL was operated in the fluorosensing mode during all of the Superflux missions. The AOL system laser (Avco Model C-5000) was entirely replaced with a frequency-doubled Nd:YAG laser having a 532.1-nm output wavelength. A high speed silicon photodiode viewed radiation extraneously scattered from the first folding mirror to provide the start pulse timing and monitoring of the analog output pulse power signal. Digitization and recording of this signal allow the data to be corrected for laser output power variations. The pulsed laser output is folded twice through 90° in the horizontal plane of the upper tier into the adjustable beam divergence/collimating lens. The laser output beam divergence of the frequency-doubled YAG laser is controllable only between 0.3 and 5 mrad. Minimum divergence was used during all of these field experiments. The beam is then folded directly downward through the main receiver folding flat, finally striking the angle-adjustable nutating scan mirror. The scan mirror is 56 cm in diameter and is connected at its center in a wheel-and-axle type configuration. This mirror is integrally connected with an adjustable concentric counterbalance wheel so that the entire mechanism does not vibrate when the mirror is rotated in nonperpendicular positions of 5, 10, or 15°. A setting of 15° off nadir was used for all Superflux missions and the data were obtained in a nonscanning mode. This scan mirror finally directs the beam to the ocean surface. The total surface, volume, and/or ocean bottom backscattered signals return through the same path but because of their uncollimated spatial extent are principally directed into the 30.5-cm Cassegrainian receiving telescope. The horizontal and vertical fields of view of the receiving telescope are each separately controlled by a pair of operator-adjustable focal plane knife-edges. The radiation is then collimated to eliminate undesirable skewing of the bandpass by subsequent narrowband interference filters. The radiation is then focused 3 cm behind the face of the EMI D-279 PMT to avoid weak photocathode areas. The combination 45° folding flat and beam splitter located between the collimating lenses and the narrowband interference filter is used only in the fluorosensing mode.

The beam-splitting mirror directs a major portion of the excitation wavelength and the fluorescent return signal into the fluorosensing detector assembly. The YAG laser excitation wavelength (532 nm) component of the return signal was rejected from the spectrometer by a Kodak 21 high-pass (wavelength) filter. This filter rejects radiation below 540 nm. A small amount of the surface return signal is allowed to pass through a small 1-cm opening in the beam splitter where it is sensed by the bathymetry photomultiplier tube and subsequently used to measure slant range and to generate the gate pulses for the analog-to-digital charge digitizers (CD). A 0.3-nm narrowband interference filter was placed into the 11-cm diameter collimated return beam just behind the beam splitter. The bathymetry photomultiplier tube portion of the system must therefore function during all modes of operation and slant range information is available at all times.

The fluorosensing detection assembly contains an 11-cm diameter transmission diffraction grating blazed for 480.0 nm having 600 grooves/mm. An 11-cm diameter simple lens brings the dispersed radiation to the entrance surface of thirty-six quartz light guides. These guides are optically coupled to two separate banks of 20 RCA C71042 phototubes of which a total of only thirty-six were used in these experiments. The front faces of the light guides are

physically located in the focal plane to receive the dispersed spectral components nominally from 390 to 800 nm. This configuration yields a spectral bandwidth of 11.25 nm for each channel. The tubes are not shuttered or gated but remain active at all times. Ambient background radiation rejection is provided by the 0-20 mrad adjustable field-of-view (FOV) knife-edge pairs located at the focal point of the receiving telescope. The optimum operational FOV for our field tests was experimentally determined to be 4 mrad by observing the water Raman SNR. The pulsed analog outputs of the entire bank of phototubes are routed to ac-coupled buffer amplifiers that drive each of the thirty-six charge digitizer (CD) input channels. The amplifiers respond only to wide bandwidth fluorescent pulses, and thus response to background noise is very minimal permitting full daylight operation.

The fluorosensor PMT analog outputs are routed through 10X buffer amplifiers and digitized. All thirty-six charge digitizers are simultaneously gated ON to obtain the entire spectral waveform at a temporal position determined by the surface return signal from the bathymetry photomultiplier tube. Additionally, the CDs can be held ON for selectable integration times of 15 to 150 nsec using a LeCroy model 161 discriminator. An integration period of approximately 30 nsec was used during all of the Superflux missions. The CDs are fundamentally the analog-to-digital converters for the AOL spectral waveform digitizing system. The charge digitizers are 10 bit yielding a maximum of 1024 counts. Their output is directed through CAMAC standard instrumentation to a Hewlett-Packard 21MX computer for recording. With proper delay adjustments relative to the bathymetry PMT-derived surface return, the spectral waveforms may be taken at any position above or below the ocean surface. In this experiment the spectral waveform data acquisition was started 3 nsec prior to encountering the surface and terminated 30 nsec later. Summary information and additional instrumentation details may be found in Refs. 1 through 4.

DESCRIPTION OF THE FIELD WORK

During the June 1980 Superflux field experiments the AOL was flown on five separate missions, however the first mission of this series was flown near the mouth of the Delaware Bay and is not included in this paper. Figures 3 and 4 are computer plots of the flightlines occupied on the remaining four missions. The purposes of the AOL participation in these missions were (1) to assess the precision and accuracy of the system in providing total chlorophyll *a* concentration in the surface layer (upper 5 m) of water column, and (2) to provide wide area, nearly synoptic maps of the distribution of water transmissivity and chlorophyll *a* concentration (as well as the relative distribution of other organic pigments) in the vicinity of the Chesapeake Bay mouth and adjacent Atlantic shelf. Further, the AOL was used to digitally record the analog output of the PRT-5 infrared thermal sensor.

The flightlines were arranged primarily to provide wide areal coverage of the study area with convergence and closer spacing around the vicinity of Cape Henry where spatial gradients of the various parameters were expected to be the most pronounced. On some of the missions however certain of the flightlines were repeated or arranged in a crossing pattern. Although the repeating lines do not appear to provide optimal use of prime flight time they do provide an effective measure of precision and repeatability for an unproven sensor as will be seen in the succeeding section of this paper. Likewise, crossing or highly converging lines can be used to assess the internal consistency of a sensor provided the temporal separation between the lines is short relative to the temporal flux in parameter concentrations. Once the precision of the sensor is documented, however, the crossing lines having larger temporal separation can be used to infer dynamic changes in parameters. Unfortunately available flight time did not permit the inclusion of many repeating or crossing lines.

The surface truthing logistics were coordinated by the LaRC experiment team. On each mission various research vessels were deployed at points designed to be coincident with the projected ground track of the P-3 aircraft. The results of surface measurements taken at these points would then serve as standards against which to test the accuracy of the onboard sensors and these measurements would subsequently allow the relative values obtained by the sensors to be converted into absolute concentrations. Once converted, the airborne sensors allow extension of the reliable surface measurements over wide areas in a reasonably synoptic manner. The utility of this technique is of course dependent on the ship's sampling the same watermass that was observed by the sensor. Temporal and spatial separation between airborne and surface sampling degrades the confidence that can be attached to the sensor data. In practice, perfect sampling coincidence is nearly impossible, therefore the relative variation in the gradients of the constituents under consideration both in time and space must be taken into account in assessing the degree of reliability to be attached to the sensor testing. This topic will be expanded in the concluding portion of the next section of this paper.

DISCUSSION OF RESULTS

This section has been divided into subsections in order to pursue discussion of several separate but related aspects of the AOL participation in the Superflux experiments. The initial subsection describes the multispectral data obtained by the AOL, the second portion of this section examines the necessity for applying corrections to the spectra for spatial variations in the transmissivity properties of the water column, and the final section examines the degree of confidence that can be placed on the AOL data obtained during the Superflux experiments. The results presented herein must be considered preliminary in that more analysis will be required before it will be a fully functional data set. As will be pointed out in the succeeding discussion, there are additional corrections to be made to the data with regard

to adjusting the spectral waveform. Beyond this there are some inherent errors for which we will not be able to compensate. These errors do not appear to seriously degrade the utility of the AOL results. Feasible solutions to these remaining problems will be presented and most of these solutions are either in the process of being implemented or can be effected by the time the next mission of this type is undertaken. The logistical difficulties described in the final portion of this section should not be construed as criticism of the experiment team but rather as suggestions for improving future efforts.

AOL Data Description

The 532.1-nm excitation wavelength provided by the frequency-doubled YAG laser yields spectra similar to those obtained from Chesapeake Bay water in work performed at the Langley Research Center (LaRC) laboratories.[6] Similar spectra were obtained by the airborne lidar system (AOL) on the Superflux experiments. Compare the laser-induced spectra obtained within the bay plume (Figure 5a) with one obtained offshore (Figure 5b). The locations of these sampling points are noted on Figure 4. Each airborne spectrum is a simple average of five seconds of data gathered at 6.25 pps or 31 waveforms. The three spectral lines of most interest are labeled in both Figures 5a and 5b. These spectral peaks correspond to the Raman backscatter, chlorophyll _a_, and organic pigment lines at 645 nm, 685 nm, and 580 nm respectively. The organic pigment line has not been fully understood and is currently being investigated in joint WFC/LaRC experiments. Openings were provided through the longpass filter to allow a small amount of on-wavelength backscatter into the spectrometer at 532 nm. These spectra have not been corrected for a slight distortion from the Kodak 21 longpass filter used to partially reject the laser wavelength from the spectra. Also, cross-channel interference between the Raman peak return and the chlorophyll _a_ return have not been deconvolved. This may produce some error in both very clear, offshore waters where our relative chlorophyll values may be slightly elevated or in turbid, nearshore waters with strong chlorophyll responses where our relative chlorophyll values may be too low.

In analytical work performed on the Superflux data sets at WFC we have produced a number of data products that we feel will be useful in interpreting the results of the field experiments and in preparing technical papers some of which are planned for joint authorship with other Superflux investigators. These products include time-series cross-sections and spatial contour plots of pigment, Raman, and chlorophyll _a_ spectral peaks. The time-series cross-sectional projections have been prepared for all passes taken during the Superflux experiment while the contoured projections have been produced only for the missions flown on June 23, 25 and 27, 1980. The mission flown on June 20th had too few flightlines to allow contouring. Figure 6 is an example of a cross-section from a pass flown on June 23rd and is typical of the plots obtained on most of the passes flown within the bay or across the bay outflow plume. Note the large increase in chlorophyll _a_ as the mouth of the bay is approached during the latter portion of the flightline. The actual location of this flightline 4 is given in Figure 3b. Figures 7-9 are individual contour plots of Raman, chlorophyll _a_ and pigment produced from the mission flown on June 23. The dotted segments indicate the actual aircraft flight ground tracks. Note that the Raman values vary inversely with attenuation, thus the higher Raman values on these

plots represent clearer water while the lower values indicate more turbidity in the upper layer of the water column. Of particular interest are the distribution of clear and turbid watermasses on the Raman contour plot and the presence of the outflow plume evident on all three contour plots. The contour plot in Figure 7 has been corrected only for altitude and laser power variations. Contour plots 8 and 9 have been corrected for altitude, laser power fluctuations, and spatial variations in the optical properties of the watermass. This latter correction has been made to the organic pigments and chlorophyll *a* response peaks by normalization with the water Raman response peak of Figure 7. This normalization procedure will be discussed in detail in the next subsection. The cross-sections as well as the contoured projections made from them are presently relative parameter values comparable only to other parameter values taken within the same data set. Through the application of available truth measurements it appears that the AOL chlorophyll *a* fluorescence data can be converted into absolute units of concentration on at least three of the four Superflux missions. This will be discussed subsequently. As we shall see, the truth data from Figure 12b can be used to convert Figure 8 to an absolute chlorophyll *a* concentration map.

Three major problems remain in the AOL Superflux data sets. These are (1) spectral distortion from the Kodak 21 filter; (2) separation of Gelbstoff fluorescence from that of the other organic pigments; and (3) the spectral overlap of the water Raman backscatter and chlorophyll *a* fluorescence signals. Correction for the Kodak 21 filter appears to be the least significant of these difficulties. The spectral properties of this filter are well known and thus corrections for distortion can be applied in a straightforward manner. The other two problems are more difficult to address. The separation of Gelbstoff fluorescence from the responses of the other organic pigments cannot be fully addressed in the Superflux data sets and will likely not be attempted. The problems due to spectral overlap of the chlorophyll *a* and Raman signals can be corrected for the most part through interpolation techniques similar to those presented in Reference 1. As will be shown in the final portion of this section, this latter problem does not appear to present a serious error in the Superflux data sets where the total chlorophyll *a* concentration primarily remained between 0.2 and 5.0 μg/ℓ. This error, however, would become significant in conditions of high total chlorophyll *a* concentration.

The solution to both of these latter problems appears to involve a shift in the laser wavelength. A field study aimed at resolving both the photo-pigments and chlorophyll might best be addressed by using a fluorosensing system equipped with two laser wavelengths. One laser could be operated at a wavelength in the 515-520 nm region. This excitation wavelength would place the Raman backscatter line in the 620- to 628-nm portion of the spectrum, thus providing a reasonable separation from the chlorophyll line at 685 nm. The other laser could be a nitrogen system at 337.1-nm excitation wavelength allowing better definition of the broad Gelbstoff response. These lasers could be alternately pulsed or be used one at a time on alternating passes made over the same flightline.

Corrections for Spatial Variations in Water Transmissivity Properties

The importance in laser fluorosensing of applying corrections to the various fluorescence responses for spatial variation in water column transmittance properties cannot be overstressed for the precise recovery of even relative concentrations of various parameters. The transmittance of the water can be measured from the participating surface truth vessels using in situ techniques for recovering α and K, the beam and diffuse attenuation coefficients respectively. Alternately, the "apparent" transmissivity of the water can be directly acquired by the laser fluorosensor itself by monitoring the 3400 cm^{-1} water Raman backscatter signal. The Raman backscatter signal is proportional to the number of water molecules accessed by the laser pulse during the receiver integration period. If the Raman line is sufficiently close to the response line of the parameter to be corrected the relative concentration of that parameter can be found by simply normalizing its response intensity with that of the water Raman. This technique has been recently demonstrated with a dual channel receiver[7,8] using a 50/50 beam splitter and respectively isolating the Raman and chlorophyll *a* lines with a 10-nm interference filter centered at 560 nm and a 23-nm filter centered at 685 nm. A dual channel receiving system is however restricted to monitoring single parameters and necessarily the resulting data cannot be corrected for spectral interference from other responses such as described in the preceding section. Further, with increasing importance potentially attached to other fluorescence response wavelengths[6,9,10] we feel that a multichannel receiving capability is the appropriate type sensor for baseline assessment and monitoring in estuarine and nearshore water bodies.

Figure 10 illustrates the importance of the normalization procedure. The cross sections shown in Figure 10 are time history plots of the peak channel amplitudes of the organic pigment, Raman, and chlorophyll *a* lines for Pass 8 of the Superflux mission flown on June 27, 1981. The location of Pass 8 is shown in Figure 4. The chlorophyll *a* and pigment profiles in Figure 10a have not been normalized with the water Raman data. In Figure 10b the chlorophyll *a* and pigment peak values have been divided (or normalized) by the corresponding 645-nm Raman peak obtained simultaneously. The amplitude of the Raman peak channel is of course not normalized and remains the same in both Figure 10a and Figure 10b. The Raman cross section is representative of the relative water transmissivity and thus increases in amplitude in areas of clearer water and correspondingly lowers in amplitude in areas of more turbid water. As expected, the Raman cross section indicates that the offshore water is more transmissive than the water just off Cape Henry where the flightline was discontinued. Notice that the raw chlorophyll *a* and organic pigment responses appear to only increase slightly over the flightline on Figure 10a. In Figure 10b however, the corrected responses of both the chlorophyll and organic pigments are decreased from their previous values offshore where the Raman signal indicates a larger volume of water was accessed by the laser pulse. They are larger nearshore in the more turbid watermass where a smaller volume of water was accessed as indicated by the lower Raman signal.

Most of the flightlines flown during the Superflux experiments had variations in the spatial distribution of water transmittance similar to that shown in Figure 10. Patchiness in water clarity and chlorophyll concentration was especially evident within the bay proper and in the bay outflow flanking the Virginia shoreline south of Cape Henry. We have found these variations typical of most watermasses overflown within the Chesapeake and Delaware Bays, on the Atlantic shelf, and in the German Bight of the North Sea.

Results of AOL Self-Consistency Tests and Comparison with Surface Truth Measurements

The internal consistency and precision of the AOL can be adequately demonstrated by the reoccupation of flightlines within short time intervals or by flying a grid pattern of flightlines with many crossing points. Of the two options available we prefer the reoccupation of the same line since this procedure furnishes considerably more overlapping points, temporal separation between overlapping points can be minimized, and uncertainties in positioning as determined by the onboard Litton LTN-51 Inertial Navigation System (INS) or the auxiliary Loran-C system are reduced. The crossing grid pattern, on the other hand, allows maximum areal coverage while still presenting enough overlapping points to insure that no drift in the AOL system has taken place.

During the course of the Superflux experiments a number of lines were reoccupied during the same experiment. Of these data sets, however, only Passes 6 and 16 of the mission flown on June 27th are usable for testing sensor precision. The locations and flight directions of Passes 6 and 16 are labeled in Figure 4b. The remaining sets were either monotonous (located too far offshore or too far south of Cape Henry), had gross temporal separation, or in one case the set was flown at the very beginning of a mission when the AOL was still being adjusted and optimized.

Cross-sectional plots of Passes 6 and 16 are shown on Figure 11. The three parameters (chlorophyll, Raman, and pigment) of interest are labeled in the figure. The two passes were flown in opposite direction with respect to one another. The chlorophyll and pigment responses have been normalized with the Raman backscatter signal. Note the agreement in all cases, even down to relatively small-scale features. At this point we have not attempted to statistically quantify the agreement although it is our intention to do so as we continue our analysis of Superflux data.

Although only one set of passes can be compared in this manner from the Chesapeake Bay Superflux missions we have been able to compare three sets of passes from the Delaware Bay Superflux mission (June 1980) and two sets from missions flown in the German Bight area of the North Sea (1979).[3] All of these comparisons have been favorable indicating that the internal consistency of the AOL is dependable from mission to mission and over a time frame of one year.

Surface truth samples are not only useful for proving the accuracy of the AOL but are also required to allow extrapolation of absolute chlorophyll concentrations from the relative values of corrected chlorophyll backscatter signal available from the pre-processed AOL data. The agreement between the AOL and surface truth chlorophyll measurements then affects both the absolute concentration values and the degree of confidence that can be placed on the AOL results. During the Superflux experiments an attempt was made to place the surface truth vessels at points that were coincident with an intended overpass as nearly in both time and space as possible. As will be subsequently shown, considerable spatial and temporal differences between airborne observations and surface truth measurements were experienced. Fortunately, reasonable agreement between the AOL and surface truth chlorophyll determinations was found during the analysis of the four Superflux missions flown in June. However, this sampling disparity is a limiting factor on both the instrument credibility and the confidence with which oceanographers can apply the AOL results.

Figure 12 shows the comparison between the AOL and surface truth chlorophyll results for all four Superflux missions conducted during June 1980. All available surface truth samples occurring within one nautical mile or within 60 minutes of an airborne observation were used in this comparison. The positions of both the surface vessels and the aircraft were obtained from their respective Loran-C receivers. A computer program was used to pick the particular AOL sample spatially nearest the surface truth observation within the arbitrarily chosen one hour time constraint. For the sampling points located well offshore both the temporal and spatial constraints were relaxed. Linear correlation coefficients determined for each of the four missions are given within their respective plots. In general, we consider the agreement reasonably good over the entire range of chlorophyll concentration with the exception of some minor disagreement found during Mission 32. The slopes are somewhat varied from mission to mission because of variations in the fluorosensor gain caused by using a different PMT high voltage setting. Also, the placement of the spectrum within the 36 fluorosensor light guides was sometimes varied from mission to mission. The placement of the spectrum upon the light guides can be adjusted by angular movement of the plane of the beamsplitting mirror immediately in front of the bathymetry PMT. The plane of this mirror was changed from mission to mission during these experiments in an attempt to optimize the spectral response of the AOL. More recent techniques in pre-flight preparation of the instrumentation and hardware improvements are expected to result in better fluorosensor spectra and considerably lower mission-to-mission variability in gain and bias.

Logistical planning and sampling coordination between airborne sensors and surface truthing vessels play a vital role in the ultimate usefulness of data from experiments such as Superflux. It is therefore worth examining the sampling coordination experienced during these experiments for utility in planning future experiments. Plots of temporal and spatial differences between airborne and surface truth sampling are given in Figure 13 for the respective passes discussed above. Although time and space cannot be equated in such a straightforward fashion for gauging the probable effects on the results of the intercomparisons, the general spread of differences between surface and airborne sampling on all

missions does indicate a significant possibility that some of these samples were extracted from different naturally occurring populations. It should be noted that, in general, those points indicating the largest differences represent offshore measurements where coincident sampling is least important. Also, the distribution of sampling differences on the plot for Mission 32, which had the poorest agreement on the regression analysis, is not much different than the distributions shown for the other missions. Perhaps this lack of agreement is due at least in part to the effect of the tidal phase in which the sampling was conducted. Mission 32 was flown during the flood cycle while the remaining missions were flown during the ebb cycle or near slack water. The higher vertical turbulence of the flood tide has been well documented as has the patchiness of various entrained parameters during that tidal cycle. This increased turbulence and attendant patchy distribution of chlorophyll and particulate matter would tend to magnify the effects of sampling differences.

The other aspect of coordinated surface and airborne sampling that appears to have been important during the Superflux experiments is the local gradient of various parameters in the vicinity of the sampling points. Figures 14 and 15 are time series cross-sections of normalized chlorophyll for passes flown during Mission 32 from which a comparative sample(s) was extracted for the preceding intercomparison. The location of the sampling point(s) on each pass is indicated by small arrows placed above the profile. The potential difference in values that could result from rather small horizontal displacement between aircraft and surface vessel sampling positions is especially apparent on Figure 15 while the lower gradients shown on Figure 14 would result in much lower potential differences. Attention should be afforded to this aspect on future missions, however it is realized that patchiness is almost an inherent problem in "high" chlorophyll areas within dynamic estuarine systems such as the lower Chesapeake Bay.

SUMMARY AND CONCLUSIONS

The results of the AOL flight tests conducted during the Superflux Experiments indicate that rapid, synoptic assessment of surface layer concentrations of chlorophyll and related pigments is feasible from an airborne laser fluorosensing system. Further, these initial tests show that the lidar system provides repeatable results with high internal consistency. Several problems have been identified in the present data set. As previously discussed the data presented herein has not been corrected for the effects of the Kodak 21 filter, the Gelbstoff component has not been separated from other fluorescent returns in the 580-nm region of the spectrum, and cross talk (caused by the low 11.25-nm AOL resolution) between the Raman and chlorophyll returns has not been deconvolved. Nevertheless, the results indicate that stimulation of natural waters with 532-nm wavelength radiation will (1) yield good results for chlorophyll concentrations ranging from 0.2 to 5 μg/ℓ, (2) provide satisfactory but not ideal Raman placement for correction of water attenuation properties, and (3) probably yield Gelbstoff fluorescence potentially mixed in an ambiguous combination with fresh biological photo-pigments.

The results of intercomparisons made between the AOL and surface truth chlorophyll measurements appear to be reasonably good with linear correlation coefficients varying between 0.81 and 0.97. Further, these comparative plots appear to have a linear fit through the distribution of points indicating that the spectral overlap of the Raman and chlorophyll has not seriously degraded the AOL chlorophyll results for the concentrations encountered in these field studies. Some problems associated with the coordination of aircraft and surface vessel sampling were discussed in the preceding section of this paper, but with the possible exception of Mission 32 the spatial and temporal disparities in coincident sampling do not appear to have produced a serious effect on the agreement between AOL and surface truth measurements of chlorophyll. However, these problems should be addressed in planning future missions of this type. Conversion of the AOL relative chlorophyll values to absolute concentration values using the slopes calculated in the linear regression analysis is practical in view of these results. Contour and cross-sectional projections of this data can be utilized by the oceanographer with reasonable confidence.

AOL hardware and software changes currently being implemented should provide improvements to the spectral problems discussed in the preceding section and are expected to significantly reduce the mission-to-mission variability experienced during the Superflux missions. The addition of a second laser wavelength (a) should also allow separation of some phytoplankton color groups as has been demonstrated with the LaRC ALOPE laser fluorosensor and (b) may facilitate the separation of Gelbstoff fluorescence from that of other organic pigments.

REFERENCES

1. Hoge, F. E.; and Swift, R. N.: Oil Film Thickness Measurement Using Airborne Laser-Induced Water Raman Backscatter. Appl. Opt., vol. 19, no. 19, 1980, p. 3269.

2. Hoge, F. E.; and Swift, R. N.: Absolute Tracer Dye Concentration Using Airborne Laser-Induced Water Raman Backscatter. Appl. Opt., vol. 20, no. 7, 1981, pp. 1191-1202.

3. Hoge, F. E.; and Swift, R. N.: Airborne Simultaneous Spectroscopic Detection of Laser-Induced Raman Backscatter and Fluorescence from Chlorophyll and Other Naturally Occurring Pigments. Appl. Opt., vol. 20, no. 18, 1981.

4. Hoge, F. E.; Swift, R. N.; and Frederick, E. B.: Water Depth Measurement Using an Airborne Pulsed Neon Laser System. Appl. Opt., vol. 19, no. 6, 1980, pp. 871-883.

5. Bressel, C.; Itzkan, I.; and Nunes, J. E.; and Hoge, F. E.: Airborne Oceanographic Lidar System. Proceedings, Eleventh International Symposium on Remote Sensing of the Environment, vol. 2, Environmental Research Institute of Michigan, Ann Arbor, 1977, pp. 1259-1268.

6. Zimmerman, A. V.; Paul, Fred W.; and Exton, R. J.: Research and Investigation of the Radiation Induced by a Laser Beam Incident on Sea Water. NASA CR-145149, 1976.

7. Bristow, M.; Nielsen, D.; Bundy, D.; Furtek, R.; and Baker, J.: Airborne Laser Fluorosensing of Surface Water Chlorophyll a. U.S. Environmental Protection Agency, Report no. 600/4-79-048. 1979.

8. Bristow, M.; Nielsen, D.; and Furtek, R.: A Laser-Fluorosensor Technique for Water Quality Assessment. Proceedings, Thirteenth International Symposium on the Remote Sensing of the Environment, vol. 1, Environmental Research Institute of Michigan, Ann Arbor, 1979, pp. 397-417.

9. Zimmerman, A. V.; and Bandy, Alan R.: The Application of Laser Raman Scattering to Remote Sensing of Salinity and Turbidity. Final Technical Report, Contract NAS1-11707 (Task 33), Old Dominion University Research Foundation, Norfolk, Virginia, 1975.

10. Bristow, M.; and Nielsen, D.: Remote Monitoring of Organic Carbon in Surface Waters. Project Report no. EPA-600-4-81-001, U.S. Environmental Protection Agency, 1981.

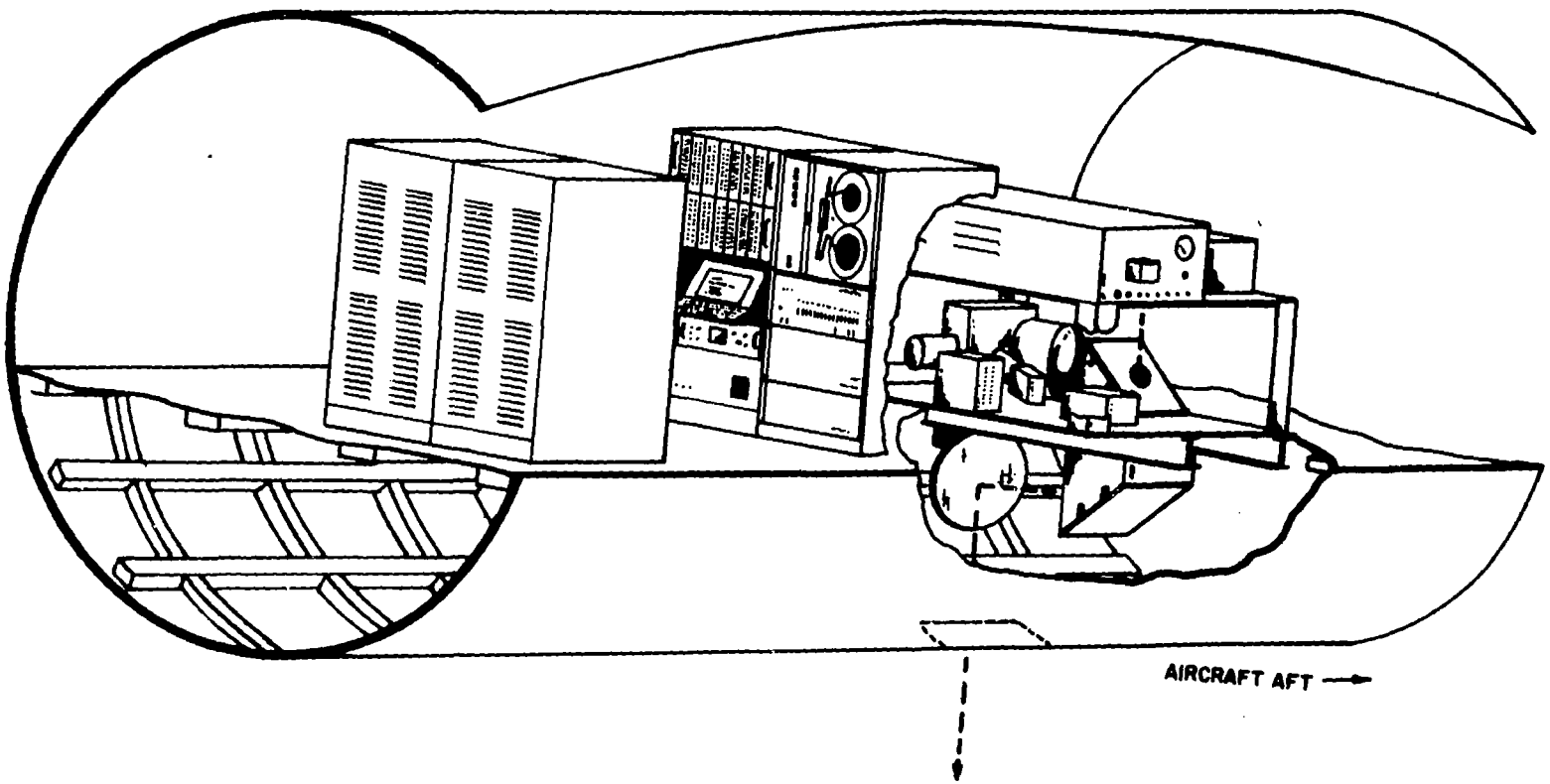

Figure 1.- Cut-away view of the AOL system as arranged on the WFC P-3 aircraft.

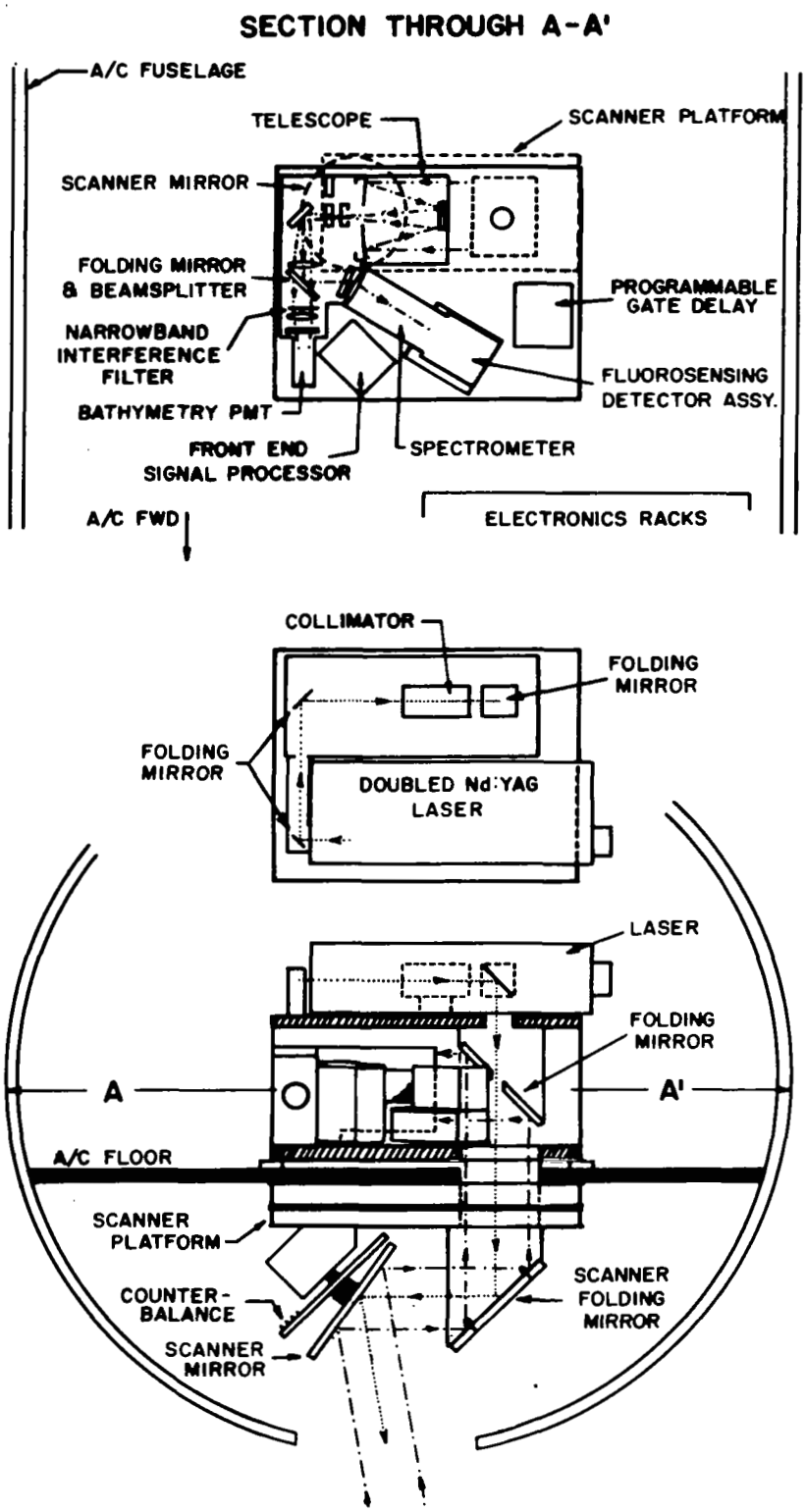

Figure 2.- Detailed view of the transmitter and receiver optics of the AOL system during the Superflux experiments.

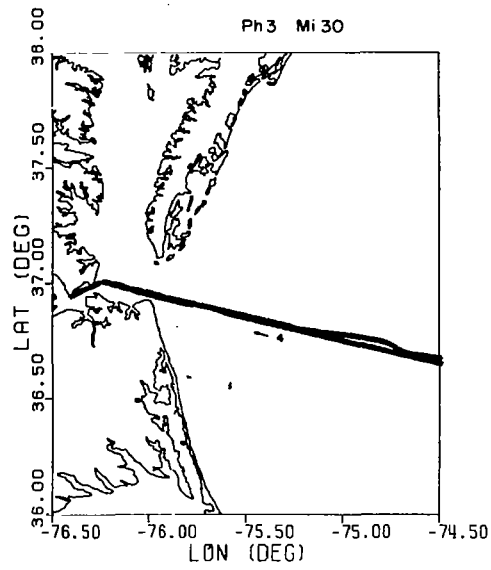

(a) June 20, 1980.

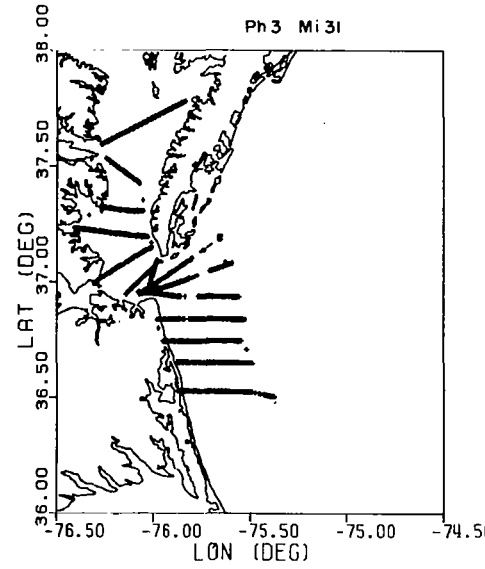

(b) June 23, 1980.

Figure 3.- Computer-drawn ground tracks for flight lines occupied on AOL missions 30 and 31 (June 20 and 23, 1980, respectively).

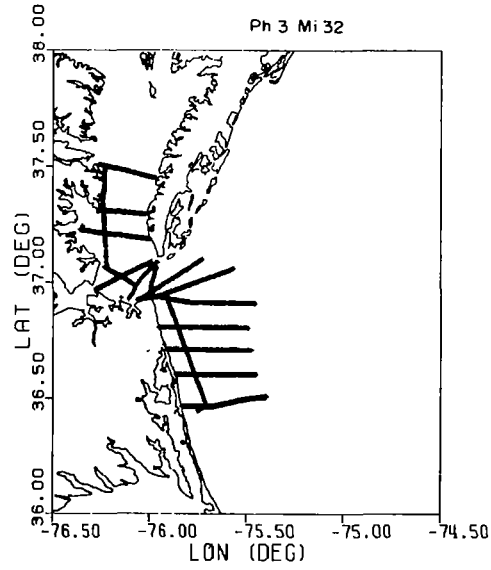

(a) June 25, 1980.

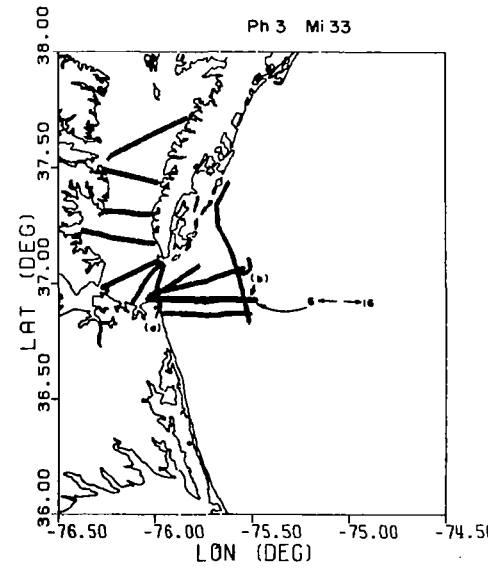

(b) June 27, 1980.

Figure 4.- Computer-drawn ground tracks for flight lines occupied on AOL missions 31 and 32 (June 25 and 27, 1980, respectively).

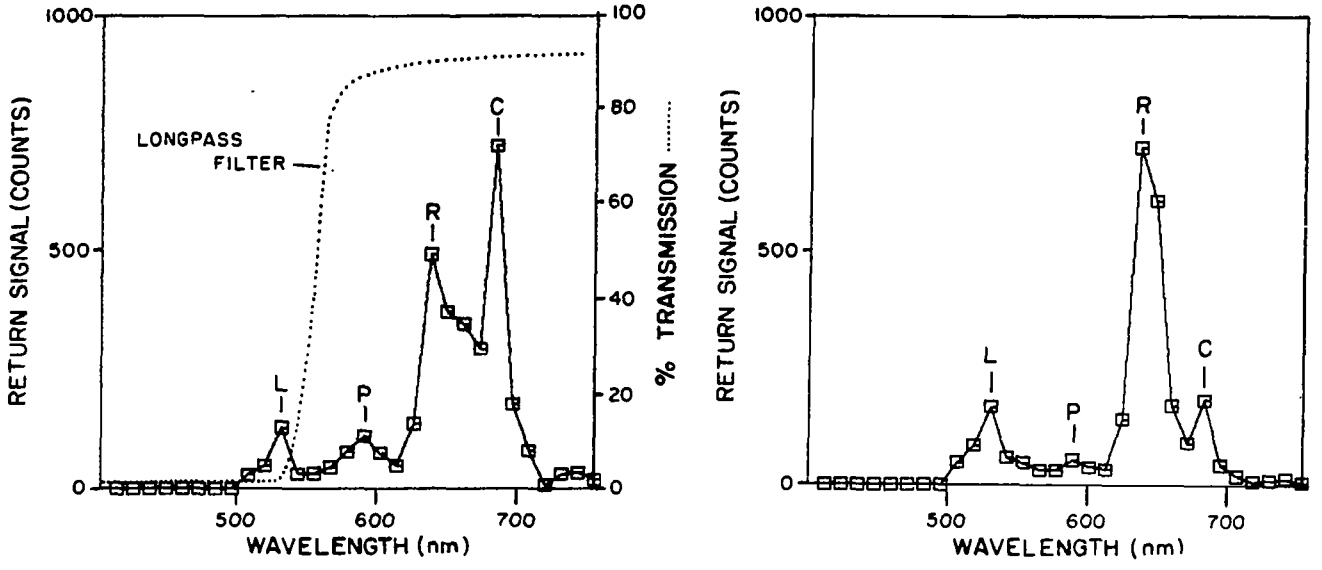

(a) Within the Bay plume.

(b) Offshore.

Figure 5.- Sample AOL spectra from within the Bay plume and offshore. The location of this flight line is given in figure 3(a). P - organic pigments; R - Raman; C - chlorophyll; L - laser.

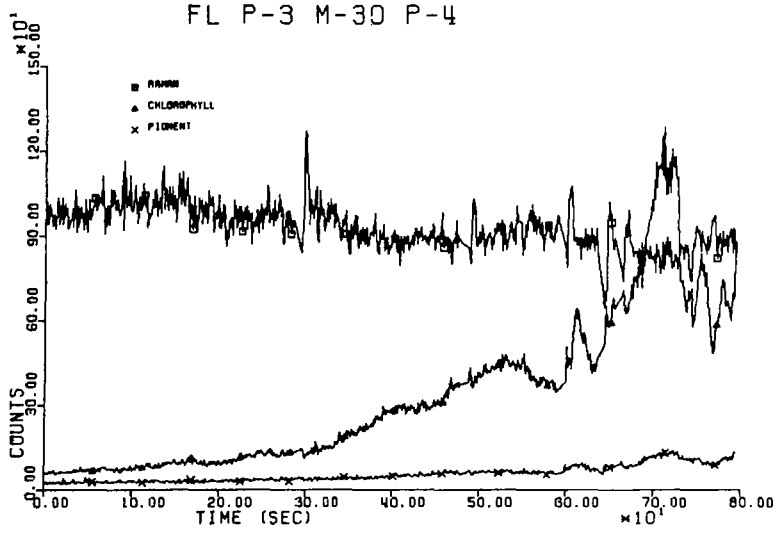

Figure 6.- Sample cross-section from a pass flown on June 23. The location of this flight line is given in figure 3(a).

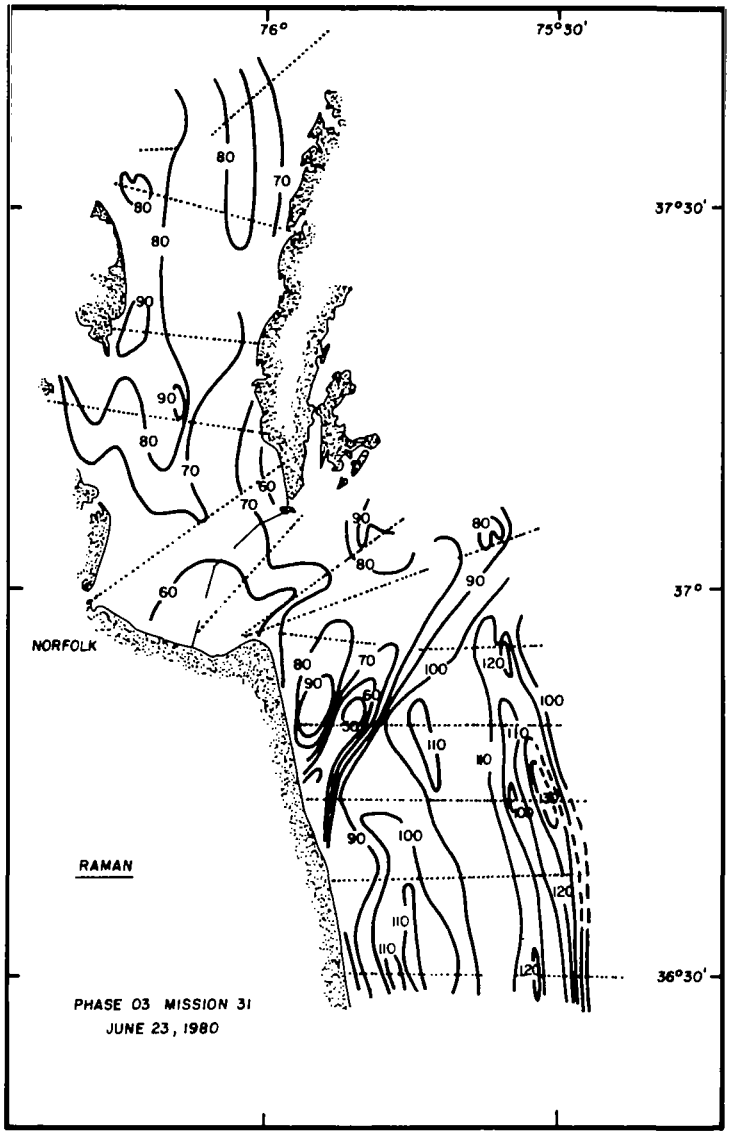

Figure 7.- Contoured plots of relative Raman backscatter from the mission flown on June 23. The dotted segments indicate the ground tracks.

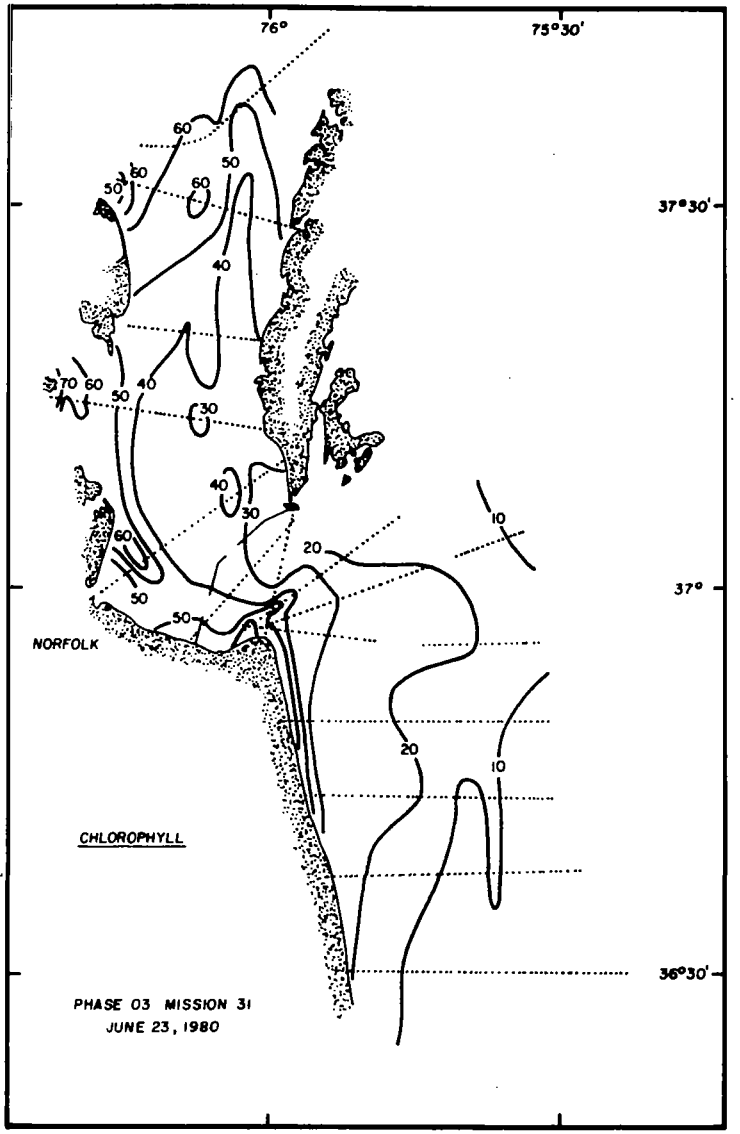

Figure 8.- Contoured plots of relative chlorophyll a fluorescence from the mission flown on June 23.

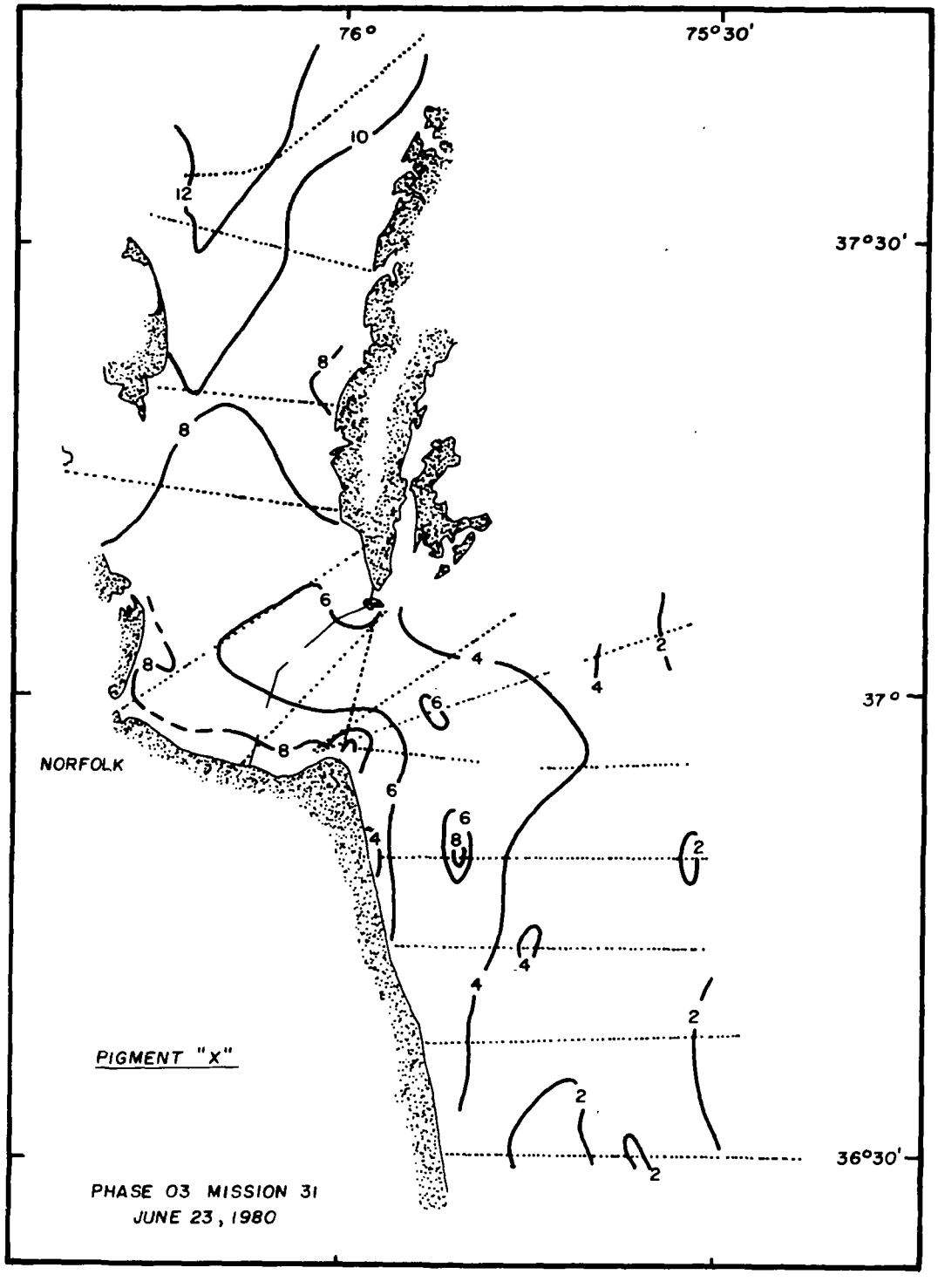

Figure 9.- Contoured plots of relative organic pigment fluorescence from the mission flown on June 23. The organic pigment response has been normalized by the Raman backscatter to remove the effects of spatial variations in water transmissivity.

(a)

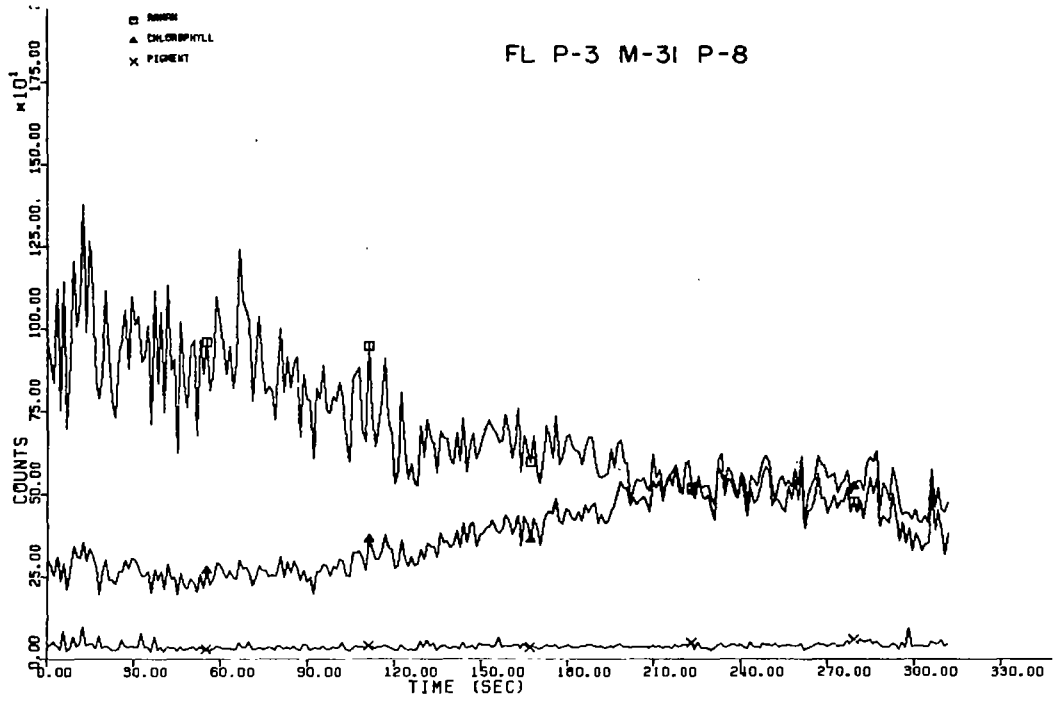

(b)

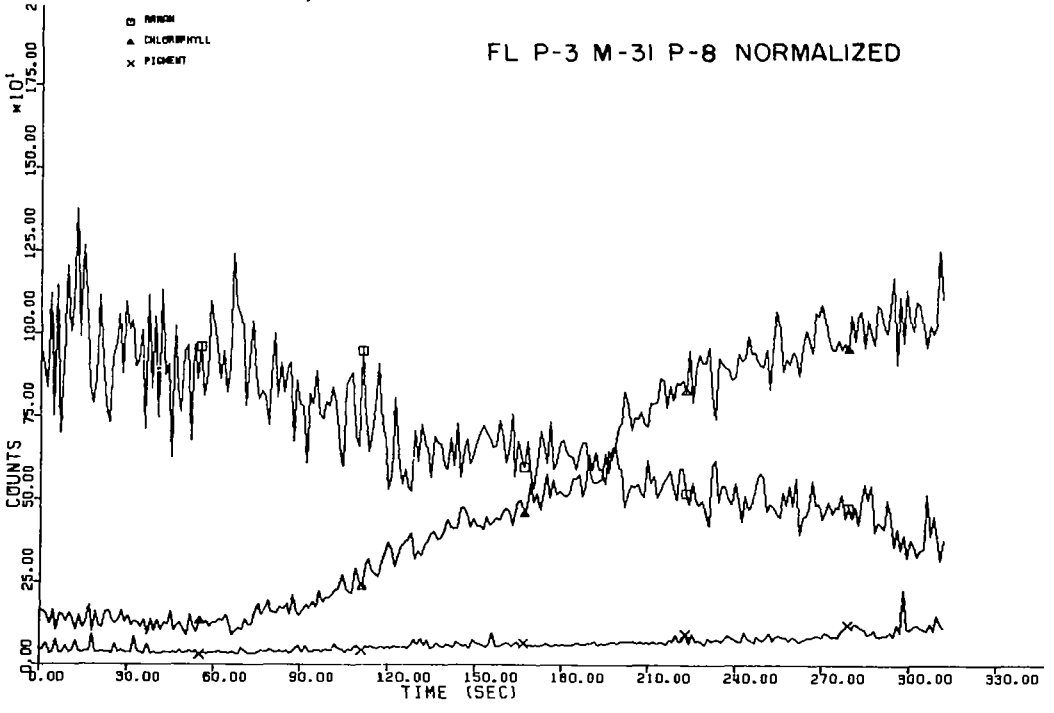

Figure 10.- Comparative cross-sections of flight line 8 from the mission flown on June 23. Figure 10(a) indicates the relative intensities of chlorophyll a and organic pigment fluorescence signals before normalization; the traces in figure 10(b) have been normalized.

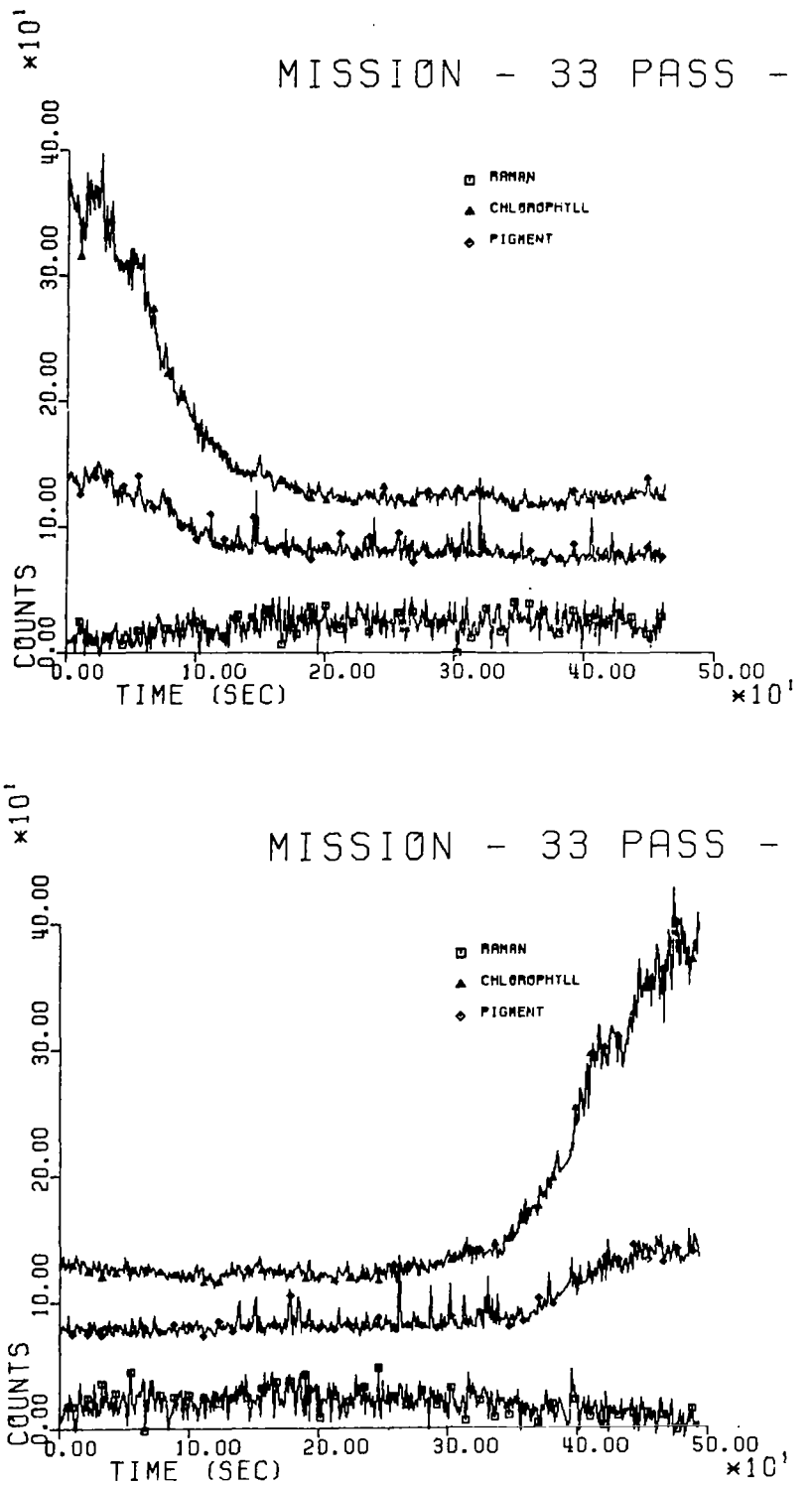

Figure 11.- Comparative cross-sections from flight lines 16 and 6 flown on June 23. Both of these flight lines were taken over the same ground track, but in the opposite direction.

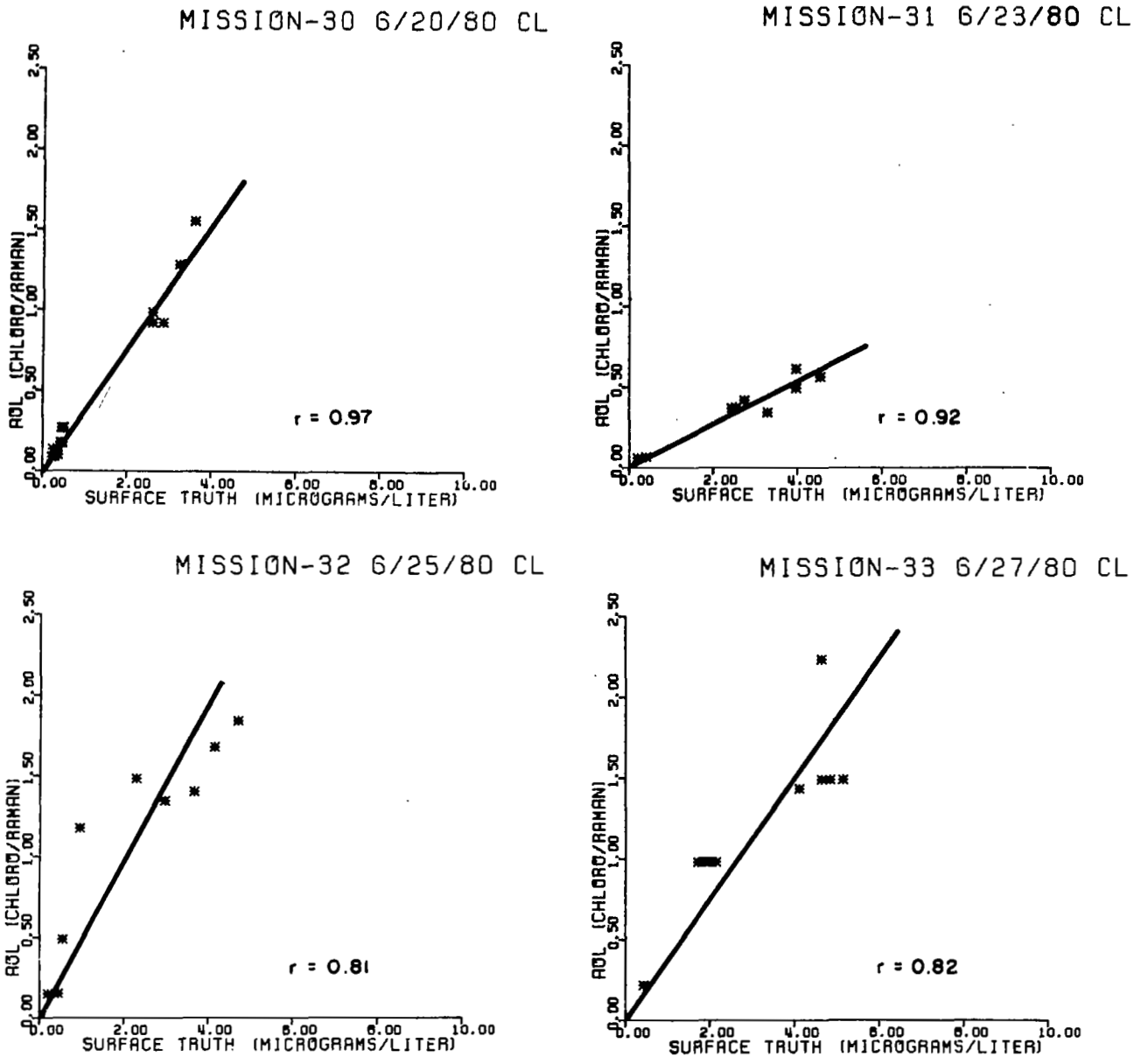

Figure 12.- Comparative plots indicating the agreement between AOL and surface truth chlorophyll a results for the four Superflux missions flown over the Chesapeake Bay mouth in June 1981.

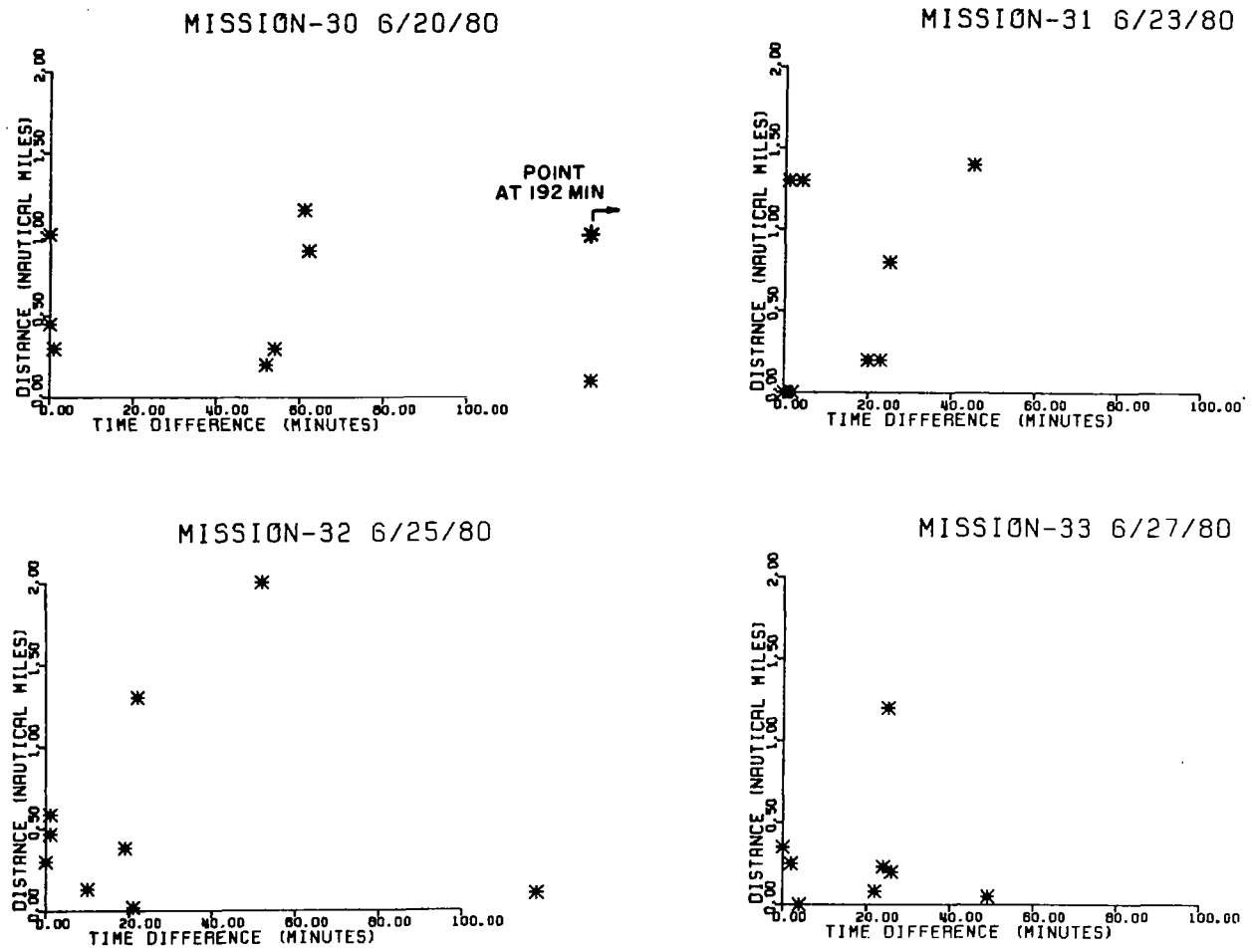

Figure 13.- Plots of temporal and spatial differences between AOL and surface truth sampling for the four Superflux missions flown over the Chesapeake Bay mouth in June 1981.

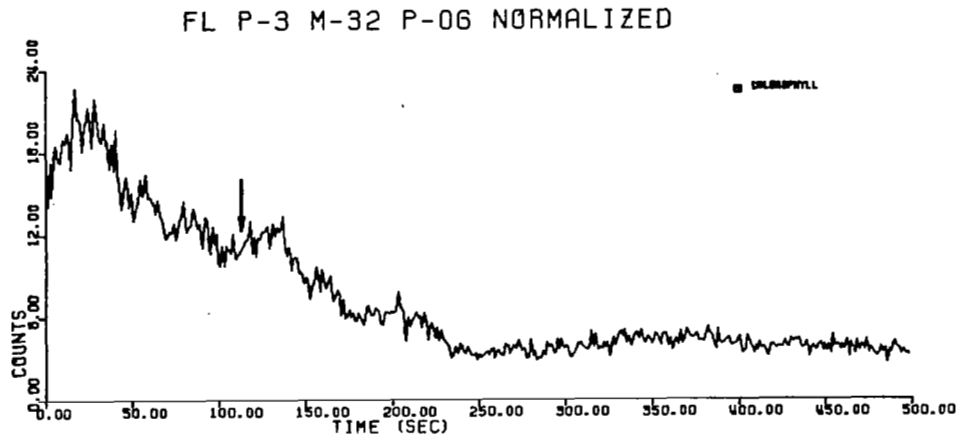

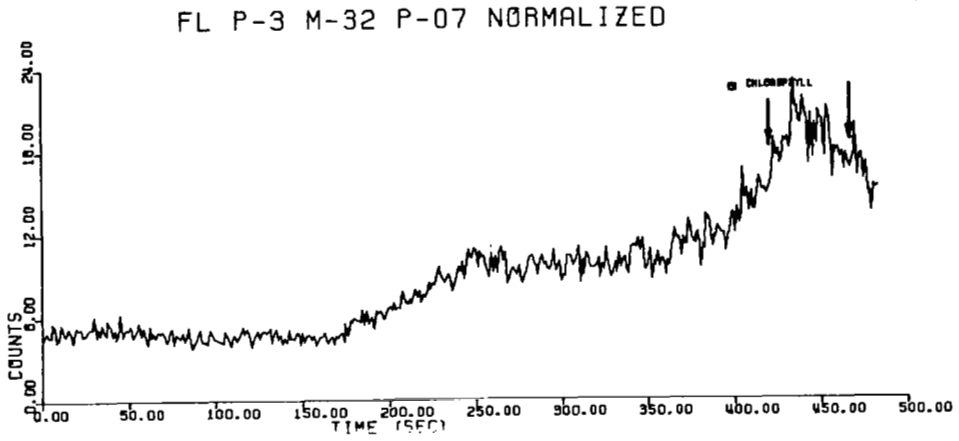

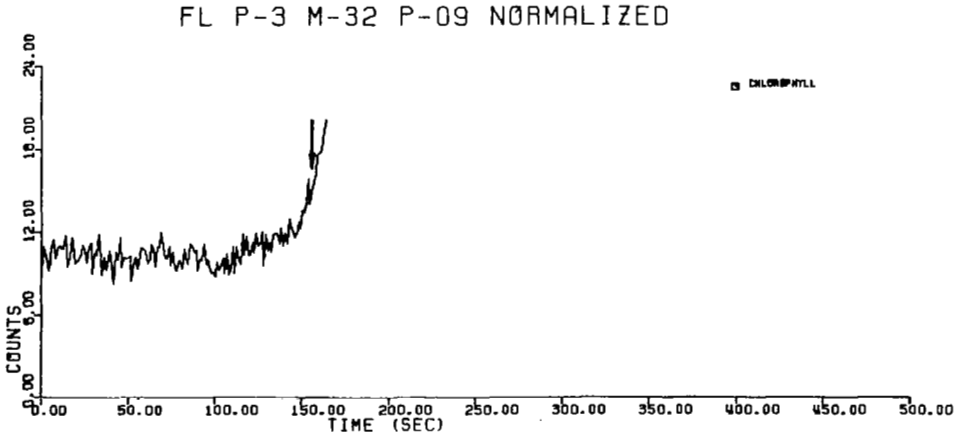

Figure 14.- Cross-sections of normalized chlorophyll a for passes taken on June 25 where surface truth sampling was available. The arrow(s) indicates the location of the high gradient sampling point on each pass.

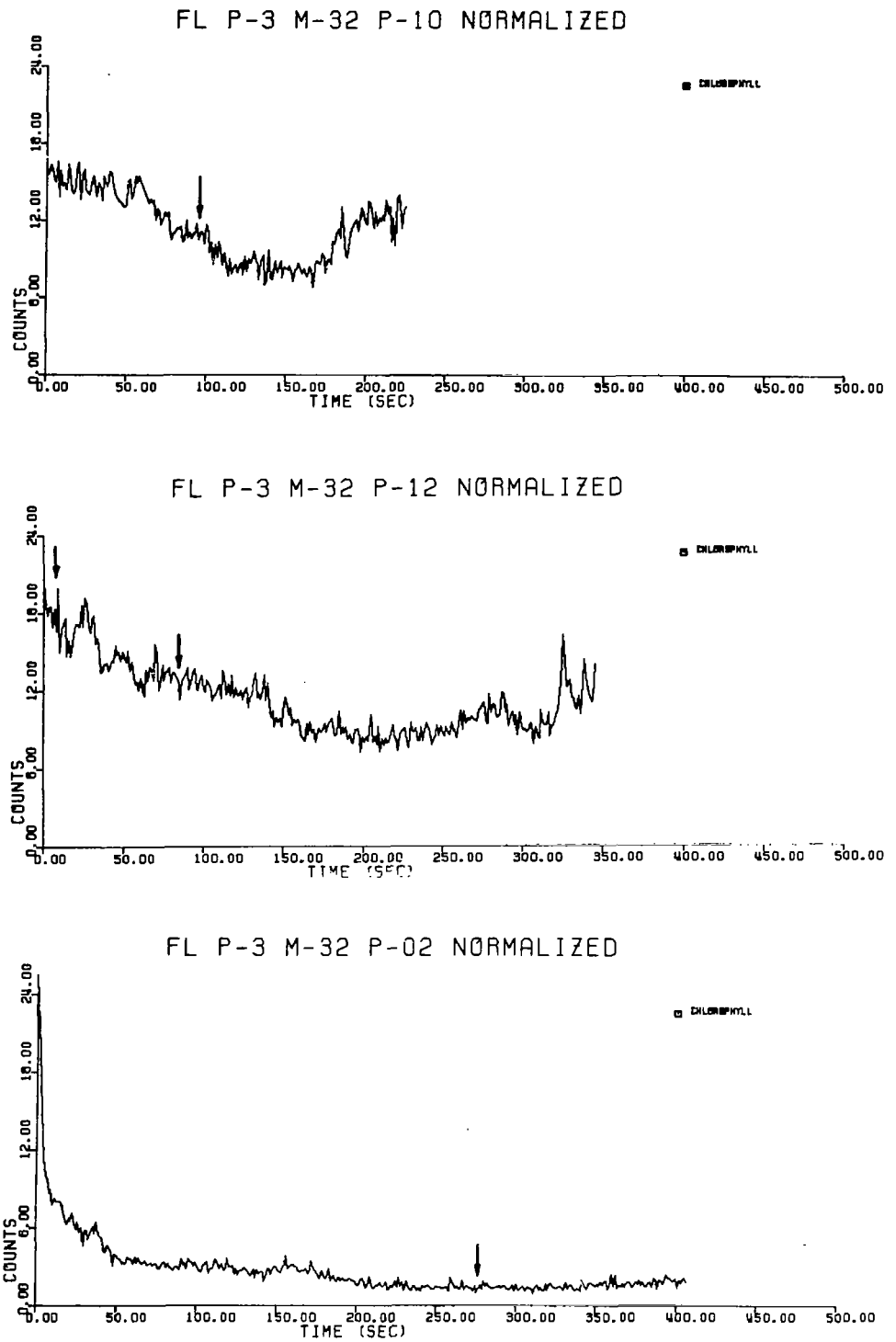

Figure 15.- Cross-sections of normalized chlorophyll a for passes taken on June 25 where surface truth sampling was available. The arrow(s) indicates the location of the low gradient sampling point on each pass.

TOTAL PLANKTON RESPIRATION IN THE CHESAPEAKE BAY PLUME

Craig N. Robertson and James P. Thomas
Sandy Hook Laboratory
Northeast Fisheries Center
National Marine Fisheries Service

SUMMARY

Total plankton respiration (TPR) was measured at 17 stations within the Chesapeake Bay plume off the Virginia coast during March, June, and October 1980. Elevated rates of TPR, as well as higher concentrations of chlorophyll *a* and phaeopigment *a*, were found to be associated with the Bay plume during each survey. TPR rates within the Bay plume were close to those found associated with the Hudson River plume for comparable times of the year. The data examined indicate that the Chesapeake Bay plume stimulates biological activity and is a source of organic loading to the contiguous shelf ecosystem.

INTRODUCTION

Total plankton respiration (TPR) is the consumption of dissolved oxygen by planktonic organisms in the water column. TPR represents the rate of assimilation and decomposition of organic matter and is partially responsible for the recycling of nutrient materials to support primary production in the marine ecosystem.

Few measurements of oxygen consumption by plankton exist for the region off the Virginia-North Carolina coast. Thus, the objective of this research was to quantify TPR in near-coastal waters off the Chesapeake Bay with particular emphasis on studying the effects of the Chesapeake Bay plume on the biological activity (TPR) of the planktonic community.

METHODS

Samples for salinity, chlorophyll *a*, phaeopigment *a*, and TPR were collected from 17 stations north of the Virginia-North Carolina border (ref. 1, figure 5) during the three Superflux cruises. The periods were March 12-15, June 18-21, and October 16-18. Samples were taken from surface (1 m) to bottom (3 to 6 depths per station) in 5-, 10-, or 12-l Niskin bottles. Water column temperatures were measured using an expendable bathythermograph (XBT) to the nearest $0.1^{\circ}C$.

Water for chlorophyll (chl *a*) and phaeopigment *a* (phaeo *a*) determinations was drawn from the Niskins into opaque polypropylene bottles after first passing the sample through a 300-μm nylon screen to remove larger zooplankton. Under subdued light each sample was filtered through a Whatman Gf/F filter. The filter

was ground in 90% spectral grade acetone for one minute and centrifuged for five minutes, and the extracted chlorophyll solution was transferred to a fluorometer. After chl *a* determination, two drops of 5% HCL were added to the tube containing the extract, mixed, and the concentration of phaeo *a* was determined fluorometrically. Corrected concentrations of chl *a* and phaeo *a* expressed in mg/m^3 were calculated by the equations in reference 2.

As soon as they were recovered, samples for TPR were drawn from the Niskins into 300-ml acid-washed and baked ($232^{\circ}C$ for one hour) BOD bottles. Five replicates were taken from each depth samples. Two (unincubated) of the five were fixed immediately for dissolved oxygen determination, while the remaining three were incubated at $\pm 1^{\circ}C$ of *in situ* temperature in the dark on shipboard for approximately 24 hours. Following incubation these three were also fixed for dissolved oxygen determination. Oxygen concentrations were measured by the method of Strickland and Parsons (ref. 2) with the modification of using 0.0375 N phenylarsine oxide (PAO) in place of sodium thiosulfate and amylose in place of soluble starch (refs. 3 and 4). Respiration rates (TPR) were calculated by the formula

$$\text{TPR (ml } O_2/m^3/h) = \left(\frac{S_u - S_i}{t}\right)(0.7 \times 1000)$$

where S_u is the mean dissolved oxygen concentration in (mg O_2/l) of the unincubated samples, S_i is the mean dissolved oxygen concentration (mg O_2/l) of the incubated sample, and t is the period of incubation in hours. The constants 0.7 and 1000 are to convert mg O_2 to ml O_2 and volume from liters to m^3, respectively. Salinity samples were taken from each Niskin and measured on a Guildline Autosal model 8400 salinometer.

RESULTS

Hydrography

Figures 1 to 3 show surface (1 m) views of σ_t, total chlorophyll, total phaeopigment, and total plankton respiration for March, June, and October 1980. Figures 4 to 7 show lengthwise sections of the Chesapeake Bay plume for σ_t, total chlorophyll, total phaeopigment, and total plankton respiration for June 1980. In March the density plume ($\sigma_t \leq 24$) exiting from the Chesapeake Bay mouth extended from the Virginia coast to 16 km offshore and from inside Cape Henry to just south of the Virginia-North Carolina border (>42 km south of Cape Henry) (fig. 1(a)). The water column was essentially isothermal but vertical salinity stratification was evident. The strongest pycnocline (halocline) was near the Bay mouth (station 69) with a six-σ_t-unit difference between surface and bottom waters. South of station 69 stratification was still present, although weaker, with only three σ_t units separating surface and bottom waters. The nearshore density plume was as deep as 14 m near station 69 and had risen to 8 m by station 71 off the Virginia-North Carolina border.

In June the water column was strongly stratified vertically due to temperature and salinity differences from the surface to bottom. The density plume extended from 22 km (station 804) to 32 km (station 813) offshore and south of the Virginia-North Carolina border (fig. 2(a)). A strong pycnocline existed throughout the entire area of study (5 σ_t units). The depth of the density plume varied from 6 to 9 m.

October's water column was essentially isopycnal except near the Bay mouth (<2 σ_t units). The density plume did not extend seaward beyond station 69 (fig. 3(a)) and was not deeper than 4 m at this station. This restricted plume extension is attributed to very low rainfall and runoff of fresh water (ref. 5).

Chlorophyll

Chl *a* and phaeo *a* in March ranged from 1.60 to 14.44 mg/m^3 ($\bar{X}$ = 5.41 ±2.97) and ~0.0 to 11.04 mg/m^3 ($\bar{X}$ = 1.61 ±2.07), respectively, within the plume waters, while in surrounding water concentrations ranged from 0.43 to 12.11 mg/m^3 ($\bar{X}$ = 2.86 ±2.57) and ~0.0 to 3.11 mg/m^3 ($\bar{X}$ = 0.70 ±0.83) (figs. 1(b) and 1(c)). Chl *a* and phaeo *a* concentrations near the Bay mouth (stations 69-802) were higher within the plume waters; however, at stations 808-809 and southward phaeo *a* concentrations had increased in waters below the plume and exceeded adjacent plume concentrations.

June chl *a* and phaeo *a* concentrations were highest in surface waters within the plume north of stations 808-809 (figs. 2(b), 2(c), 4(b), 4(c), 5(b), and 5(c)). Concentrations ranged from 0.66 to 7.75 mg/m^3 ($\bar{X}$ = 2.35 ±1.90) for chl *a* and 0.13 to 4.12 mg/m^3 ($\bar{X}$ = 0.81 ±0.88) for phaeo *a*. South of stations 808-809 chl *a* and phaeo *a* concentrations increased in waters below the plume and ranged from 0.35 to 5.27 mg/m^3 ($\bar{X}$ = 1.58 ±1.03) and 0.08 to 2.08 mg/m^3 ($\bar{X}$ = 0.64 ±0.53), respectively (figs. 6(b), 6(c), 7(b), and 7(c)).

During the October cruise measured concentrations of chl *a* and phaeo *a* within the contracted plume ranged from 2.59 to 4.58 mg/m^3 ($\bar{X}$ = 3.35 ±0.75) and 0.55 to 0.98 mg/m^3 ($\bar{X}$ = 0.78 ±0.15) (figs. 3(b) and 3(c)). In the surrounding waters, south and seaward of station 69, the ranges were 0.29 to 6.23 mg/m^3 ($\bar{X}$ = 2.13 ±1.27) and 0.11 to 3.48 mg/m^3 ($\bar{X}$ = 0.85 ±0.71). Chl *a* and phaeo *a* within the plume were fairly homogeneous from surface to bottom. Outside of the plume, chl *a* and phaeo *a* increased from surface to bottom along the transect (stations 69-804) just off Cape Henry. Throughout the remainder of the study area, chl *a* showed a nearshore-to-offshore decreasing gradient with concentrations of less than 3 mg/m^3 except at station 808 where they exceeded 4 mg/m^3. Phaeo *a* continued to show a surface-to-bottom increase with concentrations of greater than 2 mg/m^3. The exception to this occurred at stations 808-809 where values in excess of 3 mg/m^3 were measured near the bottom and a nearshore-to-offshore decreasing gradient was present.

Respiration

TPR rates in March within the area defined by the density plume ($\sigma_t \leq 24$) ranged from 0.47 to 13.36 ml O_2/m^3/h ($\bar{X}$ = 7.27 ±2.94) consumed (fig. 1(d)). In the waters surrounding the plume the range was 1.01 to 11.53 ml O_2/m^3/h ($\bar{X}$ =

5.23 ±2.18). Thus, the waters within the plume exhibited greater TPR rates than adjacent waters. Rates greater than 10 ml $O_2/m^3/h$ were found at station 805 from surface to bottom, at station 70 in the upper 5 m, and at station 800 at 5 m. TPR rates decreased south of station 805 to less than 5 ml $O_2/m^3/h$.

In June TPR rates within the plume ($\sigma_t \leq 22$) ranged between 1.46 and 20.99 ml $O_2/m^3/h$ ($\bar{X}$ = 11.29 ±4.63) and outside of it from 2.88 to 22.21 ml $O_2/m^3/h$ ($\bar{X}$ = 10.24 ±4.87) (fig. 2(d)). Highest rates occurred within or just beneath the plume, with rates decreasing southward of transect 69-804 and from surface to bottom. Rates excedded 10 ml $O_2/m^3/h$ in the upper water column from transect 808-811 northward (figs. 4(d), 5(d), and 6(d)).

TPR rates in October, although not as high as in June, were still elevated. TPR rates ranged from 6.15 to 18.02 ml $O_2/m^3/h$ ($\bar{X}$ = 10.18 ±4.32) within the plume ($\sigma_t \leq 22$) and from ∿0.0 to 15.01 ml $O_2/m^3/h$ ($\bar{X}$ = 6.19 ±4.69) in surrounding waters (fig. 3(d)). TPR rates were highest within the Bay mouth (station 801); proceeding southward, elevated rates were found approximately 12 to 17 km offshore and in the upper water column. These rates decreased southward to station 805 and then increased to station 809, where they exceeded 12 ml $O_2/m^3/h$. Further south (station 812) they exceeded 14 ml $O_2/m^3/h$. These higher rates did not appear to be related to the plume. TPR rates in bottom water (>8 m) along transects 805-807 and at station 810 were too low to detect (<0.02 ml $O_2/m^3/h$) by the method used. These were the lowest TPR rates measured during the three studies.

DISCUSSION

Few measurements of TPR have been made along the Atlantic coast of the United States (Table I and refs. 6 to 15). For comparative purposes our mean rates for March, June, and October were 6.25, 10.86, and 6.42 ml $O_2/m^3/h$, respectively. These rates were of the same magnitude, for similar time periods, as values given for the Hudson River plume (ref. 9) and the shelf south of Cape Hatteras (ref. 12). Both the Hudson River plume and Chesapeake Bay plume are regions representative of estuarine outwellings and thus one would possibly expect the rates to be similar. However, the Hudson plume is reported to be more highly eutrophic (ref. 9), and thus it would be expected to exhibit higher respiration rates than the Chesapeake plume. This may indeed be the case, but due to the lack of supporting data for other periods of the year in the Chesapeake Bay plume no clear conclusions can be made. Barlow et al. (ref. 6), Sirois (ref. 7), and Taft et al. (ref. 8) all reported rates in excess of ours. Their rates are higher based on their sampling further up estuaries where conditions are more eutrophic due to increased organic loading. Rates presented by Pomeroy and Johannes (refs. 12 and 13) are generally lower than the ones presented in this study, and their rates are more representative of shelf and oceanic conditions. Georges Bank (refs. 14 and 15) appears to be an enriched system nearly comparable to the estuarine plumes.

Elevated chl *a* and phaeo *a* concentrations and TPR rates are associated with the density plume emanating from the Bay for the three periods examined. This would tend to suggest that the Bay plume stimulates phytoplankton growth and metabolic activity.

Marshall (ref. 16) cites higher phytoplankton cell numbers within the plume waters, and Kator and Zubkoff (ref. 17) found elevated bacterial biomass and heterotrophic uptake rates for the same area. In order to support this elevated biological activity, the Bay plume has to be an area of increased organic supply to the ecosystem either from autochthonous or allochthonous sources. For October 1980, dissolved organic carbon concentrations ranged from 0.8 to 3.3 mg/l. These concentrations are similar to those for the Hudson plume (ref. 9). Additional evidence for allochthonous inputs is shown in the data presented in references 18 and 19 for increased coprostanol and hydrocarbon concentrations found within the plume. However, without primary productivity data (including released dissolved fractions) it is difficult to determine which source is responsible for providing the bulk of the energy necessary to support TPR.

During both the March and June samplings, elevated chl *a* and phaeo *a* concentrations and TPR rates were found within the plume waters north of station 808 (figs. 4(b), 4(c), 4(d), 5(b), 5(c), and 5(d)), but by station 808 there is the indication of a decoupling of the particulates from the plume (figs. 6(b), 6(c), 7(b), and 7(c)) as shown by increased concentrations of particulates in bottom waters. TPR rates are still higher in the plume, but there is also increased activity in bottom waters probably due to the "raining out" of organic material from the plume. Brown and Wade (ref. 18) also found increasing concentrations of coprostanol in bottom waters. This settling of particulate materials to the benthos down the length of the plume may be a method of transporting contaminants as well as food to the seabed and ultimately into the benthic food web.

CONCLUSIONS

Total plankton respiration rates were elevated in the Chesapeake Bay plume over those in surrounding waters, and thus the Bay plume represents a source of labile organic material to the adjacent shelf waters and seabed. This is supported by the increased biomass concentrations of chlorophyll *a*, phaeopigment *a*, phytoplankton cell numbers, and bacterial cell numbers also found associated with plume waters. This initial look also suggests that TPR rates found within the Bay plume may be nearly comparable to those in the supposedly more heavily eutrophic Hudson River plume. Based on the results of this study, it appears that the plume exiting the Chesapeake Bay acts to stimulate biological activity over the contiguous shelf.

REFERENCES

1. Thomas, James P.: Superflux I, II, and III Experiment Designs: Water Sampling and Analyses. Chesapeake Bay Plume Study - Superflux 1980, NASA CP-2188, 1981 (Paper no. 5 of this compilation).

2. Strickland, J. D. H.; and Parsons, T. R.: A Practical Handbook of Seawater Analysis. Fish. Res. Bd. Canada, Bulletin 167, Ottawa, 1972.

3. Kroner, R. C.; Longbottom, J. E.; and Gorman, R.: A Comparison of Various Reagents Proposed for Use in the Winkler Procedure for Dissolved Oxygen. PHS Water Pollut. Surveillance System Appl. Develop. Rep. 12, Public Health Service, 1964.

4. U.S. Environmental Protection Agency: Methods for Chemical Analysis of Water and Wastes. Methods Develop. Qual. Assurance Res. Lab. NERC EPA-625/6-74-003, 1974.

5. Hargis, William J., Jr.: A Benchmark Multi-Disciplinary Study of the Interaction Between the Chesapeake Bay and Adjacent Waters of the Virginian Sea. Chesapeake Bay Plume Study - Superflux 1980, NASA CP-2188, 1981 (Paper no. 1 of this compilation).

6. Barlow, J. P.; Loranzen, C. J.; and Myren, R. T.: Eutrophication of a Tidal Estuary. Limnol. Oceanogr., vol. 8, no. 2, 1963, pp. 251-262.

7. Sirois, D. L.: Community Metabolism and Water Quality in the Lower Hudson River Estuary. Third Symposium of Hudson River Ecology, G. P. Howells and G. J. Lauer, eds., Hudson River Environmental Society, Inc., New York, 1974.

8. Taft, J. L.; Taylor, W. R.; Hartwig, E. O.; and Loftus, R.: Seasonal Oxygen Depletion in Chesapeake Bay. Estuaries, vol. 3, no. 4, 1980, pp. 242-247.

9. Thomas, James P.; O'Reilly, J. E.; and Robertson, Craig N.: Synoptic Invesitgations in Nutrient Cycling. Report No. SHL 79-05, National Marine Fisheries Service, Sandy Hook Laboratory, 1979.

10. Thomas, James P.; Phoel, W. C.; Steimle, W. F.; O'Reilly, J. E.; and Evans, C. A.: Seabed Oxygen Consumption in the New York Bight Apex. Amer. Soc. Limnol. Oceanogy. Spec. Symp., vol. 2, 1976, pp. 354-369.

11. Thomas, James P.; O'Reilly, J. E.; Draxler, A.; Babinchak, J. A.; Robertson, Craig N.; Phoel, W. C.; Waldhauer, R.; Evans, C. A.; Matte, A.; Cohn, M.; Nitowski, M.; and Dudley, S.: Biological Processes: Productivity and Respiration. Chapter 10, Oxygen Depletion and Associated Benthic Mortalities in New York Bight, R. L. Swanson and C. J. Sindermann, eds., NOAA Professional Paper No. 11, 1976.

12. Pomeroy, L. R.; and Johannes, R. E.: Total Plankton Respiration. Deep-Sea Res., vol. 13, 1966, pp. 971-973.

13. Pomeroy, L. R.; and Johannes, R. E.: Occurrence and Respiration of Ultraplankton in the Upper 500 Meters of the Ocean. Deep-Sea Res., vol. 15, 1968, pp. 381-391.

14. Thomas, James P.; O'Reilly, J. E.; Robertson, Craig N.; and Phoel, W. C.: Primary Productivity and Respiration Over Georges Bank During March and July 1977. C. M. 1978/L:37, International Council for the Exploration of the Sea, 1978.

15. Riley, G. A.: Plankton Studies. IV. Georges Bank. Bull. Bingham Oceanogr. Coll., vol. 7, 1941, pp. 1-73.

16. Marshall, Harold G.: Phytoplankton Assemblages Within the Chesapeake Bay Plume and Adjacent Waters of the Continental Shelf. Chesapeake Bay Plume Study - Superflux 1980, NASA CP-2188, 1981 (Paper no. 32 of this compilation).

17. Kator, Howard I.; and Zubkoff, Paul L.: Bacterial Biomass and Heterotrophic Potential in the Waters of the Chesapeake Bay Plume and Contiguous Continental Shelf. Chesapeake Bay Plume Study - Superflux 1980, NASA CP-2188, 1981 (Paper no. 28 of this compilation).

18. Brown, Robert C.; and Wade, Terry L.: Coprostanol as a Potential Tracer of Particulate Sewage Effluent to Shelf Waters Adjacent to the Chesapeake Bay. Chesapeake Bay Plume Study - Superflux 1980, NASA CP-2188, 1981 (Paper no. 18 of this compilation).

19. Wade, Terry L.; and Oertel, George F.: Concentration of Hydrocarbons Associated with Particles in the Shelf Waters Adjacent to the Entrance of Chesapeake Bay. Chesapeake Bay Plume Study - Superflux 1980, NASA CP-2188, 1981 (Paper no. 17 of this compilation).

TABLE I.- A COMPARISON OF RESPIRATION RATES FROM COASTAL WATERS NEAR VIRGINIA WITH VALUES FROM OTHER AREAS ALONG THE NORTHEAST COAST OF THE UNITED STATES

Authors	Area	Month	Mean Respiration Rates ml $O_2/m^3/h$
Barlow et al. (ref. 6)	Forge River estuary	June-September	272.0
Sirois (ref. 7)	Hudson River (upper)	July	44.0
		September	24.0
	Hudson River (lower)	July	72.0
		September	53.0
Taft et al. (ref. 8)	Chesapeake Bay (upper)	February	9.6-37.1
		April	10.8-56.3
		August	22.5-79.6
Present study	Chesapeake Bay mouth - Virginia-North Carolina border	March	6.25
		June	10.86
		October	6.42
Thomas et al (ref. 9)	Hudson River plume	March	6.2
		May	9.5
		July	13.5
		November	4.4
Thomas et al (ref. 10)	New York Bight apex	August	35.1
Thomas et al. (ref. 11)	New York Bight apex	August-September	7.0*
Pomeroy and Johannes (ref. 12)	Cape Hatteras shelf (north)	July	0.6
	Cape Hatteras shelf (south)	July	9.5
	Cape Hatteras slope	May	0.1
Pomeroy and Johannes (ref. 13)	Cape Hatteras slope (upper 10 m)	April	1.3
Thomas et al. (ref. 14)	Georges Bank	March-April	4.1
		July	3.5

* Rate measured during an anoxic episode in 1976.

TABLE I.- Concluded

Authors	Area	Month	Mean Respiration Rates ml $O_2/m^3/h$
Riley (ref. 15)	Georges Bank	January	0.2
		March	4.0
		April	8.4
		May	5.1
		June	8.3
		September	6.5

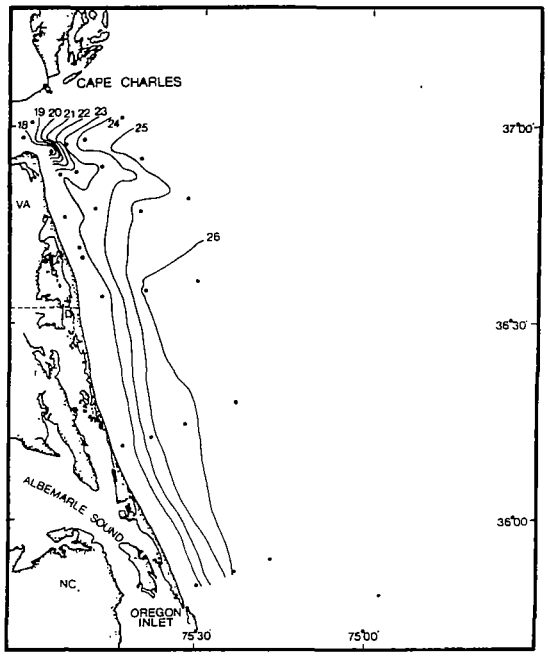

(a) σ_t.

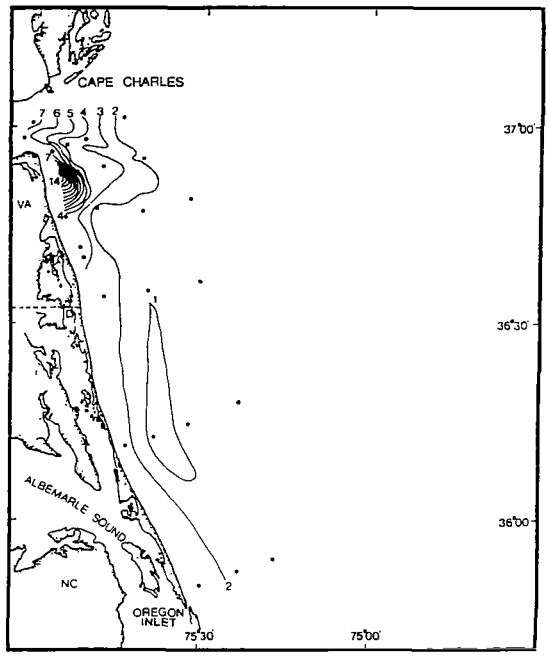

(b) Total chlorophyll (mg chl a/m^3).

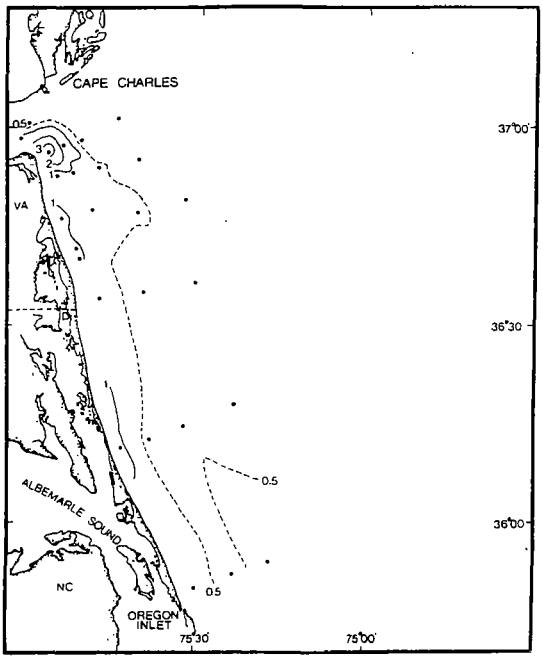

(c) Total phaeopigment (mg phaeo a/m^3).

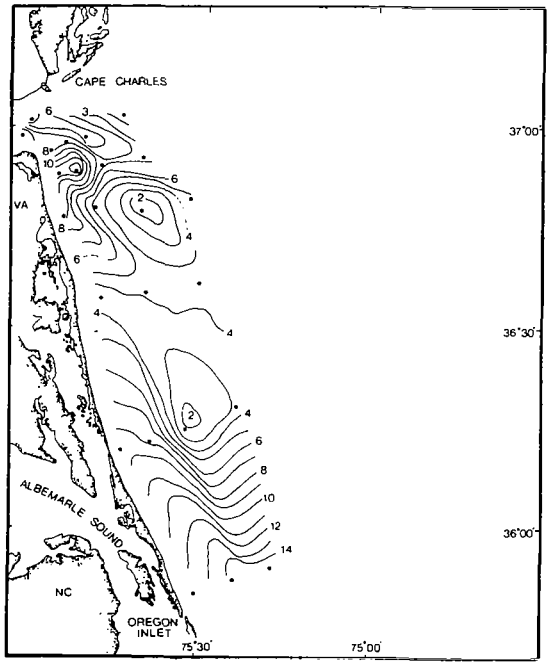

(d) Total plankton respiration (ml $O_2/m^3/h$).

Figure 1.- Surface views (1 m) of σ_t, total chlorophyll, total phaeopigment, and total plankton respiration for March 1980.

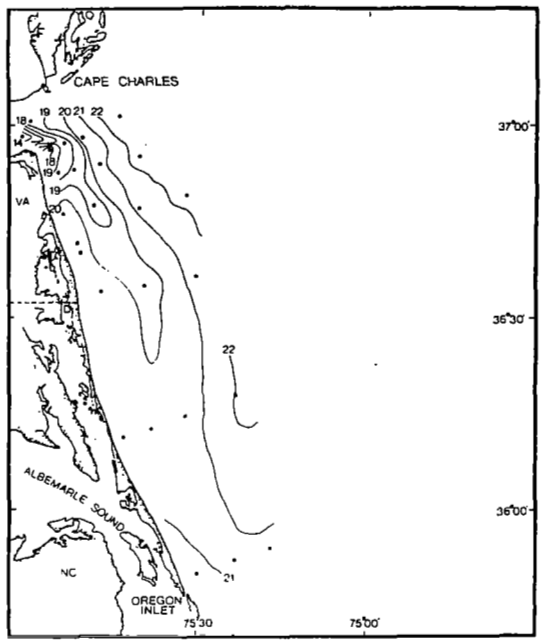

(a) σ_t.

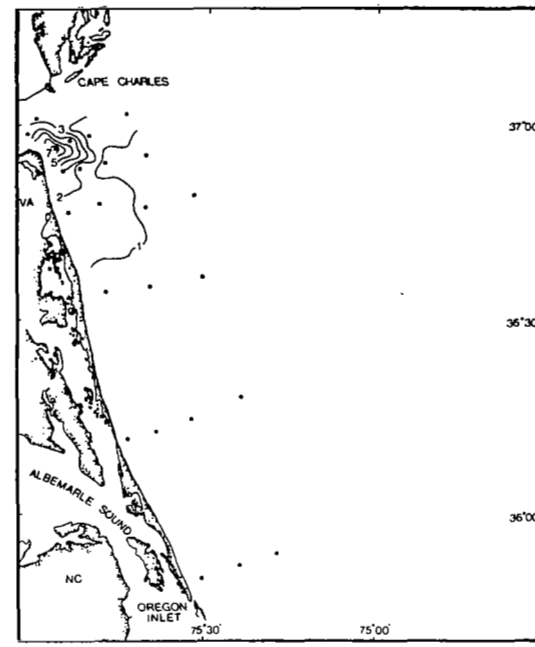

(b) Total chlorophyll (mg chl a/m^3).

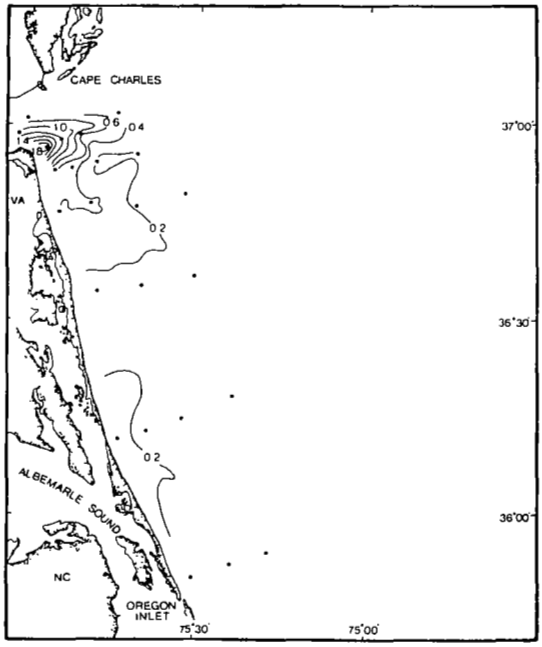

(c) Total phaeopigment (mg phaeo a/m^3).

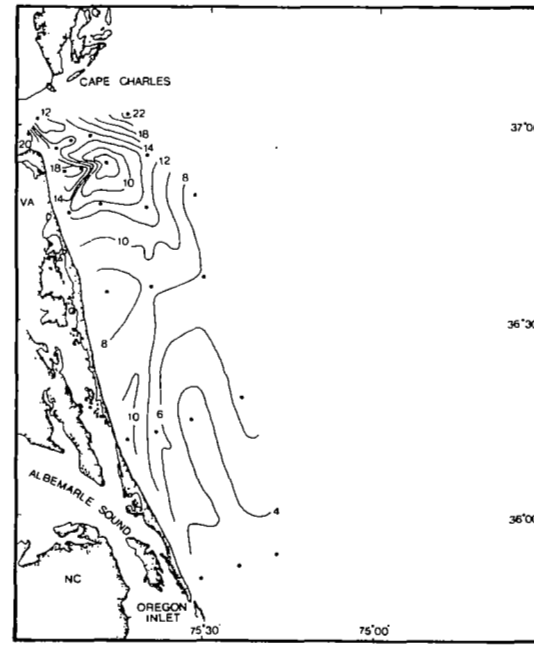

(d) Total plankton respiration (ml $O_2/m^3/h$).

Figure 2.- Surface views (1 m) of σ_t, total chlorophyll, total phaeopigment, and total plankton respiration for June 1980.

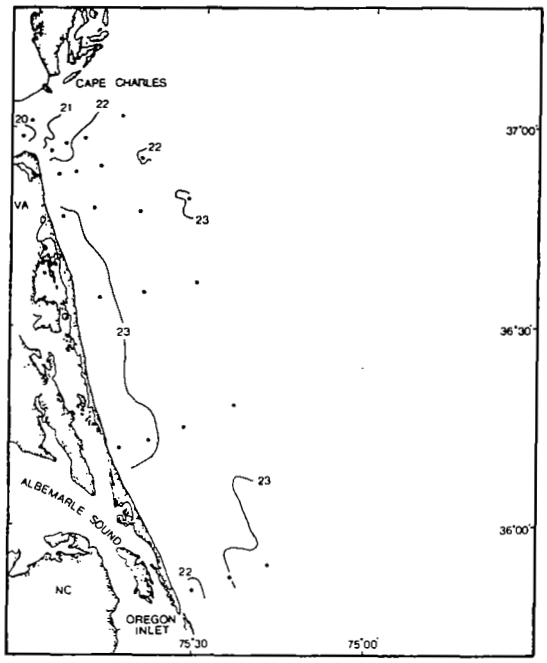

(a) σ_t.

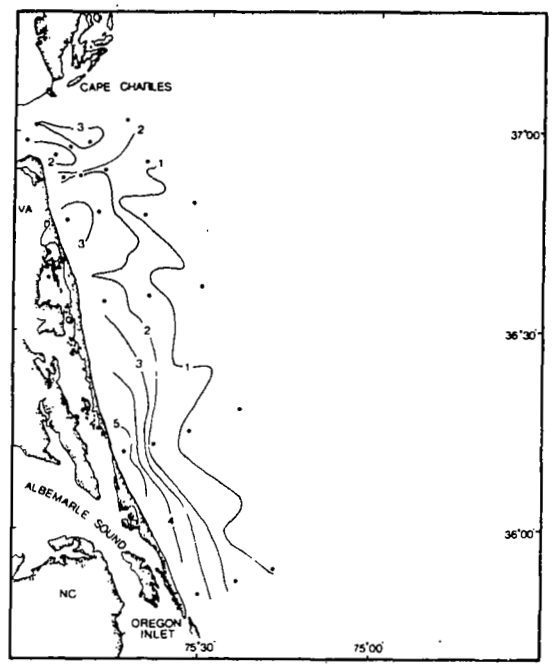

(b) Total chlorophyll (mg chl a/m^3).

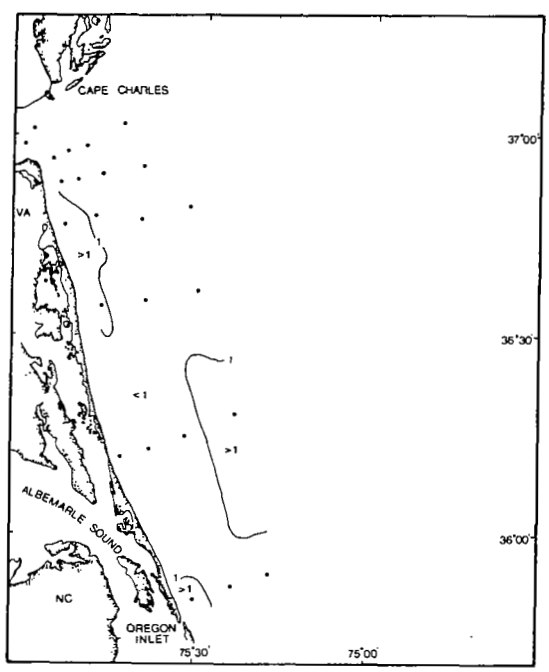

(c) Total phaeopigment (mg phaeo a/m^3).

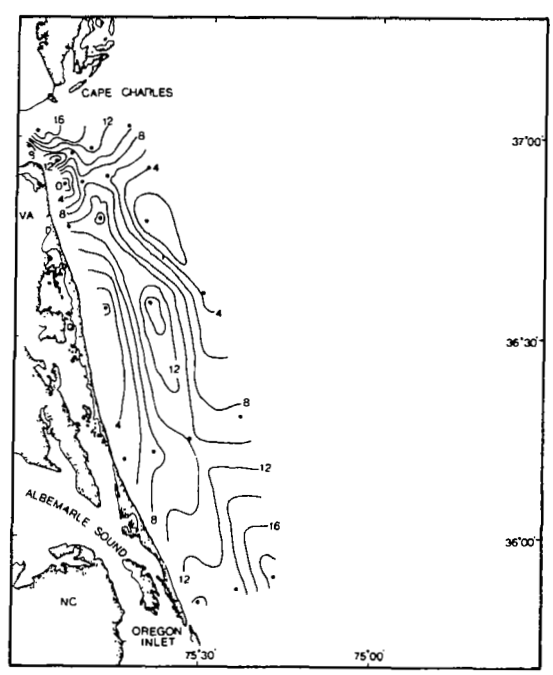

(d) Total plankton respiration (ml $O_2/m^3/h$).

Figure 3.- Surface views (1 m) of σ_t, total chlorophyll, total phaeopigment, and total plankton respiration for October 1980.

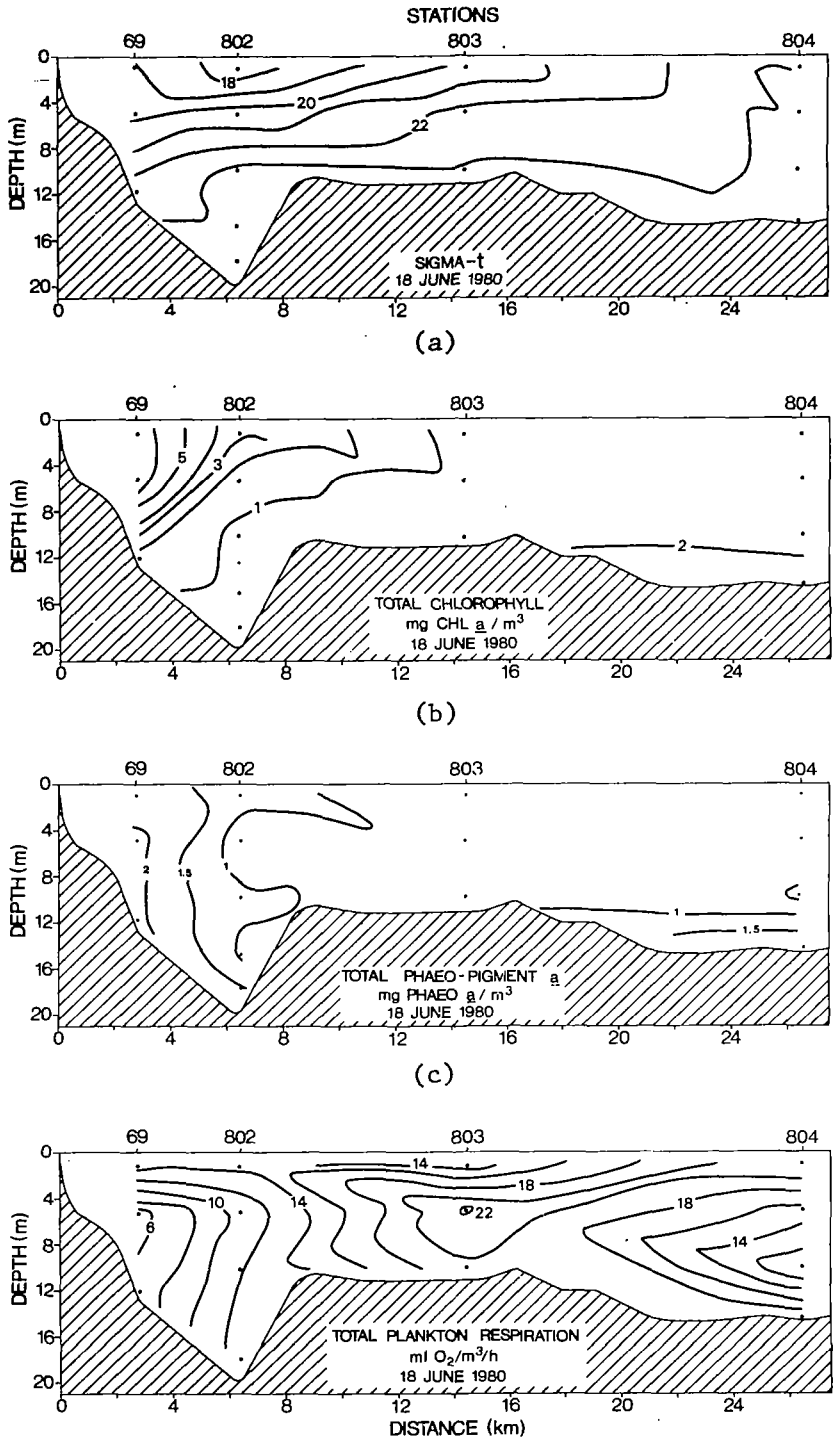

Figure 4.- Lengthwise section (stations 69-804) of the Chesapeake Bay plume for σ_t, total chlorophyll, total phaeopigment, and total plankton respiration for June 1980.

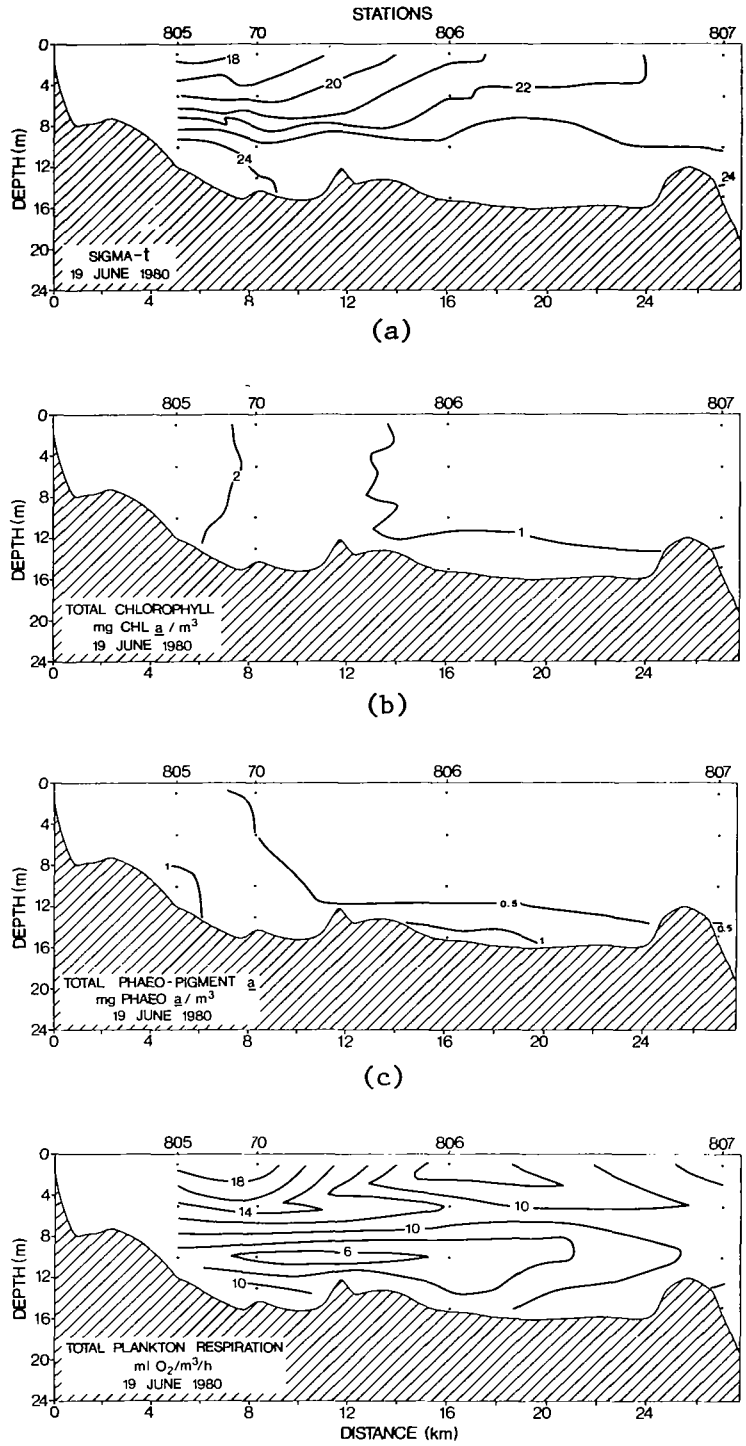

Figure 5.- Lenthwise section (stations 805-807) of the Chesapeake Bay plume for σ_t, total chlorophyll, total phaeopigment, and total plankton respiration for June 1980.

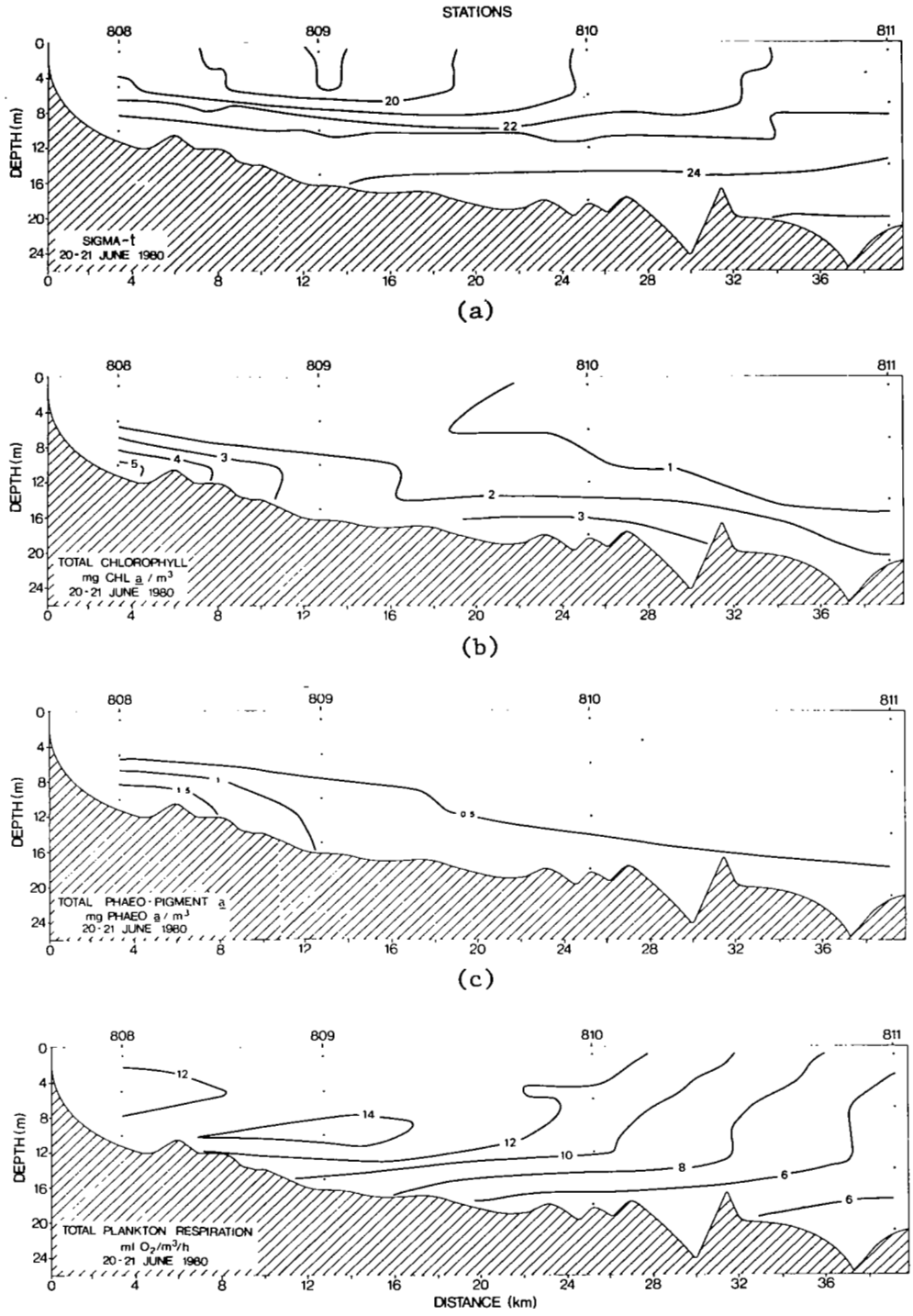

Figure 6.- Lengthwise section (stations 808-811) of the Chesapeake Bay plume for σ_t, total chlorophyll, total phaeopigment, and total plankton respiration for June 1980.

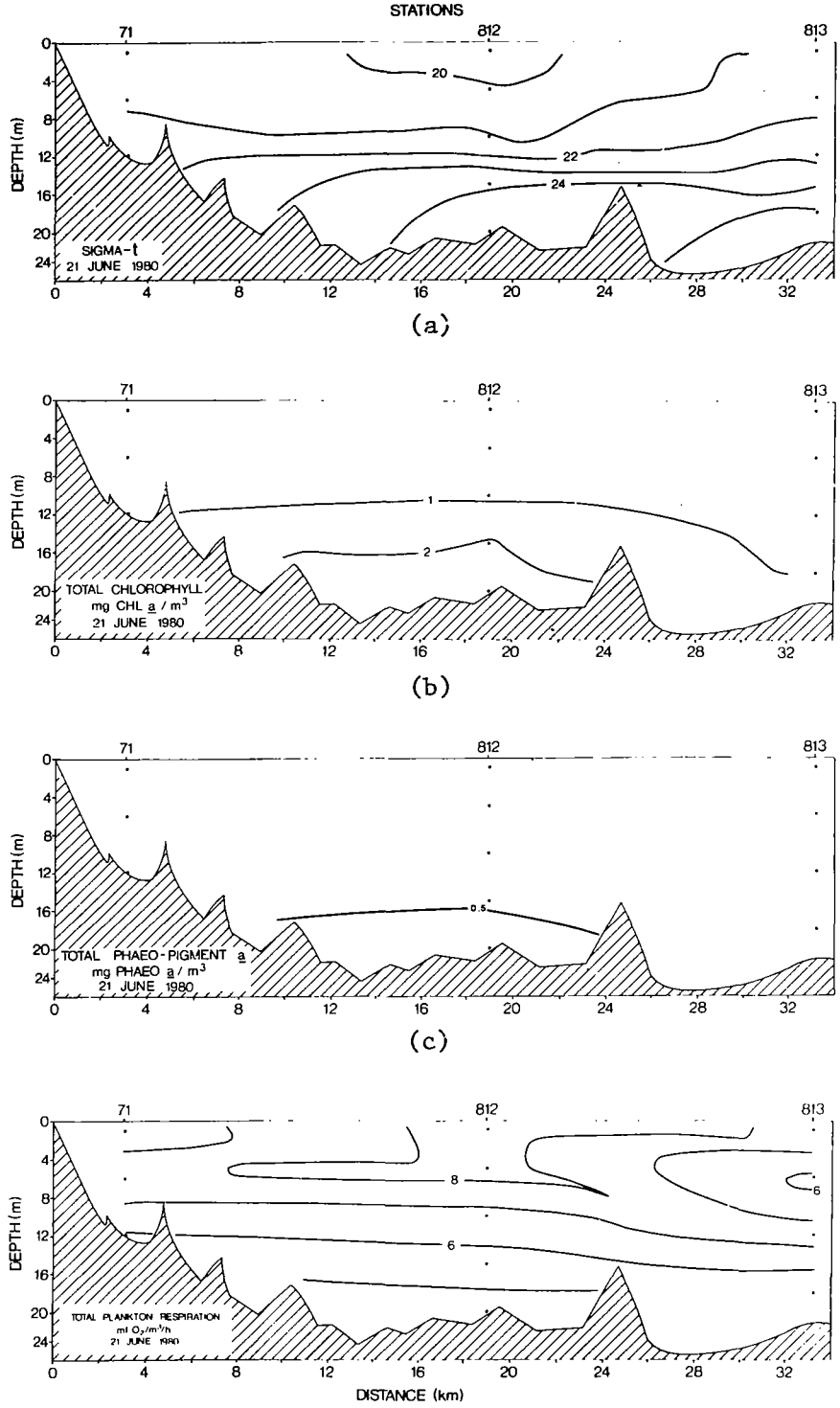

Figure 7.- Lengthwise section (stations 71-813) of the Chesapeake Bay plume for σ_t, total chlorophyll, total phaeopigment, and total plankton respiration for June 1980.

BACTERIAL BIOMASS AND HETEROTROPHIC POTENTIAL IN THE WATERS OF THE CHESAPEAKE BAY PLUME AND CONTIGUOUS CONTINENTAL SHELF[a]

Howard I. Kator and Paul L. Zubkoff
Department of Microbiology-Pathology and
Department of Environmental Physiology
Virginia Institute of Marine Science
of the
College of William and Mary

SUMMARY

Viable count bacterial numbers in surface water samples collected during June 1980 ranged from a maximum of 190×10^3 MPN (most probable number) $m\ell^{-1}$ at the Bay mouth to a minimum of 7.9×10^3 MPN $m\ell^{-1}$ offshore. Similarly, direct count densities ranged from 1800×10^3 BU (bacterial units) $m\ell^{-1}$ to 24×10^3 BU $m\ell^{-1}$. Heterotrophic potential (V_{max}) was largest at the Bay mouth (0.770 µg glucose $\ell^{-1}h^{-1}$) and lowest offshore (0.057 µg glucose $\ell^{-1}h^{-1}$). Biomass and V_{max} values usually decreased with depth although subsurface maxima were occasionally observed at inshore stations.

Correlation of biomass and heterotrophic potential data with selected hydrographic variables was determined with a non-parametric statistic (Kendall Tau). Results indicated viable counts were positively and significantly correlated with total chlorophyll, temperature, direct count and V_{max} during June 1980; significant negative correlations were obtained with salinity and depth; no correlation was observed for suspended particulates. Calculations of bacterial standing crop are discussed.

INTRODUCTION

Bacterial populations in Chesapeake Bay and contiguous shelf waters are significant to such essential processes as mineralization, nutrient recycling, degradation of pollutants and biomass production. However, our understanding of the dynamic relationships of physical and chemical factors to bacterial biomass and activities in Chesapeake Bay plume waters is limited. The availability of synoptic hydrographic (and remotely sensed physical-chemical) data obtained simultaneously with measurements of microbial biomass and activity presented an opportunity to examine such relationships.

Specific objectives of this study were: (1) to compile seasonal baseline data on bacterial biomass and heterotrophic uptake in the Chesapeake Bay plume

[a]performed under Contract #NA-80-FAC-00035 with National Marine Fisheries Service, NOAA, United States Department of Commerce.

and contiguous Atlantic Ocean shelf waters, (2) to relate bacterial data to relevant physical-chemical variables also potentially measurable by remote sensing techniques, and (3) to further evaluate and define methodology currently utilized for the measurement of bacterial biomass and heterotrophic activity at sea.

METHODS

Sample Collection

Water samples for the determinations of bacterial density and activity (heterotrophic potential) were collected by hydrocast using Niskin sterile bag samplers at appropriate depths. Samples were processed immediately after collection using aseptic techniques.

Bacterial Viable Count Determinations

Estimates of viable heterotrophic bacteria in Bay and plume waters were obtained using a five tube MPN (most probable number) technique employing a heterotrophic seawater medium. This medium consisted of a 1.0 g ℓ^{-1} peptone, 0.5 g ℓ^{-1} yeast extract, 0.01 g ℓ^{-1} ferric citrate, 0.1 g ℓ^{-1} sodium glycerol phosphate in 1000 mℓ of aged seawater adjusted to the proper salinity prior to autoclaving (121°C for 15 min). Inocula from appropriate serial dilutions of two subsamples from each water sample collected were planted in appropriate tubes and the tubes incubated at ca. 20°C for two weeks. MPN values were calculated using standard tables (1) and the values expressed as MPN mℓ^{-1} seawater.

Direct Bacterial Count

Twenty-mℓ aliquots of each water sample were aseptically transferred to sterile tubes to which 2 mℓ of a 5% glutaraldehyde seawater solution were added as a fixative. Tubes were sealed and immediately refrigerated during the period prior to filtration.

Direct counts were processed using the basic technique of Hobbie et al. (2) with some modifications. Five- or ten-mℓ aliquots of water samples were filtered through stained (Irgalan Black) Nuclepore^{R} filters (0.2 µm, 25 mm dia.) at reduced pressure (100 mm Hg). Cells were then washed by filtration with 10 mℓ of a 0.2% solution of sodium metabisulfite (aldehyde block) in distilled water. Several mℓ of sterile distilled water were then placed on the filter followed by 200 µℓ of the fluorescent dye proflavin (0.033% in distilled water). Staining was for 5 min followed by a 10-mℓ wash with distilled water. Filters were removed upon dryness, cleared with non-fluorescing immersion oil on a standard microscope slide, covered with a #1 coverslip and stored under refrigeration pending examination by epifluorescence. Using this methodology, relatively stable high contrast images without rapid bleaching were routinely obtained. All solutions and washes were filtered through 0.2-µm membrane

filters immediately prior to processing.

Cells were counted using a Zeiss Standard microscope equipped with an epi-fluorescence illuminator for FITC fluorescence (exciter filter KP 490, beam splitter FT 510 and barrier LP 520). Only recognizable bacterial cells were counted from 49 randomly chosen fields within a known area of an ocular grid. Count values were corrected for area, sample volume, dilution factors and expressed as bacterial units (BU) $m\ell^{-1}$. Replicate counts of randomly chosen samples as well as procedural blanks were performed.

Heterotrophic Potential

Heterotrophic potential or V_{max} (glucose) was determined by incubating replicate 10 $m\ell$-aliquots of each water sample with uniformly labeled ^{14}C-glucose (250-360 mCi mmole^{-1}) at final concentrations of 37.5, 75.0, 187.5 and 370.5 $\mu g\ \ell^{-1}$ in the dark at ambient water temperatures for 3 h. Control and incubated samples were inactivated by the addition of 0.1 $m\ell$ of 2% buffered formalin. ^{14}C-labeled particulate fractions were collected on cellulose acetate filters (Millipore^R EHWP 0.5 μm), the filters placed in 4.0-$m\ell$ mini-vials (Wheaton) to which 3.5 $m\ell$ of Aquasol II (New England Nuclear) was added. Counting was carried out at 88-91% efficiency using a liquid scintillation counter with external standardization (Beckman LS-150). The calculation of V_{max} (glucose) using linear regression analysis had an r value of 0.9 or greater for at least 3 of the 4 substrate concentrations used. No provision was made to trap and measure respired ^{14}C-CO_2 during the incubation period. Therefore, calculated V_{max} values represent only that portion of labeled substrate in particulate form and are minimum estimates of substrate uptake.

RESULTS

Data for viable, direct bacterial counts, V_{max} (glucose) and relevant physical-chemical measurements are compiled in Tables 1 and 2. Locations of stations are shown in Figure 1.

Viable bacterial count densities were consistently smaller than corresponding direct count densities. Viable counts in surface waters ranged from a maximum of 190×10^3 MPN $m\ell^{-1}$ at the Bay mouth to a minimum of 7.9×10^3 MPN $m\ell^{-1}$ in offshore waters. Similarly, direct count densities ranged from 1800×10^3 BU $m\ell^{-1}$ to a minimum of 24×10^3 BU $m\ell^{-1}$ offshore. Mean viable count densities were approximately 10x smaller than direct count densities (Table 2). Such a relationship is considered usual since direct counting techniques enumerate all cells present, including active, dead, and dormant cells and cells metabolically incapable of a positive response in the heterotroph medium employed. Furthermore, correction for positive bias inherent in the MPN technique would reduce the viable counts and thus increase the differential between direct and viable MPN counts.

Although a detailed quantitative analysis was not made, the majority of bacteria (80-90%) appeared as free-living cells and were not attached to

particulates. Analysis of direct count samples revealed possibilities for enumeration and identification of heterotrophic and photosynthetic flagellates and algae and the presence of sometimes abundant coccoid cells somewhat larger than bacteria. Cells resembling the latter have been reported to be coccoid cyanobacteria (3); however, the decay of natural fluorescence in stored samples prevented definitive identification. Therefore, the direct counting epifluorescence procedure will be most useful for the identification and quantification of microorganisms (other than bacteria) if preparations are processed and examined on shipboard before the naturally fluorescing photopigments decay.

Bacterial numbers and V_{max} were generally largest in surface waters and at all depths in the water column for stations closest to the Bay mouth. V_{max} values ranged from a maximum of 0.770 µg glucose $\ell^{-1}h^{-1}$ at the Bay mouth to a minimum of 0.057 µg glucose $\ell^{-1}h^{-1}$ offshore. Figure 1 shows the spatial distribution of bacterial count and V_{max} values contoured for surface (1 m) water. Smaller values were located outside the "plume" and were generally farthest offshore. These spatial distributions are "quasi-synoptic" since the data were collected over a range of tidal and meteorological conditions during a seven day cruise interval.

Biomass and V_{max} values generally decreased with depth although subsurface maxima were occasionally observed at inshore stations. Such values tended to correspond to elevated levels of particulates (Table 1). However, it was not clear if these elevated levels were due to suspension of sediment through bottoming of the sampler or cable weight during rolling, turbulence generated by the vessel, or to an actual subsurface turbidity maximum.

Non-parametric correlation analyses (4) of microbial data with selected hydrographic measurements were performed (Table 3). Viable count data were significantly correlated with direct counts and V_{max}. V_{max} was significantly correlated with both viable and direct counts. Viable counts were positively and significantly correlated with chlorophyll concentrations and temperature, negatively and significantly correlated with salinity and depth, but not correlated with suspended particulates. Absolute values of the Kendall Tau statistic are not directly comparable with correlation coefficients derived using other statistics and indicate only relative degrees of correlation or correspondence.

Table 4 indicates the relationship of sampling depth to arithmetic means of microbiological data for each depth. Both mean numbers of viable saprophytic bacteria and direct counts decreased with depth. Proportionately, the decrease in mean V_{max} at the greatest depth was closer to the decrease in mean direct count than to mean viable count. Thus, values of V_{max} and direct count at depths greater than 15 m were approximately 50% of the surface values while mean viable count was 19% of the surface.

DISCUSSION

Despite inherent limitations associated with quasi-synoptic chemical and biological sampling of a large and dynamically complex estuarine-shelf system

such as the Chesapeake Bay plume, non-parametric correlation analyses of microbial and selected hydrographic variables revealed statistically significant relationships. Furthermore, the significant correspondence of microbial variables with plume hydrographic characteristics provided (at least during this cruise) a means for detection and spatial location of plume waters using microbiological measurements.

Highly significant values of Tau ($\alpha \leq 0.001$) were obtained for viable bacterial counts with direct bacterial counts and V_{max}. Significant negative correlations of these microbial parameters with salinity and depth indicated surface or lower salinity plume water contained the largest bacterial biomass and the most active cells. This association also appeared as a significant positive correlation of microbial parameters with water temperature. A significant negative correlation of salinity with temperature suggested a stratified hydrographic regime typical of the summer period. Lack of significant correlation of microbial data with suspended particulates may have been related to the presence of subsurface suspended solids maxima or to the relatively small variation in the suspended solids data set.

Microbial analyses of Chesapeake Bay plume waters revealed a highly active population of saprophytic bacteria. Both bacterial standing crop (direct or viable count) and V_{max} activity measurements were significantly greater in surface plume waters compared with the colder shelf water. Saprophytic bacterial populations are known to require relatively high levels of natural or pollutant-derived organic solutes which must be present in Bay plume waters.

Actual bacterial biomass may be approximated on a weight basis from direct count data using an average cell volume of 0.06 μm^3 (5) and assuming a specific gravity of 1.0. Values shown in Table 5 for mean bacterial densities correspond to direct count density contours shown in Figure 1. The distribution of biomass (and V_{max}) with respect to proximity to the Bay mouth was qualitatively similar to that measured in Kiel Fjord and Bight waters in Germany (6). Mean surface bacterial biomass corresponded to 0.8% of the mean total suspended particulate load within the contour of maximum direct count density. By comparison, if one assumes that chlorophyll concentration may be converted to cellular carbon using an average weight ratio of 60:1 for carbon:chlorophyll (5), the same mean bacterial biomass was approximately equivalent to 4% of the phytoplankton standing crop. Although these estimates are extremely rough, they do suggest the instantaneous standing crop of bacterial biomass in plume waters was not insubstantial as a food source for potential consumers such as heterotrophic flagellates. An estimate of the true flux of bacterial protoplasm as a carbon and energy source to shelf waters is not possible owing to the unavailability of information on the net flux of bacterial biomass from the Bay or seasonal bacterial growth rates during transition from Bay to shelf waters. Finally, although the effect of streamflow volume into the Bay on bacterial productivity and net transport is unknown, it is probable that significantly lower streamflow volumes such as those encountered in 1980 would reduce bacterial biomass production.

In summary, Chesapeake Bay plume waters supported high levels of active saprophytic marine bacteria. These bacteria not only convert nutrients and organic matter into bacterial protoplasm, but appear to be a significant food source of unknown dimension for microorganisms such as heterotrophic flagellates and others.

REFERENCES

1. APHA-AWWA-WPCF. 1975. Part 900. Microbiological Examination of Water, 875-1004. In Standard Methods for the Examination of Water and Wastewater. 14th Ed. American Public Health Association, Washington, D. C.

2. Hobbie, J. E., O. Holm-Hansen, T. T. Packard, L. R. Pomeroy, R. W. Sheldon, J. P. Thomas, W. J. Wiebe. 1972. A study of the distribution and activity of microorganisms in ocean water. Limnol. Oceanog. 17: 544-555.

3. Sieburth, J. M. 1979. Sea Microbes. Oxford University Press, New York, 491 p.

4. Siegel, S. 1956. Ch. 9. Measures of Correlation and Their Tests of Significance, 195-239. In Non-Parametric Statistics, McGraw-Hill, New York.

5. Strickland, J. D. H. 1965. Production of organic matter in the primary stages of the marine food chain. In J. P. Riley and G. Skirrow [eds.], Chemical Oceanography. Academic Press, Ottawa.

6. Zimmermann, R. 1977. Estimation of bacterial number and biomass by epifluorescence microscopy and scanning electron microscopy. In G. Rheinheimer [ed.], Microbial Ecology of a Brackish Water Environment. Ecological Studies Volume 25. Springer-Verlag, Berlin.

Table 1. Biomass and V_{max} data and selected physical-chemical parameters used for Kendall Tau calculations. Chesapeake Bay Plume Experiment II.

NOAA Station No.	Depth m	Viable Count MPNx10^3 mℓ^{-1}	Direct Count BUx10^3 mℓ^{-1}	V_{max} µg glucose $\ell^{-1}h^{-1}$	Salinity o/oo	Temperature °C	Total Chlorophyll µg ℓ^{-1}	Suspended particulates mg ℓ^{-1}
800	1	190	1800	0.681	21.63	22.30	3.41	1.3
	7	120	1900	0.663	21.98	22.00	2.08	2.0
801	1	160	1100	0.590	26.0	20.20	2.73	3.8
	5	80	1500	0.425	27.73	20.20	2.21	1.3
	10	56	1300	-	30.48	19.50	2.57	1.4
	13	100	540	0.535	31.09	19.20	2.89	1.6
69	1	140	870	0.691	27.48	20.50	7.62	2.0
	5	110	700	0.612	28.05	19.70	7.75	3.2
	10	60	380	0.980	31.38	18.20	2.41	5.0
802	1	150	1000	0.737	25.49	20.80	4.32	1.3
	5	23	180	-	28.38	18.30	2.22	0.7
	10	23	110	0.192	31.96	17.80	1.91	2.7
	15	20	210	-	31.92	17.40	1.84	3.7
	17	25	200	0.256	32.18	16.80	1.52	1.4
803	1	150	270	0.351	29.02	20.40	1.62	2.2
	5	82	560	-	31.50	19.80	1.68	0.1
	10	57	390	0.245	32.19	18.90	1.57	0.8
804	1	31	320	0.207	32.15	18.70	1.44	0.3
	5	51	170	-	32.15	18.60	1.55	0.5
	10	48	170	0.221	32.15	18.60	1.32	0.5
	15	33	170	0.305	32.26	18.50	2.86	0.7
805	1	190	980	0.770	25.97	21.00	2.57	1.4
	5	23	120	-	28.06	18.20	2.57	1.2
	10	56	290	0.851	33.97	16.80	2.25	2.0

Table 1 (continued)

NOAA Station No.	Depth m	Viable Count MPNx10^3 mℓ^{-1}	Direct Count BUx10^3 mℓ^{-1}	V_{max} µg glucose $\ell^{-1}h^{-1}$	Salinity o/oo	Temperature °C	Total Chlorophyll µg ℓ^{-1}	Suspended particulates mg ℓ^{-1}
70	1	36	200	0.404	26.55	21.40	1.75	0.4
	5	23	240	-	27.16	17.50	1.85	1.2
	10	7.2	130	0.209	31.69	15.40	1.65	1.8
	13	6.4	220	0.222	32.21	14.80	1.51	0.4
806	1	23	130	0.189	29.58	20.00	0.66	1.2
	5	28	79	-	30.72	18.80	0.51	0.6
	10	12	120	0.103	32.16	17.50	0.68	1.0
	15	33	180	0.077	32.26	17.40	1.97	2.8
807	1	7.9	24	0.057	31.60	19.40	0.51	0.4
	5	19	44	0.043	31.60	19.35	0.51	0.2
	10	7.7	57	-	32.03	19.00	0.58	0.2
	15	9	400	0.723*	32.40	14.40	1.3	0.4
808	1	28	460	0.365	29.44	20.00	1.57	0.8
	5	40	500	-	29.41	18.30	1.53	1.0
	10	36	390	0.710	31.96	14.45	5.27	1.2
809	1	41	480	0.484	27.34	21.00	1.46	0.6
	5	56	140	-	27.36	20.80	1.18	0.4
	10	9.5	98	-	30.77	15.00	2.29	2.0
	15	14	260	0.211	31.71	13.80	2.29	0.8
810	1	9.5	57	0.164	30.08	20.20	0.80	1.4
	6	27	77	-	30.09	20.20	0.80	0.8
	12	64	180	0.240	31.28	14.50	1.22	0.4
	18	18	220	0.203	32.78	13.30	3.62	0.2
811	1	9.5	140	-	31.87	20.10	0.71	1.6
	7	18	74	-	31.92	19.20	0.40	2.2
	14	6	76	-	32.31	15.10	0.72	3.8
	21	8	160	-	33.12	12.80	2.07	6.4

Table 1 (concluded)

NOAA Station No.	Depth m	Viable Count MPNx10^3 mℓ^{-1}	Direct Count BUx10^3 mℓ^{-1}	V_{max} µg glucose $\ell^{-1}h^{-1}$	Salinity o/oo	Temperature °C	Total Chlorophyll µg ℓ^{-1}	Suspended particulates mg ℓ^{-1}
813	1	15	83	-	30.42	20.20	0.42	1.2
	6	9	130	-	30.69	19.90	0.35	1.8
	12	6.4	85	-	31.92	19.00	0.46	0.2
	18	3.3	21	-	32.97	12.20	0.86	2.2
812	1	41	110	0.294	28.68	22.00	0.63	1.4
	5	40	96	-	28.90	20.75	0.87	6.2
	10	20	72	0.164	29.65	19.30	0.87	2.0
	15	4.9	340	-	31.75	13.60	2.03	4.0
	20	-	270	0.146	32.54	13.20	2.88	0.6
71	1	25	76	0.189	29.75	21.00	0.70	0.4
	6	46	300	0.189	29.83	20.35	0.78	0.2
	12	46	290	0.252	30.30	19.40	0.98	0.4
814	1	42	510	0.219	29.80	21.20	0.68	0.8
	5	110	460	0.465	29.82	21.00	0.68	3.2
	10	95	780	0.714	30.87	16.40	0.92	0.8

*sand in sample, value discounted

Table 2. Statistical analysis of hydrographic and microbiological parameters.

VARIABLE	N	MEAN	STD DEV	MEDIAN	MINIMUM	MAXIMUM
DEPTH, M	66	7.65	5.66	6.00	1.0	21.0
VIABLE COUNT, MPN $m\ell^{-1}$	65	46901.54	47107.42	28000.00	3300.0	190000.0
DIRECT COUNT, BU $m\ell^{-1}$	66	366333.33	407183.92	210000.00	24000.0	1900000.0
VMAX, µg glucose $\ell^{-1}h^{-1}$	42	0.37	0.24	0.25	0.0	1.0
SALINITY, o/oo	66	30.22	2.47	30.82	21.6	34.0
TEMPERATURE, °C	66	18.42	2.55	19.10	12.2	22.3
CHLOROPHYLL, µg ℓ^{-1}	66	1.80	1.44	1.54	0.3	7.8
SUSPENDED SOLIDS, mg ℓ^{-1}	66	1.53	1.38	1.20	0.1	6.4

Table 3. Values of non-parametric Kendall Tau correlation coefficient calculated for biomass and V_{max} data against selected physical and chemical parameters.

	DEPTH	VIABLE	DIRECT	VMAX	SAL	TEMP	CHLOR	SS
DEPTH	1.00000[a]	-0.30595	-0.05199	-0.11746	0.57184	-0.63975	0.12728	0.05973
	0.0000[b]	0.0008	0.5646	0.3106	0.0001	0.0001	0.1580	0.5151
	66[c]	65	66	42	66	66	66	66
VIABLE COUNT	-0.30595	1.00000	0.48273	0.58477	-0.39748	0.38225	0.28488	0.01240
	0.0008	0.0000	0.0000	0.0000	0.0000	0.0000	0.0009	0.8871
	65	65	65	41	65	65	65	65
DIRECT COUNT	-0.05199	0.48273	1.00000	0.57494	-0.20094	0.08253	0.43076	0.07243
	0.5646	0.0000	0.0000	0.0000	0.0178	0.3324	0.0000	0.4019
	66	65	66	42	66	66	66	66
VMAX	-0.11746	0.58477	0.57494	1.00000	-0.31389	0.19472	0.41521	0.30512
	0.3106	0.0000	0.0000	0.0000	0.0035	0.0717	0.0001	0.0055
	42	41	42	42	42	42	42	42
SALINITY	0.57194	-0.39748	-0.20094	-0.31389	1.00000	-0.59488	-0.08206	-0.05836
	0.0001	0.0000	0.0178	0.0035	0.0000	0.0001	0.3326	0.4983
	66	64	66	42	66	66	66	66
TEMPERATURE	-0.63975	0.38225	0.08253	0.19472	-0.59488	1.00000	-0.12718	-0.03315
	0.0001	0.0000	0.3324	0.0717	0.0001	0.0000	0.1348	0.7016
	66	65	66	42	66	66	66	66
CHLOROPHYLL	0.12728	0.28488	0.43076	0.41521	-0.08206	-0.12718	1.00000	0.17632
	0.1580	0.0009	0.0000	0.0001	0.3326	0.1348	0.0000	0.0411
	66	65	66	42	66	66	66	66
SUSPENDED SOLIDS	0.05973	0.01240	0.07243	0.30512	-0.05836	-0.03315	0.17632	1.00000
	0.5151	0.8871	0.4019	0.0055	0.4983	0.7016	0.0411	0.0000
	66	65	66	42	66	66	66	66

[a]Kendall Tau correlation coefficient
[b]probability of obtaining value randomly
[c]sample size

Table 4. Mean values of selected microbiological and hydrographic variables for depths indicated.

	1 m	5 m	10 m	15 m	>15 m
Viable Count, MPN $m\ell^{-1}$	71605	52692	37492	26083	13575
Direct Count, BU $m\ell^{-1}$	478333	368384	329769	245916	212000
Vmax, µg glucose $\ell^{-1}h^{-1}$	0.40	0.39	0.44	0.26	0.20
Chlorophyll, µg ℓ^{-1}	1.87	1.93	1.87	1.67	2.19
Suspended Solids, mg ℓ^{-1}	1.25	1.52	1.65	1.60	2.16

Table 5. Estimated bacterial biomass calculated from direct count densities of the surface waters (1 m) as shown in Figure 1.

Density Contour	Mean Direct Count, BUx10^3 $m\ell^{-1}$	Estimated Mean Biomass, Wet, µg $m\ell^{-1}$	Estimated Mean Biomass, Dry, µg $m\ell^{-1}$
6.0-6.5	1300	0.078	0.016
5.5-5.9	500	0.030	0.006
5.0-5.4	160	0.0096	0.0019
4.5-4.9	79	0.0047	0.0009
4.0-4.4	25	0.0015	0.0003

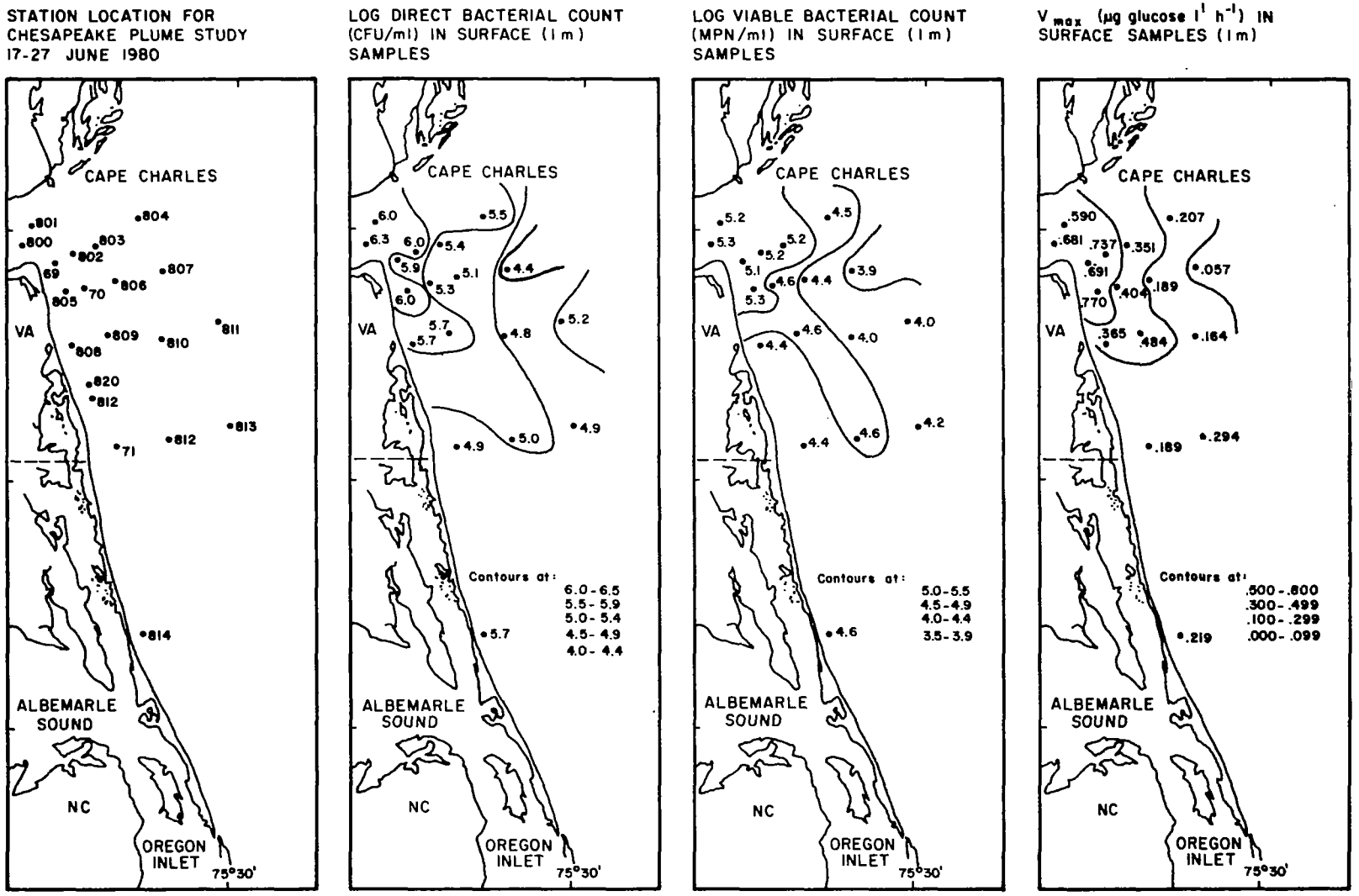

Figure 1. Location charts for observed parameters in the surface waters during Chesapeake Bay Plume Study, 17-27 June 1980. Station Locations/Direct Bacterial Count/Log Viable Bacterial Count/V_{max} (glucose).

ANALYSIS OF ALOPE DATA FROM SUPERFLUX

Olin Jarrett, Jr., Wayne E. Esaias,
Clarence A. Brown, Jr., and E. Brian Pritchard
NASA Langley Research Center

SUMMARY

Remote sensing data collected with the Airborne Lidar Oceanographic Probing Experiment (ALOPE) laser fluorosensor during the Superflux I (March 17, 1980) and Superflux II (June 23, 1980) experiments have been analyzed using two techniques. A qualitative technique which requires no supplementary data has provided a near-real-time estimate of relative abundance of the golden-brown and green phytoplankton color groups. Contour plots developed for the June 23, 1980 mission are used to demonstrate the utility of this technique. A quantitative technique which requires supplementary data to define the attenuation coefficient provides chlorophyll *a* concentration by color group. The sum of the golden-brown and green chlorophyll *a* data yields total chlorophyll *a* values which may be compared with in situ data.

Maximum values of chlorophyll *a* concentration for the golden-brown population were 0.08 g/m^3 in the vicinity of Newport News Point for the March 17, 1980 mission. Maximum values of chlorophyll *a* concentration for the green population were 0.03 g/m^3 in the vicinity of Fort Monroe and again offshore in the region of the "Green River." As expected, the golden-brown population was dominant in the Chesapeake Bay and the Bay plume whereas the green population was dominant in shelf waters.

INTRODUCTION

The Airborne Lidar Oceanographic Probing Experiment (ALOPE) remote laser fluorosensor was used in Superflux I and II to collect data on the relative abundance and chlorophyll *a* concentrations of phytoplankton species of the golden-brown and green color groups. Two analysis techniques were used in this study. The first provides a qualitative distribution of phytoplankton between the two color groups of interest (golden-brown and green) without the need for either chlorophyll *a* sea truth or measurement of attenuation coefficient. The second provides a quantitative distribution of chlorophyll *a* by color group but requires some in situ data on attenuation coefficient to define the depth of penetration of the laser beam into the water. This paper presents both qualitative and quantitative data on chlorophyll *a* concentrations and species diversity for the Superflux missions of March 17 and June 23, 1980.

Classification errors are not discussed; however, the potential for such errors is discussed by Farmer (ref. 1). In addition, correlations between

the remote fluorosensor data and in situ cell counts have not been attempted to date. The data of Marshall (ref. 2) will provide the necessary data base for such comparisons.

SENSOR AND MISSION DESCRIPTION

The ALOPE remote laser fluorosensor, originally configured for four excitation wavelengths (see ref. 3) was modified for the Superflux missions to use only two excitation wavelengths. The dominance of the golden-brown and green phytoplankton color groups in Chesapeake Bay and adjacent continental shelf waters eliminates the need for consideration of the blue-green and red color groups. For this study, excitation wavelengths of 454 and 539 nm were selected as near optimum for discrimination between the two color groups of interest. Alternating pulses of laser light at the 454 and 539 nm wavelengths are emitted with a time separation of 1.9 seconds. Laser power varies from 2 to 5 mJ with a pulse duration of 400 n sec. Laser-induced fluorescence at 685 nm is collected through a telescope-optical filter (9-nm-bandwidth) photomultiplier tube system. Laser-off data are also collected to determine background radiance.

The ALOPE sensor was mounted in the NASA-Wallops P-3 aircraft and flown at 152-meter altitude at a nominal airspeed of 350 km/hour. The data presented here are for the James/shelf mission of March 17, 1980 (identical to the mission of June 20, 1980 as presented in fig. 2 of ref. 4) and the mapping mission of June 23, 1980 (see fig. 3 of ref. 4).

The fundamental equation defining laser-induced fluorescence (as developed in ref. 5) is:

$$F(\lambda) = K(\alpha_\lambda + \alpha_F) \frac{P_{r_\lambda}}{P_{o_\lambda}} \qquad (1)$$

where $F(\lambda)$ is the chlorophyll a fluorescence at 685 nm produced by laser excitation at wavelength λ

α_λ is the water attenuation coefficient at the excitation wavelength

α_F is the water attenuation coefficient at the fluorescence wavelength (685 nm)

P_{r_λ} is the energy received by the PMT at 685 nm

P_{o_λ} is the output energy of the laser at the excitation wavelength

K is the collected geometrical and optical terms which are constant for a given flight altitude and system

Fluorescence can be related to chlorophyll a concentration by the expression

$$F(\lambda) = \sum_i n_i \sigma_{i\lambda} \tag{2}$$

where n_i is the chlorophyll a concentration, or density of a given phytoplankton color group

and $\sigma_{i\lambda}$ is the fluorescence cross-section of a given phytoplankton color group at excitation wavelength λ

Thus, for Chesapeake Bay and adjacent shelf waters where there are two dominant phytoplankton color groups, equation (2) becomes

$$F(\lambda_1) = n_1 \sigma_{1\lambda_1} + n_2 \sigma_{2\lambda_1} \tag{3}$$

Then for the two excitation wavelengths used for the Superflux experiments

$$F(454) = n_1 \sigma_{1,454} + n_2 \sigma_{2,454} \tag{4a}$$

and

$$F(539) = n_1 \sigma_{1,539} + n_2 \sigma_{2,539} \tag{4b}$$

If σ is known, then chlorophyll a concentration can be determined from equations (4a) and (4b).

The fluorescence cross-sections of a number of phytoplankton species have been measured in the laboratory by flowing well-mixed samples through a fluorescence spectrophotometer (see ref. 5). Typical values of σ for the golden-brown and green color groups as a function of excitation wavelength are shown in figure 1. Also indicated are the two excitation wavelengths selected for the Superflux experiments. Note that the two curves are significantly different in shape, thereby permitting differentiation between the two color groups through data obtained at the two indicated excitation wavelengths.

Although environmental factors are known to effect the value of σ, the shape of the $\sigma - \lambda$ curve is not significantly affected. Thus, use of laboratory-derived cross-sections with remotely sensed data can provide an estimate of the chlorophyll a concentration by color group and a qualitative determination of the relative distribution of phytoplankton between color

groups. Limited in situ data can be used to correct the laboratory-derived cross-sections for environmental effects to provide quantitative data on chlorophyll a density by color group.

Qualitative analysis.- The qualitative approach to phytoplankton color group discrimination without the need for definition of α or sea-truth data to correct laboratory-derived cross-sections is derived from examination of the fluorescence ratio

$$R = \frac{F_{539}}{F_{454}} \tag{5}$$

Substitution of equation (1) yields

$$R = \frac{\alpha_{539} + \alpha_{685}}{\alpha_{454} + \alpha_{685}} \frac{P_{r539}}{P_{o539}} \Big/ \frac{P_{r454}}{P_{o454}} \tag{6}$$

Elimination of the α dependency of equation (6) requires examination of the α term in equation (6) over a variety of conditions. Figure 2 presents measured values of the α ratio from 20 in situ samples with α values ranging from 0.43 m^{-1} to 36.9 m^{-1} (at λ = 633 nm, ref. 3) as a function of α_{633}. The α ratio is seen to be essentially constant at a value of 0.929. Those data of figure 2 for which in situ chlorophyll measurements were available are plotted in figure 3 to demonstrate that there is no significant variability of α with chlorophyll a. Thus, equation (6) can be rewritten as:

$$R \simeq 0.929 \frac{P_{r539}}{P_{o539}} \Big/ \frac{P_{r454}}{P_{o454}} \equiv 0.929\ R^* \tag{7}$$

Remotely sensed data can then be input to equation (7) to determine fluorescence ratio.

From figure 1 (and ref. 3) it can be seen that for values of R of approximately unity, the phytoplankton are essentially all golden-browns, while for values of R of approximately 0.3, the phytoplankton are all members of the green color group. Values of R between 1.0 and 0.3 would indicate mixtures of phytoplankton of the two color groups.

Quantitative Analysis.- Quantitative determination of chlorophyll a by color group is obtained by substitution of equations (4a) and (4b) into equation (1) to obtain

$$n_1\sigma_{1,454} + n_2\sigma_{2,454} = K(\alpha_{454} + \alpha_{685}) \frac{P_{r454}}{P_{o454}} \tag{8a}$$

$$n_1\sigma_{1,539} + n_2\sigma_{2,539} = K(\alpha_{539} + \alpha_{685}) \frac{P_{r539}}{P_{o539}} \tag{8b}$$

Solution of equations (8a) and (8b) for n_1 and n_2 requires measured values of α and corrections to laboratory-derived values of σ. (In these calculations, laboratory-derived values for σ were used.) For the purposes of this study, values of α were obtained from a straight-line fit between background radiance at 685 nm (laser off) and the measured in situ values of α. Under clear-sky conditions, background radiance normalized by solar elevation angle correlates well with attenuation coefficient. For future studies, however, it is recommended that the laser-induced Raman peak be used to determine α as discussed by Hoge (ref. 6).

RESULTS

Qualitative Analysis

Equation 7 was used to generate the results shown in figures 4 and 5. Figure 4 presents results for the return leg of the March 17, 1980 James/shelf mission. As discussed previously, values of R of 1.0 indicate golden-brown phytoplankton, and values of 0.3 indicate green phytoplankton. Golden-browns are seen to dominate within the Chesapeake Bay with greens dominating offshore (from about 120 km to 180 km). The increase in relative abundance of golden-browns between 180 km and 195 km corresponds to the shelf break region.

Sufficient data were collected on the mapping mission of June 23, 1980 to generate the contour plot shown in figure 5. Golden-browns clearly dominate within the Bay ($R > 0.65$). The contour for $R = 0.43$ gives a good qualitative description of the Bay plume extending along the Virginia-North Carolina coast, and is in good agreement with other data collected on this mission. The wave-like structure (wavelength $\simeq$ 25 km) of the outer edge of the plume appears to be induced by tidal effects.

Data of the type shown in figures 4 and 5 could be generated in near real time for future Chesapeake Bay plume studies. Such data would be very useful in directing seaborne systems to sampling areas of high interest.

Quantitative Analysis

Quantitative plots of chlorophyll a for the March 17, 1980 mission are presented in figures 6, 7, and 8 for the golden-brown color group, the green color group, and total chlorophyll a, respectively. These data were obtained by solution of equations (8a) and (8b). Golden-browns are seen (fig. 6) to peak at a value of about 0.08 g/m^3 in the vicinity of Newport News Point. They decrease to zero in the range of 120 to 160 km and increase slightly in the expected region of the "Green River." In figure 7, greens are seen to be low in the Bay, then increasing to a peak of 0.03 g/m^3 in the vicinity of Fort Monroe.

Total chlorophyll a, shown in figure 8, indicates significant fine structure with clearly defined peaks at 10- to 15-km intervals from 20 to 110 km distance. These data also indicate a minimum between 130

and 150 km. Further analysis of these data, in combination with the data from other remote sensors and in situ investigations, will be required to assess the significance of these results. The four sea truth data points indicated on figure 8 show consistency between remote and in situ data within the accuracy of both techniques. The results presented in figures 6 to 8 were obtained using laboratory-developed fluorescence cross sections, σ. Future analyses should incorporate a correction to these values derived from in situ data.

CONCLUSIONS

Data generated by a dual-laser-excitation-wavelength, single-wavelength-detector remote airborne fluorosensor provide a near-real-time qualitative assessment of phytoplankton distribution by color group without the need for in situ data. Quantitative chlorophyll a concentrations by color group are obtained through the use of supplementary data to define the attenuation coefficient. It is recommended that the laser-induced Raman peak be used to determine attenuation coefficient in future studies.

Results from this study demonstrate the capability of remote laser fluorosensor systems to determine fine-scale structure both within the Chesapeake Bay Plume and in shelf waters.

References

1. Farmer, Franklin H.: Interpretation of an Index of Phytoplankton Population Composition Calculated from Remote Airborne Fluorosensor (RAF) Data. Chesapeake Bay Plume Study - Superflux 1980, NASA CP-2188, 1981 (Paper no. 31 of this compilation).

2. Marshall, H. G.: Phytoplankton Assemblages Within the Chesapeake Bay Plume and Adjacent Waters of the Continental Shelf. Chesapeake Bay Plume Study - Superflux 1980, NASA CP-2188, 1981 (Paper no. 32 of this compilation).

3. Brown, Clarence A., Jr.; Jarrett, Olin, Jr.; and Farmer, Franklin H.: Laboratory Tank Studies of Single Species of Phytoplankton Using a Remote Sensing Fluorosensor. NASA TP-1821, 1981.

4. Campbell, Janet W.; Esaias, Wayne E.; and Hypes, Warren D.: Superflux I, II, and III Experiment Designs: Remote Sensing Aspects. Chesapeake Bay Plume Study - Superflux 1980, NASA CP-2188, 1981 (Paper no. 4 of this compilation).

5. Jarrett, Olin, Jr.; Mumola, Peter B.; and Brown, Clarence A., Jr.: Four-Wavelength Lidar Applied to Determination of Chlorophyll a Concentration of Algae Color Group. Remote Sensing and Water Resources Management, Keith P. B. Thomson, Robert K. Lane, and Sandor C. Csallany, eds., Proc. no. 17, American Water Resources Association, 1973, pp. 259-268.

6. Hoge, F. E.; and Swift, R. N.: Application of the NASA Airborne Oceanographic Lidar to the Mapping of Chlorophyll and Other Organic Pigments. Chesapeake Bay Plume Study - Superflux 1980, NASA CP-2188, 1981 (Paper no. 26 of this compilation).

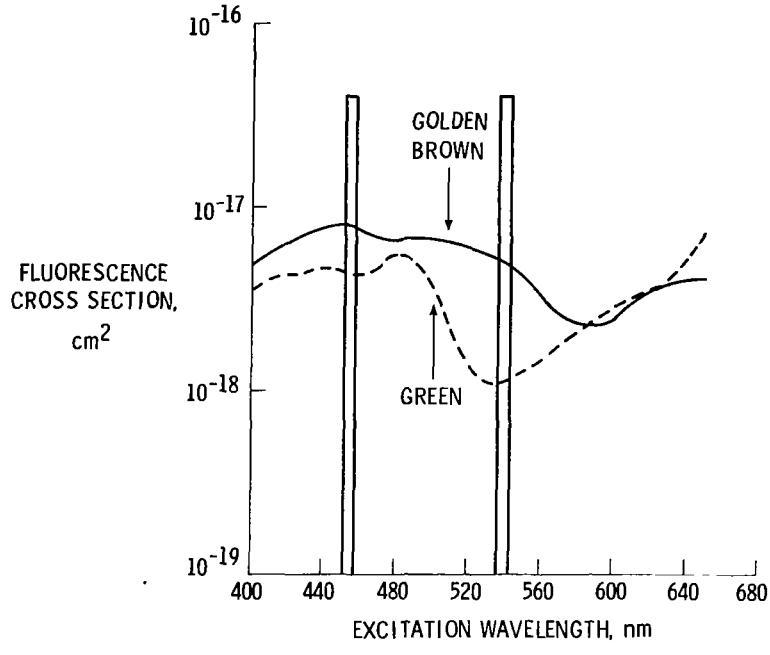

Figure 1.- Fluorescence cross-sections for single species representative of green and golden-brown phytoplankton color groups. (Vertical bars are at laser excitation wavelengths.)

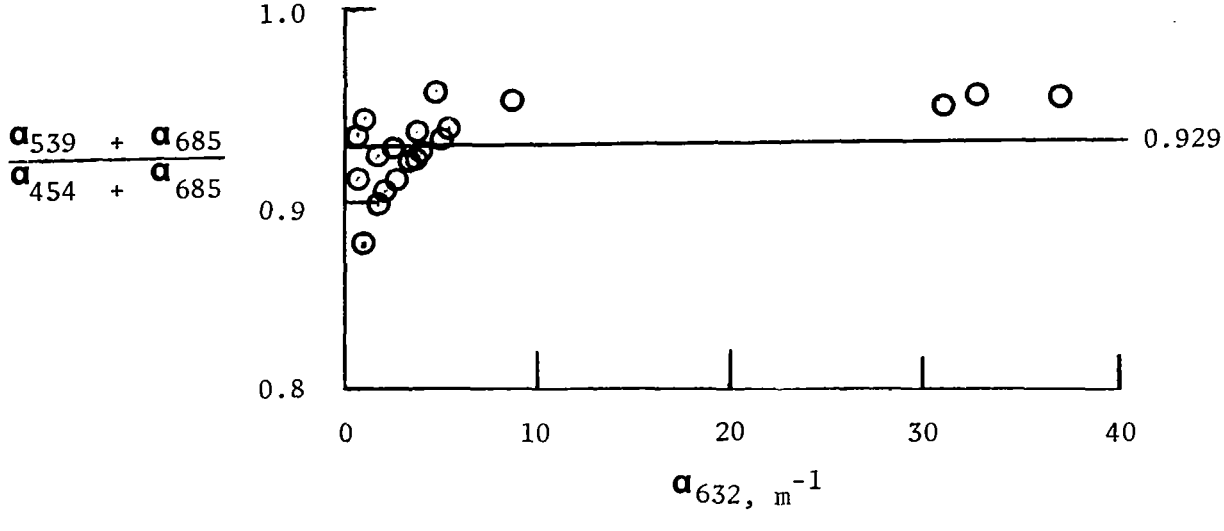

Figure 2.- In situ attenuation coefficient ratio.

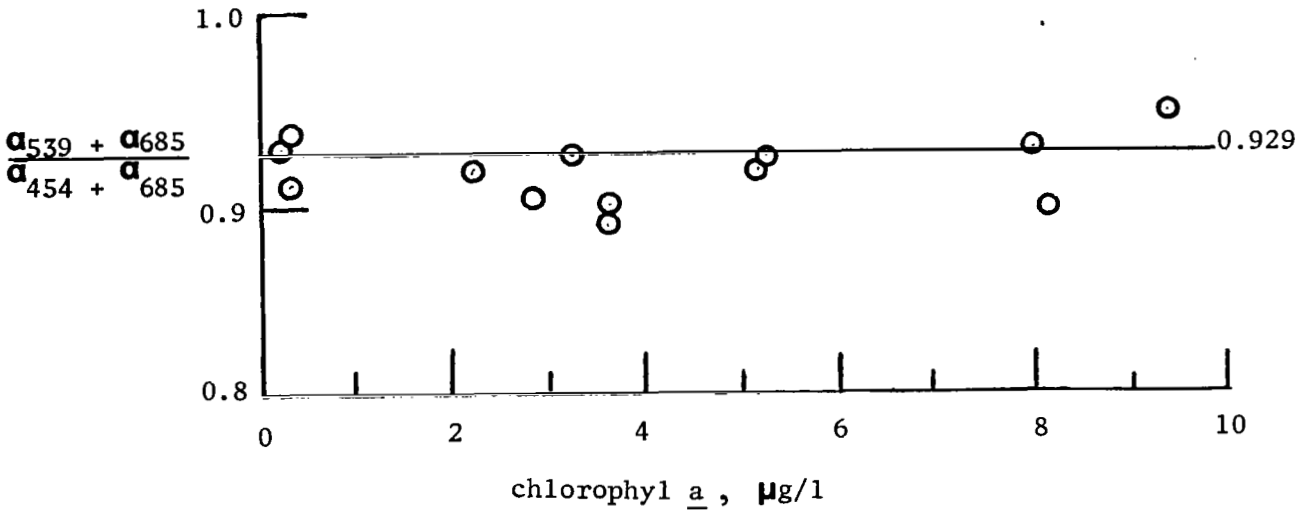

Figure 3.- In situ attenuation coefficient ratio - chlorophyll a relationship.

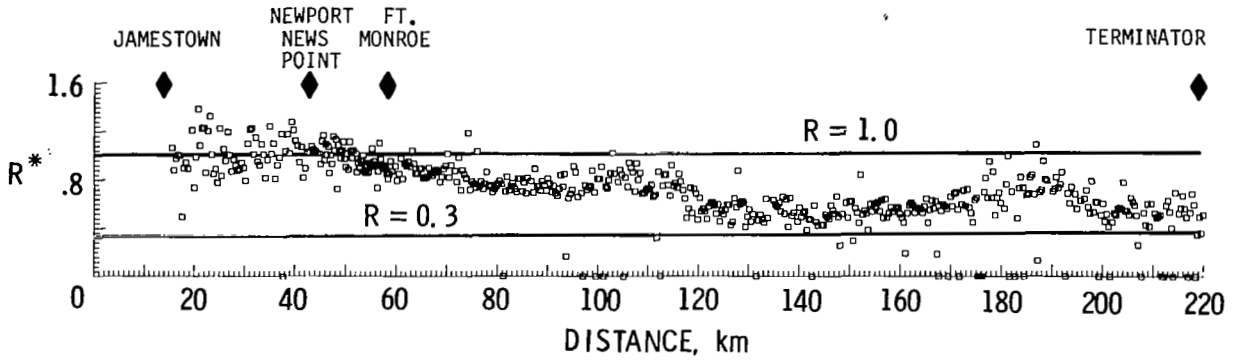

Figure 4.- Fluorescence ratio, R*, for March 17, 1980 James/shelf mission.

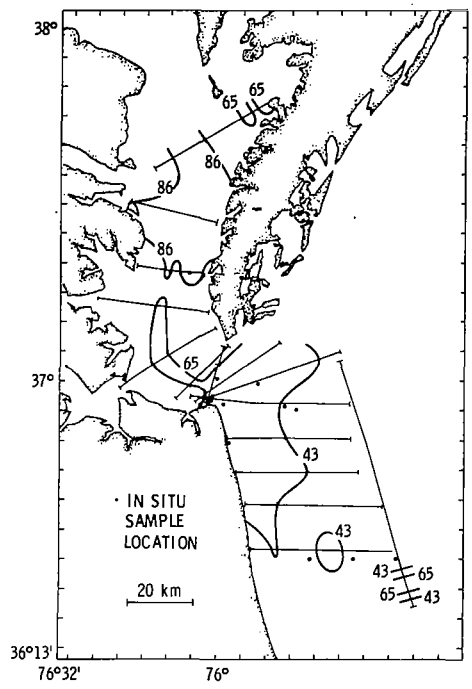

Figure 5.- Flight paths and contours from calculations of fluorescence ratios for June 23, 1980 mapping mission. (Numbers on contour lines are fluorescence ratio, R, x 10^2.)

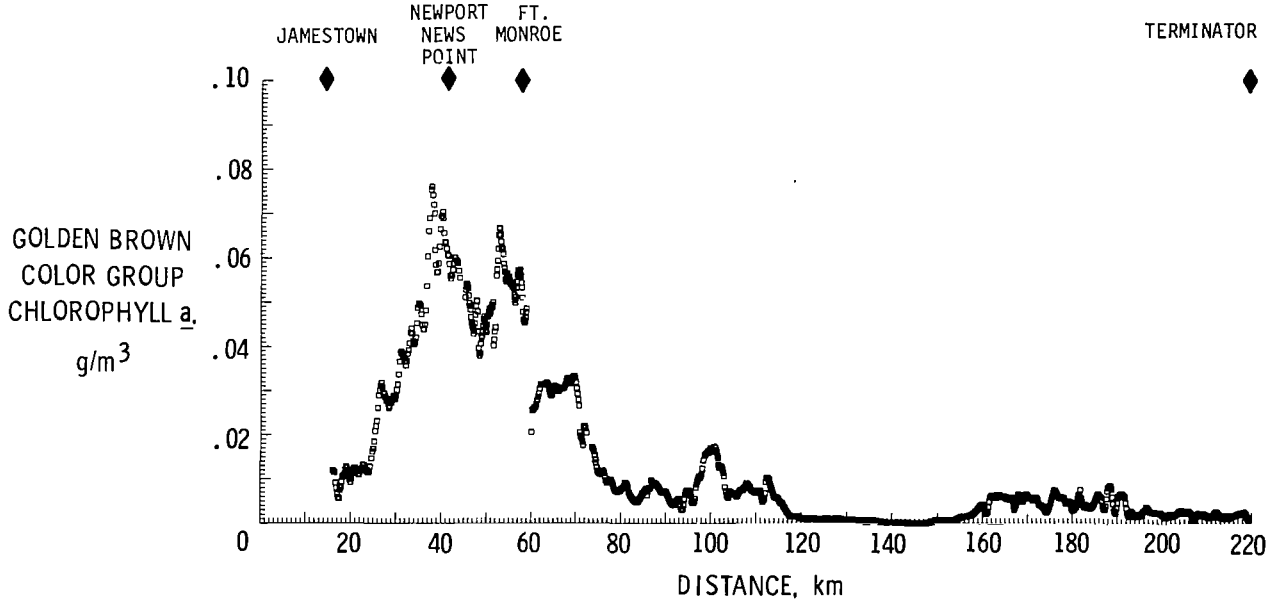

Figure 6.- Chlorophyll a density in golden-brown color group for March 17, 1980 James/shelf mission.

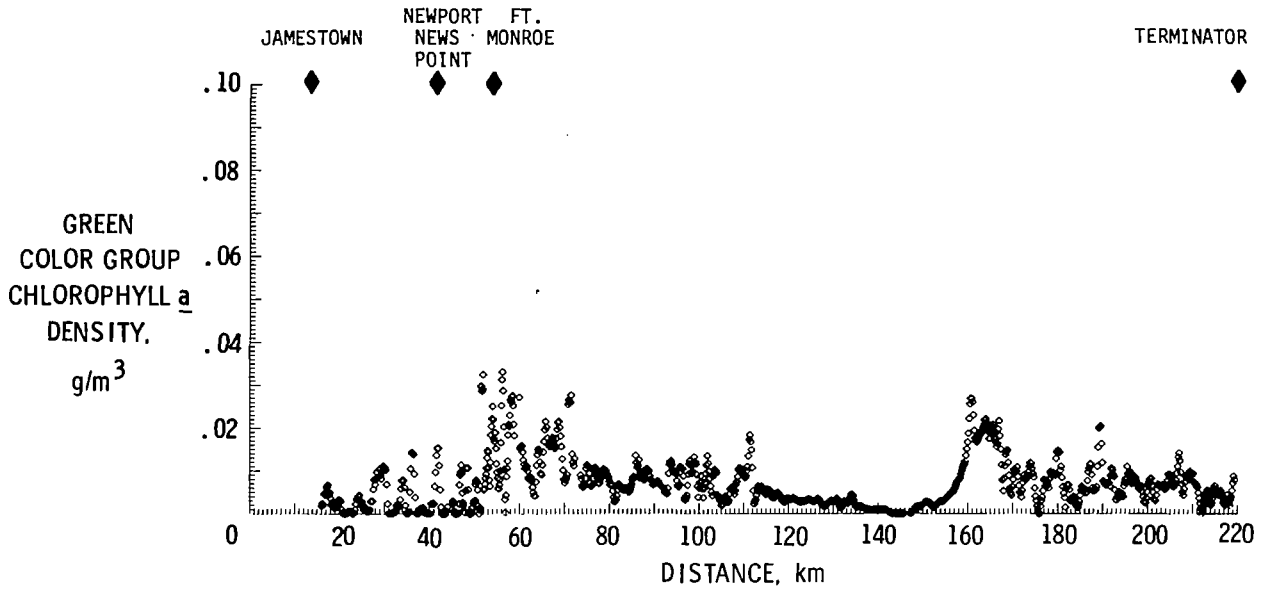

Figure 7.- Chlorophyll a density in green color group for March 17, 1980 James/shelf mission.

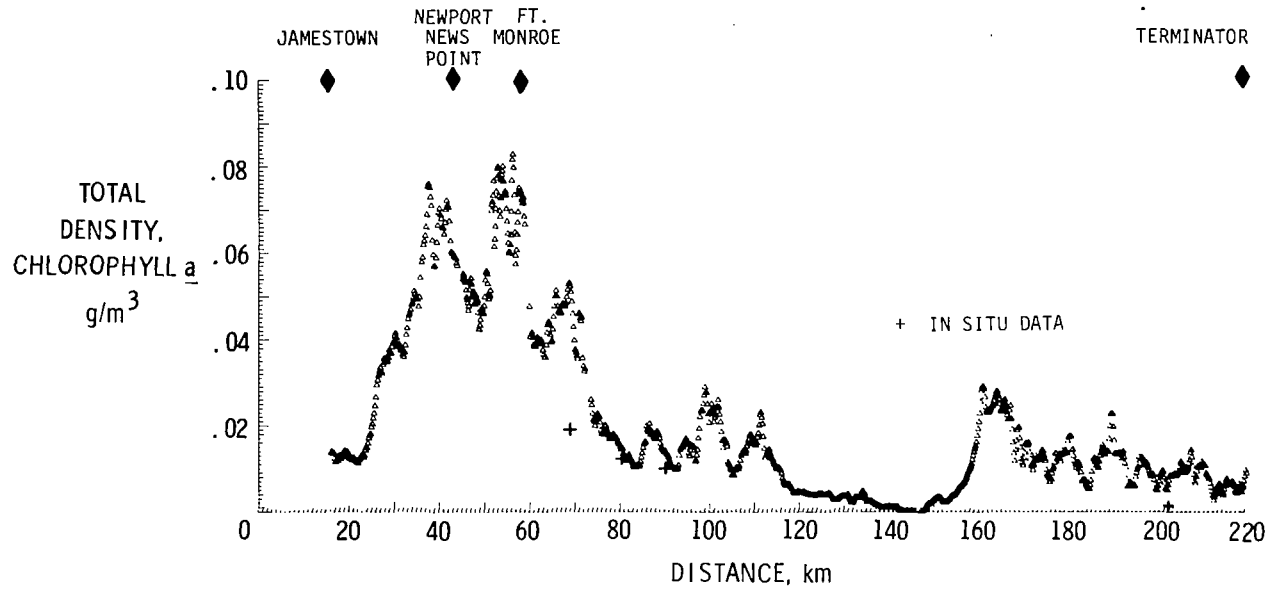

Figure 8.- Total chlorophyll a (total of data on figs. 6 and 7) for March 17, 1980 James/shelf mission.

AN ALGORITHM FOR COMPUTING CHLOROPHYLL a CONCENTRATIONS USING A DUAL-FREQUENCY FLUOROSENSOR

Janet W. Campbell
NASA Langley Research Center

INTRODUCTION

The purpose of this paper is to recommend an algorithm to be used on data from a dual-frequency fluorosensor (i.e. one using two wavelengths for excitation of chlorophyll-a fluorescence) to compute total chlorophyll-a concentration and to partition that chlorophyll between two color groups present in a mixed phytoplankton population. The recommended algorithm is based on laboratory and field-testing experience gained with the Airborne Lidar Oceanographic Probing Experiment (ALOPE) fluorosensor at NASA's Langley Research Center.

As with the single-laser fluorosensor, an assumption must be made that the fluorescence efficiency of each color group remains constant over the area being "calibrated", but the dual-frequency technique can account for a shift in the overall or net fluorescence efficiency that would result from a shift in the relative abundance of two populations having different efficiencies. Therefore, the two-frequency technique can provide more accurate total chlorophyll estimates even if there is no interest in partitioning into color groups.

Partitioning of the total chlorophyll into color group components requires knowledge of the spectral characteristics of the fluorescence excitation spectra of the color groups. Techniques used with single-laser fluorosensors to calibrate the fluorescence signal using concurrent measurements of chlorophyll a (sea truth) cannot be extended to the dual frequency technique by simply changing the dimensionality of the equations. This is because there are no reliable techniques for providing sea truth values for the chlorophyll a concentrations of the two color groups. That is, if total chlorophyll is comprised of chlorophyll from two color groups with concentrations C_1 and C_2 such that the total chlorophyll concentration is $C_T = C_1 + C_2$, sea truth does not exist for C_1 and C_2. Conventional techniques for obtaining total chlorophyll extract the pigment from all cells indiscriminately. Microscopic phytoplankton identifications or cell counts provide information on the relative abundance of the various species, and these can be classified (hopefully) into color groups, but the information on cell size distributions and chlorophyll per cell needed to translate this into component chlorophyll concentrations is virtually nonexistent. Clearly it is beyond the capability of conventional shipboard techniques.

This paper will describe algorithms for computing C_T, C_1, and C_2 at progressively more quantitative levels depending on the amount of information available or assumed. The first or least quantitative level is that of real-time data that can show, without sea truth, the relative variation

of C_T , C_1 , and C_2 along the flight track. At a higher level, an algorithm is presented for mapping total chlorophyll using two fluorescences which is more accurate than one using a single fluorescence when varying mixtures of phytoplankton color groups are present. This requires sea truth on total chlorophyll, but no additional assumptions. Finally, given sea truth on total chlorophyll and assumptions about the fluorescence excitation characteristics of the two color groups of phytoplankton present, an algorithm is presented for computing C_1 and C_2 as well as C_T . In both algorithms that use sea truth, the criterion chosen as the basis for deriving model parameters is to select those parameters that minimize the total squared error in chlorophyll a measured at the sea truth stations. That is, if $C_{T,k}$, $k = 1,\ldots,m$, are the sea truth measurements of total chlorophyll a at m sea truth stations, and $\hat{C}_{T,k}$, $k = 1,\ldots,m$, are estimates of total chlorophyll based on the algorithm used, then the algorithm parameters are selected to minimize

$$\text{Total Error} = \sum_{k=1}^{m} (C_{T,k} - \hat{C}_{T,k})^2 \qquad (1)$$

This is the conventional unweighted least-squares solution where "error" is defined in terms of total chlorophyll measurements.

GENERAL LINEAR MODEL: THEORY

Fluorometric techniques for measuring chlorophyll a concentrations in living phytoplankton cells (in vivo) are based on the assumption that if the cells in a fixed volume of water are excited by light energy, the induced fluorescent energy emitted by the chlorophyll a per unit of excitation energy will be proportional to the molecular density or volumetric concentration of chlorophyll a. The fluorescence of chlorophyll a molecules is in a narrow spectral range centered at 685 nm. If the excitation source is effectively monochromatic, such as that provided by a laser, and if the excitation light frequency is varied, a fluorescence excitation spectrum is generated. Peaks in the spectrum correspond to absorbance peaks of auxilliary pigments present in the cell. Therefore, because the four major color groups of phytoplankton are characterized by the presence or absence of the auxilliary pigments, fluorescence excitation spectra can be used as a means of classifying the color groups. It was this fact that was the basis for the development of the ALOPE fluorosensor which utilized four distinct excitation wavelengths that were selected to discriminate among the four major color groups of phytoplankton. In practice a fluorosensor flown on an aircraft at altitudes generally around 150 m (500 ft) fires light pulses from a laser into the water and senses the returned fluorescence in several spectral bands. To apply fluorometric techniques, the chlorophyll fluorescence at 685 nm must be normalized to correct for variations in the laser's penetration depth along the track. The best-known technique for accomplishing this is to divide the 685-nm fluorescence by the Raman scattering produced by the laser which, in theory, is proportional to the number of water molecules accessed

by the laser or, equivalently, the penetration depth of the laser energy. This technique also corrects for any variations in the output energy of the laser.

In a dual-excitation frequency technique corrections must also be made for spectral differences in the light penetration and for any differences in the excitation energies of the two sources. All of these corrections are accomplished if the Raman signal from each laser is used to normalize fluorescences produced by that laser. It will be assumed in the remainder of this paper that fluorescence refers to a normalized fluorescence where variations in penetration depth and excitation energy are accounted for.

The linear model used for fluorescence from a single-wavelength excitation is

$$F = b + aC_T \tag{2}$$

where the fluorescence F is a linear function of the chlorophyll-a concentration C_T. The term b represents a background fluorescence which is not related to chlorophyll a and the slope a is related to the fluorescence efficiency of the chlorophyll a. The parameters b and a are assumed to remain constant over a defined area. Concurrent measurements of C_T (sea truth) are regressed against corresponding fluorescences F, and the slope a and intercept b are estimated.

The model for a dual-frequency fluorosensor is

$$F_i = b_i + a_{i1}C_1 + a_{i2}C_2 \tag{3}$$

where fluorescence resulting from laser i, F_i, is linearly related to the chlorophyll-a concentrations of the two color groups, C_1 and C_2, and to a background fluorescence b_i induced by that laser. Again, the parameters b_i, a_{i1} and a_{i2} are assumed to be constants over the calibration area, and the parameters a_{i1} and a_{i2}, sometimes called cross sections, are related to the fluorescence efficiencies of the two color groups at excitation frequency i.

Experience with the ALOPE fluorosensor has shown that the ratio of fluorescences $R = F_2/F_1$ can be used as an indicator of the relative abundance of the two color groups. In cultures of a single species grown in the laboratory, where background fluorescences are assumed to be zero (i.e., $b_1 = b_2 = 0$), fluorescence ratios are equivalent to the cross-section ratio a_{2j}/a_{1j} for color group j. The two excitation frequencies 454 nm and 539 nm have been used extensively in ALOPE field tests to differentiate the golden-brown and green phytoplankton color groups, the two color groups commonly found in coastal and shelf waters. In the absence of any background fluorescence, the fluorescence ratio $F(539)/F(454)$ is approximately equal to 1.0 for a golden-brown population and 0.3 for a green population. Figure 1 is a plot of this fluorescence ratio along a 220-km long flight track that began in the Chesapeake Bay where a golden-brown diatom was the

predominant species and ended in clear offshore shelf waters where green species formed a significant component of the population. Note a shift in the ratio from values near 1.0 toward lower ratios around 0.45.

Before proceeding to a discussion of the algorithms, which assume that b_i and a_{ij} are constants, some discussion of this assumption is in order. The assumption that the fluorescence efficiencies of the color groups remain constant over the calibration area is necessary, just as it is in shipboard techniques that use flow-through fluorometers. Sea truth measurements of chlorophyll *a* serve essentially the same purpose as the chlorophyll extractions that are made periodically to calibrate the continuous fluorometer record.

A much more serious problem may be the assumption that background fluorescence is constant. Dissolved organic matter is known to have a broad-band emission spectrum that can significantly contribute to fluorescence at 685 nm, and, depending on the excitation wavelength used, the Raman signal can overlap the chlorophyll *a* fluorescence. Probably the best method for removing a variable background signal, i.e. isolating the fluorescence due to chlorophyll *a*, is to have sufficient spectral resolution in the emission spectrum above and below the 685 nm band. Then, as illustrated in figure 2, a varying background can be estimated and removed. In all the algorithms discussed here, b_1 and b_2 are assumed to be constants that can be estimated and removed by various techniques.

ALGORITHMS

Two situations will be considered in the algorithms that are presented. First, no assumptions will be made about the fluorescence excitation spectra of the two color groups. In this situation the algorithm can provide total chlorophyll, either its relative variation (without sea truth) or absolute variation (with sea truth). Second, it will be assumed that the ratios $R_j = a_{2j}/a_{1j}$ for both color groups ($j = 1$ and $j = 2$) are known constants. In this situation both relative and absolute estimates of C_1 and C_2 can be derived.

Situation 1. Estimation of Total Chlorophyll *a*

Without Assumptions About Cross-Section Ratios

Without sea truth data, plots of F_1 and/or F_2 versus distance provide information about the relative concentration of chlorophyll *a* along the flight track. Since a shift in the relative abundance of the two color groups with different fluorescence efficiencies can affect the assumed linearity of fluorescence with respect to total chlorophyll, a plot of F_2/F_1 versus distance can be used to delineate the portions of the flight track over which linearity can be assumed. That is, either F_1 or F_2 will be a valid relative measure of total chlorophyll over a region, provided F_2/F_1 is fairly constant.

Note that to compute fluorescence ratios the data must consist of fluorescence pairs representing the same locations along the flight track. Since the lasers are fired sequentially rather than simultaneously some preliminary interpolation is required to estimate the fluorescence return of the unfired laser to pair with a measured return.

Once sea truth values for total chlorophyll are available, it is recommended that a multiple linear regression equation

$$\hat{C}_T = \beta_0 + \beta_1 F_1 + \beta_2 F_2 \tag{4}$$

be derived rather than a simple linear regression of C_T on F_1 or F_2 alone. The reason for this is illustrated in figure 3. The symbols represent a hypothetical situation in which sea truth values of total chlorophyll concentration $C_T = C_1 + C_2$ are plotted against a fluorescence computed from the model

$$F_i = 1.0 + 1.2C_1 + 0.3C_2 \tag{5}$$

Line I represents the linear relationship that would exist if the population were exclusively from color group 1, and line II that for color group 2. Any mixture of groups 1 and 2 would result in a point lying between the two lines.

The cluster of points in figure 3 in the range $7 \leq C_T \leq 10$ was sampled from a patch that was predominantly color group 2, whereas the cluster near $C_T = 3$ was from a patch which was predominantly group 1. Since the efficiency of group 2 is lower than that of group 1, the increase in fluorescence resulting from a tripling of the chlorophyll concentration was offset almost entirely by an overall reduction in fluorescence efficiency. Clearly a regression line drawn through these data would be a poor representation of the true relationship, particularly outside the range of the measured chlorophyll, or if a high chlorophyll patch of color group 1 or a low chlorophyll region of color group 2 were encountered.

A multiple regression of C_T on F_1 and F_2 would prevent such errors. At each sea truth station, the relationship between $C_{T,k}$ and F_{1k}, F_{2k} should be modeled as

$$C_{T,k} = \beta_0 + \beta_1 F_{1k} + \beta_2 F_{2k} \tag{6}$$

for $k = 1,\ldots,m$. The least-squares solution for the coefficients that minimizes errors in $C_{T,k}$ (see equation (1)), is given by

$$\beta = [F^t F]^{-1} F^t C_T \tag{7}$$

where $\beta = (\beta_0, \beta_1, \beta_2)^t$; F is the $m \times 1$ column vector of sea truth chlorophylls $C_{T,k}$. More explicitly, the formulas for the regression coefficients are

$$\beta_1 = \frac{S_{C_T}(\rho_1 - \rho_0\rho_2)}{S_{F_1}(1 - \rho_0^2)}$$

$$\beta_2 = \frac{S_{C_T}(\rho_2 - \rho_0\rho_1)}{S_{F_2}(1 - \rho_0^2)} \tag{8}$$

$$\beta_0 = \bar{C}_T - \beta_1\bar{F}_1 - \beta_2\bar{F}_2$$

where $\bar{C}_T$ and S_{C_T} are the mean and standard deviation, respectively, of the sea truth chlorophylls; $\bar{F}_i$ and S_{F_i} are the mean and standard deviation, respectively, of the corresponding F_i sample; ρ_0 is the linear correlation coefficient of F_1 and F_2 at sea truth stations; and ρ_i is the linear correlation coefficient of F_i and C_T at the truth stations.

Situation 2. Estimating C_T, C_1, and C_2

With Assumptions About Cross-Section Ratios

It is now assumed that the ratio of cross-sections a_{2j}/a_{1j} are known constants R_1 and R_2 for color groups 1 and 2, respectively. The equations governing the fluorescences are now

$$F_1 = b_1 + a_{11}C_1 + a_{12}C_2$$

$$F_2 = b_2 + R_1a_{11}C_1 + R_2a_{12}C_2 \tag{9}$$

At this point some further assumptions must be made regarding the background terms b_1 and b_2. One cannot solve for a_{11}, a_{12}, b_1, and b_2 using total chlorophyll sea truth data alone. One solution is to find a minimum F_1 and F_2 in the entire data set, assume that chlorophyll is zero at this location, and set

$$b_1 = \min F_1$$

$$b_2 = \min F_2 \tag{10}$$

Another solution is to assume a fixed ratio $R_0 = b_2/b_1$ based on known spectral characteristics of, say, dissolved organic material.

Assume first that b_1 and b_2 are estimated by other means (e.g., equation (10)) and then subtracted from the fluorescences. The resulting chlorophyll *a* fluorescences would then be given by

$$F_1 = a_{11}C_1 + a_{12}C_2$$
$$F_2 = R_1a_{11}C_1 + R_2a_{12}C_2 \tag{11}$$

Solving these equations for C_1 and C_2 gives

$$C_1 = \frac{1}{a_{11}}\left[\frac{R_2F_1 - F_2}{R_2 - R_1}\right]$$
$$C_2 = \frac{1}{a_{12}}\left[\frac{F_2 - R_1F_1}{R_2 - R_1}\right] \tag{12}$$

and summing these gives

$$C_T = \frac{U_1}{a_{11}} + \frac{U_2}{a_{12}} \tag{13}$$

where

$$U_1 = \frac{R_2F_1 - F_2}{R_2 - R_1}$$

and (14)

$$U_2 = \frac{F_2 - R_1F_1}{R_2 - R_1}$$

Although sea truth values are required to derive estimates of a_{11} and a_{12} note that U_1 and U_2 are relative measures of C_1 and C_2, respectively, accurate to within scale factors $1/a_{11}$ and $1/a_{12}$. Thus, plots of U_1 and U_2 along a flight track can be computed to provide the relative variation of C_1 and C_2. The sum of U_1 and U_2, however, is not necessarily a good measure of total chlorophyll because the scale factors may differ significantly in magnitude. Like F_1 or F_2, the sum $U_1 + U_2$ is a good relative measure of total chlorophyll only in regions where F_2/F_1 is fairly constant, indicating a constant $C_2{:}C_1$ ratio.

Given sea truth $C_{T,k}$, $k = 1,\ldots,m$, and corresponding values of U_1 and U_2

$$U_{1k} = \frac{R_2F_{1k} - F_{2k}}{R_2 - R_1}$$
$$U_{2k} = \frac{F_{2k} - R_1F_{1k}}{R_2 - R_1} \tag{15}$$

the least-squares solution for $1/a_{11}$ and $1/a_{12}$ is

$$\begin{bmatrix} a_{11}^{-1} \\ a_{12}^{-1} \end{bmatrix} = \left[U^t U\right]^{-1} U^t C_T \tag{16}$$

where U is the $m \times 2$ matrix whose kth row is $(U_{1k}\ U_{2k})$, and C_T is the $m \times 1$ column vector of sea truth chlorophyll measurements.

More explicitly, the solution for a_{11} and a_{12} is

$$\begin{aligned} a_{11} &= \frac{\Sigma U_1^2 \Sigma U_2^2 - (\Sigma U_1 U_2)^2}{\Sigma C_T U_1 \Sigma U_2^2 - \Sigma C_T U_2 \Sigma U_1 U_2} \\ a_{12} &= \frac{\Sigma U_1^2 \Sigma U_2^2 - (\Sigma U_1 U_2)^2}{\Sigma C_T U_2 \Sigma U_1^2 - \Sigma C_T U_1 \Sigma U_1 U_2} \end{aligned} \tag{17}$$

where all sums are over $k = 1,\ldots,m$. With these parameters, then, the U_1 and U_2 values can be converted to $C_1 = U_1/a_{11}$ and $C_2 = U_2/a_{12}$.

The final case considered assumes $R_0 = b_2/b_1$ to be a known constant. Here the fluorescences are

$$\begin{aligned} F_1 &= b_1 + a_{11}C_1 + a_{12}C_2 \\ F_2 &= R_0 b_1 + R_1 a_{11} C_1 + R_2 a_{12} C_2 \end{aligned} \tag{18}$$

Solving for C_1, C_2, and C_T gives

$$\begin{aligned} C_1 &= \frac{U_1}{a_{11}} - \frac{b_1}{a_{11}}\left[\frac{R_2 - R_0}{R_2 - R_1}\right] \\ C_2 &= \frac{U_2}{a_{12}} - \frac{b_1}{a_{12}}\left[\frac{R_0 - R_1}{R_2 - R_1}\right] \end{aligned} \tag{19}$$

and

$$C_T = \frac{U_1}{a_{11}} + \frac{U_2}{a_{12}} + \beta_0 \tag{20}$$

where β_0 is the sum of the constant terms in equation (19).

A multiple linear regression of sea truth chlorophyll values on U_1 and U_2 similar to that described above in equations (6) to (8) would provide solutions for β_0 , $\beta_1 = 1/a_{11}$ and $\beta_2 = 1/a_{12}$.

Explicitly, the solutions are

$$a_{11} = \frac{S_{C_T}(\rho_1 - \rho_0\rho_2)}{S_{U_1}(1 - \rho_0^2)}$$

$$a_{12} = \frac{S_{C_T}(\rho_2 - \rho_0\rho_1)}{S_{U_2}(1 - \rho_0^2)} \qquad (21)$$

$$b_1 = \frac{\bar{C}_T - \bar{U}_1/a_{11} - \bar{U}_2/a_{12}}{U_0/a_{11} + (1 - U_0)/a_{12}}$$

where $U_0 = (R_0 - R_1)/(R_2 - R_1)$, and ρ_i are linear correlation coefficients for U_i and C_T at sea truth stations.

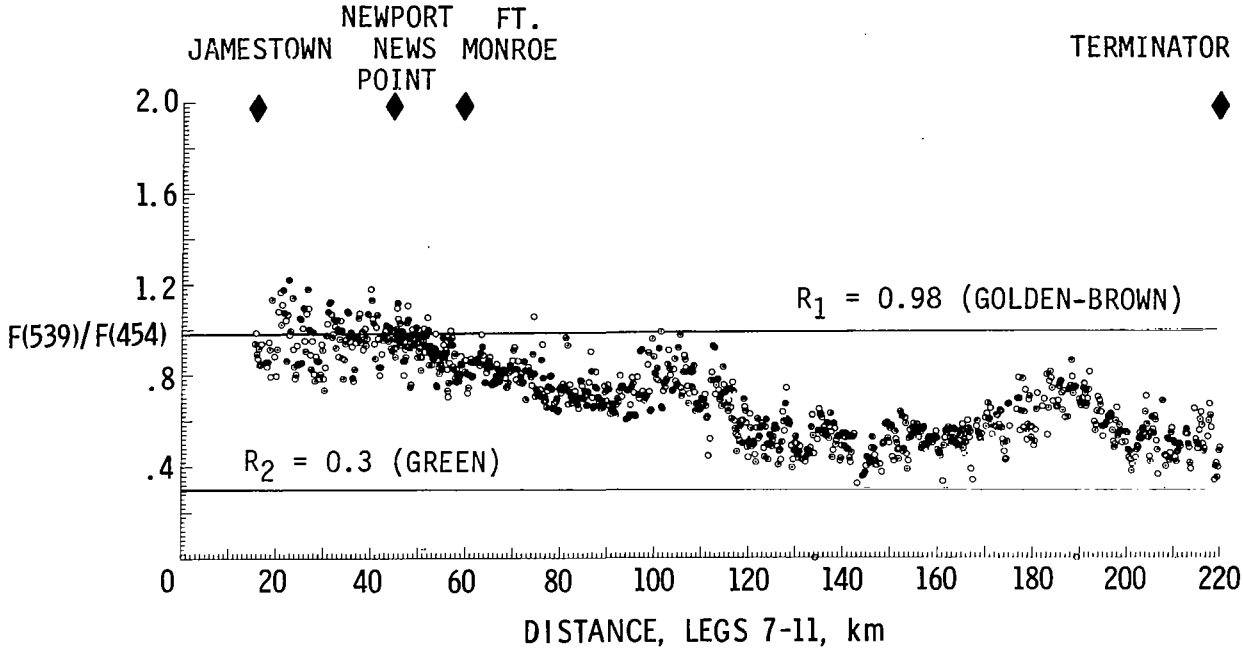

Figure 1.- Fluorescence ratios for the March 17, 1980 James River/shelf mission.

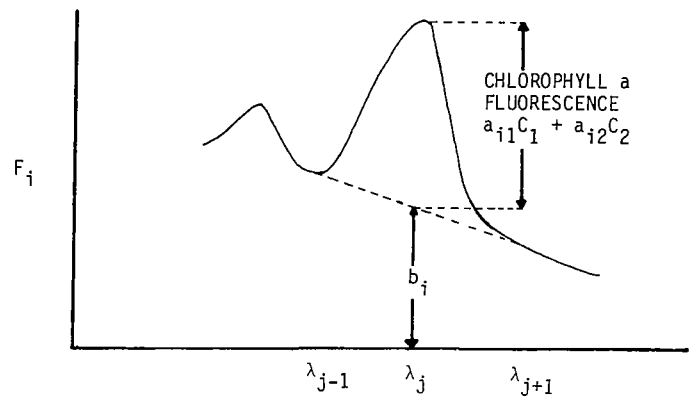

If fluorescence emission spectrum is measured at wavelengths λ_{j-1}, λ_j = 685 nm, λ_{j+1}, then an estimate of b_i = background is:

$$b_i = \frac{(\lambda_{j+1} - \lambda_j)F_{i,j-1} + (\lambda_j - \lambda_{j-1})F_{i,j+1}}{\lambda_{j+1} - \lambda_{j-1}}$$

Figure 2.- Use of neighboring bands in emission spectrum to estimate background.

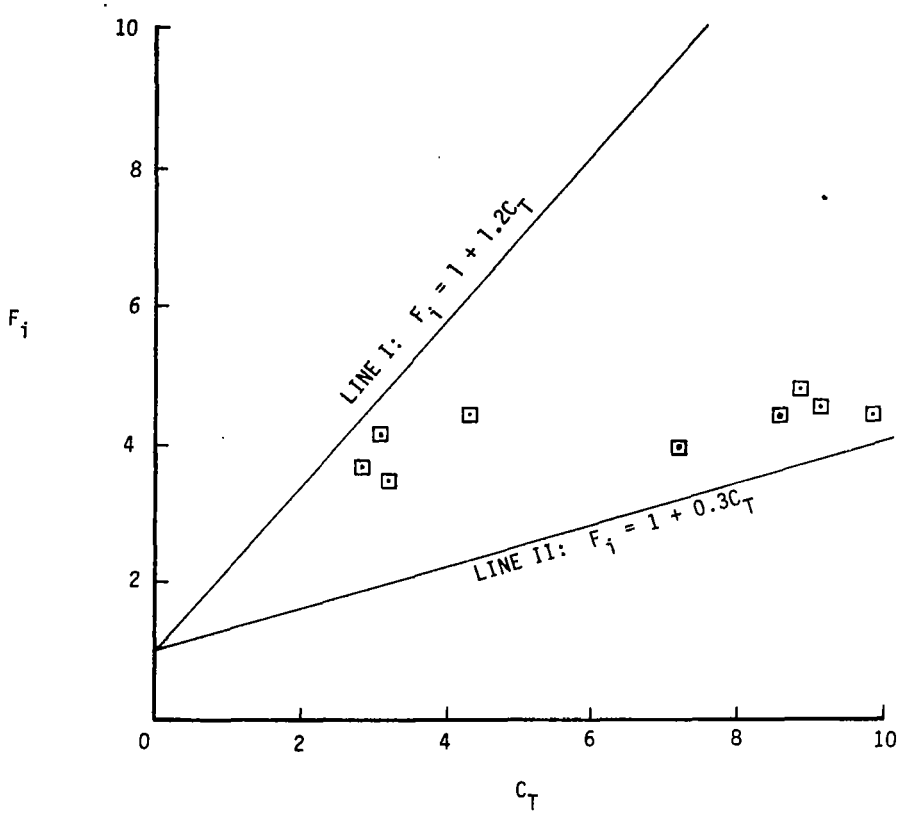

Figure 3.- Illustration of the relationship between fluorescence and total chlorophyll when there is a variation in the relative abundance of two color groups with different fluorescence efficiencies.

INTERPRETATION OF AN INDEX OF PHYTOPLANKTON POPULATION COMPOSITION CALCULATED FROM REMOTE AIRBORNE FLUOROSENSOR (RAF) DATA

Franklin H. Farmer
NASA Langley Research Center*

INTRODUCTION

Chlorophyll a fluorescence at 685nm excited by narrow band light at 454 and 539nm can be used to calculate a simple index of phytoplankton population composition. The ratio of the fluorescence excited by light of these two wavelengths is a function of the distribution of the phytoplankton between two "color" groups, designated the "golden-brown" and the "green". The "golden-brown" group consists of those species which have the highly photosynthetically active carotenoid-chlorophyll-a-protein complexes, i.e. members of the classes Bacillariophyceae, i.e. diatoms (ref. 1) Dinophyceae, i.e. dinoflagellates (ref. 2, 3 and 4), and evidently some members of the class Prymnesiophyceae (formerly Haptophyceae). The "green" color group consists of those species of phytoplankton which apparently lack those complexes, i.e. members of the classes Chlorophyceae, Euglenophyceae, Prasinophyceae, Eustigmatophyceae, Xanthophyceae, and a few members of the Prymnesiophyceae. A few species of phytoplankton appear to have intermediate characteristics, and would apparently belong to neither group. Most of these species are members of the class Cryptophyceae. The composition index varies from about 1.0, when the members of the "golden brown" color group are 100 percent of the phytoplankton population, to about 0.33, when the members of the "green" color group are 100 percent. Thus, an even distribution between the two color groups should produce an index of about 0.67.

This index of composition is similar to but not the same as a diversity index (ref. 5 and 6). The main difference between these two indexes is that the latter relates the number of phytoplankton species to the number of individuals, while the former indicates the relative concentration of two major multi-class components of the phytoplankton population. Also, the diversity index is directly tied to classical taxonomy, while the composition index is only indirectly related to it.

RECENT LABORATORY DATA

Figure 1 presents the fluorescence excitation spectra of some marine species of phytoplankton which are representative of both "color" groups, and of the intermediate species. Note that the "golden-brown" species all fluoresce strongly upon excitation with green light, while the "green" species do not. It is this characteristic, i.e. the absorption or non-absorption of green light, which produces the difference in color between members of the two groups. Since the primary difference in pigment content of these two groups is the presence or absence of fucoxanthin or peridinin based chlorophyll-a-protein complexes, it has been concluded that these complexes are responsible for the absorption/fluorescence excitation characteristics of the "golden-brown" species in the green region of the light spectrum.

* Presently stationed at Bigelow Laboratory for Ocean Sciences.

The composition index is also effected by the presence or absence of chlorophyllide c. Even though this compound is usually present in much lower concentrations than is chlorophyll a, there is evidently sufficient overlap of their in vivo spectra to produce a cumulative excitation effect at 454nm. However, the effect of chlorophyll b on the composition index is evidently negligible, as can be seen by comparing the index for the chlorophyll b containing Chlorophyceae (0.33) with that for the Eustigmatophyceae (0.33), which contain neither chlorophyll b nor chlorophyllide c.

The intermediate position of the cryptophytes is primarily due to their phycoerythrin content. This phycobilin pigment has a significant amount of absorption/fluorescence excitation in the region of 539nm, although its maximum is at a longer wavelength (570 vs. 555nm) than the fucoxanthin and peridinin complexes. Also, these organisms have alloxanthin, an xanthophyll very similar to fucoxanthin but not known to form complexes with chlorophyll a and protein. If the longer wavelength selected to compute the index were changed from 539nm to 525nm or even 530nm, the effect of the phycoerythrin would be considerably reduced and the cryptophytes would be closely aligned with the "green" species. However, since the cryptophytes are usually a minor component of the marine phytoplankton population, their effect on the composition index is usually ignored.

While there appears to be good coherence of composition index values within the "green" color group there is considerably more divergence of the index within the "golden-brown" color group. This variance is more by class than by species, and appears to be related to the relative concentrations of chlorophyll a and fucoxanthin or peridinin (possibly representative of the concentration of their respective complexes). For example, the three diatoms, two chrysophytes, and one "brown" benthic alga examined by Hagar and Stransky (ref. 7) exhibited a range of total fucoxanthin to chlorophyll a ratio (by weight) from 0.31 to 0.74. All diatoms gave essentially the same ratio (0.73/0.74), but the remaining species showed a wide variation in values. The ratio for an Isochrysis species (0.68), now included in the Prymnesiophyceae, was close to the diatoms, but the Ochromonas species (0.31), a sensu strictu chrysophyte, and the laminarian (0.40) were found to have only about half the fucoxanthin per unit chlorophyll a as did the diatoms. However, this variance should only impact the composition index when the non-diatom/dinoflagellate members of the "golden-brown" group are numerous, as occasionally happens in the coastal waters of the northwestern Atlantic during the winter months. When more spectral data is available, it may be possible to separate this group and quantitate its effect in cases when historical data indicates that these organisms may be present in large numbers.

REMOTE DATA

The ratio of fluorescence obtained by the Remote Airborne Fluorosensor (RAF) during the Chesapeake Bay Plume Study in 1980 has been presented by Jarrett (ref. 8) in the previous paper. He has also reviewed the operation of the RAF and the calculation used to obtain the fluorescence excitation ratios he presented. In this paper the primary focus will be on the data acquired on 17 March on Flight Legs 7, 9, and 11. Figure 2 presents the composition index, i.e. the ratio of fluorescence excited by light of a 539nm wavelength

(green) to that excited by light of a 454nm wavelength (blue) versus distance along the flight path starting at Jamestown Island in the James River and ending about 10 km east of the shelf break. This set of almost 1000 data points spread over 205 km reveals a number of interesting features. First, there is a general trend in the index which ranges from a 100% "golden-brown" population (1.0) in the lower James River and Hampton Roads to an equivalence, and possibly the dominance of "green" species (0.55) in the mid-shelf and east of the shelf break. Superimposed upon this general trend are two peaks of "golden-brown" dominance, at the eastern "front" of the Chesapeake Bay Plume and at the shelf break. It appears from this data that the "golden-brown" species predominate in the traditionally nutrient rich areas, while the "green" species dominate, or at least attain equivalence, in the traditionally nutrient poor regions. In the areas between the regions of dominance a gradual "linear" change in composition occurs which could simply be due to tidal mixing of the two components, or of the nutrients which support them. The variance in the index for any one area which would be expected to have constant composition seems to be uniform along the entire flight line, except in the upper region of the James River, where very high optical attenuation evidently increased the variance.

COMPARISON WITH IN SITU DATA

On the morning of the March 17th remote sensing overflight, five research vessels were positioned along the flight lines. Most of these vessels took water samples at three stations which were overflown by the aircraft, one station about an hour before overflight, one at the time of overflight, and one about an hour after the overflight. Thus a total of 16 stations were sampled in conjunction with this portion of the overflight, of which five (#2, 5, 8, 11, and 15) were at the time or very near the time of overflight. The locations of these stations are indicated in Figure 2. Surface (depth of one meter or less) samples were taken at all stations, and sub-samples for phytoplankton counts and identification were preserved with formalin at half of those. These samples were examined by Dr. Harold Marshall of Old Dominion University, who presents a detailed report of his findings in the next paper (ref. 9). His data has been summarized in Table I using a format suitable for making comparisons between the counts and the fluorescence ratio (539/454)/composition index. Note that the same general trend exists in the two data sets, i.e. a trend from highest "green" species content and lowest composition index at station #1, located just east of the shelf break, to the lowest "green" species content and highest composition index at stations #11 and 15, located at the entrance to Hampton Roads and well up the James River, respectively. Upon first examination this relationship was not obvious, because the fluorescence excitation characteristics of the coccolithophores were assumed to be the same as the other prymnesiophytes. It was later found that some of these organisms, the most predominant group of deep sea phytoplankton, have fluorescence excitation spectra very similar to the cryptophytes, but without the phycoerythrin effect. Their composition indexes range from 0.40 to 0.44. Since the only species in this group examined so far has been found to have 19'-hexanoyloxyfucoxanthin, a structural variant of fucoxanthin, as its primary carotenoid (ref. 10), it may be that these organisms do not have the

complexed fucoxanthin of the other prymnesiophytes. This makes them respond to the two wavelengths of excitation light in a manner similar to the "green" species. Exceptions to the general trend are most noticeable at stations #3 and #8 where substantially more "green" species were found than would be expected from the composition index. However, these two stations were also the only ones at which unidentified spherical shaped cells, called "small green spheres" by Dr. Marshall, dominated the "green" species component. These algae were assumed, in the absence of any further identification, to belong in the "green" component, simply on the basis of their color. If this assumption was incorrect and these organisms are actually "golden-brown" species, then the revised "green" species component would show no obvious exceptions to the general trend predicted from the remote data.

In some cases the composition index has apparently been affected by the presence of blue-green algae. Examples of this effect can be seen by a comparison of the data from station 4 with 5, and 11 with 15. The presence of phycoerythrin in some of the blue-green algae can cause a substantial increase in the fluorescence excited by green light (539nm) and thus result in a higher composition index when they are present, even though the distribution of the major components is the same. This effect could be countered by adding a third excitation wavelength in the yellow/orange region of the spectrum (570nm) which would primarily excite the phycoerythrin. This modification to the RAF could easily be made when blue-green algae are known from historical data to comprise a significant portion of the phytoplankton population.

In addition to the above points, it should be noted that the "in situ" data from Dr. Marshall supports the decision to ignore the effects of the cryptophytes, chrysophytes and prymnesiophytes in the computation of the composition index. At only one station (#3) were the cryptophytes a significant portion (5.6%) of the phytoplankton population, and species from the other two classes were not important at any of the stations. In fact, with a few minor exceptions, the phytoplankton population of the entire area could be characterized in terms of five major components (diatoms, dinoflagellates, coccolithophores, "small green spheres", and blue-green algae), with only 2-4 of these components occurring at any one station. Minor components which were occasionally important were the silicoflagellates and the "true" green species, such as members of the genera Scenedesmus and Euglena.

As an additional aid in the interpretation of the composition index for this experiment, the pigment content of the particulates in some of the water samples was determined. Separation of extracted pigments was accomplished by high pressure liquid chromatography and identification was based on location of absorption maxima. Emphasis was placed on the major pigments, i.e. the chlorophylls, fucoxanthin and peridinin. These pigment identifications were made on surface samples from four stations along the flight line, i.e. #3, 5, 6 and 10. No detectable amounts of chlorophyll b were found at any of these stations, which is not surprising as significant numbers of chlorophytes were not found at any of them. The other major pigments are presented as the amount found per unit chlorophyll a (Table II). The variation among these stations of both chlorophyll c and total primary xanthophyll (fucoxanthin + peridinin) relative to chlorophyll a was similar, as both showed highest

values in the plume area (stations #5 and 6) and lower values at the shelf break. However, at station #10, near the entrance to Hampton Roads, the normalized chlorophyll c level was considerably lower than elsewhere, and lower than would be expected from the xanthophyll level. The composition index for this station was also significantly higher than at the other three stations. A comparison of the composition index and the ratio of total primary xanthophyll to chlorophyll c revealed that neither varied much among stations #3, 5 and 6, but both were definitely higher at station #10. This agreement should be expected since the fluorescence of chlorophyll a when the organism which contains it is illuminated by blue (454nm) light is primarily a function of its total chlorophyll content, chlorophyll c being the strongest absorber at that wavelength, and since the same fluorescence when the organism is illuminated by green (539nm) light is evidently primarily a function of its complexed xanthophyll content. Thus, measurement of the pigment content of the particulates in the surface water at several stations was helpful in interpreting the variation of the composition index. However, the relationship between these two parameters was not constant and further investigation will be pursued utilizing a larger data base.

CONCLUDING REMARKS

Even though there are a number of unknowns still involved in the interpretation of the composition index, these are being resolved and hopefully within the next year or so it will have evolved into a technically and scientifically sound approach. So, the question is: How can this measurement be utilized; what is it good for? Although there are several potential areas of application, the primary use seems to be in studies of marine productivity. "Color" group and "size" group seem to be quite synonymous. The "golden-brown" species are physically larger than the "green" species, which are mostly nonoplankton. Feeding or grazing of zooplankton on the phytoplankton population is primarily keyed to size, i.e. certain zooplankton are only equipped to collect phytoplankton within a specific size range. The presence or absence of the right size of phytoplankton can mean the difference between a high and low grazing efficiency. Models of marine productivity usually take this factor into consideration, but the conventional methods of obtaining the data are extremely time consuming and labor intensive, even for the samples from a few stations. The availability of an index based on remote data which could be rapidly computed at dozens of points per square kilometer would help make the models much more spatially realistic, while reducing considerably the labor involved. If this index were to be keyed or calibrated to a few in situ stations, its accuracy would be increased to the level of other trophic measurements. In addition, the combination of the composition and "standing stock" measurements of phytoplankton, both of which can be made by the RAF or any similar remote fluorosensor, greatly increases the power of this type of tool.

REFERENCES

1. Holdsworth, E.S.; and Arshad, H.J.: A Manganese-Copper-Pigment-Protein Complex Isolated from the Photosystem II of Phaeodactylum Tricornutum. Arch. Biochem. Biophys., vol. 183, 1977, pp. 361-373.

2. Haidak, D.; Mathews, C.; and Sweeney, B.: Pigment Protein Complex from Gonyaulax. Science, vol. 152, 1966, pp. 212-213.

3. Haxo, F.T.; Kycia, J.H.; Somers, G.F.;Bennett, A.; and Siegleman, H.W.: Peridinin-Chlorophyll a-Proteins of the Dinoflagellate, Amphidinium carterae (Plymouth 450). Plant Physio., vol. 57, 1976, pp. 297-303.

4. Prezelin, B.B.; and Haxo, F.T.: Purification and Characterization of Peridinin-Chlorophyll a-Proteins from the Marine Dinoflagellates Glenodinium sp. and Gonyaulax polyedra. Planta (Berl.), vol. 128, 1976, pp. 133-141.

5. Fisher, R.A.; Corbet, A.S.; and Williams, C.B.: The Relation between the Number of Species and the Number of Individuals in a Random Sample of an Animal Population. J. Anim. Ecol., vol. 12, 1943, pp. 42-58.

6. Hulburt, E.B.: The Diversity of Phytoplankton Populations in Oceanic, Coastal, and Estuarine Regions. J. Mar. Res., vol. 21, no. 2, 1963, pp. 81-93.

7. Hager, A.; and Stransky, H.: Das Carotinoidmuster und die Verbreitung des lichtinduzierten Xanthophyllcyclus in verschiedenen Algenklassen. V. Einzelne Vertreter der Cryptophyceae, Euglenophyceae, Bacillariophyceae, Chrysophyceae, and Phaeophyceae. Arch. Mikrobiol., vol. 73, 1970, pp. 77-89.

8. Jarrett, Olin, Jr.; Esaias, Wayne E.; Brown, Clarence A., Jr.; and Pritchard, E. Brian: Analysis of ALOPE Data From Superflux. Chesapeake Bay Plume Study - Superflux 1980, NASA CP-2188, 1981 (Paper no. 29 of this compilation).

9. Marshall, Harold G.: Phytoplankton Assemblages Within the Chesapeake Bay Plume and Adjacent Waters of the Continental Shelf. Chesapeake Bay Plume Study - Superflux 1980, NASA CP-2188, 1981 (Paper no. 32 of this compilation).

10. Berger, R.; Liaaen-Jensen, S.; McAlister, V,; and Guillard, R.R.L.: Carotenoids of Prymnesiophyceae (Haptophyceae). Biochem. System. Ecol., vol. 5, 1977, pp. 71-75.

TABLE I - Summary of Phytoplankton Composition

Station #	"Golden-brown" Species (%)			"Green" Species (%)	F_{539}/F_{454}
	Diatoms	Dinoflag.	Others	Total	
1	60.2	6.2	0.4	33.2	0.54
2	75.0	15.1	-	9.9	0.54
3	50.9	3.0	5.6	38.8	0.69
5	34.4	64.5	0.8	0.3	0.73
4	84.9	0.8	10.9*	3.1	0.77
8	28.5	43.3	7.1*	21.1	0.71
11	98.9	1.1	-	-	0.84
15	56.7	41.5	1.8*	-	~1.0

* Significant content of blue-green algae.

TABLE II - Pigment Content of Particulates in Water Samples

Pigment* or Pigment Ratio	Station #			
	3	6	5	10
Chlorophyll *a*	55.1	28.8	70.1	69.9
Chlorophyll *b*	<5.0	<5.0	<5.0	<5.0
Chlorophyllide *c*	12.4	10.7	22.1	12.4
Peridinin	<2.0	13.5	27.6	21.0
Fucoxanthin	30.5	11.6	26.2	35.0
Chl *c*/Chl *a*	0.23	0.37	0.32	0.18
(Per.+Fuco.)/Chl *a*	0.55	0.87	0.77	0.80
F_{539}/F_{454} (Composition Index)	0.69	0.70	0.73	0.85

*µg/ml of extract.

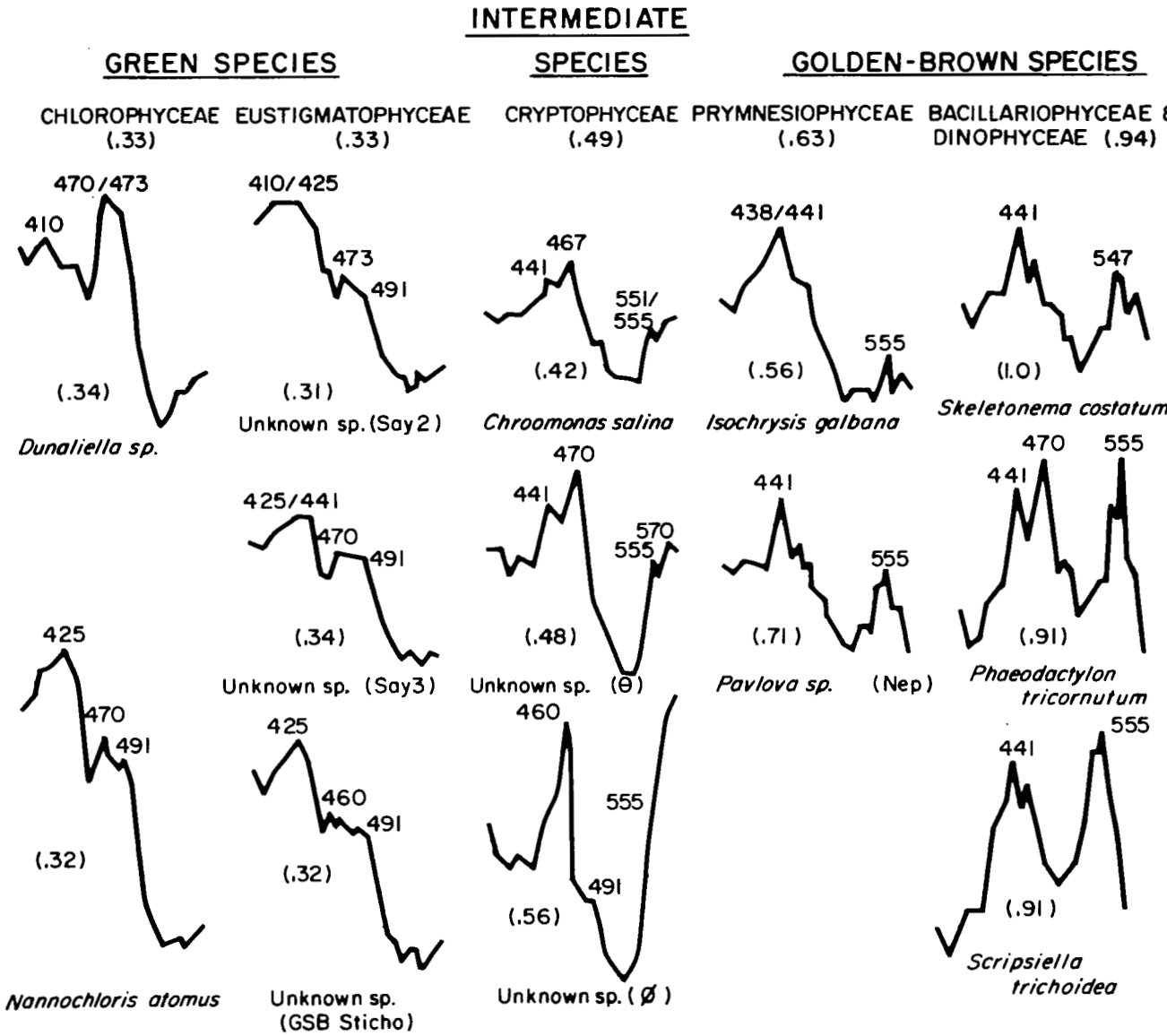

Figure 1.- Fluorescence (685 nm) excitation spectra of phytoplankton species from green, golden-brown, and intermediate color groups. Numbers in parentheses are composition indexes. Names and Greek letters in parentheses are clone names.

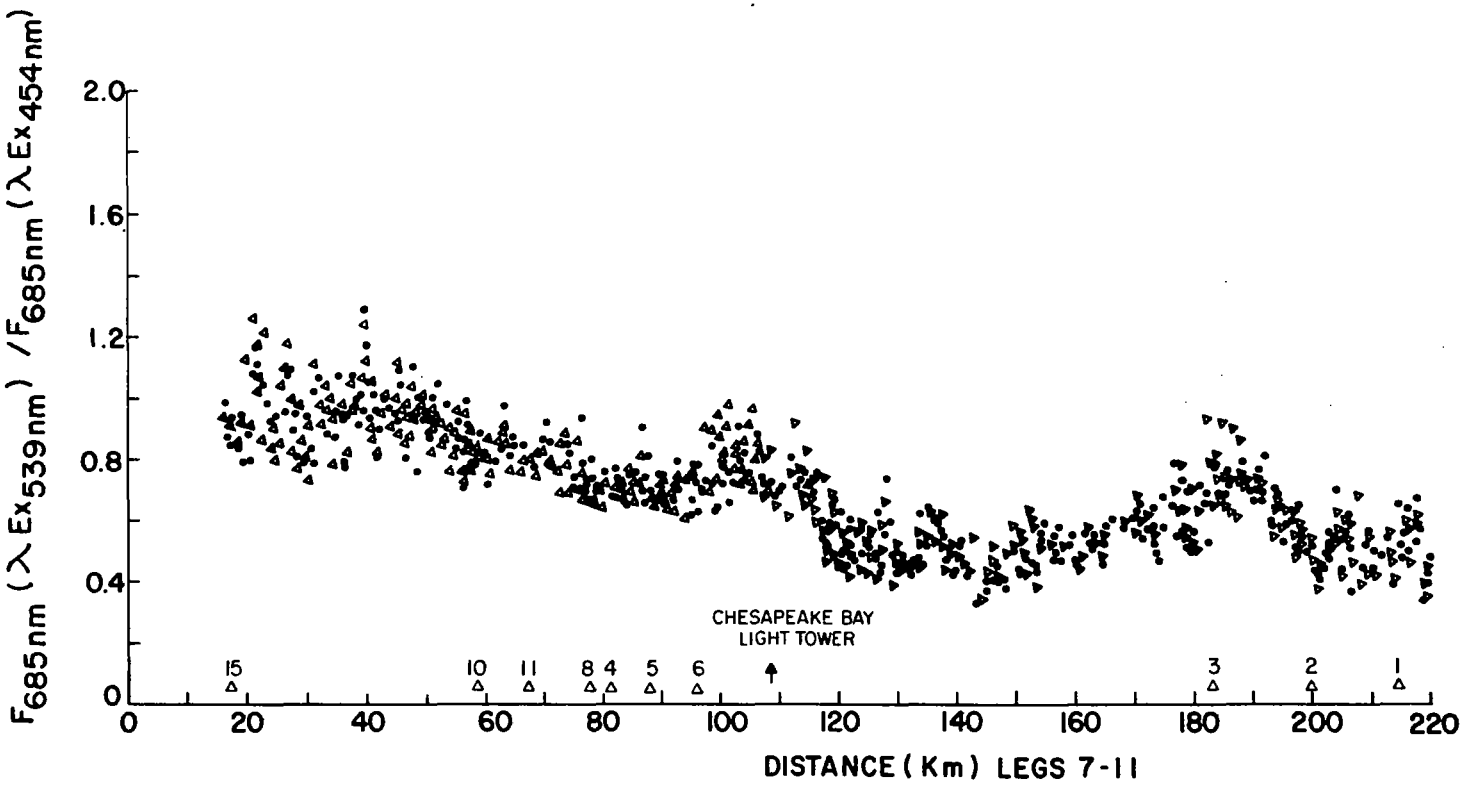

Figure 2.- Composition index (fluorescence excitation ratio) values along flight legs 7, 9 and 11. Numbers over triangles indicate sample station locations.

PHYTOPLANKTON ASSEMBLAGES WITHIN THE CHESAPEAKE BAY PLUME AND ADJACENT WATERS OF THE CONTINENTAL SHELF

Harold G. Marshall
Department of Biological Sciences
Old Dominion University

SUMMARY

The Chesapeake Bay plume was identified and plotted in relation to the presence and high concentrations of phytoplankton assemblages. Seasonal differences occurred within the plume during the collection period, with *Skeletonema costatum* and an ultraplankton component the dominant forms. Patchiness was found along the transects, with variations in composition and concentrations common on consecutive day sampling within the plume in its movement along the shelf. The presence of 236 species is noted, with their presence indicated for plume and shelf stations during the March, June, and October 1980 collections.

INTRODUCTION

The Chesapeake Bay represents the largest estuary on the United States east coast. It extends along a north-south direction from the mouth of the Susquehanna River for approximately 275 km to the Virginia Capes. Typical of other estuaries, it receives outflow and substances from tributaries and other sources along its borders. These products come from agricultural and land run-off, an assortment of industries and municipalities, and shipping and boating activities within its waters. Throughout the year, the degree that these substances are present will often vary in combination with other ecological variables, resulting in a changing milieu more favorable at times to the growth of certain species than others within the phytoplankton community. These responses to changes in water quality and environmental conditions are enhanced by the short life cycle and the potential for rapid growth present in the phytoplankton populations. These population dynamics may then result in a phytoplankton complex that would be characteristic of Chesapeake Bay waters and the effluent that passes to the continental shelf. The initial purpose of this study was to characterize the phytoplankton within the Chesapeake Bay effluent plume in relation to phytoplankton populations over the continental shelf during three seasonal collection periods in March, June, and October 1980. Another goal was to use these assemblages as index species in identifying the passage and eventual breakdown of the plume over

the continental shelf. For definition, the Chesapeake Bay plume is considered as the water outflow from the lower Chesapeake Bay onto the continental shelf which is characterized by certain phytoplankton assemblages present in the lower Chesapeake Bay. In addition, it has subsequently become apparent that these data sets may have additional significance because the collection year (1980) coincided with a period of stream flow into the Chesapeake Bay that was approximately one-half of the water entry for a typical year (ref. 1). The influence of this reduced flow on the water quality and biota is unknown, but is a factor that should be further evaluated in subsequent studies.

Past phytoplankton studies in the lower Chesapeake Bay have identified the major phytoplankters as neritic north temperate species (ref. 2, 3, 4). Seasonal fluctuations in populations are common, with the flora generally dominated by diatoms through fall, winter, and spring, with a combination of diatoms, phytoflagellates, and nanoplankters common in the summer. The importance of Chesapeake Bay nanoplankton has been previously stressed in regard to high productivity values and its composition (ref. 4, 5, 6). Other forms seasonally common to the lower Bay are found over the continental shelf (ref. 4).

METHODS

Water samples were obtained from the participating vessels in the Superflux program. These included vessels from the National Marine Fisheries Service of NOAA, Old Dominion University, and the Virginia Institute of Marine Science. Additional launches were provided by the NASA Langley Research Center, the U.S. Coast Guard, and others. All collections were made during March, June and October 1980. These months were originally selected to coincide with periods of high, moderate, and low outflow from the Bay. However, as previously mentioned, this was an atypical year of very low stream inflow, so the quantity of outflow to the shelf was below seasonal averages. Samples for phytoplankton analysis were obtained at stations presented in Figures 1-4. These stations were located within the lower Bay, at the Bay entrance, and eastward to the shelf break and south to Oregon Inlet. Station coordinates, with salinity and temperature values, are also presented in Tables 1-3. In addition to the surface samples taken at each station, a series of vertical collections were also obtained at selected stations during each cruise. Several other side experiments were made, but will not be discussed at this time. Standard hydrographic water bottle casts were used to obtain the samples, of which 500 ml were placed directly in polyethylene bottles containing a buffered formalin solution. Using a settling and siphoning procedure, a 20 ml concentrate was obtained and subsequently examined with a Zeiss inverted plankton microscope. Random fields and minimal numbers were counted at 312X to provide a statistical accuracy of 85% (ref. 7). Species diversity was determined using the Shannon-Weaver diversity index. Identification was in accordance with the classification followed by Hendey (ref. 8) and Parke and Dixon (ref. 9). Salinity and temperature measurements were taken by personnel from the participating vessels. Special acknowledgement is given to Charles K. Rutledge, Stephen Cibik, and Laurie Kalenak for their assistance in this project.

RESULTS

During the three collection periods in March, June, and October 1980 a total of 223 water samples were analyzed for phytoplankton composition and concentration. A total of 236 phytoplankters were noted from these collections (Table 4). These consisted of Bacillariophyceae (126), Pyrrhophyceae (74), Haptophyceae (15), Cyanophyceae (9), Chlorophyceae (4), Cryptophyceae (3), Euglenophyceae (2), and Chrysophyceae (3). In addition, there was an unidentified ultraplankton component prominent in the plume and at the near shore stations. The ultraplankton are defined according to the classification given by Strickland (ref. 10), who placed cells within the size range of 0.5 to 10 μm as ultraplankton. These cells consisted of three size groups: less than 3 μm, 3-5 μm, and 5-10 μm. Several samples of these cells exhibited fluorescence when stained with acridine orange and examined under a fluorescent microscope, whereas other cells did not fluoresce. This ultraplankton component is considered to be composed of several species, including coccoid cyanophyceans and chlorophyceans.

Concentrations of the phytoplankton were consistently higher in samples from the lower Bay and the Bay entrance area. Progressing eastward over the shelf there was a decrease in cell numbers and a change in the phytoplankton composition. Most typical was the transition in dominance from diatoms and ultraplankton cells (described above) in the Bay entrance area, to coccolithophores, with another diatom assemblage seaward. Evidence was also found of an increase in phytoplankton concentration near the shelf break. Moving southward from the Bay entrance to Oregon Inlet, the higher phytoplankton concentrations taper off, remaining larger near shore. Evidence for the breakdown of the plume and for mixed populations of shelf and plume phytoplankton increases toward Oregon Inlet. Throughout the collection period the phytoplankton composition within the Bay entrance and the Bay plume contained assemblages that could distinguish the plume from adjacent shelf waters.

March 1980

The dominant phytoplankton found in Bay entrance waters and the Chesapeake Bay plume included the diatoms: *Asterionella glacialis*, *Cyclotella* sp., *Skeletonema costatum*, *Leptocylindrus minimus*, a pyrrhophycean *Prorocentrum minimum*, a cyanophycean *Gomphosphaeria aponina*, and the ultraplankton group of unidentified cells. In the Bay entrance, the concentration of *Prorocentrum minimum* was over 1.2 million cells per liter, with *Cyclotella* sp. at approximately 434,000 cells per liter. The different size categories of the ultraplankton group varied in their concentrations. Cells smaller than 3.0 μm averaged approximately 200,000 cells/l in the Bay entrance and 770,000 cells/l in the near shelf stations. The cells in the 3-5 μm range averaged approximately 100,000 cells/l in the Bay entrance, with numbers markedly reduced beyond the entrance. The larger sized ultraplankton (5-10 μm) did not reach

the concentrations of the other size classes near shore, but had highest concentrations (29,318 cells/l) at far shelf stations.

The phytoplankton composition and concentrations changed beyond the Bay entrance. The cell concentrations dropped significantly, only to increase dramatically at Station 22 where cell counts were over 1.1 million cells per liter. Dominant species at this station, located about 33 km beyond the Bay entrance, consisted of *Prorocentrum minimum*, several small-sized diatoms, dinoflagellates, cyanophyceans, and the ultraplankton green cells 5-10 μm in size. In a clustering analysis of stations in this study, it was shown that Station 22 and Stations 7 and 8 (located in the lower Bay entrance area), which were sampled two days apart, have very close species relationships. This gives the impression that Station 22 waters may represent a pulse, or remnant, of an earlier plume outflow from the Bay. Continuing seaward the phytoplankton concentrations generally decreased. However, there was a population increase farther out over the shelf at Station 3. Here, the cell counts were over 394,000 cells per liter. At this station, small chain-forming diatoms were dominant with the most abundant forms being *Rhizosolenia delicatula* and *Thalassiosira nordenskioldii*. The diatoms *Nitzschia longissima* and *Thalassiosira rotula* and the coccolithophore *Emiliania huxleyi* were also in high concentrations. A similar composition but in lower cell concentrations was found at the two most distant stations (1 and 2) along the transect.

Vertical Distribution

Differences were noted in the vertical distribution of the phytoplankton. Similar species composition over the vertical series was found at several of the stations with other stations having a mixed assemblage (Table 5). *Leptocylindrus danicus* and *Leptocylindrus minimus* were common dominants or sub-dominants at several of these stations. At scattered surface locations there were also high cell concentrations for *Emiliania huxleyi* (Station 1), *Prorocentrum minima* (Station 5), green cells, 5-10 μm (Station 22), and *Guinardia flaccida* (Station 33). When no dominant form was present, the composition was a mixed selection of predominantly diatoms. Species diversity was characteristically lower in plume waters, or where a few species were present in high concentrations. The higher diversity readings were noted in samples where concentrations were more uniform among a greater variety of species. Differences in station counts over the vertical range were mainly attributed to a higher concentration of one or two species that were typically dominant within the vertical sampling range. The unidentified green cells and *Prorocentrum minimum* were found in highest numbers at the surface, decreasing significantly with depth. With the exception of several samples where a single species dominated the counts, there was a similarity in composition over the vertical range of sampling. This was found in the Bay entrance and at stations located over the shelf.

Plume Phytoplankton

The outflow from the Chesapeake Bay is directed southward, moving as a narrow band along the Virginia and North Carolina coast (ref. 11). This flow

would be altered seasonally in its extent eastward over the shelf and southward toward Cape Hatteras. The results of the March study associated highest cell concentrations with the plume at the entrance of the Bay, directly south of the entrance (Station 12), with an apparent isolated segment of the plume east of the Bay entrance at Station 22 (Figure 5). Beyond this area eastward increased concentrations of coccolithophores and other typical shelf species occurred. The plume phytoplankton assemblage was distinct for this sampling period in contrast to phytoplankton at the far shelf stations. Various degrees of mixing and phytoplankton patchiness were also identified in the shelf areas.

To summarize the results of the March collections, the dominant constituents of the Bay plume were the unidentified green cells, found in the three ultraplankton size groups. This component was significant in regard to its high concentrations and wide distribution. These were found to be more prevalent in the surface collections, with the majority of these cells believed to be either cyanophyceans or chlorophyceans. The vertical distribution patterns and concentrations of the phytoplankton were generally homogeneous, with the exception of several stations where there occurred high concentrations of single species (and green cells) at surface collections. The plume phytoplankton included *Asterionella glacialis*, *Cyclotella* sp., *Skeletonema costatum*, *Leptocylindrus minimus*, *Prorocentrum minimum*, *Gomphosphaeria aponia*, and unidentified ultraplankton-sized green cells. This assemblage was distinguished from the shelf populations.

June 1980

Distinct differences were also apparent in the phytoplankton composition of the plume compared to other shelf stations in June 1980. The plume waters of the Chesapeake Bay were identified as extending from the Bay entrance southward and close to the Virginia coastline (Figure 6). The phytoplankton within the plume reached concentrations of over 7.9 million cells/liter. These waters were dominated by diatoms and the unidentified green cells in the 3-5 μm size range. *Skeletonema costatum* was the major constituent, with sub-dominants being *Nitzschia pungens*, *Leptocylindrus danicus*, *Rhizosolenia delicatula*, and *Chaetoceros* spp. The pyrrhophyceans, coccolithophores and other representatives were in low concentrations within the plume. The diversity index for these stations ranged from 0.8351 to 2.1241. Because the sampling protocol placed specific restrictions on each vessel, collections were made over a six-day period, preventing short term synoptic coverage of the area. This was unfortunate because the location of the plume is known to fluctuate in its passage southward (ref. 11). Thus, the data used as a basis to identify the plume in Figure 3 were obtained over a six-day period and do not represent the plume outline for a specific date. Even with these limitations, the direction of plume flow is easily identified as moving south of the Virginia Capes and along the Virginia coastline. These waters apparently favor the growth of *Skeletonema costatum* and the green cell component. These are plankters of small cell size (ultraplankton) and high reproductive potential. Larger sized diatoms and the pyrrhophyceans were rare

at these stations. A more southern extension of the plume was noted off the North Carolina coast that was separated from the plume directly south of the Bay entrance by an area of lower cell count and mixed composition. The plume segment off the North Carolina coast was dominated by *Skeletonema costatum*, but contained a mixture of other forms, such as *Emiliania huxleyi* which is considered a common shelf species. This mixed composition is accompanied by increased species diversity values. During 23-27 June 1980 another leg of the cruise series was conducted that included stations near the Bay entrance and over the shelf (Figure 3). Even in this abbreviated collection series, large phytoplankton concentrations were noted in an identifiable plume south of the Bay entrance, with these larger concentrations directed southward (Figure 7). These stations have a similar assemblage of dominant species, as was found in the 17-22 June 1980 collections.

There was an increase in the species diversity at stations bordering the plume that ranged from 1.7258 to 2.8403. These waters also differed from the plume by having an increased number of co-dominant species. These included *Emiliania huxleyi*, *Leptocylindrus danicus*, the various sized green cells, *Chaetoceros* sp., *Nitzschia pungens*, *Cryptomonas* sp., *Gymnodinium* sp., and *Rhizosolenia fragilaria*. The stations nearest the Bay entrance had greater concentrations of *Skeletonema costatum* and *Emiliania huxleyi*, in contrast to what was found along the North Carolina coastline. *Skeletonema costatum* was noted at stations off the Carolina coast nearest to the shoreline. However, green cells that were less than 3 μm and 3-5 μm in size were the most abundant form in the near shore waters. These more southern plume waters indicate a degree of mixing between shelf waters and the Bay plume by the changing concentrations of *Skeletonema costatum* and *Emiliania huxleyi*. The concentrations of *Skeletonema costatum* in the plume decrease with movement of the plume southward and eastward over the shelf. The mixing and transformation of the plume phytoplankton increase both southward and eastward, with the concentrations of *Emiliania huxleyi* and other coccolithophores increasing.

Stations located near the shelf break and far east of the Bay plume contain a phytoplankton assemblage distinct from the plume waters and the near shelf mixing zone. These stations also show a trend of a decreasing species diversity in comparison to the near shore stations (ranging from 1.4187 to 2.3112). The dominant components at these stations were the coccolithophores with several dinoflagellates and green cells (3-5 μm) the sub-dominants. The major coccolithophores were *Emiliania huxleyi*, *Syracosphaera pulchra*, *Rhabdosphaera* sp. and *Pontosphaera* sp. Prominent diatoms included *Rhizosolenia alata*, *R. styliformis*, and *R. delicatula*, with an increased variety of the pyrrhophyceans. These included *Ceratium fusus*, *C. extensum*, *C. tripos*, *C. macroceros*, *Prorocentrum micans*, and *Protoperidinium* spp. The high concentration of coccolithophores in these waters supports the use of appropriate preservatives that would not destroy these populations prior to examination.

High concentrations of cells were commonly found in the sub-surface samples within the Bay plume (Table 6). *Skeletonema costatum* was the major

constituent with green cells (3-5 μm) in high concentrations throughout the water column. Species diversity remained low below the surface, having lowest concentrations in the Bay entrance area, increasing slightly below Cape Henry. In the shelf areas on either side of the plume, numerous co-dominants provided a mixture of major species at the various depths that included green cells (3-5 μm), *Leptocylindrus danicus*, *Emiliania huxleyi*, and reduced numbers of *Skeletonema costatum*. The vertical sampling was limited to the surface and 3 meters at the far shelf stations, with the major constituents being the coccolithophores at both depths. The number of different species represented at these stations was much less (56) than at the near shore stations (155).

In summary, the June phytoplankton within the plume contained high concentrations of the diatom *Skeletonema costatum*, in association with unidentified green cells. Sub-dominants included *Chaetoceros* sp., *Cylindrotheca closterium*, *Leptocylindrus danicus*, *Nitzschia pungens*, and *Rhizosolenia delicatula*. The plume extended slightly eastward beyond the Bay entrance, with its flow to the south along the Virginia and North Carolina coastline. There was basically a homogeneous vertical distribution of dominants within the plume near the Bay entrance. This condition gradually broke down with the movement of the plume southward, with increasing numbers of coccolithophores and a decrease in *Skeletonema costatum*. A similar decrease in the various "green cells" within the plume did not occur. Numbers remained high for this group over the near shelf waters between the Virginia Capes and Oregon Inlet.

October 1980

The highest phytoplankton concentrations for October were found at the Chesapeake Bay entrance (Station 801), off Cape Henry (Stations 69, 803), and to the south (Stations 808, 809, 811). Dominant phytoplankters were *Skeletonema costatum* and unidentified green cells (<3 microns in size). The concentrations at these stations were generally above a million cells per liter, with the highest counts found at Station 808 (October 15, 1980) where there were approximately 13.8 million cells/liter. South of the False Cape area to Oregon Inlet, the cell counts remained above one million cells/liter at the near shore stations, decreasing in numbers rapidly seaward. The Bay plume appears to extend over these stations, tapering from the area beyond the Bay entrance toward the North Carolina coastline (Figure 8). Beyond this plume area and extending over the shelf, the concentrations of *Skeletonema costatum* declined, but the ultraplankton component was present in reduced but significant concentrations. Diatoms also found in high concentrations at the plume stations were *Asterionella glacialis*, *Nitzschia pungens*, *Chaetoceros* sp., *Lauderia borealis*, *Leptocylindrus danicus*, *Nitzschia delicatissima*, *Rhizosolenia stolterfothii*, *R. delicatula*, *R. fragilissima*, *Thalassiothrix mediterranea*, and *Cylindrotheca closterium*. Other plume phytoplankters were *Anacystis* sp., *Cryptomonas* sp., and *Emiliania huxleyi*. The dinoflagellates were common throughout the sampling area, but were consistently found in low concentrations. An apparent patchiness in cell concentrations and composition was also noted at stations along transects,

with variations in concentrations at some of the same stations on subsequent sampling days.

An example of patchiness occurred on October 15, 1981 along transect Stations 69-805. At Station 802, the total cell count was approximately 121,000 with dominant species being *Asterionella glacialis* and *Chaetoceros costatum*. *Skeletonema costatum* was not found in the sample. At adjacent stations (69 and 803) located approximately 2 km to the east and west, cell counts for both stations were over 2 million cells per liter with *Skeletonema costatum* at concentrations of 1.9 and 1.7 million cells per liter. In contrast, the pattern along the 808-811 transect on October 15, 1981 indicated a decline in cell concentrations seaward along the first four stations in this series. However, there was a significant rise in population numbers (3.2 million) at Station 811, the station most distant from shore in this transect (Table 7). The presence of *Emiliania huxleyi* throughout the plume differs from the results of the June samples. This species was more common over the shelf and outside of the plume area in June, with its degree of entry along the peripheral areas of the plume more indicative of the extent of mixing and breakdown of the plume structure.

The shelf waters beyond the area of the plume contained a variety of phytoplankters, with many dominants similar to those in the plume waters. These included *Skeletonema costatum*, *Leptocylindrus danicus*, *Nitzschia pungens*, *Anacystis* sp., *Emiliania huxleyi*, and the unidentified ultraplankton components. The composition for the major phytoplankton groups along the transects is given in Table 7. The diatoms consistently have the highest concentrations of cells in the Bay entrance and in the plume directly south of Cape Henry. The green cell component is also significant, becoming more abundant than the diatoms southward. On October 22, samples were taken from an additional 4 stations along a transect from Cape Henry 125 km eastward and beyond the continental shelf. The general pattern in this series, as in the other transects seaward, was a marked reduction in the concentration of the phytoplankton. Cell concentrations dropped from 1.4 million cells per liter at Station 15 off Cape Henry to about 24,000 cells per liter at the far shelf station.

In summary, the dominant species for October at near shore stations and within the Bay plume was *Skeletonema costatum*. Also prominent in the majority of the samples were ultraplankton sized cells which were unidentified but appeared similar to coccoid cyanophyceans and chlorophycean species previously mentioned. The pyrrhophyceans were common but not abundant in the samples. Coccolithophores were common within the plume waters and were the dominant forms in the more distant stations over the shelf. *Cryptomonas* sp. was the dominant species at several stations with several cyanophyceans also abundant in the samples. In general, species diversity reflected the degree of dominance by *Skeletonema costatum* (or the other dominants), being lower where a large population concentration was the product of one or a few species, and usually found near shore. A higher diversity index value was more typical in assemblages of lower population numbers and lacking a significantly dominant form (Station 802).

PHYTOPLANKTON ASSEMBLAGES

The Chesapeake Bay plume was characterized by its phytoplankton composition and high concentration of cells. Seasonal assemblages within the plume and in adjacent shelf waters for March, June, and October are given in Table 8. The predominant species throughout the year in the plume waters was *Skeletonema costatum*, in association with certain ultraplankton forms. These included several unidentified round, green cells of three different size groups (<3 μm, 3-5 μm, 5-10 μm) that appear to be coccoid cyanophycean and chlorophycean species. The plume species were dominated by ultraplankton and nanoplankton components, generally characteristic of enriched areas, and capable of rapid growth. Beyond the plume, the shelf waters contained a variety of diatoms, the green cell component, and phytoflagellates, but were generally dominated by coccolithophores. Transects from near shore stations seaward were characterized by decreasing phytoplankton populations, from mainly a diatom floral assemblage to a mixed group with coccolithophores most prominent. The coccolithophores were useful indicators of the degree of plume mixing with the shelf waters for March and June, but to a lesser degree in October, when they were also common in the plume. The dominant species within the plume were similar to species previously noted for waters of this region (ref. 4, 12), with the high concentrations of *Skeletonema costatum* at near shore stations not unusual (ref. 4, 13). However, a high concentration of *Skeletonema costatum* was one of the characteristics that identified the plume. The ultraplankton group is also associated with the plume and to a lesser extent the shelf waters outside of the plume. Greater recognition has been given this group in recent years as a common and often major component of estuaries and marine waters (ref. 12, 13, 14, 15). There is need for many of these ultraplankton cells to be isolated, cultured, and identified to assure uniformity in the reporting of these species by various investigators.

The extent and permanence of the plume over the shelf varied during the sampling periods. Generally, there was a bulge area of high cell concentration just beyond the Bay entrance, with the southward extension of the plume close to the Virginia shoreline, tapering off toward Oregon Inlet. Although populations decreased in numbers seaward, there was also evidence along several transects of a moderate increase in cell concentration near the shelf break. Patchiness was also common along transects, indicating areas of both high and low concentrations, or dominant species development, along a series of stations. Significant variations in the composition and concentrations of the phytoplankton were also noted during consecutive-day sampling at the same station. Such changes occurred near shore, at the Bay entrance, and within the plume in its extent south toward Oregon Inlet. This implies a dynamic state for the area, in which water movement will be influenced by local wind patterns, tidal currents, and offshore upwelling and current action. Since the degree to which these activities are present will vary, fluctuations in the concentration and composition of the phytoplankton in these waters may be expected over short time periods, and may be included in the seasonal assemblages.

REFERENCES

1. U.S. Dept. Interior Geological Survey. Estimated Stream Flow Entering Chesapeake Bay. Monthly Report. Jan. 2, 1981.

2. Wolfe, J., B. Cunningham, N. Wilkerson, and J. Barnes. 1926. An investigation of the microplankton of Chesapeake Bay. J. Elisha Mitchell Sci. Soc. 42: 25-54.

3. Patten, B., R. Mulford, and J. Warinner. 1963. An annual phytoplankton cycle in the lower Chesapeake Bay. Ches. Sci. 4: 1-20.

4. Marshall, H. G. 1980. Seasonal phytoplankton composition in the lower Chesapeake Bay and Old Plantation Creek. Estuaries. 3: 207-216.

5. McCarthy, J. J., W. R. Taylor, and J. Loftus. 1974. Significance of nanoplankton in the Chesapeake Bay estuary and problems associated with the measurement of nanoplankton productivity. Mar. Biology. 24: 7-16.

6. VanValkenburg, S. E. and D. A. Flemer. 1974. The distribution and productivity of nanoplankton in a temperate estuarine area. Estuarine and Coastal Marine Science. 2: 311-322.

7. Venrick, E. L. 1978. How many cells to count. In: A. Sournia, Ed. Phytoplankton Manual. pp. 167-180. Unesco Publ. Page Brothers, Ltd. Paris.

8. Hendey, N. I. 1974. A revised check-list for British marine diatoms. J. Mar. Biol. Ass. U.K. 56: 277-400.

9. Parke, M. and P. Dixon. 1976. Checklist of British marine algae. J. Mar. Biol. Ass. U.K. 56: 527-594.

10. Strickland, J. D. H. 1960. Measuring the production of marine phytoplankton. Bull. Fish. Res. Bd. Canada.No. 122. 42 p.

11. Boucourt, W. C. 1973. The circulation of water on the continental shelf from Chesapeake Bay to Cape Hatteras. Ph.D. dissertation. Johns Hopkins University. Baltimore, Md. 147 p.

12. Marshall, H. G. 1978. Phytoplankton along the eastern coast of the USA. Part II. Seasonal assemblages north of Cape Hatteras, North Carolina. Marine Biology. 45: 203-208.

13. Marshall, H. G., K. Nesius, and S. Cibik. 1981. Phytoplankton studies within the Virginia Barrier Islands. II. Seasonal study of phytoplankton within the Barrier Islands Channels. Castanea. 46: 1-10.

14. Marshall, H. G. 1981. Occurrence of bluegreen algae (Cyanophyta) in the phytoplankton off the southeastern coast of the United States. J. Plankton Research. 3(2): 163-166.

15. Waterbury, J., S. Watson, R. Guillard, and L. Brand. 1979. Widespread occurrence of a unicellular, marine, planktonic, cyanobacterium. Nature.Vol. 277: 293-294.

Table 1. Station coordinates with surface salinity, temperature, and date sampled, for March 1980 collections.

Station	Coordinates		Salinity °/oo	Temp. °C	Date
4	36°57,6N	76°01.7W	21.5	12.5	17 March 1980
7	36°57.6	76°02.2	21.0	4.1	17 March 1980
8	36°57.6	76°02.2	20.2	4.3	17 March 1980
5	36°56.9	75°57.2	22.2	5.9	17 March 1980
15	36°56.0	75°57.1	24.0	6.0	19 March 1980
12	36°56.1	75°57.5	25.0	6.1	19 March 1980
6	36°55.9	75°51.7	22.5	--	17 March 1980
21	36°50.1	75°42.9	29.5	16.1	19 March 1980
22	36°55.1	75°34.8	24.0	6.0	19 March 1980
11	36°52.5	75°30.7	23.9	6.0	19 March 1980
16	36°52.4	75°30.6	27.8	6.0	19 March 1980
33	36°51.9	75°29.8	--	6.2	19 March 1980
34	36°52.0	75°29.8	--	6.3	19 March 1980
3	36°45.0	74°54.2	30.5	9.6	17 March 1980
2	36°43.3	74°42.3	30.5	12.4	17 March 1980
1	36°41.2	74°33.0	30.5	15.2	17 March 1980

Table 2. Station coordinates, with surface salinity, temperature, and date sampled for June 1980.

Station	Coordinates		Salinity °/oo	Temp. °C	Date
800	36°57.3N	76°02.9W	21.63	22.3	17 June 1980
801	36°59.2	76°00.6	26.00	20.2	18 June 1980
69	36°55.0	75°58.0	27.48	20.5	18 June 1980
802	36°56.0	75°55.8	25.49	20.8	18 June 1980
803	36°58.0	75°51.5	29.02	20.4	18 June 1980
804	37°00.6	75°44.4	32.15	18.7	18 June 1980
805	36°52.0	75°56.0	25.97	21.0	19 June 1980
70	36°52.4	75°53.5	26.5	21.4	19 June 1980
806	36°53.2	75°48.6	29.58	20.0	19 June 1980
807	36°54.4	75°41.8	31.60	19.4	19 June 1980
808	36°45.5	75°54.7	29.44	20.0	20 June 1980
809	36°46.4	75°49.0	27.34	21.0	20 June 1980
810	36°47.6	75°41.2	30.08	20.2	20 June 1980
811	36°48.7	75°32.6	31.87	20.1	21 June 1980
813	36°35.9	75°31.2	30.42	20.2	21 June 1980
812	36°34.5	75°40.2	28.68	22.0	21 June 1980
71	36°33.7	75°48.1	29.75	21.0	21 June 1980
814	36°11.5	75°44.1	27.80	21.2	21 June 1980
815	36°13.1	75°38.7	29.36	21.2	21 June 1980
72	36°15.0	75°32.6	29.66	20.6	21 June 1980
1	36°57.6	75°59.0	28.02	20.0	19 June 1980
2	36°56.6	75°58.9	24.25	20.8	19 June 1980
3	36°56.6	75°59.0	24.37	21.5	19 June 1980
66	36°40.2	74°30.0	34.48	19.4	20 June 1980
67	36°41.6	74°36.4	34.56	19.8	20 June 1980
68	36°42.9	74°42.6	33.62	18.4	20 June 1980
81	36°43.9	74°49.2	32.67	18.6	20 June 1980
82	36°45.3	74°55.7	32.47	19.0	20 June 1980
83	36°46.5	75°02.6	32.35	19.6	20 June 1980
46	36°30.0	75°23.3	31.17	19.9	23 June 1980
47	36°30.0	75°31.9	29.77	21.1	23 June 1980
48	36°30.0	75°40.7	30.28	20.8	23 June 1980
49	36°52.0	75°31.0	30.59	21.3	27 June 1980
50	36°52.0	75°43.0	30.21	21.9	27 June 1980
51	36°52.0	75°55.6	25.65	22.1	27 June 1980
816	36°18.1	75°23.1	31.50	20.0	22 June 1980
818	35°54.3	75°17.1	29.86	20.8	22 June 1980
817	35°52.3	75°23.9	30.01	21.5	22 June 1980
73	35°50.2	75°30.2	30.73	21.7	22 June 1980
805b	36°52.0	75°56.1	25.07	21.8	25 June 1980
70	36°52.3	75°53.6	29.02	21.5	25 June 1980
819	36°40.0	75°52.8	31.45	20.5	26 June 1980
820	36°42.4	75°53.9	27.96	2.4	26 June 1980

Table 3. Station coordinates, with surface salinity, temperature and date sampled for October 1980 collections.

Station	Coordinates		Salinity °/oo	Temp. °C	Date
800	36°57.2N	76°02.8W	27.09	18.6	14 October 1980
801	36°59.0	76°01.2	28.32	18.3	14 October 1980
69	36°54.8	75°57.0	29.60	18.1	16 October 1980
802	36°55.9	75°55.4	30.47	18.3	16 October 1980
803	36°58.2	75°51.6	31.37	19.5	16 October 1980
804	37°01.2	75°44.2	31.71	19.3	16 October 1980
805	36°52.2	75°55.8	31.98	19.5	17 October 1980
70	36°52.5	75°53.1	31.64	19.4	17 October 1980
806	36°53.4	75°48.5	32.33	20.2	17 October 1980
807	36°54.8	75°41.0	31.09	19.9	17 October 1980
808	36°45.7	75°54.6	32.60	18.4	15 October 1980
809	36°46.3	75°48.7	--	18.3	15 October 1980
821	36°47.4	75°42.6	--	19.8	15 October 1980
810	36°47.6	75°41.1	--	19.3	15 October 1980
811	36°48.7	75°32.2	--	19.6	15 October 1980
808	36°46.1	75°54.6	32.71	20.4	18 October 1980
809	36°46.5	75°48.6	32.47	20.3	18 October 1980
810	36°48.0	75°41.1	31.78	20.1	18 October 1980
811	36°48.8	75°31.9	32.61	20.2	17 October 1980
71	36°34.0	75°47.2	32.88	20.8	18 October 1980
812	36°35.0	75°39.9	32.34	20.6	18 October 1980
813	36°36.2	75°30.8	32.61	20.9	18 October 1980
814	36°11.6	75°44.0	32.81	20.4	19 October 1980
815	36°13.2	75°38.9	32.85	20.8	19 October 1980
72	36°15.2	75°33.1	32.32	20.8	19 October 1980
816	36°17.7	75°23.4	32.71	20.9	19 October 1980
73	35°50.0	75°30.4	31.48	21.4	19 October 1980
817	35°52.3	75°24.1	32.17	21.6	19 October 1980
15	36°56.11	75°50.0	--	19.3	22 October 1980
14	36°55.8	75°33.0	--	19.8	22 October 1980
13	36°56.0	75°18.0	--	19.5	22 October 1980
1	36°56.0	74°30.0	--	20.1	22 October 1980

Table 4. Phytoplankton observed during the March, June, and October 1980 Superflux cruises. The degree of numerical dominance for each period, within the plume at the Bay entrance and at shelf stations, is indicated by A, B, C (with A the most dominant) and X noting presence in the samples.

	March		June		October	
	Plume	Shelf	Plume	Shelf	Plume	Shelf
BACILLARIOPHYCEAE						
Actinoptychus sp.	-	-	-	X	-	-
Actinoptychus senarius Ehrenberg	-	-	X	X	-	-
Amphora cuneata Cleve	-	-	-	X	-	X
Amphora sp.	X	-	-	X	-	X
Asterionella glacialis Castracane	A	X	X	X	C	C
Bacillaria paxillifer (Muller) Hendey	-	-	X	-	-	-
Bacteriastrum delicatulum Cleve	-	X	-	-	-	-
Bacteriastrum hyalinum Lauder	-	X	-	-	-	X
Bacteriastrum sp.	-	X	-	-	-	-
Bellochea horologicalis Von Stosch	-	-	-	X	X	-
Biddulphia alternans (Bailey) Van Heurck	-	X	X	X	X	X
Biddulphia aurita (Lyngbye) Brebisson	-	-	X	-	-	-
Biddulphia longicruris Greville	-	-	-	-	-	-
Biddulphia mobiliensis (Bailey) Grunow	-	X	X	X	X	X
Biddulphia rhombus f. *trigona* Hustedt	-	-	-	-	-	X
Biddulphia sinensis Greville	-	-	-	X	-	X
Biddulphia sp.	-	-	-	-	-	X
Campylosira cymbelliformis (Schmidt) Grunow	-	-	-	-	-	X
Chaetoceros pelagica (Cleve) Hendey	X	X	X	X	X	C
Chaetoceros affine Lauder	-	X	-	-	X	X
Chaetoceros atlanticum Cleve	-	-	X	X	X	X
Chaetoceros coarctatum Lauder	-	-	-	-	X	X
Chaetoceros compressum Lauder	X	X	-	X	X	-
Chaetoceros costatum Pavillard	-	-	-	X	-	X
Chaetoceros curvisetum Cleve	-	X	-	X	X	X
Chaetoceros danicum Cleve	X	X	X	X	-	-
Chaetoceros decipiens Cleve	-	X	X	X	X	X
Chaetoceros gracile Schutt	-	X	X	X	X	-
Chaetoceros lorenzianum Grunow	-	-	-	-	X	-
Chaetoceros pendulum Karsten	-	-	-	X	X	-
Chaetoceros peruvianum Brightwell	-	-	X	X	-	X
Chaetoceros sociale Lauder	X	X	-	X	-	-
Chaetoceros sp.	X	C	X	X	B	-
Climacodium frauenfeldianum Gurnow	-	-	-	-	X	X

Table 4. Continued.

	March		June		October	
	Plume	Shelf	Plume	Shelf	Plume	Shelf
Cocconeis sp.	-	-	-	X	X	X
Corethron criophilum Castracane	C	X	-	-	X	-
Coscinodiscus asteromphalus Ehrenberg	-	X	-	-	-	-
Coscinodiscus centralis Ehrenberg	-	X	-	-	-	-
Coscinodiscus grani Gough	-	-	-	-	-	X
Coscinodiscus gigas Ehrenberg	-	X	X	X	-	-
Coscinodiscus granulosus Grunow	-	X	-	X	-	-
Coscinodiscus lineatus Ehrenberg	X	X	X	X	-	X
Coscinodiscus marginatus Ehrenberg	-	-	-	-	-	-
Coscinodiscus nitidus Gregory	-	X	-	X	-	-
Coscinodiscus oculus iridis Ehrenberg	-	-	-	X	-	-
Coscinodiscus radiatus Ehrenberg	-	-	-	-	-	X
Coscinodiscus sp.	-	X	-	-	X	X
Coscinodiscus wailesii Gran and Angst	X	-	-	X	X	X
Coscinosira polychorda (Gran) Gran	-	-	-	X	-	-
Cyclotella sp.	Z	X	X	X	X	-
Cylindrotheca closterium (Ehrenberg) Reimann and Lew	X	X	C	X	C	-
Cymatosira belgica Grunow	-	-	-	-	-	X
Dactyliosolen mediterraneus Peragallo	-	-	-	X	-	-
Diploneis crabro Ehrenberg	X	-	-	-	-	-
Diploneis smithii (Brebisson) Cleve	X	-	-	-	-	-
Ditylum brightwellii (West) Grunow	X	X	-	X	X	X
Eucampia zoodiacus Ehrenberg	-	-	-	X	X	X
Fragilaria pinnata Ehrenberg	-	X	-	-	-	-
Fragilaria sp.	-	X	-	-	-	-
Grammatophora sp.	-	X	X	-	-	X
Guinardia flaccida (Castracane) Pergallo	C	X	X	X	X	X
Gyrosigma balticum similis (Grunow) Cleve	X	-	-	-	-	-
Gyrosigma sp.	-	-	-	X	X	-
Hemiaulus hauckii Grunow	-	X	-	X	X	-
Hemiaulus sinensis Greville	-	X	-	X	X	X
Lauderia borealis Gran	-	-	-	-	C	X
Leptocylindrus danicus Cleve	C	B	B	A	B	B
Leptocylindrus minimus Gran	B	B	X	C	X	-
Licmophora sp.	-	X	-	-	-	X

Table 4. Continued.

	March		June		October	
	Plume	Shelf	Plume	Shelf	Plume	Shelf
Navicula cancellata Donkin	-	-	X	X	-	X
Navicula lyra Ehrenberg	-	-	-	X	X	-
Navicula sp.	-	X	-	X	X	X
Navicula transitans var. *asymmetrica* (Cleve) Cleve	-	-	-	X	-	-
Nitzschia delicatissima Cleve	-	B	-	-	C	X
Nitzschia gracillima Heiden and Kolbe	-	-	X	X	-	-
Nitzschia insignis Gregory	-	-	-	-	-	-
Nitzschia longissima (Brebisson) Ralfs	-	X	-	X	-	-
Nitzschia panduriformis Gregory	-	-	-	-	-	X
Nitzschia pungens Grunow	C	C	B	X	C	C
Nitzschia seriata Cleve	X	X	-	X	X	X
Nitzschia sp.	X	X	-	X	X	X
Nitzschia spathulata Brebisson	-	-	X	X	-	-
Paralia sulcata (Ehrenberg) Cleve	C	X	X	X	X	X
Plagiogramma sp.	-	X	-	X	-	-
Plagiogramma staurophorum (Gregory) Heilberg	-	X	X	X	-	X
Plagiogramma vanheurckii Grunow	-	-	X	X	X	X
Pleurosigma angulatum (Quekett) W. Smith	-	X	-	X	-	-
Pleurosigma naviculaceum Brebisson	X	-	-	-	-	-
Pleurosigma nicobaricum (Grunow) Grunow	-	X	-	-	-	-
Pleurosigma normanii Ralfs	-	-	-	X	-	-
Pleurosigma sp.	X	X	X	X	X	X
Rhaphoneis amphiceros Ehrenberg	X	-	X	X	X	X
Rhaphoneis sp.	-	-	X	-	-	-
Rhaphoneis surirella (Enrenberg) Grunow	-	-	-	X	-	X
Rhizosolenia alata Brightwell	X	X	-	C	X	X
Rhizosolenia alata f. *gracillima* (Cleve) Grunow	X	-	-	X	X	-
Rhizosolenia alata f. *indica* (Peragallo) Gran	-	X	-	X	X	X
Rhizosolenia bergonii Peragallo	-	-	-	X	X	X
Rhizosolenia calcar-avis Schultze	-	X	X	X	X	X
Rhizosolenia delicatula Cleve	B	A	C	X	C	C
Rhizosolenia fragilissima Gergon	B	X	X	X	B	B
Rhizosolenia hebetata f. *semispina* (Hensen) Gran	-	-	-	-	-	X
Rhizosolenia imbricata Brightwell	X	X	-	X	X	X
Rhizosolenia robusta Norman	-	-	-	X	X	-
Rhizosolenia setigera Brightwell	-	-	X	X	X	X
Rhizosolenia sp.	X	-	-	-	-	X
Rhizosolenia stolterfothii Peragallo	-	X	-	X	B	B

Table 4. Continued.

	March		June		October	
	Plume	Shelf	Plume	Shelf	Plume	Shelf
Rhizosolenia styliformis Brightwell	X	-	X	X	X	X
Schroederella delicatula (Peragallo) Pavillard	-	-	-	-	X	-
Skeletonema costatum (Greville) Cleve	A	X	A	B	A	B
Stephanopyxis palmeriana (Greville) Grunow	-	-	-	X	X	X
Stephanopyxis turris (Greville) Ralfs	-	-	-	X	X	-
Striatella unipunctata (Lyngbye) Agardh	X	-	-	-	X	X
Synedra sp.	X	X	-	-	-	X
Tabellaria fenestrata var. *asterionelloides* Grunow	X	X	X	-	-	-
Tabellaria fenestrata (Lyngbye) Kutzing	-	X	-	X	-	-
Thalassionema nitzschioides Hustedt	C	X	X	X	X	X
Thalassiosira eccentrica (Ehrenberg) Cleve	-	-	X	X	-	-
Thalassiosira gravida Cleve	C	X	X	X	-	-
Thalassiosira nordenskioldii Cleve	B	B	-	X	-	-
Thalassiosira pseudonana (Hustedt) Hasle and Heimdal	-	-	X	X	-	-
Thalassiosira rotula Meunier	-	B	X	X	X	-
Thalassiosira sp.	-	-	X	-	-	-
Thalassiothrix frauenfeldii Grunow	X	X	-	X	-	X
Thalassiothrix mediterranea Pavillard	-	-	-	-	C	X
Tricetatium acutum Ehrenberg	-	-	-	X	-	-
Unidentified centric diatoms <20 microns	-	X	-	X	X	X
Unidentified centric diatoms 20 to 100 microns	-	X	-	X	-	X
Unidentified pennate diatoms <20 microns	X	X	X	X	X	X
Unidentified pennate diatoms >20 microns	-	-	X	X	X	X
PYRRHOPHYCEAE						
Amphidinium acutum Lahmann	-	X	-	X	X	X
Amphidinium acutissimum Schiller	-	X	-	X	-	-
Amphidinium schroederi Schiller	-	-	-	X	-	-
Amphidinium sp.	X	X	-	X	-	X
Ceratium arcticum (Ehrenberg) Cleve	-	-	-	-	-	X
Ceratium buceros (Zacharias) Schiller	-	-	X	X	-	-
Ceratium contortum (Gourret) Cleve	-	-	-	-	X	-
Ceratium extensum (Gourret) Cleve	-	-	-	X	X	X

Table 4. Continued.

	March		June		October	
	Plume	Shelf	Plume	Shelf	Plume	Shelf
Ceratium furca (Ehrenberg) Claparede and Lachmann	-	-	-	X	-	-
Ceratium fusus (Ehrenberg) Dujardin	X	X	X	X	X	X
Ceratium lineatum (Ehrenberg) Cleve	X	C	X	X	X	X
Ceratium macroceros (Ehrenberg) Vanhoffen	-	X	X	X	X	X
Ceratium massiliense (Gourret) Jorgensen	-	-	X	X	-	X
Ceratium minutum Jorgensen	-	X	X	X	-	X
Ceratium pentagonum Gourret	-	-	-	X	X	X
Ceratium sp.	-	X	-	-	-	-
Ceratium trichoceros (Ehrenberg) Kofoid	X	X	-	X	-	X
Ceratium tripos (Muller) Nitzsch	-	X	X	X	X	X
Ceratium tripos var. *atlanticum* (Ostenfeld) Paulsen	X	X	X	X	X	-
Cladopyxis brachiolata Stein	-	-	-	-	X	-
Dinophysis acuminanta Claparede and Lachmann	X	-	-	X	-	-
Dinophysis acuta Ehrenberg	-	X	X	X	-	X
Dinophysis caudata Kent	-	-	-	X	X	X
Dinophysis fortii Pavillard	X	X	X	X	-	X
Dinophysis hastata Stein	-	-	-	X	-	-
Dinophysis norvegica Claparede and Lachmann	-	-	X	X	-	-
Dinophysis ovum Schutt	-	X	X	X	X	X
Dinophysis punctata Jorgensen	-	-	X	X	-	X
Dinophysis rotundata Claparede and Lachmann	-	-	X	X	-	-
Dinophysis sp.	-	-	-	X	X	-
Dinophysis tripos Gourret	-	-	-	X	-	-
Goniaulax diegensis Kofoid	-	-	-	X	-	-
Goniaulax digitalis (Pouchet) Kofoid	-	-	-	X	-	X
Goniaulax sp.	X	X	-	X	-	-
Goniaulax spinifera (Claparede and Lachmann) Diesing	-	-	-	X	-	-
Gymnodinium arcticum Wulff	-	-	X	X	-	X
Gymnodinium breve Davis	-	-	X	X	-	-
Gymnodinium sp.	X	X	X	X	X	X
Gyrodinium estuariale Hulburt	-	-	-	-	X	-
Gyrodinium sp.	-	X	X	X	X	X
Heterocapsa triquetra (Ehrenberg) Stein	X	-	-	-	-	-

Table 4. Continued.

	March		June		October	
	Plume	Shelf	Plume	Shelf	Plume	Shelf
Oxytoxum elegans Pavillard	-	-	-	X	-	-
Oxytoxum milneri Murray and Whitting	-	-	-	X	X	-
Oxytoxum parvum Schiller	-	-	-	-	X	-
Oxytoxum sceptrum (Stein) Schroder	-	-	-	X	-	-
Oxytoxum scolopax Stein	-	-	-	X	X	X
Oxytoxum sp.	-	-	-	-	X	X
Oxytoxum turbo Kofoid	-	-	-	-	X	-
Podolampas palmipes Stein	-	-	-	-	X	-
Prorocentrum aporum (Schiller) Dodge	-	-	-	-	X	-
Prorocentrum balticum (Lohmann) Loeblich III	-	X	X	X	-	X
Prorocentrum cassubicum (Woloszynska) Dodge	-	-	-	-	X	X
Prorocentrum compressum (Bailey) Abe	-	-	-	X	-	-
Prorocentrum dentatum Stein	X	X	-	-	X	-
Prorocentrum micans Ehrenberg	X	X	X	X	X	X
Prorocentrum minimum (Pavillard) Schiller	A	X	X	X	-	X
Prorocentrum nanum Schiller	-	X	-	-	-	-
Prorocentrum scutellum Schroder	-	-	X	X	-	-
Prorocentrum sp.	-	X	-	X	-	-
Prorocentrum triestinum Schiller	-	-	-	X	X	-
Protoperidinium sp.	X	X	X	X	X	X
Protoperidinium breve (Paulsen) Balech	-	X	-	-	-	-
Protoperidinium cerasus (Paulsen) Balech	-	X	-	X	-	-
Protoperidinium depressum (Bailey) Balech	X	-	X	X	X	X
Protoperidinium oceanicum (Vanhoffen) Balech	-	-	X	X	-	-
Protoperidinium punctulatum (Paulsen) Balech	-	-	-	X	-	-
Protoperidinium claudicans (Paulsen) Balech	-	-	-	X	-	-
Protoperidinium steinii (Jorgensen) Balech	-	-	-	X	X	X
Protoperidinium minutum (Kofoid) Loeblich III	-	-	-	X	-	-
Protoperidinium divergens (Ehrenberg) Balech	-	-	-	X		
Pyrocystis fusiformis (Wyville-Thomson) Murray	-	-	-	-	-	X
Pyrophacus horologium Stein	-	-	-	X	X	-
Pyrophacus sp.	-	-	-	X	-	-

Table 4. Continued.

	March		June		October	
	Plume	Shelf	Plume	Shelf	Plume	Shelf
Scrippsiella trochoidea (Stein) Loeblich III	-	-	-	-	X	-
Unidentified dinoflagellate cysts	X	X	X	X	X	X
Unidentified dinoflagellates	-	C	-	X	X	X
HAPTOPHYCEAE						
Acanthoica quattrospina Lohmann	-	-	-	X	-	-
Calciocolenia granii Schiller	-	-	-	X	X	-
Calciosolenia murrayi Gran	-	-	-	-	X	-
Discosphaera tubifer (Murray and Blackman) Ostenfeld	-	-	-	-	X	X
Emiliania huxleyi (Lohmann) Hay and Mohler	X	A	X	A	C	B
Michaelsarsia elegans Gran	-	X	-	-	-	-
Monodus sp.	X	-	-	-	-	-
Ophiaster hydroides (Lohmann) Lohmann	-	X	-	X	X	-
Pontosphaera sp.	-	-	-	X	-	-
Pontosphaera syracusana Lohmann	-	-	-	C	-	X
Rhabdosphaera claviger Murray and Blachman	-	-	-	-	X	X
Rhabdosphaera hispida Lohmann	-	X	-	-	X	-
Rhabdosphaera stylifer Lohmann	-	-	-	X	-	-
Rhabdosphaera sp.	-	X	-	C	-	X
Syracosphaera pulchra Lohmann	-	X	-	B	X	X
Unidentified coccolithophores	-	X	X	X	X	X
CHRYSOPHYCEAE						
Dictyocha fibula Ehrenberg	-	X	X	X	X	X
Distephanus speculum (Ehrenberg) Haekel	-	X	X	X	X	X
Ebria tripartita (Schumann) Lemmermann	X	-	-	X	-	-

Table 4. Concluded.

	March		June		October	
	Plume	Shelf	Plume	Shelf	Plume	Shelf
CYANOPHYCEAE						
Anacystis aeruginosa Drouet and Daily	-	X	-	-	-	-
Anacystis sp.	-	-	-	-	B	C
Gomphosphaeria aponina Kutzing	A	X	-	-	-	-
Johannesbaptistia pellucida (Dickie) Taylor and Drouet	-	X	-	X	-	-
Merismopedia sp.	-	-	-	-	-	X
Nostoc commune Vaucher	B	X	-	-	X	X
Oscillatoria erythraea (Ehrenberg) Kutzing	-	-	-	-	X	X
Oscillatoria sp.	X	X	-	-	-	-
Oscillatoria submembranacea Ardissone and strafforella	X	-	-	-	-	-
EUGLENOPHYCEAE						
Euglena sp.	X	X	-	-	X	X
Eutreptia sp.	-	-	-	X	X	X
CHLOROPHYCEAE						
Chlorella sp.	-	-	X	X	X	X
Crucigenia tetrapedia (Kirchner) West and West	-	-	-	-	X	-
Pediastrum simplex (Meyer) Lemmermann	-	-	-	X	-	-
Scenedesmus sp.	X	-	-	-	-	-
CRYPTOPHYCEAE						
Chroomonas sp.	X	X	-	X	X	X
Cryptomonas sp.	C	C	X	X	C	B
Ochromonas variabilis Meyer	-	X	-	-	-	-
OTHERS						
Green cells (<3.0 microns)	A	A	X	A	A	A
Green cells (3-5 microns)	A	C	A	B	C	B
Green cells (5-10 microns)	X	B	X	X	X	-

Table 5. Total cell concentrations for surface, 3 meter and 7 meter depths at stations with species diversity and dominant species noted for each station for March 1980. Samples lacking a universally dominant single species are indicated as mixed sample.

Station		Surface	3 meters	7 meters
Bay Entrance	5	*Prorocentrum minima* 1,046,697 cells/l 2.308	*Leptocylindrus danicus* 62,700 cells/l 1.986	Mixed 43,890 cells/l 2.983
Shelf	11	*Leptocylindrus danicus* 247,248 cells/l 0.939	*Leptocylindrus minimus* 171,296 cells/l 1.931	*Leptocylindrus minimus* 397,631 cells/l 2.690
Shelf	16	*Leptocylindrus danicus* 19,920 cells/l 2.527	*Leptocylindrus danicus* 36,022 cells/l 2.065	*Leptocylindrus danicus* 51,975 cells/l 2.543
Shelf	21	Mixed 40,283 cells/l 3.781	Mixed 31,050 cells/l 3.488	Mixed 39,105 cells/l 3.870
Shelf	22	Green cells 1,546,185 cells/l 0.647	*Leptocylindrus danicus* 36,630 cells/l 2.495	Mixed 39,765 cells/l 3.723
Shelf	33	*Guinardia flaccida* 53,130 cells/l 2.107	*Leptocylindrus danicus* 54,450 cells/l 2.289	*Leptocylindrus danicus* 43,725 cells/l 2.014
Shelf	34	*Leptocylindrus danicus* 42,735 cells/l 2.500	*Leptocylindrus danicus* 109,890 cells/l 1.946	*Leptocylindrus danicus* 34,485 cells/l 2.635
Far Shelf	1	*Emiliania huxleyi* 32,576 cells/l 3.776	Mixed 16,040 cells/l 3.878	Mixed 11,700 cells/l 3.746
Far Shelf	2	Mixed 29,100 cells/l 3.505	Mixed 34,815 cells/l 3.155	Mixed 26,712 cells/l 3.080

Table 6. The dominant species, total cell concentrations (cells/1 x 10^4), and species diversity at various depths for stations within the plume, shelf and far shelf for June 1980.

	Stations	Surface	3-5 meters	7-12 meters	13-15 meters
Plume	800	*S. costatum* 363.4 1.1286	*S. costatum* 377.8 0.8449	*S. costatum* 424.3 0.5929	
	802	*S. costatum* 166.2 2.1864	*S. costatum* 87.0 1.5723	Green cells 97.0 1.6851	Green cells 28.3 1.3973
	69	*S. costatum* 687.9 1.1119	*S. costatum* 740.0 1.2272	*S. costatum* 217.6 1.2699	
	70	*S. costatum* 370.2 1.2068	*S. costatum* 367.7 1.0645	*S. costatum* 188.7 2.1251	*L. danicus* 76.1 2.1516
	809	*S. costatum* 233.4 1.3133	*S. costatum* 320.9 1.2772	*S. costatum* 240.4 1.8871	
Shelf	807	Green cells *E. huxleyi* 14.0 2.6515	Green cells 12.7 2.1013	Green cells *E. huxleyi* 155.3 2.3160	Green cells *E. huxleyi* 27.9 2.0051
	812	*L. danicus* *S. costatum* 77.1 2.8104	Mixture 153.2 2.0961	Mixture 73.4 2.7542	Mixture 121.5 2.4503
	817	Mixture 59.5 2.4880	*E. huxleyi* *L. danicus* 39.0 2.4052	*E. huxleyi* Mixture 41.0 2.2177	Mixture 43.1 2.5666
	818	Mixture 56.7 2.5176	*E. huxleyi* Mixture 26.8 2.0901	Mixture 61.6 2.4303	Mixture 39.05 3.0197
Far Shelf	66	Coccolithophores 18.9 2.3113	Coccolithophores 39.5 1.8696		
	67	Coccolithophores 23.7 1.9474	Coccolithophores 44.0 1.5609		

Table 7. Representative composition at stations during the October 1980 Superflux collections. Concentrations are in numbers per liter x 10^4.

	Stations									
	800	801	69	802	803	804	69	802	803	804
Diatoms	72.5	169.1	207.7	9.5	200.3	142.7	287.2	92.1	145.0	3.3
Pyrrhophyceae	.4	.1	.1	<.1	<.1	.3	.3	.2	.4	<.1
Coccolithophores	0	0	.7	0	6.5	0	0	.7	1.9	.2
Cyanophyceae	0	0	0	0	3.9	18.5	9.7	3.9	2.9	.1
Cryptophyceae	0	6.9	13.6	.8	.1	2.3	2.3	1.7	.3	<.1
Green cells	23.9	61.5	50.7	1.2	24.4	21.4	40.0	39.0	29.7	93.7
Others	.9	5.1	.9.9	.4	0	0	0	6.3	0	0
Total cells/l	97.9	242.9	274.0	12.1	235.3	185.5	339.7	144.1	180.4	97.4
Diversity Index	1.776	1.863	1.521	3.394	1.673	2.282	1.306	2.194	1.560	1.022
Date	10/14	10/14	10/15	10/15	10/15	10/15	10/16	10/16	10/16	10/16

	808	809	821	810	811	808	809	810	811
Diatoms	1169.0	170.7	20.7	18.8	294.4	91.2	148.8	5.4	1.1
Pyrrhophyceae	.5	.7	.3	<.1	0	3.6	.4	.2	.2
Coccolithophores	3.0	4.5	0	.4	1.1	.5	7.0	.3	.4
Cyanophyceae	19.5	3.9	4.8	1.4	3.9	0	13.6	.4	1.5
Cryptophyceae	2.2	15.9	.8	1.9	.1	.6	.7	.9	1.0
Green cells	191.3	66.4	32.4	3.0	28.8	59.5	167.9	5.7	18.9
Others	0	0	0	0	0	5.1	13.7	0	.2
Total cells/l	1385.4	262.3	59.1	25.7	328.4	160.6	352.2	13.0	23.6
Diversity Index	1.262	2.306	2.617	3.319	1.006	2.459	3.155	3.103	1.488
Date	10/15	10/15	10/15	10/15	10/15	10/18	10/18	10/18	10/17

Table 7. Concluded.

	Stations								
	805	70	806	807	15	14	13	1	
Diatoms	41.4	72.1	21.9	81.4	75.7	2.6	.1	<.1	
Pyrrhophyceae	<.1	.2	.8	1.1	.4	.5	.2	.3	
Coccolithophores	0	3.2	1.1	1.1	1.7	<.1	.2	1.2	
Cyanophyceae	9.7	0	.6	3.9	0	<.1	.7	<.1	
Cryptophyceae	3.4	5.2	<.1	0	7.5	.1	7.7	<.1	
Green cells	66.8	93.7	12.3	34.1	52.7	12.0	6.1	.5	
Others	5.8	.3	2.5	34.1	1.9	.1	0	.3	
Total cells/l	127.5	175.0	39.5	121.8	140.4	15.6	15.2	2.4	
Diversity Index	2.976	2.777	2.909	1.728	2.918	1.448	1.892	2.985	
Date	10/17	10/17	10/17	10/17	10/22	10/22	10/22	10/22	
	71	812	813	814	815	72	816	73	817
Diatoms	81.7	10/9	8.9	123.7	10.5	3.2	.6	54.0	5.3
Pyrrhophyceae	.2	.1	<.1	<.1	<.1	.5	<.1	<.1	.1
Coccolithophores	5.8	1.3	3.4	.7	<.1	2.2	1.8	1.3	1.2
Cyanophyceae	1.4	3.9	4.9	0	0	4.4	<.1	14.6	.2
Cryptophyceae	2.6	.4	.9	3.3	0	.2	3.2	13.9	<.1
Green cells	83.9	10.6	23.2	22.5	15.4	29.1	13.8	46.7	8.9
Others	.9	1.7	.2	0	0	1.2	.9	.8	.7
Total cells/l	176.8	29.1	41.6	150.3	26.0	41.0	20.4	119.2	16.6
Diversity Index	2.932	3.413	2.562	2.723	2.493	2.433	1.778	2.942	3.140
Date	10/18	10/18	10/18	10/19	10/19	10/19	10/19	10/19	10/19

Table 8. Phytoplankton assemblages within the Chesapeake Bay plume and adjacent shelf waters for March, June, and October 1980. Numerical dominance is indicated for each collection period.

	Bay Entrance - Plume	Shelf
March	*Asterionella glacialis*	*Bacteriastrum hyalinum*
	Cyclotella sp.	*Chaetoceros costatum*
	Guinardia flaccida	*Nitzschia longissima*
	Leptocylindrus danicus	*Rhizosolenia delicatula*
	Leptocylindrus minimus	*Thalassiosira nordenskioldii*
	Nitzschia pungens	*Thalassiosira rotula*
	Paralia sulcata	**Emiliania huxleyi*
	Rhizosolenia delicatula	Green cells 5-10 microns
	Rhizosolenia fragilissima	
	**Skeletonema costatum*	
	Thalassiosira nordenskioldi	
	Gomphosphaeria aponina	
	Nostoc commune	
	**Prorocentrum minimum*	
	*Green cells <3 microns	
	*Green cells 3-5 microns	
June	*Chaetoceros* spp.	*Rhizosolenia alata*
	Cylindrotheca closterium	**Emiliania huxleyi*
	Leptocylindrus danicus	*Pontosphaera* sp.
	Nitzschia pungens	*Rhabdosphaera* sp.
	Rhizosolenia delicatula	*Syracosphaera pulchra*
	**Skeletonema costatum*	
	*Green cells 3-5 microns	
October	**Asterionella glacialis*	*Nitzschia pungens*
	Cerataulina pelagica	*Rhizosolenia delicatula*
	Cylindrotheca closterium	*Rhizosolenia fragilissima*
	Lauderia borealis	*Skeletonema costatum*
	Leptocylindrus danicus	**Emiliania huxleyi*
	Nitzschia pungens	*Green cells <3 microns
	Rhizosolenia delicatula	*Green cells 3-5 microns
	**Skeletonema costatum*	Mixed phytoflagellates
	**Emiliania huxleyi*	
	*Green cells <3 microns	
	*Green cells 3-5 microns	
	Anacystis sp.	
	Cryptomonas sp.	

*Dominant phytoplankters

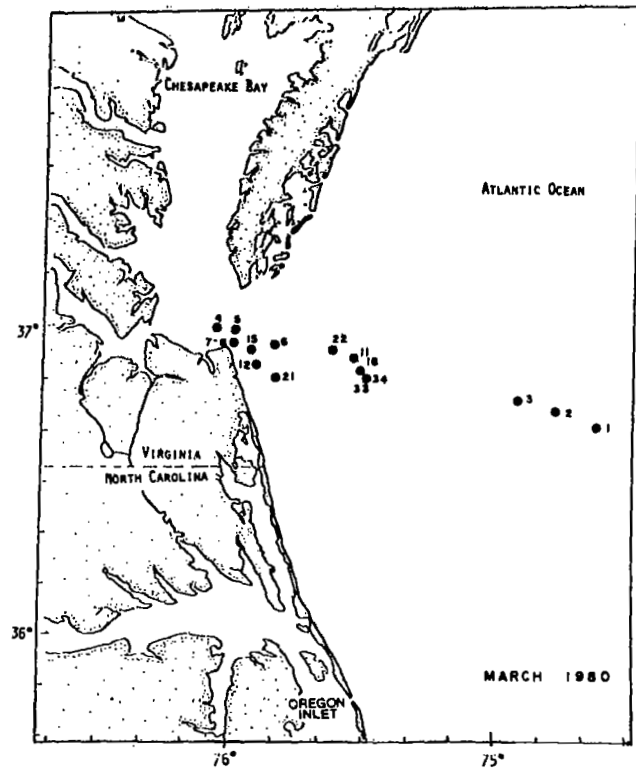

Figure 1.- Station locations.

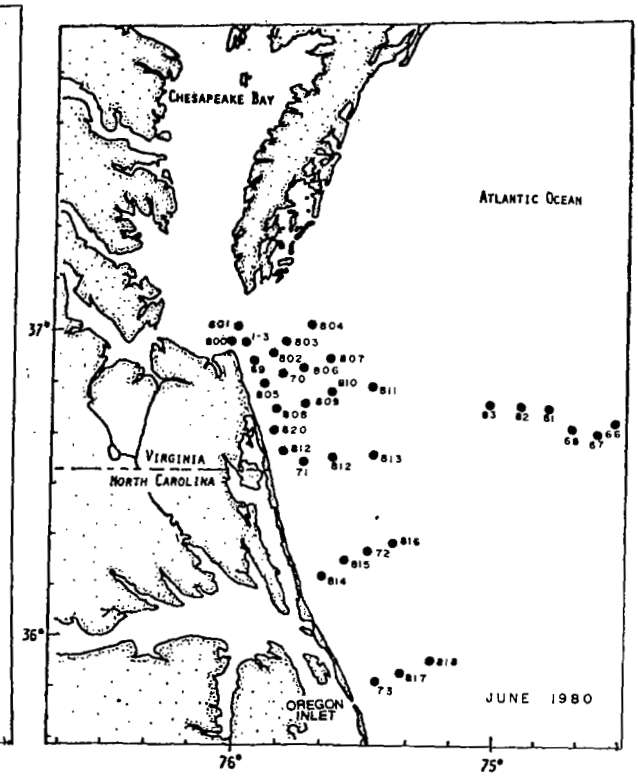

Figure 2.- Station locations.

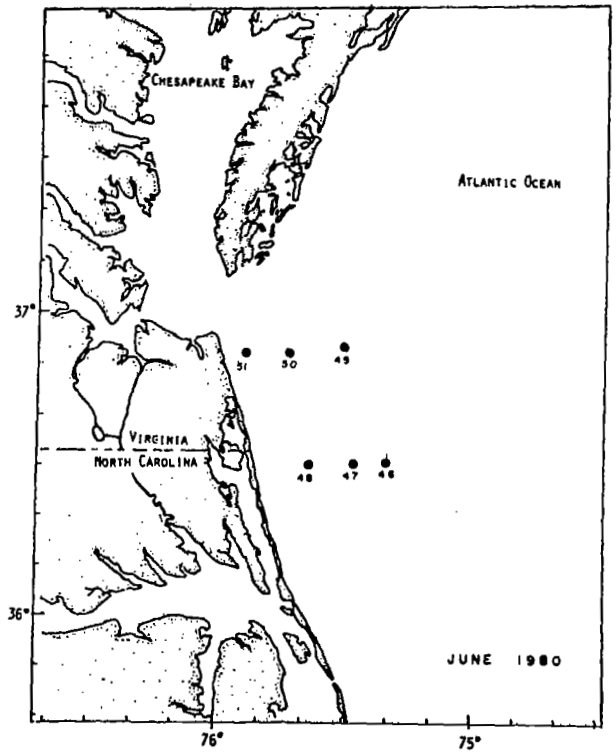

Figure 3.- Station locations.

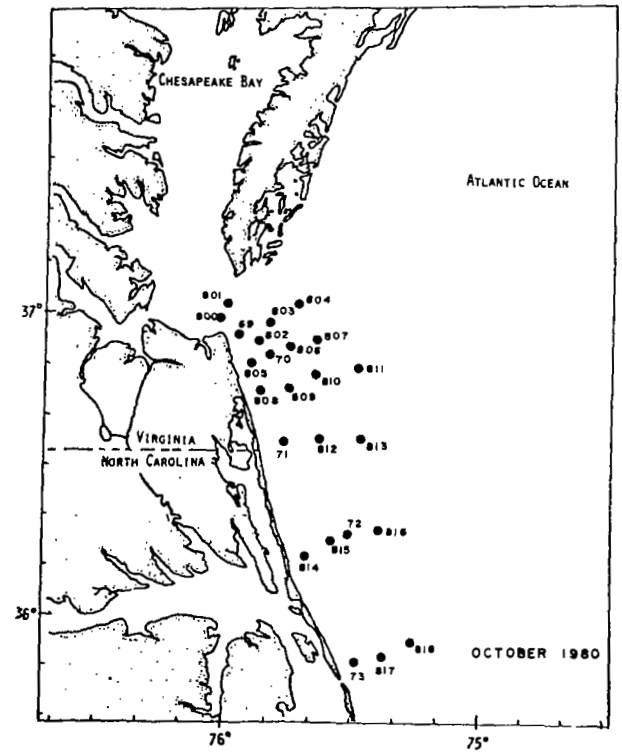

Figure 4.- Station locations.

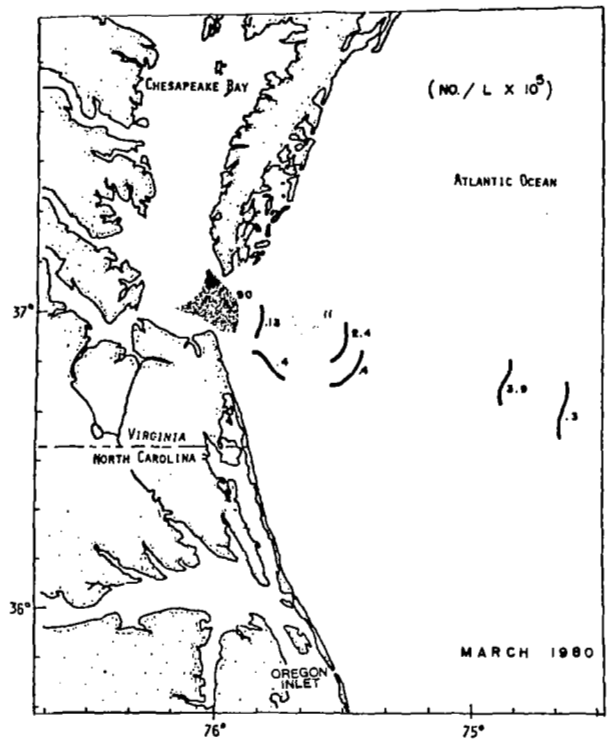

Figure 5.- Cell concentrations.

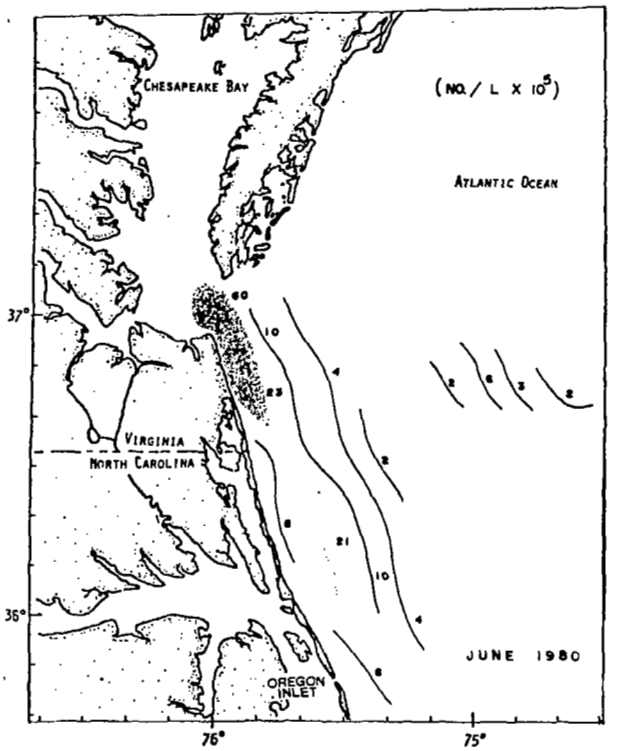

Figure 6.- Cell concentrations.

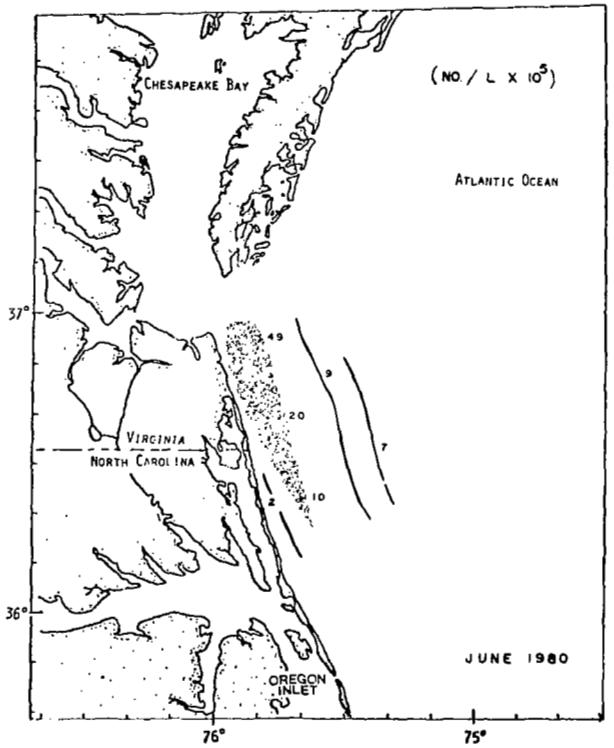

Figure 7.- Cell concentrations.

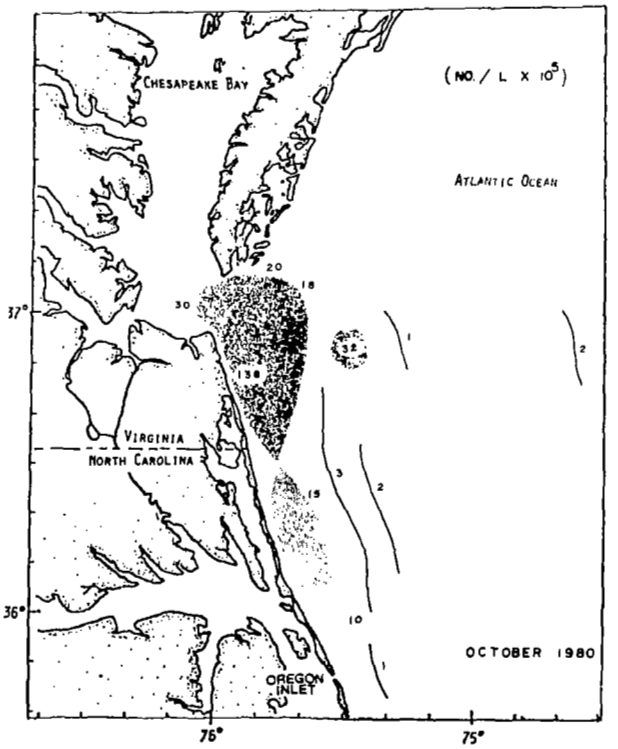

Figure 8.- Cell concentrations.

USE OF ORDINATION AND CLASSIFICATION PROCEDURES TO EVALUATE PHYTOPLANKTON COMMUNITIES DURING SUPERFLUX II

Charles K. Rutledge and Harold G. Marshall
Department of Biological Sciences
Old Dominion University

SUMMARY

Cluster analysis and an ordination procedure were performed on two data matrices to investigate real and environmental spatial relationships. Multiple regression analysis was used to relate the measured environmental variables to the phytoplankton community changes. Qualitative type phytoplankton data proved to be less structured in both of these spaces, relative to the biomass data. The salinity gradients of the northern transects covaried significantly with the phytoplankton association changes. In the southern transects the light variable was most important in explaining the variance in the ordination axes. These data suggest the close relationships between phytoplankton community changes and the physical hydrology of the area.

INTRODUCTION

The purposes of this study were: 1) to investigate phytoplankton community structure within the three-dimensional spatial confines of the Chesapeake Bay plume and 2) to examine the changes of community structure in a multidimensional environmental space. To realize the first objective, cluster analysis was used. A similar approach was followed in the study of plankton associations in the North Sea (ref. 1, 2), and to associate phytoplankton assemblages with major water masses in the West Indian Ocean (ref. 3). More recently cluster analysis has been applied in the impact assessment field and community structure studies (ref. 4, 5, 6, 7).

An ordination procedure was performed for the second objective. Polar ordination was used to place collection sites into a theoretically continuous environmental space (ref. 8). Eigenvector ordination techniques have also been used to investigate phytoplankton associations without any real efficiency (ref. 2, 9). Similar techniques were followed with more success to ordinate species samples from transient beach ponds (ref. 10). Polar ordination was selected for this study because of its relative simplicity (ref. 11) and the general failure of the other techniques previously applied in plankton research (ref. 12). The merits of this procedure with respect to

other ordination techniques have been previously discussed (ref. 13, 14, 15). A major assumption made by environmental ordination techniques is that species distributions in space and time are a result of specific responses to environmental variables. The assessment of such a multidimensional space could provide insight into the controlling factors of phytoplankton interrelationships.

The use of two data matrices in the following analysis allows the investigation of two fundamentally different questions. From the qualitative presence-absence matrix, species presence without reference to quantity is investigated. Are the species lists at the observed stations different within the sampling regime? Are there pronounced different qualitative regions within the study area relative to phytoplankton populations? The other matrix, the cell volume matrix, assesses the quantities of the phytoplankton species at the stations.

MATERIALS AND METHODS

Sampling Program

The phytoplankton samples for this study were collected during the June 1980 Chesapeake Bay plume studies aboard the NOAA vessels Kelez and Delaware II. The study area has a complex circulatory system represented by a southward flowing, low salinity mass of water originating from the Chesapeake Bay which generally holds to the Virginia and North Carolina coasts (ref. 16, 17). Such circulatory systems may be responsible for major phytoplankton dispersions (ref. 18), with areas of contrasting community structure.

The station numbers used in this study represent the 24 standard stations (see Marshall, Figure 2, paper no. 32 of this compilation) with each depth being assigned a station number. A total of 101 such station depth events occurred during the cruises. The samples were collected over a five day period. The study area was located between 37.00.6' and 35.50.2' N latitude and 76.02.9' and 75.17.1' W longitude. Parameters measured during the cruises were secchi depth, salinity, water temperature, dissolved oxygen, total suspended matter, nitrites, nitrates, ammonia, silicon, phosphates, and light. Appreciation is expressed to Dr. George Wong of Old Dominion University for supplying the station concentrations of nitrites, nitrates, phosphates, ammonia, and silicates; to Dr. Paul Zubkoff of the Virginia Institute of Marine Science for the daily isolation curves; and to Dr. James Thomas and Craig Robertson of NOAA for the salinity, dissolved oxygen, and temperature data. Special appreciation is given to Dr. James Matta of Old Dominion University in reference to the application of the multivariate techniques in this study. These data were selected for this study because of their historic relationships to phytoplankton dynamics.

The samples were collected with 20-liter Niskin sampling bottles. Different depths were selected at each station in relation to the thermostructure of the water column as assessed by using an expendable bathythermographic probe.

Phytoplankton Analysis

For phytoplankton analysis a measured subsample (500 ml) of seawater was withdrawn from the Niskin sampler at each station depth and transferred directly into a polypropylene bottle which contained 20 ml of buffered formalin. Upon returning to the laboratory, the bottles were allowed at least 72 hours for the sedimentation of cells. A siphoning procedure followed that resulted in a 20-ml concentrate for each sample. For quantifying and identifying the cells either aliquots or whole concentrates were placed into settling chambers and allowed to re-settle; they were then examined and counted using a Zeiss inverted plankton microscope. Random fields of the chamber were selected and counts were made to give 85% confidence intervals on the mean concentration (ref. 19). A total of 168 species were identified from the 101 station depths.

To compute cell volumes, the identified species were assigned geometric shapes according to Kovala and Larrance (ref. 20). This scheme allowed for 18 phytoplankton shapes to choose from to approximate the shape of each species, with up to 10 dimensions applicable for the more complex forms. Average cell dimensions were determined from the literature with spot measurements also made for major species in the collections. A FORTRAN program was written to compute these volumes using the cell dimensions and appropriate formulae from Kovala and Larrance (ref. 20). Cell volumes per liter were computed for each station by multiplying the species volume by the number of cells per liter. This data base formed the volumetric matrix. This matrix was reduced to 64 × 101 (species × station-depths) by arbitrarily setting a cut-off criterion of 1%. Volumetric percentages for each species-station possibility were calculated and if a species did not account for at least 1% of the volume at any station it was removed from the matrix.

The qualitative matrix consisted of ones and zeroes. Wherever a species was present within the 168 by 101 matrix a value of 1 represented presence, zero for absence. This matrix was reduced to a 72 × 101 dimension by setting the cut-off criterion to 5%.

Other Variables

The light variable at each station was calculated using Riley's (ref. 21) equation:

$$\langle I \rangle = \frac{I_0}{kZ}(1 - e^{-kZ})$$

where $\langle I \rangle$ is the amount of light received by the phytoplankton in a well-mixed water column of depth Z and extinction coefficient k. I_0 is the surface radiation.

The extinction coefficient, k, was determined using the equation of Poole and Atkins (ref. 22):

$$k = \frac{1.41}{Z_{sd}}$$

where Z_{sd} is the depth of disappearance of the secchi disc (m.). Stations performed during darkness were assigned values of 0 at each depth.

A tide-related variable was also calculated. From standard tide tables (ref. 23) the tidal height at collection time for each station was determined. Values for the tide-related variable (TRV) were also calculated for offshore stations using the station time and the calculated tidal height (ft) for the closest subordinate standard tidal station. The variable was calculated as follows:

$$TRV = \left(\frac{TH}{2DS \cdot DBM} \right)^{0.5}$$

where TRV is the tide-related variable, TH is tidal height at the closest subordinate station, DS is the distance from the collection station to the subordinate tidal station and DBM is the distance to the bay mouth (distances used were relative map units). This computation allows a simple approach for viewing the nonsynoptic nature of the sampling schedule as it relates to the tidal variable. The variable assigns smaller values for offshore stations. The variable is also inversely proportional to the distance from the bay mouth. Figure 1A shows the behavior of the variable if synoptic data were taken, Figure 1B is the variable calculated for the actual times of the standard stations.

NUMERICAL METHODS

Cluster Analysis Techniques

The purpose of the cluster analysis in this study was to segregate the 101 station depth events into a fewer number of station clusters. The intention of this technique is that stations within a defined cluster of stations are more closely related to each other than they are to stations of other clusters, relative to phytoplankton composition.

The computer program used was ORDANA (ref. 24). It has a sequential, agglomerative, heirarchical, non-overlapping algorithm.

For the qualitative data in this study the Jaccard coefficient was used. The Jaccard coefficient (D_{ij}) was computed as follows:

$$D_{ij} = \frac{C_{ij}}{N_i + N_j - C_{ij}}$$

where C_{ij} is the number of conjoint presences within the two stations i and j. N_i and N_j are the numbers of species at the respective stations. The theoretical maximum value of 1.0 would indicate qualitatively perfect matching of species at the two stations.

For quantitative data the Czekanowsky similarity coefficient was used according to the following formula where S_{jk} = similarity between samples j and k, X_{ij} = abundance of i-th species in the j-th sample, and n = the total number of species.

$$S_{jk} = \frac{\sum_{j=1}^{n} MIN(X_{ij}, X_{ik})}{\sum(X_{ij} + X_{ik}) - \sum MIN(X_{ij}, X_{ik})}$$

Again the theoretical maximum value for this coefficient was 1.0, indicating like species in similar quantities at each station.

The sorting strategy selected was group average, which is a space-conserving algorithm (ref. 11). This sorting strategy was chosen as it generally maximizes the correlation between the similarity values and the cluster analysis results.

All quantitative data (volume matrix) were transformed using $X = (\ln X + 1)$ to reduce the scale problem inherent in the data and to rid the matrix of zeroes.

Ordination Techniques

Polar ordination, developed by Bray and Curtis (ref. 8), is one of the simplest and most effective techniques available. Its major drawback is the required knowledge of endpoints along the ordination axis. To perform the ordination the following steps were taken:

1. Computation of a dissimilarity coefficient (determined by subtracting each similarity value from its theoretical maximum).

2. Selection of station endpoints which reflect the most dissimilar species populations. The endpoints were selected using the dissimilarity matrix. As hypothesized, the most dissimilar station-depth pair was between a bay mouth station (Standard station #801) and an offshore station (Standard station #816), where D=0.924. These two points are the anchors of the ordination axis with the distance between them, L.

3. The distances for all other stations were assessed from the dissimilarity matrix relative to the endpoints.

4. The positions of the other i samples, X_i, along the ordination axis were computed as follows:

$$X_i = \frac{L^2 - D_{1i}^2 - D_{2i}^2}{2L}$$

and the distance E_i of the sample from the axis is:

$$E_i = \left(D_{1i}^2 - X_i^2 \right)^{0.5}$$

The X_i values are an ordering of the species along a continuous axis. The E_i values are related to possible distortion of the axes. Second and subsequent axes may be calculated by selecting those two points which are closest to the median x-axis value for the next endpoints.

Multiple linear regression of environmental variables on these axes was performed to ascertain those variables which account for most of the variance in these axes. Violations in the assumptions of regression analysis were assessed by graphical interpretation of the residual plots. The light variable was transformed using the common log function.

RESULTS

Cluster Analysis

The results of the cluster analysis for the qualitative 72 X 101 (species x station-depths) matrix are schematically represented in dendogram form in Figure 2. Two major clusters were observed to fuse at a similarity value of 0.317. Table 1 is a listing of the station-depth sites which are grouped under the major sub-groups in the dendogram. Six clusters were observed (labeled A-F). These clusters are presented relative to their geographical locations in Figure 3. The two major clusters (B and C) accounted for 83.16% of the stations. The remaining 17 stations were grouped among 4 clusters which appeared to be randomly distributed among the stations. The depth stations at

each location generally grouped together indicating vertical homogeneity of plankton populations. The qualitative phytoplankton associations do not appear to be related to major water masses as might be expected from this region.

The results of the cluster analysis for the 64 X 101 cell volume matrix are presented in Table 2. In this matrix, phytoplankton biomass as measured by cell volumes is assessed. Two major clusters again result in 92 of the 101 station-depths being grouped to form a major dichotomy. These two major sub-groups fused at a similarity value of 0.493. A general large scale relationship between these sub-groups and their relation to a "plume" may be inferred (Figure 4). All standard stations closest to the coast clustered in one of these groups. Of the northernmost 21 standard stations only 2 standard stations (including their depths) seem to be outlyers. Considering the possible patchy nature of phytoplankton populations these results appear to be representative of a plume or an onshore/offshore pattern. Three standard stations (801, 69 and 805) at the bay mouth clustered in such a way as to suggest that phytoplankton associations there are indicative of microscale changes within the water column. These results appear plausible considering the complexity of the currents in this general vicinity (ref. 16, 17). The southernmost transect seems to represent a reversal of the onshore versus offshore generality. It is noted that the results of the cluster analysis, as have been used here, are not hypothesis concluding. The procedure only allows a more objective approach at developing complex associations.

Polar Ordination

Polar ordination was performed on both of the matrices with varying results. As indicated by the results of the cluster analysis, the qualitative data were characterized by somewhat random distributions. Consequently, the ordination axes computed for these data were not significantly related to the environmental variables as assessed by multiple linear regression analysis. These results suggest the interactions by the species with the environmental variables measured are not sufficient to explain their qualitative distribution.

From the triangular dissimilarity matrix representing the 64 X 101 (species-volumes x station-depths) pairs a polar ordination was performed. Two ordination axes were computed. Regression analysis showed the first ordination axis was only weakly related to salinity which accounted for 23.3% of its variance (Table 3). A significant ($\alpha = 0.05$) correlation between salinity and the first polar ordination axis existed. None of the remaining variables was significantly related to the dependent variable. There was no significant regression relationship between any of the environmental variables and the second polar ordination axis.

These results indicate a weak association between salinity and the change in species associations as assessed by the ordination technique. The general failure of environmental ordination procedures in cases involving many sites has been suggested by Boesch (ref. 25). As the number of sites increases, so does the inefficiency.

Ordinations of transect data were individually performed to decrease the site number and increase the efficiency of the ordination procedure. The station-depths from the six major transects (omitting standard stations #800 and 801) were ordinated (Figure 5A-F). The first polar ordination axes were observed to generally order the sites into an onshore versus offshore transition. The second polar ordination axes are not so easily generalized from the graphical presentation.

The results of the regression analyses of environmental variables on both the first and second axes are presented in Table 4. Of the measured variables, salinity was observed to account for most of the variance in the computed first polar ordination axes in two of the three northernmost transects and was significantly related to the second transect. Inorganic nutrients were observed to explain most of the variance in the second polar ordination axes for these northern transects. In the southern three transects the light and tide variables account for most of the variance in the ordination axes.

DISCUSSION

The existence of a biotic plume, as measured by phytoplankton volumes, is supported by the results of the classification and ordination analyses. While being a non-conservative property within the environment, phytoplankton biomass associations were observed to significantly covary with some conservative variables (salinity, silicates and phosphates).

The six major transects may be conveniently divided into two regions (northernmost three, southernmost three) which appear to have fundamentally different factors affecting their endemic phytoplankton populations. The basic environments of the populations within these two major regions appear to be different in lieu of the ordination results. The low salinity plume of water originating from the Chesapeake Bay which generally holds to the coast is a region of high division rates and standing crops (see Marshall, paper no. of this compilation). Within the southern three transects, of the measured variables, the light variable is most important in accounting for the variance in the population biomass shifts.

These results suggest relationships between the physical hydrology of the region and the phytoplankton communities. As indicated by the salinity data and previous summer studies (ref. 16) the water columns of the study area are generally stratified with a pronounced salinity gradient seaward. This gradient has an influence on the biomass associations as far south as the North Carolina border. Further south this effect is superseded by the summer stratification as indicated by the large proportion of variance in the ordination axes explained by the light variable.

The linear models used in this study were not expected to accurately describe the biological events. Walsh (ref. 26) has stated the problems of using linear models in biology most succinctly:

> "Linear regression analysis is appropriate for preliminary insight into a complex system, but is an inadequate description of biological phenomenon. Linear relations...cannot be expected to fully describe or predict biological relationships which are basically non-linear and consist of thresholds, timelags, and saturation and inhibition effects."

NUMERICAL SUMMARY

1. The volumetric-biomass data proved more informative as related to environmental variables using regression analysis. These data more closely approximate the "plume" situation than the qualitative data.

2. The factors which influence phytoplankton populations within the region appeared to be complex.

3. A salinity gradient which was present within the northern transects covaried significantly with the phytoplankton biomass association changes.

4. Within the southern transects the normal summer stratification was related to phytoplankton populations with the light variable most important in explaining the variance.

5. The results suggest the importance of the physical hydrology in this system in influencing the phytoplankton associations.

6. Of secondary importance, the inorganic nutrients (silicates and phosphates) significantly covaried with the biomass changes within the northern transects.

7. The numerical methods, borrowed from the social scientists and the terrestrial phyto-sociologist, seemed to perform moderately well to extract information from large complex phytoplankton data matrices.

REFERENCES

1. Colebrook, J. M. and G. A. Robinson. 1964. Continuous Plankton Records: Annual Variations of Abundance of Plankton, 1948-60. Bull. Mar. Ecol. 6: 52-69.

2. Ibanez, F. 1972. Interpretation De Donnes Ecologiques Par L'analyse Des Composantos Principales: Ecology Planktonique de la Mer du Nord. J. Cons. CEIM. 34: 323-340.

3. Thorrington-Smith, M. 1971. West Indian Ocean Phytoplankton: A Numerical Investigation of Phytogeographic Regions and Their Characteristic Phytoplankton Associations. Mar. Biol. 9: 115-137.

4. Boesch, D. F. 1973. Classification and Community Structure of Macrobenthos in the Hampton Roads Area, Virginia. Marine Biology. 21: 226-244.

5. Kaisler, R. L. and J. Cairns. 1972. Cluster Analysis of Data from Limnological Surveys of the Upper Potomac River. American Naturalist. 88: 56-67.

6. Day, J. H. and J. G. Field. 1971. The Use of Numerical Methods to Determine the Distribution of Benthic Fauna Across the Continental Shelf of North Carolina. J. Anim. Ecol. 40: 93-125.

7. Sandilands, R. G. 1977. Effect of Pulp Mill Effluent on the Surficial Sediments of Western Nipigon Bay, Lake Superior. J. Fish. Res. Board Can. 34: 817-823.

8. Bray, J. R. and J. T. Curtis. 1957. An Ordination of the Upland Forest Communities of Southern Wisconsin. Ecol. Monogr. 27: 325-349.

9. Margalef, R. and F. Gonzales Bernaldez. 1969. Grupos de Especies Asociades en el Fitoplancton del Mar Caribe (N.E. de Venezuela). Invest. Pesq. 33: 287-312.

10. Levandowsky, M. 1972. An Ordination of Phytoplankton Populations in Ponds of Varying Salinity and Temperature. Ecology. 53: 398-407.

11. Pimentel, R. A. 1979. MORPHOMETRICS: The Multivariate Analysis of Biological Data. Kendall/Hunt Publishing Company, 276 pp.

12. Legendre, L. and P. Legendre. 1978. Associations. In Phytoplankton Manual: Monographs on Oceanographic Methodology, ed. by A. Sourina. UNESCO. 337 pp.

13. Gauch, H. G., R. H. Whittaker, and T. R. Wentworth. 1977. A Comparative Study of Reciprocal Averaging and Other Ordination Techniques. J. Ecology. 65: 157-174.

14. Fasham, M. J. R. 1977. A Comparison of Nonmetric Multidimensional Scaling, Principal Components and Reciprocal Averaging for the Ordination of Coenoclines and Coenoplanes. Ecology. 58: 551-561.

15. Beals, E. W. 1973. Ordination: Mathematical Elegance and Ecological Naivete. J. Ecology. 61: 551-561.

16. Boicourt, W. C. and P. W. Hacker. 1978. Circulation on the Atlantic Continental Shelf of the U.S. from Cape May to Cape Hatteras. Contribution # 218 from Johns Hopkins Univ., Chesapeake Bay Institute, Baltimore.

17. Boicourt, W. C. 1973. The Circulation of Water on the Continental Shelf from Chesapeake Bay to Cape Hatteras. Ph.D. Thesis, The Johns Hopkins University, Baltimore, Maryland. 183 pp.

18. Okuba, A. 1978. Horizontal Dispersion and Critical Scales for Phytoplankton Patches. In SPATIAL PATTERN IN PLANKTON COMMUNITIES ed. by J. H. Steele, Plenum Press. 470 pp.

19. Venrick, E. L. 1978. How Many Cells to Count? In Phytoplankton Manual: Monographs on Oceanographic Methodology, ed. by A. Sourina, UNESCO. 337 pp.

20. Kovala, P. E. and J. D. Larrance. 1966. Computation of Phytoplankton Cell Numbers, Cell Volumes, Cell Surface and Plasma Volume per Liter, from Microscopical Counts. Dept. Oceanog., University of Washington. (Special Report #38). 91 pp.

21. Riley, G. A. 1957. Phytoplankton of the North Central Sargasso Sea. Limnol. and Oceanog. 2: 252-270.

22. Poole, H. H. and W. R. Atkins. 1929. Photoelectric Measurements of Submarine Illumination Through Out the Year. J. Mar. Biol. Assoc. U.K. 16: 297-324.

23. N.O.A.A. 1980. High and Low Water Predictions, East Coast of North and South America. U.S. Department of Commerce. 297 pp.

24. Bloom, S. A., S. L. Santos, and J. G. Day. 1977. A Package of Computer Programs for Benthic Community Analyses. Bulletin of Marine Science. 27: 577-580.

25. Boesch, D. F. 1977. Application of Numerical Classification in Ecological Investigations of Water Pollution. Special Scientific Report No. 77, Virginia Institute of Marine Science. 113 pp.

26. Walsh, J. J. 1971. Relative Importance of Habitat Variables in Predicting the Distribution of Phytoplankton at the Ecotone of the Antarctic Upwelling Ecosystem. Ecol. Monogr. 41: 291-309.

Table 1. Order of depth-sites from dendogram: qualitative data.

	Station Sequences
Group A S = .336	101, 100, 33, 24, 7, 5, 6, 23, 25, 15
Group B S = .339	98, 92, 97, 96, 95, 44, 43, 67, 51, 61, 40, 94, 49, 65, 59, 57, 58, 50, 42, 41, 30, 38, 66, 93, 91, 31, 87, 86, 85, 32, 52, 90, 89, 88, 39, 78, 77, 28, 76, 75, 60, 74, 63, 62, 73, 64, 26, 27, 29, 3, 2, 1
Group C S = .330	84, 83, 56, 72, 71, 70, 45, 55, 37, 48, 35, 36, 54, 53, 20, 19, 18, 47, 46, 34, 69, 68, 17, 16, 13, 12, 11, 4, 82, 81, 80, 79
Group D S = .367	22, 21, 14
Group E S = .259	10, 9, 8
Group F S = .209	99

Table 2. Order of depth-sites from dendogram: quantitative data.

	Station Sequences
Group A S = .455	97, 90, 92, 88, 96, 95, 94, 51, 61, 40, 52, 44, 43, 93, 91, 67, 59, 57, 66, 58, 30, 50, 49, 31, 89, 88, 87, 85, 65, 32, 42, 41, 38, 39, 1, 2, 3, 78, 60, 77, 28, 29, 76, 75, 63, 62, 74, 73, 64, 26, 27, 24, 7, 6, 5, 23, 9, 8
Group B S = .482	84, 83, 72, 71, 48, 70, 55, 45, 69, 68, 56, 20, 19, 54, 53, 46, 36, 34, 18, 37, 35, 47, 17, 16, 13, 12, 11, 4, 33, 15, 25, 22, 21, 14
Group C S = .420	101, 100, 10
Group D S = .348	99, 98
Group E S = .310	82, 81, 80, 79

Table 3. Multiple regression results: polar ordination of 101 station-depths.

Dependent variable: polar ordination axis #1				
Independent Variables	F	R^2	R^2 Change	Simple R
Salinity	29.13*	0.23283	0.23281	0.48253*
Temperature	20.52	0.30169	0.06885	-0.09978
Dissolved oxygen	15.17	0.32624	0.02456	0.09680
Total suspended matter	12.06	0.34151	0.01526	-0.23809*
Light	9.79	0.34731	0.00580	0.10983
Si	8.20	0.35110	0.00379	0.05055
Ammonia	7.04	0.35379	0.00269	0.07745
Nitrates	6.15	0.35615	0.00239	0.05675
Tide variable	5.44	0.35744	0.00125	-0.19218
Nitrites	4.85	0.35823	0.00079	-0.05649
Phosphates	4.38	0.35937	0.00114	-0.16556

* = Significant, $\alpha = 0.05$

Table 4. Multiple regression results: polar ordination of transect data.

Transect	Dependent Variable	Independent Variable	R^2	F
69-804	P.O. axis 1	Salinity	0.62609	18.418*
69-804	P.O. axis 2	Silicates	0.70027	25.699*
805-807	P.O. axis 1	Light	0.60840	20.203*
805-807	P.O. axis 1	Salinity	0.11008 (increase)	15.318*
805-807	P.O. axis 2	Silicates	0.46809	11.441*
808-811	P.O. axis 1	Salinity	0.43780	9.838*
808-811	P.O. axis 2	Phosphates	0.58076	18.008*
71-813	P.O. axis 1	Tide variable	0.73793	28.154*
71-813	P.O. axis 2	- - - - - -	- - - -	- - -
814-816	P.O. axis 1	Light	0.57611	24.514*
814-816	P.O. axis 2	- - - - - -	- - - -	- - -
73-818	P.O. axis 1	Light	0.60177	16.622*
73-818	P.O. axis 2	Tide variable	0.34562	5.809*

* = Significant, $\alpha = .05$

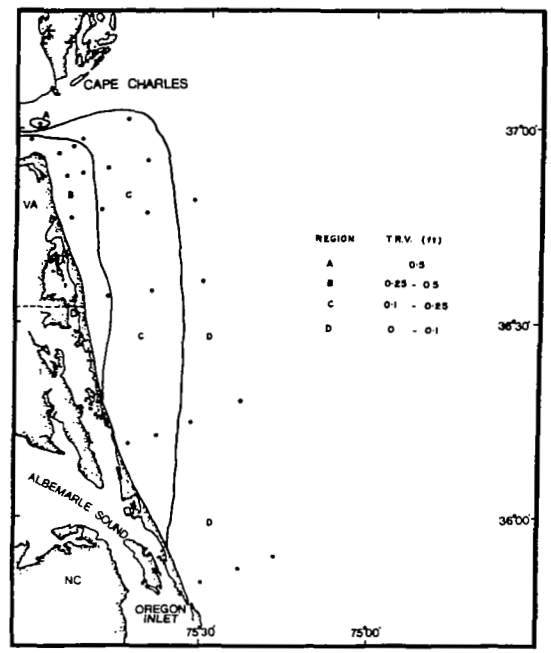

(a) Synoptic sampling.

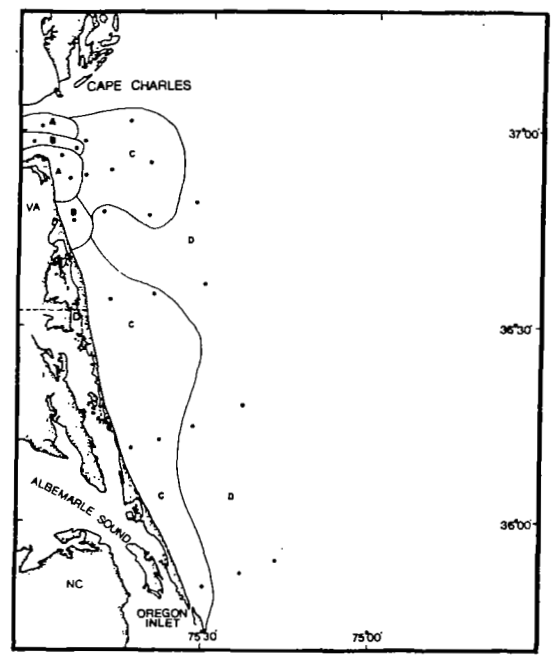

(b) Superflux II sampling.

Figure 1.- Tide-related variable.

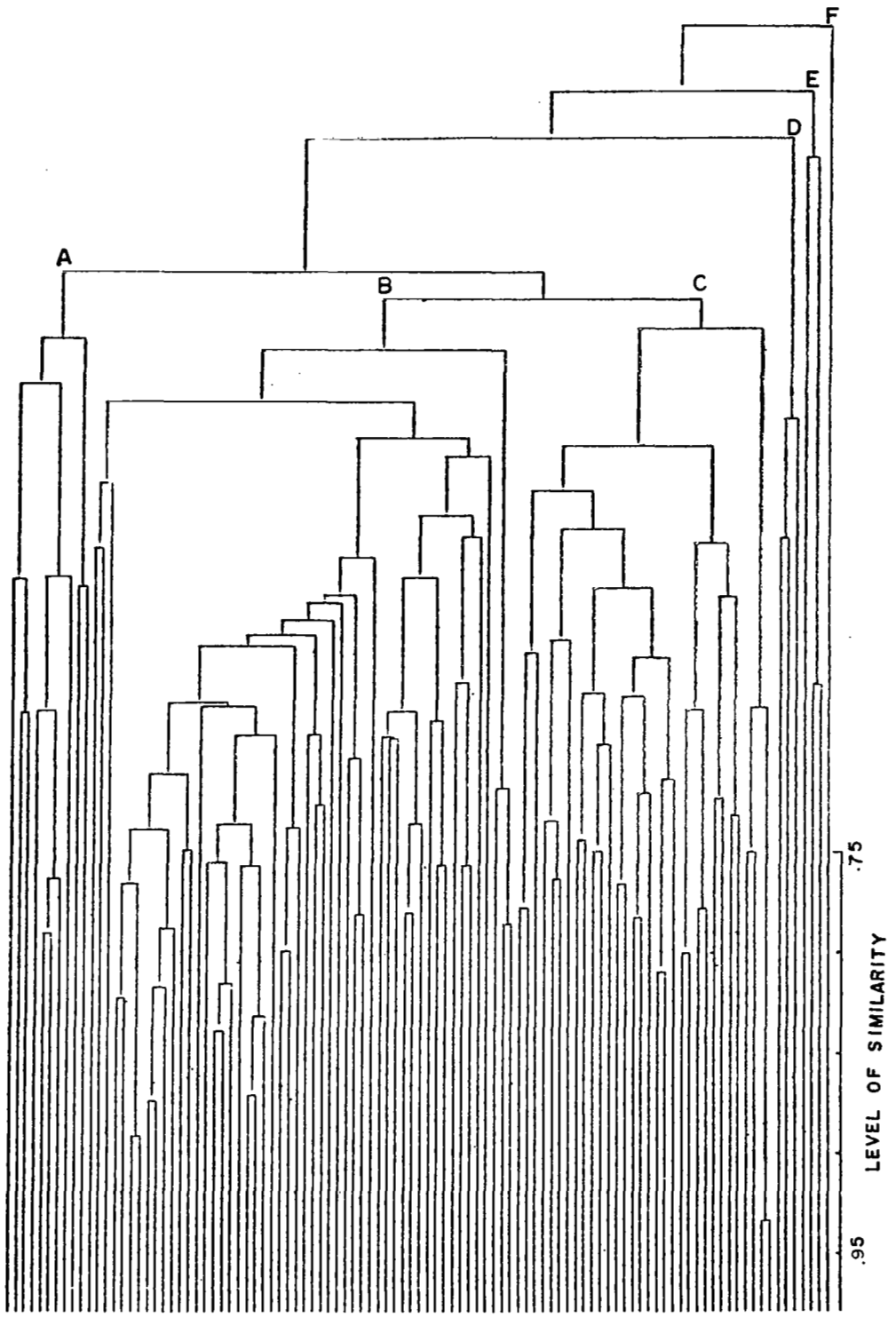

Figure 2.- Dendogram sequence of stations.

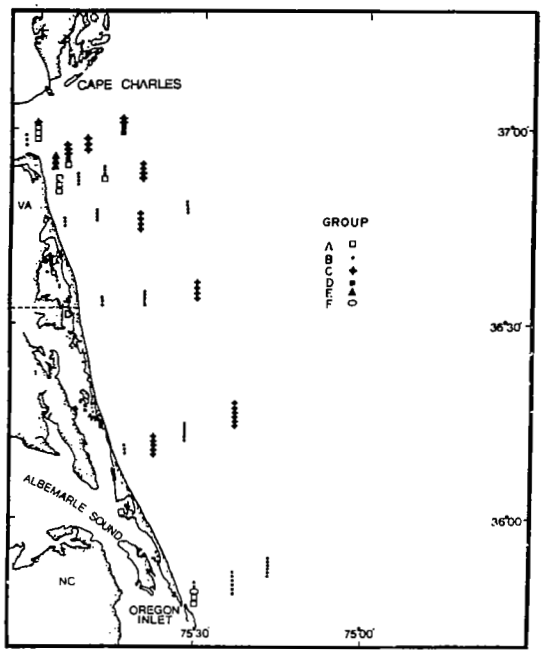

Figure 3.- Major qualitative clusters.

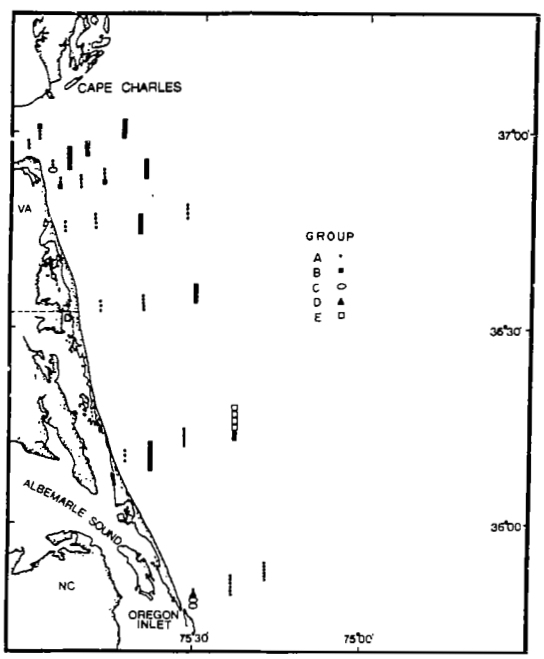

Figure 4.- Major qualitative clusters.

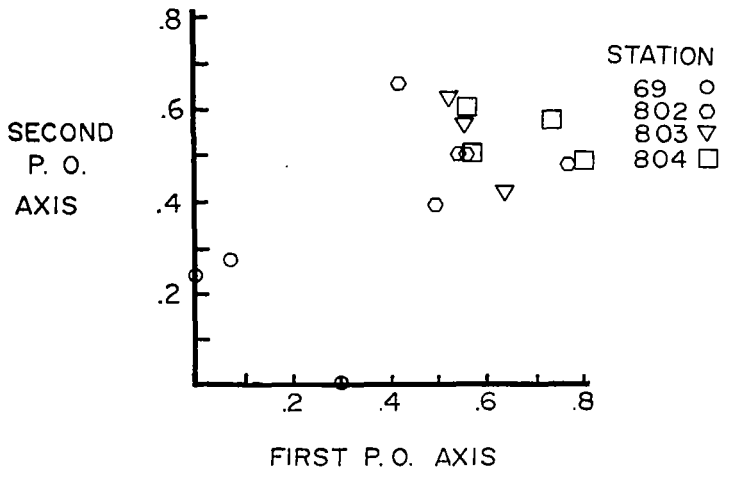

(a) Transect 69-804.

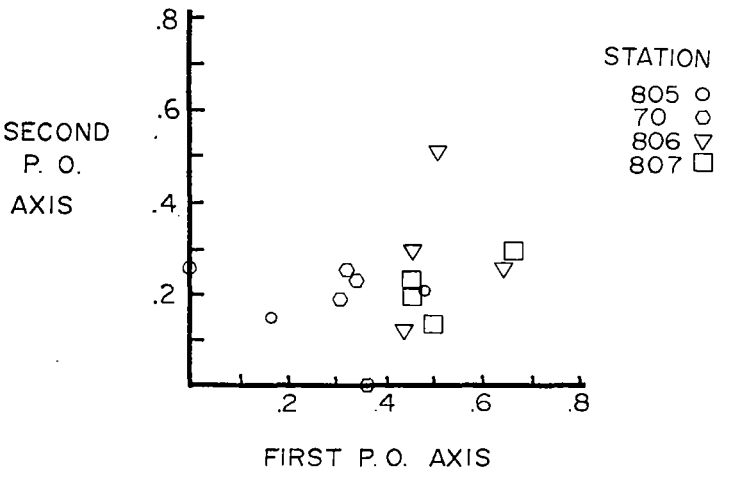

(b) Transect 805-807.

Figure 5.- Site ordination.

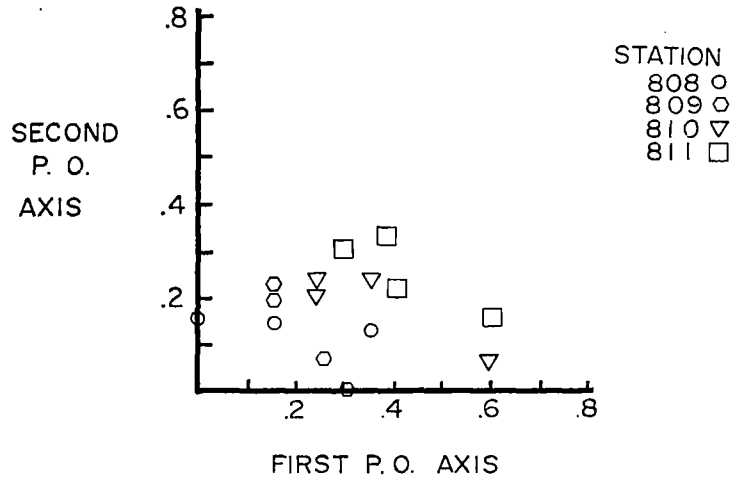

(c) Transect 808-811.

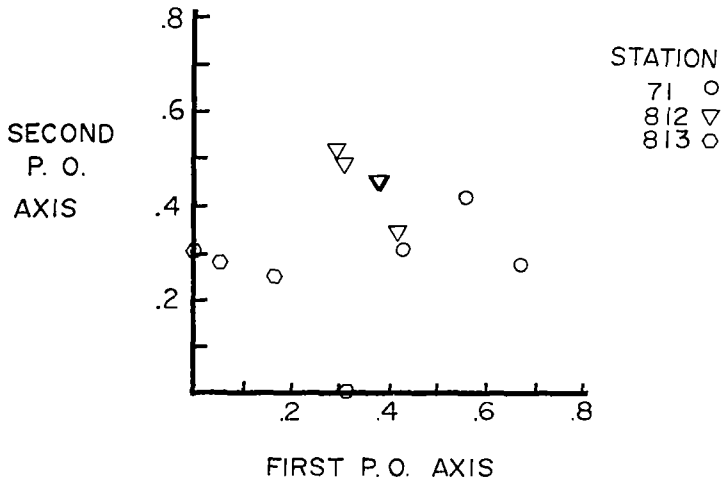

(d) Transect 71-813.

Figure 5.- Continued.

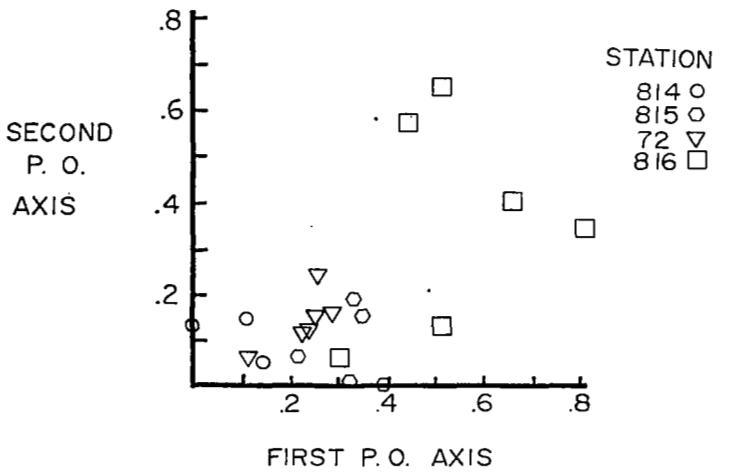

(e) Transect 814-816.

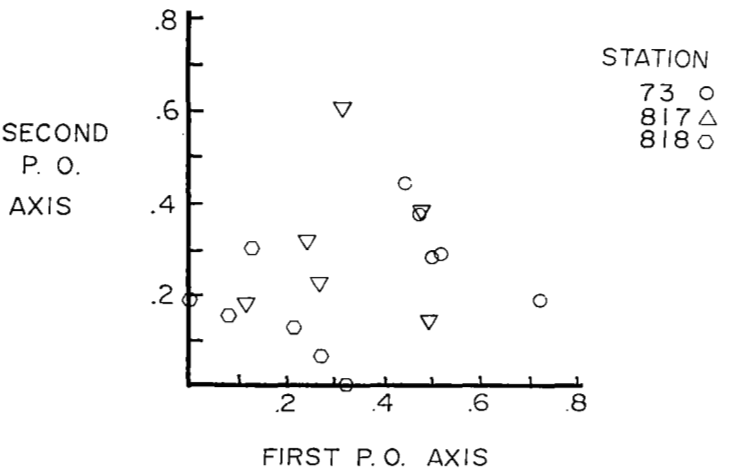

(f) Transect 73-818.

Figure 5.- Concluded.

SUPERFLUX CHLOROPHYLL *a* ANALYSIS:

AN ASSESSMENT OF VARIABILITY IN RESULTS

INTRODUCED PRIOR TO FLUOROMETRIC ANALYSIS

S. J. Cibik and C. K. Rutledge
Department of Biological Sciences
Old Dominion University
Norfolk, Virginia

C. N. Robertson
NOAA, NMFS, Northeast Fisheries Center
Sandy Hook Laboratory
Highlands, New Jersey

SUMMARY

During the Superflux II cruise (June 17-27, 1980), several experiments were undertaken to identify variability in results that came from procedural differences in the processing of chlorophyll samples prior to fluorometric analysis. Specifically, the questions to be addressed were: a) did failure to initially pass the seawater sample through a 300-μm mesh nylon screen to remove large zooplankton cause significant differences in chlorophyll *a* and phaeopigment *a* concentrations over a specified period of time; b) did samples which were immediately filtered through the Whatman glass fiber filters and held for a specified time period yield significantly different results from unfiltered seawater samples held for the same period; c) is there a significant difference in results of samples processed immediately and those held for a 24-hour extraction period?

T-tests on group means indicated that significant differences ($\alpha = 0.05$) in phaeopigment *a* concentrations did result in samples not initially screened, but not in the chlorophyll *a* concentrations. Highly significant differences ($\alpha = 0.001$) in group means were found in samples which were held in acetone after filtering as compared to unfiltered seawater samples held for the same period. No difference in results was found between the 24-hour extraction and samples which were processed immediately.

INTRODUCTION

The intent of the Superflux program was to monitor the fate of the effluent from the Chesapeake Bay. In an attempt to achieve a synoptic view of the plume, smaller support craft were utilized for simultaneous sampling. The samples for fluorometric evaluation were then transferred to the R/V *Kelez* for

subsequent analysis. One result of this program was the introduction of a time variable between sampling and chlorophyll a determination. In addition, samples exhibited various degrees of preparation, i.e., some arrived as just samples of seawater without any processing, some were initially screened with a 300-μm mesh screen to remove larger zooplankton, and, if facilities were available, some were further processed by filtration, the filters placed in acetone, and held in the dark.

An attempt was made to design experiments aboard ship to simulate these factors and possibly indicate whether they contributed to variability in pigment analysis results. The tests were not an extensive study of the situation; however, they provided some insight into the conditions under which the analyses were conducted and may provide the groundwork for further investigation.

MATERIALS AND METHODS

In order to investigate the effects of larger zooplankton being included in a seawater sample during transport, ten replicate samples without initial screening were held for a period of three hours along with ten replicates in which the seawater had been passed through a 300-μm mesh screen. The samples were held in the one-liter opaque containers which were being used for sample transport.

At the end of the time period the unscreened seawater was passed through the 300-μm mesh screen prior to analysis. Chlorophyll a and phaeopigment a were measured using the standard fluorometric techniques as described by Strickland and Parsons (ref. 1). Extraction was facilitated by the use of a tissue grinder. In each test 400 ml of seawater were filtered for analysis.

To contrast samples which arrived aboard ship already filtered with screened seawater samples, five replicate samples were held in 0.5-l light-proof bottles for six hours. At the same time five 400-ml replicate samples from the same source were filtered through the glass fiber filters, the filters were then folded with the plankton inside, placed in 15-ml centrifuge tubes, and held in the dark in 10 ml of 90% acetone for a similar period. Subsequently, the seawater samples were filtered and processed as described above.

The 24-hour extraction technique was compared with immediate processing by filtering five 400-ml replicates and holding the filters in acetone for 24 hours in a freezer. Five 400-ml samples were processed immediately for comparison.

Experimental results were subjected to a standard t-test to identify significant differences in group means.

RESULTS

The mean chlorophyll *a* concentration for the ten replicate samples which had been screened prior to analysis was 6.52 ± 0.435 mg/m^3*; the mean for the unscreened replicates was 6.88 ± 0.435 mg/m^3. These group means are not significantly different ($\alpha = 0.05$). The mean concentrations for phaeopigments *a* for screened vs. non-screened samples were 2.42 ± 0.244 mg/m^3 and 2.99 ± 0.328 mg/m^3, respectively, which are significantly different at $\alpha = 0.05$.

A highly significant difference ($\alpha = 0.001$) was found between group means for both chlorophyll *a* and phaeopigment *a* concentrations for the samples in which the filters were held for six hours vs. the seawater samples held for the same period. The group means for chlorophyll *a* were 0.76 ± 0.025 mg/m^3 for the filtered samples and 0.45 ± 0.106 mg/m^3 for the non-filtered samples. Group means for phaeopigments *a* were 0.20 ± 0.024 mg/m^3 and 0.10 ± 0.022 mg/m^3, respectively.

No significant difference ($\alpha = 0.05$) was found between the 24-hour technique and those samples processed immediately. Group means for chlorophyll *a* were 0.68 ± 0.068 mg/m^3 and 0.75 ± 0.107 mg/m^3, and those for phaeopigment *a* concentrations were 0.15 ± 0.018 mg/m^3 and 0.17 ± 0.045 mg/m^3.

In summary, the results of these experiments indicate that significant variability in results can be introduced in chlorophyll *a* analysis by differences in the processing of samples prior to fluorometric analysis. It is therefore recommended that uniformity in handling be emphasized when transferring samples from the support craft. Specifically, samples should be filtered aboard the support craft and transported under refrigeration in the absence of light.

REFERENCE

1. Strickland, J. D. H., T. R. Parsons. A Practical Handbook of Seawater Analysis, 2nd ed. Ottawa: Fisheries Research Board of Canada (Bull. 167), 1972.

*Group means are given with their associated standard deviations.

ASSESSMENT OF SUPERFLUX

RELATIVE TO MARINE SCIENCE AND OCEANOGRAPHY

Wayne E. Esaias
NASA Langley Research Center

It is clearly much too early in the stage of data analysis to attempt a real synthesis of results from Superflux with respect to oceanography and marine science. It is equally impractical to attempt a synthesis of such a diverse and complex program in a short time. That work will require a great deal of effort and will result in at least as much information as has already been presented during this symposium. What is clear is that there are certain threads of scientific commonality which run through all the presentations and indeed were a result of the design of the Superflux experiments.

It has been said that if one has no clear idea of testable hypotheses, no clear idea of how the data will be used to test those hypotheses, and no idea of how the data will look, then one has no business collecting the data to begin with. While Superflux may have been somewhat guilty of this, the experiments produced meaningful and useful data which would not have been gathered otherwise. Most importantly, showing that the data could be collected, and with meaningful results, is in support of the hypothesis that interactive ship, aircraft, and satellite measurements form a mutually exclusive and complementary data set, and further that this data set is required to properly investigate highly dynamic coastal systems.

In some respects Superflux did not produce as complete a data set as would be required to attempt a flux-type calculation, but this was not an expected accomplishment for the first year of a study. We understand much more clearly now the small-scale variances in Bay and plume properties which need to be addressed to properly perform the rather herculean task of quantifying the flux of materials, pollutants, salt, water, carbon, nitrogen, etc., across the transect from Cape Charles to Cape Henry. This information is also essential to understand the dynamics of how coastal waters mix with the waters of the Bay and how the plume affects the environment and resources on the adjacent continental shelf.

The concept of space and time domains is important here. Referring to figure 1 of Campbell et al. (ref. 1), recall that synoptic aircraft measurements sampled a space-time domain unapproachable by ship platforms. Ships cannot cover enough distance in a given time to assess the coherence of conservative (passive) and non-conservative (growth- and time-dependent) properties over regions as large as the Bay and plume. Shipboard measurements can show this coherence where some relatively slowly varying biological entities such as phytoplankton behave as passive contaminants, but only over short times and distances. References 2 and 3 contain several good examples.

This coherence is readily apparent on much larger scales of time and space, such as in the satellite imagery presented in references 4 and 5. These images again demonstrate the existence of a plume, because the data were collected synoptically. However, spatial resolution and time delays inherent in satellite imagery do not lend themselves to aiding real-time experiments by ships, which are required to perform the complicated and lengthy physical, biological, and physiological measurements to determine how organisms are interacting with their environment.

Superflux addressed the middle range of the space and time domain. The excellent shipboard data sets show that the concept of a plume, really the coherence of conservative and nonconservative properties, is not apparent in the data. For some properties, however, this coherence is readily apparent in the aircraft data sets. Figure 1 compares the microwave salinity and the chlorophyll mappings of Kendall (ref. 6) and Hoge (ref. 7), respectively. Further analysis of the data sets (cross-correlations, etc.) will serve to substantiate the existence of such a coherence. The major impact of Superflux was the demonstration, for the first time, of the ability to collect such data sets at subtidal frequencies. This shows that many properties can be treated as passive contaminants within plumes if synopticity is maintained.

The importance of vertical mixing due to tidal energy in the plume area and how it affects the distribution of properties is a topic which has not received much attention in this symposium. Two facts can be pointed out which may be relevant as the data are analyzed further. First, the dates of the Superflux studies were biased toward spring tidal cycles, or periods of relatively high tidal energy dissipation and tidal mixing (fig. 2). Secondly, the bathymetry of the adjacent shelf is such that, for reasonable tidal velocities, the water column should be well mixed during spring tides for a considerable distance offshore. The shelf break occurs approximately at the 50-m isobath (fig. 3). The ratio of water column depth to the cube of the tidal velocity amplitude is within the range which indicates marginal stratification for much of the shelf. Thirdly, 1980 was a year of unusually low runoff, and added buoyancy in the form of fresh water was at a ten-year low for the plume region. It is interesting to match a conceptual diagram of water column density and other properties based upon these facts (fig. 3) with cross-shelf distributions (ref. 2). In particular, attention should be drawn to the band of cooler, clearer water seaward of the plume which was observed in several of the remote sensing images and transects. This may result from tidal mixing of the water column at this point, and is a hypothesis to be tested in the future.

In summary, the Superflux program clearly demonstrated the effectiveness of state-of-the-art technology required to study highly dynamic estuarine plumes, and the necessity of a broadly interdisciplinary, interactive remote sensing and shipboard program required to significantly advance our understanding of transport processes and impacts of estuarine outflows. The scientific accomplishments which have been presented here, and those which will come from additional detailed analysis, support the conceptual and programmatic accomplishments in the areas of experiment design and planning, and have paved the way for future studies in these and similiar areas.

REFERENCES

1. Campbell, Janet W.; Esaias, Wayne E.; and Hypes, Warren: Superflux I, II, and III Experiment Designs: Remote Sensing Aspects. Chesapeake Bay Plume Study - Superflux 1980, NASA CP-2188, 1981 (Paper no. 4 of this compilation).

2. Ruzecki, Evon P.: Temporal and Spatial Variations of the Chesapeake Bay Plume. Chesapeake Bay Plume Study - Superflux 1980, NASA CP-2188, 1981 (Paper no. 9 of this compilation).

3. Oertel, George F.; and Wade, Terry L.: Characteristics of Total Suspended Matter and Associated Hydrocarbon Concentrations Adjacent to the Chesapeake Bay Entrance. Chesapeake Bay Plume Study - Superflux 1980, NASA CP-2188, 1981 (Paper no. 19 of this compilation).

4. Munday, John C., Jr.; and Fedosh, Michael S.: Chesapeake Bay Plume Dynamics from Landsat. Chesapeake Bay Plume Study - Superflux 1980, NASA CP-2188, 1981 (Paper no. 7 of this compilation).

5. Vukovich, Fred M.; and Crissman, Bobby W.: Monitoring the Chesapeake Bay Using Satellite Data for Superflux III. Chesapeake Bay Plume Study - Superflux 1980, NASA CP-2188, 1981 (Paper no. 8 of this compilation).

6. Kendall, Bruce M.: Remote Sensing of the Chesapeake Bay Plume Salinity Via Microwave Radiometry. Chesapeake Bay Plume Study - Superflux 1980, NASA CP-2188, 1981 (Paper no. 10 of this compilation).

7. Hoge, F. E.; and Swift, R. N.: Application of the NASA Airborne Oceanographic Lidar to the Mapping of Chlorophyll and Other Organic Pigments. Chesapeake Bay Plume Study - Superflux 1980, NASA CP-2188, 1981 (Paper no. 26 of this compilation).

8. National Ocean Survey: Tidal Current Tables 1980. Atlantic Coast of North America. U.S. Dept. of Commerce, NOAA, 1979.

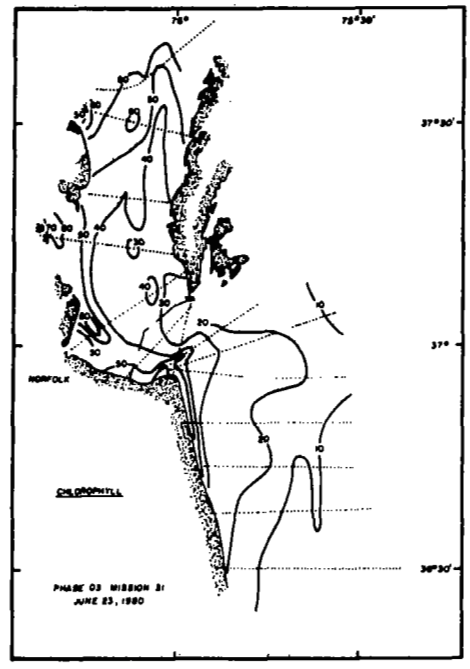

(a) Relative chlorophyll a (from ref. 6).

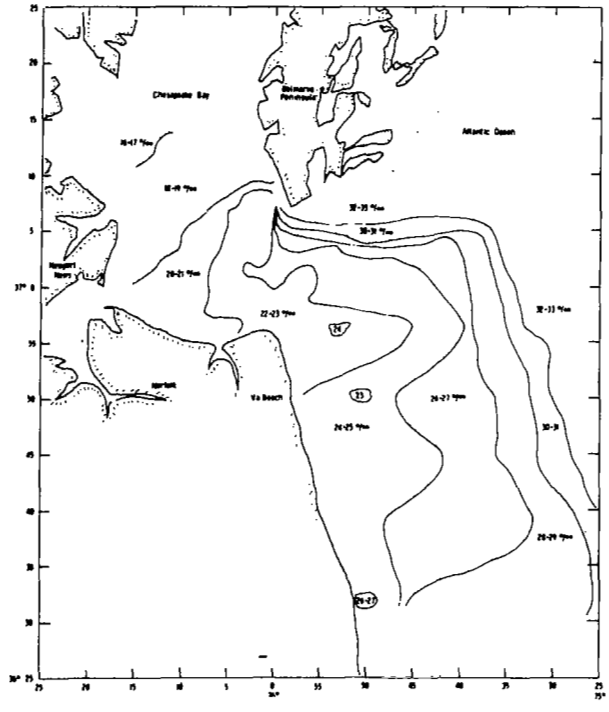

(b) Salinity (from ref. 7).

Figure 1.- Simultaneous measurements of relative chlorophyll a fluorescence and salinity on June 23, 1980.

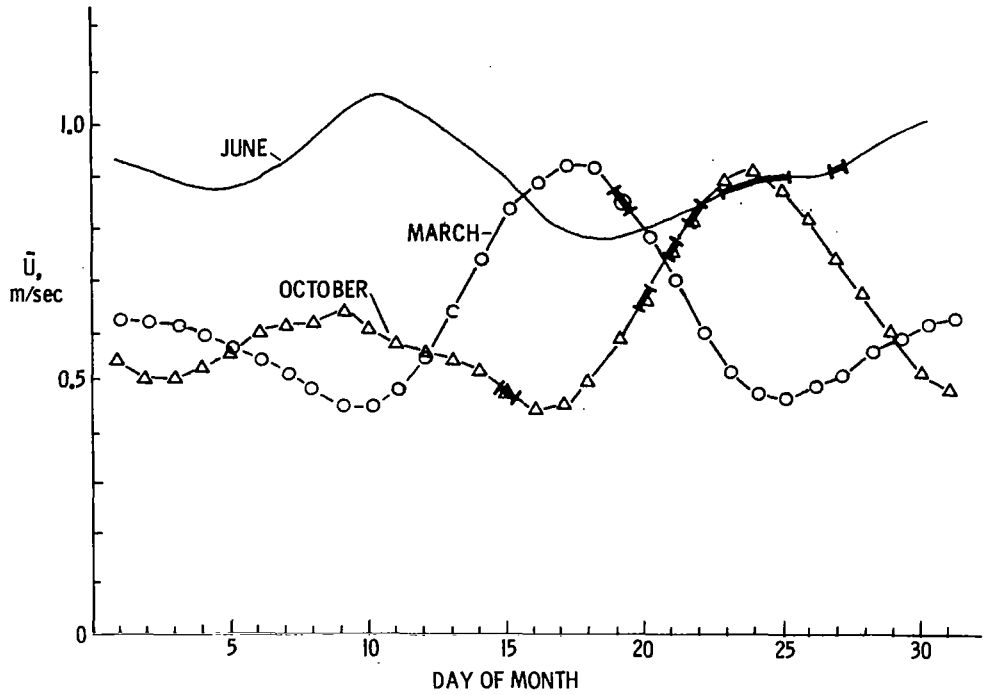

Figure 2.- Daily averages of tidal current maxima at Chesapeake Bay entrance for months of Superflux experiments. Portions of lines inked heavily are dates of specific NASA overflights, illustrating the bias toward periods of strong tidal flow (data from ref. 8).

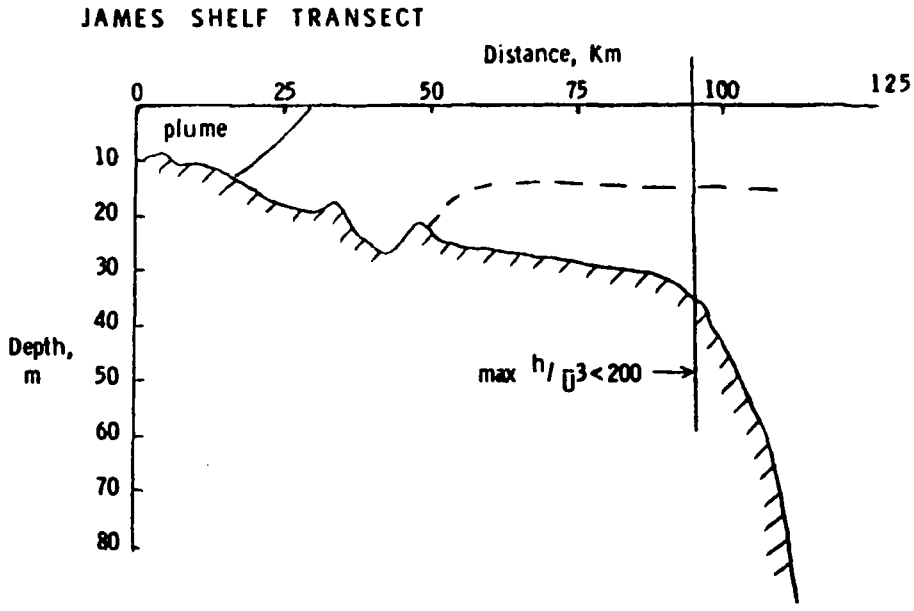

Figure 3.- Profile of depth along the James/shelf transect.

ASSESSMENT OF SUPERFLUX RELATIVE TO REMOTE SENSING

Janet W. Campbell
NASA Langley Research Center

One of the objectives of Superflux was to advance the state of the art in remote sensor technology, thereby hastening the day when remote sensing can be used operationally for fisheries research and monitoring. This goal has certainly been achieved, both in terms of individual sensors as well as in the design of remote sensor systems.

There were three major individual sensor technologies that benefited from the program: laser fluorosensors, optical-range scanners, and passive microwave sensors. Under Superflux, the first convincing evidence was obtained that the AOL fluorosensor can map chlorophyll, i.e., is linear, over a wide range from less than 0.5 to 5.0 mg/m^3. The ALOPE dual-excitation concept for addressing phytoplankton color group composition was also demonstrated convincingly. The result has been that NASA's support for laser fluorosensor technology has increased significantly (comparing 1981 to 1980 research funds) and the AOL will acquire a second laser, thus adopting the dual-frequency excitation technique of the ALOPE.

In the area of optical-range scanners (MOCS, TBAMS, and AOL), 1980 was the year that the 3-band MOCS algorithm came to our attention. It appears to be an extremely successful algorithm for eliminating extraneous effects (e.g., atmospheric and other variations) while retaining the water color information. Superflux provided many hours of flight verification for the MOCS algorithm at altitudes ranging from 150 to 6000 m and with the best and most comprehensive sea truth MOCS has ever had. This added significantly to empirical evidence that the MOCS algorithm works, but there still needs to be analytical ("first principles") and laboratory validation. The MOCS algorithm was applied to TBAMS data and was highly successful in eliminating off-nadir asymmetries.

Advances in the area of passive microwave sensors were not as dramatic because that technology had already been well established before 1980. Superflux did provide the opportunity, however, to demonstrate that a single microwave band could be used with a modified commercially-available infrared radiometer (PRT-5) to map salinity and temperature. This decreases the complexity of the microwave sensor compared to the 2-band microwave systems used before Superflux.

The real-time capability of several of the sensors is worthy of mention. The analog displays of the AOL, MOCS, L-Band, and OCS, which were generated in real time onboard the aircraft or near real time (in the case of the OCS which has a 5-minute lag time) at a ground station, made aircraft-boat interactions highly successful. The location of fronts and patches could be relayed to the boats to enable better in situ sampling of these features.

The most significant accomplishment of Superflux was its initiation of the systems approach, that is, the integration of sensors into systems and the synergism that resulted. Regarding the validity or "proof" of individual sensors, there is nothing more convincing than witnessing the synchrony of two or more sensors. For example, when all the sensors onboard the P-3 detect a front with simultaneous increases in chlorophyll *a*, turbidity, and temperature, the validity of each sensor is enhanced.

The remote-sensing technology that was advanced by Superflux is still a long way from being ready for operational use in fisheries research and monitoring. To this end, the design for a more operational airborne remote sensor system is beginning to emerge. It would be comprised of sensors of the same type as those used in the low-altitude system during Superflux, but it would be a true system in the sense that it would have common electronics (e.g., data acquisition and display hardware, etc.) and be linking to a common time code generator and Loran C tracker. Thus, the so-called "registration" of the data would be made simpler and more operational. In addition, the sensor system would be made as compact and light as possible so that it could be flown on a smaller and operationally less expensive aircraft than the P-3.

In conclusion, the effort that went into the Superflux experiments has resulted in a stronger scientific underpinning of the technologies in this area. The high degree of interaction between NASA technologists and the scientists, who will ultimately be the beneficiaries of the technology development, contributed immeasurably to that scientific underpinning. By supporting Superflux, the National Marine Fisheries Service has enabled the pursuit of some remote-sensing technology development which otherwise would have been postponed or even cancelled. The many successes that resulted have put this technology in a much better position to compete for limited financial resources in the future.

ASSESSMENT OF SUPERFLUX RELATIVE TO FISHERIES RESEARCH AND MONITORING

James P. Thomas
U. S. Department of Commerce
National Oceanic and Atmospheric Administration
National Marine Fisheries Service
Northeast Fisheries Center
Sandy Hook Laboratory
Highlands, New Jersey

INTRODUCTION

The National Marine Fisheries Service (NMFS) mission is to "achieve a continued optimum utilization of living marine resources for the benefit of the nation". These resources include oceanic, coastal, estuarine, and anadromous fisheries, their forage species, and habitats. An essential aspect of this mission is to promote the conservation, restoration, and enhancement of the productivity of these resources and the habitats upon which they depend, through scientific research, monitoring, analysis and application of findings.

The purposes of Superflux were to: 1) advance the development and transfer of improved remote sensing systems and techniques for monitoring environmental quality and effects on living marine resources; 2) increase our understanding of the influence of estuarine "outwellings" (plumes) on contiguous shelf ecosystems; and 3) provide a synoptic, integrated, and timely data base for application to problems of marine resources and environmental quality.

In terms of fishery research and monitoring we would like to know where the Chesapeake Bay plume goes offshore, how it behaves, what it carries, what it deposits, and what its effects are on the biota. We would like to know what area of the shelf the plume influences through time and what the influences are. Such information is necessary to more effectively direct our research and monitoring programs.

We have believed that new methods and approaches are needed for the resolution of these and other matters of interest to the NMFS. Synoptic sampling of dynamic systems with relatively short-lived events has been a problem with the use of conventional techniques. Therefore, Superflux was conceived to respond to the need for new methods and approaches to better carry out our various missions.

ASSESSMENT OF ACTIVITIES

This paper reviews some of the findings of the Superflux program relative to fishery research and monitoring. My plan is to 1) demonstrate that there is a relatively well-defined area over the continental shelf that is influenced by the Chesapeake Bay plume, 2) describe some of the actual and potential influences of the plume on the shelf ecosystem contiguous to the mouth of

Chesapeake Bay, 3) present new insights derived from the combined use of *in situ* and remotely sensed data, and 4) say something about all of this in terms of fishery research and monitoring.

Definition of the Chesapeake Bay Plume

We have, through Superflux, demonstrated that a definable area exists over the continental shelf that is influenced by the Chesapeake Bay plume. We have been interested in defining such an area in relation to long-term monitoring and for planning an initial strategy for combatting catastrophic spills of toxic substances or other such occurrences. Boicourt (ref. 1) examined the plume area from February 1971 to August 1972, and determined that the major influence of the Chesapeake Bay plume was southward from the mouth of the Bay along the Virginia coast.

Munday and Fedosh (ref. 2) examined the historical data from Landsat available since 1972 to define an area influenced by the Chesapeake Bay plume over the contiguous shelf. From the 81 images they examined, covering all seasons of the year, they defined areas of influence based on various wind and tidal conditions (see ref. 2, Figures 7 and 8). In general, they found that the plume frequented a relatively well-defined area east and south of the Bay mouth, along the Virginia coast.

A similar pattern is exhibited in terms of the *in situ* data as indicated by σ_t (ref. 3, Figure 2(a)); total suspended material (ref. 4, Figure 2); biostimulants such as the phytoplankton nutrient orthophosphate (ref. 5, Figure 3); biomass such as bacterial numbers (ref. 6, Figure 1), chlorophyll *a* (ref. 3, Figure 2(b)), and phytoplankton cell counts (ref. 7, Figure 6); community structure in terms of phytoplankton assemblages (ref. 7, Table 8); and ecosystem function such as heterotrophic potential ((ref. 6, Figure 1) and total plankton respiration (ref. 3, Figure 2(d)). Contaminants such as hydrocarbons (ref. 8, Figure 2) and heavy metals (Figure 1) associated with total suspended matter, had similar distributions.

Likewise, remotely sensed data, as evidenced by salinity derived from the L-band microwave radiometer in conjunction with the PRT-5 infrared radiometer (ref. 9, Figure 5), turbidity based on the Ocean Color Scanner (OCS) (ref. 10, Figure 9), chlorophyll (relative fluorescense) based on the Airborne Oceanographic Lidar (AOL) (ref. 11, Figure 8) and the Testbed Airborne Multispectral Scanner (TBAMS) (ref. 12, Figure 9), and phytoplankton community composition derived from an Airborne Lidar Oceanographic Probing Experiment (ALOPE) fluorosensor (ref. 13, Figure 5) confirmed a very similar distribution of variables. Thus a rather well-defined plume or outwelling area from Chesapeake Bay extends over the continental shelf.

The area of influence, however, may contract or expand depending on freshwater discharge from the Bay mouth. During the latter half of 1980, a severe drought caused the plume to contract (Figure 2). Eight years previous, Boicourt (ref. 1) found a greatly expanded plume caused by excessive rainfall and freshwater runoff following hurricane Agnes (Figure 2).

Influence of Chesapeake Bay Plume on Contiguous Shelf Ecosystem

The waters emanating from the mouth of Chesapeake Bay exert an influence on the contiguous shelf ecosystem. Some examples of the kinds of influence that the Chesapeake Bay plume has or could have on the shelf system, based on information obtained during the Superflux experiments, are presented here. We are interested in defining the actual and potential influences of the plume so that with increased understanding our ability to assess and manage the system might be improved.

Flowing out of the Bay with the estuarine water (ref. 3, Figure 2(a)) are higher concentrations of total suspended matter (ref. 4, Figure 2) which not only affect light penetration for primary production, but also provide a source of both food and contaminants for particulate feeders, both in the water column and on the seabed. Evidence suggests that particulate material outwelling from the Bay settles to the seabed down the length of the plume (Figure 3 and ref. 3, Figures 4, 5, and 6). See reference 14, Figure 8 for station locations.

The Bay also is a source of nutrients for primary producers (ref. 5, Figure 3). These nutrients stimulate primary production, resulting in increased biomass and higher concentrations of phytoplankton and chlorophyll over the area influenced (ref. 7, Figure 6, and ref. 3, Figure 2(b)). This increased biomass, plus particulate and dissolved organic material from the estuary, acts as a food source to stimulate and support other trophic levels (ref. 6, Figure 1). Functionally, the response is a biologically more active system in the plume than in adjacent shelf waters. We see this with heterotrophic potential (ref. 6, Figure 1) and total plankton respiration (ref. 3, Figure 2(d)), both indicators of rates of utilization and decomposition of organic matter.

In terms of community structure the phytoplankton assemblage of the Chesapeake Bay plume is different from surrounding shelf waters (ref. 7, Table 8, and ref. 13, Figure 5). Thus not only do quantitative and functional differences arise between the plume and surrounding shelf waters, but there are also qualitative differences which would affect higher trophic levels through their feeding habits.

Oertel and Wade (ref. 8) reported on the characteristics of total suspended matter and associated hydrocarbon concentrations in shelf waters adjacent to Chesapeake Bay. Of particular interest was the fact that there was no congruence in the plumes of total suspended matter, hydrocarbons, and salinity (ref. 8, Figures 3 and 4). Each was characteristic of a separate, definable subplume emanating from the Bay mouth. During the June 1980 experiment the total suspended matter subplume was closest to the beach, the hydrocarbon subplume was furthest away, and the salinity subplume was in the middle (ref. 8, Figures 3 and 4). Such a distribution, with all flowing from one single Bay mouth, suggests different primary sources from within the estuary and the maintenance of the continuity with each of these sources as the materials are carried from the Bay to the shelf. Thus, not

only is there stratification or vertical layering and partitioning (between the plume surface waters and the benthos) as suggested earlier in the paper, but also separation of the various stimulating and contaminating influences on a horizontal basis, as demonstrated by Oertel and Wade. This means that the potential exists for different biological responses to occur in different parts of the outwelled water as well as on the seabed beneath the several subplumes emanating from the Bay mouth. Oertel and Dunstan (ref. 15) describe a similar phenomenon for the Georgia estuaries with foam-line fronts forming between the various sources within the estuary and subsequent "uncoupling" at the seaward ends of the plumes offshore. Therefore, this phenomenon is not unique to Chesapeake Bay, but probably is found with most dendritic-patterned estuaries and their offshore plumes.

Distance or length of the outwelling plume from the Bay mouth is related to time, and depends on the volume of water discharged and the interaction of the meteorological and physical factors affecting the shelf. With time, organic materials are oxidized (hydrocarbons weathered) and inorganic materials are reduced. Nutrients are incorporated into phytoplankton during photosynthesis and released during respiration and decomposition. Contaminants may be inactivated or detoxified by binding or destructive mineralization. However, they may also be concentrated on suspended particulates which then may be fed upon by plankton and nekton or sink to the seabed, to be consumed by benthos. Thus distance down the outwelling allows time for physical, chemical, and biological processes to function to modify the dissolved and particulate materials emanating from the Bay mouth. Such modification leads to further fractionation and partitioning of the various constituents which in turn affect the biota of the contiguous shelf ecosystem.

Combined Use of in situ and Remotely Sensed Data

The combined use of in situ and remotely sensed data and comparisons between the two provide insight into the potential use of remote sensing in fishery research and monitoring programs such as those described by Pearce (ref. 16). During the June 1980 experiment a salinity plume was defined east and south of the Chesapeake Bay mouth along the Virginia coast based on data collected from a research ship over a period of several days and a number of tidal cycles (Figure 4). The result was a smoothly contoured plume which gave the impression of a discrete tongue of water with a central core emanating from the Bay mouth.

During this same experiment, but lasting for periods of two hours instead of several days, an L-band microwave radiometer was flown over the Chesapeake Bay plume area on several different days to map the distribution of surface salinity (ref. 9, Figures 5 and 6). These data are nearly synoptic compared with the in situ data collected over several days. The contouring is not as smooth and regular, even though the same general pattern is seen in both the in situ and remotely sensed data. Notice the change in salinity distribution between 23 June and 25 June (ref. 9, Figures 5 and 6). The low salinity water still ranges from the Bay mouth south along the Virginia shore. However, what is particularly interesting is the presence of high-salinity water between two tongues of low-salinity water exiting southeastward from the Bay

mouth (ref. 9, Figure 6). Isolated pockets of lower or higher salinity water are present. This so-called "pocketing", added detail in contouring, and the rather large change in salinity distribution over a period of several days were not in evidence in the more generalized in situ data (Figure 4). This is new information in terms of understanding the dynamics of an estuarine plume; we are unable to obtain this kind of synoptic, repeated, and detailed information using a single surface ship.

Similar detail is seen in the Ocean Color Scanner (OCS) data (ref. 10, Figures 7, 8 and 9). The outline of the plume is not regular, nor is the plume of uniform density. The satellite imagery of sea surface temperature presented by Vukovich (ref. 17, Figures 1, 2 and 10) has less resolution, but covers a very much larger area. The shelf/slope front is jagged in appearance and the continental shelf surface waters are highly heterogeneous. This kind of imagery is changing our perspective of the oceans by allowing us to see and understand some of their structural and dynamic complexity.

Additionally, remote sensors have the capability of providing real-time or near-real-time output of data sufficiently reduced to be useful in directing operations during the course of an experiment. The Ocean Color Scanner data collected by Ohlhorst during June 1980 (ref. 10, Figures 7, 8, and 9) were transmitted in real time from the aircraft to a ground station and used to direct operations. The Airborne Oceanographic Lidar, the L-band microwave radiometer, the PRT-5 infrared radiometer, and the Multichannel Ocean Color Scanner all produced data capable of being reduced in near-real-time for purposes of directing operations.

A particularly graphic example illustrating the usefulness of airborne remote sensing for defining major regions of the shelf and then directing surface ship sampling was presented by Grew (ref. 18, Figure 14). He used real-time output from a Multichannel Ocean Color Scanner (MOCS) to define the shelf regions and then direct a surface ship to each of the key areas. Approximately 8 to 9 hours prior to the aircraft-directed sampling, the NOAA Ship Kelez was requested to collect and process surface bucket samples (one every 10 to 15 minutes) for chlorophyll and phaeopigment (for Fo/Fa ratio) from the mouth of Chesapeake Bay east across the shelf to the continental rise (ref. 14, Figure 13). Data from the in situ samples were to be compared with the MOCS remotely sensed data. Although processed immediately, the data from these samples were not graphed until after the cruise. Consequently, the shape of the cross-shelf profile was unknown to those of us on the surface ship until much later. Thus no guidance was provided to aircraft personnel for directing in situ sampling. Once offshore over the continental rise we were asked to proceed back toward the mouth of the Bay along the same line we had just sampled (ref. 14, Figure 14). The difference, however, was that we took many fewer samples and those we did take were at locations selected by airborne MOCS operators on the basis of the real-time output they observed from MOCS.

In our charted data, notice that the cross-shelf profiles, as defined by both the remotely sensed and the in situ data, are similar (Figure 5), and that the in situ data derived from the aircraft-directed sampling (Figure 5b)

do describe the basic features of the chlorophyll a cross-shelf profile. Thus a degree of confidence can be had in the remotely sensed data to 1) characterize in real time the major features of the shelf and slope surface waters and 2) direct in situ sampling of these waters. This is particularly relevant to fishery research and monitoring in that the ability to define major type areas in real time enhances our ability to effectively utilize our ships and personnel.

CONCLUDING REMARKS

In terms of fishery research and monitoring, the combined use of in situ and remotely sensed data has enabled us to define, for each experiment as well as over time, the area of the continental shelf that is influenced by the Chesapeake Bay plume. Based on historical as well as present information we know that this area contracts and expands based on freshwater discharge from the Bay mouth and meteorological and physical factors affecting the shelf. From Superflux we know that the waters emanating from Chesapeake Bay contain biostimulants, contaminants and other materials as well as increased biomass and biological activity and structurally different assemblages of organisms. These waters emanating from the Bay are not homogeneous, but rather appear to be a series of discrete subplumes each with its own set of characteristics. We also see evidence to suggest that particulate materials settle from plume waters to the seabed down the length of the plume. Thus by way of expansion, contraction, changes in direction, and the fractionation or partitioning of materials, the Chesapeake Bay plume exerts greater or lesser positive and negative influences on the living marine resources of the contiguous shelf.

From remote sensing we have learned something of the complexity of the Chesapeake Bay plume and adjacent shelf surface waters. Remote sensing of the plume and neighboring shelf waters provided us with more synoptic and more detailed information concerning the distributions of temperature, salinity, turbidity, chlorophyll a, and phytoplankton assemblages in these surface waters than was obtainable using a single surface ship. In certain cases, repeated coverage by remote sensors informed us of some of the dynamic changes that took place over a period of several days. Additionally, sufficiently reduced real-time output from the remote sensors enabled definition of surface water masses over the continental shelf. Such ability to define the various water masses was used to direct in situ sampling of surface waters in near real time. Thus remote sensing adds to our ability to understand complex and dynamic areas by 1) providing synoptic and detailed information for the surface field in which in situ measurements at isolated locations are being made, and 2) directing surface ships to key areas to maximize their sampling ability.

Surface ships, however, not only provide sea truth for the remote sensors, but also examine the vertical structure of the water column and investigate variables not directly relatable to those measured by remote sensors. Thus it is the flow of information back and forth between remote sensing and in situ sampling that provides the real power to 1) overcome the temporal-spatial problems of in situ sampling and 2) expand the interpretability of the remotely sensed data to variables not measured directly by the remote sensors.

Johnson (ref. 19) has stated, "The exciting prospect is that remote sensing will be [is] a logical bridge between intensive ecological research on small areas and the application of principles thus revealed to planning and management of large political units such as townships, counties or states or whole natural units such as watersheds, tropical rain forests, or ocean basins." In future years remote sensing will be used more heavily in research. It will be used to monitor environmental quality and to assist in managing resources (e.g. directing fishing operations) and habitats (e.g. ecological zoning for development or waste disposal). Finally, because of its perspective vantage point and ability to describe surface flow and transport of materials, remote sensing will be utilized increasingly to respond to catastrophic events and major spills of toxic substances.

REFERENCES

1. Boicourt, W. C.: The Circulation of Water on the Continental Shelf from Chesapeake Bay to Cape Hatteras. Ph. D. Thesis, Johns Hopkins University, 1973.

2. Munday, John C.; and Fedosh, Michael S.: Chesapeake Bay Plume Dynamics from Landsat. Chesapeake Bay Plume Study - Superflux 1980, NASA CP-2188, 1981 (Paper no. 7 of this compilation).

3. Robertson, Craig N.: and Thomas, James P.: Total Plankton Respiration in the Chesapeake Bay Plume. Chesapeake Bay Plume Study - Superflux 1980, NASA CP-2188, 1981 (Paper no. 27 of this compilation).

4. Gingerich, Kathryn J.; and Oertel, George F.: Suspended Particulate Matter in the Chesapeake Bay Entrance and Adjacent Shelf Waters. Chesapeake Bay Plume Study - Superflux 1980, NASA CP-2188, 1981 (Paper no. 15 of this compilation).

5. Wong, George T. F.; and Todd, James F.: Nutrients in Waters on the Inner Shelf Between Cape Charles and Cape Hatteras. Chesapeake Bay Plume Study - Superflux 1980, NASA CP-2188, 1981 (Paper no. 20 of this compilation).

6. Kator, Howard I.; and Zubkoff, Paul L.: Bacterial Biomass and Heterotrophic Potential in the Waters of the Chesapeake Bay Plume and Contiguous Shelf. Chesapeake Bay Plume Study - Superflux 1980, NASA CP-2188, 1981 (Paper no. 28 of this compilation).

7. Marshall, Harold G.: Phytoplankton Assemblages Within the Chesapeake Bay Plume and Adjacent Waters of the Continental Shelf. Chesapeake Bay Plume Study - Superflux 1980, NASA CP-2188, 1981 (Paper no. 32 of this compilation).

8. Oertel, George F.; and Wade, Terry L.: Characteristics of Total Suspended Matter and Associated Hydrocarbon Concentrations Adjacent to the Chesapeake Bay Entrance. Chesapeake Bay Plume Study - Superflux 1980, NASA CP-2188, 1981 (Paper no. 19 of this compilation).

9. Kendall, Bruce M.: Remote Sensing of the Chesapeake Bay Plume Salinity via Microwave Radiometry. Chesapeake Bay Plume Study - Superflux 1980, NASA CP-2188, 1981 (Paper no. 10 of this compilation).

10. Ohlhorst, Craig W.: Preliminary Analysis of Ocean Color Scanner Data from Superflux III. Chesapeake Bay Plume Study - Superflux 1980, NASA CP-2188, 1981 (Paper no. 12 of this compilation).

11. Hoge, R. E.; and Swift, R. N.: Application of the NASA Airborne Oceanographic Lidar to the Mapping of Chlorophyll and Other Organic Pigments. Chesapeake Bay Plume Study - Superflux 1980, NASA CP-2188, 1981 (Paper no. 26 of this compilation).

12. Bowker, David E.; Hardesty, Charles A.; Jobson, Daniel S.; and Bahn, Gilbert S.: Analysis of Testbed Airborne Multispectral Scanner Data from Superflux II. Chesapeake Bay Plume Study - Superflux 1980, NASA CP-2188, 1981 (Paper no. 24 of this compilation).

13. Jarrett, Olin, Jr.; Esaias, Wayne E.; Brown, Clarence A., Jr.; and Pritchard, E. Brian: Analysis of ALOPE Data from Superflux. Chesapeake Bay Plume Study - Superflux 1980, NASA CP-2188, 1981 (Paper no. 29 of this compilation).

14. Thomas, James P.: Superflux I, II, and III Experiment Designs: Water Sampling and Analyses. Chesapeake Bay Plume Study - Superflux 1980, NASA CP-2188, 1981 (Paper no. 5 of this compilation).

15. Oertel, George F.; and Dunstan, W. M.: Suspended-Sediment Distribution and Certain Aspects of Phytoplankton Production off Georgia, U.S.A. Marine Geol., vol. 40, 1981, pp. 171-197.

16. Pearce, John B.: A Marine Environmental Monitoring and Assessment Program. Chesapeake Bay Plume Study - Superflux 1980, NASA CP-2188, 1981 (Paper no. 3 of this compilation).

17. Vukovich, Fred M.; and Crissman, Bobby W.: Monitoring the Chesapeake Bay Using Satellite Data for Superflux III. Chesapeake Bay Plume Study - Superflux 1980, NASA CP-2188, 1981 (Paper no. 8 of this compilation).

18. Grew, Gary W.: Real-Time Test of MOCS Algorithm During Superflux 1980. Chesapeake Bay Plume Study - Superflux 1980, NASA CP-2188, 1981 (Paper no. 23 of this compilation).

19. Johnson, P. L.: Remote Sensing as a Tool for Study and Management of Ecosystems. Chapter 18. Fundamentals of Ecology, E. P. Odum, ed., Saunders Co., Philadelphia, 1971.

20. Harris, R. L.: Metal Distributions in Suspended Sediment in the Chesapeake Bay Plume and Adjacent Atlantic Continental Shelf. Northeast Monitoring Program Office, Sandy Hook Laboratory, Highlands, New Jersey, Contract no. NA-80-FA-C-00034, 1980.

21. Wade, Terry L.; and Oertel, George F.: Concentration of Hydrocarbons Associated with Particles in the Shelf Waters Adjacent to the Entrance of Chesapeake Bay. Chesapeake Bay Plume Study - Superflux 1980, NASA CP-2188, 1981 (Paper no. 17 of this compilation).

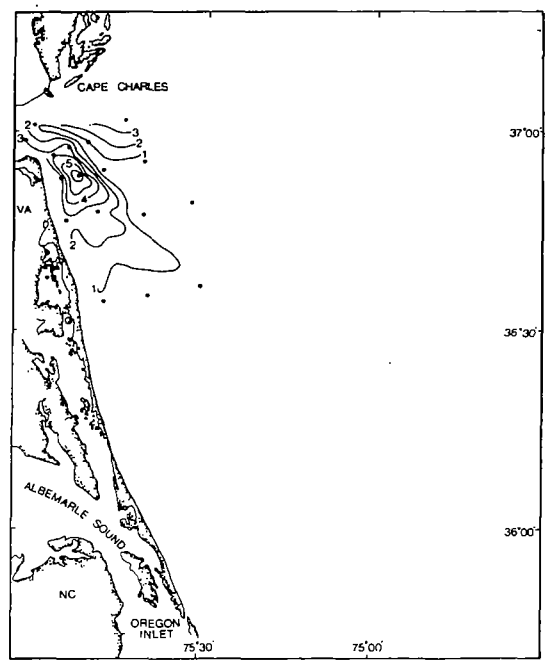

(a) Particulate manganese (mg Mn/g dry wt. sus. sed.) at 1 m depth for June 1980.

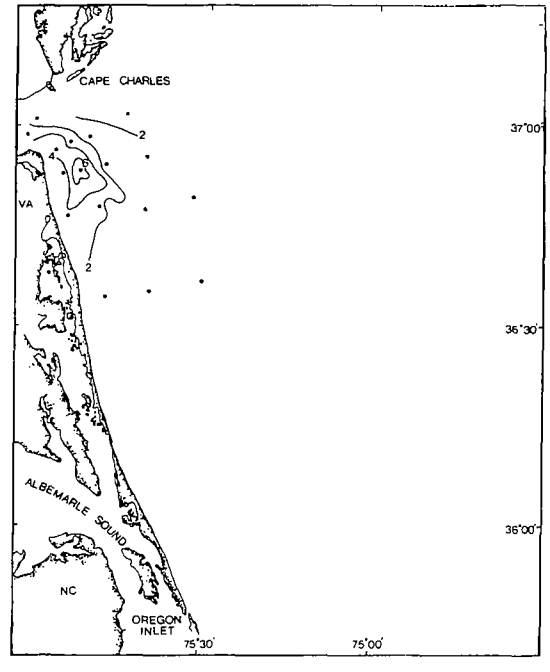

(b) Particulate iron (Fe in % dry wt. sus. sed.) at 1 m depth for June 1980.

Figure 1.- Heavy metals associated with total suspended matter (from ref. 20).

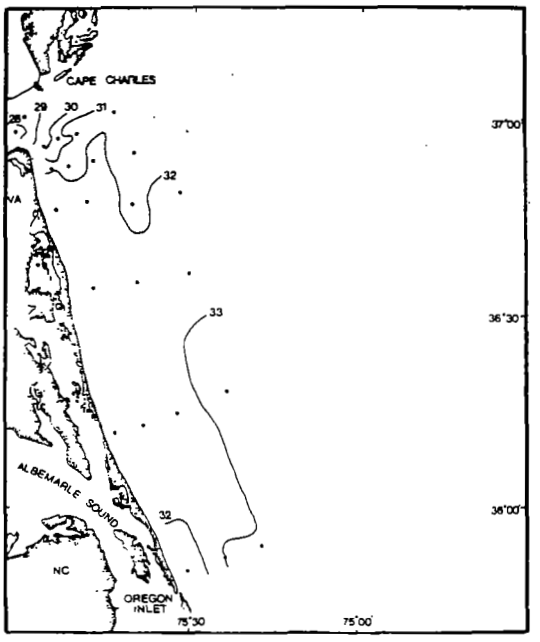

(a) October 1980.

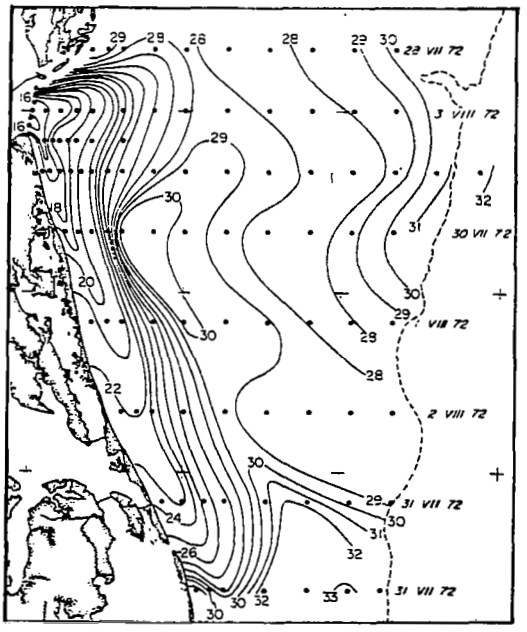

(b) July-August 1972.

Figure 2.- Surface (1 m) salinity distributions (°/oo) for October 1980 and July-August 1972 (from ref. 1).

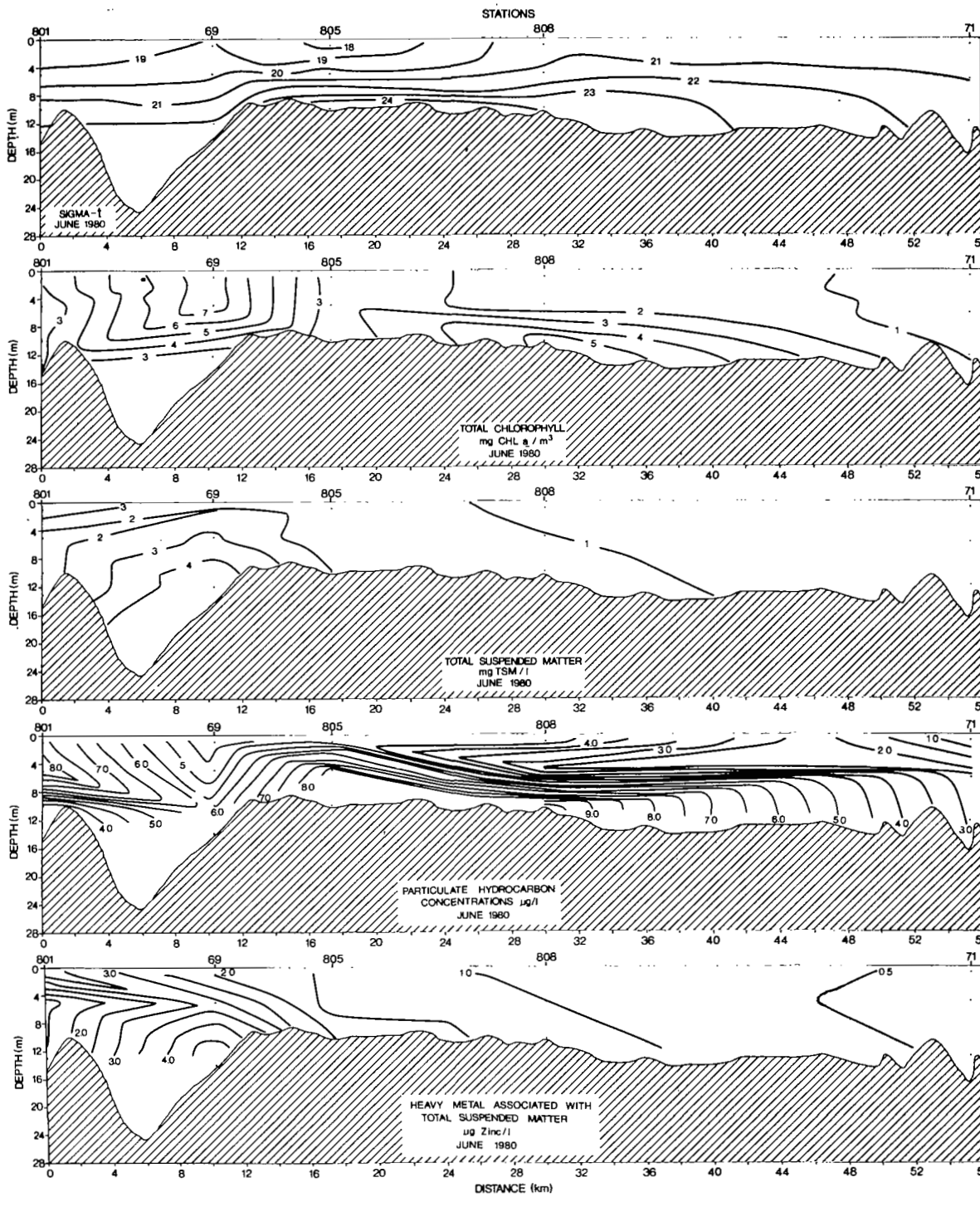

Figure 3.- Lengthwise section of the Chesapeake Bay plume for σ_t, total chlorophyll a, total suspended matter, particulate hydrocarbons (data from ref. 21), and heavy metal concentrations (ref. 20). See reference 14, Figure 8 for station locations.

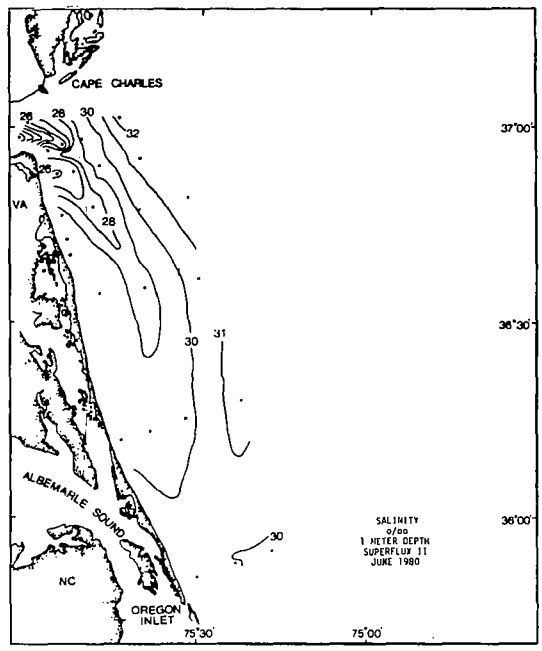

Figure 4.- Surface (1 m) salinity distribution (°/oo) for period 17-22 June 1980.

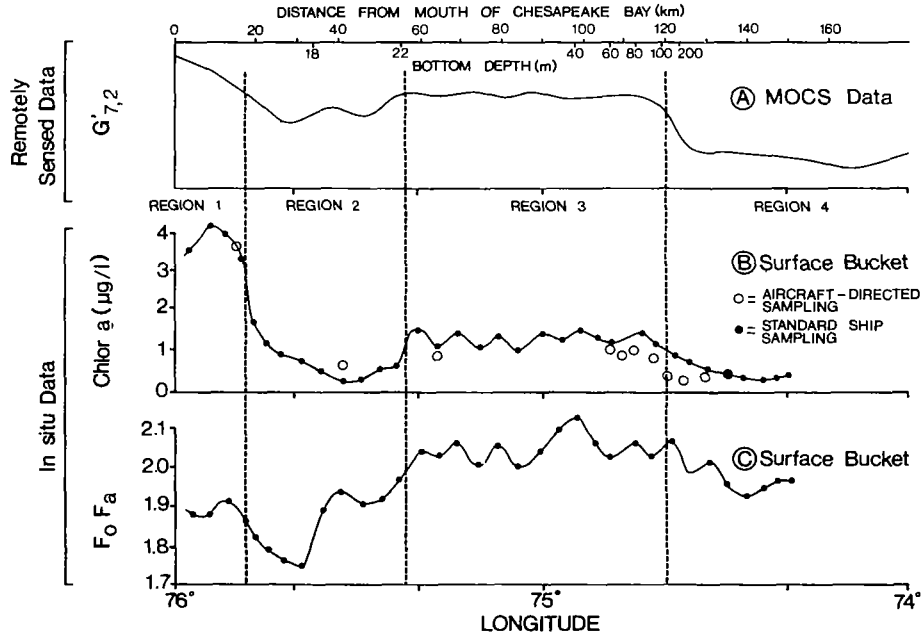

Figure 5.- Multichannel Ocean Color Scanner (MOCS) data, in situ surface chlorophyll a, and Fo/Fa ratios along transect from the mouth of Chesapeake Bay across shelf to continental rise and return on 21 October 1980 (after ref. 18).

*U.S. GOVERNMENT PRINTING OFFICE: 1981--735-006/12--1-3

1. Report No.	2. Government Accession No.	3. Recipient's Catalog No.
NASA CP-2188 NOAA/NEMP III 81 ABCDFG 0042		

4. Title and Subtitle	5. Report Date
Chesapeake Bay Plume Study - Superflux 1980	October 1981
	6. Performing Organization Code 146-40-15-50
7. Author(s)	8. Performing Organization Report No.
Janet W. Campbell and James P. Thomas, editors	L-14680
	10. Work Unit No.
9. Performing Organization Name and Address NASA Langley Research Center Hampton, VA 23665	11. Contract or Grant No.
	13. Type of Report and Period Covered Conference Publication
12. Sponsoring Agency Name and Address National Aeronautics and Space Administration Washington, DC 20546 and National Oceanic and Atmospheric Administration Washington, DC 20230	14. Sponsoring Agency Code

15. Supplementary Notes

16. Abstract

A symposium was convened in Williamsburg, Virginia, January 21-23, 1981, to present the results of three interactive aircraft-boat experiments which were conducted during March, June, and October 1980 in the Chesapeake Bay. The study, called Superflux, concentrated on the use of airborne remote sensors to characterize the spatial extent, variability, and biological and chemical properties of the Chesapeake Bay plume during periods of high, moderate, and low runoff. The program, which was sponsored jointly by the Northeast Fisheries Center (NEFC) of NOAA and NASA Langley Research Center, had three objectives: (1) to understand the influence of estuarine outflow on continental shelf ecosystems, (2) to determine the role of remote sensing in future marine monitoring and assessment programs, and (3) to advance the state of the art in remote sensing systems toward the day when remote sensing can be used operationally for monitoring and assessment.

17. Key Words (Suggested by Author(s))	18. Distribution Statement
Remote sensing Airborne remote sensing Pollution monitoring Fisheries management Estuarine flux Estuarine flow Ecosystem Continental shelf ecosystems	Unclassified - Unlimited Subject Category 48

19. Security Classif. (of this report)	20. Security Classif. (of this page)	21. No. of Pages	22. Price
Unclassified	Unclassified	522	A22

N-305

For sale by the National Technical Information Service, Springfield, Virginia 22161